BNL -73847-2005
Formal Report

Hunting the Quark Gluon Plasma

Results from the first 3 years at RHIC

Assessments by the experimental collaborations

April 18, 2005

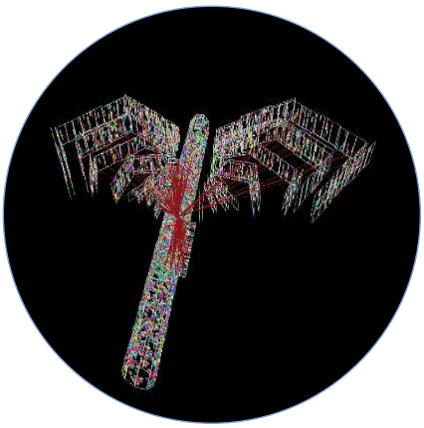

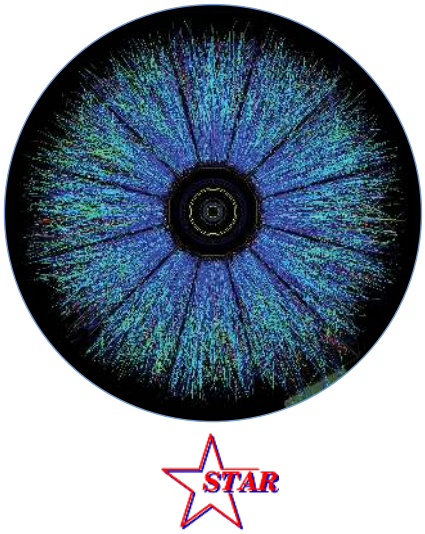

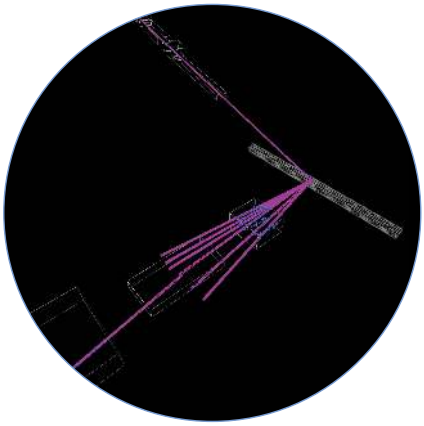

Relativistic Heavy Ion Collider (RHIC) • Brookhaven National Laboratory, Upton, NY 11974-5000

Office of Science
U.S. Department of Energy

BROOKHAVEN
NATIONAL LABORATORY

DISCLAIMER

CONTENTS

Forward

The U.S. Department of Energy's Relativistic Heavy Ion Collider (RHIC) construction project was completed at BNL in 1999, with the first data-taking runs in the summer of 2000. Since then the early measurements at RHIC have yielded a wealth of data, from four independent detectors, each with its international collaboration of scientists: BRAHMS, PHENIX, PHOBOS, and STAR [1].

For the first time, collisions of heavy nuclei have been carried out at colliding-beam energies that have previously been accessible only for high-energy physics experiments with collisions of "elementary" particles such as protons and electrons. It is at these high energies that the predictions of quantum chromodynamics (QCD), the fundamental theory that describes the role of quarks and gluons in nuclear matter, come into play, and new phenomena are sought that may illuminate our view of the basic structure of matter on the sub-atomic scale, with important implications for the origins of matter on the cosmic scale.

The RHIC experiments have recorded data from collisions of gold nuclei at the highest energies ever achieved in man-made particle accelerators. These collisions, of which hundreds of millions have now been examined, result in final states of unprecedented complexity, with thousands of produced particles radiating from the nuclear collision. All four of the RHIC experiments have moved quickly to analyze these data, and have begun to understand the phenomena that unfold from the moment of collision as these particles are produced. In order to provide benchmarks of simpler interactions against which to compare the gold-gold collisions, the experiments have gathered comparable samples of data from collisions of a very light nucleus (deuterium) with gold nuclei, as well as proton-proton collisions, all with identical beam energies and experimental apparatus.

The early measurements have revealed compelling evidence for the existence of a new form of nuclear matter at extremely high density and temperature – a medium in which the predictions of QCD can be tested, and new phenomena explored, under conditions where the relevant degrees of freedom, over nuclear volumes, are expected to be those of quarks and gluons, rather than of hadrons. This is the realm of the quark gluon plasma, the predicted state of matter whose existence and properties are now being explored by the RHIC experiments.

Many theorists have concluded that the results to date provide sufficient evidence that the quark gluon plasma has indeed been observed. [2] They state that the analyses of all four experiments point to the existence, in the evolution of the system immediately following a gold-gold collision, of a near-thermal, strongly interacting medium whose energy-density and temperature clearly exceed the critical values predicted by QCD calculations for a transition from ordinary hadronic states to a quark gluon plasma. However, detailed analyses of the data also make it clear that this hot, dense medium has properties that are surprising, and not yet fully understood in terms of the early expectations for the quark gluon plasma. For example, it was often stated, prior to the RHIC data, that the quark gluon plasma should behave like an ideal gas of quarks and gluons (i.e., like a weakly-coupled plasma state). The data now indicate that the observed medium behaves more like an ideal *fluid*, in analogy to a strongly coupled plasma state. Some theorists have referred to this state as the *strongly coupled quark gluon plasma*, or sQGP.

The "white papers" collected here represent the independent assessments from each of the experimental collaborations of what has been learned so far from their respective experiments regarding the existence and properties of the quark gluon plasma. The four collaborations state that the new phenomena they observe are signals of the creation of a new form of nuclear matter. However, they argue that the surprising properties of this collective medium seen in the present data need to be augmented with additional key measurements and also need to be better understood in terms of theoretical models for the formation, evolution, and freeze-out of a quark gluon plasma. These white papers are very much in the nature of status reports, providing a "snapshot" of rapidly evolving programs of data analysis. Much more will be learned over the next year from the analysis of Run IV data, obtained in the early months of 2004, which exceed the previous full-energy gold-gold data samples by a factor of ten.

A key result of the early measurements at RHIC is the demonstration that detailed exploration of the properties of new matter produced in the collisions can be carried out using experimental probes that are sensitive to the properties of the initial collective medium. What is more, it has been demonstrated that certain experimental probes are accessible that carry information directly from the thermal volume of hot matter during its lifetime. Such probes include the spectra of heavy quarks (charm and bottom) that are formed in the earliest stages of the collision, and are so massive that their dynamical properties would not be lost to thermalization at the temperatures and densities that prevail in the plasma of light quarks and gluons. Another class of such probes is the measurement and classification of high-momentum jets of particles and high-momentum photons corresponding to energetically scattered quarks and gluons. Accurate measurements of large samples allow experiments to perform tomography on the initial dense matter with "beams" of quarks and gluons.

These measurements, and others like them, along with continued progress in theory as the data become more precise, will provide the key to identifying and understanding the new form of matter produced at RHIC, and what it can reveal about the fundamental properties of the strong interaction.

S. Aronson and T. Ludlam
Brookhaven National Laboratory
April 2005

References:

1. "The Relativistic Heavy Ion Collider Project: RHIC and its Detectors", M. Harrison et al., ed., Nuclear Instruments and Methods in Physics Research A 499 (2003)
2. See, for example, "New Discoveries at RHIC – A Case for the Strongly Interactive Quark-Gluon Plasma", a collection of presentations at the RIKEN BNL Research Center, May 14-15, 2004, D. Rischke and G. Levin, ed., Nuclear Physics A750, issue 1 (2005)

BRAHMS

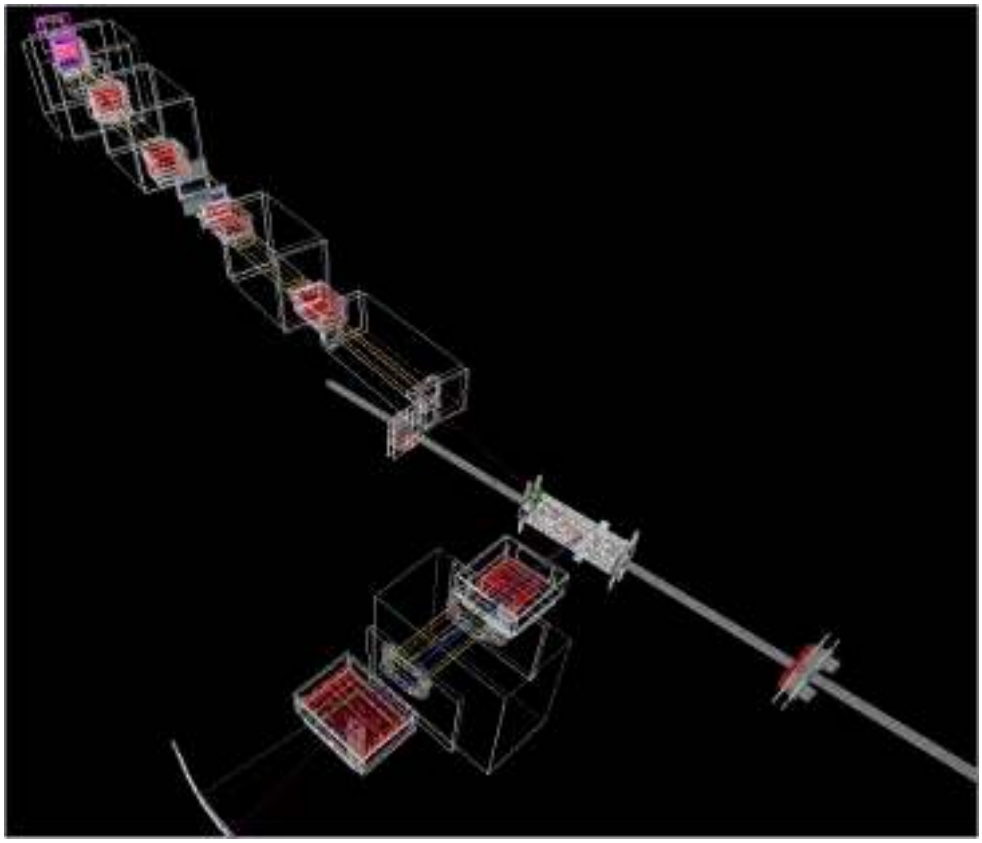

Quark Gluon Plasma and Color Glass Condensate at RHIC? The perspective from the BRAHMS experiment.

I. Arsene [j], I. G. Bearden [g], D. Beavis [a], C. Besliu [j], B. Budick [f], H. Bøggild [g], C. Chasman [a], C. H. Christensen [g], P. Christiansen [g], J. Cibor [c], R. Debbe [a], E. Enger [ℓ], J. J. Gaardhøje [g], M. Germinario [g], O. Hansen [g], A. Holm [g], A. K. Holme [ℓ], K. Hagel [h], H. Ito [a], E. Jakobsen [g], A. Jipa [j], F. Jundt [b], J. I. Jørdre [i], C. E. Jørgensen [g], R. Karabowicz [e], E. J. Kim [a,k], T. Kozik [e], T. M. Larsen [g,ℓ], J. H. Lee [a], Y. K. Lee [d], S. Lindahl [ℓ] G. Løvhøiden [ℓ], Z. Majka [e], A. Makeev [h], M. Mikelsen [ℓ], M. J. Murray [h,k], J. Natowitz [h], B. Neumann [k], B. S. Nielsen [g], D. Ouerdane [g], R. Płaneta [e], F. Rami [b], C. Ristea [g,j], O. Ristea [j], D. Röhrich [i], B. H. Samset [ℓ], D. Sandberg [g], S. J. Sanders [k], R. A. Scheetz [a], P. Staszel [g], T. S. Tveter [ℓ], F. Videbæk [a], R. Wada [h], Z. Yin [i], I. S. Zgura [j],

[a] *Brookhaven National Laboratory, Upton, New York 11973, USA*

[b] *Institut de Recherches Subatomiques et Université Louis Pasteur, Strasbourg, France*

[c] *Institute of Nuclear Physics, Krakow, Poland*

[d] *Johns Hopkins University, Baltimore 21218, USA*

[e] *M. Smoluchkowski Inst. of Physics, Jagiellonian University, Krakow, Poland*

[f] *New York University, New York 10003, USA*

[g] *Niels Bohr Institute, University of Copenhagen, Copenhagen 2100, Denmark*

[h] *Texas A&M University, College Station, Texas, 17843, USA*

[i] *University of Bergen, Department of Physics, Bergen, Norway*

[j] *University of Bucharest, Romania*

[k] *University of Kansas, Lawrence, Kansas 66045, USA*

[ℓ] *University of Oslo, Department of Physics, Oslo, Norway*

Preprint submitted to Elsevier Science *25 January 2005*

Abstract

We review the main results obtained by the BRAHMS collaboration on the properties of hot and dense hadronic and partonic matter produced in ultrarelativistic heavy ion collisions at RHIC. A particular focus of this paper is to discuss to what extent the results collected so far by BRAHMS, and by the other three experiments at RHIC, can be taken as evidence for the formation of a state of deconfined partonic matter, the so called quark-gluon-plasma (QGP). We also discuss evidence for a possible precursor state to the QGP, i.e. the proposed Color Glass Condensate.

Key words:
PACS: 25.75.q, 25.40.-h, 13.75.-n

---

1 Introduction

From the onset of the formulation of the quark model and the first understanding of the nature of the binding and confining potential between quarks about 30 years ago it has been conjectured that a state of matter characterized by a large density of quarks and gluons (together called partons) might be created for a fleeting moment in violent nuclear collisions [1]. This high energy density state would be characterized by a strongly reduced interaction between its constituents, the partons, such that these would exist in a nearly free state. Aptly, this proposed state of matter has been designated the quark gluon plasma (QGP)[2]. It is now generally thought that the early universe was initially in a QGP state until its energy density had decreased sufficiently, as a result of the expansion of the universe, that it could make the transition to ordinary (confined) matter.

Experimental attempts to create the QGP in the laboratory and measure its properties have been carried out for more than 20 years, by studying collisions of heavy nuclei and analyzing the fragments and produced particles emanating from such collisions. During that period, center of mass energies per pair of colliding nucleons have risen steadily from the $\sqrt{s_{NN}} \approx 1\,\mathrm{GeV}$ domain of the Bevalac at LBNL, to energies of $\sqrt{s_{NN}} = 5$ GeV at the AGS at BNL, and to $\sqrt{s_{NN}} = 17$ GeV at the SPS accelerator at CERN. No decisive proof of QGP formation was found in the experiments at those energies, although a number of signals suggesting the formation of a very dense state of matter, possibly partonic, were found at the SPS [3,4].

With the Relativistic Heavy Ion Collider, RHIC, at Brookhaven National Laboratory, the center of mass energy in central collisions between gold nuclei at $100\,\mathrm{AGeV} + 100\,\mathrm{AGeV}$ is almost $40\,\mathrm{TeV}$, the largest so far achieved in nucleus-nucleus collisions under laboratory conditions. This energy is so large

that conversion of a sizeable fraction of the initial kinetic energy into matter production creates many thousands of particles in a limited volume leading to unprecedented large energy densities and thus presumably ideal conditions for the formation of the quark gluon plasma.

RHIC started regular beam operations in the summer of year 2000 with a short commissioning run colliding Au nuclei at $\sqrt{s_{NN}} = 130\,\mathrm{GeV}$. The first full run at the top energy ($\sqrt{s_{NN}} = 200\,\mathrm{GeV}$) took place in the fall/winter of 2001/2002. The third RHIC run during the winter/spring of 2003 focussed on d+Au and p+p reactions. Recently, in 2004, a long high luminosity Au+Au run at $\sqrt{s_{NN}} = 200\,\mathrm{GeV}$ and a short run at $\sqrt{s_{NN}} = 62.4\,\mathrm{GeV}$ have been completed. The collected data from the most recent runs are currently being analyzed and only a few early results are thus available at the time of writing of this document.

The aim here is to review the available information obtained from the first RHIC experiments with the purpose of determining what the experimental results, accumulated so far, allow us to say about the high energy density matter that is created at RHIC in collisions between heavy atomic nuclei.

We concentrate primarily on results from the BRAHMS detector, one of the four detectors at RHIC, but naturally also refer to results obtained by the other three experiments (STAR, PHENIX and PHOBOS) insofar as they complement or supplement information obtained from BRAHMS. The BRAHMS experiment is a two arm magnetic spectrometer with excellent momentum resolution and hadron identification capabilities. The two spectrometers subtend only a small solid angle (a few msr) each, but they can rotate in the horizontal plane about the collision point to collect data on hadron production over a wide rapidity range (0-4), a unique capability among the RHIC experiments. For details about the BRAHMS detector system we refer the reader to [5,6]. The large number of articles already produced by the four experiments at RHIC may be found on their respective homepages [7]. Recent extensive theoretical reviews and commentaries may be found in refs. [8–10].

2 What is the QGP and what does it take to see it?

The predicted transition from ordinary nuclear matter, which consists of hadrons inside which quarks and gluons are confined, to the QGP, a state of matter in which quarks and gluons are no longer confined to volumes of hadronic dimensions, can in the simplest approach, be likened to the transition between two thermodynamic states in a closed volume.

As energy is transferred to the lower energy state a phase transition to the

higher energy state occurs, akin to a melting or an evaporation process. For a first order phase transition (PT), the transformation of one state into the other occurs at a specific temperature, termed the critical temperature, and the process is characterized by absorption of latent heat during the phase conversion, leading to a constancy or discontinuity of certain thermodynamic variables as the energy density or temperature is increased. In this picture, it is tacitly assumed that the phase transition occurs between states in thermodynamic equilibrium. From such thermodynamical considerations, and from more elaborate models based on the fundamental theory for the strong interaction, Quantum Chromo Dynamics (e.g. lattice QCD calculations), estimates for the critical temperature and the order of the transition can be made. Calculations indicate that the critical temperature should be $T_c \approx 175\,\mathrm{MeV}$ in the case of a vanishing baryon chemical potential [11]. The order of the transition at various values of the chemical potential is not known. In general, a decreasing critical temperature with increasing chemical potential is expected. Likewise, at non-zero chemical potential a mixed phase of coexisting hadron gas, HG, and QGP is predicted to exist in a certain temperature interval around the critical temperature. Recently calculational techniques have progressed to the point of allowing an extension of the lattice methods also to finite chemical potential. Such calculations also suggest the existence of a critical point at larger chemical potential above which, the transition may be of first order.

The transition from ordinary matter to the QGP is thus primarily a deconfinement transition. However, it is also expected, due to the vanishing interaction between partons in the QGP phase, that hadron masses will be lowered. In the limit of chiral symmetry the expectation value of the quark condensate, $< q\bar{q} >$, vanishes and opposite parity states (chiral partners) are degenerate. As a consequence of the QGP to HG transition, the chiral symmetry is broken and the hadrons acquire definite and nondegenerate masses. According to lattice QCD calculations chiral symmetry should be restored at sufficiently high temperature ($T >> T_c$).

It is, however, at the onset not at all clear that the transition to the QGP, as it is expected to be recreated in nucleus-nucleus collisions, proceeds between states of thermodynamic equilibrium as sketched above. The reaction, from first contact of the colliding nuclei to freeze-out of the created fireball, occurs on a typical timescale of about 10 fm/c and is governed by complex reaction dynamics so that non-equilibrium features may be important. Likewise there can be significant rescattering of the strongly interacting components of the system, after its formation, that tends to obscure specific features associated with a phase transition.

Many potential experimental signatures for the existence of the QGP have been proposed. These can be roughly grouped into two classes: 1) *evidence*

for bulk properties consistent with QGP formation, e.g. large energy density, entropy growth, plateau behavior of the thermodynamic variables, unusual expansion and lifetime properties of the system, presence of thermodynamic equilibration, fluctuations of particle number or charge balance etc, and 2) *evidence for modifications of specific properties of particles thought to arise from their interactions with a QGP*, e.g. the modification of widths and masses of resonances, modification of particle production probabilities due to color screening (e.g. J/Ψ suppression) and modification of parton properties due to interaction with other partons in a dense medium (e.g. jet quenching), etc.

We may ask the following questions: *1) What is the requirement for calling a state of matter a QGP*, and *2) What would constitute proof of QGP formation according to that definition?*

As far as the first question is concerned it would seem obvious that the determining factor is whether the high density state that is created in the nuclear collisions clearly has properties that are determined by its partonic composition, beyond what is known at the nucleon level in elementary nucleon-nucleon collisions (e.g. p+p collisions). It has often been presupposed that the 'plasma' should be in thermodynamical equilibrium. However, this may not be realized within the short time scales available for the evolution of the reaction from first contact to freeze-out, and is perhaps not necessary in the definition of the version of the QGP that may be observable in relativistic heavy ion collisions. Finally, it may be asked whether chiral symmetry restoration is essential. It would seem that even in a situation in which the partons of the system are still (strongly) interacting one may speak of a QGP as long as the constituents are not restricted to individual hadrons. Thus it would appear that *deconfinement* is the foremost property needed to define the QGP state, and the one that needs to be demonstrated by experiment.

Clearly, the observation of all, or at least of a number of the effects listed above, in a mutually consistent fashion, would serve to constitute a strong case for the formation of a QGP. Ideally, the observed effects must not be simultaneously describable within other frameworks, e.g. those based on purely hadronic interactions and not explicitly involving the partonic degrees of freedom. This suggests the requirement that a 'proof', in addition to having consistency with QGP formation, also must contain elements that are *only* describable in terms of QGP formation, phase transition etc.

Finally, if a sufficiently good case exists, we may also ask if there are any specific features that may *falsify* the conclusion. To our knowledge no tests have been proposed that may allow falsification of either a partonic scenario or a hadronic scenario, but it would be important if any such exclusive tests were to be formulated.

In this report we address some of the signatures discussed above, notably the energy density, which can be deduced from the measured particle multiplicities, the thermal and dynamical properties of the matter at freeze-out which may be inferred from the abundances and spectral properties of identified particles, and the modifications of spectral properties arising from the interaction of particles with the high energy-density medium.

3 Reactions at RHIC: how much energy is released?

The kinetic energy that is removed from the beam and which is available for the production of a state such as the QGP depends on the amount of stopping between the colliding ions.

The stopping can be estimated from the rapidity loss experienced by the baryons in the colliding nuclei. If incoming beam baryons have rapidity, y_b relative to the CM (which has $y = 0$) and average rapidity

$$< y >= \int_0^{y_b} y \frac{dN}{dy} dy / \int_0^{y_b} \frac{dN}{dy} dy \qquad (1)$$

after the collision, the average rapidity loss is $\delta y = y_b - < y >$ [12,13]. Here dN/dy denotes the number of net-baryons (number of baryons minus number of antibaryons) per unit of rapidity. Thus, for the case of full stopping: $\delta y = y_b$.

At AGS energies the number of produced antiprotons is quite small and the net-baryon distribution is similar to the proton distribution [15–17]. The net-proton rapidity distribution is centered around $y = 0$ and is rather narrow. The rapidity loss for central collisions is about 1 for a beam rapidity of approx. 1.6. At CERN-SPS energies ($\sqrt{s_{NN}} = 17\,\mathrm{GeV}, 158\,\mathrm{AGeV}$ Pb+ Pb central reactions) the rapidity loss is slightly less than 2 for a beam rapidity of 2.9 [18], about the same relative rapidity loss as at the AGS. The fact that the rapidity loss is large on an absolute scale means, however, that there is still a sizeable energy loss of the colliding nuclei. This energy is available for particle production and other excitations, transverse and longitudinal expansion. Indeed, in collisions at the SPS, multiplicities of negatively charged hadrons are about $dN/dy = 180$ around $y = 0$. At SPS another feature is visible (see fig. 1): the net proton rapidity distribution shows a double 'hump' with a dip around $y = 0$. This shape results from the finite rapidity loss of the colliding nuclei and the finite width of each of the humps, which reflect the rapidity distributions of the protons after the collisions. This picture suggests that the reaction at the SPS is beginning to be transparent in the sense that fewer of the original baryons are found at midrapidity after the collisions, in contrast to the situation at lower energies.

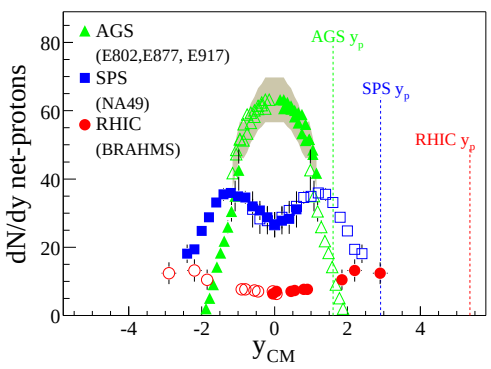

Fig. 1. Rapidity density of net protons (i.e. number of protons minus number of antiprotons) measured at AGS, SPS, and RHIC (BRAHMS) for central collisions [19]. At RHIC, where the beam rapidity is $y = 5.4$, the full distribution cannot be measured with current experiments, but BRAHMS will be able to extend its unique results to y=3.5 from the most recent high statistics Au+Au run, corresponding to measurements extending to 2.3 degrees with respect to the beam direction.

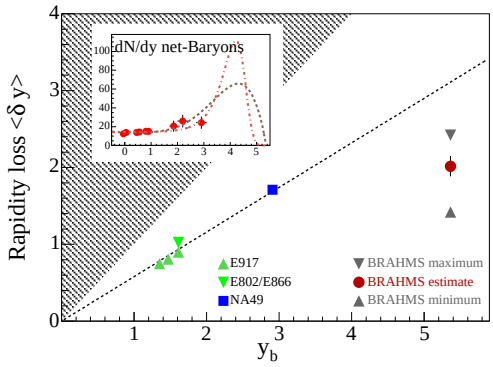

Fig. 2. Insert: fit of the data to two possible net-baryon distributions (Gaussian in p_L and 6'th order polynomial) respecting baryon number conservation. In going from net-proton to net-baryon distributions we have assumed that $N(n) \approx N(p)$ and have scaled hyperon yields known at midrapidity to forward rapidity using HIJING. Even assuming that all missing baryons are located just beyond the acceptance edge or at the beam rapidity, quite tight limits on the rapidity loss of colliding Au ions at RHIC can be set [19] (main panel).

BRAHMS has measured [19] the net proton rapidity distribution at RHIC in the interval $y = 0-3$ in the first run with $(0-10\%)$ central Au+Au collisions at full energy. The beam rapidity at RHIC is about 5.4. Details of the analysis can be found in [19]. The results are displayed in fig. 1 together with the previously discussed net-proton distributions measured at AGS and SPS. The distribution measured at RHIC is both qualitatively and quantitatively very different from those at lower energies indicating a significantly different system is formed near midrapidity.

The net number of protons per unit of rapidity around $y = 0$ is only about 7 and the distribution is flat over at least the ± 1 unit of rapidity. The distribution rises in the rapidity range $y = 2-3$ to an average $dN/dy \approx 12$. We have not yet completed the measurements at the most forward angles (highest rapidity) allowed by the geometrical setup of the experiment, but we can exploit baryon conservation in the reactions to set limits on the relative rapidity loss at RHIC. This is illustrated in fig. 2, which shows two possible distributions whose integral areas correspond to the number of baryons present in the overlap between the colliding nuclei. From such distributions one may deduce a set of upper and lower limits for the rapidity loss at RHIC. Furthermore the situation is complicated by the fact that not all baryons are measured. The limits shown in the figure includes estimates of these effects [19]. The

conclusion is that the *absolute* rapidity loss at RHIC ($\delta y = 2.0 \pm 0.4$) is not appreciably larger than at SPS. The value is close to expectations from extrapolations of pA data at lower energies [13,14]. In fact the *relative* rapidity loss is significantly reduced as compared to an extrapolation of the low energy systematics [12].

It should be noted that the rapidity loss is still significant and that, since the overall beam energy (rapidity) is larger at RHIC than at SPS, the *absolute energy loss* increases appreciably from SPS to RHIC thus making available a significantly increased amount of energy for particle creation in RHIC reactions.

In particular we have found that the average energy loss of the colliding nuclei corresponds to about 73 ± 6 GeV per nucleon [19]. From our measurements of the particle production as a function of rapidity (pions, kaons and protons and their antiparticles) we can deduce not only the number of produced particles but also their average transverse momentum and thus their energy. Within systematic errors of both measurements we find that the particle production is consistent with the energy that is taken from the beam.

Thus, the energy loss measurements clearly establish that as much as 26 TeV *of kinetic energy is removed from the beam per central Au+Au collision. This energy is available for particle production in a small volume immediately after the collision.*

4 Energy density

The collision scenario that we observe at RHIC and which was outlined in the previous section indicates that the reaction can be viewed as quite transparent. After the collision, the matter and energy distribution can be conceptually divided up into two main parts, a so–called fragmentation region consisting of the excited remnants of the colliding nuclei which have experienced an average rapidity loss, $\delta y \approx 2$, and a central region in which few of the original baryons are present but where significant energy density is collected.

This picture is in qualitative agreement with the schematic one already proposed by Bjorken 20 years ago [20]. The central region (an interval around midrapidity) is decoupled from the fragments. In that theoretical scenario the energy removed from the kinetic energy of the fragments is initially stored in a color field strung between the receding partons that have interacted. The linear increase of the color potential with distance eventually leads to the production of quark-antiquark pairs. Such pairs may be produced anywhere between the interacting partons leading to an approximately uniform particle

production as a function of rapidity and similar spectra characteristics in each frame of reference (boost invariance).

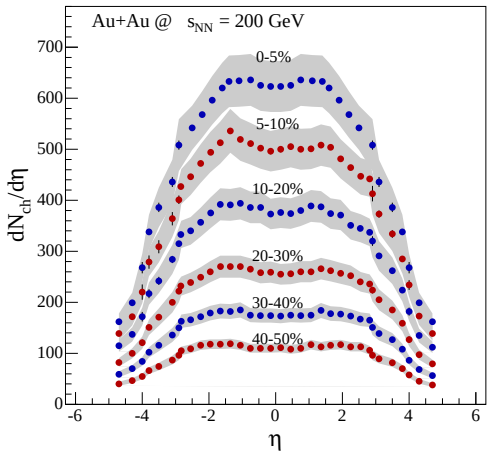

Fig. 3. Pseudorapidity densities (multiplicities) of charged particles measured by BRAHMS for $\sqrt{s_{NN}} = 200\,GeV$ Au+Au collisions for various centralities. The integral of the most central distribution $0-5\%$ corresponds to about 4600 charged particles [6].

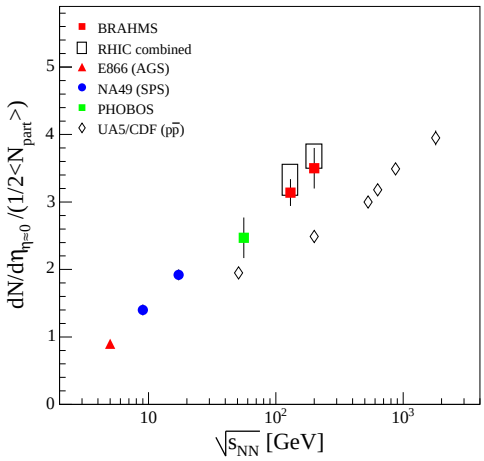

Fig. 4. Multiplicity of charged particles per participant pair around midrapidity, as a function of $\sqrt{s_{NN}}$. The figure shows that the particle production in Au+Au collisions at the RHIC top energy , around $\eta = 0$, exceeds that seen in p+p collisions by 40-50%.

Figure 3 shows the overall multiplicity of charged particles observed in Au+Au collisions at RHIC [6] for various collision centralities and as a function of pseudorapidity. The figure shows that the multiplicity at RHIC is about $dN/d\eta = 625$ charged particles per unit of rapidity around $\eta = 0$ for central collisions. Figure 4 shows that the production of charged particles in central collisions exceeds the particle production seen in p+p collisions at the same energy by 40-50%, when the yield seen in Au+Au collisions is divided by the number of pairs of participant nucleons (participant scaling). Also we note that the average rapidity loss in p+p collisions is $\delta y \approx 1$. The energy available for particle production in p+p is thus about 50% of the beam energy, to be compared to the 73% found for Au+Au collisions.

Integration of the charged particle pseudorapidity distributions corresponding to central collisions tells us that about 4600 charged particles are produced in each of the 5% most central collisions. Since we only measure charged particles, and not the neutrals, we multiply this multiplicity by 3/2 to obtain the total particle multiplicity of about 7000 particles.

From the measured spectra of pions, kaons and protons and their antiparticles as a function of transverse momentum we can determine the average transverse mass for each particle species (fig. 5). This allows us to estimate the initial

energy density from Bjorkens formula [20]

$$\epsilon = \frac{1}{\pi R^2 \tau} \frac{d\langle E_T \rangle}{dy} \tag{2}$$

where we can make the substitution $d\langle E_T \rangle = \langle m_T \rangle dN$ and use quantities from the measured spectral distributions. Since we wish to calculate the energy density in the very early stages of the collision process we may use for R the radius of the overlap disk between the colliding nuclei, thus neglecting transverse expansion. The formation time is more tricky to determine [21,22]. From the uncertainty relation and the typical relevant energy scale (200 MeV) one infers a formation time of the order of 1 fm/c. This leads to $\epsilon \approx 5\,\mathrm{GeV/fm^3}$, which should be considered as a lower limit. Alternatively, one may use the average transverse momentum of produced particles around midrapidity (see fig. 5) to set the energy scale. This leads to estimates of the energy density that are 3-4 times higher. The $\epsilon \approx 5\,\mathrm{GeV/fm^3}$ value for the initial energy exceeds the energy density of a nucleus by a factor of 30 the energy density of a baryon by a factor of 10, and the energy density for QGP formation that is predicted by lattice QCD calculations by a factor of 5 [23,24].

The particle multiplicities that are observed at RHIC indicate that the energy density associated with particle production in the initial stages of the collisions largely exceeds the energy density of hadrons.

5 Is there thermodynamical and chemical equilibrium at RHIC?

It has traditionally been considered crucial to determine whether there is thermodynamical equilibration of the "fireball" in relativistic collisions. The main reason is that, if there is thermalization, the simple two phase model may be invoked and the system should evidence the recognizable features of a phase transition.

In nuclear collisions, however, the time scale available for equilibration is very short and the entire system only lives in the order of 10 fm/c. Consequently, it is not evident that the system will evolve through equilibrated states. If equilibrium is established, it would suggest that the system existed for a short time in a state with sufficiently short mean free path. A central issue is whether equilibrium is established in the hadronic cloud in the later stages of the collisions just prior to freeze-out or whether it is established on the partonic level prior to hadronization [25]. Thus, even if equilibration *per se* is probably not a requirement for defining the QGP, it may prove to be an important tool in *identifying* the QGP.

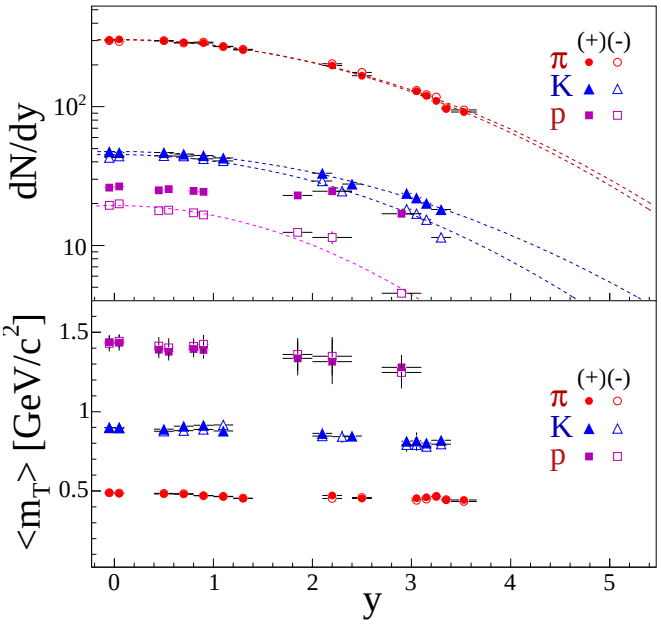

Fig. 5. Top panel: rapidity density distribution for positive and negative pions, kaons and protons measured by Brahms. The shown data have not been corrected for feed down. The lines show Gaussian fits to the measured distributions. Bottom panel: average m_T distributions as a function of rapidity. From [26].

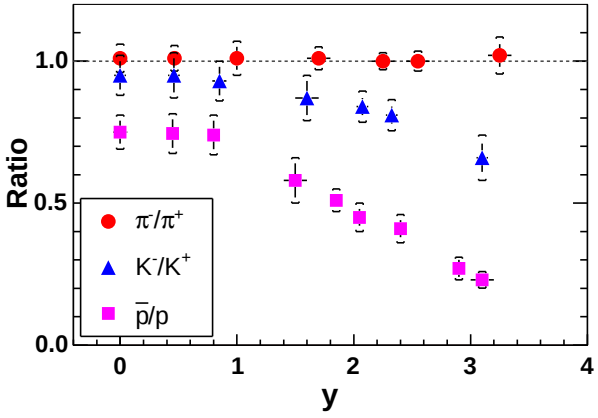

Fig. 6. Ratios of antiparticles to particles (pions, kaons and protons) as a function of rapidity for $\sqrt{s_{NN}} = 200\,\mathrm{GeV}$ Au+Au collisions measured by the BRAHMS experiment [27]. For the first time in nuclear collisions an approximate balance between particles and antiparticles is seen around midapidity. Statistical and systematic errors are indicated.

Figure 5 shows the results of a recent and more detailed study of particle production in central collisions as a function of rapidity [19,26]. The figure shows the rapidity densities of pions, kaons and protons for central collisions. From such distributions we can construct the ratio of the yields of particles

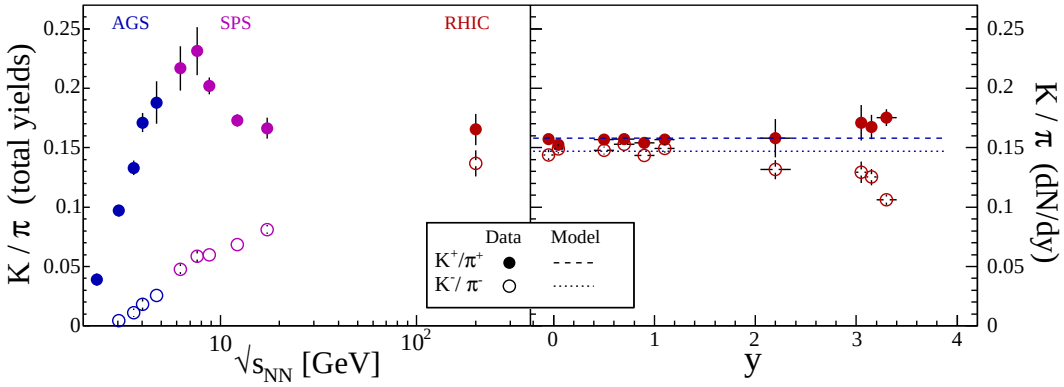

Fig. 7. Left panel: ratios of kaons and pions of both charge signs and in the full phase space (i.e. integrated over azimuthal angles and over rapidity) as a function of center of mass energy in the nucleon-nucleon system. Right panel: the ratios at the top RHIC energy as a function of rapidity. At midrapidity the two ratios are about the same and equal to 0.15 [26], while at forward rapidity the ratio of positive kaons and pions increases as expected for a larger baryochemical potential. The lines show statistical model predictions assuming a temperature of 177 MeV and $\mu_B = 29$ MeV.

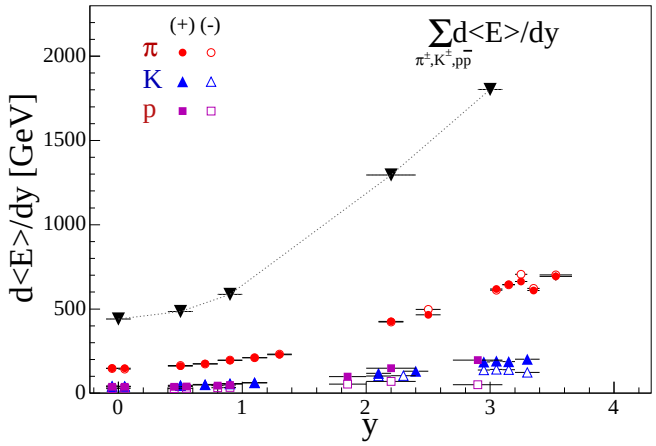

Fig. 8. Total relativistic energy carried by charged hadrons (pions, kaons, protons and their antiparticles) in the rapidity interval $0 < y < 3$ deduced from the information in fig. 5 and using the relationship $E = m_t cosh(y)$. The triangles show the sum of the individual distributions. Adding the expected contribution from unobserved neutral particles it can be concluded that particles in the range $-3 < y < 3$ carry about 9 TeV of total energy whereas particle in the range $-1 < y < 1$ carry about 1.5 TeV.

and their antiparticles as a function of rapidity. Figure 6 shows the ratios of yields of antihadrons to hadrons (posititive pions, kaons and protons and their antiparticles). The ratio is seen to be approaching unity in an interval of about 1.5 units of rapidity around midrapidity, suggesting that the particle production in the central region is predominantly from pair creation. This

is true for pions (ratio of 1), but less so for kaons (ratio=0.95) and protons (ratio= 0.76). There are processes that break the symmetry between particles and antiparticles that depend on the net-baryon content discussed in the previous section. One such process that is relevant for kaons is the associated production mechanism (e.g. $p+p \rightarrow p+\Lambda+K^+$) which leads to an enrichment of positive kaons in regions where there is an excess of baryons. Support for this view is given by fig. 7, which shows the systematics of kaon production relative to pion production as a function of center of mass energy. At AGS, where the net proton density is high at midrapidity, the rapidity density of K^+ strongly exceeds that of K^-. In contrast, at RHIC, production of K^+ and K^- is almost equal. This situation changes, however, at larger rapidities where the net proton density increases.

From the measured yields of identified particles as a function of rapidity and their momentum spectra we may calculate the total relativistic energy carried by particles in the rapidity interval $y = 0 - 3$. This is shown in fig. 8. By integrating and reflecting the total energy distribution around $y = 0$ and adding the estimate contribution from neutrals we may deduce that about 9 TeV are carried by the particles in the rapidity range $|y| < 3$.

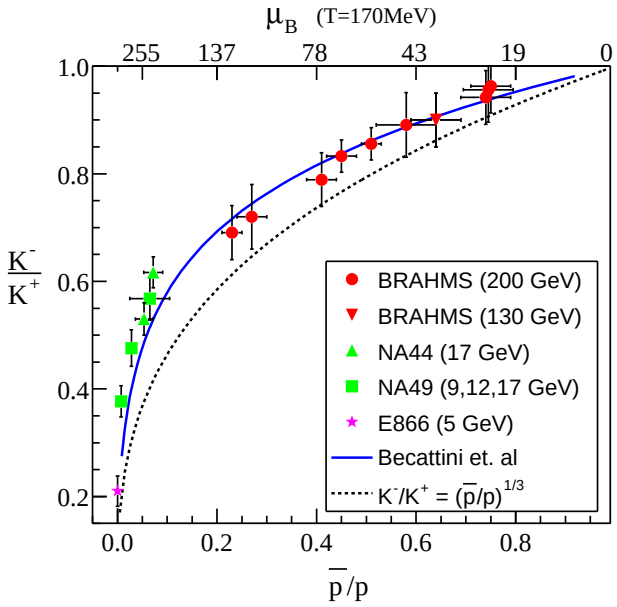

Fig. 9. Correlation between the ratio of charged kaons and the ratio of antiprotons to protons. The dashed curve corresponds to equation 4 in the text using $\mu_s = 0$. The full drawn curve is a statistical model calculation with a chemical freeze-out temperature fixed to 170 MeV [27,32] but allowing the baryochemical potential to vary. The circles denote ratios measured by BRAHMS at the top RHIC energy at different rapidities in the range $0 < y < 3$. At midrapidity the baryochemical potential has decreased to $\mu_B \approx 25 MeV$.

The particle yields measured by BRAHMS also lend themselves to an analysis of the charged particle production in terms of the statistical model [27–33].

Figure 9 shows the ratios of negative kaons to positive kaons as a function of the corresponding ratios of antiprotons to protons for various rapidities at RHIC. The data are for central collisions, and the figure also displays similar ratios for heavy ion collisions at AGS and SPS energies. There is a striking correlation between the RHIC/BRAHMS kaon and proton ratios over 3 units of rapidity. Assuming that we can use statistical arguments based on chemical and thermal equilibrium at the quark level, the ratios can be written

$$\frac{\rho(\bar{p})}{\rho(p)} = exp(\frac{-6\mu_{u,d}}{T}) \tag{3}$$

and

$$\frac{\rho(K^-)}{\rho(K^+)} = exp(\frac{-2(\mu_{u,d} - \mu_s)}{T}) = exp(\frac{2\mu_s}{T}) \times [\frac{\rho(\bar{p})}{\rho(p)}]^{\frac{1}{3}} \tag{4}$$

where ρ, μ and T denote number density, chemical potential and temperature, respectively. From equation 3 we find the chemical potential for u and d quarks at midrapidity to be around 25 MeV, the lowest value yet seen in nucleus-nucleus collisions. Equation 4 tells us that for a vanishing strange quark chemical potential we would expect a power law relation between the two ratios with exponent 1/3. The observed correlation deviates from the naive expectation suggesting a finite value of the strange quark chemical potential.

A more elaborate analysis assuming a grand canonical ensemble with charge, baryon and strangeness conservation can be carried out by fitting these and many other particle ratios observed at RHIC in order to obtain the chemical potentials and the temperature. It is found that a very large collection of such particle ratios are extremely well described by the statistical approach [31,33]. An example of such a procedure is shown in fig. 9 and displayed with the full line [32]. Here the temperature is 170 MeV. The point to be made is that the calculation agrees with the data over a wide energy range (from SPS to RHIC) and over a wide range of rapidity at RHIC. This may be an indication that the system is in chemical equilibrium over the considered $\sqrt{s}$ and y ranges (or at least locally in the various y bins). However, that statistical fits reproduce particle ratios is only a necessary condition for equilibration. Separate measurements at RHIC of, for example, elliptical flow also suggest that the system behaves collectively and thus that the observed ratios are not just due to the filling of phase space according to the principle of maximum entropy.

5.2 Flow

The properties of the expanding matter in the later stages of the collisions up to the moment when interactions cease (kinetic freeze out) can be studied from

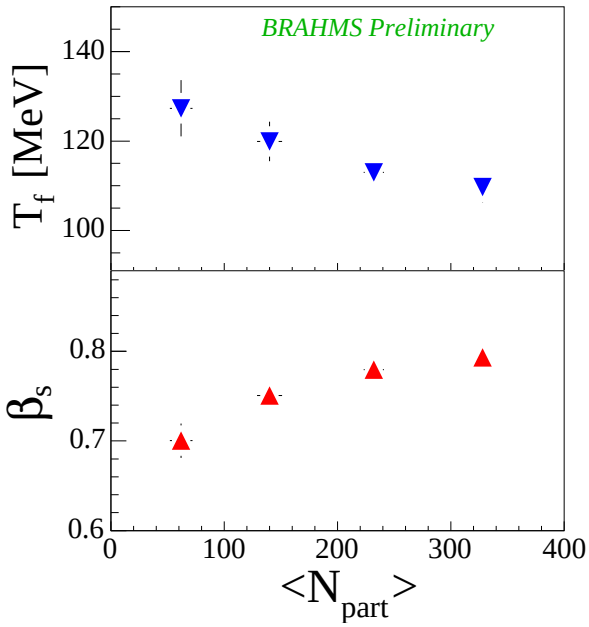

Fig. 10. Temperature and (surface) transverse flow velocity at the kinetic freezeout as a function of collision centrality for Au+Au collisions at midrapidity. The values have been obtained from blastwave fits to measured transverse momentum spectra. BRAHMS preliminary [40].

the momentum distribution of the emitted particles. The slopes of spectra of emitted particles depend in general on the temperature of the source from which they were created and on kinetic effects that may alter the expected Maxwellian distribution, such as a velocity component resulting from an overpressure leading to an outwards flow of the matter. This flow is expected, in the case of (at least local) thermal equilibrium and sufficient density, to be describable by concepts derived from fluid dynamics. One should note that the slopes of spectra reflect the particle distributions at the time of freeze-out when interactions have ceased.

In the so-called blastwave approach the spectrum shape is parametrized by a function depending on the temperature and on the transverse expansion velocity which in turn depends on the radius. The result of such analyses for several particle/antiparticle species indicates that the thermal (freezeout) temperature is in the range $T = 120 - 140\,\mathrm{MeV}$ and that the maximum flow velocity is about $0.70c - 0.75c$ as displayed in Fig. 10. The first quantity is found, as expected, to be lower than the temperature of the chemical freeze out discussed in the previous subsection. Indeed, it would be expected that the freeze-out of particle ratios occurs earlier than the kinetic freeze out of the particles. The flow velocity component is larger than what was observed at SPS energies. This is consistent with a large pressure gradient in the transverse direction resulting from a large initial density. Fig.10 shows results from analysis of midrapidity particle spectra from the BRAHMS experiment using

the blastwave approach.

Another powerful tool to study the thermodynamic properties of the source is the analysis of the azimuthal momentum distribution of the emitted particles relative to the event plane (defined as the direction of the impact parameter). This distribution is usually parametrized as a series of terms depending on $cos(n(\phi - \phi_r))$, where ϕ and ϕ_r denote the azimuthal angles of the particle and of the reaction plane, respectively. The coefficient (v_1) to the n=1 term measures the so-called directed flow and the coefficient (v_2) to the n=2 term measures the elliptic flow. Elliptic flow has been analyzed at RHIC [34–39] and has been found to reach (for many hadron species) large (v_2) values consistent with the hydrodynamical limit and thus of equilibration. Model calculations suggest [41–47] that the observed persistence of azimuthal momentum anisotropy indicates that the system has reached local equilibrium very quickly and that the equilibrium can only be established at the *partonic* level when the system is very dense and has many degrees of freedom. This explanation presupposes however that there are many interactions and thus that the dense partonic phase is strongly interacting.

The particle ratios observed at RHIC can be well described by concepts from statistical physics applied at the quark level, thus assuming thermodynamical equilibrium. However this is only a necessary condition and not a sufficient condition for equilibration. The observation of a strong elliptic flow at RHIC and comparison to model calculation suggests that the system is strongly collective as must be the case for an equilibrated system.

6 High p_T suppression. The smoking gun of QGP?

The discussion in the previous sections indicates that the conditions for particle production in an interval $|y| \lesssim 1.5$ at RHIC are radically different than for reactions at lower energies. At RHIC the central zone is baryon poor, the considered rapidity interval appears to approximately exhibit the anticipated boost invariant properties, the particle production is large and dominated by pair production and the energy density appears to exceed significantly the one required for QGP formation. The overall scenario is therefore consistent with particle production from a color field, formation of a QGP and subsequent hadronization. Correlation and flow studies suggest that the lifetime of the system is short ($< 10 fm/c$) and, for the first time, there is evidence suggesting thermodynamic equilibrium already at the partonic level.

But, is this interpretation unique? And, can more mundane explanations based on a purely hadronic scenario be excluded? In spite of the obvious difficulties in reconciling the high initial energy density with hadronic volumes, a com-

prehensive answer to this question requires the observation of an effect that is directly dependent on the partonic or hadronic nature of the formed high density zone.

6.1 High p_T suppression at midrapidity: final state partonic energy loss?

Such an effect has recently been discovered at RHIC and is related to the suppression of the high transverse momentum component of hadron spectra in central Au+Au collisions as compared to scaled momentum spectra from p+p collisions [48–51]. The effect, originally proposed by Bjorken, Gyulassy and others [52–55] is based on the expectation of a large energy loss of high momentum partons, scattered in the initial stages of the collisions, in a medium with a high density of color charges [56]. According to QCD colored objects may lose energy by radiating gluons as bremsstrahlung. Due to the color charge of the gluons, the energy loss is proportional to the square of the length of color medium traversed. Such a mechanism would strongly degrade the energy of leading partons resulting in a reduced transverse momentum of leading particles in the jets that emerge after fragmentation into hadrons. The STAR experiment has shown that the topology of high p_T hadron emission is consistent with jet emission, so that we may really speak about jet-suppression [57].

The two upper rows of fig. 11 show our measurements [48,58] of the so-called nuclear modification factors for *unidentified* charged hadrons from Au+Au collisions at rapidities $\eta = 0$ and 2.2. The nuclear modification factor is defined as:

$$R_{AA} = \frac{d^2N^{AA}/dp_t d\eta}{< N_{bin} > d^2N^{NN}/dp_t d\eta}. \tag{5}$$

It involves a scaling of measured nucleon-nucleon transverse momentum distributions by the calculated number of binary nucleon-nucleon collisions, N_{bin}. In the absence of medium effects, the nuclear collisions can, at high p_T be viewed as a superposition of elementary hard nucleon-nucleon collisions. Consequently we expect $R_{AA} = 1$ at high p_T. At low p_T, where the particle production follows a scaling with the number of participants, the above definition of R_{AA} leads to $R_{AA} < 1$ for $p_T < 2\,\mathrm{GeV/c}$.

In fact, it is found that $R_{AA} > 1$ for $p_T > 2\,\mathrm{GeV/c}$ in nuclear reactions at lower energy. This enhancement, first observed by Cronin, is associated with multiple scattering of partons [59,60].

Figure 11 demonstrates that, surprisingly, $R_{AA} < 1$ also at high p_T for central collisions at both pseudorapidities, while $R_{AA} \approx 1$ for more peripheral collisions. It is remarkable that the suppression observed at $p_T \approx 4\,\mathrm{GeV/c}$ is very large, amounting to a factor of 3 for central Au+Au collisions as compared to

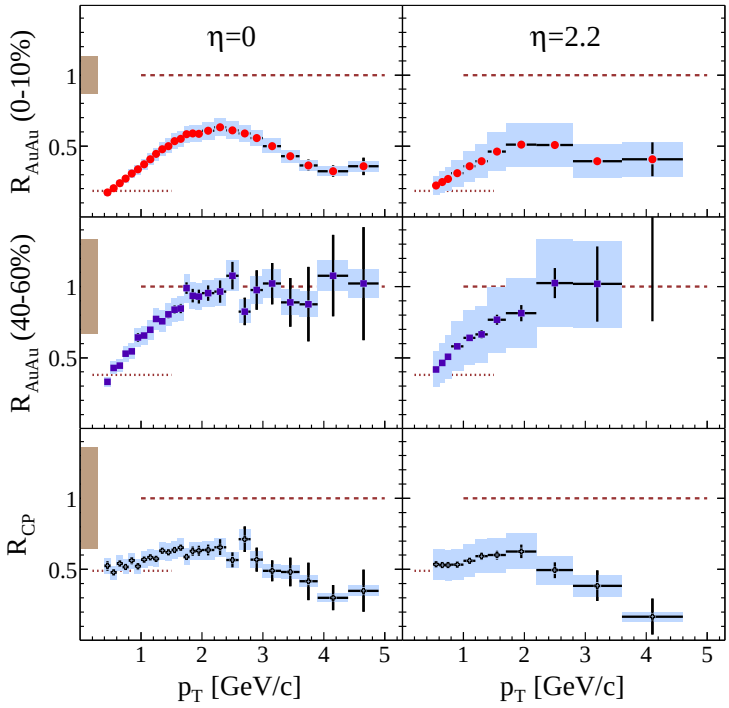

Fig. 11. Nuclear modification factors R_{AuAu} as defined in the text,measured by BRAHMS for central (top row) and semi-peripheral (middle row) Au+Au collisions at midrapidity (left) and forward pseudorapidity (right). Note the strong suppression of the high p_T component above $p_T > 2\ GeV$ seen at both rapidities. The lower row shows the factor R_{cp}, i.e. the ratio of the R_{AuAu} for central and peripheral collisions. This ratio has the property of being independent of the p+p reference spectrum [48].

p+p and a factor of more than 4 as compared to the more peripheral collisions. Such large suppression factors are observed at both pseudorapidities.

The very large suppression observed in central Au+Au collisions must be quantitatively understood and requires systematic modelling of the dynamics. At $\eta = 0$ the particles are emitted at 90 degrees relative to the beam direction, while at $\eta = 2.2$ the angle is only about 12 degrees. In a naive geometrical picture of an absorbing medium with cylindrical symmetry around the beam direction, the large suppression seen at forward angles suggests that the suppressing medium is extended also in the longitudinal direction. Since the observed high p_T suppression is similar or even larger at forward rapidity as compared to midrapidity (see fig. 12) one might be tempted to infer a longitudinal extent of the dense medium which is approximately similar to its transverse dimensions. However, the problem is more complicated, due to the significant transverse and in particular longitudinal expansion that occurs as the leading parton propagates through the medium, effectively reducing the densities of color charges seen. Also other high p_T suppressing mechanisms

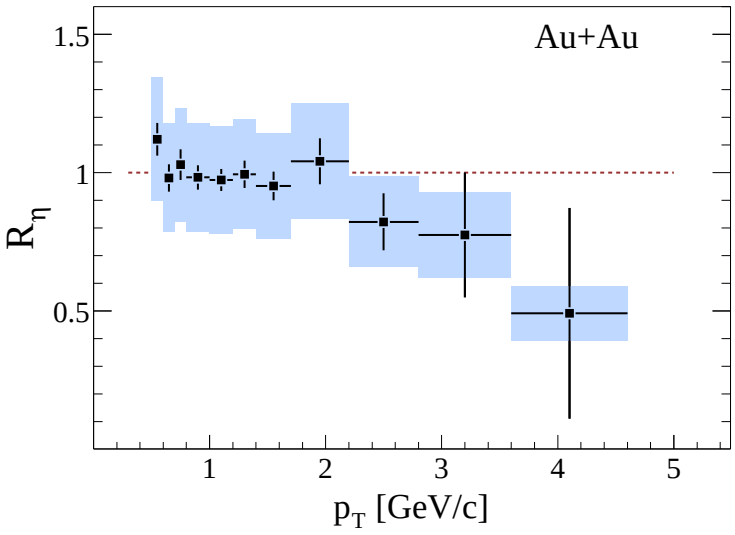

Fig. 12. Ratio R_η of the suppression factors R_{cp} at pseudorapidities $\eta = 0$ and $\eta = 2.2$ that are shown in figure 11. The figure suggest that high p_T suppression persists (and is even more important) at forward rapidity than at $\eta = 0$ [48].

may come into play at forward rapidities (see discussion on the Color Glass Condensate in the following chapter).

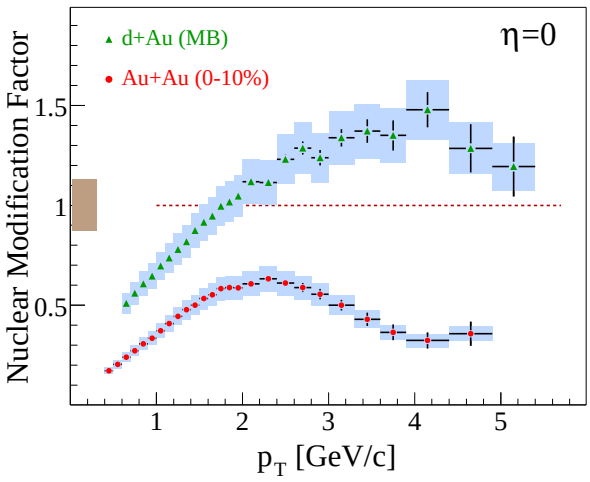

Fig. 13. Nuclear modification factors measured for central Au+Au collisions and minimum bias d+Au collisions at $\sqrt{s_{NN}} = 200\,\text{GeV}$, evidencing the important high p_T suppression observed in central Au+Au collisions [48] which is absent in the d+Au reactions. The shaded band around the points indicates the systematic errors. The shaded box on the ordinate around unity shows the estimated uncertainty on the value of N_{bin}.

It has been conjectured that the observed high p_T suppression might be the result of an entrance channel effect, for example as might arise from a limitation of the phase space available for parton collisions related to saturation effects [61] in the gluon distributions inside the swiftly moving colliding nucleons

(which have $\gamma = 100$). As a test of these ideas we have determined the nuclear modification factor for d+Au minimum bias collisions at $\sqrt{s_{NN}} = 200\,\mathrm{GeV}$. The resulting R_{dAu} is shown in fig. 13 where it is also compared to the R_{AuAu} for central collisions previously shown in fig. 11. No high p_T jet suppression is observed for d+Au [48,63–65]. The R_{dAu} distribution at $y = 0$ shows a Cronin enhancement similar to that observed at lower energies [18,66,67]. At $p_T \approx 4\,\mathrm{GeV/c}$ we find a ratio $R_{dAu}/R_{AuAu} \approx 4 - 5$. These observations are consistent with the smaller transverse dimensions of the overlap disk between the d and the Au nuclei and also appear to rule out initial state effects as the cause of the observed high p_T yield reduction observed in Au+Au collisions.

High p_T suppression at forward rapidities may also be expected to arise from the possible Color Glass Condensate phase in the colliding nuclei (see the discussion in the next section). There is little doubt that systematic studies of the high p_T jet energy loss as a function of the thickness of the absorbing medium obtained by varying the angle of observation of high p_T jets relative to the event plane and the direction of the beams will be required in order to understand in detail the properties of the dense medium.

6.2 The flavor composition

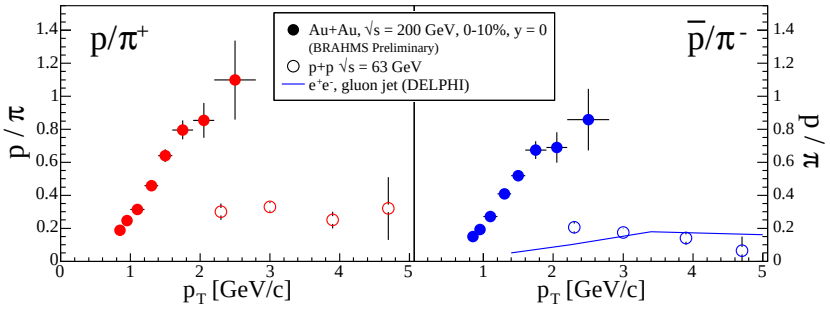

Fig. 14. Ratios of particle yields p/π^+ (left) and $\bar{p}/\pi^-$ (right) measured at mid-rapidity for 0-10% central Au+Au collisions at $\sqrt{s_{NN}} = 200\,\mathrm{GeV}$. The error bars show the statistical errors. The systematic errors are estimated to be smaller than 8%. Data at $\sqrt{s} = 63\,\mathrm{GeV}$ for $p+p$ collisions [69] are also shown (open circles). The solid line in the right hand panel is the $(p+\bar{p})/(\pi^+ + \pi^-)$ ratio measured for gluon jets [70] in $e^+ + e^-$ collisions.

With its excellent particle identification capabilities BRAHMS can also study the dependence of the high p_T suppression on the type of particle. Preliminary results [58,68] indicate that mesons (pions and kaons) experience high p_T suppression while baryons (protons) do not. The reason for this difference is at present not well understood.

The observed differences may be a consequence of baryons being more sensitive to flow, because of their larger mass, than mesons. The flow contribution leads

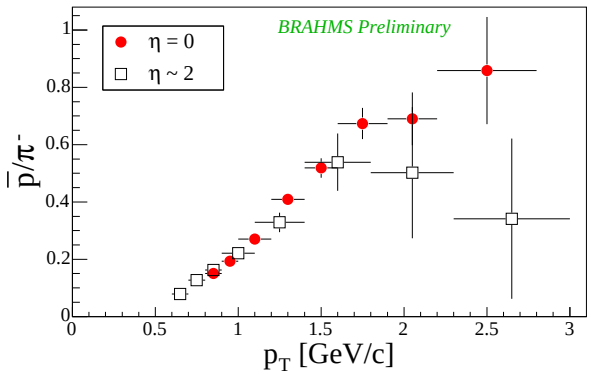

Fig. 15. Comparison of the ratios yields of $\bar{p}/\pi^-$ at rapidities $y = 0$ and $y = 2.2$. In spite of small statistics the data suggest that a forward rapidity the flow may be weaker resulting in a derecreased yield of antiprotons relative to pions above $p_T \approx 2$ GeV. BRAHMS preliminary [68]

a flatter transverse momentum spectrum for baryons than for mesons, thus possibly compensating for a high p_T suppression effect similar to that of the mesons. It is also possible that the difference reflects details associated with the fragmentation mechanism that leads to different degrees of suppression of the high p_T component for 2 and 3 valence quark systems. Finally the difference may reflect the mechanism of recombination for 3 quarks relative to that for 2 quarks in a medium with a high density of quarks.

Figure 14 shows a recent investigation by BRAHMS (ref. [68]) of the baryon to meson ratios at mid-rapidity p/π^+ and $\bar{p}/\pi^-$, as a function of p_T for the 0-10% most central Au+Au collisions at $\sqrt{s_{NN}} = 200$ GeV. The ratios increase rapidly at low p_T and the yields of both protons and anti-protons are comparable to the pion yields for $p_T > 2\,\mathrm{GeV/c}$. The corresponding ratios for $p_T > 2\,\mathrm{GeV/c}$ observed in $p + p$ collisions at $\sqrt{s} = 62$ GeV [69] and in gluon jets produced in $e^+ + e^-$ collisions [70] are also shown. The increase of the p/π^+ and $\bar{p}/\pi^-$ ratios at high p_T, seen in central Au+Au collisions, relative to the level seen in $p + p$ and $e^+ + e^-$ indicates significant differences in the overall description, either at the production or fragmentation level.

Figure 15 shows the comparison of BRAHMS data for the ratio of antiprotons to negative pions at $\eta = 0$ and 2.2. Although statistics at high transverse momentum are low there are indications that the ratio is smaller at the higher rapidity for $p_T > 2$ GeV. Recent calculations based on a parton recombination scenario [71–73] with flow at the partonic level appear to be able to describe the data at midrapidity, while calculations omitting flow fall short of the data already at $p_T \approx 1.5\,GeV$.

The experimental and theoretical investigation of these questions is, however, still in its infancy. These issues can and will be addressed in depth through the analysis of the large data set collected by BRAHMS in the high luminosity

Au+Au run of year 2004.

6.3 High p_T suppression at lower energy?

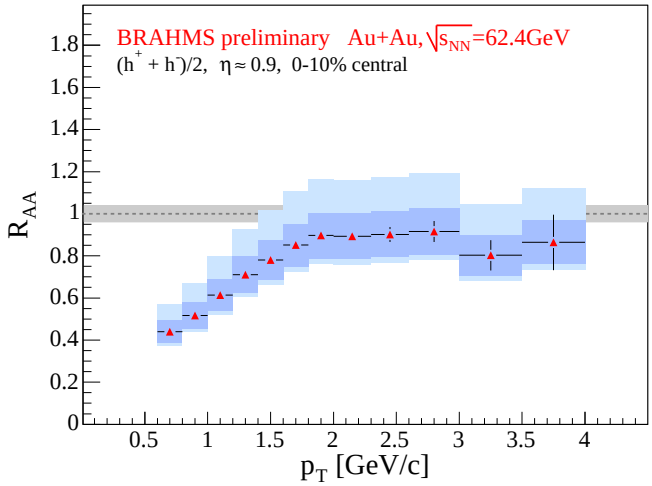

Fig. 16. Nuclear modification factor R_{AuAu} measured by BRAHMS for charged hadrons at $\eta = 0.95$ for $0-10\%$ central Au+Au collisions at $\sqrt{s_{nn}} = 62.4GeV$ [74]. The dark shaded band indicates the systematic errors on the data, the lighter shaded band the combined estimated systematic error on the Au+Au data data and the p+p reference.

The short commissioning run for Au+Au collisions at $\sqrt{s_{NN}} = 62.4\,\mathrm{GeV}$ has allowed us to carry out a first analysis of the high p_T suppression of charged hadrons at an energy of about 1/3 the maximum RHIC energy and about 3.5 times the maximum SPS energy. Preliminary results are shown in figure 16 for nuclear modification factor calculated for the sum of all charged hadrons measured at 45 degrees($\eta = 0.9$) with respect to the beam direction. The data have been compared to reference spectra measured in $\sqrt{s_{NN}} = 63\,\mathrm{GeV}$ p+p collisions at the CERN-ISR. The figure shows that the high p_T data are less suppressed at $\sqrt{s_{NN}} = 62.4\,\mathrm{GeV}$ than at $\sqrt{s_{NN}} = 200\,\mathrm{GeV}$. This is consistent with recent results from PHOBOS [75]. For comparison, at SPS energies no high p_T suppression was observed (albeit a discussion has surfaced regarding the accuracy of the reference spectra at that energy [62]). It thus seems the suppression increases smoothly with energy.

The remarkable suppression of high p_T jets at mid-rapidity seen at RHIC is an important signal that evidences the interaction of particles originating from hard parton scatterings with the high energy density medium created in the collisions. The quantitative understanding of the observed high p_T suppression, as a function of energy, should be able to determine whether this suppression occurs at the partonic or hadronic level. This needs to be supplemented by detailed studies of the flavor dependence of the suppression mechanism.

7 The color glass condensate: a model for the initial state of nuclei?

As part as the study of the high p_T suppression in nucleus-nucleus collisions BRAHMS has investigated the rapidity dependence of the nuclear modification factors as a function of rapidity ($\eta = 0, 1, 2.2, 3.2$) in d+Au collisions at $\sqrt{s_{NN}} = 200\,\mathrm{GeV}$. As discussed in the previous section the measured nuclear modification factors for d+Au are consistent with the absence of high p_T suppression around midrapidity. This may be taken as direct evidence for the fact that the strong high p_T suppression seen in Au+Au collisions around $y = 0$ is not due to particular conditions of the colliding nuclei (initial state effects) [63,64,63] and [48].

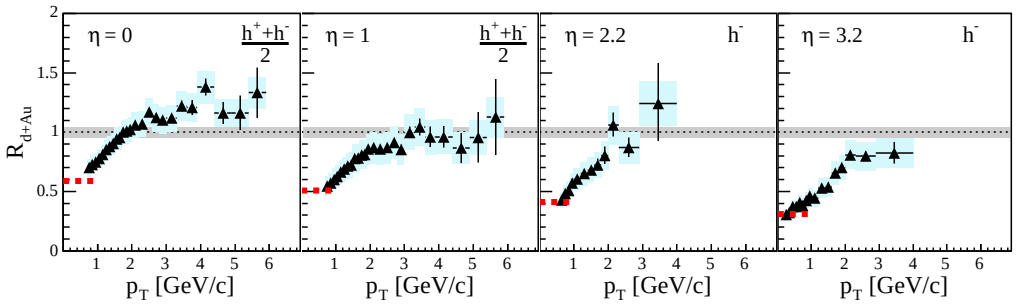

Fig. 17. Evolution of the nuclear modification factors measured by BRAHMS for the 10% most central d+Au collisions at $\sqrt{s_{NN}} = 200\,\mathrm{GeV}$, as a function of pseudorapidity η [76].

At forward rapidity in d+Au collisions, however, BRAHMS has observed [76] a marked high p_T suppression starting already at $\eta = 1$ (see Fig. 17) and increasing smoothly in importance with increasing pseudorapidity (up to $\eta = 3.2$). It has been proposed that this effect at forward rapidity [77] is related to the initial conditions of the colliding d and Au nuclei, in particular to the possible existence of the Color Glass Condensate (CGC).

The CGC is a description of the ground state of swiftly moving nuclei prior to collisions [78]. Due to the non Abelian nature of QCD, gluons self interact which results in nuclei containing a large number of low–x gluons (x is the fraction of the longitudinal momentum carried by the parton) that appears to diverge (grow) with decreasing x. There is however, a characteristic momentum scale, termed the saturation scale, below which the gluon density saturates. This effect sets in when x becomes small and the associated gluon wave length ($\frac{1}{m_p x}$) increases to nuclear dimensions. In such a regime gluons may interact and form a coherent state reminiscent of a Bose-Einstein condensate. Early indications for the formation of such non-linear QCD systems have been found in lepton-hadron or lepton-nucleus collisions at HERA [79] and have been described by the so called "Geometric Scaling" model [80].

The density of gluons $\frac{dN_g}{d(ln(1/x))} \sim \frac{1}{\alpha_s}$ in such a saturated system is high, since α_s, the strong interaction running coupling constant, decreases as the energy increases. The system can therefore be described as a (semi)classical field, and techniques borrowed from field theory can be employed to find the functional form of the parton distributions in the initial state [82].

Saturation in the wave function sets in for gluons with transverse momentum $Q^2 < Q_s^2 = A^{\frac{1}{3}}(\frac{x_0}{x})^{\lambda} \sim A^{\frac{1}{3}}e^{\lambda y}$. A value of $\lambda \sim 0.3$ is estimated from fits to HERA data [81]. The dependence of the saturation scale Q_s on the atomic number of the target and rapidity suggests that saturation effects can be best studied at RHIC with heavy nuclei at large rapidities, although larger beam energy will also make it possible in the future to study low x phenomena in nuclear collisions closer to midrapidty.

Collisions between heavy ions with energies $E = 100\,\mathrm{AGeV}$ may therefore provide a window to the study of low–x gluon distributions of swiftly moving nuclei. In particular, head-on collisions between deuterons and gold nuclei in which hadrons, produced mostly in quark-gluon collisions, are detected, close to the beam direction but away from the direction of motion of the gold nuclei, allow the low–x components (mostly gluons) of the wave function of the gold nuclei to be probed.

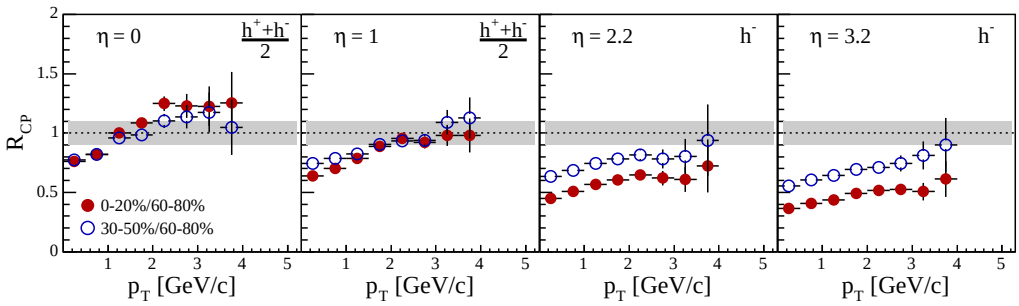

Fig. 18. Central to peripheral ratios R_{CP} as a function of pseudorapidity measured by BRAHMS for d+Au collisions at the RHIC top energy [76]. The filled circles represent the central-to-peripheral (0-20% over 60-80%) ratio. The open circles the semicentral-to-peripheral (30-50% over 60-80%) ratio. The shaded band around unity indicates the uncertainty associated with the values of the number of binary collisions at the different centralities.

The centrality dependence of the nuclear modification factors provides additional information on the mechanism underlying the observed suppression. Fig. 18 shows the R_{CP} factors, defined as the ratios of the nuclear spectra for central (0-20%) and peripheral (60-80%) collisions (closed points) and for semicentral (30-50%) and peripheral collisions(open points), suitably scaled by the corresponding number of binary collisions, versus p_T and η. There is a substantial change in R_{CP} as a function of η. At $\eta = 0$ the central-to-peripheral collisions ratio is larger than the semicentral-to-peripheral ratios suggesting an

increased Cronin type multiple scattering effect in the more violent collisions. In contrast, the ratio of the most central collisions relative to the peripheral, as compared to the semicentral-to-peripheral, is the most suppressed at forward rapidities, suggesting a suppression mechanism that scales with the centrality of the collisions.

The observed suppression of yields in d+Au collisions (as compared to p+p collisions) has been qualitatively predicted by various authors [83–86], within the Color Glass Condensate scenario. Recently, a more quantitative calculation has been carried out [87] which compares well with the data. Other authors [88,89] have estimated the nuclear modification factors based on a two component model that includes a parametrization of perturbative QCD and string breaking as a mechanism to account for soft coherent particle production using HIJING. HIJING uses the mechanism of gluon shadowing to reduce the number of gluon-gluon collisions and hence the multiplicity of charged particles a lower p_t. HIJING has been shown to give a good description of the overall charged particle multiplicity in d+Au collisions. A similar approach was followed by Barnafoldi et al. [90]. Vogt has used realistic parton distribution functions and parametrizations of nuclear shadowing to give a reasonable description of the minimum bias data though not of the centrality dependence [91]. Guzey et al. have suggested that isospin effects may increase the suppression [92]. Hwa et al. have reproduced the measured nuclear modification factors in calculations based on quark recombination in the final state [93].

The high p_T-suppression in Au+Au collisions at large rapidites discussed earlier suggests that there may be two competing mechanisms responsible for the observed high p_T suppression in energetic Au+Au collisions, each active in its particular rapidity window. It has been proposed [8] that the high p_T suppression observed around midrapidity reflects the presence of an incoherent (high temperature) state of quarks and gluons while the the high p_T suppression observed at forward rapidities bears evidence of a dense coherent partonic state. Clearly, additional analysis of recent high statistics data for Au +Au collisions at high rapidites, as well as firmer theoretical predictions are needed to understand the quantitative role of gluon saturation effects in energetic nucleus-nucleus collisions.

The suppression of high p_T particles seen at forward rapidities in nucleus-nucleus collisions is a novel and unexpected effect and may be related to a new collective partonic state that describes nuclei at small x, and hence the initial conditions for the reaction in energetic nucleus-nucleus collisions.

8 Conclusions and perspectives

The results from the first round of RHIC experiments clearly show that studies of high energy nucleus-nucleus collisions have moved to a qualitatively new physics domain characterized by a high degree of reaction transparency leading to the formation of a near baryon free central region. There is appreciable energy loss of the colliding nuclei, so the conditions for the formation of a very high energy density zone with approximate balance between matter and antimatter, in an interval of $|y| \lesssim 1.5$ around midrapidity are present.

The indications are that the initial energy density is considerably larger than 5 GeV/fm ^{3}, i.e. well above the energy density at which it is difficult to conceive of hadrons as isolated and well defined entities. Analysis within the framework of the statistical model of the relative abundances of many different particles containing the three lightest quark flavors suggest chemical equilibrium at a temperature in the vicinity of T=175 MeV and a near-zero light quark chemical potential. The temperature thus determined for the chemical freeze-out compares well with the prediction for the critical temperature obtained from lattice QCD calculations. The conditions necessary for the formation of a dense system of quarks and gluons therefore appear to be present.

However, there are a number of features, early on considered as defining the concept of the QGP, that do not appear to be realized in the current reactions, or at least have not (yet?) been identified in experiment. These are associated with the expectations that a QGP would be characterized by a vanishing interaction betweens quarks and exhibit the features of chiral symmetry restoration and, furthermore, that the system would exhibit a clear phase transition behavior. Likewise, it was originally expected that a QGP phase created in nuclear collisions would be characterized by a long lifetime (up to 100 fm/c) and by the existence of a mixed phase exhibiting large fluctuations of characteristic parameters. In contrast, the present body of measurements compared to theory suggest a short lifetime of the system, a large outward pressure, and significant interactions most likely at the parton level that result in a (seemingly) equilibrated system with fluid-like properties. Thus, the high density phase that is observed, is not identical to the QGP with properties of an ideal gas that was imagined a decade or two ago.

However, the central question is whether the properties of the matter as it is created in today's high energy nucleus–nucleus collisions clearly bears the imprint of a system characterized by quark and gluon degrees of freedom over a range larger that the characteristic dimensions of the nucleon. We know that in nuclei the strong interaction is mediated by a color neutral objects (mesons). Is there experimental evidence that clearly demonstrates interactions based on the exchange of objects with color over distances larger than

those of conventional confined objects?

The best candidate for such an effect is clearly the suppression of high transverse momentum particles observed in central Au+Au collisions by the four experiments at RHIC. The remarkably large effect that is observed (a suppression by a factor of 3-5 as compared to peripheral and d+Au collisions) appears readily explainable by radiation losses due to the interaction of high p_T partons with an extended medium (of transverse dimensions considerably larger than nucleon dimensions) consisting of deconfined color charges. Current theoretical investigations, which recently have progressed to attempt first unified descriptions of the reaction evolution, indicate that scenarios based on interactions between hadronic objects cannot reproduce the magnitude of the observed effect.

The interpretation of current data relies heavily on theoretical input and modelling, in particular on the apparent necessity to include partonic degrees of freedom in order to arrive at a consistent description of many of the phenomena observed in the experimental data. Seen from a purely experimental point of view this situation is somewhat unsatisfying, but probably not unexpected, nor avoidable, considering the complexity of the reaction and associated processes.

It is also clear that the unravelling of the physics of the matter state(s) observed at RHIC has just begun. In spite of the impressive advances that have been made in the last three years there are still many issues to be understood in detail, such as the differences in the high p_T suppression of baryons and mesons and the quantitative energy and rapidity dependence of the final and initial state high p_T suppression. Undoubtedly future measurements will shed new light on these and many other questions. We should not forget, however, that there are also significant challenges for theory. In the opening chapters of this document we remarked on the requirement that scientific paradigms must be falsifiable. We have yet to see a fully self consistent calculation of the entire reaction evolution at RHIC that in an unambiguous way demonstrates the impossibility of a hadronic description.

In conclusion, we find that the body of information obtained by BRAHMS and the other RHIC experiments in conjunction with the available theoretical studies is strongly suggestive of a high density system that cannot be characterized solely by hadronic degrees of freedom but requires a partonic description. Indications are that such a partonic state is not characterized by vanishing interaction of its constituents, but rather by a relatively high degree of coherence such as the one characterizing fluids. At the same time indications of a coherent partonic state at low x in the colliding nuclei has been found.

There is no doubt that the experiments at RHIC have revealed a plethora of

new phenomena that for the most part have come as a surprise. In this sense it is clear that the matter that is created at RHIC differs from anything that has been seen before. Its precise description must await our deeper understanding of this matter.

9 Acknowledgements

This work was supported by the Division of Nuclear Physics of the Office of Science of the U.S. Department of Energy under contracts DE-AC02-98-CH10886, DE-FG03-93-ER40773, DE-FG03-96-ER40981, and DE-FG02-99-ER41121, the Danish Natural Science Research Council, the Research Council of Norway, the Jagiellonian University Grants, the Korea Research Foundation Grant and the Romanian Ministry of Education and Research (5003/1999, 6077/2000). We thank the staff of the Collider-Accelerator Division at BNL for their excellent and dedicated work to deploy RHIC and their support to the experiment.

References

[1] J. C. Collins, M. J. Perry, Phys. Rev. Lett. **34**, 1353 (1975); G. Baym, S. A. Chin, Phys. Lett. **B88**, 241 (1976); B. A. Freedman, L. D. McLerran, Phys. Rev. **D16**, 1196 (1977); G. Chapline, Nauenberg, Phys. Rev. **D16**, 450 (1977); E. V. Shuryak, Phys. Lett. **B78**, 150 (1978); O. K. Kalashnikov, V. V. Klimov, Phys. Lett. **B88**, 328 (1979); J. I. Kapusta, Nucl. Phys. **B148**, 461 (1979).

[2] E. V. Shuryak, Phys. Rep. 61, 71(1980).

[3] H. Satz, Nucl. Phys. **A715**, 3 (2003).

[4] CERN press release 2000, http://pressold.web.cern.ch/ PressOld/Releases00/ PR01.00EQuarkGluonMatter.html.

[5] M. Adamczyk *et al.*, BRAHMS Collaboration, Nucl. Instr. and Meth. **A499**, 437 (2003).

[6] I. G. Bearden *et al.*, BRAHMS Collaboration, Phys. Lett. **B523**, 227 (2001) and Phys. Rev. Lett. **88**, 202301 (2002).

[7] BRAHMS homepage: http://www4.rcf.bnl.gov/brahms/WWW/brahms.html; PHENIX homepage: http://www.phenix.bnl.gov/; PHOBOS homepage: http://www.phobos.bnl.gov/; STAR homepage: http://www.star.bnl.gov/.

[8] M. Gyulassy, L. McLerran, nucl-th/0405013.

[9] E. V. Shuryak, hep-ph/0405066.

[10] P. Jacobs and X. Wang, hep-ph/0405125.

[11] C. R. Allton *et al.*, Phys. Rev. **D68**, 014507 (2003), F. Karsch, E. Laermann and A. Peikert, Phys. Lett. **B478**, 447 (2000), F. Karsch, Lect. Notes Phys. **583**, 209 (2002), C. W. Bernard *et al.*, Phys. Rev. **D55**, 6861 (1997), S. Gupta, Pramana **61**, 877 (2003), Z. Fodor and S. D. Katz, hep-lat/0402006, F. Csikor *et al.*, hep-lat/0401022.

[12] F. Videbæk and O. Hansen, Phys. Rev. **C52**, 26 (1995).

[13] W. Busza and A. S. Goldhaber, Phys. Lett. **B139**, 235 (1984).

[14] W.Busza and R.Ledoux, Ann.Rev.Nucl.Science **38** 150 (1988).

[15] B. B. Back *et al.*, Phys. Rev. Lett. **86**, 1970 (2001).

[16] L. Ahle *et al.*, Phys. Rev. **C60**, 064901 (1999).

[17] J. Barette *et al.*, Phys. Rev. **C62**, 024901 (2000).

[18] H. Appelshauser *et al.*, Phys. Rev. Lett. **82**, 2471 (1999).

[19] BRAHMS collaboration, Nucl. Phys.**A715**, 171c (2003) and *ibid* p. 482c, BRAHMS collaboration PRL **93**, 1020301 (2004), and P. Christiansen, Ph. D. thesis, Univ. Copenhagen, June 2003. Phys. Rev. Lett. **89**, 092301 (2002) and K. Adcox *et al.*, PHENIX collaboration, ibid p. 092302.

[20] J. D. Bjorken, Phys. Rev. D**27**, 140 (1983). PHOBOS Collaboration, Phys. Rev. Lett. **88**, 022302 (2002).

[21] J. W. Harris and B. Müller, Ann. Rev. Nucl. Part. Sci. **46**, 71 (1996).

[22] K. J. Eskola and Xin-Nian Wang, Phys. Rev. **D49**, 1284 (1994).

[23] F. Karsch, Nucl. Phys. **A698**, 199 (2002).

[24] M. Gyulassy and T. Matsui, Phys. Rev. **D29**, 419 (1984).

[25] R. Stock, Phys. Lett. **B456**, 277 (1999).

[26] D. Ouerdane, Ph.D. thesis, Univ. Copenhagen, August 2003, I. G. Bearden *et al.*, BRAHMS Collaboration, nucl-ex/0403050 and references therein.

[27] I. G. Bearden *et al.*, BRAHMS Collaboration, Phys. Rev. Lett. **90**, 102301 (2003).

[28] P. Koch *et al.*, Phys. Rep. **142**, 167 (1986).

[29] J. Cleymans *et al.* Z. Phys. **C57**, 135 (1993).

[30] J. Cleymans *et al.* Nucl. Phys. **A566**, 391 (1994).

[31] P. Braun-Munzinger *et al.*, Phys. Lett. B **518**, 41 (2001).

[32] F. Becattini *et al.*, Phys. Rev. C**64**, 024901 (2001) and private communication.

[33] J. Cleymans, J. Phys. **G28**, 1576 (2002).

[34] S. S. Adler *et al.*, PHENIX collaboration, Phys. Rev. Lett. **91**, 182301 (2003).

[35] S. S. Adler *et al.*, PHENIX collaboration, Phys. Rev. Lett. **89**, 212301 (2002).

[36] B. B. Back *et al.*, PHOBOS collaboration, Phys. Rev. Lett. **89**, 222301 (2002).

[37] C. Adler *et al.*, STAR collaboration, Phys. Rev. **C66**, 034904 (2002).

[38] C. Adler *et al.*, STAR collaboration, Phys. Rev. Lett. **87**, 182301 (2001).

[39] C. Adler *et al.*, STAR collaboration, Phys. Rev. Lett. **86**, 402 (2001).

[40] I. Arsene et al., BRAHMS collaboration, J. Phys. **G30**, S667, (2004).

[41] P. F. Kolb, J. Sollfrank, U. Heinz, Phys. Lett. **B459**, 667 (1999).

[42] P. Huovinen, P. F. Kolb, U. Heinz, P.V. Ruuskanen, S. A. Voloshin, Phys. Lett. **B503**, 58 (2001).

[43] D. Molnar, S. A. Voloshin, Phys. Rev. Lett. **91**, 092301 (2003).

[44] D. Teaney, J. Lauret, E. V. Shuryak, Phys. Rev. Lett. **86**, 4783 (2001).

[45] H. Sorge, Phys. Rev. Lett. **82**, 2048 (1999).

[46] H. Heiselberg and A. M. Levy, Phys. Rev. **C59**, 2716 (1999).

[47] P. F. Kolb, P. Huovinen, U. Heinz, H. Heiselberg, Phys. Lett. **B500**, 232 (2001).

[48] I. Arsene *et al.*, BRAHMS collaboration, Phys. Rev. Lett **91**, 072305 (2003).

[49] J. Adams *et al.*, Phys. Rev. Lett. **91**, 172302 (2003).

[50] S. S. Adler *et al.*, Phys. Rev. **C69**, 034910 (2004).

[51] B. Back *et al.*, Phys. Lett. **B578**, 297 (2004).

[52] R. Baier *et al.*, Phys. Lett. **B345**, 277 (1995).

[53] M. Gyulassy and M. Plümer, Phys. Lett.**B243**, 432 (1990).

[54] X. N. Wang and M. Gyulassy, Phys. Rev. Lett. **68**, 1480(1992).

[55] J. D. Bjorken, Report No. Fermilab-Pub-82/59-THY (1982).

[56] R. Baier, D. Schiff, B.G. and Zakharov, Ann. Rev. Nucl. Part. Sci. **50**, 37 (2000).

[57] C. Adler *et al.*, Phys. Rev. Lett. **90**, 082302 (2003).

[58] C. E. Jørgensen *et al.*, BRAHMS collaboration, Nucl. Phys. A715 741c (2003).

[59] J. W. Cronin *et al.*, Phys. Rev. **D11** 3105 (1975).

[60] A. Accardi, hep-ph/0212148.

[61] D. Kharzeev, E. Levin, L. McLerran, Phys. Lett. **B561**, 93 (2003) and references therein.

[62] D. d'Enterria, Phys. Lett. **B596**, 32 (2004).

[63] J. Adams *et al.*, Phys. Rev. Lett. **91**, 072304 (2003).

[64] B. B. Back *et al.* nucl-ex/0302015 and Phys. Rev. Lett. **91**, 072302 (2003).

[65] S. S. Adler *et al.*, Phys. Rev. Lett. **91**, 072303 (2003).

[66] M. M. Aggarwal *et al.*, Eur. Phys. J. **C18**, 651 (2001).

[67] G. Agakishiev *et al.*, hep-ex/0003012.

[68] Z. Yin, BRAHMS Collaboration, J. Phys. **G30**, S983 (2004).

[69] B. Alper *et al.*, Nucl. Phys. **B100**, 237 (1975).

[70] P. Abreu *et al.*, Eur. Phys. J. **C17**, 207 (2000).

[71] R. C. Hwa and C. B. Yang, Phys. Rev. **C67**, 034902 (2003).

[72] R. J. Fries *et al.*, Phys. Rev. **C68**, 044902 (2003).

[73] V. Greco, C. M. Ko and P. Levai, Phys. Rev. Lett. **90**, 202302 (2003).

[74] BRAHMS Collaboration, in preparation; C.Ekman, Ph.D. Thesis, University of Copenhagen, 2004.

[75] B. Back *et al.*, submitted to Phys. Rev. Lett. (nucl-ex/0405003).

[76] I. Arsene *et al.*, BRAHMS collaboration, Phys. Rev. Letters, 93, 242303 (2004).

[77] D. Kharzeev, E. Levin and L. McLerran Phys. Lett. **B561** 93-101 (2003).

[78] L. V. Gribov, E. M. Levin and M. G. Ryskin, Phys. Rept. **100**, 1 (1983), A. H. Mueller and Jian-wei Qiu, Nucl. Phys. **B268**, 427 (1986), L.N. Lipatov, Sov. J. Nucl. Phys. **23** (1976), 338, E.A. Kuraev, L.N. Lipatov and V.S. Fadin, Sov. Phys. JETP 45 (1977), 199G Ya.Ya. Balitsky and L.N. Lipatov, Sov. J. Nucl. Phys. **28**, 822 (1978), L. D. McLerran and R. Venugopalan, Phys. Rev. **D49**, 2233(1994) 3352 (1994); D50, 2225 (1994), E. Iancu, A. Leonidov and L. D. McLerran, Nucl. Phys. **A692**, 583 (2001), E. Iancu and L. McLerran, Phys.Lett. **B510**, 145 (2001).

[79] J. Breitweg *et al.* Eur. Phys. J. C7 609-630, (1999); ZEUS Collaboration, J. Breitweg *et al.*, Phys. Lett. **B487** (2000) 53; ZEUS Collaboration, S. Chekanov *et al.*, Eur. Phys.J. **C21** (2001) 443; H1 Collaboration, C. Adloff *et al.*, Eur. Phys. J. **C21** (2001) 33.

[80] A. M. Staśto, K. Golec-Biernat, and J. Kwieciński Phys. Rev. Lett. 86 596-599 (2001).

[81] J. Breitweg *et. al.*, Phys. Lett. **B407**, 432 (1997).

[82] L. McLerran and R. Venugopalan, Phys. Rev. **D49**, 2233(1994); Phys. Rev. **D59**, 094002 (1999); E. Iancu, A. Leonidov and L. D. McLerran, Nucl. Phys. **A692**, 583 (2001), and references therein.

[83] A. Dumitru and J. Jalilian-Marian, Phys. Lett. B **547**, 15 (2002)

[84] J. Jalilian-Marian, Y. Nara and R. Venugopalan, Phys. Lett. B **577**, 54 (2003); A. Dumitru and J. Jalilian-Marian Phys. Rev. Lett. 89 022301 (2002).

[85] R. Baier *et al.* Phys. Rev. D68, 054009, (2003); J. Albacete, *et. al.*, hep-ph/0307179.

[86] D. Kharzeev, Y. V. Kovchegov and K. Tuchin Phys. Rev. D68, 094013, (2003); D. Kharzeev, E. Levin and L. McLerran, Phys. Lett. B **561**, 93 (2003).

[87] D. Kharzeev, Y. V. Kovchegov, and K. Tuchin, hep-ph/0405045.

[88] I. Vitev, Phys. Lett. **B562**, 36 (2003)

[89] Xin-Nian Wang, Phys. Lett. **B565**, 116-122, (2003).

[90] G.G. Barnafoldi et al., J. Phys. G**30** S1125, (2004).

[91] R. Vogt hep-ph/0405060.

[92] V. Guzey, M. Strickman and W. Vogelsang, Phys. Lett. B**603** 173, (2004).

[93] R. Hwa, C.B. Yang and R. J. Fries, nucl-th/0410111; R. Hwa and C.B. Yang. Phys. Rev. C**70**, 024905, (2004).

PHENIX

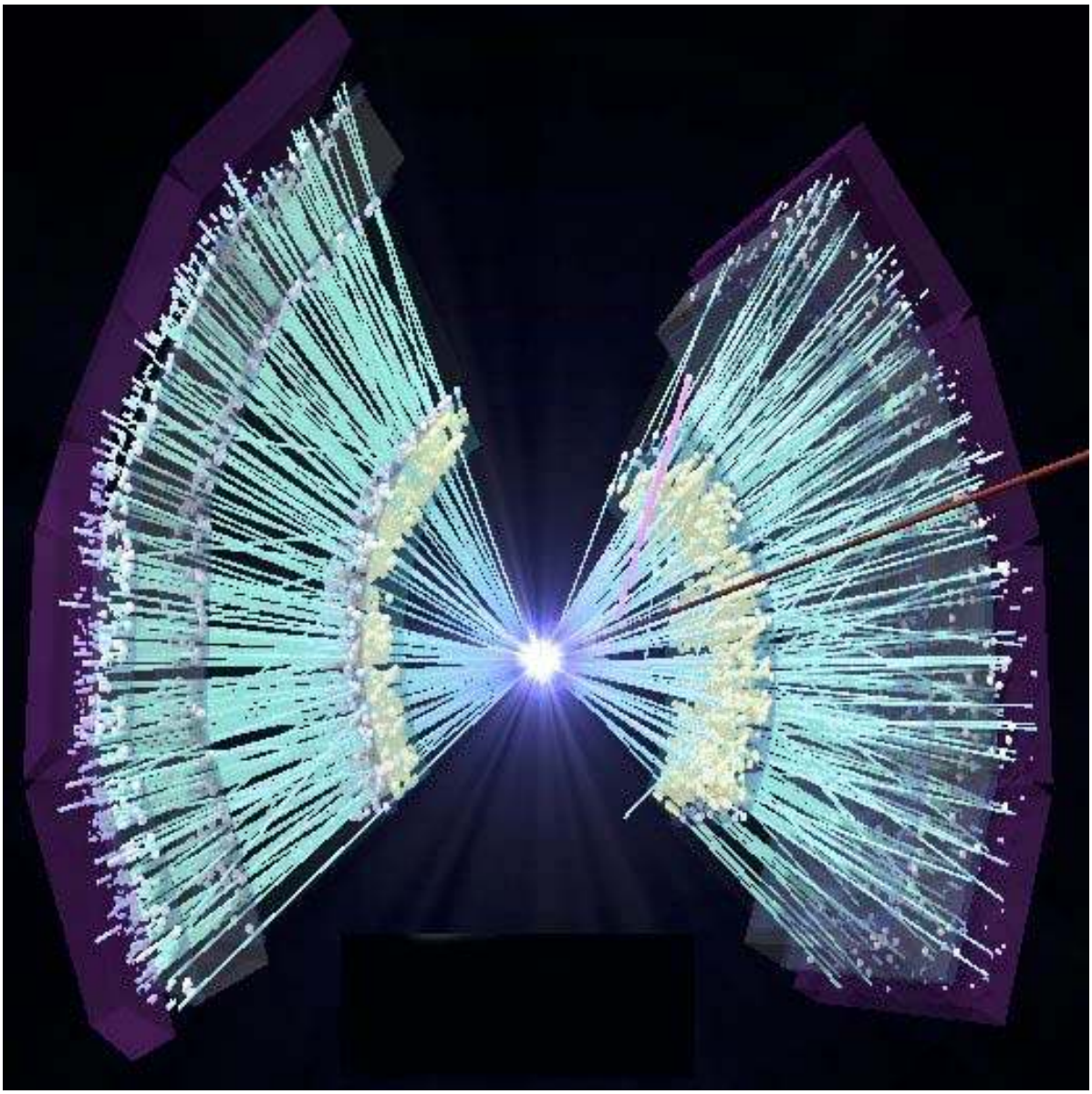

Formation of dense partonic matter in relativistic nucleus-nucleus collisions at RHIC: Experimental evaluation by the PHENIX collaboration

K. Adcox [be] S.S. Adler [e] S. Afanasiev [t] C. Aidala [e,j]
N.N. Ajitanand [aw] Y. Akiba [w,aq,ar] A. Al-Jamel [aℓ] J. Alexander [aw]
R. Amirikas [n] K. Aoki [aa,aq] L. Aphecetche [az] Y. Arai [w]
R. Armendariz [aℓ] S.H. Aronson [e] R. Averbeck [ay] T.C. Awes [am]
R. Azmoun [e,ay] V. Babintsev [q] A. Baldisseri [k] K.N. Barish [f]
P.D. Barnes [ad] J. Barrette [ag] B. Bassalleck [ak] S. Bathe [f,ah]
S. Batsouli [j] V. Baublis [ap] F. Bauer [f] A. Bazilevsky [e,q,ar]
S. Belikov [e,q,s] F.G. Bellaiche [am] S.T. Belyaev [z] M.J. Bennett [ad]
Y. Berdnikov [at] S. Bhagavatula [s] M.T. Bjorndal [j]
J.G. Boissevain [ad] H. Borel [k] S. Borenstein [ab] S. Botelho [au]
M.L. Brooks [ad] D.S. Brown [aℓ] N. Bruner [ak] D. Bucher [ah]
H. Buesching [e,ah] V. Bumazhnov [q] G. Bunce [e,ar]
J.M. Burward-Hoy [ac,ad,ay] S. Butsyk [ap,ay] X. Camard [az]
T.A. Carey [ad] J.-S. Chai [u] P. Chand [d] J. Chang [f] W.C. Chang [b]
L.L. Chavez [ak] S. Chernichenko [q] C.Y. Chi [j] J. Chiba [w] M. Chiu [j]
I.J. Choi [bh] J. Choi [v] R.K. Choudhury [d] T. Christ [ay]
T. Chujo [e,bd,be] M.S. Chung [y,ad] P. Chung [aw] V. Cianciolo [am]
C.R. Cleven [o] Y. Cobigo [k] B.A. Cole [j] M.P. Comets [an]
P. Constantin [s] M. Csanád [m] T. Csörgő [x] J.P. Cussonneau [az]
D. d'Enterria [j] T. Dahms [ay] K. Das [n] G. David [e] F. Deák [m]
H. Delagrange [az] A. Denisov [q] A. Deshpande [ar,ay] E.J. Desmond [e]
A. Devismes [ay] O. Dietzsch [au] B.V. Dinesh [d] J.L. Drachenberg [a]
O. Drapier [ab] A. Drees [ay] A.K. Dubey [bg] R. du Rietz [af]
A. Durum [q] D. Dutta [d] V. Dzhordzhadze [ba] K. Ebisu [aj]
Y.V. Efremenko [am] J. Egdemir [ay] K. El Chenawi [be]
A. Enokizono [p] H. En'yo [aa,aq,ar] B. Espagnon [an] S. Esumi [bd]
L. Ewell [e] T. Ferdousi [f] D.E. Fields [ak,ar] C. Finck [az] F. Fleuret [ab]
S.L. Fokin [z] B. Forestier [ae] B.D. Fox [ar] Z. Fraenkel [bg]

J.E. Frantz [j] A. Franz [e] A.D. Frawley [n] Y. Fukao [aa,aq,ar]
S.-Y. Fung [f] S. Gadrat [ae] S. Garpman [af,1] F. Gastineau [az]
M. Germain [az] T.K. Ghosh [be] A. Glenn [ba] A.L. Godoi [au]
G. Gogiberidze [ba] M. Gonin [ab] J. Gosset [k] Y. Goto [aq,ar]
R. Granier de Cassagnac [ab] N. Grau [s] S.V. Greene [be]
M. Grosse Perdekamp [r,ar] T. Gunji [h] S.K. Gupta [d] W. Guryn [e]
H.-Å. Gustafsson [af] T. Hachiya [p,aq] A. Hadjhenni [az]
J.S. Haggerty [e] M.N. Hagiwara [a] H. Hamagaki [h] A.G. Hansen [ad]
H. Hara [aj] H. Harada [p] E.P. Hartouni [ac] K. Haruna [p] M. Harvey [e]
E. Haslum [af] K. Hasuko [aq] R. Hayano [h,bc] N. Hayashi [aq] X. He [o]
M. Heffner [ac] T.K. Hemmick [ay] J.M. Heuser [aq,ay] M. Hibino [bf]
P. Hidas [x] H. Hiejima [r] J.C. Hill [s] D.S. Ho [bh] R. Hobbs [ak]
M. Holmes [be] W. Holzmann [aw] K. Homma [p] B. Hong [y]
A. Hoover [aℓ] T. Horaguchi [aq,ar,bb] H.M. Hur [u] T. Ichihara [aq,ar]
V.V. Ikonnikov [z] K. Imai [aa,aq] M. Inaba [bd] M. Inuzuka [h]
M.S. Ippolitov [z] D. Isenhower [a] L. Isenhower [a] M. Ishihara [aq,ar]
T. Isobe [h] M. Issah [aw] A. Isupov [t] B.V. Jacak [ar,ay] W.Y. Jang [y]
Y. Jeong [v] J. Jia [j,ay] J. Jin [j] O. Jinnouchi [aq,ar] B.M. Johnson [e]
S.C. Johnson [ac,ay] K.S. Joo [ai] D. Jouan [an] F. Kajihara [h,aq]
S. Kametani [h,bf] N. Kamihara [aq,bb] M. Kaneta [ar] J.H. Kang [bh]
M. Kann [ap] S.S. Kapoor [d] K. Katou [bf] T. Kawabata [h]
T. Kawagishi [bd] A.V. Kazantsev [z] S. Kelly [i,j] B. Khachaturov [bg]
A. Khanzadeev [ap] J. Kikuchi [bf] D.H. Kim [ai] D.J. Kim [bh]
D.W. Kim [v] E. Kim [av] G.-B. Kim [ab] H.J. Kim [bh] S.Y. Kim [bh]
Y.-S. Kim [u] Y.G. Kim [bh] E. Kinney [i] W.W. Kinnison [ad]
A. Kiss [m] E. Kistenev [e] A. Kiyomichi [aq,bd] K. Kiyoyama [aj]
C. Klein-Boesing [ah] S. Klinksiek [ak] H. Kobayashi [aq,ar]
L. Kochenda [ap] V. Kochetkov [q] D. Koehler [ak] T. Kohama [p]
R. Kohara [p] B. Komkov [ap] M. Konno [bd] M. Kopytine [ay]
D. Kotchetkov [f] A. Kozlov [bg] P.J. Kroon [e] C.H. Kuberg [a,ad]
G.J. Kunde [ad] N. Kurihara [h] K. Kurita [aq,ar,as] Y. Kuroki [bd]
M.J. Kweon [y] Y. Kwon [bh] G.S. Kyle [aℓ] R. Lacey [aw] V. Ladygin [t]
J.G. Lajoie [s] J. Lauret [aw] Y. Le Bornec [an] A. Lebedev [s,z]
S. Leckey [ay] D.M. Lee [ad] M.K. Lee [bh] S. Lee [v] M.J. Leitch [ad]
M.A.L. Leite [au] X.H. Li [f] Z. Li [g,aq] D.J. Lim [bh] H. Lim [av]

A. Litvinenko [t] M.X. Liu [ad] X. Liu [g] Y. Liu [an] Z. Liu [g]
C.F. Maguire [be] J. Mahon [e] Y.I. Makdisi [e] A. Malakhov [t]
M.D. Malik [ak] V.I. Manko [z] Y. Mao [g,ao,aq] S.K. Mark [ag]
S. Markacs [j] G. Martinez [az] M.D. Marx [ay] A. Masaike [aa]
H. Masui [bd] F. Matathias [ay] T. Matsumoto [h,bf] M.C. McCain [a,r]
P.L. McGaughey [ad] E. Melnikov [q] M. Merschmeyer [ah]
F. Messer [ay] M. Messer [e] Y. Miake [bd] J. Milan [aw] T.E. Miller [be]
A. Milov [ay,bg] S. Mioduszewski [e,ba] R.E. Mischke [ad] G.C. Mishra [o]
J.T. Mitchell [e] A.K. Mohanty [d] D.P. Morrison [e] J.M. Moss [ad]
T.V. Moukhanova [z] F. Mühlbacher [ay] D. Mukhopadhyay [be,bg]
M. Muniruzzaman [f] J. Murata [aq,ar,as] S. Nagamiya [w]
Y. Nagasaka [aj] Y. Nagata [bd] J.L. Nagle [i,j] M. Naglis [bg]
Y. Nakada [aa] T. Nakamura [p] B.K. Nandi [f] M. Nara [bd]
J. Newby [ac,ba] M. Nguyen [ay] L. Nikkinen [ag] P. Nilsson [af]
S. Nishimura [h] B. Norman [ad] A.S. Nyanin [z] J. Nystrand [af]
E. O'Brien [e] C.A. Ogilvie [s] H. Ohnishi [e,p,aq] I.D. Ojha [c,be]
H. Okada [aa,aq] K. Okada [aq,ar] O.O. Omiwade [a] M. Ono [bd]
V. Onuchin [q] A. Oskarsson [af] L. Österman [af] I. Otterlund [af]
K. Oyama [h,bc] K. Ozawa [h] L. Paffrath [e,1] D. Pal [be,bg]
A.P.T. Palounek [ad] V. Pantuev [ay] V. Papavassiliou [aℓ] J. Park [av]
W.J. Park [y] A. Parmar [ak] S.F. Pate [aℓ] H. Pei [s] T. Peitzmann [ah]
V. Penev [t] J.-C. Peng [r,ad] H. Pereira [k] V. Peresedov [t]
D.Yu. Peressounko [z] A.N. Petridis [s] A. Pierson [ak]
C. Pinkenburg [e,aw] R.P. Pisani [e] P. Pitukhin [q] F. Plasil [am]
M. Pollack [ay,ba] K. Pope [ba] M.L. Purschke [e] A.K. Purwar [ay]
H. Qu [o] J.M. Qualls [a] J. Rak [s] I. Ravinovich [bg] K.F. Read [am,ba]
M. Reuter [ay] K. Reygers [ah] V. Riabov [ap,at] Y. Riabov [ap]
G. Roche [ae] A. Romana [ab] M. Rosati [s] A.A. Rose [be]
S.S.E. Rosendahl [af] P. Rosnet [ae] P. Rukoyatkin [t] V.L. Rykov [aq]
S.S. Ryu [bh] M.E. Sadler [a] B. Sahlmueller [ah] N. Saito [aa,aq,ar]
A. Sakaguchi [p] T. Sakaguchi [h,bf] M. Sakai [aj] S. Sakai [bd]
H. Sako [bd] T. Sakuma [aq,bb] V. Samsonov [ap] L. Sanfratello [ak]
T.C. Sangster [ac] R. Santo [ah] H.D. Sato [aa,aq] S. Sato [e,w,bd]
S. Sawada [w] B.R. Schlei [ad] Y. Schutz [az] V. Semenov [q] R. Seto [f]
D. Sharma [bg] M.R. Shaw [a,ad] T.K. Shea [e] I. Shein [q]

T.-A. Shibata [aq,bb] K. Shigaki [p,w] T. Shiina [ad] M. Shimomura [bd]
Y.H. Shin [bh] T. Shohjoh [bd] K. Shoji [aa,aq] I.G. Sibiriak [z]
A. Sickles [ay] C.L. Silva [au] D. Silvermyr [ad,af,am] K.S. Sim [y]
J. Simon-Gillo [ad] C.P. Singh [c] V. Singh [c] M. Sivertz [e] S. Skutnik [s]
W.C. Smith [a] A. Soldatov [q] R.A. Soltz [ac] W.E. Sondheim [ad]
S.P. Sorensen [am,ba] I.V. Sourikova [e] F. Staley [k] P.W. Stankus [am]
N. Starinsky [ag] P. Steinberg [j] E. Stenlund [af] M. Stepanov [aℓ]
A. Ster [x] S.P. Stoll [e] M. Sugioka [aq,bb] T. Sugitate [p] C. Suire [an]
J.P. Sullivan [ad] Y. Sumi [p] Z. Sun [g] M. Suzuki [bd] J. Sziklai [x]
T. Tabaru [ar] S. Takagi [bd] E.M. Takagui [au] A. Taketani [aq,ar]
M. Tamai [bf] K.H. Tanaka [w] Y. Tanaka [aj] K. Tanida [aq,ar]
E. Taniguchi [aq,bb] M.J. Tannenbaum [e] A. Taranenko [aw]
P. Tarján [ℓ] J.D. Tepe [a,ad] J. Thomas [ay] J.H. Thomas [ac]
T.L. Thomas [ak] W. Tian [g,ba] M. Togawa [aa,aq] J. Tojo [aa,aq]
H. Torii [aa,aq,ar] R.S. Towell [a,ad] V-N. Tram [ab] I. Tserruya [bg]
Y. Tsuchimoto [p,aq] H. Tsuruoka [bd] A.A. Tsvetkov [z] S.K. Tuli [c]
H. Tydesjö [af] N. Tyurin [q] T.J. Uam [ai] T. Ushiroda [aj] H. Valle [be]
H.W. van Hecke [ad] C. Velissaris [aℓ] J. Velkovska [e,ay,be]
M. Velkovsky [ay] R. Vertesi [ℓ] V. Veszprémi [ℓ] L. Villatte [ba]
A.A. Vinogradov [z] M.A. Volkov [z] A. Vorobyov [ap]
E. Vznuzdaev [ap] M. Wagner [aa] H. Wang [f] X.R. Wang [o,aℓ]
Y. Watanabe [aq,ar] J. Wessels [ah] S.N. White [e] N. Willis [an]
D. Winter [j] C. Witzig [e] F.K. Wohn [s] C.L. Woody [e] M. Wysocki [i]
W. Xie [f,ar,bg] K. Yagi [bd] Y. Yang [g] A. Yanovich [q] S. Yokkaichi [aq,ar]
G.R. Young [am] I. Younus [ak] I.E. Yushmanov [z] W.A. Zajc [j]
O. Zaudkte [ah] C. Zhang [j] Z. Zhang [ay] S. Zhou [g] S.J. Zhou [bg]
J. Zimányi [x] L. Zolin [t] X. Zong [s] (PHENIX Collaboration)

[a] *Abilene Christian University, Abilene, TX 79699, USA*

[b] *Institute of Physics, Academia Sinica, Taipei 11529, Taiwan*

[c] *Department of Physics, Banaras Hindu University, Varanasi 221005, India*

[d] *Bhabha Atomic Research Centre, Bombay 400 085, India*

[e] *Brookhaven National Laboratory, Upton, NY 11973-5000, USA*

[f] *University of California - Riverside, Riverside, CA 92521, USA*

[g] *China Institute of Atomic Energy (CIAE), Beijing, People's Republic of China*

[h] *Center for Nuclear Study, Graduate School of Science, University of Tokyo, 7-3-1*

Hongo, Bunkyo, Tokyo 113-0033, Japan

[i] *University of Colorado, Boulder, CO 80309*

[j] *Columbia University, New York, NY 10027 and Nevis Laboratories, Irvington, NY 10533, USA*

[k] *Dapnia, CEA Saclay, F-91191, Gif-sur-Yvette, France*

[ℓ] *Debrecen University, H-4010 Debrecen, Egyetem tér 1, Hungary*

[m] *ELTE, Eötvös Loránd University, H - 1117 Budapest, Pázmány P. s. 1/A, Hungary*

[n] *Florida State University, Tallahassee, FL 32306, USA*

[o] *Georgia State University, Atlanta, GA 30303, USA*

[p] *Hiroshima University, Kagamiyama, Higashi-Hiroshima 739-8526, Japan*

[q] *Institute for High Energy Physics (IHEP), Protvino, Russia*

[r] *University of Illinois at Urbana-Champaign, Urbana, IL 61801*

[s] *Iowa State University, Ames, IA 50011, USA*

[t] *Joint Institute for Nuclear Research, 141980 Dubna, Moscow Region, Russia*

[u] *KAERI, Cyclotron Application Laboratory, Seoul, South Korea*

[v] *Kangnung National University, Kangnung 210-702, South Korea*

[w] *KEK, High Energy Accelerator Research Organization, Tsukuba-shi, Ibaraki-ken 305-0801, Japan*

[x] *KFKI Research Institute for Particle and Nuclear Physics (RMKI), H-1525 Budapest 114, POBox 49, Hungary*

[y] *Korea University, Seoul, 136-701, Korea*

[z] *Russian Research Center "Kurchatov Institute", Moscow, Russia*

[aa] *Kyoto University, Kyoto 606, Japan*

[ab] *Laboratoire Leprince-Ringuet, Ecole Polytechnique, CNRS-IN2P3, Route de Saclay, F-91128, Palaiseau, France*

[ac] *Lawrence Livermore National Laboratory, Livermore, CA 94550, USA*

[ad] *Los Alamos National Laboratory, Los Alamos, NM 87545, USA*

[ae] *LPC, Université Blaise Pascal, CNRS-IN2P3, Clermont-Fd, 63177 Aubiere Cedex, France*

[af] *Department of Physics, Lund University, Box 118, SE-221 00 Lund, Sweden*

[ag] *McGill University, Montreal, Quebec H3A 2T8, Canada*

[ah] *Institut für Kernphysik, University of Muenster, D-48149 Muenster, Germany*

[ai] *Myongji University, Yongin, Kyonggido 449-728, Korea*

[aj] *Nagasaki Institute of Applied Science, Nagasaki-shi, Nagasaki 851-0193, Japan*

[ak] *University of New Mexico, Albuquerque, NM 87131, USA*

[aℓ] *New Mexico State University, Las Cruces, NM 88003, USA*

[am] *Oak Ridge National Laboratory, Oak Ridge, TN 37831, USA*

[an] *IPN-Orsay, Universite Paris Sud, CNRS-IN2P3, BP1, F-91406, Orsay, France*

[ao] *Peking University, Beijing, People's Republic of China*

[ap] *PNPI, Petersburg Nuclear Physics Institute, Gatchina, Russia*

[aq] *RIKEN (The Institute of Physical and Chemical Research), Wako, Saitama 351-0198, JAPAN*

[ar] *RIKEN BNL Research Center, Brookhaven National Laboratory, Upton, NY 11973-5000, USA*

[as] *Physics Department, Rikkyo University, 3-34-1 Nishi-Ikebukuro, Toshima, Tokyo 171-8501, Japan*

[at] *St. Petersburg State Technical University, St. Petersburg, Russia*

[au] *Universidade de São Paulo, Instituto de Física, Caixa Postal 66318, São Paulo CEP05315-970, Brazil*

[av] *System Electronics Laboratory, Seoul National University, Seoul, South Korea*

[aw] *Chemistry Department, Stony Brook University, Stony Brook, SUNY, NY 11794-3400, USA*

[ay] *Department of Physics and Astronomy, Stony Brook University, SUNY, Stony Brook, NY 11794, USA*

[az] *SUBATECH (Ecole des Mines de Nantes, CNRS-IN2P3, Université de Nantes) BP 20722 - 44307, Nantes, France*

[ba] *University of Tennessee, Knoxville, TN 37996, USA*

[bb] *Department of Physics, Tokyo Institute of Technology, Tokyo, 152-8551, Japan*

[bc] *University of Tokyo, Tokyo, Japan*

[bd] *Institute of Physics, University of Tsukuba, Tsukuba, Ibaraki 305, Japan*

[be] *Vanderbilt University, Nashville, TN 37235, USA*

[bf] *Waseda University, Advanced Research Institute for Science and Engineering, 17 Kikui-cho, Shinjuku-ku, Tokyo 162-0044, Japan*

[bg] *Weizmann Institute, Rehovot 76100, Israel*

[bh] *Yonsei University, IPAP, Seoul 120-749, Korea*

Abstract

Extensive experimental data from high-energy nucleus-nucleus collisions were recorded using the PHENIX detector at the Relativistic Heavy Ion Collider (RHIC). The comprehensive set of measurements from the first three years of RHIC operation includes charged particle multiplicities, transverse energy, yield ratios and spectra of identified hadrons in a wide range of transverse momenta (p_T), elliptic flow, two-particle correlations, non-statistical fluctuations, and suppression of particle production at high p_T. The results are examined with an emphasis on implications for the formation of a new state of dense matter. We find that the state of matter created at RHIC cannot be described in terms of ordinary color neutral hadrons.

1 INTRODUCTION

1.1 Historical Introduction

A recurring theme in the history of physics is the desire to study matter under extreme conditions. The latter half of the twentieth century saw this quest extended from 'ordinary' atomic systems to those composed of nuclear matter. Even prior to the identification of Quantum Chromodynamics (QCD) as the underlying theory of the strong interaction, there was considerable interest in the fate of nuclear matter when subjected to density and temperature extremes [1–3]. Particularly intriguing was the suggestion that new phases of nuclear matter could be associated with a corresponding change in the structure of the vacuum [4]. These considerations gained additional impetus with the realizations that a) QCD was the correct theory of the strong interaction, b) the phenomena of quark confinement was a consequence of the nonperturbative structure of the vacuum and c) this vacuum structure is modified at high temperatures and/or densities, suggesting that quarks and gluons under such conditions would be deconfined. Taken together, these facts suggest that QCD is a fundamental theory of nature containing a phase transition *that is accessible to experimental investigation.*

It is quite remarkable that this understanding was achieved very early in the development of QCD. Collins and Perry noted in 1975 [5] that the reduction of the coupling constant at small distances indicated that the dense nuclear matter at the center of neutron stars would consist of deconfined quarks and gluons [2] . Their treatment focused on the high-density, low-temperature regime of QCD, but they did note that similar arguments might apply to the high temperatures present in the early universe. An extensive review by Shuryak in 1980 [7] is the first to have examined the high-temperature phase in detail, and is also notable for proposing the phrase "quark-gluon plasma" (QGP) to describe the deconfined state:

> *When the* energy *density* ε *exceeds some typical hadronic value (*~ 1 GeV/fm^3*), matter no longer consists of separate hadrons (protons, neutrons, etc.), but*

Email address: PHENIXSpokesperson: zajc@nevis.columbia.edu (W.A. Zajc).

[1] Deceased

[2] In fact, prior to the development of QCD the quark hypothesis raised serious issues concerning the stability of neutron stars [6].

as their fundamental constituents, quarks and gluons. Because of the apparent analogy with similar phenomena in atomic physics we may call this phase of matter the QCD (or quark-gluon) plasma.

Developing a quantitative understanding of the deconfining phase transition in hadronic matter and of QGP properties has proven to be a challenging task. While simple dimensional arguments suffice to identify both the critical energy density $\varepsilon_C \sim 1\text{GeV/fm}^3$ and the associated critical temperature $T_C \sim 170\text{MeV}$, these values also imply that the transition occurs in a regime where the coupling constant is of order unity, thereby making perturbative descriptions highly suspect.

Progress in understanding QCD in the extremely non-perturbative domain near the critical temperature has relied on an essential contribution by Creutz [8], who showed that numerical implementations of Wilson's lattice formulation [9] could be used to study phase transition phenomena. This work, together with the continued exponential increases in computing power, stimulated the development of lattice QCD, which in turn has led to detailed investigations of the thermodynamic properties of quarks and gluons [10].

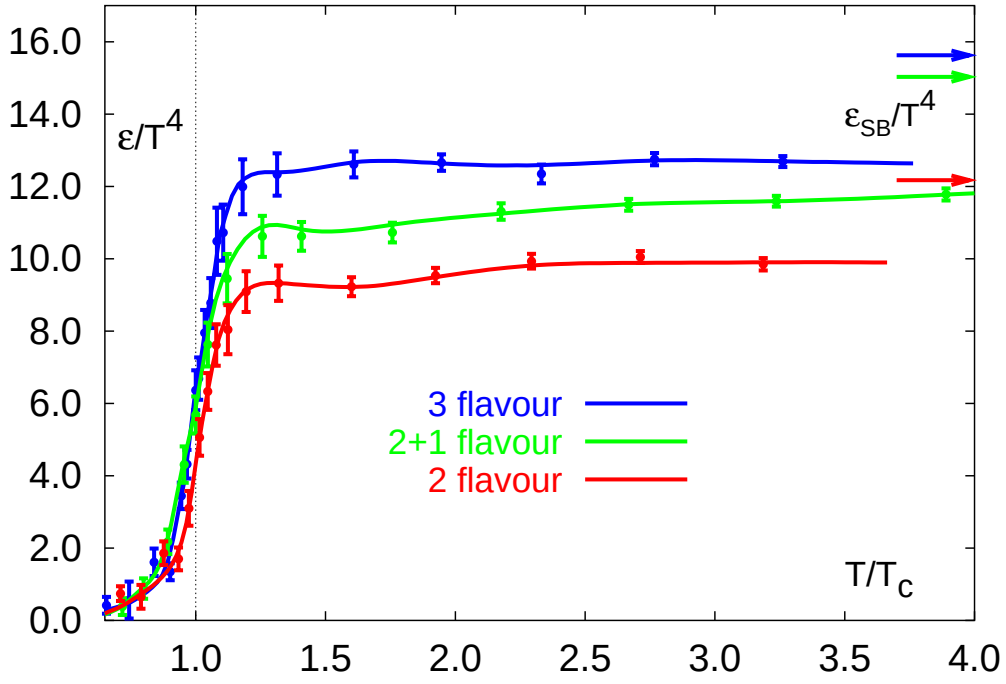

Fig. 1. Lattice QCD results [11] for the energy density / T^4 as a function of the temperature scaled by the critical temperature T_C. Note the arrows on the right side indicating the values for the Stefan-Boltzmann limit.

Lattice QCD predicts a phase transformation to a quark-gluon plasma at a temperature of approximately $T \approx 170\text{MeV} \approx 10^{12}$ K, as shown in Fig. 1 [11].

This transition temperature corresponds to an energy density $\varepsilon \approx 1\text{GeV/fm}^3$, nearly an order of magnitude larger than that of normal nuclear matter. As noted above, this value is plausible based on dimensional grounds, since such densities correspond to the total overlap of several (light) hadrons within a typical hadron volume of 1–3 fm^3. No plausible mechanism exists under which hadrons could retain their *in vacuo* properties under these conditions. Lattice calculations also indicate that this significant change in the behavior of the system occurs over a small range in temperature (∼20 MeV), and suggest that the change of phase includes the restoration of approximate chiral symmetry resulting from greatly reduced or vanishing quark constituent masses.

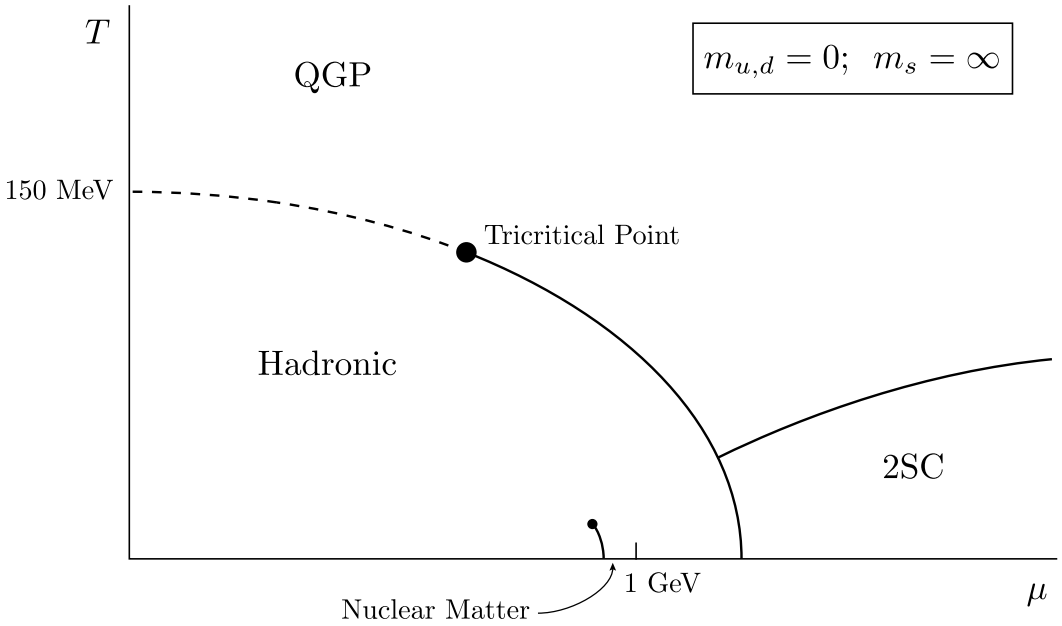

Fig. 2. Theoretical phase diagram of nuclear matter for two massless quarks as a function of temperature T and baryon chemical potential μ [12].

In the limit of massless noninteracting particles, each bosonic degree of freedom contributes $\frac{\pi^2}{30}T^4$ to the energy density; each fermionic degree of freedom contributes $\frac{7}{8}$ this value. The corresponding "Stefan-Boltzmann" limits of the energy density ε_{SB} for the case of 2(3) active flavor quark-gluon plasma is then

$$\varepsilon_{SB} = \{2_f \cdot 2_s \cdot 2_q \cdot 3_c \frac{7}{8} + 2_s \cdot 8_c\} \frac{\pi^2}{30} T^4 = 37\ \frac{\pi^2}{30} T^4 \tag{1}$$

$$\{3_f \cdot 2_s \cdot 2_q \cdot 3_c \frac{7}{8} + 2_s \cdot 8_c\} \frac{\pi^2}{30} T^4 = 47.5\ \frac{\pi^2}{30} T^4 \tag{2}$$

after summing over the appropriate flavor, spin, quark/antiquark and color factors for quarks and spin times color factors for gluons. The large numerical

coefficients (37 and 47.5) stand in stark contrast to the value of $\sim$3 expected for a hadron gas with temperature $T < T_C$, in which case the degrees of freedom are dominated by the three pion species π^-, π^0, π^+.

The exact order of this phase transition is not known. In a pure gauge theory containing only gluons the transition appears to be first order. However, inclusion of two light quarks (up and down) or three light quarks (adding the strange quark) can change the transition from first order to second order to a smooth crossover. These results are obtained at zero net baryon density; dramatic changes in the nature of the transition and in the medium itself are expected when the net baryon density becomes significant. A schematic version of the phase diagram for an idealized form of nuclear matter with vanishing light quark (up and down) masses and infinite strange quark mass is presented in Fig. 2 [12]. For sufficiently large values of the baryon chemical potential μ this system exhibits a first order phase transition between hadronic matter and QGP, along with a tricritical point below which the transition becomes second order. However, non-zero values of the light quark masses dramatically alter this simple picture: The second order phase transition denoted by the dashed line in Fig. 2 becomes a smooth crossover, and the tricritical point correspondingly becomes a critical point designating the end of the first order transition found at higher values of μ. For example, recent calculations [13,14] indicate that the transition is a crossover for values of $\mu <\sim 400$ MeV. Given that both theoretical arguments and experimental data suggest that nucleus-nucleus collisions at RHIC (at least near mid-rapidity) are characterized by low net baryon density, we will restrict our attention to this regime, while noting that the predicted smooth nature of the transition in this region increases the experimental challenges of unambiguously establishing that such a transition has occurred. We also note that while Fig. 2 shows that the region of low temperature and high baryon density is expected to show a transition to a color superconducting phase of matter, this regime is not accessible to RHIC collisions and will not be discussed further.

While the lattice results plotted in Fig. 1 show that the energy density reaches a significant fraction (~ 0.8) of the Stefan-Boltzmann values in the deconfined phase, the deviation from ε_{SB}, and the reason for the persistence of that deviation to the highest studied values of T/T_C, are of great interest. For instance, Greiner has noted [15] that "in order to allow for simple calculations the QGP is usually described as a free gas consisting of quarks and gluons. This is theoretically not well founded at $T \approx T_c$". In fact, analysis of the gluon propagator in a thermal system [16,17] has demonstrated that effective masses of order $g(T)T$ are generated, suggesting that the relevant degrees of freedom are in fact massive near T_C. $m_g \approx T_c$ could be generated by gluons. Especially interesting is recent work which indicates that both heavy [18–20] and light [21] flavor states may remain bound above T_C, calling into question the naive interpretation of $\varepsilon(T)$ as an indicator of the explicit appearance of

quark and gluon degrees of freedom. This is supported by explicit calculations of the spectrum of bound states above T_C [22] which predict a rich structure of states that belies a description as a weakly interacting parton gas.

To emphasize this point, consider the standard measure of the degree of coupling in a classical plasma, obtained by comparing the relative magnitudes of the average kinetic and potential energies:

$$\Gamma \equiv \frac{\langle V(r) \rangle}{\langle E_{kin} \rangle}. \tag{3}$$

In the case of the QCD plasma the mean inter-particle spacing should scale as some numerical coefficient times $1/T$. Naively, this gives a mean potential energy $\langle V(r) \rangle \sim \alpha_s(T) \langle 1/r \rangle \sim \alpha_s(T) T$, leading to

$$\Gamma \sim \frac{\alpha_s(T) T}{3T} \sim \alpha_s(T). \tag{4}$$

Any reasonable estimate for the numerical coefficients leads to $\Gamma > 1$, which is the condition for a "strongly-coupled" plasma. In reality, the screening present at such densities (or equivalently, the generation of effective gluon masses) modifies the mean potential energy to $\langle V(r) \rangle \sim g(T) T$, which only increases the estimated value of Γ [23]. Considerations such as these have led some authors [24,25] to denote quark-gluon plasma in this regime as "sQGP" for "strongly interacting QGP".

It is worth noting that this state of affairs has been anticipated by many authors. Whether the argument was based on the divergence of perturbative expansions [26], on phenomenological descriptions of confinement [27], on the development of effective gluon masses from plasmon modes [28] or on general principles [15], it is clear that the QGP near T_C should not be regarded as an ideal gas of quarks and gluons.

How high a temperature is needed not just to form a quark-gluon plasma, but to approach this "weakly" interacting plasma? A calculation of the pressure of hot matter within perturbative QCD [29] is shown in Fig. 3. The pressure result oscillates significantly as one considers contributions of different orders. These oscillations are an indication that the expansion is not yielding reliable results. However at temperatures approaching 1000 times of T_C ($\approx \Lambda_{\bar{M}S}$), they appear to be converging toward the Stefan-Boltzmann limit (asymptotically free partons). It is interesting that in considering the highest-order term, the results are still nonconvergent though one seems to approach the lattice calculated pressure. Unlike the case of single parton-parton scattering at zero temperature, the infrared problems of finite-temperature field theory prevent further analytic progress even for very small values of the coupling constant

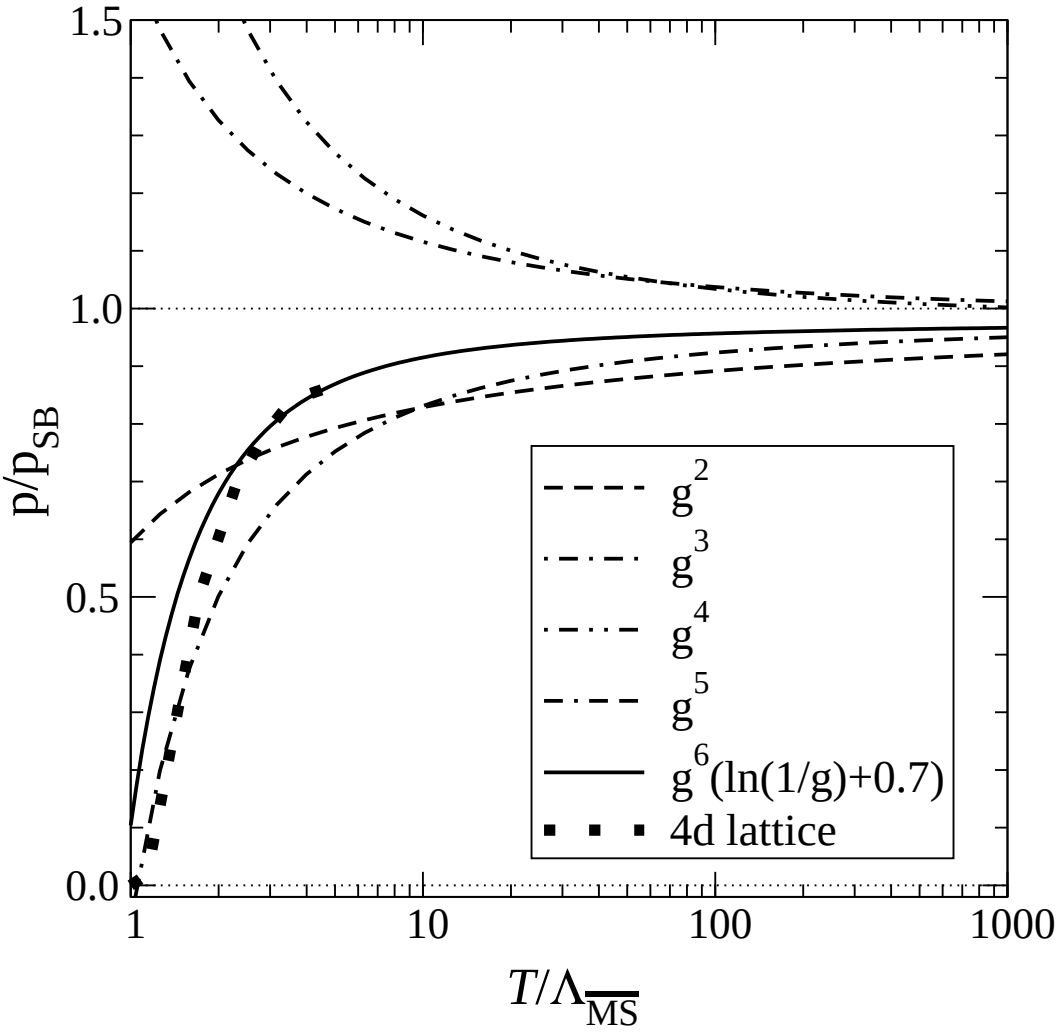

Fig. 3. Perturbative QCD results for the pressure as a function of temperature at various orders normalized to the Stefan-Boltzmann value p_{SB} [29].

[29–31].

The goal of relativistic heavy ion physics is the experimental study of the nature of QCD matter under conditions of extreme temperature. A great emphasis has been placed on "the discovery of the quark-gluon plasma", where the terminology "quark-gluon plasma" is used as a generic descriptor for a system in which the degrees of freedom are no longer the color neutral hadron states observed as isolated particles and resonances. This definition is limited since high-energy proton-proton reactions cannot be described purely in terms of color-neutral hadrons, but rather require analysis of the underlying partonic interactions. The hoped-for essential difference in heavy ion collisions is the dominance of the partonic-level description for essentially all momentum scales and over nuclear size distances. Beyond this simple criterion, in order to characterize the produced system as a state of matter it is necessary to establish that these non-hadronic degrees of freedom form a statistical ensemble,

so that concepts such as temperature, chemical potential and flow velocity apply and the system can be characterized by an experimentally determined equation of state. Additionally, experiments eventually should be able to determine the physical characteristics of the transition, for example the critical temperature, the order of the phase transition, and the speed of sound along with the nature of the underlying quasi-particles. While at (currently unobtainable) very high temperatures $T \gg T_c$ the quark-gluon plasma may act as a weakly interacting gas of quarks and gluons, in the transition region near T_c the fundamental degrees of freedom may be considerably more complex. It is therefore appropriate to argue that the quark-gluon plasma must be defined in terms of its unique properties *at a given temperature*. To date the definition is provided by lattice QCD calculations. Ultimately we would expect to validate this by characterizing the quark-gluon plasma in terms of its experimentally observed properties. However, the real discoveries will be of the fascinating properties of high temperature nuclear matter, and not the naming of that matter.

1.2 Experimental Program

The theoretical discussion of the nature of hadronic matter at extreme densities has been greatly stimulated by the realization that such conditions could be studied via relativistic heavy ion collisions [32]. Early investigations at the Berkeley Bevalac (c. 1975–1985), the BNL AGS (c. 1987–1995) and the CERN SPS (c. 1987–present) have reached their culmination with the commissioning of BNL's Relativistic Heavy Ion Collider (RHIC), a dedicated facility for the study of nuclear collisions at ultra-relativistic energies [33].

The primary goal of RHIC is the experimental study of the QCD phase transition. The 2002 Long-Range Plan for Nuclear Science [34] clearly enunciates this objective:

> *...the completion of RHIC at Brookhaven has ushered in a new era. Studies are now possible of the most basic interactions predicted by QCD in bulk nuclear matter at temperatures and densities great enough to excite the expected phase transition to a quark-gluon plasma. As the RHIC program matures, experiments will provide a unique window into the hot QCD vacuum, with opportunities for fundamental advances in the understanding of quark confinement, chiral symmetry breaking, and, very possibly, new and unexpected phenomena in the realm of nuclear matter at the highest densities.*

The RHIC accelerator and its four experiments were commissioned and brought online in the summer of 2000. The initial operation of both RHIC and the experiments has been remarkably successful. In these first three years the ac-

celerator has collided, and the experiments have acquired data on, Au+Au collisions at five energies, an essential $p + p$ baseline data set, and a critical d+Au comparison. The analyses of these various systems have resulted in a correspondingly rich abundance of results, with over 90 publications in the refereed literature.

It is therefore appropriate to reflect on the physics accomplishments to date, with a particular emphasis on their implications for the discovery of a new state of matter. At the same time, it is essential to identify those features of the data (if any) that are at odds with canonical descriptions of the produced matter, to specify those crucial measurements which remain to be made, and to outline a program for continued exploration and characterization of strongly interacting matter at RHIC. The PHENIX collaboration [35] has performed such an assessment; this document represents a summary of its findings.

The PHENIX Conceptual Design Report [36], submitted to BNL/RHIC management on January 29th, 1993, outlined a comprehensive physics program focused on the search for and characterization of new states of nuclear matter. The measurement of electromagnetic probes and high-transverse-momentum phenomena formed a major thrust of the proposed program. It was also realized that the measurement of global variables and soft identified hadron spectra in the same apparatus was essential to the goal of understanding the evolution of the produced matter over all relevant timescales. These diverse criteria required combining an unprecedented number of subsystems together with a high-bandwidth trigger and data-acquisition system into an integrated detector design. Particular attention was given to minimizing the conflicting design criteria of the central arm spectrometers, with their requirement for minimal mass in the aperture, and those of the muon spectrometers which require maximal absorption of the incident hadron flux. The data acquisition and trigger system was designed to accommodate the great variety of interaction rates and event sizes provided by RHIC. Every effort was made to provide for future upgrades, both in the geometry of the experiment and in the architecture and design parameters of the read-out system.

The published PHENIX results of Au+Au collision at a center-of-mass energy per nucleon pair, $\sqrt{s_{NN}}$, of 130 GeV [37–48] and at $\sqrt{s_{NN}} = 200$ GeV [49–55], $p+p$ collisions at $\sqrt{s} = 200$ GeV [56,57], and d+Au at $\sqrt{s_{NN}} = 200$ GeV [58] clearly demonstrate that PHENIX's goal to make high-quality measurements in both hadronic and leptonic channels for collisions ranging from $p + p$ to Au+Au has been realized. A summary of these results illustrates this point:

- Systematic measurement of the dependence of the charged particle pseudorapidity density [37] and the transverse energy [38] on the number of participants in Au+Au collisions at $\sqrt{s_{NN}}$=130 GeV.
- Discovery of suppressed production for π^0's and charged particles at high

p_T in Au+Au collisions at $\sqrt{s_{NN}}$=130 GeV [39] and a systematic study of the scaling properties of the suppression [47]; extension of these results to much higher transverse momenta in Au+Au collisions at $\sqrt{s_{NN}}$=200 GeV [49,53].

- Co-discovery (together with BRAHMS[59], PHOBOS[60] and STAR[61]) of absence of high-p_T suppression in d+Au collisions at $\sqrt{s_{NN}}$=200 GeV [58].
- Discovery of the anomalously large proton and anti-proton yields at intermediate transverse momentum in Au+Au collisions at $\sqrt{s_{NN}}$=130 GeV through the systematic study of $\pi^{\pm}$, $K^{\pm}$, p and $\bar{p}$ spectra [40]; measurement of Λ's and $\bar{\Lambda}$'s in Au+Au collisions at $\sqrt{s_{NN}}$=130 GeV [43]; study of the scaling properties of the proton and anti-proton yields in Au+Au collisions at $\sqrt{s_{NN}}$=200 GeV [52]; measurement of deuteron and anti-deuteron spectra at $\sqrt{s_{NN}}$=200 GeV [62].
- Measurement of Hanbury-Brown-Twiss (HBT) correlations in $\pi^+\pi^+$ and $\pi^-\pi^-$ pairs in Au+Au collisions at $\sqrt{s_{NN}}$=130 GeV [41] and 200 GeV [63], establishing that the "HBT puzzle" of $R_{\rm out} \approx R_{\rm side}$ extends to high pair momentum.
- First measurement of single electron spectra in Au+Au collisions at $\sqrt{s_{NN}}$=130 GeV, suggesting that charm production scales with the number of binary collisions [42].
- Sensitive measures of charge fluctuations [44] and fluctuations in mean p_T and transverse energy per particle [45,55] in Au+Au collisions at $\sqrt{s_{NN}}$=130 GeV and 200 GeV.
- Measurements of elliptic flow for charged particles from Au+Au collisions at $\sqrt{s_{NN}}$=130 GeV [46] and identified charged hadrons from Au+Au collisions at $\sqrt{s_{NN}}$=200 GeV [50].
- Extensive study of hydrodynamic flow, particle yields, ratios and spectra from Au+Au collisions at $\sqrt{s_{NN}}$=130 GeV [48] and 200 GeV [54].
- First observation of J/ψ production in Au+Au collisions at $\sqrt{s_{NN}}$=200 GeV [51].
- Measurement of crucial baseline data on π^0 spectra [56] and J/ψ production [57] in $p+p$ collisions at $\sqrt{s}$=200 GeV.

These publications encompass physics from the barn to the picobarn level; their very breadth precludes a detailed presentation here. These data, together with a rich program of future RHIC measurements, will allow us to address many of the features that would characterize a quark-gluon plasma:

- Temperature
- Parton number density
- Energy density
- Opacity
- Collective behavior
- Thermalization leading to the quark-gluon phase
- Deconfinement

- Number and nature of degrees of freedom
- Recombination of quarks and gluons to form final-state hadrons
- Chiral symmetry restoration
- Time evolution of system parameters
- Equation of state
- Color and thermal transport properties
- Critical behavior

As emphasized above, the present PHENIX data set from RHIC runs in year 2000 to 2003 already provides an extensive set of measurements on global variables: (transverse energy and multiplicity, elliptic flow); correlations and fluctuations: (fluctuations in charge and $\langle p_T \rangle$, HBT measurements), hadron spectra: (low-p_T single-hadron spectra and radial flow, particle ratios, resonances, anomalous p/π ratio at intermediate p_T); high-p_T physics: (high-p_T singles spectra, suppression phenomena in $A + A$, nonsuppression in $d + A$, high-p_T two-particle correlations, nuclear suppression/enhancement in forward/backward directions), heavy flavor production: (charm, J/ψ), and electromagnetic probes: (direct photons). However, an important conclusion of this report is that systematic studies of these observables (vs. collision species and energy) are needed to extract unambiguous information on most of these features.

1.3 Organization of this Document

As a result, this paper concentrates on those aspects of the present data that address the broad features of energy density, thermalization, deconfinement and critical behavior. The focus in most cases will be on the data of the PHENIX experiment, but the data of the other RHIC experiments will be cited to support and to extend the discussion [3]. The experimental tools that allow the systematic study of all phenomena as a function of the inferred impact parameter are presented in the context of hard-scattering phenomena. These methods and the associated data are then used to discuss the experimental evidence for the formation of a state of high-density matter. The measured abundances, spectra and flow patterns are used to analyze the degree of thermalization and collectivity in the produced matter. These results are then examined for evidence establishing the role of deconfined quarks and gluons in the produced system, along with the implications for its description as a quark-gluon plasma. A concluding section summarizes the findings and identifies key future measurements required to further refine our observations.

[3] An underappreciated aspect of the RHIC program is the excellent agreement between the various experiments in almost all measured channels.

2 ENERGY DENSITY AND E_T, N_{CH}

A prerequisite for creating a quark-gluon plasma is producing a system with sufficiently large energy density. From both elementary estimates [22] and from extensive numerical studies in lattice QCD [11,10], the required density is known to be on the order of 1 GeV/fm^3. Establishing that this energy density is created in RHIC collisions is a basic ingredient in establishing the creation of a QGP at RHIC.

In this section we explore what can be deduced about the energy densities achieved in RHIC A+A collisions from measurements of the global transverse energy and multiplicity. In later sections these estimates will be compared to densities inferred from hydrodynamics-based models (Section 3) and from jet quenching evidence (Section 6).

Specifically, we will address three different energy density estimates, and introduce two distinct time scales: (i) The peak *general energy density* that is achieved when the incoming nuclei overlap; (ii) The peak *formed energy density* involving created particles at proper time τ_{Form}; and (iii) The peak *thermalized energy density* present at proper time τ_{Therm} when local thermal equilibrium is first achieved (assuming that this occurs). The values and time scales for formed and thermalized energy densities are indicated schematically in Fig 4; detailed explanations follow in Sections 2.3 and 2.4.

In this Section we will also review data on overall particle multiplicities, and through them distinguish between different models of the initial particle production.

2.1 General Energy Density

The simplest definition of "energy density" is the total mass-energy within some region of space divided by the volume of that region, as seen at some instant of time in some Lorentz frame. However, this definition is not satisfactory since we can "trivially" raise any simple energy density by viewing the system in a different frame. For example, a static system with constant energy density ρ_0 in its rest frame—say, a gold nucleus—will appear to have energy density $\gamma^2\rho_0$ when viewed in a frame boosted by Lorentz γ. Accordingly, we can only calculate a *meaningful* energy density $\langle\varepsilon\rangle$ as mass-energy/volume for some region *in the case* when the total momentum in the region is zero.

Now let us imagine a symmetric RHIC A+A collision at a moment when the two original nuclei are overlapping in space, as seen in the lab/CMS frame. The total momentum in any overlap region is zero by symmetry, so we can

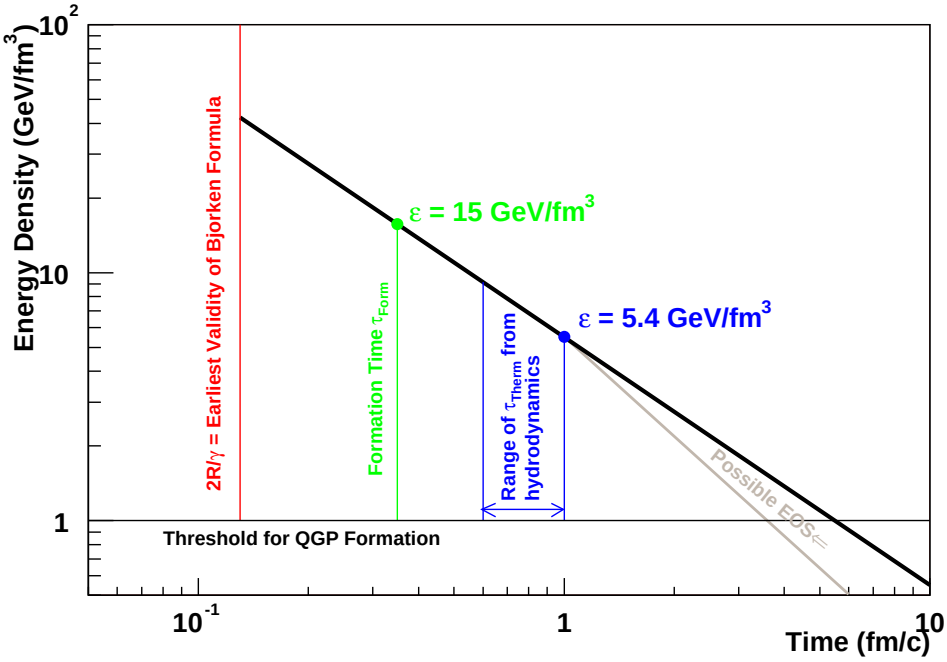

Fig. 4. Schematic drawing of the time and energy density scales derived through the Bjorken picture.

calculate a meaningful—if short-lived—energy density for such a region. If each nucleus has energy density ρ_0 in its rest frame then the total energy density in the overlap region is just $\langle\varepsilon\rangle = 2\rho_0\gamma^2$. If we take a nominal ρ_0=0.14 GeV/fm^3 for a nucleus at rest and $\gamma = 106$ for a full-energy RHIC collision, then the result for the peak general energy density is $\langle\varepsilon\rangle$ =3150 GeV/fm^3. This is a spectacularly, almost absurdly high number on the scale of ∼1 GeV/fm^3 associated with the familiar transition described by lattice QCD.

This energy density is of course artificial, in that it would be temporarily present even in the case of no interactions between the two nuclei. It is instructive to consider the (again artificial) case where the nucleons in the two nuclei have only elastic interactions. Then the time during which a high energy density is present over *any* volume cannot last longer than $t = 2R/\gamma$, where R is the rest-frame radius of the nucleus. With R =7 fm for Au this time is only 0.13 fm/c at RHIC, and after this time all energy densities will fall precipitously back to ρ_0 if no secondary particles are created. The scale of this interval is so short that a scattering cannot even be said to have occurred within that volume unless its momentum transfer scale Q exceeds at least 1.5 GeV/c, or more.

Accordingly, we will turn our attention instead to energy densities involving only produced particles, as the potential source for a QCD transition.

In any frame (not just the CMS frame) where the two incoming nuclei have very high energies the region when/where the nuclei overlap will be very thin in the longitudinal direction and very short in duration. In this limit, then, it is fair to describe all secondary produced particles as having been radiated out from a very thin "disk", and that they are all created at essentially the same time. These realizations lead directly to the picture described by Bjorken [64], whose original diagram is reproduced in Fig. 5 and whose derivation we retrace briefly here.

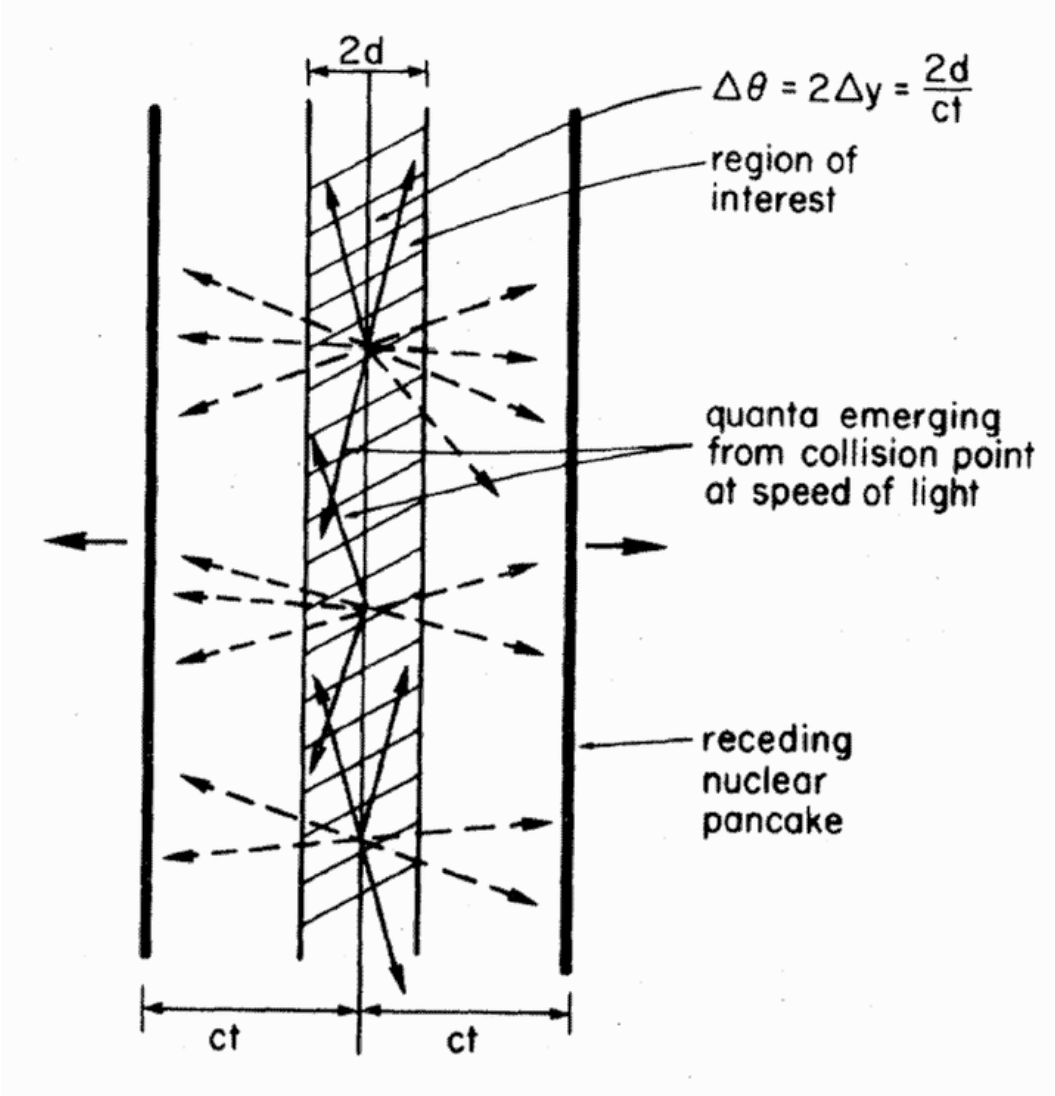

Fig. 5. Figure from Bjorken [64] illustrating the geometry of initially produced particles at a time t after the overlap of the incoming nuclei in some frame. The picture is valid in any frame in which the incoming nuclei have very high energies and so are highly Lorentz contracted.

Once the beam "pancakes" recede after their initial overlap, the region between them is occupied by secondaries at intermediate rapidities. We can calculate the local energy density of these created particles if we make one further assumption: that the secondaries can be considered "formed" at some proper time τ_{Form} after they are radiated out from the thin source disk.

Our region of interest, in any frame, will be a slab perpendicular to the beam direction, with longitudinal thickness dz, with one face on the "source" plane in this frame, and transverse extent with area A covering the nuclear overlap region [4]. At time $t = \tau_{Form}$ this volume will contain all the (now-formed) particles with longitudinal velocities $0 \leq \beta_{\|} \leq dz/\tau_{Form}$ (since we assume that the particles cannot scatter before they are formed!). We can then write this number of particles as $dN = (dz/\tau_{Form})\frac{dN}{d\beta_{\|}}$, or equivalently $dN = (dz/\tau_{Form})\frac{dN}{dy}$, where y is longitudinal rapidity, since $dy = d\beta_{\|}$ at $y = \beta_{\|} = 0$. If these particles have an average total energy $\langle m_T \rangle$ in this frame ($E = m_T$ for particles with no longitudinal velocity), then the total energy divided by the total volume of the slab at $t = \tau_{Form}$ is just

$$\begin{aligned} \langle \varepsilon(\tau_{Form}) \rangle &= \frac{dN\langle m_T \rangle}{dz\, A} = \frac{dN(\tau_{Form})}{dy}\frac{\langle m_T \rangle}{\tau_{Form} A} \\ &= \frac{1}{\tau_{Form} A}\frac{dE_T(\tau_{Form})}{dy} \end{aligned} \tag{5}$$

where we have equated $\frac{dE_T}{dy} = \langle m_T \rangle \frac{dN}{dy}$ and emphasized that Eq.5 is true for the transverse energy density present at time $t = \tau_{Form}$.

Equation 5 here is essentially identical [5] to Eq. 4 of Bjorken's result [64], and so is usually referred to as the *Bjorken energy density* ε_{Bj}. It should be valid as a measure of peak energy density in created particles, on very general grounds and in all frames, as long as two conditions are satisfied: (1) A finite formation time τ_{Form} can meaningfully be defined for the created secondaries; and (2) The thickness/"crossing time" of the source disk is small compared to τ_{Form}, that is, $\tau_{Form} \gg 2R/\gamma$. In particular, the validity of Eq. 5 is completely independent of the shape of the $dE_T(\tau_{Form})/dy$ distribution to the extent that $\beta_{\|}$ is infinitesimally small in a comoving frame; a plateau in dE_T/dy is *not* required. For present practical purposes, we will consider condition (2) above to be satisfied as long as $\tau_{Form} > 2R/\gamma$ is true, corresponding to τ_{Form} >0.13 fm/c for full-energy Au+Au collisions at RHIC.

[4] The region described here corresponds to half the shaded region shown in Fig. 5. Since $\beta_{\|} \simeq 0$ for particles near the source location, this is an appropriate region over which we can calculate a meaningful energy density.

[5] A (well-known) factor of 2 error appears in the original.

Bjorken's original motivation was to estimate, in advance of data, the energy densities that would be reached in high-energy A+A collisions, using knowledge of $p(\bar{p})+p$ collisions to estimate $\langle m_T \rangle$ and dN/dy, and choosing $\tau_{Form} \sim 1$ fm/c without any particular justification other than as an order-of-magnitude estimate. With A+A collision data in hand, attempts have been made to use Eq. 5 to estimate the energy densities that are actually achieved in the collisions. Historically, ε_{Bj} has been calculated using the final-state dE_T/dy and simply inserting a nominal value of 1 fm/c for τ_{Form}. In addition, fixed target experiments have been using $dE_T/d\eta$ as an estimate for dE_T/dy, which is a good approximation for these experiments; at RHIC a correction is made for the Jacobian $dy/d\eta$ which is important for a collider geometry. These "nominal Bjorken energy density" estimates, which we term $\varepsilon_{Bj}^{Nominal}$, range for central event samples from about 1.5 GeV/fm^3 in Au+Au collisions at AGS energies [65] ($\sqrt{s_{NN}}$ =5 GeV), to about 2.9 GeV/fm^3 in Pb+Pb collisions at SPS energies [66,38] ($\sqrt{s_{NN}}$ =17 GeV; and see also [67]) to about 5.4 GeV/fm^3 in Au+Au collisions at full RHIC energy [67] ($\sqrt{s_{NN}}$ =200 GeV).

It has often been noted that all of these values are similar to, or higher than, the 1 GeV/fm^3 scale required for the QCD transition. However, we cannot take these $\varepsilon_{Bj}^{Nominal}$ estimates seriously as produced energy densities without some justification for the value of 1 fm/c taken for τ_{Form}. An indication of potential problems with this choice arises immediately when considering AGS Au+Au and SPS Pb+Pb collisions, where the CMS "crossing times" $2R/\gamma$ are 5.3 fm/c and 1.6 fm/c respectively, which implies that this choice for τ_{Form} =1 fm/c actually violates the validity condition $\tau_{Form} > 2R/\gamma$ we set for the use of Eq. 5. So we will deprecate the use of $\varepsilon_{Bj}^{Nominal}$ as an quantitative estimate of actual produced energy density, and instead treat it only as a compact way of comparing $dE_T/d\eta$ measurements across different systems, centralities and beam energies.

2.3 Realistic τ_{Form} and ε_{Bj} estimates

Can we justify a better estimate for τ_{Form}? We might say, on general quantum mechanical grounds, that in a frame where its motion is entirely transverse a particle of energy m_T can be considered to have "formed" after a time $t = \hbar/m_T$ since its creation in that frame. To estimate the average transverse mass, we can use the final-state $dE_T/d\eta$ to estimate $dE_T(\tau_{Form})/dy$ and, correspondingly, use the final-state $dN/d\eta$ as an estimate for $dN(\tau_{Form})/dy$ to obtain

$$\langle m_T \rangle = \frac{dE_T(\tau_{Form})/dy}{dN(\tau_{Form})/dy} \simeq \frac{dE_T/d\eta}{dN/d\eta} \text{ (Final state).} \quad (6)$$

PHENIX has measured the ratio of final-state transverse-energy density to charged-particle density, each per unit pseudorapidity, and the results are shown in Fig. 6. For a wide range of centralities the ratio is remarkably constant at about 0.85 GeV for full-energy central Au+Au collisions, and shows very little change with beam energy, decreasing to only 0.7 GeV when $\sqrt{s_{NN}}$ is decreased by an order of magnitude down to 19.6 GeV.

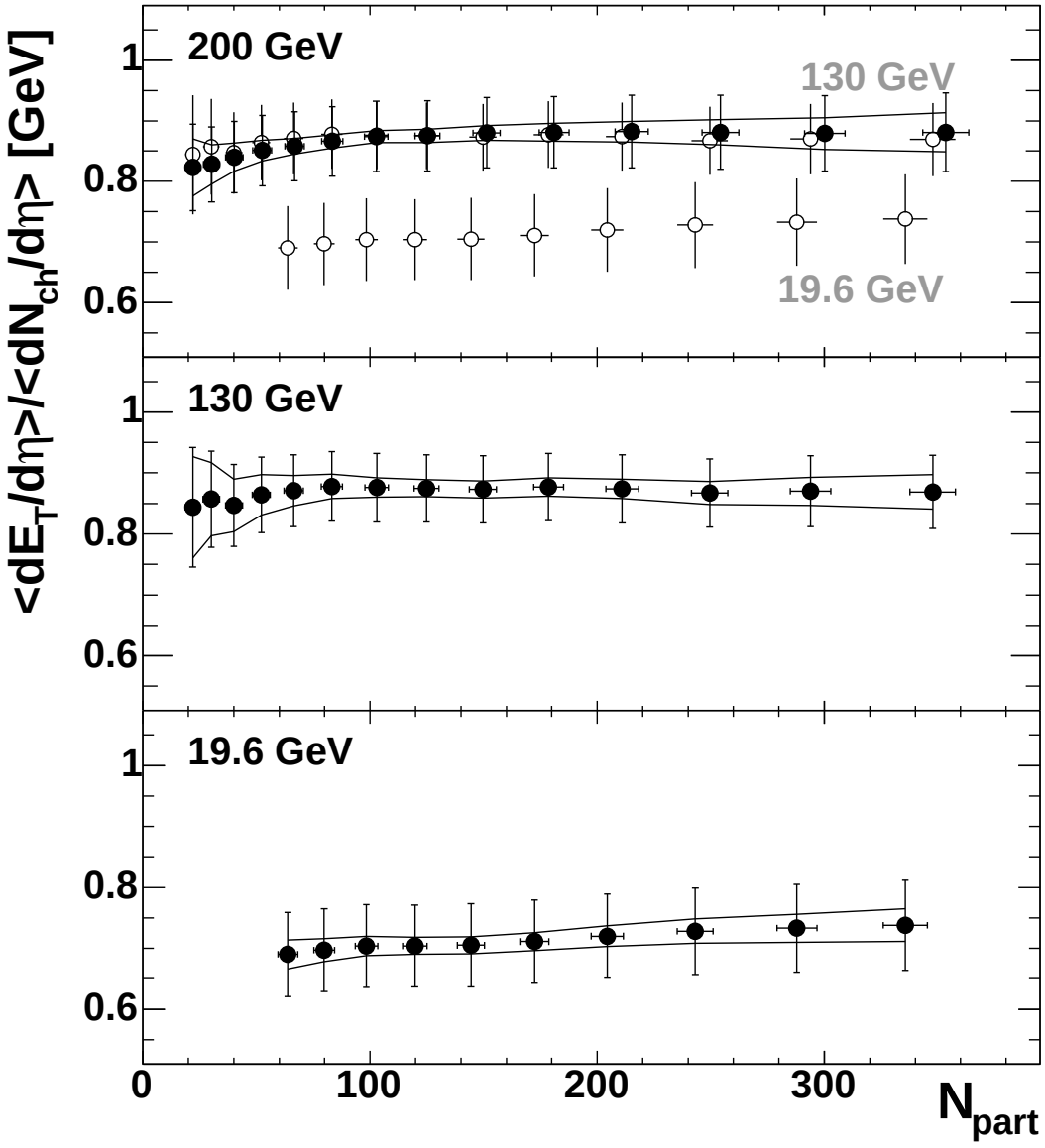

Fig. 6. The ratio of transverse energy density in pseudorapidity to charged particle density in pseudorapidity, at mid-rapidity; shown as a function of centrality, represented by the number of nucleons participating in the collision, N_{part}, for three different RHIC beam energies [67].

If we approximate $dN^{Ch}/d\eta = (2/3)dN/d\eta$ in the final state then Eq. 6 would imply $\langle m_T \rangle \simeq$0.57 GeV and corresponding $\tau_{Form} \simeq$0.35 fm/c, a value shorter

than the "nominal" 1 fm/c but still long enough to satisfy our validity condition $\tau_{Form} > 2R/\gamma$ at RHIC. Inserting this value into Eq. 5, along with the highest $dE_T/d\eta = 600$ GeV for 0–5% central events as measured by PHENIX [67], yields a value of $\langle\varepsilon\rangle = 15$ GeV/fm^3 for the energy density in initially produced, mid-rapidity particles in a central RHIC Au+Au collision, that is, roughly 100 times the mass-energy density of cold nuclear matter.

It is important to note that this large value of the energy density as obtained from Eq. 5 represents a conservative *lower* limit on the actual $\langle\varepsilon(\tau_{Form})\rangle$ achieved in RHIC collisions. This follows from two observations: (1) The final-state measured $dE_T/d\eta$ is a solid lower limit on the $dE_T(\tau_{Form})/dy$ present at formation time; and (2) The final-state ratio $(dE_T/d\eta)/(dN/d\eta)$ is a good lower limit on $\langle m_T\rangle$ at formation time, and so yields a good *upper* limit on τ_{Form}. We justify these statements as follows:

Several mechanisms are known that will decrease dE_T/dy as the collision system evolves after the initial particle formation, while no mechanism is known that can cause it to increase (for $y = 0$, at least). Therefore, its final-state value should be a solid lower limit on its value at any earlier time. A partial list of the mechanisms through which dE_T/dy will decrease after $t = \tau_{Form}$ includes: (i) The initially formed secondaries in any local transverse "slab" will, in a comoving frame, have all their energy in transverse motion and none in longitudinal motion; if they start to collide and thermalize, at least some of their E_T will be converted to longitudinal modes in the local frame; (ii) Should rough local thermal equilibrium be obtained while the system's expansion is still primarily longitudinal, then each local fluid element will lose internal energy through pdV work and so its E_T will decrease; (iii) If there are pressure gradients during a longitudinal hydrodynamic expansion then some fluid elements may be accelerated to higher or lower rapidities; these effects are complicated to predict, but we can state generally that they will always tend to *decrease* dE_T/dy where it has its maximum, namely at $y = 0$. Given that we have strong evidence that thermalization and hydrodynamical evolution do occur in RHIC collisions (Section 3), it is likely that all these effects are present to some degree, and so we should suspect that final-state $dE_T/d\eta$ is substantially lower than $dE_T(\tau_{Form})/dy$ at mid-rapidity.

Turning to our estimate of τ_{Form}, the assumption that $\tau_{Form} = \hbar/\langle m_T\rangle$ cannot be taken as exact, even if the produced particles' m_T's are all identical, since "formed" is not an exact concept. However, if we accept the basic validity of this uncertainty principle argument, then we can see that the approximation in Eq. 6 provides a lower limit on $\langle m_T\rangle$. First, the numerator $dE_T/d\eta$ is a lower limit on $dE_T(\tau_{Form})/dy$, as above. Second, the argument is often made on grounds of entropy conservation that the local number density of particles can never decrease [68], which would make the final-state denominator in Eq. 6 an upper limit on its early-time value.

With these limits in mind, then, it is not unreasonable for us to claim that the peak energy density of created particles reached in central Au+Au collision at RHIC is at least 15 GeV/fm^3, and in all likelihood is significantly higher.

2.4 Thermalized Energy Density

We have arrived at a reasonably solid, lower-limit estimate for the energy density in produced particles in a RHIC Au+Au collision, and it is more than enough to drive a QCD transition. But the situation at $t = \tau_{Form}$ pictured in Fig. 5 looks nothing like local thermal equilibrium. It is an important question, then, to ask: if and when the system evolves to a state of local thermal equilibrium, is the energy density still sufficient to drive the transition to a QGP?

To answer this we begin by looking at the state of the system at $t = \tau_{Form}$ and immediately afterward. At the time they are formed the particles have sorted themselves out automatically, with all the particles on a "sheet" at a longitudinal position z having the same longitudinal velocity $\beta_\parallel = z/t$; and so in the rest frame of a sheet all the sheet's particles have only transverse motion. If the particles continue free-streaming and never reinteract then the energy density will continue to fall as $\varepsilon \sim 1/t$ and the Bjorken formula in Eq. 5 will be valid, with t in place of τ_{Form}, as long as the expansion is primarily longitudinal [6].

For thermalization to occur the particles will have to start interacting and/or radiating. Once this happens the particles which were originally together on one "sheet" will start to spread in longitudinal velocity, though on short time scales we would expect their group average longitudinal velocity to remain the same. If the thermalization process is fast enough, then, we would expect that at time $t = \tau_{Therm}$ these groups will have formed locally equilibrated fluid elements, with a velocity profile following $\beta_\parallel^{Fluid} = z/t$. The energy density at this time will be reduced from the energy density at formation time $\varepsilon(\tau_{Form})$ by a factor τ_{Form}/τ_{Therm}; *i.e.* the ε_{Bj} of Eq. 5 but with τ_{Therm} in place of τ_{Form}. This evolution is illustrated in Fig. 4.

Once local equilibration is achieved we would then expect the system to evolve hydrodynamically, and the behavior of $\varepsilon(t)$ will depend on the details of the local equations of state (EOS). Without knowing those details, though, we can say that in the limit of low pressure, $p/\varepsilon \sim 0$, the energy density will continue to evolve (during longitudinal expansion) as $\varepsilon \sim 1/t$, while in the limit of high pressure, $p/\varepsilon \sim 1/3$, the energy density will decrease somewhat more

[6] For long times $t > R$ transverse expansion will become significant and the energy density will decrease as $\varepsilon \sim 1/t^3$.

quickly, $\varepsilon \sim 1/t^{4/3}$, within a fluid element. This range of possible behaviors for $t > \tau_{Therm}$ is indicated schematically in Fig. 4.

A direct theoretical determination of τ_{Therm} would require a detailed description of both the parton-parton interactions and the resulting evolution of the system density. However, other lines of reasoning may provide information on τ_{Therm}. For example, it has been argued [69] that the strong elliptic flow in RHIC collisions can be taken as evidence for fast thermalization (see Section 3.3). In a hydrodynamic picture the source of elliptic flow is the spatial anisotropy of the energy density in the transverse plane at the time hydrodynamics becomes valid. If local equilibration and the onset of hydrodynamics is delayed because interactions between the initially produced particles are weak at first, then the spatial anisotropy which could give rise to elliptic flow will be reduced (see Fig. 14). This, in effect, limits how high τ_{Therm} can be if hydrodynamics is the mechanism for generating elliptic flow.

We can see from Table 1 in Section 3.5 that hydrodynamical models typically require quite short thermalization times, in the range of 0.6–1.0 fm/c, in order to reproduce the magnitude of elliptic flow which is observed at RHIC. If we take this range as typical of what hydrodynamics would imply for τ_{Therm}, then we can calculate the corresponding "typical" implied energy densities at thermalization time as in range of 5.4 GeV/fm^3 to 9.0 GeV/fm^3. These densities are well above that required to drive the QCD transition, so the combination of our transverse energy measurements and the fast thermalization times from hydrodynamics can be taken, to some degree, as evidence that conditions to create the equilibrated upper phase of QCD matter are achieved at RHIC.

2.5 What Are the Initial Quanta?

With our extensive use of the picture in Fig. 5 it is only natural to ask, "What are these initially produced particles?" that Bjorken referred to, nonspecifically, as "quanta". What models do we have for initial production, and what can we say about them using our data on E_T and multiplicity?

The simplest assumption is that the initially produced particles in a RHIC collision are scattered partons at mid- to low-p_T, traditionally known as "mini-jets". For a long period in advance of RHIC data, it was widely expected that mini-jets would be the dominant channel for E_T and particle production, and this led to two further, general expectations: first, that multiplicity and E_T per interacting nucleon would go up sharply at collider energies, as compared to fixed-target energies, since jet and mini-jet cross sections are increasing quickly with $\sqrt{s}$ (see Fig. 7); and, secondly, that E_T and multiplicity per participating nucleon would increase steeply in more central events, since the

rate of hard pQCD scatterings goes up faster with centrality than does the number of interacting nucleons.

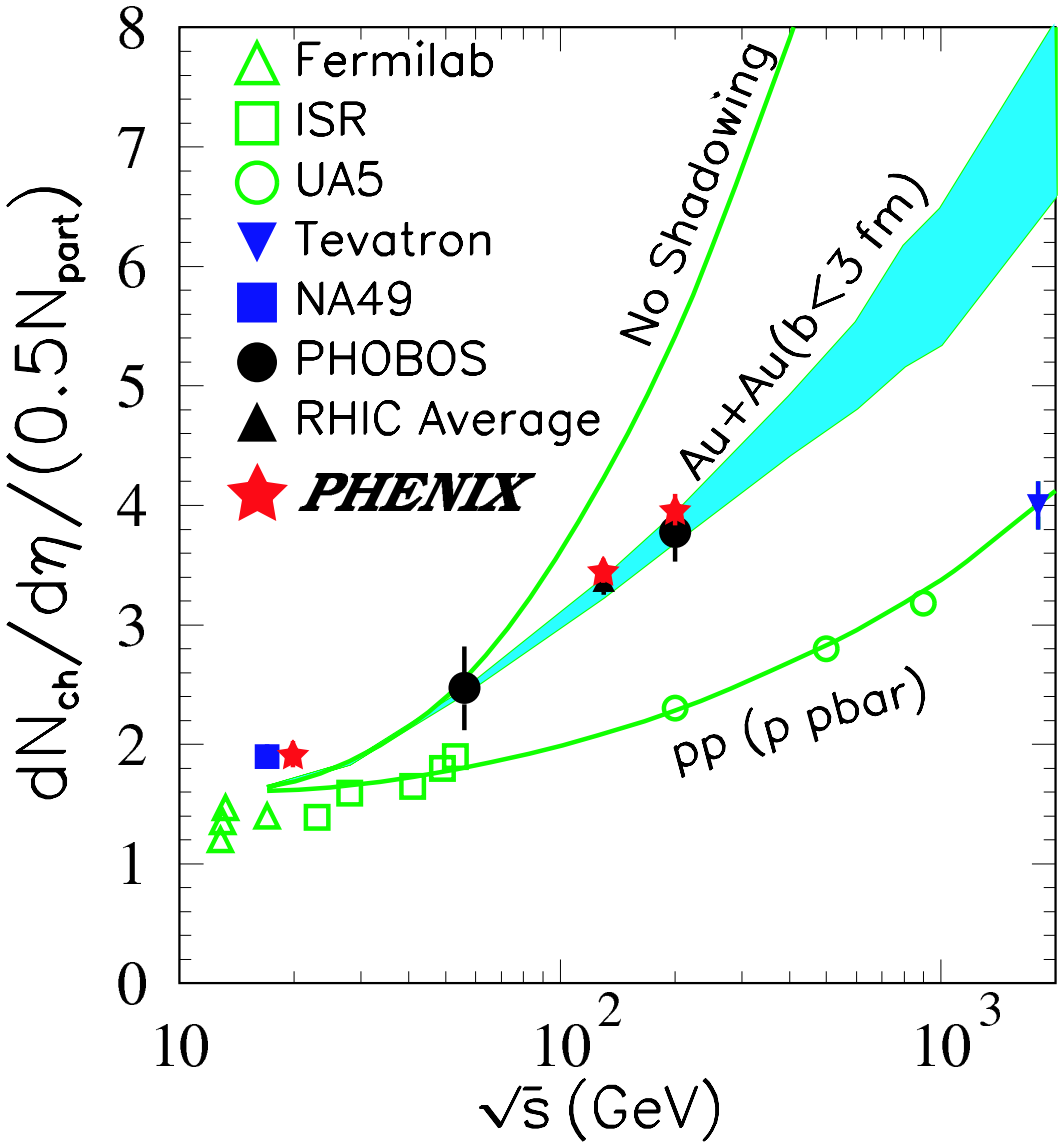

Fig. 7. Figure from Li and Wang [70] showing trends in final-state charged multiplicity per participant pair vs. (nucleon-nucleon) beam energy. (PHENIX data points have been added.) The curves are the result of their two-component "hard/soft" model, which reproduces well the multiplicities from elementary $p(\bar{p}) + p$ collisions at RHIC energies. The same model extended to nuclear collisions with no regulating mechanism on hard processes (the "No Shadowing" line) over-predicts the multiplicities in central RHIC collisions, while the data can be matched if substantial nuclear shadowing of gluons is invoked (shaded band).

It was therefore quite surprising when the first RHIC data [71,37,38] showed lower multiplicities than had been predicted from mini-jet models, and only a modest increase in E_T and multiplicity per participant as functions of centrality. Compared to the sharp rise, shown in Fig. 7, predicted by straightforward

factorized pQCD, it was clear that some mechanism must be acting at RHIC energies to restrict, or regulate, particle production [72,70].

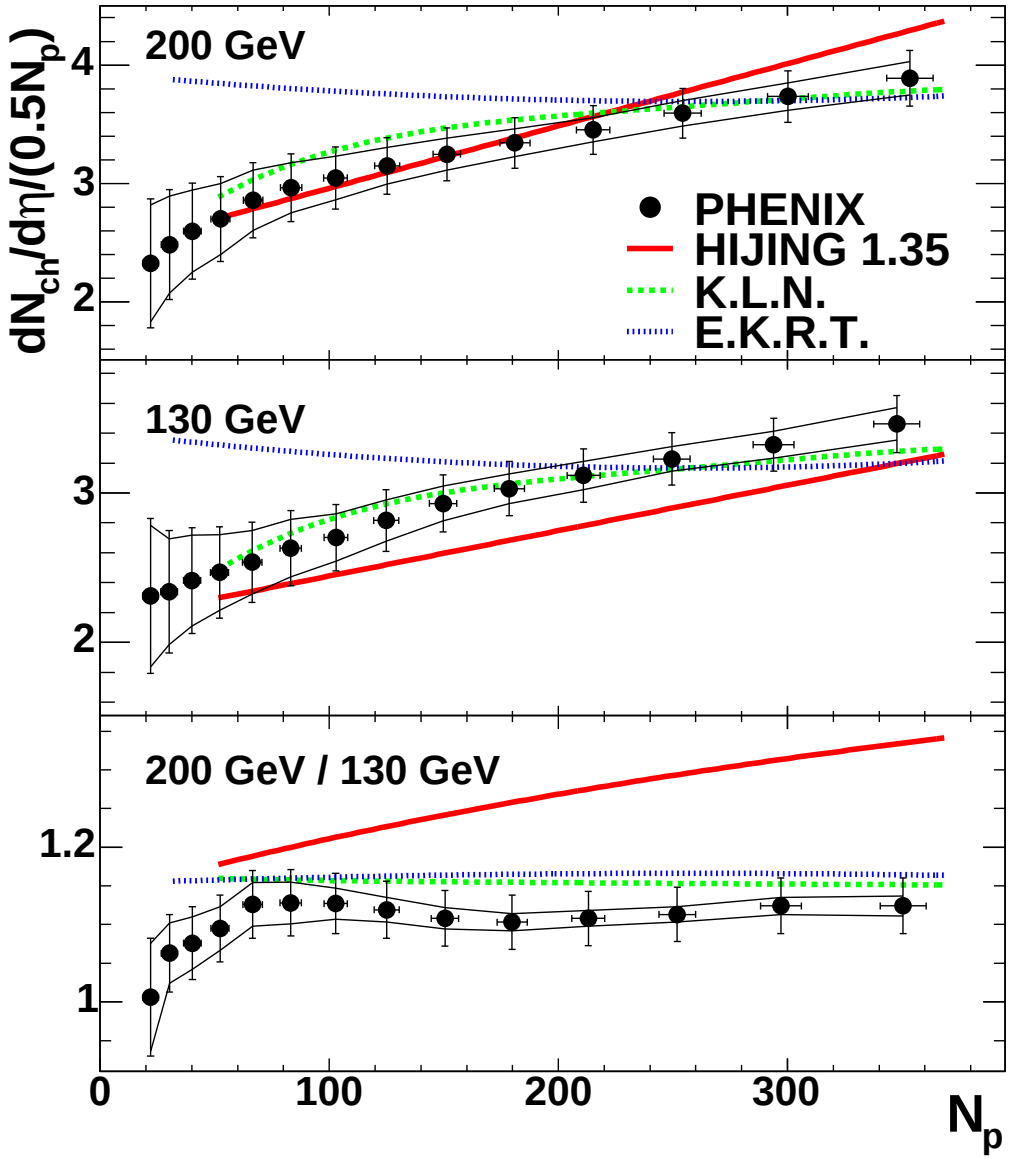

Fig. 8. Multiplicity per participant nucleon pair, as a function of centrality, for $\sqrt{s_{NN}}$ =130 GeV and 200 GeV Au+Au collisions as measured in PHENIX [73]; compared to theoretical predictions available in 2002. "HIJING" is a pQCD-based model [74], while "KLN" features gluon saturation in the initial state [75,76]; "EKRT" assumes saturation in the final state [77,78].

pQCD-based models have parameters regulating the momentum scales; these include a lower-momentum cutoff, and the factorization and fragmentation scales. Figure 8 shows that the pQCD-based HIJING model, circa 2002, was able to reproduce 130 GeV and 200 GeV $dN_{ch}/d\eta$ reasonably well. However, in that model jet production via hard scattering is an important mechanism

for particle production, and the combination of the $\sqrt{s}$ dependence of hard-scattering cross sections with the growth of the nuclear overlap with centrality causes the model to predict an increase in the ratio between the two data sets with centrality. The observed ratio is, instead, quite constant. Thus the authors found it necessary to introduce a centrality-dependent shadowing to regulate the jet growth [70].

An alternative to models which use collinearly factorized pQCD is found in the "color glass condensate" picture, in which the gluon population of low-x, low-p_T states in the initial nuclear wave function is limited by transverse overlap and fusion of these low-p_T gluons. The phase-space density saturates because of the competition between extra gluon radiation from higher-x gluons and nonlinear fusion of the gluons at high density. Au+Au collisions are then collisions of two sheets of colored glass, with the produced quarks and gluons materializing at a time given by the inverse of the saturation momentum, $\tau = 1/Q_s$. Saturation of gluons with momenta below Q_s provides a regulating mechanism that limits the rise in gluon—and later, hadron—multiplicity with centrality and beam energy. Models featuring this initial-state gluon saturation agree well with essentially all RHIC data on the multiplicity density, which is dominated by low-momentum particles [75,76]. This is seen, for instance, in Fig. 8.

In this picture, the total gluon multiplicity is proportional to $1/\alpha_s \cdot Q_s^2$, which limits the number of low-momentum charged particles produced. Q_s evolves slowly with collision centrality and beam energy. For central Au+Au collisions, it has been estimated that the typical m_T scale of the gluons "liberated" from the colored glass is about 1 GeV per particle [68], which is above the lower limit of 0.53 GeV per particle that we set above using the PHENIX data. Though there are fewer predictions of E_T than total charged-particle production from gluon-saturation models, the existing models are broadly consistent with data at RHIC. Consequently, gluon saturation is considered to be a promising candidate for describing the initial state of RHIC collisions.

2.6 Conclusions

Using reasoning similar to that of Bjorken [64], combined with some simple formation-time arguments, we can draw the following conclusions from the PHENIX data on transverse energy production and overall particle multiplicity:

• The peak energy density in created secondary particles is at least 15 GeV/fm^3, and this is most likely an underestimate. This is well in excess of the $\sim$1 GeV/fm^3 required, according to lattice QCD predictions, to drive a QCD

transition to QGP.

• We note that hydrodynamical calculations which reproduce the magnitude of elliptic flow observed at RHIC require local thermalization to occur very quickly, typically by 1 fm/c or earlier (see Section 3.5). If the system does reach local equilibrium on this time scale then the energy density of the first thermalized state would be in excess of 5 GeV/fm^3, well above the amount required to create the QGP.

• Pre-RHIC expectations that E_T and charged particle production would be dominated by factorized pQCD processes were contradicted by data, which showed only very modest increases with centrality and beam energy. A new class of models featuring initial-state gluon saturation compares well with RHIC multiplicity and E_T data, and are also consistent with our Bjorken-style arguments for estimating energy densities at early times.

3 THERMALIZATION

A key question is whether the matter formed at RHIC is thermalized, and if so when in the collision was equilibration achieved. If thermalization is established early then evidence for strong transverse expansion can be potentially related to the equation of state of the dense matter produced at RHIC. To explore these issues we review several experimental observables from integral quantities (numbers of particles produced and in what ratios), to differential distributions (measured p_T and azimuthal distributions), to two-particle (HBT) correlations.

3.1 Chemical Equilibrium

For many years it has been known that the abundances of different hadron species in $e^+ + e^-$ and $p + \overline{p}$ reactions can be reproduced by statistical models [79,80]. This success is often attributed to hadronization statistically filling the available phase space. At RHIC there is also the possibility that the strong scattering deduced from the measurements of elliptic flow (section 3.3) may prove sufficient to establish chemical equilibrium.

The production of strange particles provides a means to check whether chemical equilibrium is achieved. For $e^+ + e^-$ and $p + \overline{p}$ reactions strange particle production is suppressed due to the small size of the system. This canonical suppression is largely removed for central heavy-ion collisions. If the mea-

sured strangeness yields are still lower than full equilibrium predictions, then the partial equilibrium can be quantified by a multiplicative factor of γ_s for each strange quark in a hadron, where $\gamma_s = 1$ for complete equilibration and $\gamma_s < 1$ for partial equilibration.

Figure 9 shows the centrality dependence of K/π and p/π ratios in Au+Au collisions at $\sqrt{s_{NN}} = 200$ GeV [54]. Both K^+/π^+ and K^-/π^- increase rapidly for peripheral collisions, and then saturate or rise slowly from mid-central to the most central collisions. The ratios p/π^+ and $\overline{p}/\pi^-$ also increase from peripheral collisions but appear flatter than the K/π ratios. Canonical statistical models [81] predict an increase in these ratios with centrality, as the larger system-size effectively places less of a constraint on conserved quantities. In addition the chemical parameters, T_{chem} and μ_B, can also vary with centrality [82,83].

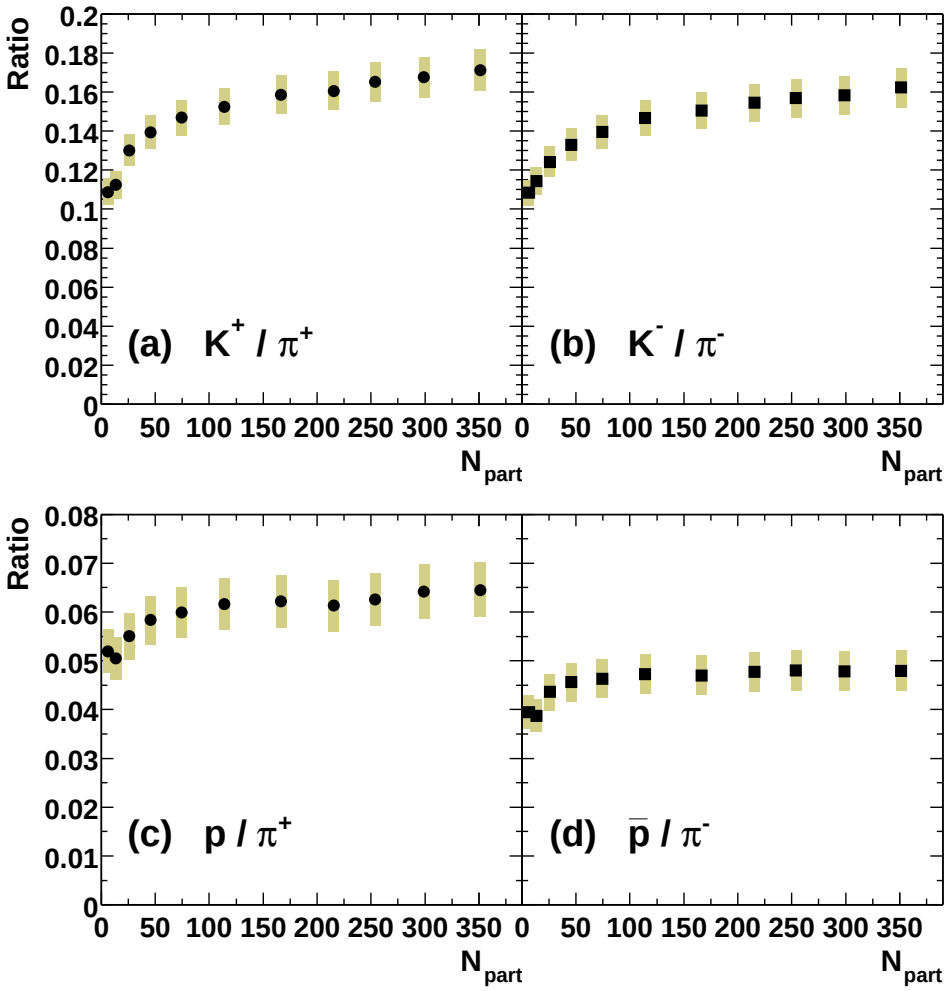

Fig. 9. Centrality dependence of particle ratios for (a) K^+/π^+, (b) K^-/π^-, (c) p/π^+, and (d) $\overline{p}/\pi^-$ in Au+Au collisions at $\sqrt{s_{NN}} = 200$ GeV [54].

Focusing on the ratios from central collisions at $\sqrt{s} = 200$ GeV, the data are compared to the thermal model data analysis of Kaneta and Xu [82] in Fig. 10. The extracted thermal parameters from this fit are $T_{chem} = 157 \pm 3$ MeV, $\mu_B = 23 \pm 3$ MeV, and $\gamma_s = 1.03 \pm 0.04$. A large γ_s is also found by STAR [84] who extract $\gamma_s = 0.96 \pm 0.06$, while Cleymans *et al.* [83] extract γ_s that increases from $\gamma_s \simeq 0.85$ in peripheral collisions to $\gamma_s \simeq 0.95$ for central collisions at RHIC. Similar fits to the central RHIC data are obtained by Braun-Munzinger *et al.* [85] who assume complete chemical equilibration, *i.e.* $\gamma_s = 1$.

We note that there are differences in the temperature parameter extracted by the different authors. Kaneta and Xu [82] extract $T_{chem} = 157 \pm 3$ MeV which is lower than that extracted by both Braun-Munzinger *et al.* [81] of $T_{chem} = 177 \pm 7$ MeV, and Cleymans *al.* [83] of $T_{chem} = 165 \pm 7$ MeV. However, both Braun-Munzinger *et al.* [81] and Magestro [86] discuss the sensitivity of the extracted temperature to corrections from feed-down from decays. Cleymans *et al.* [83] estimate that over 70% of π^+ in the thermal model fits come from the decay of resonances.

At lower beam energies there is controversy over whether strangeness is in full chemical equilibrium. Becattini *et al.* [87] use data that is integrated over the full rapidity and find that strangeness is in partial equilibrium, *i.e.* at the AGS $\gamma_s = 0.65 \pm 0.07$ and at the SPS $\gamma_s = 0.84 \pm 0.03$. Braun-Munzinger *et al.* [81] instead use ratios measured at mid-rapidity which typically have larger strange/nonstrange values and hence they obtain acceptable fits with $\gamma_s = 1$ at both AGS and SPS energies. At RHIC energies thermal model comparisons all use mid-rapidity data; a choice that is motivated in part by the separation between fragmentation regions and central particle production.

In contrast to the controversies at lower beam energies, the observation that strangeness is equilibrated is common to all thermal calculations that reproduce RHIC data. This is consistent with chemical equilibrium being obtained before hadronization, though does not prove that this is the case. An alternative explanation is that scattering in the hadronic phase could increase γ_s to 1, though small interaction cross sections imply that it may be difficult to equilibrate the multistrange baryons before the hadrons freezeout.

3.2 Spectra

Hadron spectra reflect conditions late in the reaction, as well as the integrated effects of expansion from the beginning of the collision. Figure 11 shows the p_T distributions for pions, kaons, protons, and anti-protons in both central (top panel) and peripheral collisions (bottom panel) [54]. The pion spectra have a

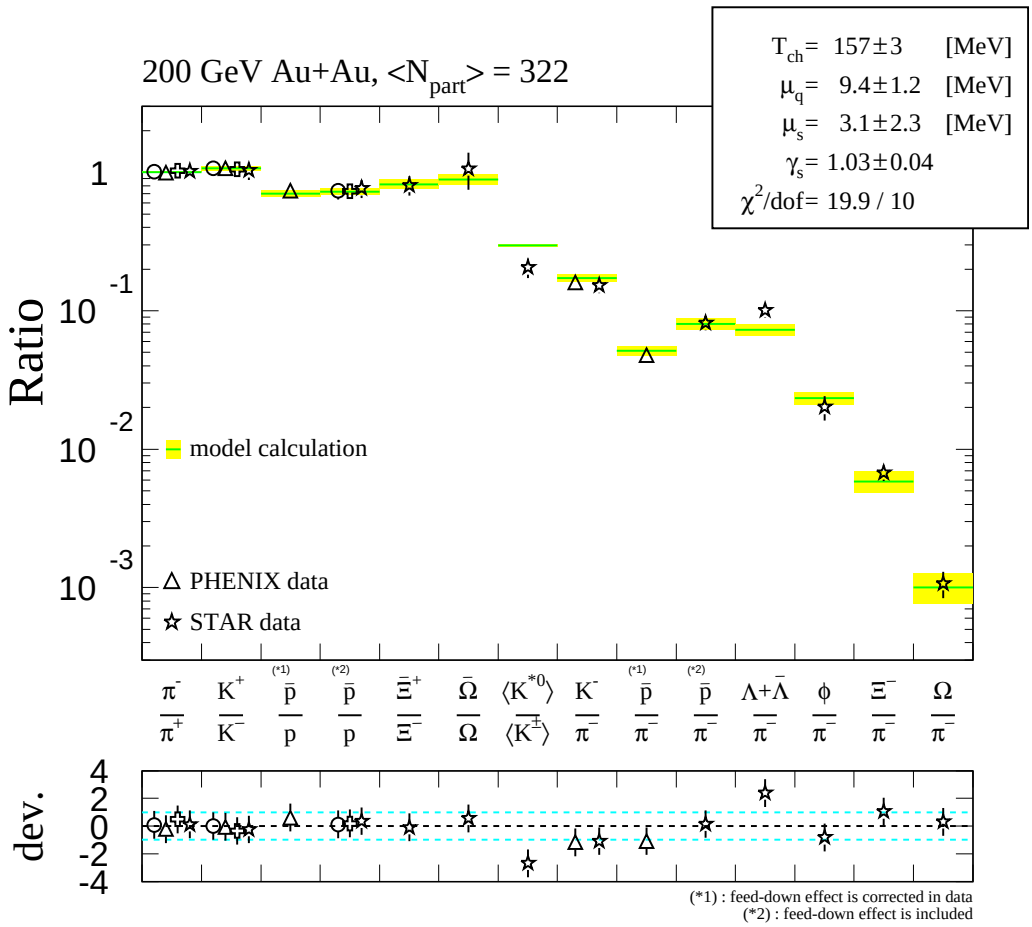

Fig. 10. Comparison of PHENIX (triangles), STAR (stars), BRAHMS (circles), and PHOBOS (crosses) particle ratios from central Au+Au collisions at $\sqrt{s_{NN}} = 200$ GeV at mid-rapidity. The thermal model descriptions from Kaneta [82] are also shown as lines. See Kaneta [82] for the experimental references.

concave shape at low p_T where many of the pions may come from the decay of resonances, Δ, ρ etc.. The kaon spectra are approximately exponential over the full measured p_T range, whereas the proton spectra flatten at low p_T for the most central collisions. A striking feature is that the proton and anti-proton spectra in central collisions become comparable in yield to the pion spectra above 2 GeV/c. This is more fully discussed in Section 7.

One way to characterize the change in spectra as a function of centrality is to calculate $\langle p_T \rangle$ for each spectrum [54] as shown in Fig. 12. The $\langle p_T \rangle$ increases for all particles as a function of centrality with the largest change occurring in peripheral collisions ($N_{part} < 100$). Across the different particles the increase is largest for protons and anti-protons. This is consistent with a collective expansion velocity that increases with centrality to produce the largest increase in $\langle p_T \rangle$ for the heaviest particles.

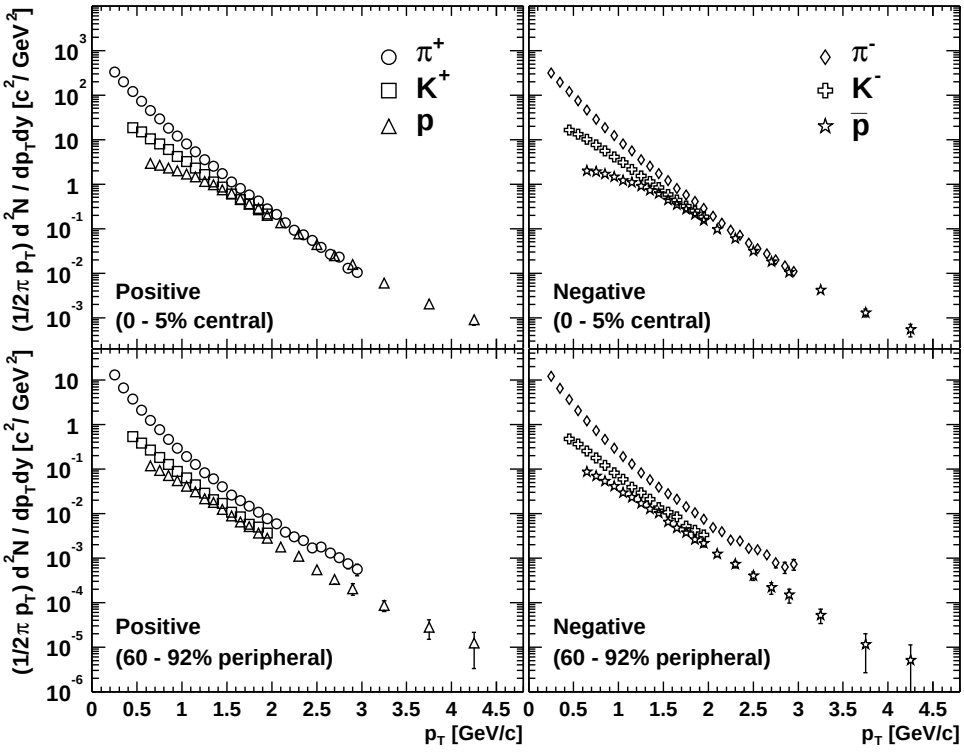

Fig. 11. Transverse momentum distributions for pions, kaons, protons, and anti-protons in Au+Au collisions at $\sqrt{s_{NN}}$=200 GeV [54].

The pion, kaon, and proton spectra can all be fit using an ansatz of a thermal, expanding source [88,48] to extract the collective transverse expansion velocity $\langle\beta_T\rangle$ as well as the temperature at freezeout T_{fo}. Figure 13 shows $\langle\beta_T\rangle \sim 0.45$ at AGS energies [89,90], which increases to $\langle\beta_T\rangle \sim 0.5$ at the SPS [91–93] and RHIC [48,94]. All the above fits use similar model assumptions of a linear velocity profile and a Woods-Saxon density profile. That the spectra at these beam energies can be reproduced by a thermal source is necessary but not sufficient evidence for thermal equilibrium at each of these energies. However it is difficult to draw strong conclusions from the increase in $\langle\beta_T\rangle$ as a function of beam energy since the parameters $\langle\beta_T\rangle$ and T_{fo} are strongly anticorrelated and their values depend on fit ranges and treatment of decays.

3.3 Elliptic Flow

At the beginning of the collision the spatial distribution of the colliding matter resembles an ellipsoid due to the incomplete overlap of the two colliding nuclei. Any strong scattering in this early stage converts the spatial anisotropy to a momentum anisotropy which is observable as an elliptic flow of the emitted hadrons. Elliptic flow is a self-limiting phenomenon, which is readily under-

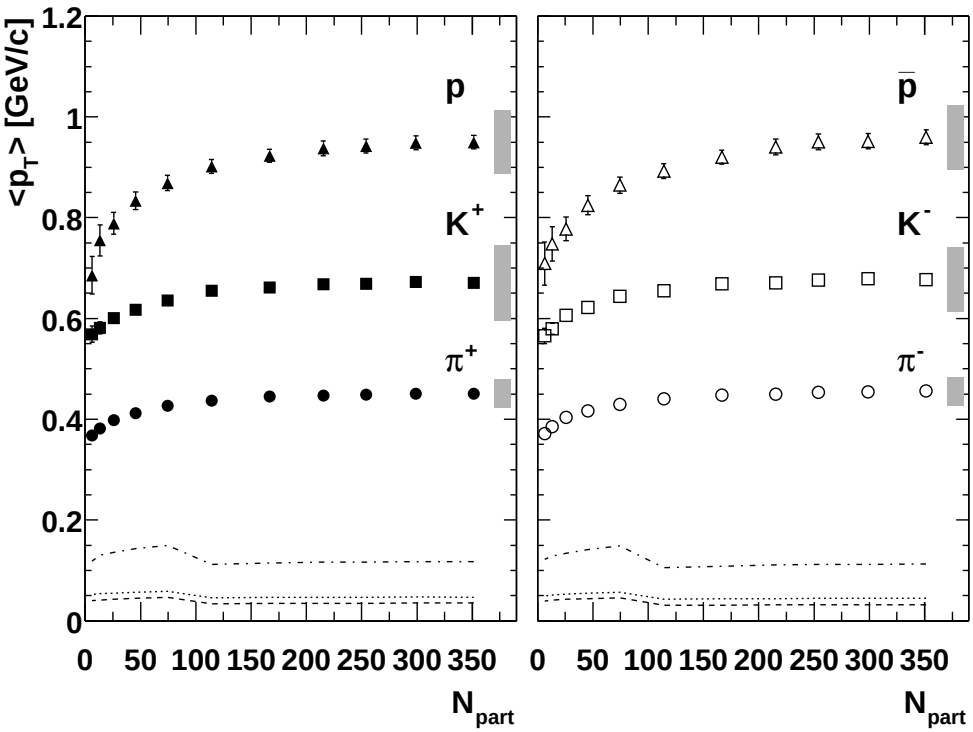

Fig. 12. Mean transverse momentum as a function of N_{part} for pions, kaons, protons and anti-protons in Au+Au collisions at $\sqrt{s_{NN}}$=200 GeV [54]. The systematic errors from extrapolation, which are scaled by a factor of two for clarity, are shown in the bottom for protons and anti-protons (dashed-dotted lines), kaons (dotted lines), and pions (dashed lines). The shaded bars to the right represent the systematic error due to cuts *etc.*

stood in the thermodynamic limit. If strong scattering is sufficient to establish local thermal equilibrium, then the pressure gradient is largest in the shortest direction of the ellipsoid. This produces higher momenta in that direction, quickly reducing the spatial asymmetry.

The absence of any strong scattering in the early stage would reduce the amount of elliptic flow that could be created. If the initially produced particles are allowed to free-stream at first and reach local equilibrium only after some time delay, then the spatial anisotropy at the start of hydrodynamic behavior will be reduced; and the longer the delay, the greater the reduction. Following the prescription of Kolb *et al.* [69] we plot in Fig. 14 the eccentricity after a time delay Δt compared to its value at formation time, as a function of Au+Au collision centrality. The eccentricity (ε) of the reaction zone is

$$\varepsilon = \frac{\langle y^2 \rangle - \langle x^2 \rangle}{\langle y^2 \rangle + \langle x^2 \rangle}. \tag{7}$$

The eccentricity can be analytically calculated once the density profile of the

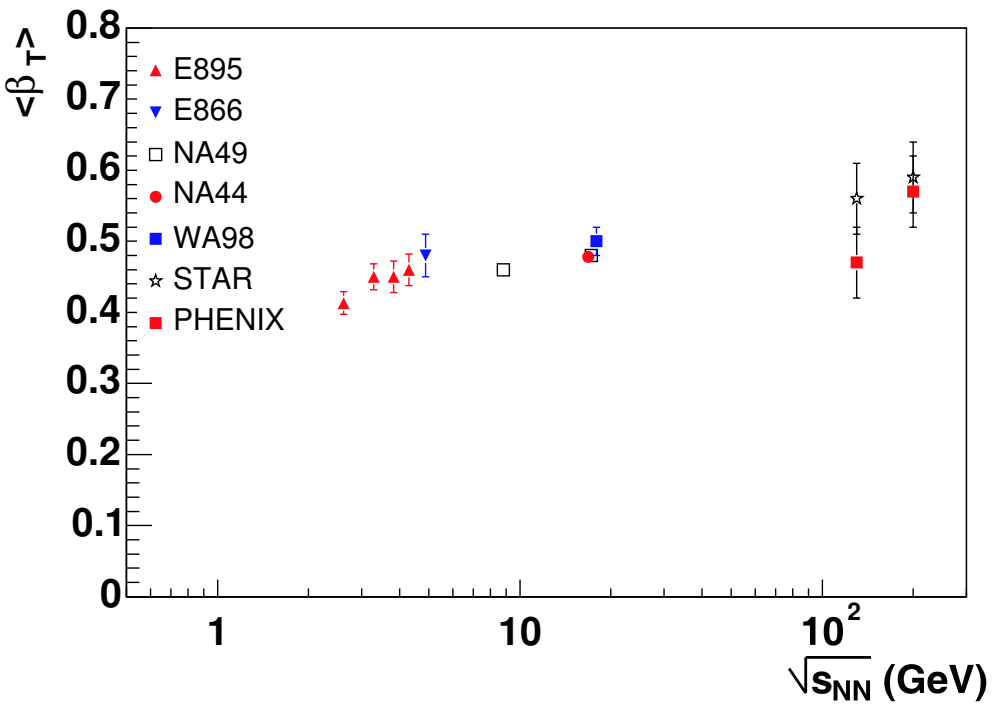

Fig. 13. Beam-energy dependence of the extracted mean transverse expansion velocity as a function of beam energy from simultaneous fits to spectra of different mass.

nuclei is chosen (typically a Woods-Saxon shape). It can also be calculated using Monte Carlo techniques, where the positions of those nucleons that participate in the reaction are used to calculate the averages in Eq. 7. From Fig. 14 we can see that for time delays of 2 fm/c or greater the magnitude of the eccentricity is significantly reduced, and its shape vs. centrality is also altered.

If locally equilibrated hydrodynamics is taken as the mechanism for generating elliptic flow, then the observation of *any* substantial amount of elliptic flow can be taken as evidence that local thermal equilibrium is achieved on a time scale before the spatial anisotropy would be completely erased. The general order of this time scale would be $t \sim R/c$, where R is the nuclear radius; however, the hydrodynamical calculations we will examine here (see Sec. 3.5 and Table 1) all require quite short thermalization times, from 0.6–1.0 fm/c, in order to reproduce the magnitude of elliptic flow observed at RHIC.

The azimuthal anisotropy of the spectra can be characterized in terms of Fourier coefficients, which at RHIC is dominated by the elliptic flow, the second Fourier coefficient $v_2(p_T)$, where

$$\frac{d^2N}{d\phi dp_T} = N_0(1 + 2v_2(p_T)\cos(2\phi)) \quad . \tag{8}$$

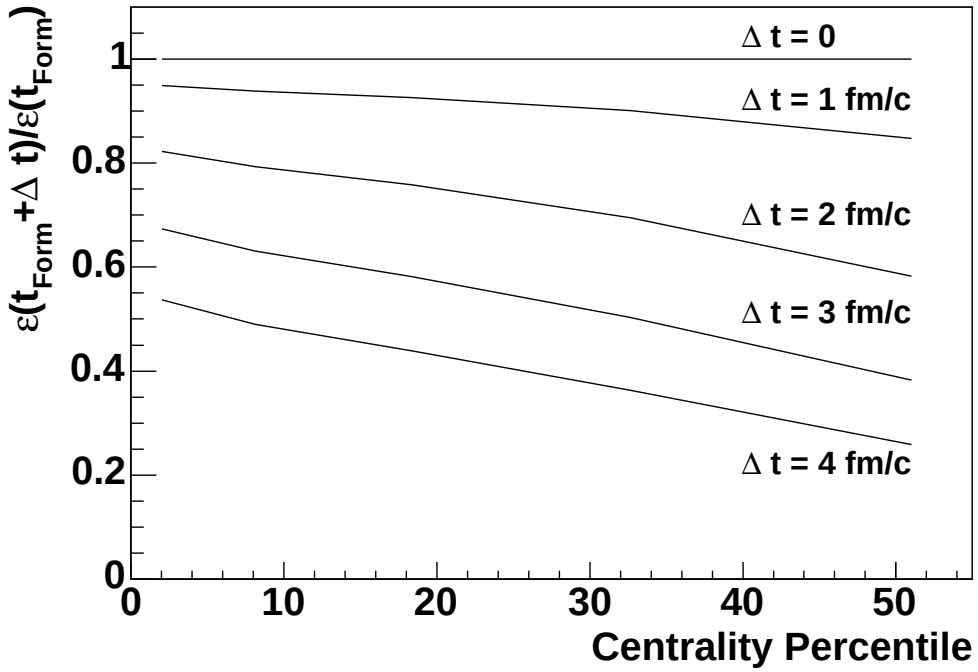

Fig. 14. The ratio of the eccentricity after a time delay Δt compared to its value at formation time, as a function of Au+Au collision centrality. The calculations follow the prescription of [69] where the produced particles are allowed to free-stream at first and reach local equilibrium only after some time delay.

Both the first Fourier coefficient v_1 and higher order coefficients have been neglected in the above expression.

The most direct evidence that v_2 is related to spatial asymmetries present early in the reaction is that v_2 at low p_T approximately scales with the initial eccentricity (ε) of the reaction zone. The measured values of v_2 normalized by ε are shown in Fig. 15 vs. centrality for two different p_T ranges [46]. At low momentum v_2/ε is independent of centrality to within 20%. This scaling is increasingly broken at higher p_T.

The measured values of the integrated v_2 at RHIC are larger than those at lower energies, but this is in part due to the fact that $v_2(p_T)$ increases with p_T and $\langle p_T \rangle$ increases as a function of beam energy. To remove this effect we will concentrate on the differential flow, *i.e.* the shape of $v_2(p_T)$ vs. p_T.

To make a uniform comparison between different colliding nuclei (Pb+Pb at SPS and Au+Au at RHIC) as well as different impact pararmeter selections from the different experiments, we normalize v_2 by the eccentricity ε, Eq. 7. The values of ε have been calculated via a Glauber Monte Carlo using Woods-Saxon nuclear profiles for both Pb and Au. The averages in Eq. 7 are over the participating nucleons, hence ε is calculated at the start of the collision. The pion data in Fig. 16 show that $v_2(p_T)/\varepsilon$ increases approximately linearly

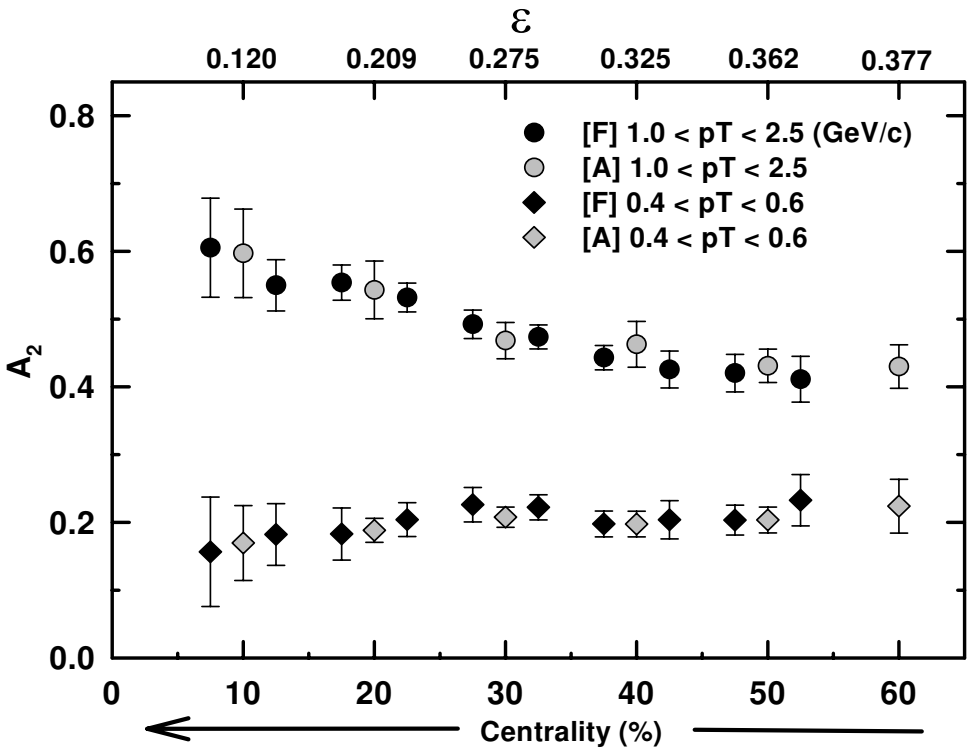

Fig. 15. $A_2 = v_2/\varepsilon$ vs. centrality for Au+Au collisions at $\sqrt{s}$=130 GeV [46]. The data points come from two different types of two-particle correlations: "fixed" p_T correlations when both particles are at the same p_T (points are labeled as "F"), and "assorted" p_T correlations when the two particles have different p_T (points are labeled as "A"). In this case the labeled p_T range is for the higher-momentum particle of the pair.

for low p_T. The increase of v_2/ε as a function of p_T is larger at RHIC [50,95] than at SPS [96,97]. This can most easily be seen by calculating the slope of v_2/ε below p_T =1 GeV/c (Fig. 17). The slope $(dv_2/dp_T)/\varepsilon$ increases from SPS to RHIC by approximately 50%. Hydrodynamical calculations [98] shown in this figure reproduce the data both at RHIC and at CERN SPS within one standard deviation. More extensive comparisons with hydro calculations will be discussed in section 3.5 while the behavior of v_2 at higher p_T, which follows a scaling with respect to the number of quarks, is discussed in Section 7.

Further insight into the expansion dynamics can be obtained from the mass dependence of $v_2(p_T)$ shown in Fig. 18 for pions, kaons and protons [50] along with a comparison with an early hydrodynamic model calculation [99]. The $v_2(p_T)$ for pions is larger than for kaons and protons at low p_T, and this mass ordering is a consequence of radial expansion shifting a given elliptic flow out to higher p_T for the heavier masses [99]. However, as will be discussed in Section 3.5, this calculation fails to reproduce the proton spectra, and attempts to remedy this failing lead to calculations that do no longer reproduce the

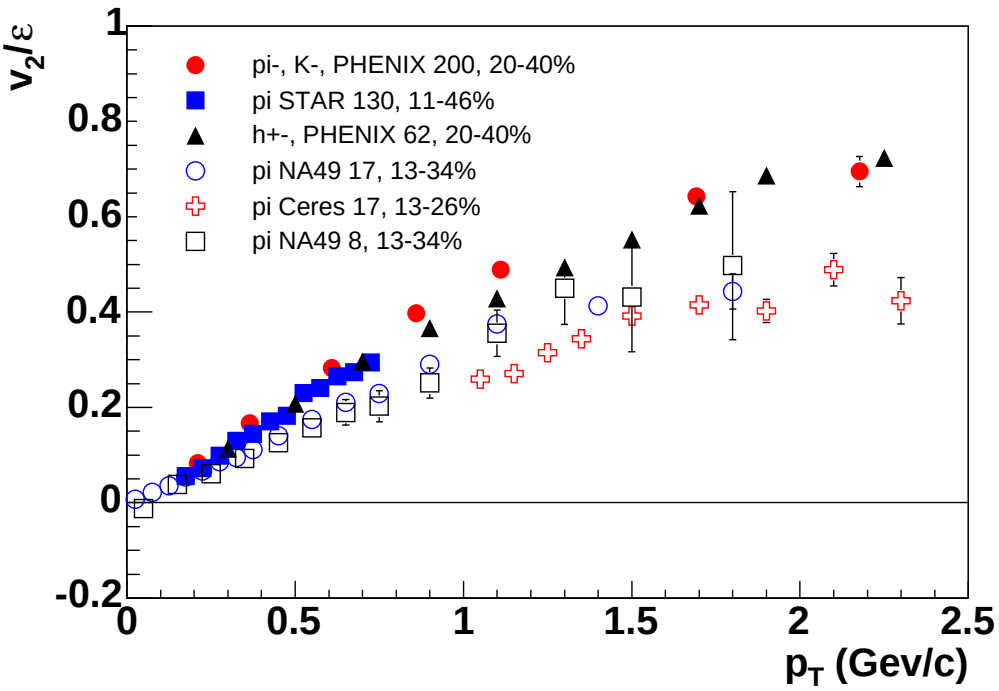

Fig. 16. $v_2(p_T)/\varepsilon$ vs. p_T for mid-central collisions at RHIC (filled symbols) and SPS (open symbols). Dividing by eccentricity removes to first order the effect of different centrality selections across the experiments.

measured v_2 for pions and protons.

3.4 HBT

Bose-Einstein correlations between identical particles provide a measure of the space-time extent of the source at the end of the reaction. Because the extracted source parameters as measured by the HBT technique are driven by space-time correlations, HBT results are sensitive to expansion dynamics integrated throughout the collision. HBT measurements were originally motivated by theoretical predictions of a large source size and/or a long duration of particle emission [100–102]—which would result from the presence of a long-lived mixture of phases in the matter as it undergoes a first-order phase transition from a quark-gluon plasma back to the hadronic phase.

In HBT analyses, multidimensional Gaussian fits are made to the normalized relative momentum distributions yielding fit parameters, $R_{\rm long}$, $R_{\rm side}$, $R_{\rm out}$ [103], also referred to as HBT radii, where

$$C_2 = 1 + \lambda \exp(-R^2_{\rm side}q^2_{\rm side} - R^2_{\rm out}q^2_{\rm out} - R^2_{\rm long}q^2_{\rm long}). \quad (9)$$

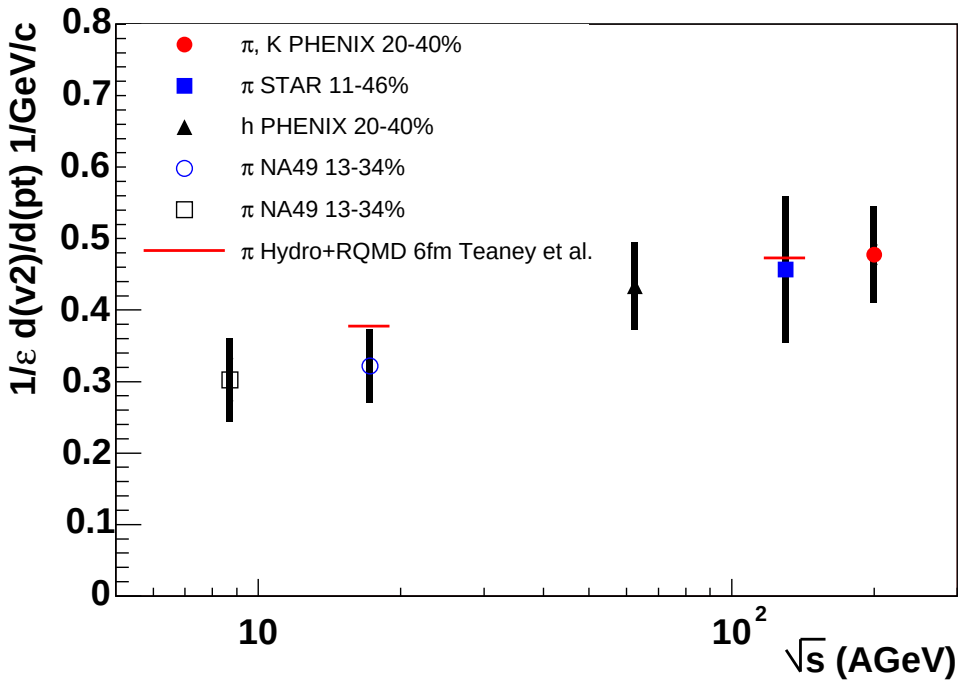

Fig. 17. The slope of the scaled elliptic flow, $(dv_2/dp_T)/\varepsilon$, for mid-central collisions at RHIC (filled symbols) and the SPS (open symbols). The slope is calculated for the data $p_T < 1$ GeV/c. The solid error bars are the systematic errors that include the systematic error on v_2 and ε.

The coordinate system is chosen so that the longitudinal direction is parallel to the beam axis, the out direction is in the direction of the pair's total transverse momentum, and the side direction is in the transverse plane perpendicular to the out axis. For dynamic (*i.e.* expanding) sources, the HBT radii depend on the mean transverse momentum of the particle pairs, $k_T = |\mathbf{p}_{1\mathrm{T}} + \mathbf{p}_{2\mathrm{T}}|/2$, and correspond to lengths of homogeneity: regions of the source which emit particles of similar momentum [104]. Measuring the k_T dependence of HBT radii provides essential constraints on dynamical models [105]. In particular, the ratio $R_{\mathrm{out}}/R_{\mathrm{side}}$ is predicted to be larger than unity for sources which emit particles over a long time.

The measured k_T dependence of all radii [63] and the ratio $R_{\mathrm{out}}/R_{\mathrm{side}}$ are shown in Fig. 19, along with STAR results [106]. The data from PHENIX and STAR are in excellent agreement. Both sets of data have been corrected for Coulomb repulsion between the detected particles.

The measured radii all decrease with increasing k_T as expected for a rapidly expanding source. The ratio $R_{\mathrm{out}}/R_{\mathrm{side}}$ was measured to be 1 within errors, with a slight systematic decrease for increasing k_T. As is discussed in the next section, these data have excluded the validity of a large majority of hydrodynamical models developed to describe Au+Au collisions at RHIC,

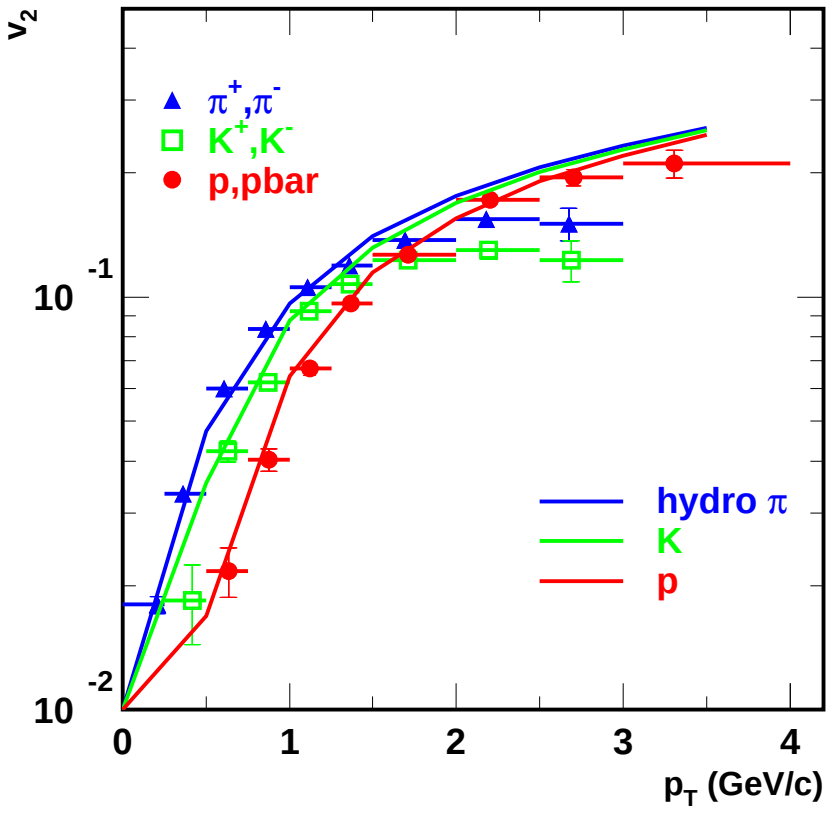

Fig. 18. $v_2(p_T)$ for pions, kaons and protons produced in minimum-bias collisions at RHIC [50] compared to hydro calculations from Huovinen *et al.* [99].

indicating that in their present form these models do not describe well the space-time evolution of the Au+Au collisions.

3.5 Hydrodynamic Model Comparisons

Many of the experimental features in the spectra and elliptic flow are consistent with equilibrium being established early in the collision with large pressure gradients that drive a strong expansion. Moving from a statement of "consistency" to a statement that equilibrium has been "established" is difficult. Some progress can be made by comparing the data to hydrodynamic models that assume full equilibrium early in the collision.

A variety of hydrodynamic models have been published. Our approach is to

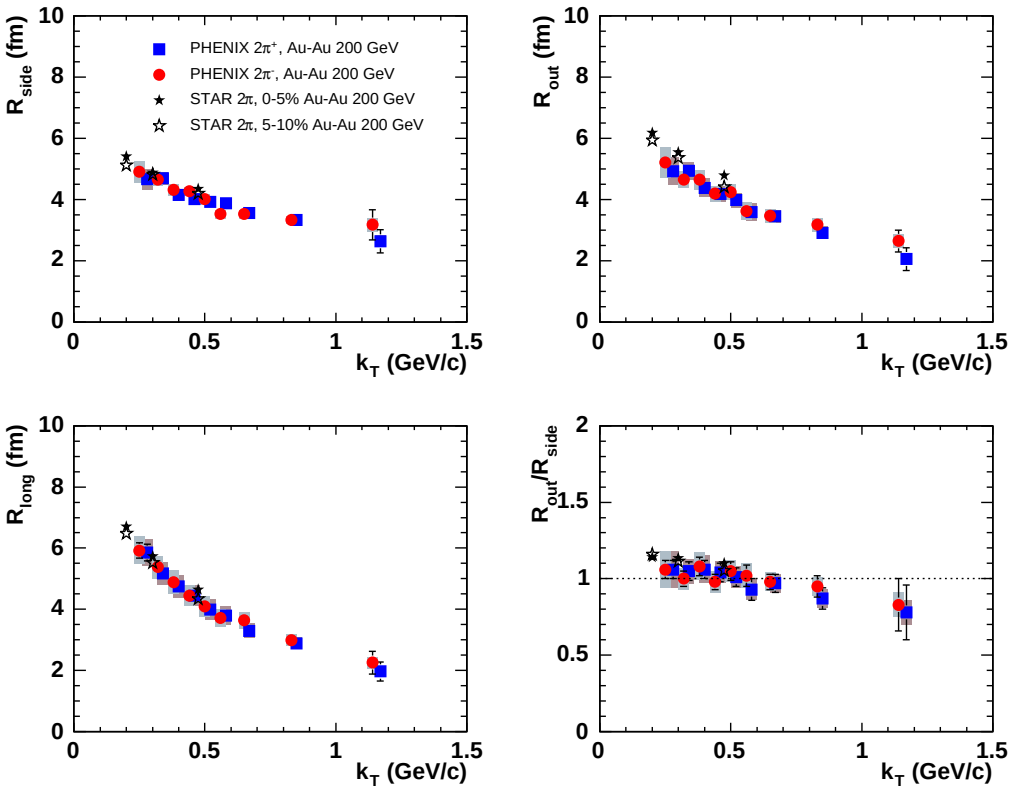

Fig. 19. The k_T dependence of the Bertsch-Pratt parameters for $\pi^+\pi^+$ (blue square) and $\pi^-\pi^-$ (red circle) for 0−30% centrality with statistical error bars and systematic error bands. Results from PHENIX [63] and STAR [106] are overlaid.

confront these models with the following broad set of data; $v_2(p_T)$, spectra, and HBT. In this paper we will not compare the data with hydro-inspired parameterized fits, *e.g.* blast-wave [107] or Buda-Lund [108] models, but will restrict ourselves to dynamical hydro models.

In Figs. 20 and 21, hydro calculations that include a phase transition from the QGP phase to a hadronic phase are shown with solid lines, while hydro calculations that do not include a pure QGP phase at any stage in the dynamics are drawn with dashed lines. The four calculations that include a QGP phase all assume an ideal gas EOS for the QGP phase, a resonance gas for the hadronic phase and connect the two using a first-order phase transition and a Maxwell construction. These calculations use latent heats that range from 0.8 GeV/fm^3 (Teaney *et al.* [98]) to 1.15 GeV/fm^3 (Huovinen *et al.* [99] and Kolb *et al.* [109]), to 1.7 GeV/fm^3 (Hirano *et al.* [110,111]). For comparison the bag model of the nucleon with external bag pressure $B = (230MeV)^4$ and a T_{crit} = 164 MeV produces a latent heat of 1.15 GeV/fm^3 [112]. The calculations that do not include a QGP phase (dashed lines) either include a hadron phase and a phase mixture by forcing the latent heat of the transition to infinity [98], or use an hadronic resonance gas equation of state, *i.e.* no mixed or QGP

phases [99].

The calculations also differ in how they solve the hydro equations and how they treat the final hadronic phase. The work of Hirano, Tsuda, and Nara cited here are the only calculations in this paper that solve the hydro equations in 3D [110,111]. For the final hadronic stage Teaney [98] uses a hybrid model that couples the hadronic phase to RQMD to allow hadrons to freezeout according to their cross section, *i.e.* for chemical equilibrium to be broken in the hadronic phase. Hirano [110] and Kolb [112] both allow for partial chemical equilibrium by chemically freezing out earlier than the kinetic freezeout. This has been done in order to reproduce the large proton yield measured at RHIC (see later in this section). In contrast, Huovinen [99] maintains full chemical equilibrium throughout the hadronic phase.

Figure 20 compares these calculations to the measured minimun-bias proton and pion $v_2(p_T)/\varepsilon$. Minimim-bias results were chosen in order to have the broadest set of data and model calculations for comparison. The four calculations that include a phase transition from the QGP phase to a hadronic phase (solid lines) reproduce the low-p_T proton data better than the two hydro calculations that do not have a QGP phase at any stage in the dynamics (dashed lines). The presence of the first-order QGP phase transition softens the EOS which reduces the elliptic flow. At higher p_T there is considerable variation between the models. Part of this is due to how the final hadronic stage is modeled. For example, Kolb's (solid light-blue line) and Hirano's (solid dark-blue line) calculations allow for partial chemical equilibrium in the final stage compared to Huovinen (solid green line) which chemically freezes out late in the collision. The difference is observable above $p_T \sim 1$ GeV/c.

The same hydro models are compared to the pion $v_2(p_T)/\varepsilon$ measurements from STAR and PHENIX in Fig. 20. The Kolb (solid light-blue line) and Hirano (solid dark-blue line) calculations fail completely by predicting too strong a v_2. These two models have very similar partial chemical equilibrium assumptions in the late hadronic stage. It is worth noting that the Kolb calculation is the same as the Huovinen (solid green line) calculation with the exception of the final hadronic stage.

All the above models have assumed ideal hydrodynamics, *i.e.* with no viscosity and zero mean free path. Non-zero viscosity in the QGP reduces v_2 [113,114] and since the early hydro calculations from Teaney and Huovinen reproduced the magnitude of the pion v_2 data, it is often stated that viscosity of the matter at RHIC must be small [24]. However recent calculations from Hirano (3D) (solid dark-blue line) and Kolb (solid light-blue line) overpredict the measured v_2. As these do not include dissipative effects, such as those present in hadronic interactions in the final state, their failure implies that the amount of viscosity at RHIC is still an open issue. Progress will require both theoretical

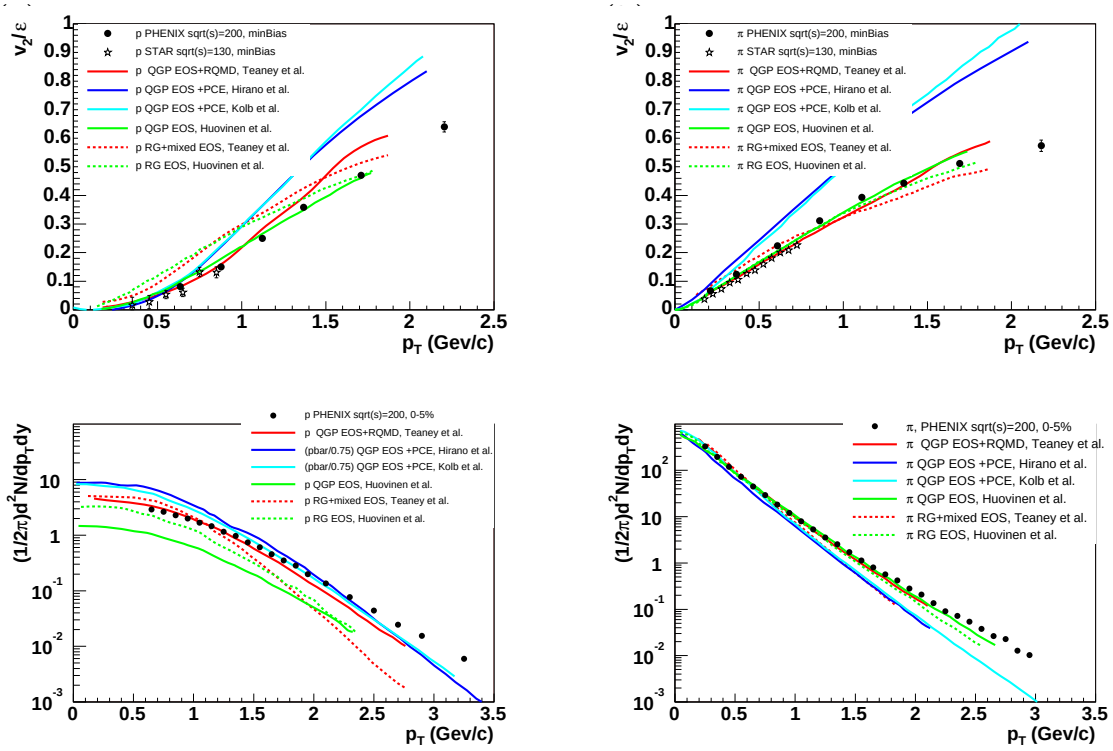

Fig. 20. Top two panels: On the left, proton $\frac{1}{\varepsilon}v_2(p_T)$ vs. p_T for minimum-bias collisions at RHIC are compared with hydro calculations, and on the right is the same comparison for pions. Bottom two panels: On the left, proton spectra for 0–5% collisions at RHIC are compared with the same hydro calculations and on the the right is the same comparison for pions.

development and experimental measures that are less sensitive to how the azimuthal asymmetry of the energy-momentum tensor is distributed between different particles in the final stage of the reaction, *e.g.* the elliptic flow of the total transverse energy.

The same hydro models are now compared to the measured spectra from central collisions. The bottom right panel of Fig. 20 shows that all the hydro models reproduce the pion spectra below $p_T \sim 1$ GeV/c; at higher p_T the particles are less likely to be equilibrated and hydro models are not expected to work well. In the bottom left panel the calculated proton spectra from Huovinen [99] (solid green line) are consistently lower than the data, due to the calculation maintaining chemical equilibrium throughout the hadronic phase. The lower temperature chemical freezeout suppresses the final calculated yield of heavier particles such as protons. Of the two calculations from Teaney [98] the calculation that includes the QGP phase (solid red line) reproduces the proton spectra, presumably because of the increased transverse flow from the stronger early pressure gradients. Hirano's and Kolb's (solid dark and light-blue lines) calculations break chemical equilibrium during the hadronic phase

	QGP+mixed+RG				*mixed+RG*	*RG*
	Teaney	*Hirano*	*Kolb*	*Huovinen*	*Teaney*	*Huovinen*
Reference	[98]	[110]	[109,115]	[99]	[98]	[99]
latent heat (GeV/fm^3)	0.8	1.7	1.15	1.15	0.8	
init. ε_{max} (GeV/fm^3)	16.7		23	23	16.7	23
init. $\langle\varepsilon\rangle$ (GeV/fm^3)	11.0	13.5			11.0	
τ_0 fm/c	1.0	0.6	0.6	0.6	1.0	0.6
hadronic stage	RQMD	partial chemical equil.	partial chemical equil.	full equil.	RQMD	full equil.
proton v2	yes	$<$ 0.7 GeV/c	$<$ 0.7 GeV/c	yes	no	no
pion v2	yes	no	no	yes	yes	yes
proton spectra	yes	overpredict	overpredict	no	no	no
pion spectra	yes	$<$ 1 GeV/c	$<$ 1 GeV/c	yes	$<$ 0.7 GeV/c	yes
HBT	Not available	No	No	No	Not available	Not available

Table 1
Summary of various hydro model assumptions and a comparison between measurements and hydro calculations. Two initial energies are tabulated, either the maximum energy density at the center of the collision or the energy density averaged over the transverse profile.

and overpredict the proton spectra at low p_T.

One difficulty is that the spectra comparison with hydrodynamic models is for central collisions while the v_2 comparison is for minimum-bias collisions. It is dificult to use central collisions for the v_2 comparison since the collisions are nearly symmetric and hence v_2 is small. In addition, hydrodyamic calculations that reproduce v_2 values over a broad range of centrality (from 0-45% in Ref. [95]) tend to overpredict the data for more peripheral collisions by approximately 25%, presumably because of a breakdown in the hydrodynamic assumptions. Hence when comparing to minimum-bias data sets, an overprediction of v_2 from the hydro models of less than 20

These comparisons between data and hydro models are summarized in Table 1 and in the following conclusions;

- $v_2(p_T, PID)$ is sensitive to all stages of the reaction. Elliptic flow is produced by strong scattering in the initial phase, while the detailed shape of $v_2(p_T)$ and how the momentum asymmetry is distributed to different particles is affected by the transition from a QGP to hadronic phase and scattering in the final hadronic stage.
- The hydro models that reproduce the low-p_T proton v_2 are those that include both a QGP and hadronic phase.
- The hadronic phase critically affects the final values of $v_2(p_T, PID)$. Models (Hirano, Kolb) that include partial chemical equilibrium to reproduce the baryon yield, completely fail on the pion v_2.
- The only model that survives this comparison with measured v_2 and spectra is Teaney's (solid red line) which includes a strong expansion in a QGP phase, a phase transition to a mixed phase, and then a hadronic cascade in the final hadronic state. There are open questions in this hybrid model, *e.g.* the sensitivity of the results to the matching conditions between hydro and RQMD. All other models fail in at least one v_2 or spectra comparison, partially due to differences in modeling the final hadronic state.
- Until the model uncertainty in the final state is reduced, it is not yet possible to use the measured splitting between proton and pion $v_2(p_T)$ to extract quantitative information on the EOS during the reaction, including the possible softening of the EOS due to the presence of a mixed phase.

A comparison with the HBT data and some of the hydro models is shown in Fig. 21. It is unfortunate that not all hydro models have been compared to HBT data, *e.g.* the hydro+RQMD model from Teaney [98] has not been confronted with this observable. The hydro calculation from Kolb, Heinz and Huovinen [115] (solid green line) includes a first-order phase transition which leads to a long lifetime for the system. The source parameter $R_{\rm long}$ is considered most sensitive to the duration of the whole collision, *i.e.* from initial overlap to final particle emission, and the Kolb/Huovinen hydro calculation [115] (solid green line) overpredicts the measured $R_{\rm long}$ data. Changing to partial chemical equilibrium in the hadronic stage [110], indicated with the dark blue line, reduces the lifetime of the collision which improves the agreement with $R_{\rm long}$. However the ratio $R_{\rm out}/R_{\rm side}$, which is sensitive to the duration over which particles are emitted, is still overpredicted.

There have been many attempts to understand what may be causing the disagreement with data (known collectively as the HBT puzzle);

- Sinyukov *et al.* [116] and Grassi et al. [117] have suggested that the sharp Cooper-Frye freezeout condition [118] should be replaced by an emission function that decouples hadrons depending on their hadronic cross section.

- However when this has been effectively implemented by using a hadronic cascade (URQMD) for the final hadronic stage, the predicted ratio $R_{\rm out}/R_{\rm side}$ increases and diverges further from the data [119]. Modeling the final stage with a hadronic cascade effectively includes dissipative effects which should increase the duration of emission and produce a larger ratio $R_{\rm out}/R_{\rm side}$.
- One method to reduce the lifetime of the reaction is to change the QGP EOS. Using a crossover instead of a first-order transition reduces the ratio $R_{\rm out}/R_{\rm side}$ by about 50% to $R_{\rm out}/R_{\rm side} \sim 1.5$ [120] which is still larger than the data. Because the calculation was restricted to $\eta = 0$ Zschiesche *et al.* were unable to compare with the measured values of $R_{\rm long}$.

In summary, model comparisons seem to be closer to the HBT data when the lifetime of the collision is made smaller than the long time resulting from a first-order phase transition. The small values of $R_{\rm out}/R_{\rm side}$ may indicate that there is little to no mixed phase present in the reactions. One possible direction for future comparisons with data is to include a more realistic EOS into the hydro models, *e.g.* to take the EOS from lattice QCD calculations [121]. Such a calculation needs to be compared with all the available data, including spectra and v_2, as well as HBT.

3.6 Conclusions

In summary we can make the following conclusions

- The measured yields and spectra of hadrons are consistent with thermal emission from a strongly expanding source.
- Strangeness is fully saturated at RHIC, consistent with full chemical equilibrium.
- The scaling of v_2 with eccentricity shows that collective behavior is established early in the collision.
- Elliptic flow is stronger at RHIC than at the SPS, since the measured slope of $v_2(p_T)$ for pions is 50% larger at RHIC.
- The measured proton $v_2(p_T)$ is less than that for pions at low p_T; the small magnitude of the proton v_2 at low p_T is reproduced by hydro models that include both a QGP and hadronic phase.
- However several of the hydro models that reproduce the proton $v_2(p_T)$ fail for the pion $v_2(p_T)$.
- The HBT source parameters, especially the small value of $R_{\rm long}$ and the ratio $R_{\rm out}/R_{\rm side}$, suggest that the mixed phase is too long-lived in the current hydro calculations.

Hence we currently do not have a consistent picture of the space-time dynamics of reactions at RHIC as revealed by spectra, v_2, and HBT. The lack of a

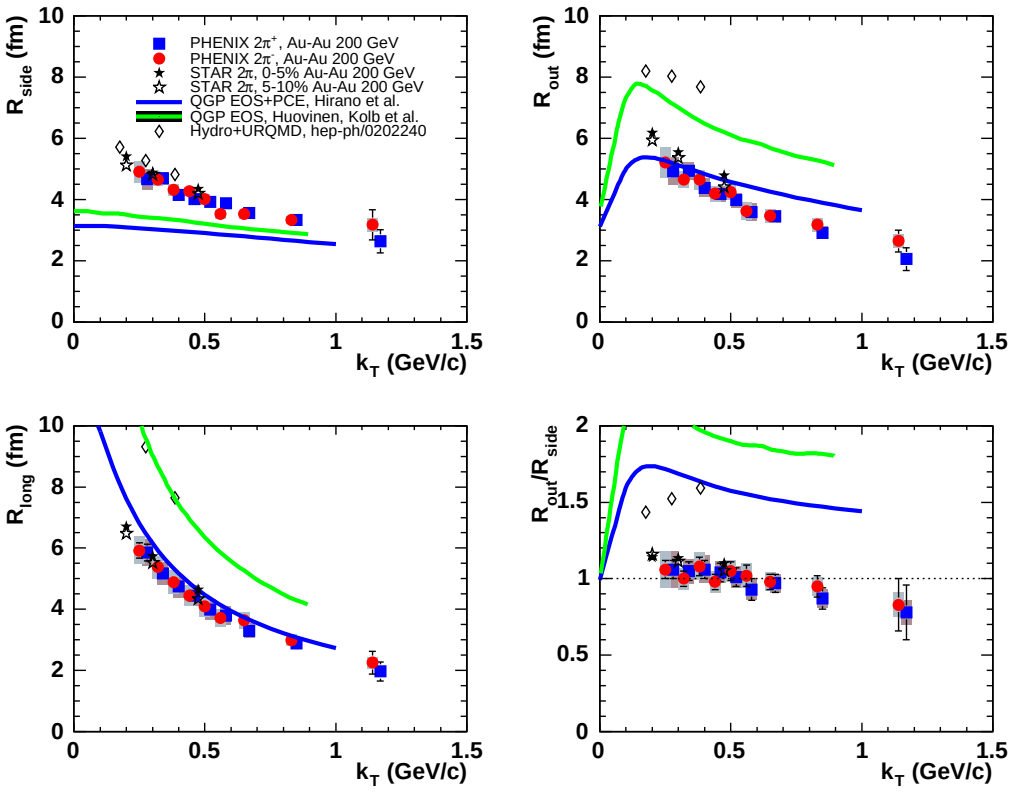

Fig. 21. The k_T dependence of the Bertsch-Pratt parameters for $\pi^+\pi^+$ (blue square) and $\pi^-\pi^-$ (red circle) for 0–30% centrality with statistical error bars and systematic error bands. Results from PHENIX [63], STAR [106] and hydrodynamics models (Hirano [110], Kolb/Huovinen [115] and Soff [122], diamonds) are overlaid.

consistent picture of the dynamics means that it is not yet possible to extract quantitative properties of the QGP or mixed phase using the observables v_2, spectra, or HBT.

4 FLUCTUATIONS

4.1 Net-Charge Fluctuations

In the study of the fluctuations of multiplicity as a means to understand the dynamics of charged particle production, one important realization was to use small regions of phase space, where energy-momentum conservation constraints would not be significant [123–125]. Such studies led to the important observation that the distribution of multiplicity, even in small intervals near mid-rapidity, was Negative Binomial rather than Poisson, which indicated large multiplicity correlations even in small $\delta\eta$ intervals [126]. No such studies

are yet available at RHIC.

Based on predictions that event-by-event fluctuations of the net charge in local phase space regions would show a large decrease as a signature of the QGP [127–129], net-charge fluctuations were measured in PHENIX [44]. The idea is that in a QGP composed of fractionally charged quarks, the larger number of fractionally charged particles compared to unit-charged hadrons would result in smaller relative net-charge fluctuations in a QGP than for a pure gas of hadrons and that this original fluctuation would survive the transition back to ordinary hadrons.

It is important to realize that the study of net-charge fluctuations represents the study of fluctuations in a quantity that is conserved over all phase space. Consider $N = N_+ + N_-$ charged particles produced in the full phase space. By charge conservation $N_+ = N_- = N/2$, and the net charge $Q \equiv N_+ - N_-$ is identically zero so that there are no net-charge fluctuations—the variance $V(Q) = 0$, where

$$V(Q) \equiv \langle Q^2 \rangle - \langle Q \rangle^2 \,. \tag{10}$$

In a smaller region of phase space, where p is the fraction of N observed in a stochastic scenario, the mean and variance of the number of positive n_+ and negative n_- particles are equal, but the variance of Q is no longer identically zero:

$$\langle n_+ \rangle = \langle n_- \rangle = pN/2 \,, \tag{11}$$

$$V(n_+) = V(n_-) = p(1-p)N/2 \,, \tag{12}$$

from which it follows that

$$V(Q) = (1-p)n_{ch} \,, \tag{13}$$

where $n_{ch} = pN$ is the expected number of charged particles on the interval. Thus the normalized variance in Q (normalized to Poisson statistics) is defined as:

$$v(Q) = \frac{V(Q)}{n_{ch}} = (1-p) \,. \tag{14}$$

In the limit $n_{ch} \gg 0$, the variance of the charge ratio $R = n_+/n_-$ approaches $V(R) = 4(1-p)/n_{ch}$. However, it is well known in mathematical statistics that moments of the inverse of a stochastic variable, e.g. $1/n_-$, diverge if there is

any finite probability, no matter how small, for $n_- = 0$. Thus, the charge ratio is not a stable measure of fluctuations.

The previous arguments are based on fixed N. The results where N varies according to a specified distribution are also interesting. If n_- is Poisson distributed, with mean value $\mu = N/2$ over the whole phase space, then in the region of phase space with probability p the distribution is also Poisson, with mean $\langle n_- \rangle|_p = \mu_p = pN/2$. If, on the other hand n_- is Negative Binomial distributed, with mean value $\mu = N/2$ and NBD parameter $\sigma^2/\mu^2 - 1/\mu = 1/k$ for the whole phase space, then in the region of phase space with probability p, the distribution is Negative Binomial with mean $\langle n_- \rangle|_p = \mu_p = pN/2$ and the same value of $1/k$.

Actually, the binomial division preserves $\sigma_p^2/\mu_p^2 - 1/\mu_p = 1/k$, for any distribution [130]. This appears to indicate that smaller intervals, which tend to have larger values of σ_p^2/μ_p^2 would be less sensitive to the global $1/k$, the long-range correlation. This would be true except for the fact that there are short-range correlations which are better seen on small intervals of phase space. Another important thing to note regarding a binomial split of a Negative Binomial distribution is that the two subintervals are not statistically independent. The conditional probability distribution on the interval $(1-p)$ depends upon the outcome on the interval p [131]. It is unfortunate that these elegant arguments can not be applied to the net-charge fluctuations since $\langle Q \rangle = 0$.

The PHENIX measurement [44] of the normalized variance $v(Q)$ of net-charge fluctuations is shown in Fig. 22 in the interval $-0.35 \leq \delta\eta \leq +0.35$ as a function of the azimuthal angular interval of reconstructed tracks, either at the detector, $\Delta\phi_d$, or at the vertex, $\Delta\phi_r$, chosen symmetrically around the detector acceptance. For smaller $\Delta\phi_r$ the data agree with the purely stochastic $(1-p)$ dependence shown as the solid line, but deviate from the stochastic prediction at larger values due to correlations from resonance decay, such as $\rho^0 \rightarrow \pi^+ + \pi^-$ as nicely explained by RQMD [132].

Absent new theoretical insight, it is difficult to understand how quark-level net-charge fluctuations in a QGP can be related to net-charge fluctuations of hadrons, where, by definition, strong correlations exist, e.g., in the formation of a meson from a $q - \bar{q}$ pair. Also, the study of the fluctuations of net charge, which is conserved, may not be as useful to detect interesting fluctuations as the study of fluctuations of the total charged multiplicity, which is much less constrained by conservation laws. This has yet to be tried at RHIC.

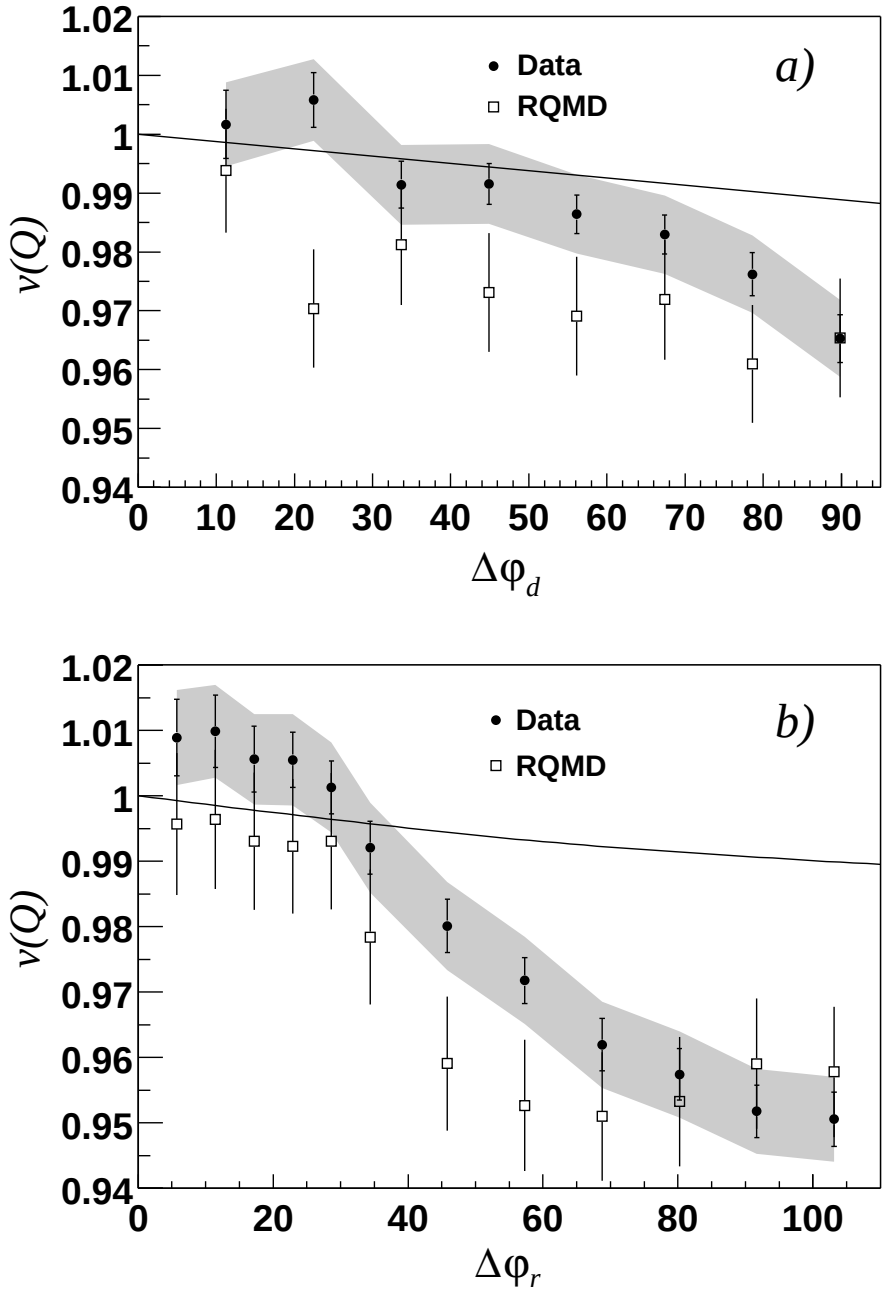

Fig. 22. $v(Q)$ for the 10% most central events in data and RQMD, as a function of the azimuthal interval in degrees of reconstructed tracks, either a) at the detector, $\Delta\phi_d$, or b) at the vertex, $\Delta\phi_r$, chosen symmetrically around the detector acceptance. For data, the error band shows the total statistical error, whereas the error bars indicate the uncorrelated part. The solid line shows the expected reduction in $v(Q)$ in the stochastic scenario when global charge conservation is taken into account [44].

Fluctuations in the event-by-event average p_T, denoted M_{p_T}, have been measured and provide a severely small limit on possible fluctuations from a sharp phase transition. For events with n detected charged particles with magnitudes of transverse momenta, p_{T_i}, the event-by-event average p_T, denoted M_{p_T} is defined as:

$$M_{p_T} = \overline{p_T} = \frac{1}{n}\sum_{i=1}^{n} p_{T_i} \, . \tag{15}$$

Mixed events are used to define the baseline for random fluctuations of M_{p_T} in PHENIX [45,55]. This has the advantage of effectively removing any residual detector-dependent effects. The event-by-event average distributions are very sensitive to the number of tracks in the event (denoted n or N_{tracks}), so the mixed event sample is produced with the *identical* N_{tracks} distribution as the data. Additionally, no two tracks from the same data event are placed in the same mixed event in order to remove any intra-event correlations in p_T. Finally, $\langle M_{p_T} \rangle$ must exactly match the semi-inclusive $\langle p_T \rangle$.

For the case of statistical independent emission, where the fluctuations are purely random, an analytical formula for the distribution in M_{p_T} can be obtained assuming Negative Binomial distributed event-by-event multiplicity, with Gamma distributed semi-inclusive p_T spectra [133]. The formula depends on the four semi-inclusive parameters $\langle n \rangle$, $1/k$, b and p which are derived from the means and standard deviations of the semi-inclusive p_T and multiplicity distributions, $\langle n \rangle$, σ_n, $\langle p_T \rangle$, σ_{p_T}:

$$f(y) = \sum_{n=n_{\min}}^{n_{\max}} f_{\mathrm{NBD}}(n, 1/k, \langle n \rangle)\, f_{\Gamma}(y, np, nb) \, , \tag{16}$$

where $y = M_{p_T}$. For fixed n, and purely random fluctuations, the mean and standard deviation of M_{p_T} follow the expected behavior, $\langle M_{p_T} \rangle = \langle p_T \rangle$, $\sigma_{M_{p_T}} = \sigma_{p_T}/\sqrt{n}$. In PHENIX, Eq. 16 is used to confirm the randomness of mixed events which are used to define the baseline for random fluctuations of M_{p_T} [45,55].

The measured M_{p_T} distributions for the data in two centrality classes for $\sqrt{s_{NN}} = 200$ GeV Au+Au collisions in PHENIX [55] are shown in Fig. 23 (data points) compared to the mixed-event distributions (histograms). The non-Gaussian, Gamma-distribution shape of the M_{p_T} distributions is evident. The difference between the data and the mixed-event random baseline distributions is not visible to the naked eye. The nonrandom fluctuation is quantified

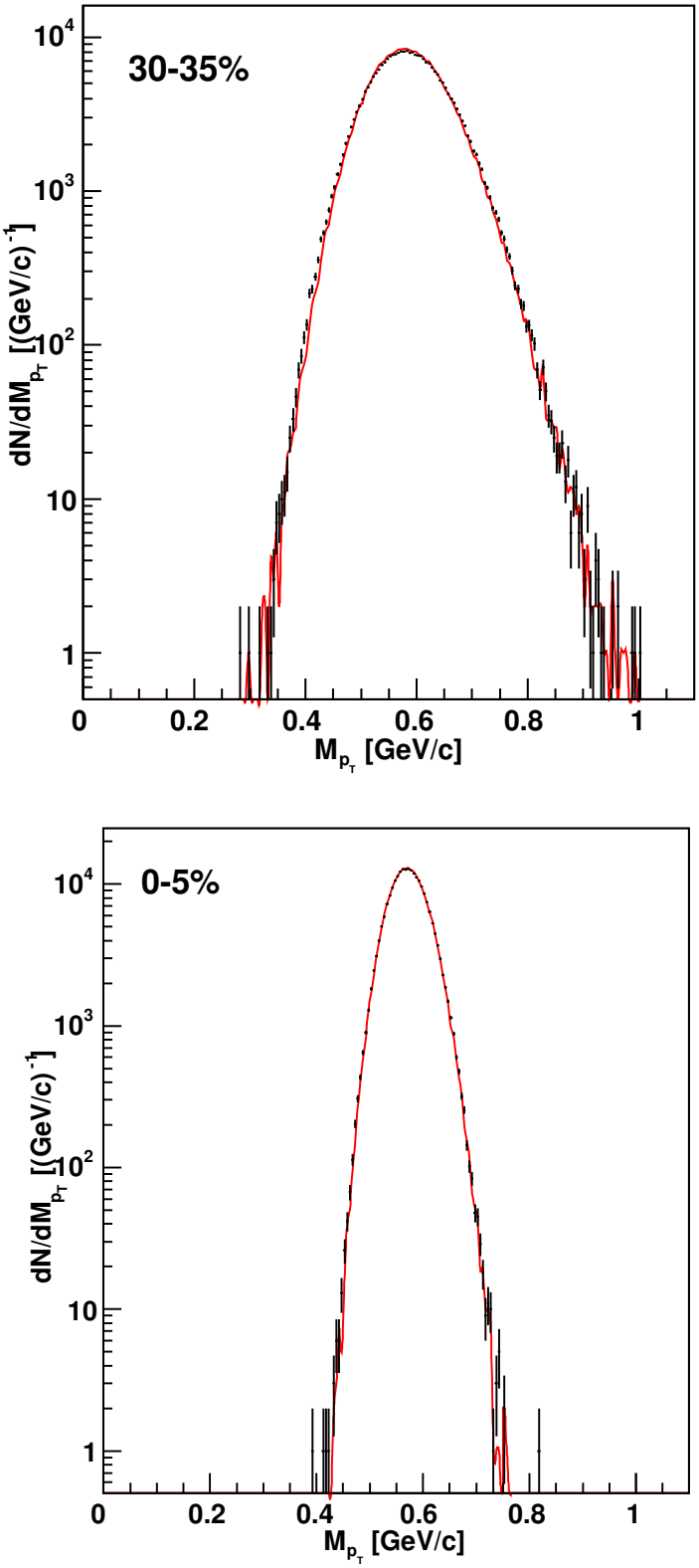

Fig. 23. M_{pT} for 30–35% and 0–5% centrality classes: data (points) mixed events (histogram) [55].

by the fractional difference of ω_{p_T}, the normalized standard deviation of M_{p_T}, for the data and the mixed-event (random) samples:

$$\omega_{p_T} = \frac{\sigma_{M_{p_T}}}{\langle M_{p_T} \rangle} \,, \tag{17}$$

$$F_{p_T} = \frac{\omega_{p_T,\mathrm{data}} - \omega_{p_T,\mathrm{mixed}}}{\omega_{p_T,\mathrm{mixed}}} \,. \tag{18}$$

The results are shown as a function of centrality, represented by N_{part} in Fig. 24.

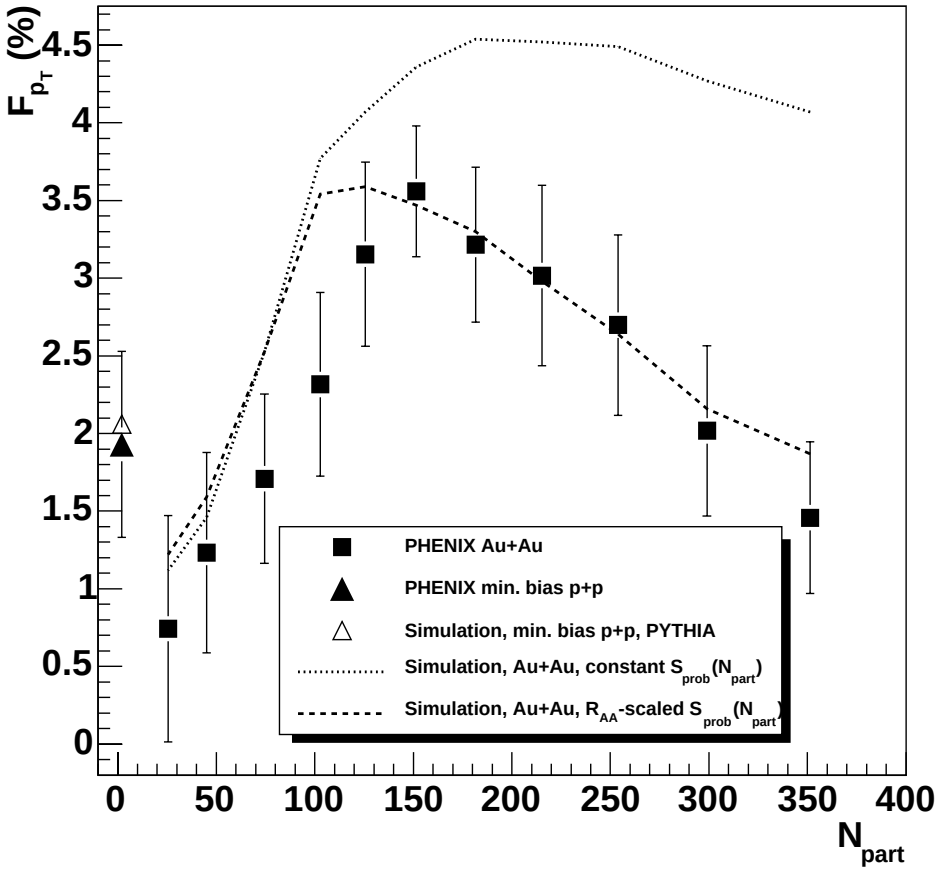

Fig. 24. F_{p_T} vs. centrality, represented as the average number of participants (N_{part}) in a centrality class, compared to jet simulation [55].

The dependence of F_{p_T} on N_{part} is striking. To further understand this dependence and the source of these nonrandom fluctuations, F_{p_T} was measured over a varying p_T range, 0.2 GeV/c $\leq p_T \leq p_T^{\max}$ (Fig. 25), where $p_T^{\max} = 2.0$ GeV/c for the N_{part} dependence.

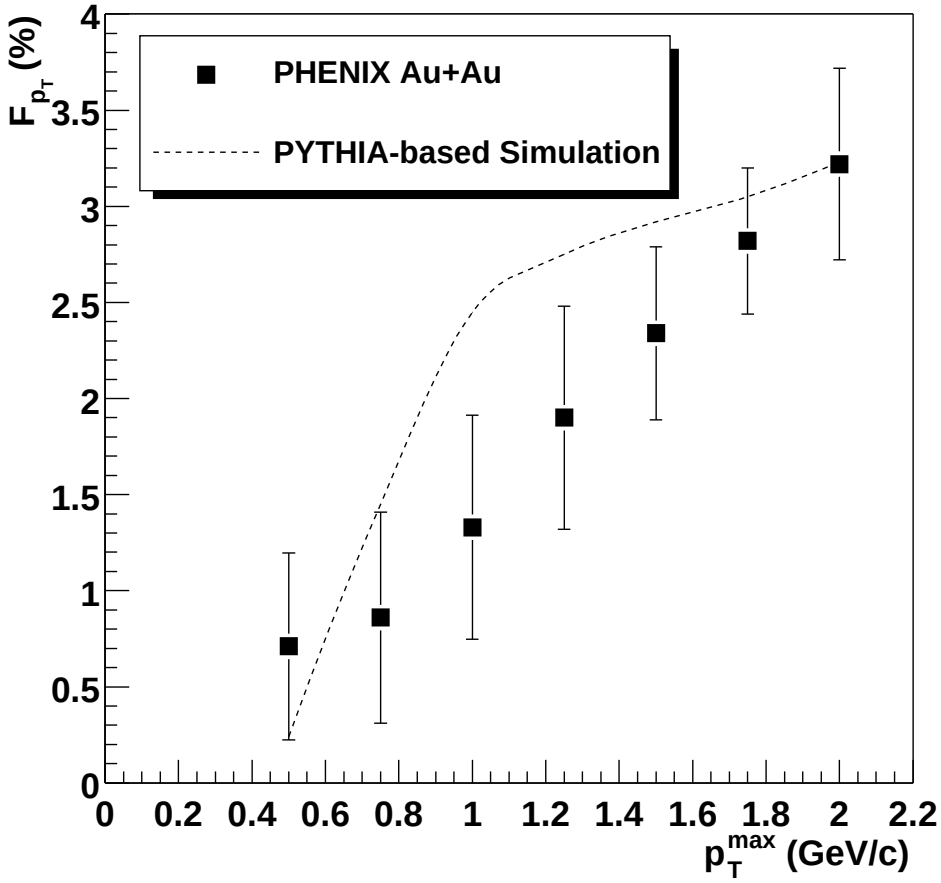

Fig. 25. F_{p_T} vs. $p_T^{\max}$ compared to R_{AA}-scaled jet simulation for the 20–25% centrality class ($N_{part} = 181.6$) [55].

The increase of F_{p_T} with $p_T^{\max}$ suggests elliptic flow or jet origin. This was investigated using a Monte Carlo simulation of correlations due to elliptic flow and jets in the PHENIX acceptance. The flow was significant only in the lowest centrality bin and negligible ($F_{p_T} < 0.1\%$) at higher centralities. Jets were simulated by embedding (at a uniform rate per generated particle, $S_{prob}(N_{part})$) $p+p$ hard-scattering events from the PYTHIA event generator into simulated Au+Au events assembled at random according to the measured N_{tracks} and semi-inclusive p_T distributions. This changed $\langle p_T \rangle$ and σ_{p_T} by less than 0.1%. $S_{prob}(N_{part})$ was either constant for all centrality classes, or scaled by the measured hard-scattering suppression factor $R_{AA}(N_{part})$ for $p_T > 4.5$ GeV/c [49]. A value $F_{p_T} = 2.06\%$ for $p+p$ collisions was extracted from pure PYTHIA events in the PHENIX acceptance in agreement with the $p+p$ measurement (Fig. 24). The value of $S_{prob}(N_{part})$ was chosen so that the simulation with $S_{prob}(N_{part}) \times R_{AA}(N_{part})$ agreed with the data at $N_{part} = 182$. The centrality and $p_T^{\max}$ dependences of the measured F_{p_T} match the

simulation very well, but only when the R_{AA} scaling is included.

A less experiment-dependent method to compare nonrandom fluctuations is to assume that the entire F_{p_T} is due to temperature fluctuations of the initial state, with RMS variation $\sigma_T/\langle T\rangle$ [134,45]. Then,

$$\omega^2_{p_T,\mathrm{data}} - \omega^2_{p_T,\mathrm{mixed}} = (1 - \frac{1}{\langle n\rangle})\frac{\sigma_T^2}{\langle T\rangle^2} = 2F_{p_T}\omega^2_{p_T,\mathrm{mixed}}\ , \tag{19}$$

This yields $\sigma_T/\langle T\rangle$=1.8% for central collisions in PHENIX with similarly small values for the other Relativistic Heavy Ion experiments [135], 1.7% in STAR, 1.3% in CERES, and 0.6% in NA49. These results put severely small limits on the critical fluctuations that were expected for a sharp phase transition, both at SPS energies and at RHIC, but are consistent with the expectation from lattice QCD that the transition is a smooth crossover [12].

Other proposed explanations of the centrality and p_T^{max} dependences of F_{p_T} include: overlapping color strings which form clusters so that the number of sources and $\langle p_T\rangle$ per source is modified as a function of centrality [136]; and near equilibrium p_T correlations induced by spatial inhomogeniety [137].

4.3 Conclusions

Critical behavior near the phase boundary can produce nonrandom fluctuations in observables such as the net-charge distribution and the average transverse momentum distribution. Our search for net-charge fluctuations has ruled out the most naive model of charge fluctuations in a QGP, but it is unclear whether the charge fluctuation signature can survive hadronization. Our measurement of the event-by-event average p_T distribution shows a nonrandom fluctuation that is consistent with the effect expected from high-p_T jets. This puts a severe constraint on the critical fluctuations that were expected for a sharp phase transition but is consistent with the expectation from lattice QCD that the transition is a smooth crossover [12].

5 BINARY SCALING

5.1 Hard Scattering and pQCD

One way to get a partonic probe into the midst of an $A + A$ collision is to use the high-p_T partons produced by hard scattering. For $p + p$ collisions in the

RHIC energy range, hard scattering is considered to be the dominant process of particle production with $p_T \geq 2$ GeV/c at mid-rapidity. Typically, particles with $p_T \geq 2$ GeV/c are produced from states with two roughly back-to-back jets which are the result of scattering of constituents of the nucleons (partons) as described by pQCD [138].

The overall $p+p$ hard-scattering cross section in "leading logarithm" pQCD is the sum over parton reactions $a+b \rightarrow c+d$ (e.g. $g+q \rightarrow g+q$) at parton-parton center-of-mass (c.m.) energy $\sqrt{\hat{s}}$:

$$\frac{d^3\sigma}{dx_1 dx_2 d\cos\theta^*} = \frac{1}{s}\sum_{ab} f_a(x_1) f_b(x_2) \frac{\pi\alpha_s^2(Q^2)}{2x_1x_2}\Sigma^{ab}(\cos\theta^*) \,, \tag{20}$$

where $f_a(x_1)$, $f_b(x_2)$, are parton distribution functions, the differential probabilities for partons a and b to carry momentum fractions x_1 and x_2 of their respective protons (e.g. $u(x_2)$), and where θ^* is the scattering angle in the parton-parton c.m. system. The parton-parton c.m. energy squared is $\hat{s} = x_1x_2s$, where $\sqrt{s}$ is the c.m. energy of the $p+p$ collision. The parton-parton c.m. system moves with rapidity $y = 1/2\ln(x_1/x_2)$ in the $p+p$ c.m. system.

Equation 20 gives the p_T spectrum of outgoing parton c, which then fragments into hadrons, e.g. π^0. The fragmentation function $D_c^{\pi^0}(z,\mu^2)$ is the probability for a π^0 to carry a fraction $z = p^{\pi^0}/p^c$ of the momentum of outgoing parton c. Equation 20 must be summed over all subprocesses leading to a π^0 in the final state. The parameter μ^2 is an unphysical "factorization" scale introduced to account for collinear singularities in the structure and fragmentation functions [138,139].

In this formulation, $f_a(x_1,\mu^2)$, $f_b(x_2,\mu^2)$ and $D_c^C(z,\mu^2)$ represent the "long-distance phenomena" to be determined by experiment; while the characteristic subprocess angular distributions, $\Sigma^{ab}(\cos\theta^*)$, and the coupling constant, $\alpha_s(Q^2) = \frac{12\pi}{25}\ln(Q^2/\Lambda^2)$, are fundamental predictions of QCD [140–142] for the short-distance, large-Q^2, phenomena. The momentum scale $Q^2 \sim p_T^2$ for the scattering subprocess, while $Q^2 \sim \hat{s}$ for a Compton or annihilation subprocess, but the exact meaning of Q^2 tends to be treated as a parameter rather than a dynamical quantity. The transverse momentum of a scattered constituent is:

$$p_T = p_T^* = \frac{\sqrt{\hat{s}}}{2}\,\sin\theta^* \,. \tag{21}$$

Equation 20 leads to a general 'x_T-scaling' form for the invariant cross section of high-p_T particle production:

$$E\frac{d^3\sigma}{d^3p} = \frac{1}{p_T^n}F(x_T) = \frac{1}{\sqrt{s}^n}G(x_T) \,, \tag{22}$$

where $x_T = 2p_T/\sqrt{s}$. The cross section has two factors, a function $F(x_T)$ ($G(x_T)$) which 'scales', i.e. depends only on the ratio of momenta, and a dimensioned factor, $1/p_T^n$ ($1/\sqrt{s}^n$), where n equals 4 in lowest-order (LO) calculations, analogous to the $1/q^4$ form of Rutherford Scattering in QED. The structure and fragmentation functions are all in the $F(x_T)$ ($G(x_T)$) term. Due to higher-order effects such as the running of the coupling constant, $\alpha_s(Q^2)$, the evolution of the structure and fragmentation functions, and the initial-state transverse momentum k_T, n is not a constant but is a function of x_T, $\sqrt{s}$. Measured values of $n(x_T, \sqrt{s})$ in $p+p$ collisions are between 5 and 8.

5.2 Mid-Rapidity p_T Spectra from $p+p$ Collisions

The scaling and power-law behavior of hard scattering are evident from the $\sqrt{s}$ dependence of the p_T dependence of the $p+p$ invariant cross sections. This is shown for nonidentified charged hadrons, $(h^+ + h^-)/2$, in Fig. 26a. At low

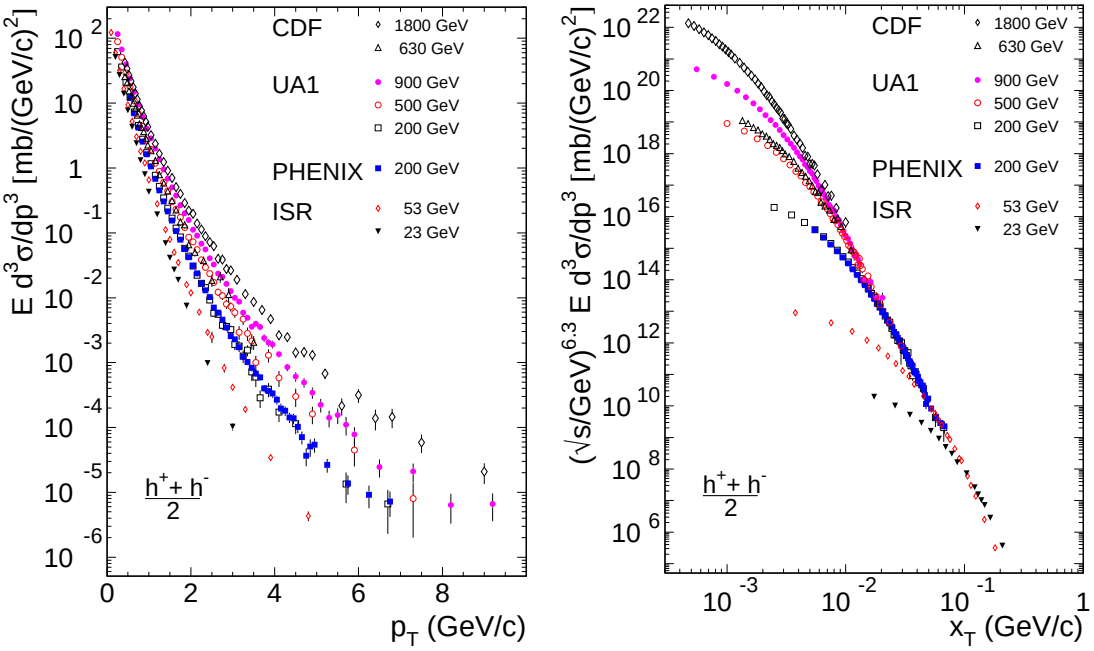

Fig. 26. (left) $Ed^3\sigma(p_T)/d^3p$ at mid-rapidity as a function of $\sqrt{s}$ in $p+p$ collisions. (right) $\sqrt{s}(\mathrm{GeV})^{6.3} \times Ed^3\sigma/d^3p$ vs. $x_T = 2p_T/\sqrt{s}$ [53] (and references therein).

$p_T \leq 1$ GeV/c the cross sections exhibit a "thermal" $\exp(-6p_T)$ dependence, which is largely independent of $\sqrt{s}$, while at high p_T there is a power-law tail, due to hard scattering, which depends strongly on $\sqrt{s}$. The characteristic variation with $\sqrt{s}$ at high p_T is produced by the fundamental power-law and scaling dependence of Eqs. 20, 22. This is best illustrated by a plot of

$$\sqrt{s}^{\,n(x_T,\sqrt{s})} \times E\frac{d^3\sigma}{d^3p} = G(x_T)\,, \tag{23}$$

as a function of x_T, with $n(x_T, \sqrt{s}) = 6.3$, which is valid for the x_T range of the present RHIC measurements (Fig. 26b). The data show an asymptotic power law with increasing x_T. Data at a given $\sqrt{s}$ fall below the asymptote at successively lower values of x_T with increasing $\sqrt{s}$, corresponding to the transition region from hard to soft physics in the p_T region of about 2 GeV/c.

The PHENIX measurement of the invariant cross section for π^0 production in $p+p$ collisions at $\sqrt{s} = 200$ GeV [56] agrees with NLO pQCD predictions over the range $2.0 \leq p_T \leq 15$ GeV/c (Fig. 27).

5.3 Scaling Hard Scattering from $p+p$ to $p+A$ and $A+B$ Collisions

Since hard scattering is point like, with distance scale $1/p_T \leq 0.1$ fm, and the hard-scattering cross section factorizes as shown in Eq. 20, the cross section in $p+A$ or $A+B$ collisions, compared to $p+p$, is proportional to the relative number of possible point-like encounters. The number of encounters of point-like constituents of nucleons is then proportional to A (AB), for $p+A$ ($A+B$) minimum-bias collisions. For $A+B$ collisions at impact parameter b, it is proportional to $T_{AB}(b)$, the nuclear thickness function, which is the integral of the product of nuclear thickness over the geometrical overlap region of the two nuclei. In detail, the semi-inclusive invariant yield of e.g. high-p_T π^0's for $A+B$ inelastic collisions, with centrality f, is related to the $p+p$ cross section by:

$$\left.\frac{1}{N_{AB}^{\rm evt}}\frac{d^2N_{AB}^{\pi^0}}{dp_T dy}\right|_f = \langle T_{AB}\rangle_f \times \frac{d^2\sigma_{pp}^{\pi^0}}{dp_T dy}\,. \tag{24}$$

Note that

$$\langle T_{AB}\rangle_f = \frac{\int_f T_{AB}(b)\,d^2b}{\int_f (1-e^{-\sigma_{NN}\,T_{AB}(b)})\,d^2b} = \frac{\langle N_{coll}\rangle_f}{\sigma_{NN}}\,, \tag{25}$$

where $\langle N_{coll}\rangle_f$ is the average number of binary nucleon-nucleon inelastic collisions, with cross section σ_{NN}, in the centrality class f. This leads to the description of the scaling for point-like processes as binary-collision (or N_{coll}) scaling.

Nuclear medium effects, either in the initial or final state, can modify the expected scaling. These modifications can be quantitatively studied by measurement of the *Nuclear modification factor* R_{AB}, which is defined as

$$R_{AB} = \frac{dN_{AB}^P}{\langle T_{AB}\rangle_f \times d\sigma_{NN}^P} = \frac{dN_{AB}^P}{\langle N_{coll}\rangle_f \times dN_{NN}^P}\,, \tag{26}$$

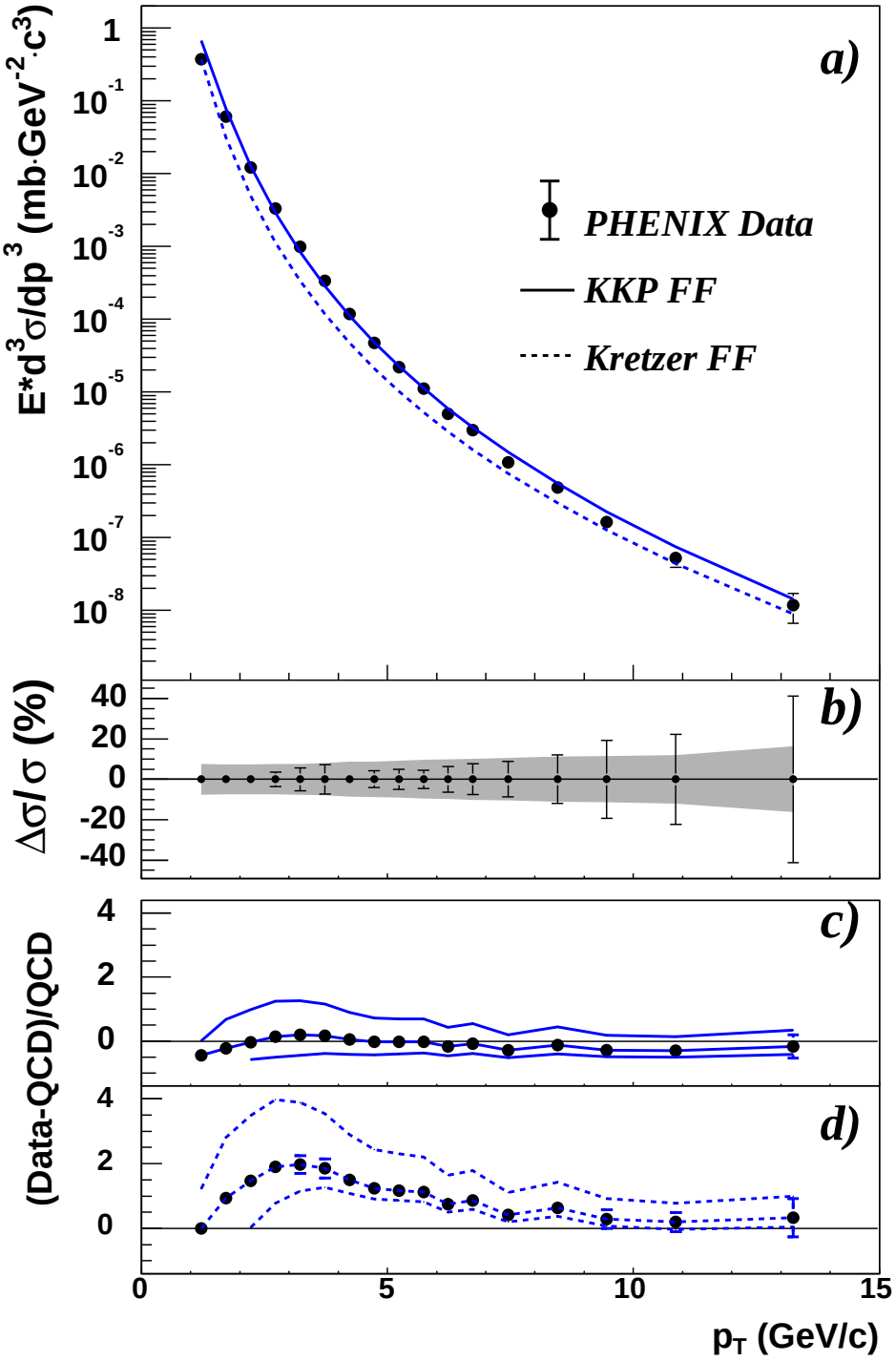

Fig. 27. PHENIX π^0 invariant cross section at mid-rapidity from $p+p$ collisions at $\sqrt{s} = 200$ GeV, together with NLO pQCD predictions from Vogelsang [143,144]. a) The invariant differential cross section for inclusive π° production (points) and the results from NLO pQCD calculations with equal renormalization and factorization scales of p_T using the "Kniehl-Kramer-Pötter" (solid line) and "Kretzer" (dashed line) sets of fragmentation functions. b) The relative statistical (points) and point-to-point systematic (band) errors. c,d) The relative difference between the data and the theory using KKP (c) and Kretzer (d) fragmentation functions with scales of $p_T/2$ (lower curve), p_T, and $2p_T$ (upper curve). In all figures, the normalization error of 9.6% is not shown[56].

where dN_{AB}^{P} is the differential yield of a point-like process P in a $A+B$ collision and $d\sigma_{NN}^{P}$ is the cross section of P in $N+N$ collision. If there are no initial- or final-state effects that modify the yield of P in $A+B$ collisions, the process P scales with $\langle T_{AB}\rangle_f$ and $R_{AB} = 1$. Sometimes, the central to peripheral ratio, R_{CP}, is used as an alternative to R_{AB}. The central to peripheral ratio is defined as

$$R_{CP} = \frac{dN^{Central}/\langle N_{coll}^{Central}\rangle}{dN^{Peripheral}/\langle N_{coll}^{Peripheral}\rangle}\,, \tag{27}$$

where $dN^{Central}$ and $dN^{Peripheral}$ are the differential yield per event of the studied process in a central and peripheral collision, respectively. If the yield of the process scales with the number of binary collisions, $R_{CP} = 1$.

5.4 Binary Scaling in $l + A$, $p + A$, and Low-Energy $A + A$

In deeply inelastic lepton scattering, where hard scattering was discovered [145–147], the cross section for μ-A collisions is indeed proportional to $A^{1.00}$ (Fig. 28). This indicates that the structure function of a nucleus of mass A is simply A times the structure function of a nucleon (with only minor deviations, $\leq 10\%$ for $0.02 \leq x \leq 0.50$ [149]), which means that the nucleus acts like an incoherent superposition of nucleons for hard scattering of leptons.

The situation is rather different in $p + A$ collisions: the cross section at a given p_T also scales as a power law, $A^{\alpha(p_T)}$ (Fig. 29), but the power $\alpha(p_T)$ is greater than 1. This is called the "Cronin Effect" [150]. The enhancement (relative to $A^{1.00}$) is thought to be due to the multiple scattering of the incident partons while passing through the nucleus A before the collision [151,152], which smears the axis of the hard scattering relative to the axis of the incident beam, leading to the characteristic "Cronin Effect" shape for $R_A(p_T)$ (Fig. 30). At low $p_T < 1$ GeV/c, the cross-section is no longer point like, so the scattering is shadowed ($\propto A^{2/3}$), thus $R_A < 1$. At larger $p_T > 2$ GeV/c, as the hard-scattering, power-law p_T spectrum begins to dominate, the multiple scattering smears the spectrum to larger p_T leading to an enhancement relative to binary-scaling which dissipates with increasing p_T as the influence of the multiple scattering diminishes.

Previous measurements of high-p_T particle production in $A + A$ collisions at $\sqrt{s_{NN}} \leq 31$ GeV (Fig. 31) and in $p+A$ (or $d+A$) collisions (Fig. 30) including measurements at RHIC [58] at mid-rapidity (Fig. 32) all show binary scaling or a Cronin effect.

This establishes that the initial condition for hard scattering at RHIC at

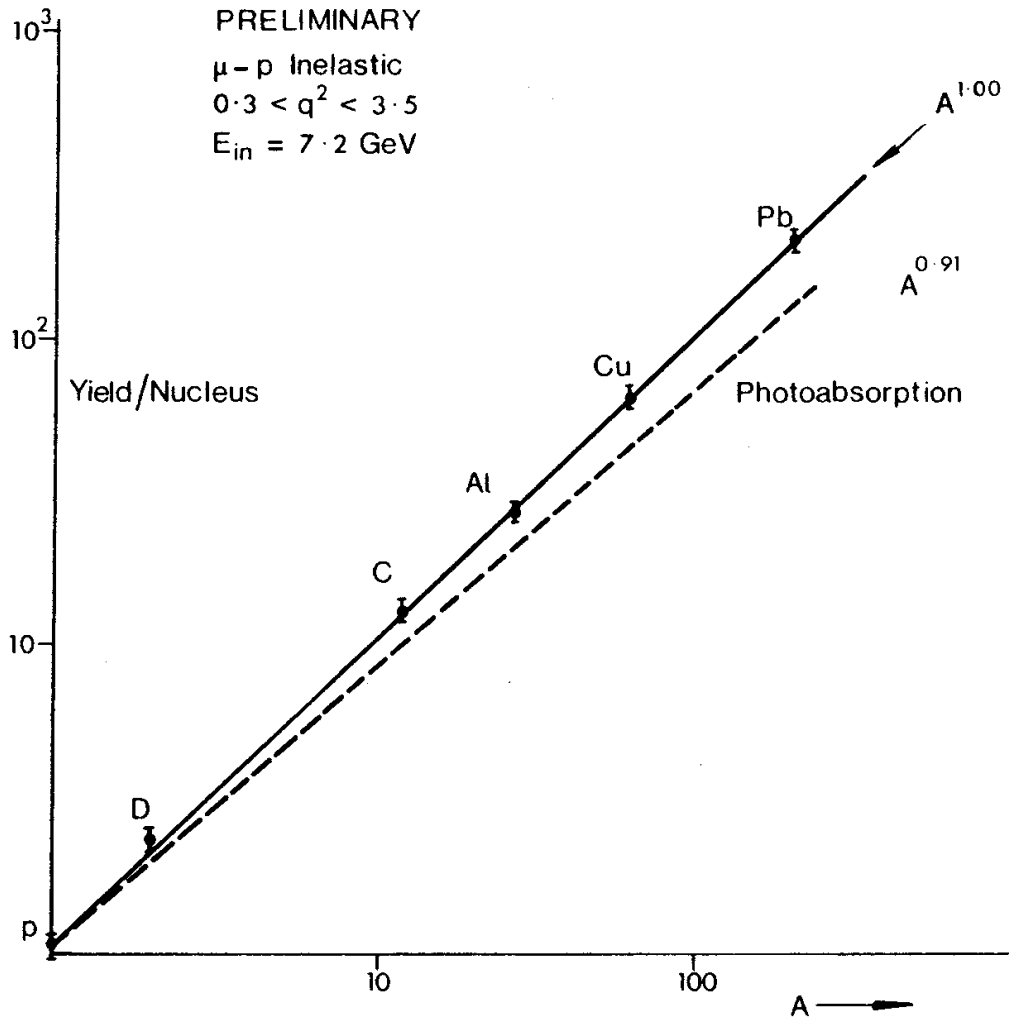

Fig. 28. μ-A cross section vs. A [148].

mid-rapidity is an incoherent superposition of nucleon structure functions, including gluons, where multiple scattering before the hard collision smears the p_T spectrum of scattered particles to be somewhat above the simple point-like binary (N_{coll}) scaling.

An alternative view of the initial state of a nucleus at RHIC is provided by the color glass condensate (CGC), in which the gluon population at low x is not an incoherent superposition of nucleon structure functions but is limited with increasing A by non-linear gluon-gluon fusion resulting from the overlap of gluons from several nucleons in the plane of the nucleus transverse to the collision axis [159]. A Cronin effect in d+A collisions, as shown in Fig. 32, can be reproduced in the CGC with a suitable choice of initial state parameters, which must also reproduce quantitatively the observed binary scaling of the direct photon production and total charm production in Au+Au collisions to be shown below (Figs. 33, 34). However, at this writing, no detailed quantita-

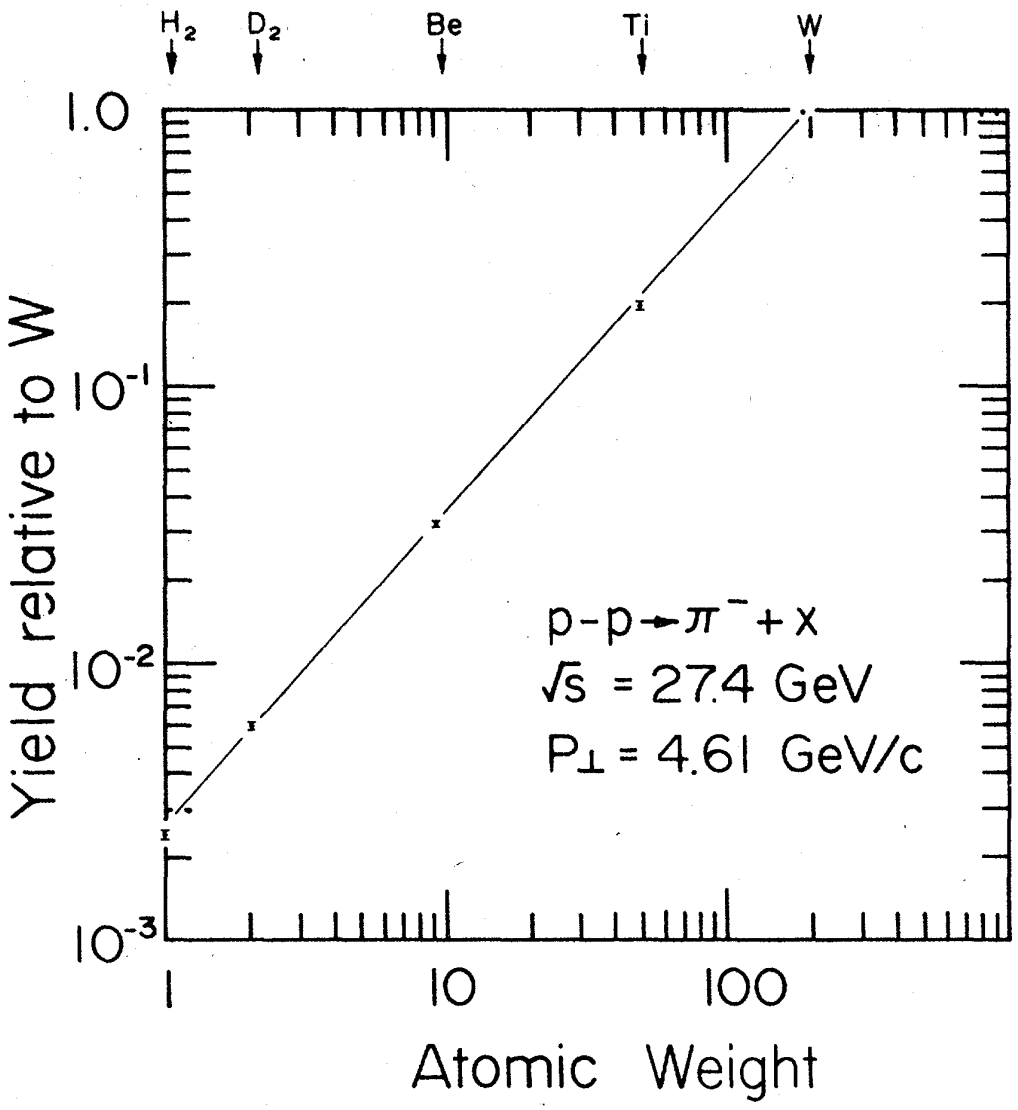

Fig. 29. Cronin Effect in $p+A$, for π^- with $p_T = 4.61$ GeV/c. $\alpha(p_T) = 1.148 \pm 0.010$ [150].

tive description of the CGC initial state which satisfies these three conditions has been published.

5.5 Binary Scaling in Au+Au Collisions at RHIC—Direct Photons and Charm Yield

The production of hard photons in Au+Au collisions at RHIC via the constituent reactions (e.g. $g + q \to \gamma + q$) is a very important test of QCD and the initial state, because the photons only interact electromagnetically, hence hardly at all, with any final-state medium produced. The direct-photon cross section and centrality dependence should then reflect only the properties of the

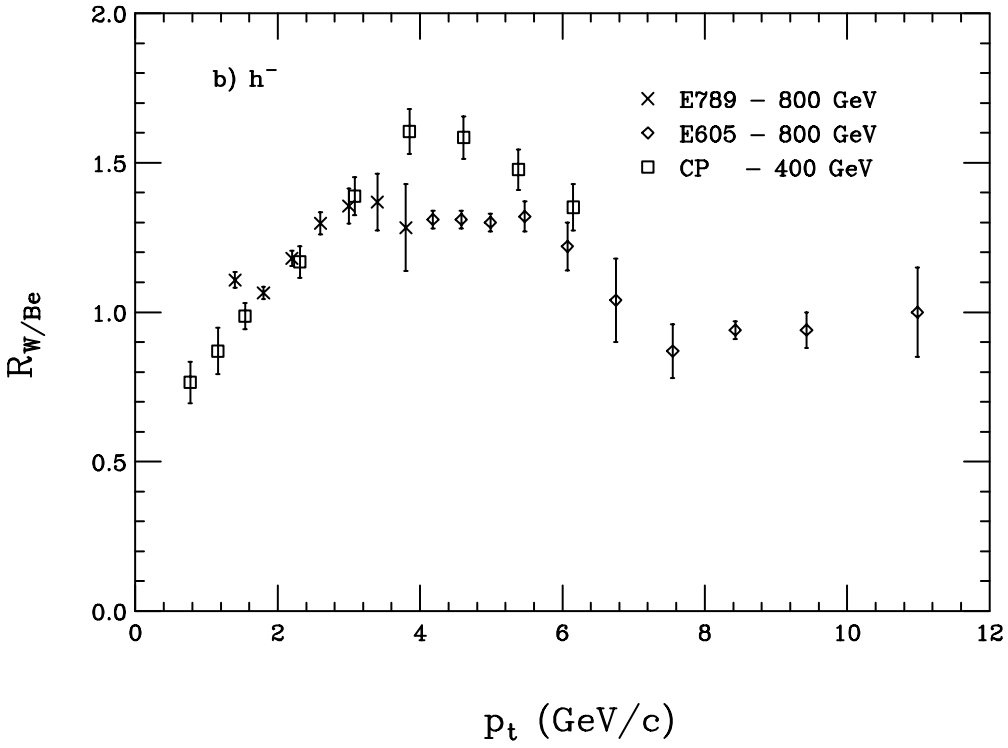

Fig. 30. Cronin effect at fixed target energies expressed as $R_{\mathrm{W/Be}}$, the ratio of the point-like scaled cross sections in $p + W$ and $p + Be$ collisions vs. p_T [153].

initial state, notably the product of the gluon and quark structure functions of the Au nuclei.

The first measurement of direct photon production in Au+Au collisions at RHIC was presented by the PHENIX collaboration at Quark Matter 2004 (Fig. 33) [165]. The data exhibit pure point-like (N_{coll}) scaling as a function of centrality relative to a pQCD calculation for $p+p$ collisions. The statistical and systematic errors still leave some room for a small Cronin effect and/or some thermal photon production. The observation of direct photon production establishes the importance of gluon degrees of freedom at RHIC.

PHENIX measured the single-electron yield from nonphotonic sources in Au+Au collision at 130 GeV [42] and 200 GeV [166]. Since semi-leptonic decay of charm is the dominant source of the non-photonic electrons at low p_T ($p_T \leq 3$ GeV/c), the total yield of charm can be determined from the integrated yield of non-photonic electrons in the low-p_T region. Figure 34 shows the yield of non-photonic electrons ($0.8 < p_T < 4.0$ GeV/c) per NN collision in Au+Au reactions at $\sqrt{s_{NN}} = 200$ GeV as a function of N_{coll} [166]. The N_{coll} dependence of the yield is fit to N_{coll}^{α}, where $\alpha = 1$ is the expectation for binary scaling. We find $\alpha = 0.938 \pm 0.075(\mathrm{stat.}) \pm 0.018(\mathrm{sys.})$, showing that the total yield of charm-decay electrons is consistent with binary scaling. It should

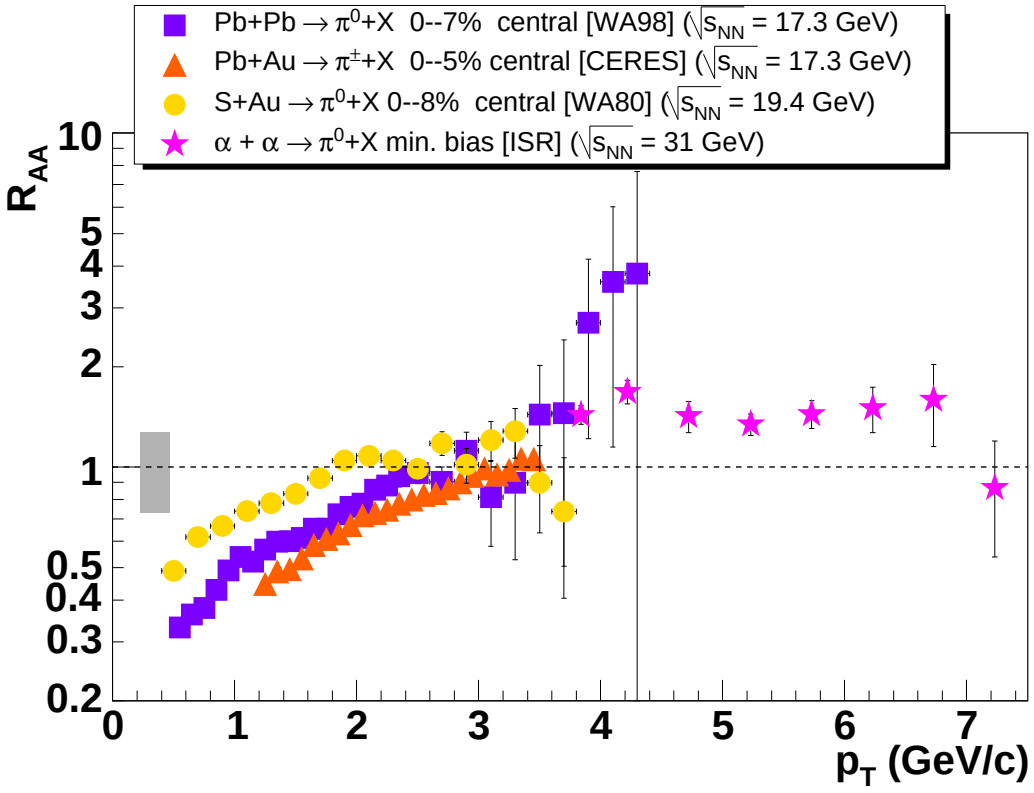

Fig. 31. Nuclear modification factors for π^0 production at the CERN-ISR in minimum-bias $\alpha + \alpha$ reactions at $\sqrt{s_{NN}} = 31$ GeV [154] and for pion production at the CERN-SPS in central Pb+Pb [155], Pb+Au [156], and S+Au [157] reactions at $\sqrt{s_{NN}} \approx 20$ GeV. The R_{AA} from SPS are obtained using the p+p parametrization proposed in ref. [158]. The shaded band around $R_{AA} = 1$ represents the overall fractional uncertainty of the SPS data (including in quadrature the 25% uncertainty of the p+p reference and the 10% error of the Glauber calculation of N_{coll}). There is an additional overall uncertainty of ±15% for the CERES data not shown in the plot [156].

be noted that medium effects, such as energy loss of charm in the dense hot medium, can only influence the momentum distribution of charm, and have little effect on the total yield of charm. Initial-state effects, such as shadowing, and other effects, such as thermal production of charm, are believed to be very small for charm production at RHIC energy. Therefore, the observation of binary scaling of the total charm yield in Au+Au collisions at RHIC may also be considered as an experimental verification of the binary scaling of a point-like pQCD process.

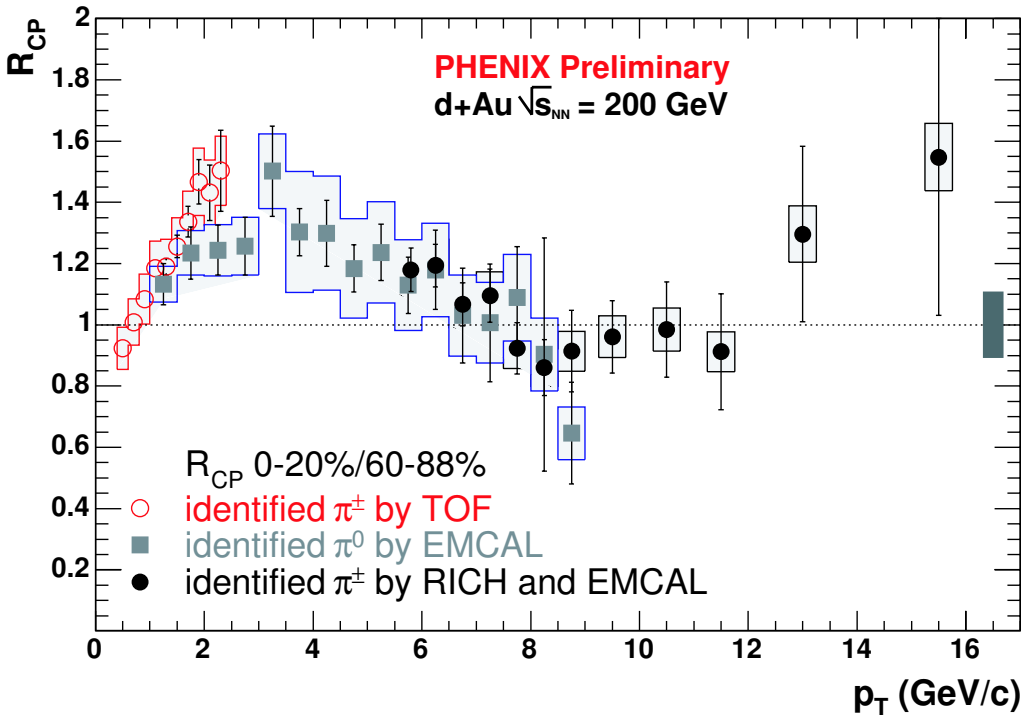

Fig. 32. Cronin effect in R_{CP}, the ratio of point-like scaled central to peripheral collisions for pions in d+Au at $\sqrt{s_{NN}} = 200$ GeV. Data points for low p_T are $\pi^{\pm}$ identified by Time of Flight (TOF). Data at medium p_T are for π^0 identified by reconstruction in the Electromagnetic Calorimeter (EMCAL). Highest p_T data are for $\pi^{\pm}$ identified by a count in the Ring Imaging Cerenkov Counter (RICH) and a deposited energy/momentum and shower shape in the EMCAL inconsistent with those of a photon or electron. The shaded band on the right represents the overall fractional systematic uncertainty due to N_{coll}.

5.6 Conclusions

In this section evidence has been presented to show that the initial condition for hard-scattering at RHIC at mid-rapidity is an incoherent superposition of nucleon structure functions, including gluons, where multiple scattering before the hard collision can smear the p_T spectrum of scattered particles to be somewhat above the simple point-like binary (N_{coll}) scaling. This was demonstrated using the reactions: pion production in d+Au collisions, where there is no final-state medium, and direct photon production in Au+Au collisions, where the outgoing photons interact electromagnetically, hence hardly at all, with any final-state medium produced. The total charm yield in Au+Au, a reaction dominated by the subprocess $g + g \rightarrow c + \bar{c}$, and which is not sensitive to final-state medium effects for the total yield of $c + \bar{c}$ pairs, also exhibits binary scaling. The latter two measurements provide experimental evidence for the binary scaling of point-like pQCD processes in Au+Au collisions.

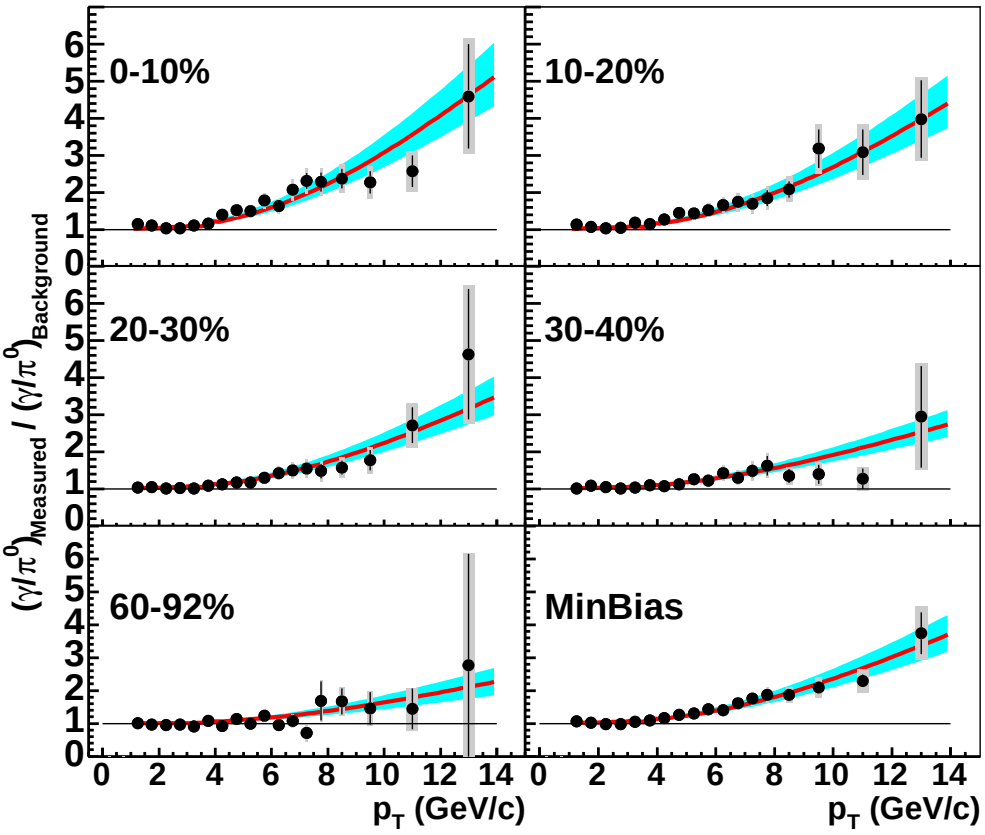

Fig. 33. PHENIX direct photon measurements relative to the background for for minimum bias and for five centralities of Au+Au collisions at $\sqrt{s_{NN}}$ = 200 GeV (0-10% is the most central). Statistical and total errors are indicated separately on each data point by the vertical bar and shaded region, respectively. The curves represent a pQCD calculation of direct photons in $p + p$ collisions from Vogelsang [160–163] scaled to Au+Au assuming pure point-like ($N_{\rm coll}$) scaling, with no suppression. The shaded region around the curves indicate the variation of the pQCD calculation for scale changes from $p_T/2$ to $2p_T$, plus the $\langle N_{coll} \rangle$ uncertainty [164].

The color glass condensate (CGC) provides an alternative view of the initial state of a nucleus at RHIC in which coherence of gluons due to non-linear gluon-gluon fusion can produce a Cronin-like effect, depending on the initial conditions and the kinematic range covered. However, at the present writing, there is no CGC description of the initial state nuclear structure function which reproduces the observed Cronin effect for pions in d+Au collisions and the observed binary scaling for both direct photon production and the total charm yield in Au+Au collisions.

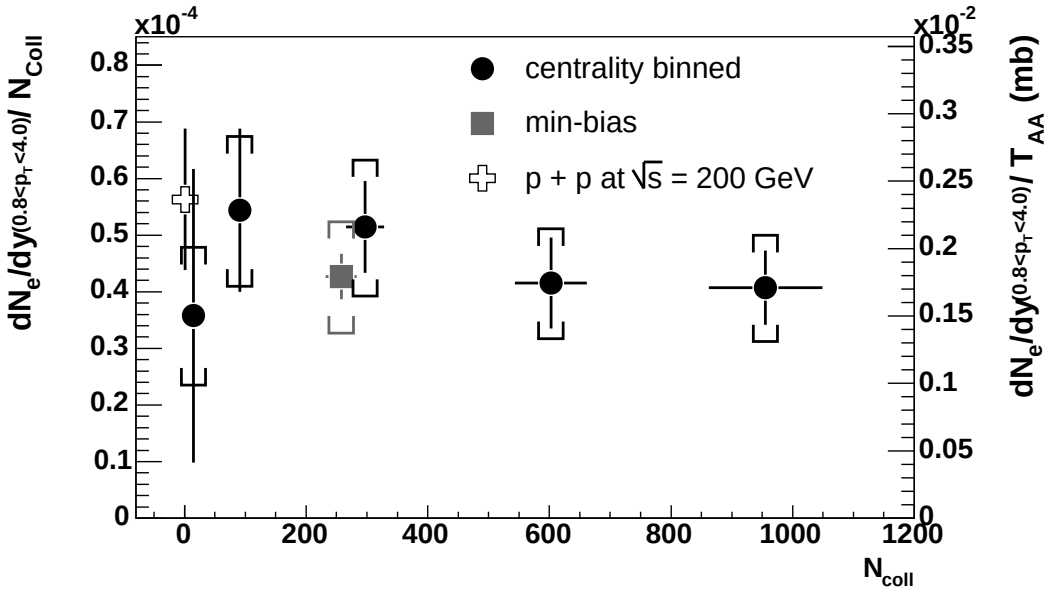

Fig. 34. Non-photonic electron yield ($0.8 < p_T < 4.0$ GeV/c), dominated by semi-leptonic charm decays, measured in Au+Au collisions at $\sqrt{s_{NN}} = 200$ GeV scaled by N_{coll} as a function of N_{coll}. The right-hand scale shows the corresponding electron cross section per NN collision in the above p_T range. The yield in $p + p$ collision at 200 GeV is also shown [166].

6 NUMBER DENSITY AND HIGH p_T SUPPRESSION

To study the initial properties of the matter created in heavy ion collisions we need a probe that is already present at earliest times and that is directly sensitive to the properties of the medium. Partons resulting from hard scatterings during the initial crossing of the two nuclei in A+A collisions provide such a probe. Energetic partons propagating through a dense medium are predicted to lose energy [167–175] thus producing a suppression in the yield of high-p_T hadrons produced from the fragmentation of these partons. Initial measurements from RHIC Run 1 [39,47,176] and Run 2 [49,53,177,178] demonstrated such a suppression, and the results of d+Au measurements [58,61,60,59] showed that the suppression was not due to initial-state effects. Further measurements have indicated a modification of di-jet angular correlations [61] that has also been attributed to in-medium parton energy loss [179,180].

While the energy loss of hard-scattered partons was originally proposed as a signature of the quark-gluon plasma and deconfinement, it has been argued recently that the energy loss is sensitive only to the density of unscreened color charges and not directly to deconfinement [171–175,181,182]. Ideally, a measurement of initial parton densities together with constraints on initial energy density might allow an estimate of the temperature of the medium. As will be seen below, the current high-p_T measurements and theoretical tools for

interpreting the experimental data are not yet sufficient to take such a step. Instead, the energy loss results are currently being used to provide estimates of the initial energy density. The remainder of this section summarizes PHENIX experimental data related to high-p_T suppression, discusses the current state of theoretical understanding of the energy loss process and concludes with a statement of estimates for initial parton number and energy densities that currently can be made.

6.1 Single particle spectra, R_{AA}

As described in Section 5, in the absence of modifications due to initial-state or final-state effects, the rate for the production of particles through hard-scattering processes in nucleus-nucleus collisions is expected to be given by the equivalent $p+p$ hard-scattering cross section multiplied by T_{AB}. Figure 35 shows PHENIX π^0 spectra, d^2N/dp_Tdy, measured in 200 GeV [49] peripheral (80–92%) and central (0–10%) Au+Au collisions compared to measured [56] $p+p$ cross sections multiplied by the peripheral and central T_{AB} values estimated using the procedure described in Section 5. The error bands on the $p+p$ data points reflect both the systematic errors on the $p+p$ cross sections and the uncertainties in the T_{AB} values. As the figure clearly demonstrates, the central Au+Au π^0 yields are strongly suppressed relative to the "expected" yields over the entire measured p_T range. In contrast, the peripheral yields compared to the T_{AB}-scaled $p+p$ cross sections show little or no suppression. The results incontrovertibly demonstrate that there is a strong and centrality-dependent suppression of the production of high-p_T pions relative to pQCD-motivated expectations. This is quite different from measurements of R_{AA} in Pb+Pb collisions at $\sqrt{s_{NN}} = 17.3$ GeV where in semi-peripheral Pb+Pb collisions there is a nuclear enhancement increasing with p_T similar to the well-known Cronin effect, while in central collisions the Cronin enhancement appears to be weaker than expected.

To better quantitatively demonstrate the suppression in central collisions indicated in Fig. 35, we show in Fig. 36 $R_{AA}(p_T)$ for mid-rapidity π^0's in central and peripheral 200 GeV Au+Au collisions. We also show the values obtained from minimum-bias 200 GeV d+Au collisions [58] which provide a stringent test of the possible contribution of initial-state nuclear effects to the observed suppression in Au+Au collisions. The error bands on the data indicate combined statistical and point-to-point systematic errors and the bars shown next to the different data sets indicate common systematic errors due to uncertainties in the $p+p$ cross section normalization and T_{AB}.

Figure 36 shows that the central Au+Au π^0 suppression changes only slightly over the measured p_T range and reaches an approximately p_T-independent

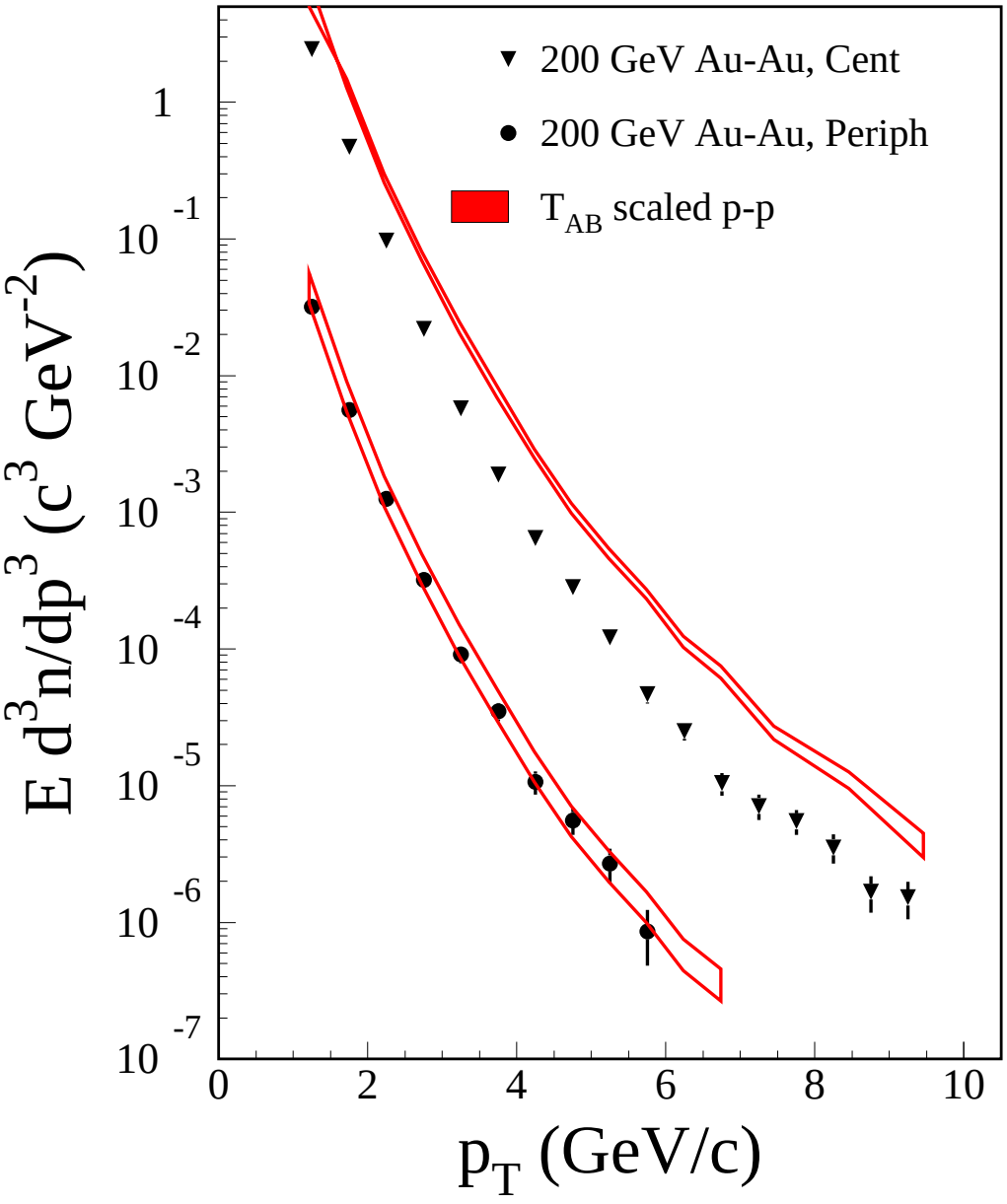

Fig. 35. π^0 p_T spectra in 200 GeV Au+Au collisions [49] compared to a T_{AB} scaling of the 200 GeV $p+p$ π^0 differential cross section [56]. The central data were obtained with a 0–10% centrality cut while the peripheral data were obtained with an 80–92% cut.

factor of 5 ($R_{AA} \approx 0.2$) for $p_T > 4-5$ GeV/c. The peripheral Au+Au R_{AA} values are consistent with one after taking into account systematic errors but we cannot rule out a slight suppression suggested by the peripheral R_{AA} values. In all of the data sets R_{AA} decreases with decreasing p_T for $p_T < 2$ GeV/c. This decrease, known since the original measurements of the A dependence of particle production in pA collisions is due to contributions of soft hadronic processes at low p_T that are expected to increase more slowly than proportional to T_{AB}. The d+Au R_{dA} values are also consistent with one within systematic uncertainties, but in contrast to the Au+Au results, the data suggests a slight

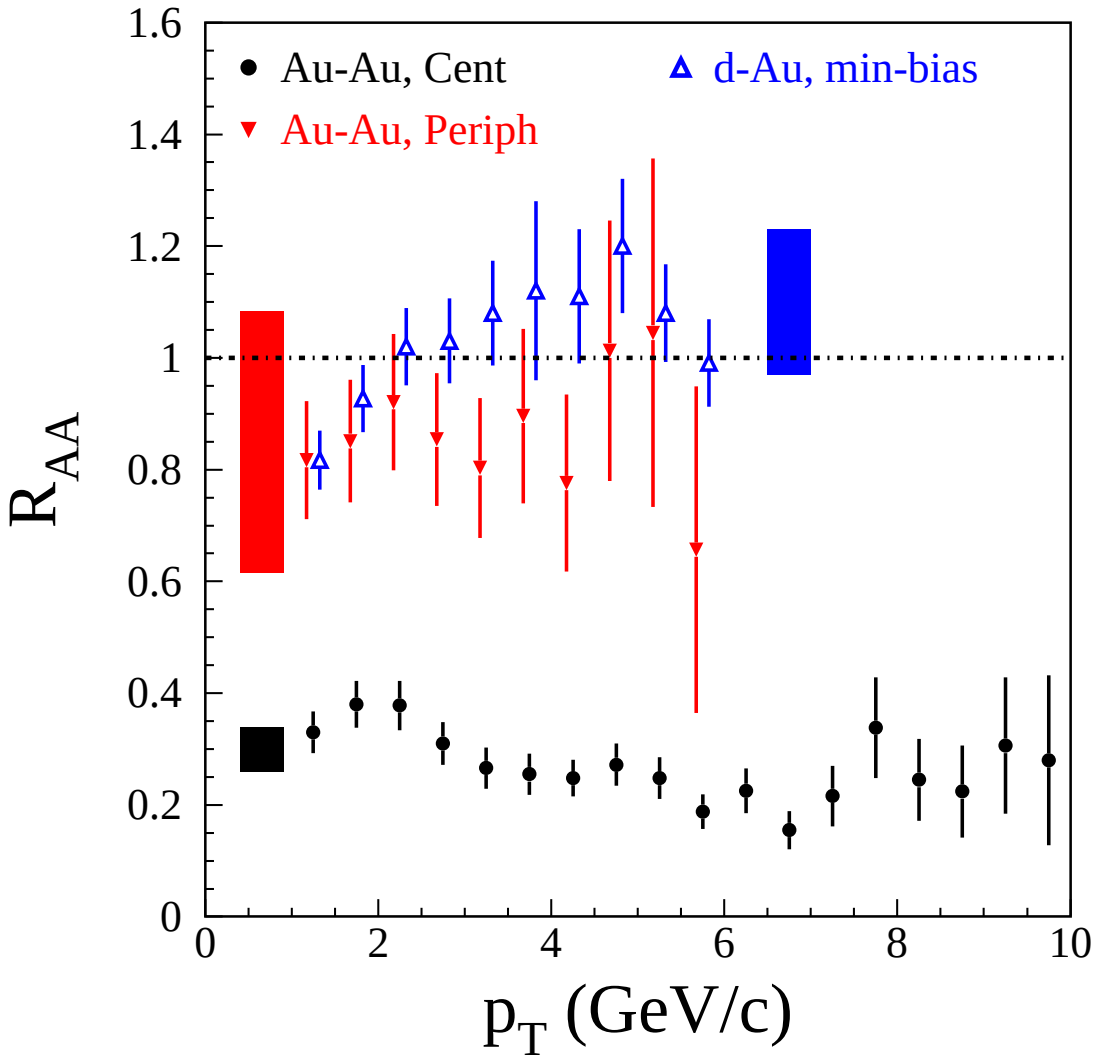

Fig. 36. π^0 $R_{AA}(p_T)$ for central (0–10 %) and peripheral (80–92 %) Au+Au collisions [49] and minimum-bias d+Au collisions [58]. The shaded boxes on the left show the systematic errors for the Au+Au R_{AA} values resulting from overall normalization of spectra and uncertainties in T_{AB}. The shaded box on the right shows the same systematic error for the d+Au points.

enhancement. The d+Au R_{dA} values above 2 GeV/c exceed one for nearly the entire experimentally covered p_T range. As shown previously in Fig. 32, only for $p_T \gtrsim 6$ GeV/c does the d+Au pion yield return to the T_{AB}-scaling expectation. Such a small enhancement is consistent with expectations based on prior measurements of the Cronin effect [183,184], and it is also quantitatively consistent with calculations incorporating the initial-state multiple scattering that is thought to produce the Cronin effect [185–191]. Therefore the Cronin effect at RHIC cannot mask a strong initial-state suppression of the parton distributions in the Au nucleus [192].

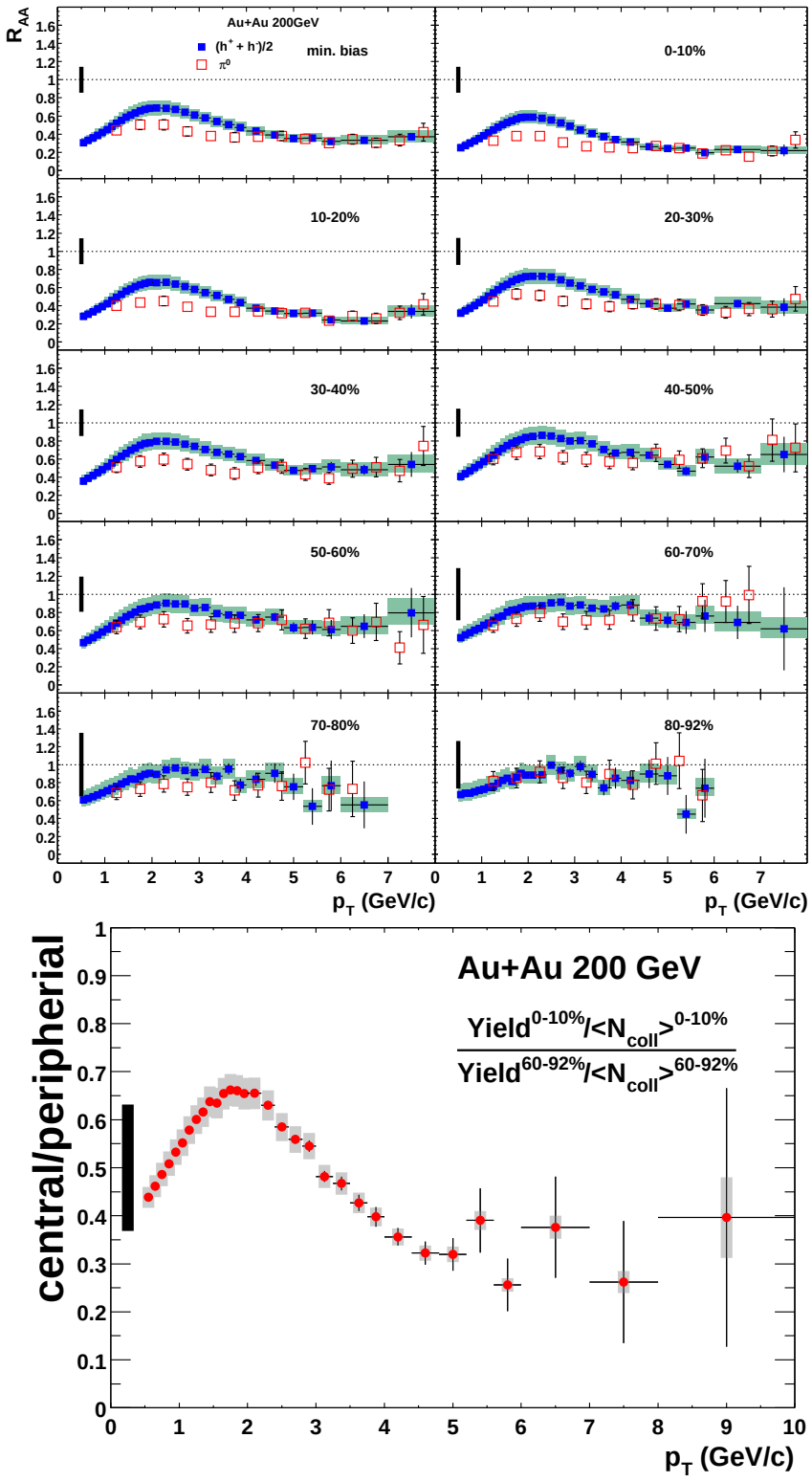

Fig. 37. Centrality and p_T dependence of nuclear modification factors in 200 GeV Au+Au collisions[53]. Top panel: π^0 and charged particle $R_{AA}(p_T)$ for ten centrality bins. Bottom panel: charged particle R_{CP} vs. p_T.

To better demonstrate the systematic behavior of the high-p_T suppression we show in Fig. 37 π^0 [49] and unidentified charged particle R_{AA} values [53] as a function of p_T for various centrality bins. While for moderate p_T values ($2 < p_T < 5$ GeV/c) total charged particle production is suppressed less than pion production, the charged particle and π^0 R_{AA} values become equal, within errors, at high p_T. This evolution in the charged particle suppression is related to contributions from the (anti)protons that will be discussed further below. Despite the differences resulting from the protons, the charged particles and π^0's exhibit very similar trends in the suppression vs. p_T and vs. centrality. The suppression increases smoothly with centrality though the change in R_{AA} values at high p_T is most rapid in the middle of the centrality range. Figure 37 also shows that the suppression is approximately constant as a function of p_T for $p_T > 4.5$ GeV/c in all centrality bins. We take advantage of this feature of the data to better illustrate the centrality dependence of the suppression by integrating both the Au+Au spectra and the reference $p+p$ cross sections over $p_T > 4.5$ GeV/c and using these integrated quantities to determine an average suppression factor, R_{AA} for $p_T > 4.5$ GeV/c. We plot the charged particle and π^0 R_{AA} values vs. $N_{\rm part}$ in Fig. 38(top). This figure suggests that the suppression evolves smoothly with $N_{\rm part}$, showing no abrupt onset of suppression. The charged particles and π^0's exhibit similar evolution of suppression with $N_{\rm part}$. In the most central collisions we obtain R_{AA} values of $0.24 \pm 0.04(total)$ and $0.23 \pm 0.05(total)$ for charged particles and π^0's respectively. In peripheral collisions, R_{AA} approaches one, but the systematic errors on the most peripheral T_{AB} values are sufficiently large that we cannot rule out $\sim 20\%$ deviations of the peripheral Au+Au hard-scattering yields from the T_{AB}-scaled $p+p$ cross sections.

An alternative method for evaluating the evolution of the high-p_T suppression with centrality is provided in Fig. 38(bottom) which presents the charged and π^0 yields per participant integrated over $p_T > 4.5$ GeV/c as a function of $N_{\rm part}$ [53] divided by the same quantity in $p+p$ collisions. Also shown in the figure are curves demonstrating the $N_{\rm part}$ dependence that would result if the π^0 and charged particle yields exactly T_{AB} scaled and what an $N_{\rm part}$ scaling from $p+p$ collisions would imply. As Fig. 38 demonstrates, the high-p_T yields of both charged hadrons and π^0's *per participant* increase proportional to T_{AB} for small $N_{\rm part}$ but level off and then decrease with increasing $N_{\rm part}$ in more central collisions. The PHENIX measurements do not naturally support an approximate $N_{\rm part}$ scaling of high-p_T particle production suggested in an analysis of PHOBOS data. The PHENIX $R_{AA}^{N_{\rm part}}$ values decrease from mid-peripheral ($N_{\rm part} \approx 75$) to central collisions by an amount larger than the systematic errors in the measurement. For more peripheral collisions, $R_{AA}^{N_{\rm part}}$ increases with $N_{\rm part}$ consistent with the modest suppression of high-p_T production shown for peripheral collisions in the top panel of Fig. 38. The initial rise and subsequent decrease of $R_{AA}^{N_{\rm part}}$ with increasing $N_{\rm part}$ suggests that the high-p_T hadron yield

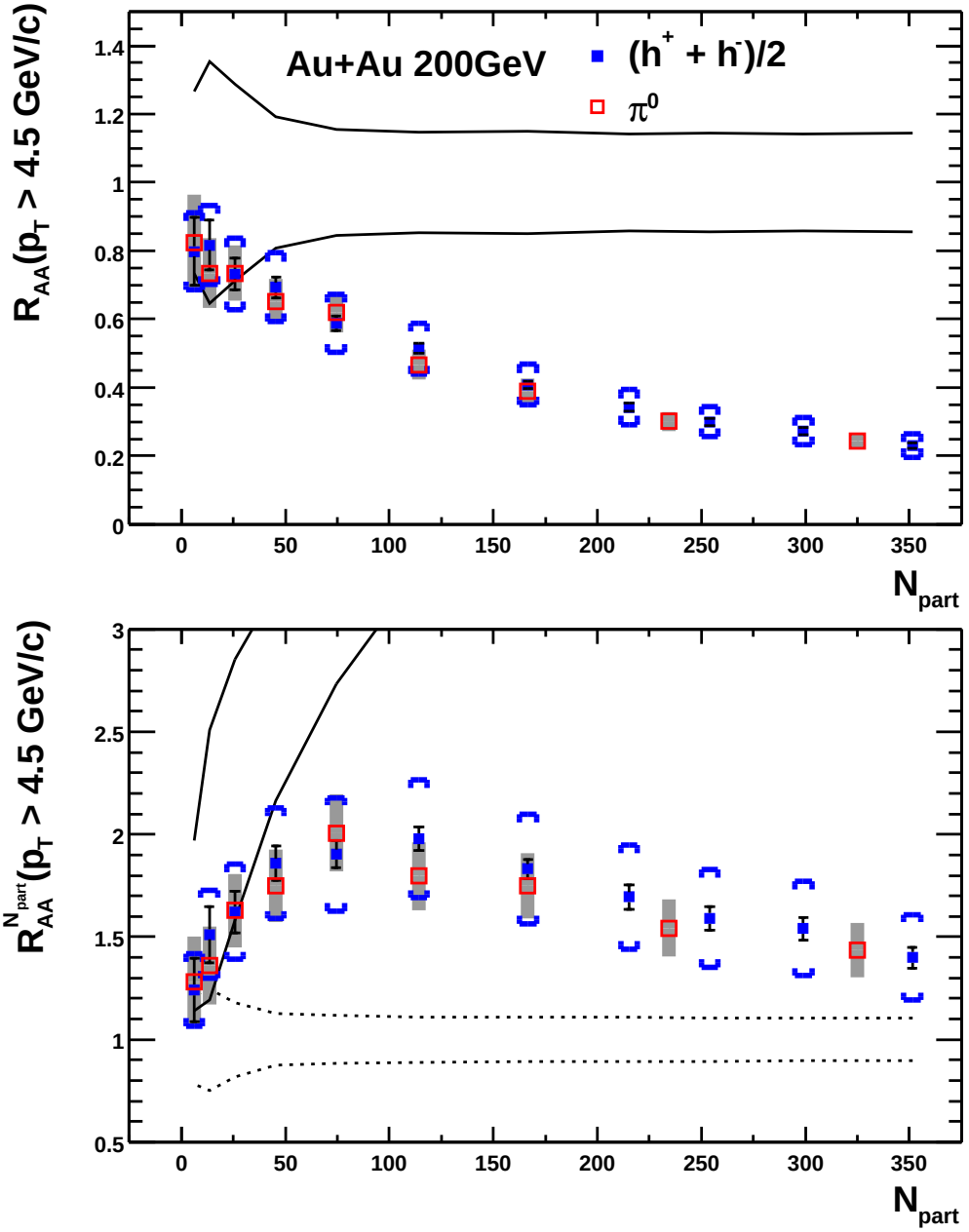

Fig. 38. Top panel: R_{AA} vs. $N_{\rm part}$ obtained from p_T-integrated ($p_T > 4.5$ GeV/c) Au+Au π^0 and charged-hadron spectra. The band indicates the systematic error bands on a hypothetical T_{AB} scaling of the $p+p$ p_T-integrated cross section. Bottom panel: π^0 and charged hadron yield per participant vs. $N_{\rm part}$ divided by the same quantity in $p+p$ collisions ($R_{AA}^{N_{\rm part}}$). The solid band shows the same band as in the top panel expressed in terms of yield per participant pair while the dashed band indicates the systematic error bands around a hypothetical $N_{\rm part}$ scaling. Both plots are from [53].

in Au+Au collisions has no simple dependence on $N_{\rm part}$. The observation that the high-p_T yields initially increase proportional to T_{AB} demonstrates that in the most peripheral Au+Au collisions the hard-scattering yields are consistent with point-like scaling. However, the deviation from T_{AB} scaling sets in rapidly, becoming significant by $N_{\rm part} = 50$. By $N_{\rm part} = 100$ the high-p_T suppression is so strong that high-p_T yields grow even more slowly than proportional to $N_{\rm part}$.

6.2 x_T scaling in Au+Au collisions at RHIC

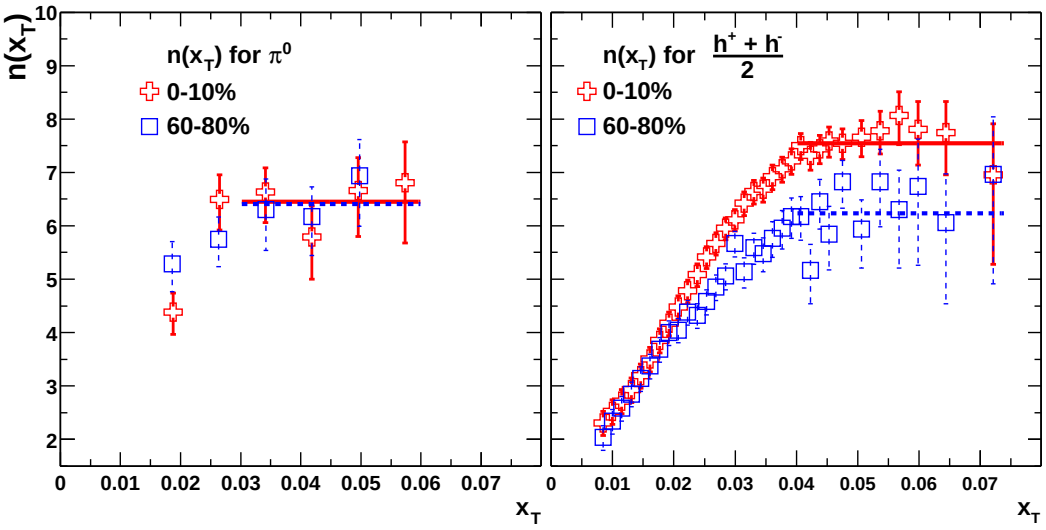

Fig. 39. Power-law exponent $n(x_T)$ for π^0 and h spectra in central and peripheral Au+Au collisions at $\sqrt{s_{NN}} = 130$ and 200 GeV [53].

If the production of high-p_T particles in Au+Au collisions is the result of hard scattering according to pQCD, then x_T scaling should work just as well in Au+Au collisions as in $p + p$ collisions and should yield the same value of the exponent $n(x_T, \sqrt{s})$. The only assumption required is that the structure and fragmentation functions in Au+Au collisions should scale, in which case Eq. 23 still applies, albeit with a $G(x_T)$ appropriate for Au+Au. In Fig. 39, $n(x_T, \sqrt{s_{NN}})$ in Au+Au is derived from Eq. 23, for peripheral and central collisions, by taking the ratio of $Ed^3\sigma/dp^3$ at a given x_T for $\sqrt{s_{NN}} = 130$ and 200 GeV, in each case. The π^0's exhibit x_T scaling, with the same value of $n = 6.3$ as in p+p collisions, for both Au+Au peripheral and central collisions, while the non-identified charged hadrons x_T-scale with $n = 6.3$ for peripheral collisions only. Notably, the $h^{\pm}$ in Au+Au central collisions exhibit a significantly larger value of n, indicating different physics, which will be discussed below. The x_T scaling establishes that high-p_T π^0 production in peripheral and central Au+Au collisions and $h^{\pm}$ production in peripheral Au+Au collisions follow pQCD as in $p + p$ collisions, with parton distributions and fragmenta-

tion functions that scale with x_T, at least within the experimental sensitivity of the data.

6.3 Two-hadron azimuthal-angle correlations

We argued in Sec. 5 that the production of hadrons at high-p_T results predominantly from hard scattering followed by fragmentation of the outgoing parton(s). While this result is well established in $p(\bar{p}) + p$ collisions, it might not be true in Au+Au collisions when the yield of high-p_T particles is modified so dramatically compared to expectations. Since a hard-scattered parton fragments into multiple particles within a restricted angular region (i.e. a jet) a reasonable way to check the assumption that high-p_T hadron production in Au+Au collisions is due to hard scattering is to directly observe the angular correlations between hadrons in the jets. None of the experiments at RHIC are currently capable of reconstructing jets in the presence of the large soft background of a Au+Au collision. However, both STAR [193,194] and PHENIX [195,196] have directly observed the presence of jets by studying two-hadron azimuthal-angle correlations. Figure 40 shows preliminary distributions [195] of the relative azimuthal angle ($\Delta\phi$) between pairs of charged particles detected within the PHENIX acceptance in d+Au collisions and peripheral (60–90%) and central (0–10%) Au+Au collisions after the subtraction of combinatoric background. The pairs of particles are chosen such that one particle lies within a "trigger" p_T range ($2.5 < p_{T\,\mathrm{trig}} < 4$ GeV/c) while the other "associated" particle falls within a lower p_T window $1.0 < p_T < 2.5$ GeV/c. The distributions show the differential yield per $\Delta\phi$ of associated particles per detected trigger particle within the given p_T ranges and within the η acceptance of the PHENIX central arms ($-0.35 < \eta < 0.35$).

The peaks observed at $\Delta\phi = 0$ (near side) reflect the correlation between hadrons produced within the same jet while the broader peaks observed at $\Delta\phi = \pi$ (away side) reflect the correlations between hadrons produced in one jet and hadrons produced in the "balance" jet. In the Au+Au cases, a $\cos 2\Delta\phi$ modulation underlies the jet angular correlations due to the elliptic flow of particles in the combinatoric background and possibly also in part due to azimuthal anisotropies in the jets themselves (see below). Nonetheless, the $\cos 2\Delta\phi$ contribution has little effect on the narrow same-jet (near-side) peak in the $\Delta\phi$ distribution.

We observe that the angular widths of the same-jet correlations are the same, within errors, in all three data sets in spite of the factor of two larger yield of associated hadrons in central Au+Au collisions compared to d+Au and peripheral Au+Au collisions. This result is demonstrated more quantitatively in Fig. 41 which shows the centrality dependence of the Gaussian widths of

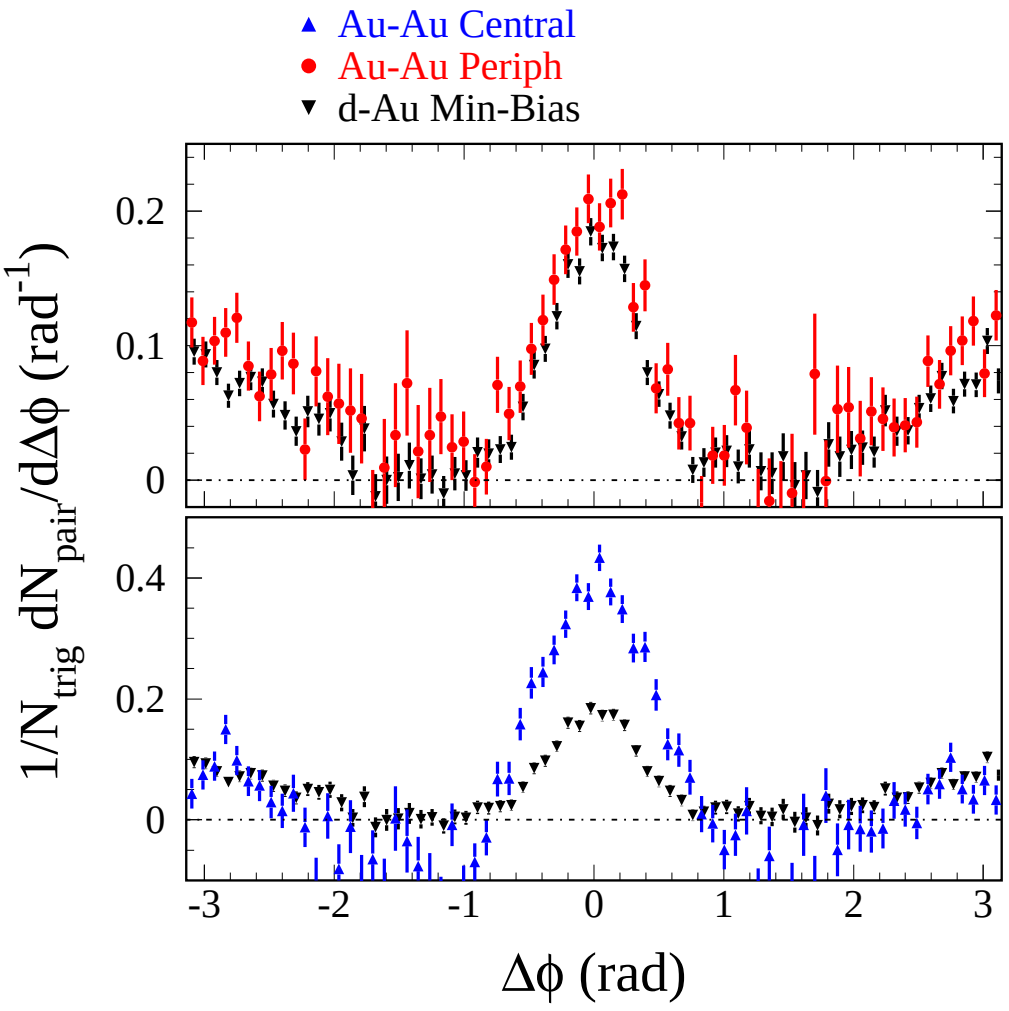

Fig. 40. Differential yields per $\Delta\phi$ and per trigger particle of pairs of charged hadrons in d+Au, peripheral Au+Au and central Au+Au collisions at $\sqrt{s_{NN}} = 200$ GeV. The pairs were selected with the higher-momentum "trigger" particle in the range $2.5 < p_T < 4.0$ GeV/c and the lower-momentum "associated" particle in the range $1.0 < p_T < 2.5$ GeV/c. A constant background has been subtracted for all three distributions.

the same-jet peaks in the Au+Au $\Delta\phi$ compared to the jet widths extracted from d+Au collisions [195]. We see that the Au+Au two-hadron correlation functions show peaks with the same jet width as d+Au collisions. Since this width is a unique characteristic of the parton fragmentation process, we conclude that high-p_T hadrons in Au+Au collisions result from hard scattering followed by jet fragmentation regardless of any medium modifications of the fragmentation multiplicity.

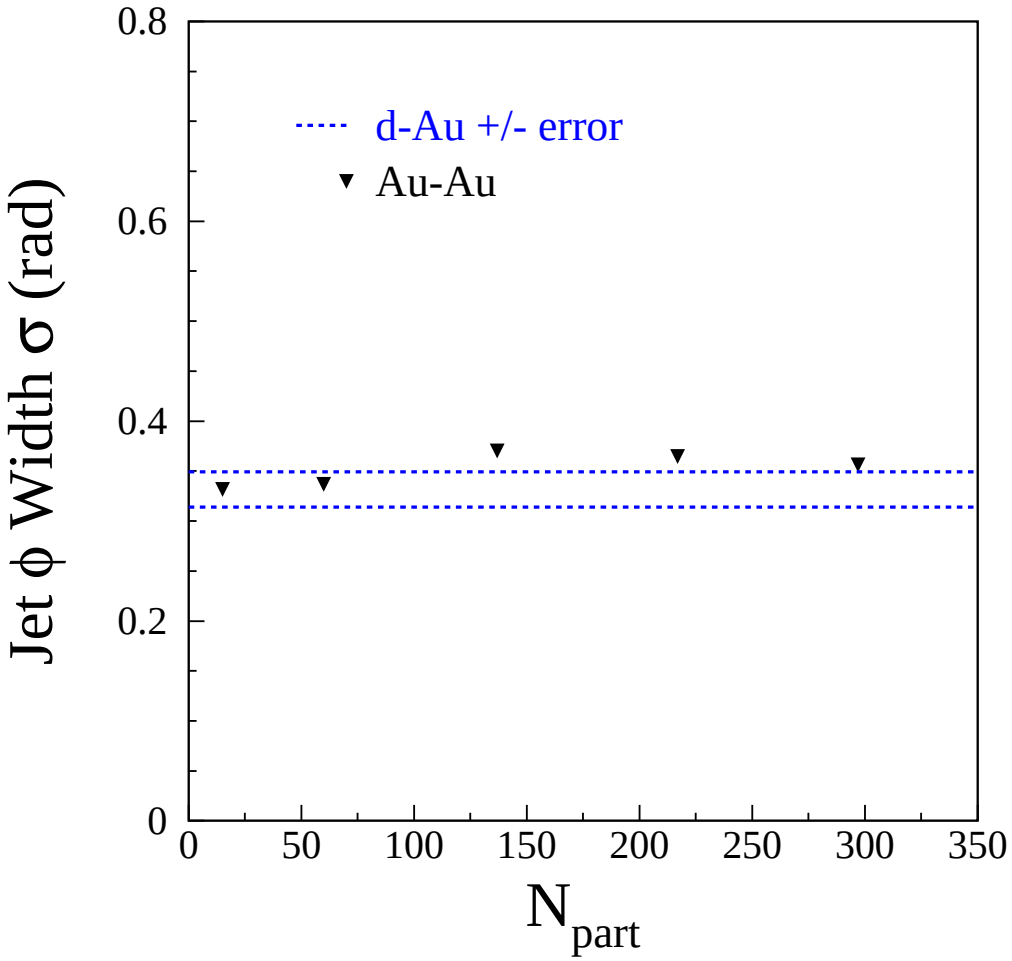

Fig. 41. The azimuthal angle width of jets in 200 GeV Au+Au collisions extracted as the σ's of Gaussian fits to the 0° peak in the two-charged-hadron azimuthal-angle ($\Delta\phi$) correlation functions [195]. The correlation functions were formed from pairs with trigger hadron in the p_T range $2.5 < p_T < 4.0$ GeV/c and the associated hadron in the range $1.0 < p_T < 2.5$ GeV/c. The dashed lines show the $\pm 1\sigma$ range of the jet widths in d+Au collisions using the same momentum bins. In the Au+Au data, the effect of the elliptic flow has been subtracted in the extraction of the jet width.

6.4 High-p_T suppression and energy loss

The suppression of the production of high-p_T hadrons in heavy ion collisions at RHIC had been predicted long before RHIC started running [167,168,170,169,171–173,197]. It is now generally accepted that partons propagating in colored matter lose energy predominantly through medium-induced emission of gluon radiation [198,199]. An energetic parton scatters off color charges in the high-parton-density medium and radiates gluon bremsstrahlung. The reduction in

the parton energy translates to a reduction in the average momentum of the fragmentation hadrons, which, in turn, produces a suppression in the yield of high-p_T hadrons relative to the corresponding yield in $p+p$ collisions. The power-law spectrum for $p_T \geq 3$ GeV/c implies that a modest reduction in fragmenting parton energy can produce a significant decrease in the yield of hadrons at a given p_T. Thus, the suppression of the yield of high-p_T hadrons is generally believed to provide a direct experimental probe of the density of color charges in the medium through which the parton passes [200,182,188]. However, before proceeding to an interpretation of our results, we briefly discuss the theoretical understanding of the radiative energy loss mechanism and limitations in that understanding.

The dominant role of radiative gluon emission was identified early on [169], but it took several years and much effort before rigorous calculations of the energy loss taking into account Landau-Pomeranchuk-Migdal suppression [170] and the time evolution of the medium were available. Initial estimates of the radiative energy loss suggested an approximately constant $\Delta E/\Delta x$ [168,170], but later calculations [171,201,174,175] showed that the quantum interference can produce a loss of energy that grows faster than linearly with the propagation path length, L, of the parton in the medium. However, this ideal growth of $\Delta E/\Delta x$ with increasing path length is never realized in heavy ion collisions due to the rapid decrease of the energy density and the corresponding color charge density with time [173,182,188,179]. Generally, all energy loss calculations predict that the fractional energy loss of a propagating parton decreases with increasing parton energy. However, the precise evolution with parton energy depends on the assumptions in the energy loss models and on the treatment of details like kinematic limits and non-leading terms in the radiation spectrum [199,198]. There are many different calculations of medium-induced energy loss currently available based on a variety of assumptions about the thickness of the medium, the energy of the radiating parton, and the coherence in the radiation process itself (see [202,199,198] for recent reviews). The p_T dependence of the PHENIX π^0 R_{AA} values has ruled out the possibility of a constant (energy independent) $\Delta E/\Delta x$ [197] and the original BDMS energy loss formulation (which the authors argued should not be applied at RHIC energies). In fact, the only detailed energy loss model that *predicted* the flat p_T dependence of R_{AA} over the p_T range covered by RHIC data was the GLV prescription [175,203–205,188]. In the GLV formulation, the fractional energy loss for large jet energies varies approximately as $\log(E)/E$ but the authors observe that below 20 GeV the full numerical calculation of the energy loss produces a nearly constant $\Delta E/E$ [199]. However, the same authors argue that the flat $R_{AA}(p_T)$ observed at high p_T at 200 GeV also requires an accidental cancellation of several different contributions including the separate p_T dependences of the quark and gluon jet contributions, the p_T dependence of the Cronin enhancement, and shadowing/EMC effect. A comparison of the GLV results for the p_T dependence of the π^0 suppression to the PHENIX data

is shown in Fig. 42.

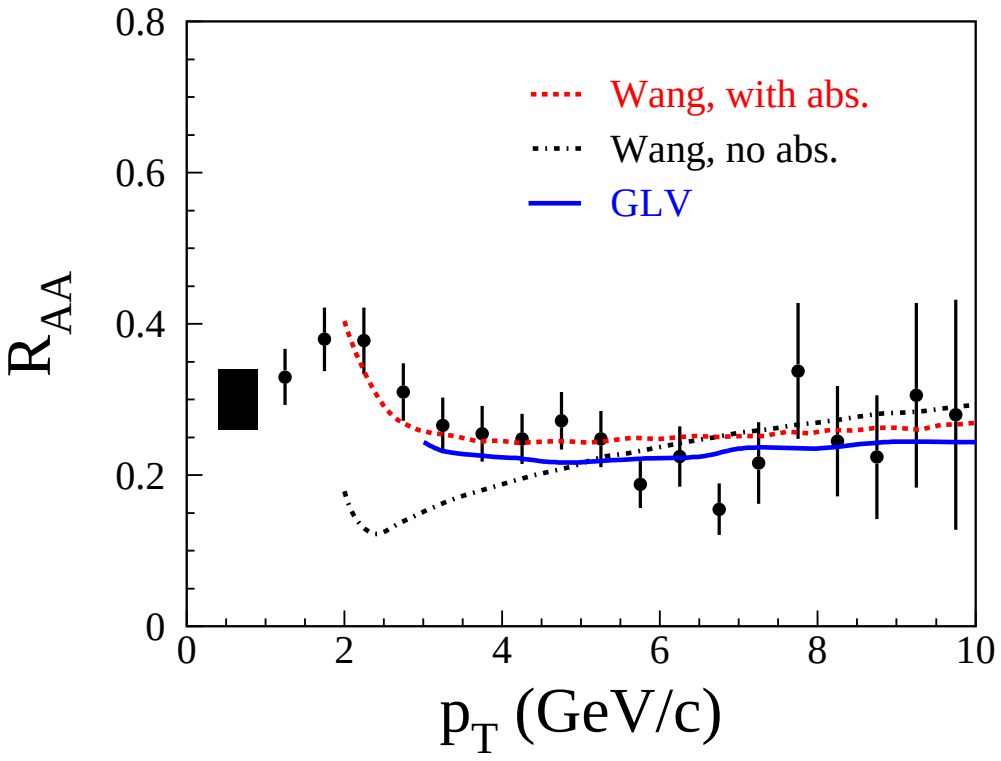

Fig. 42. Comparisons of energy loss calculations [206,179] used to extract estimates for the initial parton number or energy density (see text for details) to the central 200 GeV/c Au+Au π^0 $R_{AA}(p_T)$ measured by PHENIX. The Wang curves compare results with and without energy absorption from the medium.

One of the most critical issues in the energy loss calculation is the treatment of the time evolution of the energy density of the matter through which the radiating parton is propagating. Even if transverse expansion of the created matter is ignored, the longitudinal expansion produces a rapid reduction in the energy density as a function of time. Most energy loss calculations assume that the color charge density decreases as a function of proper time as $\rho(\tau) = \rho_0\tau_0/\tau$ in which case the measured R_{AA} can be used to infer the product $\rho_0\tau_0$. Here τ_0 represents the formation time of the partons from which the medium is composed and ρ_0 the initial number density of those partons. Since the gluons have the largest cross section for scattering with other partons, the initial color-charge density is interpreted as the gluon density. Making the usual assumption that the produced partons are spread over a longitudinal spatial width $\delta z = \tau_0\delta y$, the GLV authors relate the product $\rho_0\tau_0$ to the initial dn_g/dy and obtain $dn_g/dy = 1000 \pm 200$ from the PHENIX π^0 R_{AA} values [188]. The sensitivity of the GLV calculations to the details of the description of the transverse parton density and the transverse expansion of the matter has been tested by using the results of hydrodynamic calculations of the energy density

as a function of position and time [207]. The average energy loss for partons in central Au+Au collisions evaluated under dramatically different assumptions was shown to be remarkably insensitive to details of the description of the parton density. The GLV results are also potentially sensitive to a "screening mass" that determines both the transverse momentum distributions of the virtual gluons absorbed from the medium in the bremsstrahlung process and an energy cutoff for the radiated gluons. This mass is related to the local energy density using lattice QCD calculations of the plasma screening mass [188]. However, it was shown by the authors that a factor of two change in the screening mass produces only a 15% change in the dn_g/dy needed to describe the data.

An alternative analysis of parton energy loss [208] starts from explicit calculation of higher-twist matrix elements for $e + A$ collisions that account for coherent rescattering of the struck quark in the nucleus. The contributions of these higher-twist terms can be incorporated into modified jet fragmentation functions, producing an effective energy loss. This calculation can reproduce [182] the HERMES measurements of modified jet fragmentation in nuclear deep-inelastic scattering [209]. By relating the modified fragmentation functions from the higher-twist calculation to energy-loss results obtained from the leading term in an opacity expansion calculation (e.g. GLV) of medium-induced energy loss the parameters describing the rescattering in the nucleus in $e + A$ collisions can be related to the parameters describing the medium in an explicit energy-loss calculation. By relating the two sets of parameters, the parton density in the hot medium can be related to the parton density in a cold nucleus [182]. Results of this analysis are shown in Fig. 42 for parameters that give an initial energy loss per unit length of 13.8 ± 3.9 GeV/fm when the HIJING [70] parameterization of shadowing is used [179] (Note: this result is a factor of two larger that in [182] which was based on analysis of the 130 GeV results). However, an alternative (EKS) [210] shadowing description results in an initial energy loss of 16.1 ± 3.9 GeV/fm [179] in the same calculation indicating at least a 25% systematic error in the energy loss estimates due to uncertainties in the description of nuclear shadowing. Nonetheless, these initial-energy-loss values are much larger than the time-averaged energy loss extracted from the calculation, 0.85 ± 0.24 GeV/fm for HIJING shadowing [179], due to the assumed $1/\tau$ decrease in the color-charged density. In fact, the average energy loss per unit path length in central Au+Au collisions [182] is comparable to the value for cold nuclear matter extracted from HERMES data [182]. However, the initial energy loss is estimated by Wang to be a factor of ~ 30 larger than that in a cold nucleus [179] implying that the initial Au+Au parton density is larger by a factor > 30 than in cold nuclear matter [211].

As shown in Fig. 42 the Wang higher-twist calculation predicts a suppression that varies strongly with p_T over the range where the experimental $R_{AA}(p_T)$

values are flat. However, Wang and Wang have argued that absorption of energy from the medium needs to be accounted for in calculating the energy loss of moderate-p_T partons [181]. They provide a formula which incorporates both parton energy loss and "feedback" from the medium that can reproduce the shape of the observed high-p_T suppression as shown by the lower curve in Fig. 42. This formula, then, provides the energy loss estimate given above. This explanation for the observed p_T independence of R_{AA}, a crucial feature of the experimental data, is disquieting, however, because it contradicts the explanation provided by the GLV model which provides a consistent estimate of the initial energy density. The feedback of energy from the medium is *not* included in the GLV calculations and if this contribution is significant, then the agreement of the GLV predictions with the π^0 $R_{AA}(p_T)$ over the entire p_T range would have to be considered "accidental". Also, the variation of the suppression in the Wang higher-twist calculation with p_T reflects the $\Delta E \propto \log E$ variation of parton energy loss naturally obtained from approximations to the full opacity expansion [199]. As noted above, the GLV approach finds that incorporating non-leading terms in the opacity expansion produces $\Delta E \propto E$. Thus, while the absorption of energy from the medium in the Wang et al. approach may only be significant below $p_T = 5$ GeV/c, the differences between the variation of energy loss with parton energy in the two approaches will not be confined to low p_T.

One source of uncertainty in the interpretation of the high-p_T suppression is the role of possible inelastic scattering of hadrons after fragmentation. It was originally argued that final-state inelastic scattering of hadrons could produce all of the observed suppression [212]. The persistence of the jet signal with the correct width in Au+Au collisions would be difficult to reconcile with this hypothesis. Indeed, more recent analyses [213] discount the possibility that hadronic re-interaction could account for the observed high-p_T suppression and indicate that only $\sim 1/3$ of fragmentation hadrons undergo final-state inelastic scattering [213]. Wang has also argued [214] that the complete pattern of high-p_T phenomena observed in the RHIC data cannot be explained by hadronic rescattering. However, this leaves open the question of whether hadronic re-interactions after jet fragmentation can be partially responsible for the observed high-p_T suppression. There are a number of other open issues with the quantitative interpretation of the observed high-p_T suppression. The calculations all assume that the jets radiate by scattering off static color charges while the typical initial gluon p_T is often assumed to be ~ 1 GeV. Also the radiated gluons are assumed to be massless though a plasmon cutoff equal to the screening mass is applied. The systematic errors introduced by these and other assumptions made in the current energy loss calculations have not yet been evaluated though the gluon screening mass is being included in analyses of heavy-quark energy loss.

The observation that the suppression of high-p_T particle production is approximately independent of p_T above 4 GeV/c and that the $p+p$ p_T spectra are well described by a pure power-law function in the same p_T range allows a simple empirical estimate of the energy loss of hard-scattered partons in the medium. The π^0 invariant cross section measured by PHENIX in $p+p$ collisions [56] is found to be well described by a power law

$$E\frac{d^3n}{dp^3} = \frac{1}{2\pi}\frac{d^2n}{p_T dp_T dy} = \frac{A}{{p_T}^n} \tag{28}$$

for $p_T > 3.0$ GeV/c with an exponent $n = 8.1 \pm 0.1$. If we assume that none of the hard-scattered partons escape from the medium without losing energy, then the approximately p_T-independent suppression above 4.5 GeV/c can be interpreted as resulting from an average fractional shift in the momentum of the final-state hadrons due to energy loss of the parent parton. The suppressed spectrum can be evaluated from the unsuppressed $(p+p)$ spectrum by noting that hadrons produced in Au+Au collisions at a particular p_T value, would have been produced at a larger p_T value ${p_T}' = p_T + S(p_T)$ in $p+p$ collisions. If the energy loss is proportional to p_T then we can write $S(p_T) = S_0 p_T$ so ${p_T}' = (1+S_0)p_T$ Then, the number of particles observed after suppression in a given Δp_T interval is given by

$$\frac{dn}{dp_T} = \frac{dn}{d{p_T}'}\frac{d{p_T}'}{dp_T} = \frac{A}{(1+S_0)^{(n-2)}\,{p_T}^{(n-1)}}. \tag{29}$$

We note that the factor $\frac{d{p_T}'}{dp_T}$ accounts for the larger relative density of particles per measured p_T interval due to the effective compression of the p_T scale caused by the induced energy loss; this factor is necessary for the total number of particles to be conserved. The nuclear modification factor then can be expressed in terms of S_0,

$$R_{AA}(p_T) = \frac{1}{(1+S_0)^{(n-2)}}. \tag{30}$$

Using this very simple picture, we can estimate the fraction of energy lost by hard-scattered partons in the medium from our measured R_{AA} values. First we obtain S_0 from Eq. 30

$$S_0 = \frac{1}{{R_{AA}}^{1/(n-2)}} - 1. \tag{31}$$

Then we observe that the hadrons that would have been produced in $p+p$ collisions at a momentum $(1+S_0)p_T$ were actually produced at p_T, implying a fractional energy loss

$$S_{\rm loss} = 1 - 1/(1+S_0) = 1 - {R_{AA}}^{1/(n-2)}. \tag{32}$$

Figure 43 shows the centrality dependence of $S_{\rm loss}$ obtained from the p_T-averaged R_{AA} values shown in Fig. 38. For the most central Au+Au collisions at 200 GeV we obtain $S_{\rm loss} = 0.2$, which naively implies that an average 20% reduction in the energy of partons in the medium will produce the suppression observed in the π^0 spectra above 4.5 GeV/c. The extracted $S_{\rm loss}$ values are well described by an ${N_{\rm part}}^{2/3}$ dependence using the most central bin to fix the proportionality constant. This result agrees with the GLV prediction for the centrality dependence of the medium-induced energy loss.

It has been shown previously [215,216] that fluctuations in the radiation process can distort an estimate of parton energy loss using the procedure described above. Because of the steeply falling p_T spectrum, the partons that lose less energy dominate the yield at a given p_T so our determination of $S_{\rm loss}$ will significantly underestimate the true energy loss. However, it has also been observed that this distortion can largely be compensated by a single multiplicative factor of value $\sim 1.5-2$ [215]. While we cannot use the empirically extracted energy loss to estimate an initial gluon density, we can evaluate the consistency of our results with estimates of $\langle dE/dx \rangle$ in the medium. If we take into account the factor of $1.5-2.0$ renormalization of the $S_{\rm loss}$, we estimate that 10 GeV partons lose $\sim 3-4$ GeV of energy. If the typical path length of these partons is on the order of the nuclear radius then we can infer a $\Delta E/\Delta x \sim 0.5$ GeV/fm which is in good agreement with the estimate from Wang [182]. We can also use the above empirical energy loss approach to evaluate possible systematic errors in the estimate of the initial gluon density. For example, if one third of the observed suppression were a result of final-state hadronic interactions in the medium, then the suppression due to energy loss would be a factor of 1.5 smaller than that implied by the measured R_{AA} values, assuming that every fragmentation hadron that interacts effectively "disappears" by being shifted to much lower momentum. As a result, S_0 in central Au+Au collisions would be reduced from 0.25 to 0.17, implying 30% reduction in the estimated energy loss. If the energy loss is indeed proportional to the initial gluon density then the uncertainty in the effect of the final-state hadronic interactions would introduce a 30% systematic error in dn_g/dy.

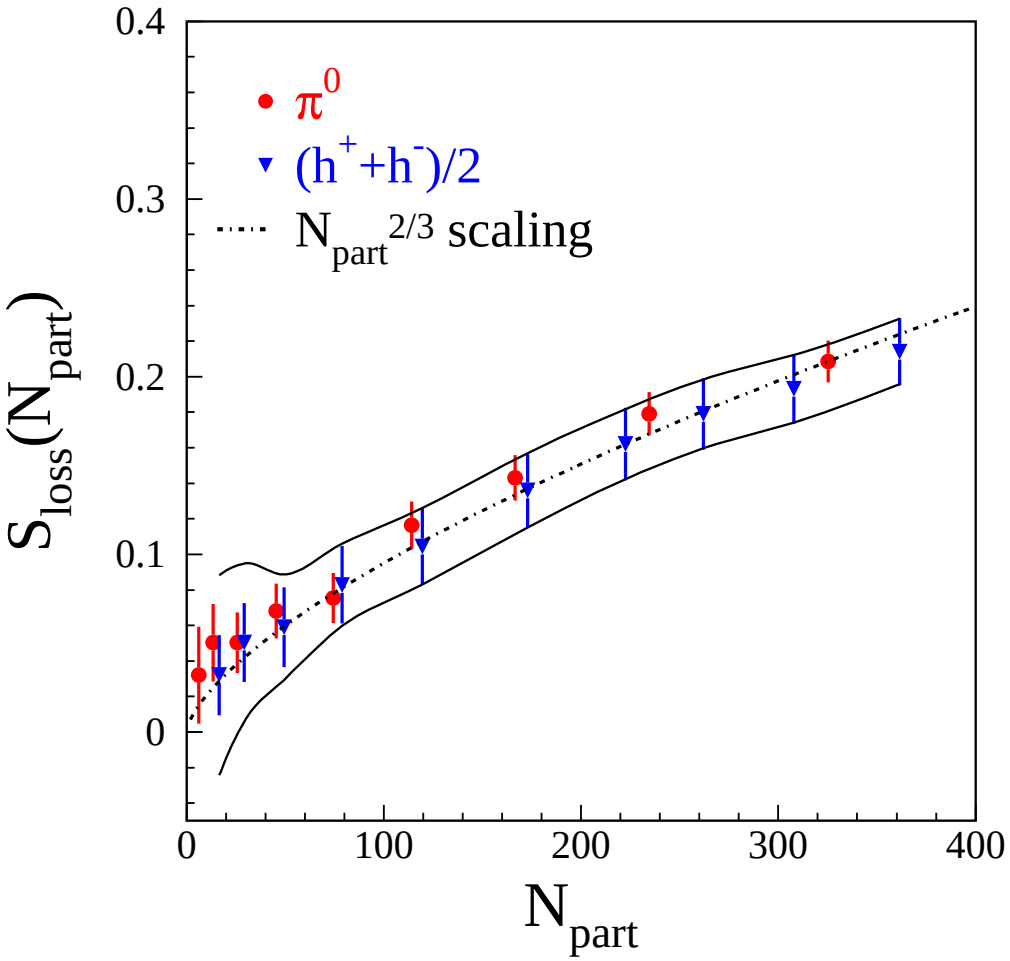

Fig. 43. Calculated energy loss shift factor, $S_{\rm loss}$ vs. $N_{\rm part}$ for π^0 and charged hadron production in 200 GeV Au+Au collisions. The band around the values indicates systematic errors resulting from uncertainties in T_{AB} and the normalization of the $p+p$ spectrum. The dot-dashed curve shows an ${N_{\rm part}}^{2/3}$ scaling of $S_{\rm loss}$ using the most central bin to fix the proportionality constant.

6.6 Conclusions

The observed suppression of high-p_T particle production at RHIC is a unique phenomenon that has not been previously observed in any hadronic or heavy ion collisions at any energy. The suppression provides direct evidence that Au+Au collisions at RHIC have produced matter at extreme densities, greater than ten times the energy density of normal nuclear matter and the highest energy densities ever achieved in the laboratory. Medium-induced energy loss, predominantly via gluon bremsstrahlung emission, is the only currently known physical mechanism that can fully explain the magnitude and p_T dependence

of the observed high-p_T suppression. This conclusion is based on evidence provided above that we summarize here:

- Observation of the x_T scaling of the high-p_T hadron spectra and measurements of two-hadron azimuthal-angle correlations at high p_T confirm the dominant role of hard scattering and subsequent jet fragmentation in the production of high-p_T hadrons.
- d+Au measurements demonstrate that any initial-state modification of nuclear-parton distributions has little effect on the production of hadrons with $p_T > 2$ GeV/c at mid-rapidity.
- This conclusion is further strengthened by preliminary PHENIX measurements showing that the yield of direct photons with $p_T > 5$ GeV/c is consistent with a T_{AB} scaling of a pQCD-calculated $p + p$ direct-photon spectrum.
- Analyses described above indicate that final-state hadronic interactions can only account for a small fraction of the observed high-p_T suppression.

Interpreted in the context of in-medium energy loss, the high-p_T suppression data rule out the simplest energy loss prescription—a jet energy independent $\Delta E/\Delta x$. The approximately flat $R_{AA}(p_T)$ was predicted by the GLV energy loss model from which the most explicit estimates of the initial gluon-number density, $dn_g/dy = 1000 \pm 200$ and a corresponding initial energy density $\varepsilon_0 \approx 15\text{GeV/fm}^3$ [188], have been obtained. An alternative estimate from the analysis of Wang et al. [182] yields a path-length-averaged energy loss of 0.5 GeV/fm. Assuming a $1/\tau$ time evolution of the energy density a much larger initial energy loss of 13–16 GeV/fm is obtained. That estimate combined with the estimated 0.5 GeV/fm energy loss of partons in cold nuclear matter yields an initial Au+Au gluon density > 30 times larger than that in nuclei [211]. From this result, Wang concludes that the initial energy density is a factor of ~ 100 times larger than that of a nucleus which would correspond to 16GeV/fm^3 [211]. While this conclusion is consistent with the independent estimate from GLV, we note that the two models provide completely different explanations for the nearly p_T-independent R_{AA} – the most unique feature of the single-particle high-p_T suppression – and the differences between the approaches may not be confined to low p_T. An empirical analysis of the parton energy loss suggests that the Wang estimate of > 0.5 GeV/fm for the average parton $\Delta E/\Delta x$ is consistent with the measured R_{AA} values in central Au+Au collisions. However, some outstanding issues with current energy loss calculations and the interpretation of high-p_T suppression were noted above. Most notably, rescattering of hadrons after parton fragmentation could affect the observed high-p_T suppression even if such rescattering cannot explain the pattern of jet quenching observations. Using results from [213] and our empirical energy loss analysis, we estimated that hadronic interactions *could* modify extracted values for initial parton densities by only 30%. However, we cannot evaluate the potential systematic error in extracted parton densities due to other untested assumptions of the energy loss calculations. Therefore, to be

conservative we interpret the extracted initial gluon number and energy densities as order-of-magnitude estimates. Even then, the 15GeV/fm^3 estimated by Gyulassy and Vitev from the central 200 GeV Au+Au π^0 $R_{AA}(p_T)$ measurements indicates that the matter produced in central Au+Au collision has an energy density > 10 times normal nuclear matter density.

7 HADRON PRODUCTION

Descriptions of heavy ion collisions have provided an understanding of early energy densities, production rates and medium effects of hard partons, and collective flow of matter. However, hadronization—the process by which partons are converted into hadrons—is not well understood. The process of hadronization is particularly important since it includes both the dressing of the quarks from their bare masses, i.e. the breaking of approximate chiral symmetry, and the confinement of quarks into colorless hadrons. One could conclude that a quark-gluon plasma had been formed if one had conclusive evidence of hadronization occurring from a thermal distribution of quarks and gluons.

Hadronization processes have been studied over many years in proton-proton and electron-positron reactions. Hadron formation, by its very nature a non-perturbative process, has often been parameterized from data (e.g. fragmentation functions $D(z)$) or phenomenologically described (e.g. string models) [217]. From QCD one expects that hadron production at high transverse momentum is dominated by hard scattering of partons followed by fragmentation into "jets" or "mini-jets" of hadrons. Following the assumptions of collinear factorization, the fragmentation functions should be universal. This universality has proved a powerful tool in comparing e^+e^- annihilation to hadron-hadron reactions. One feature of jet fragmentation is that baryons and antibaryons are always suppressed relative to mesons at a given p_T [218,219]. Phenomenologically this can be thought of as a large penalty for creating a diquark-antidiquark pair for baryon formation vs. a quark-antiquark pair for meson formation.

In hadron-hadron reactions, hard scattering followed by fragmentation is considered to be the dominant process of hadron production for particles with $p_T \geq 2$ GeV/c at mid-rapidity. At low transverse momentum, where particles have $p_T < 2$ GeV/c, particle interactions are often referred to as "soft". In small momentum transfer reactions the effective wavelength of interactions is longer than the spacing of individual partons in a nucleon or nucleus. Thus coherence effects are expected to result in large violations of factorization and universality of fragmentation functions. Hadron formation mechanisms in this "soft" regime are poorly understood. We are particularly interested in the study of hadron formation in the region of $p_T \approx 2$–5 GeV/c, where production

is expected to make the transition from "soft" to "hard" mechanisms.

7.1 Baryons and Antibaryons

One of the most striking and unexpected observations in heavy ion reactions at RHIC is the large enhancement of baryons and antibaryons relative to pions at intermediate $p_T \approx 2$–5 GeV/c. As shown in Fig. 44, the (anti)proton to pion ratio is enhanced by almost a factor of three when one compares peripheral reactions to the most central gold-gold reactions [220] [7]. This of course is in sharp contrast to the suppression of pions in this region.

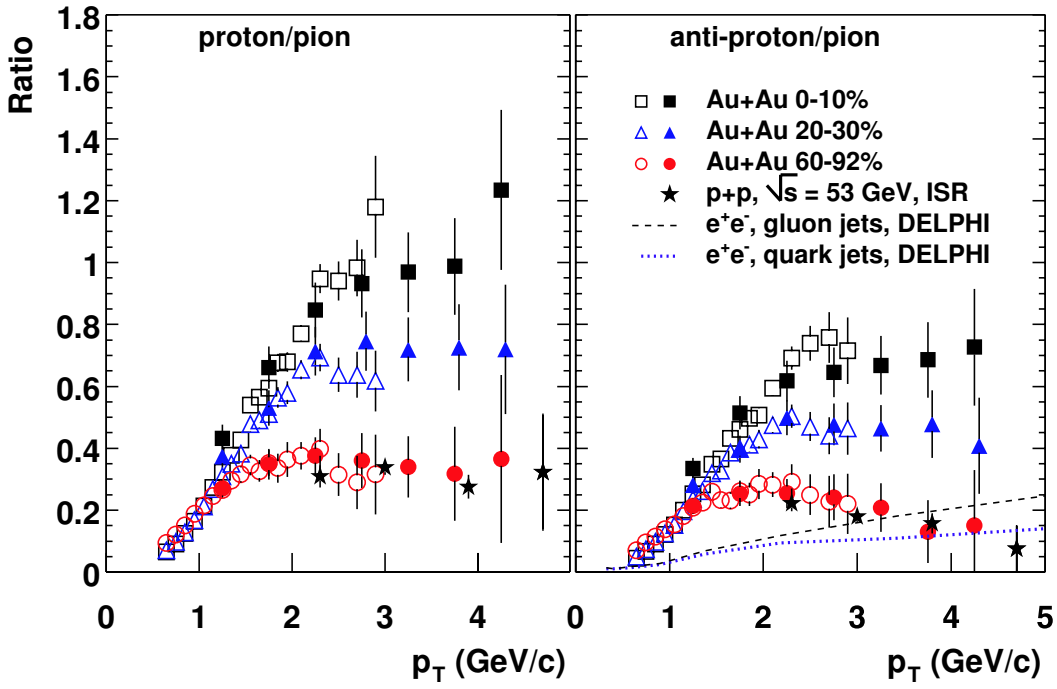

Fig. 44. p/π (left) and $\overline{p}/\pi$ (right) ratios for central (0–10%), mid-central (20–30%) and peripheral (60–92%) Au+Au collisions at $\sqrt{s_{NN}} = 200$GeV. Open (filled) points are for $\pi^{+/-}$ (π^0), respectively. Data from $\sqrt{s} = 53$GeV $p+p$ collisions [218] are shown with stars. The dashed and dotted lines are $(\overline{p}+p)/(\pi^+ + \pi^-)$ ratio in gluon and in quark jets [219].

We can investigate this (anti)baryon excess to much higher p_T by comparing our inclusive charged spectra (primarily pions, kaons and protons) with our neutral pion measurements [220]. Shown in Fig. 45 is the charged hadron to π^0 ratio as a function of transverse momentum in ten centrality bins. We observe a significant increase of the $(h^+ + h^-)/\pi^0$ ratio above 1.6 in the p_T range 1–5 GeV/c that increases as a function of collision centrality. The ratio

[7] All PHENIX (anti)proton spectra shown in this section are corrected for feed down from heavier resonances.

of $h/\pi = 1.6$ is the value measured in $p + p$ reactions [218], and is thought to arise from jet fragmentation. In Au+Au central reactions, above $p_T \approx 5$GeV/c, h/π returns to the $p+p$ measured baseline. This implies that the (anti)baryon excess occurs only in the limited p_T window ≈2–5 GeV/c, and then returns to the universal fragmentation function expectation.

As discussed in section 6, pions in this p_T range are suppressed by almost a factor of five relative to binary collision scaling for central Au+Au reactions. Thus, one possible interpretation of the large (anti)proton to pion ratio is that somehow the baryons are not suppressed in a manner similar to the pions. Figure 46 shows that in fact (anti)proton production appears to follow binary collision scaling over the transverse momentum range $p_T = 2$–5 GeV/c [220]. However, the h/π^0 ratios shown in Fig. 45 imply that above $p_T > 5$ GeV/c, the (anti)protons must be as suppressed as the pions.

Characteristics of the intermediate p_T (anti)protons are:

- A large enhancement of the p/π and $\overline{p}/\pi$ ratios in central Au+Au collisions.
- A ratio in peripheral collisions which is in agreement with that from $p + p$ collisions.
- A smooth increase from peripheral to central Au+Au collisions.
- A similar effect for protons and antiprotons.
- Approximate scaling of (anti)proton production at $p_T \approx 2$–4 GeV/c with the number of binary nucleon-nucleon collisions.
- Suppression relative to binary collision scaling similar for (anti)protons and pions for $p_T > 5$ GeV/c.

Large proton to pion ratios have also been observed in heavy ion collisions at lower energies. Figure 47 shows p_T distributions of protons, antiprotons, and pions in central Pb+Pb collisions at the SPS and in central Au+Au collisions at the AGS. The p/π ratio in central Pb+Pb collisions at the SPS is greater than unity for $p_T \geq 1.3$ GeV/c. At the AGS, the proton spectrum crosses pion spectra at $p_T \sim 0.5$ GeV/c, and the p/π ratio is about 20 at $p_T = 1.6$ GeV/c. The p/π ratios in the low-energy heavy-ion collisions are also enhanced compared with $p + p$ collisions at the same energy.

Most of the protons in these lower-energy heavy-ion collisions are not produced in the collision. Rather they are protons from the beam or target nucleus (Pb or Au) that are transported to large p_T at mid-rapidity. As discussed in section 3, a strong radial flow with velocity $\beta_T \sim 0.5$ is produced in heavy ion collisions at AGS and SPS energies. The large p/π ratio can be interpreted as a result of this radial flow. Since the proton is heavier, a fixed velocity boost results is a larger momentum boost than for pions, and thus enhances p/π ratio at higher p_T. In contrast, at RHIC energies, most of protons are produced particles [40]. The anomalously large antibaryon-to-meson ratio $\bar{p}/\pi \sim 1$ at high $p_T \geq 2$

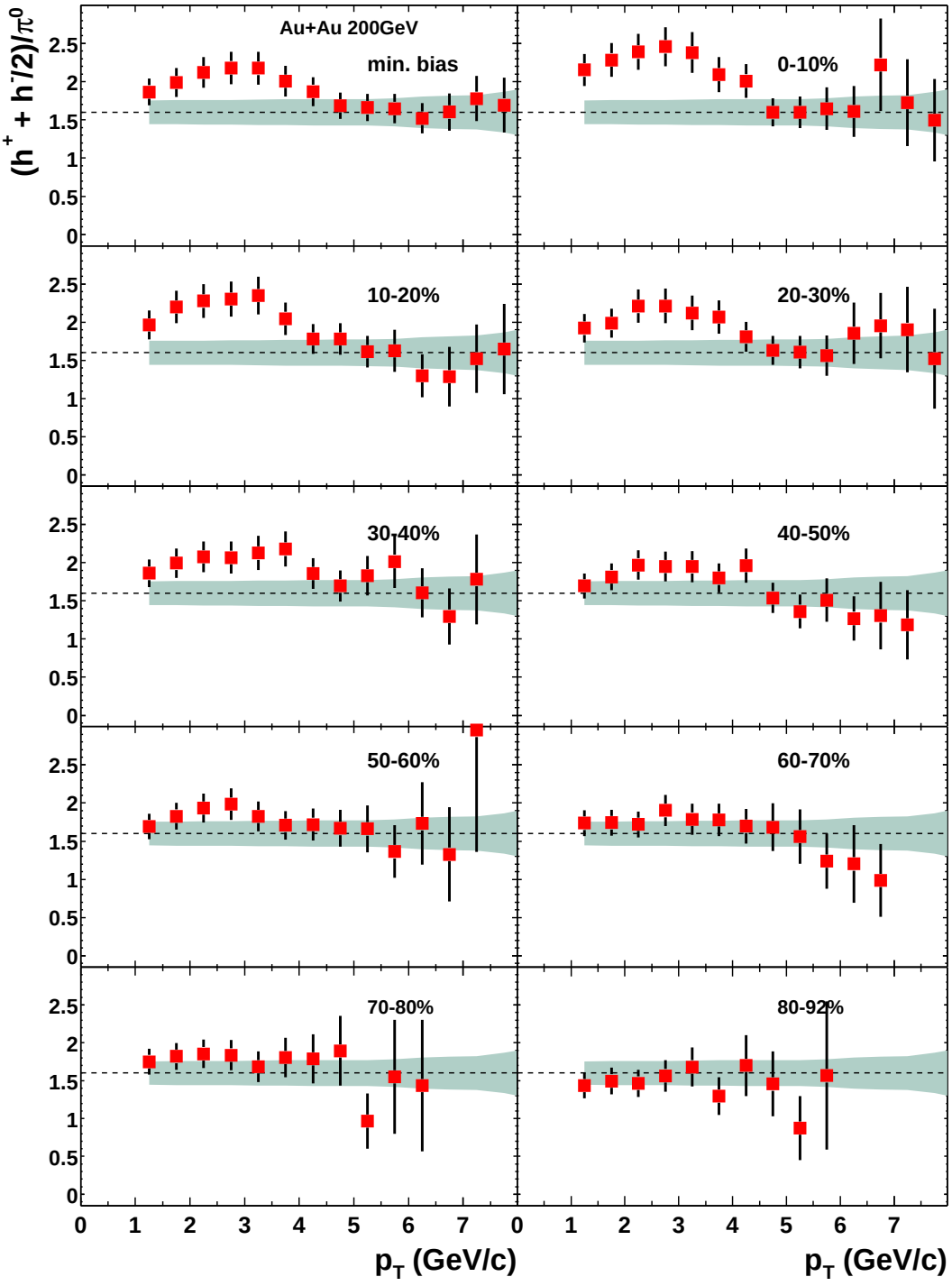

Fig. 45. Charged hadron to π^0 ratio for different centrality classes for Au+Au collisions at $\sqrt{s_{NN}} = 200$GeV. Error bars represent the quadratic sum of statistical and point to point systematic errors. The shaded band shows the normalization error common to all centrality classes. The line at 1.6 is the h/π ratio measured in $p+p$ collisions at $\sqrt{s} = 53$GeV [218] and e+e- collisions [219].

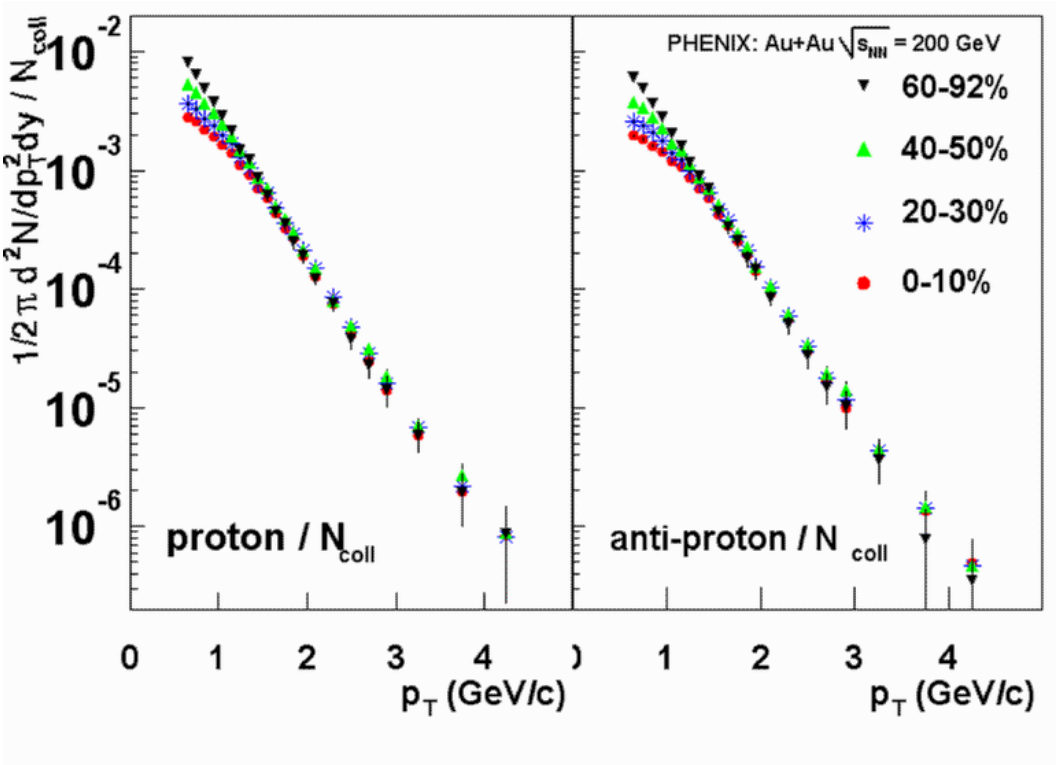

Fig. 46. p and $\overline{p}$ invariant yields scaled by N_{coll}. Error bars are statistical. Systematic errors on N_{coll} range from ≈10% for central to ≈28% for 60–92% centrality. Multiplicity dependent normalization errors are ≈3%.

GeV/c is a unique result from RHIC. Such a large $\bar{p}/\pi$ ratio has not been observed in any other collision system. Figure 47 shows that $\bar{p}/\pi$ is less than ~ 0.1 at the SPS, and it is less than 1/100 at the AGS. It should also be noted that the measurements from the AGS/SPS are limited to lower p_T ($p_T < 2$ GeV/c), where soft physics is still dominant, while at RHIC we observe a large $p(\bar{p})/\pi$ ratio in $p_T \approx 2$–5 GeV/c where hard processes are expected to be the dominant mechanism of particle production.

7.2 The ϕ Meson

We have extended our identified hadron studies to include the ϕ vector meson as measured in the K^+K^- decay channel. The ϕ is a meson, and is in that sense similar to the pion with a valence quark and antiquark, and yet its mass is comparable to that of the proton.

Figure 48 shows R_{CP}, the ratio of production in central to peripheral Au+Au collisions scaled by binary collisions, for protons, pions and ϕ mesons detected via its KK decay channel [225] in Au+Au collisions at $\sqrt{s_{NN}} = 200$GeV. A large suppression of pions at $p_T > 2$GeV/c is observed (as detailed in Section

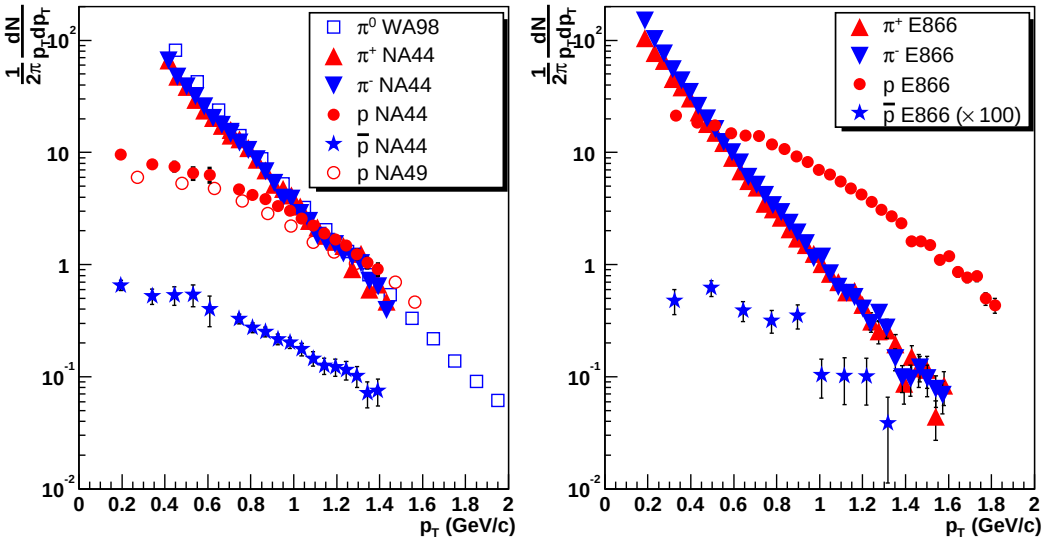

Fig. 47. Invariant yields of p, $\bar{p}$, and π as function of p_T in central Pb+Pb collisions at the SPS ($\sqrt{s_{NN}} = 17$ GeV) (left panel) and in central Au+Au collisions at the AGS ($\sqrt{s_{NN}} = 5$ GeV) (right panel). The $\bar{p}$ spectrum from the AGS is scaled up by a factor 100. All data are at mid-rapidity ($y - y_{cm} \approx 0$) and are from W98 [155], NA44 [221], NA49 [222], and E866 [223,224].

6), and a lack of suppression for the protons and antiprotons as expected from Fig. 46. The ϕ follows the suppression pattern of the pions within errors, indicating that the surprising behavior of the protons is not followed by the ϕ. Figure 49 shows a comparison between the p_T spectral shape for protons and the ϕ in central and peripheral Au+Au reactions. The two spectra agree with each other within errors for the most central events. Thus, although the yields are evolving differently with collision centrality, giving rise to the deviation from unity of R_{CP}, the p_T distributions appear quite similar.

7.3 Jet Correlations

A crucial test of the origin for the enhanced (anti)proton to pion ratio is to see if baryons in this intermediate p_T regime exhibit correlations characteristic of the structure of jets from hard-scattered partons. Particles which exhibit these correlations are termed "jet-like". Figure 50 shows the associated partner particle yield within the relative angular range $0.0 < \phi < 0.94$ radians on the same side as trigger baryons and mesons [226]. Correlated pairs are then formed between the trigger particle and other particles within the above mentioned angular range. Mixed events are used to determine the combinatorial (i.e. non-jet-like) background distribution, which is subtracted after modulation according to the measured v_2.

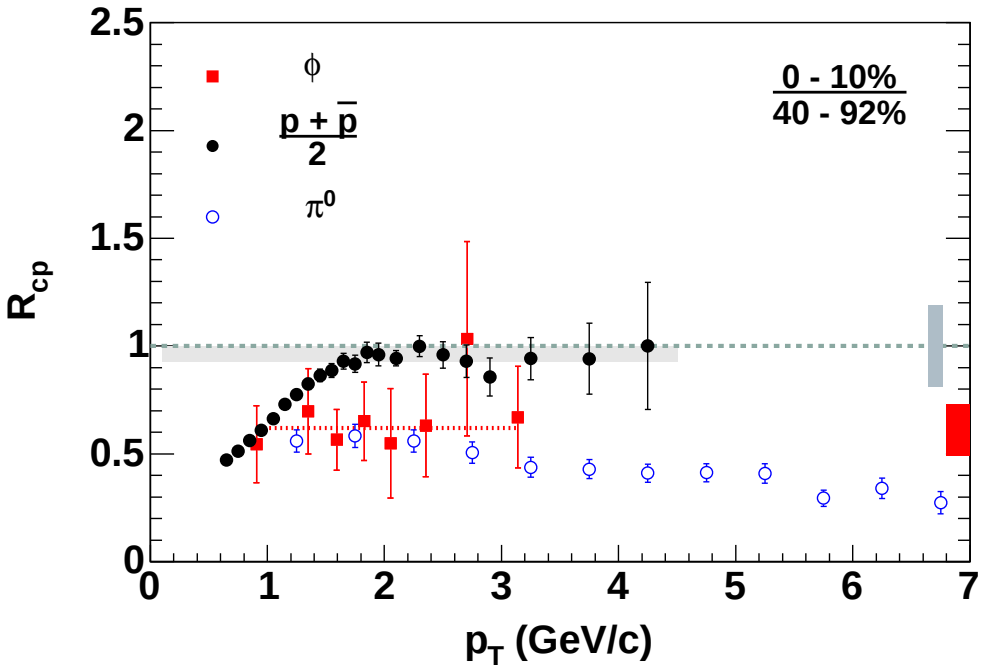

Fig. 48. The R_{CP} of the ϕ as measured in the KK channel, compared to the protons and pions for Au+Au collisions at $\sqrt{s_{NN}} = 200$GeV.

The partner yield increases for both trigger baryons and mesons by almost a factor of two from deuteron-gold to peripheral and mid-central Au+Au reactions. We then observe a decrease in the jet-like correlations for baryons relative to mesons for the most central collisions. It is notable that this observation is of limited significance within our current statistical and systematic errors. Over a broad range of centrality 10-60% the partner yield is the same for protons and pions within errors. This is notable since the (anti)proton to pion ratio has already increased by a factor of two for mid-central Au+Au relative to proton-proton reactions, with the implication that the increase in the p/π ratio is inclusive of the particles with jet-like correlations.

The dashed line in Figure 50 shows the expected centrality dependence of partners per baryon if all the "extra" baryons which increase the p/π over that in p+p collisions were to arise solely from soft processes. Baryons from thermal quark recombination should have no jet-like partner hadrons and would dilute the per-trigger conditional yield. Because this simple estimate does not allow for meson production by recombination, which must also occur along with baryon production, it represents an upper limit to the centrality dependence of jet partner yield from thermal recombination. The data clearly disagree with both the centrality dependence and also the absolute yields of this estimation, indicating that the baryon excess has the same jet-like origin as the mesons, except perhaps in the highest centrality bin.

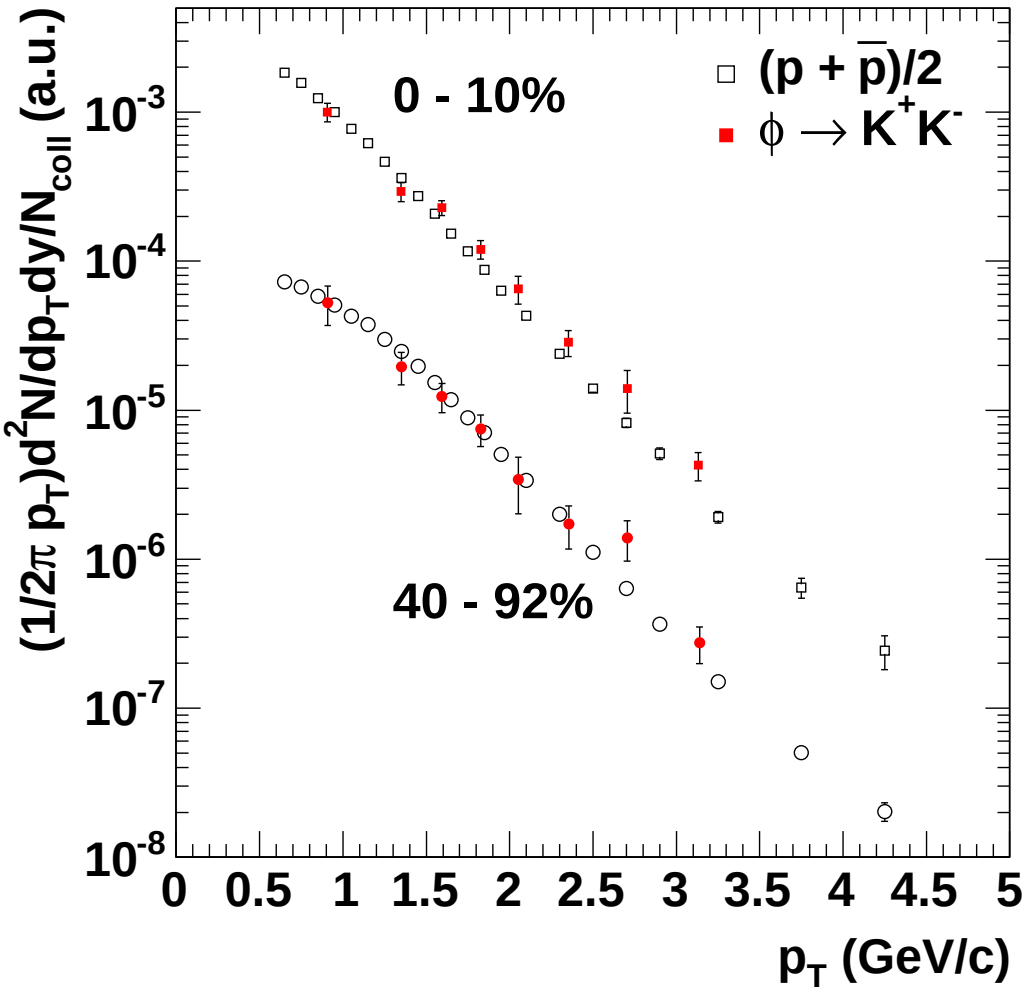

Fig. 49. $(p+\overline{p})$ and ϕ invariant yield as a function of transverse momentum for central 0–10% and peripheral 40–92% Au+Au reactions at $\sqrt{s_{NN}}$ = 200GeV. The two distributions for each centrality class are given an arbitrary relative normalization to allow for comparison of the p_T dependent shapes.

The characteristics of the jet-like particles are compared to inclusive hadrons in Fig. 51, which shows the centrality dependence of the p_T distributions of jet-like partners and inclusive hadrons. One can see that, within the statistics available, the slopes of the associated particle spectra in $p+p$, d+Au, peripheral and mid-central Au+Au collisions are very similar for both trigger mesons and trigger baryons. The partner spectra are harder than the inclusive hadron spectra, as expected from jet fragmentation. In the most central collisions, the number of particles associated with trigger baryons is very small, resulting in large statistical error bars. However, the inverse slopes of the jet-like partners and inclusive hadron distributions agree better in central collisions than in peripheral collisions.

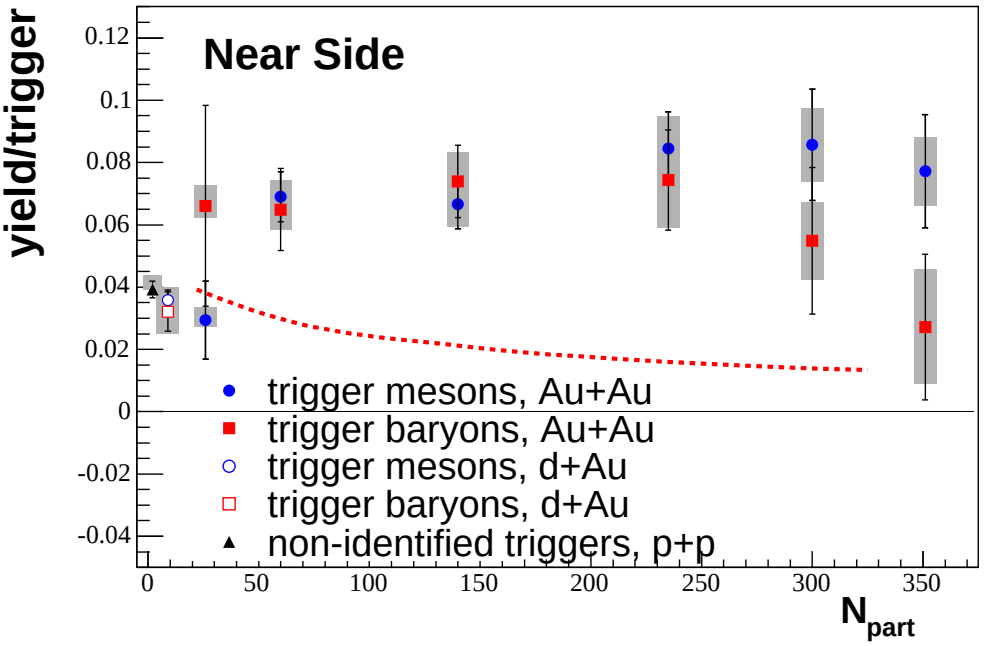

Fig. 50. Centrality dependence of associated charged hadron yield ($1.7 < p_T < 2.5 GeV/c$) above combinatorial background for trigger baryons and trigger mesons in the p_T range 2.5-4.0 GeV/c in a 54° cone around the trigger particle in Au+Au collisions at $\sqrt{s_{NN}} = 200$GeV. The error bars are statistical errors and the gray boxes are systematic errors. The dashed line represents an upper limit of the centrality dependence of the near-side partner yield from thermal recombination (see text).

We can then make the following general observations:

- Trigger (anti)protons and mesons have comparable near-side associated-particle yields over a broad range in centrality, indicating a significant jet-like component for both.
- There is an indication that the proton partner yield tends to diminish for the most central collisions, unlike for leading mesons.
- Within the limited statistics available for the measurement, the inverse slopes of the associated particles are similar for both mesons and baryons. These are harder than for the inclusive spectra.
- Trigger particles in Au+Au collisions appear to have *more* associated particles than in d+Au collisions. This is true for all centralities aside from the most peripheral, and except for leading baryons in central collisions.

7.4 Soft Physics

In hadron-hadron reactions, hard scattering followed by fragmentation is considered to be the dominant process of hadron production with $p_T \geq 2$ GeV/c

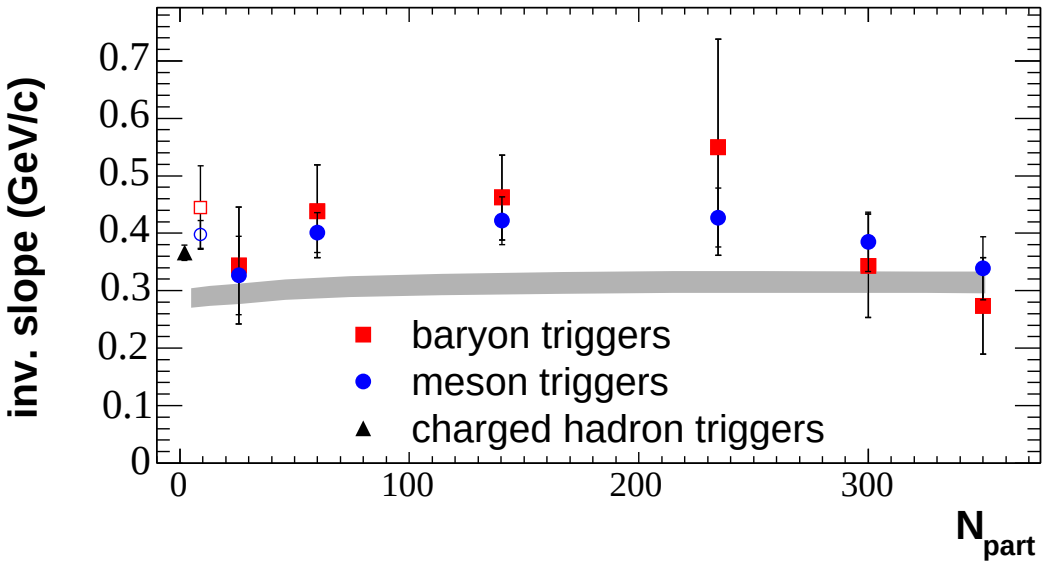

Fig. 51. The inverse slopes for the momentum distributions of the associated particles shown in Fig. 50. The gray band is the inverse slope of the momentum distribution of the inclusive hadrons from Au+Au collisions at $\sqrt{s_{NN}} = 200$GeV.

at mid-rapidity. However, as detailed in section 3, there is strong evidence for explosive collective motion of particles in the medium. If the mean free path for particles in the medium is small, then all particles must move with a common local velocity as described by hydrodynamics. Therefore, heavier particles receive a larger momentum boost than lighter particles. This effective shifting of particles to higher p_T results in a "shoulder-arm" shape for the (anti)proton p_T spectra, visible in Fig. 49.

7.4.1 Hydrodynamics

Is it possible that this soft hadron production extends to higher p_T for baryons than mesons? Hydrodynamic boosting of "soft" physics for heavier particles into the $p_T > 2$GeV/c offers a natural explanation for the enhanced p/π and $\overline{p}/\pi$ ratios [98].

As seen in Section 3, some hydrodynamical models can describe both the proton and the pion spectra. Consequently, the p/π ratio is also reproduced (Fig. 52). It is clear that the description of the p/π ratio is not unique and different calculations yield quite different results. Above some p_T, hydrodynamics should fail to describe the data and fragmentation should dominate. Pure hydrodynamics predicts that this ratio would continue to increase essentially up to $p_T \to \infty$. However, these particles cannot have a zero mean free path in the medium. Any finite mean free path and a finite volume will limit the number of p_T "kicks" a particle can receive. For this reason many of the hydrodynamic calculations are not extended into the p_T region 2–5 GeV/c in which we are

interested.

Hydrodynamic calculations do not specify the quanta that flow; rather they assume an equation of state. When applied at RHIC, most calculations start with a quark-gluon-plasma equation of state and transition to a resonance gas. The mapping of the fluid onto hadrons is somewhat *ad hoc,* and often uses the Cooper-Frye freezeout [118], giving the typical hierarchies of momenta one sees where heavier particles receive a larger boost.

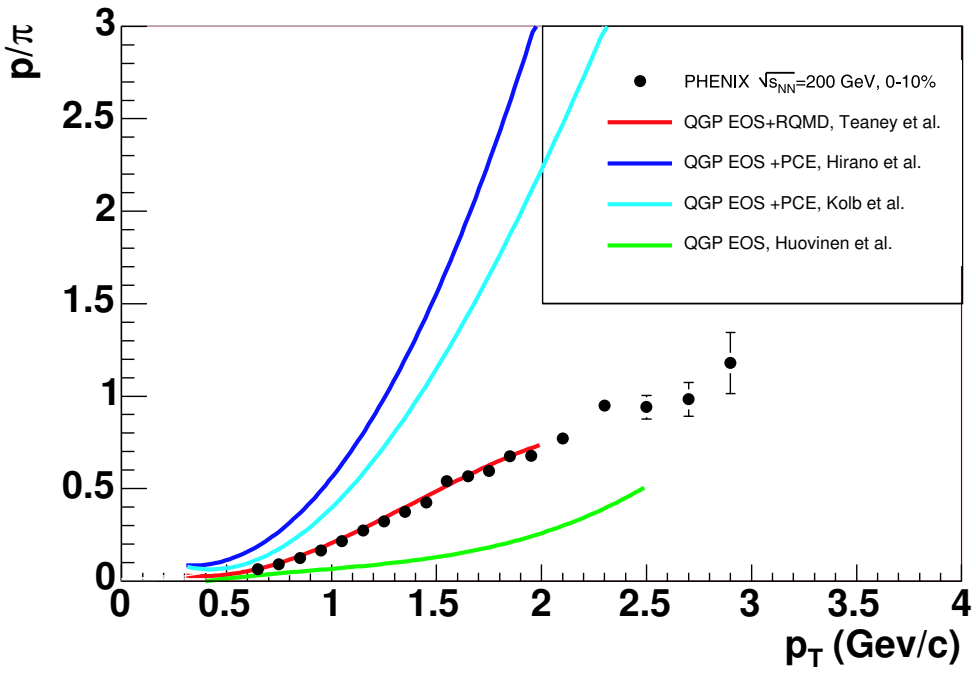

Fig. 52. p/π ratios for central (0–10%) Au+Au collisions at $\sqrt{s_{NN}} = 200$GeV compared to hydrodynamic models [98,99,109–111].

As mentioned previously, this generic feature of a transverse velocity boost yielding an increase in the baryon to meson ratio relative to proton-proton reactions is not unique to RHIC as shown in Fig. 47. However, a major difference between lower-energy results and those at $\sqrt{s_{NN}} = 200$ GeV is that at these highest energies there is a significant hard-process contribution. If the source of the excess baryons is the transport of soft baryons to the intermediate p_T range, then it is purely coincidental that the baryons scale with binary collisions. More importantly, we should expect a significant decrease in the jet-like partner yield for baryons relative to mesons. Although there may be a hint of this for the most central reactions, one expects this decrease to follow the centrality dependence of the increase in p/π ratio. Thus, this effect should already reduce the partner yield by a factor of two in mid-central Au+Au reactions. This is ruled out by the data.

7.4.2 Recombination Models

The quark recombination or coalescence model is a different physics framework in which baryons receive a larger p_T boost than mesons. These models were frequently invoked in the 1970's [227,228] in an attempt to describe the rapidity distribution of various hadronic species in $hadron - hadron$ reactions. More recently, these models have been applied to describe the forward charm hadron production in $hadron - nucleus$ reactions at Fermilab [229]. In this case they calculate a significant probability for D meson formation from a hard-scattering-created charm quark with a light valence quark in the projectile. The quark coalescence mechanisms have some similarities to light nuclei coalescence. However, wave functions are relatively well determined for light nuclei, whereas the hadron wave functions are neither easily described by partons nor directly calculable from QCD.

Recently, quark recombination has been successfully applied to describe a number of features of heavy ion collisions [230,231] (Duke model). In this picture, quarks in a densely populated phase space combine to form the final-state hadrons. This model uses the simplifying assumption that the mass is small relative to the momentum giving a prediction largely independent of the final hadron wave function [8]. The coalescing parton distribution was assumed to be exponential, i.e. thermal, and recombination applied for hadrons where $m^2/p_T^2 << 1$. At very high p_T particles are assumed to arise from fragmentation of hard partons with a standard power law distribution; the relative normalization of the thermal source with respect to this process is an important external parameter to the model. A crucial component of recombination models is the assumption that the partons which recombine carry a mass which is essentially equal to the mass of the dressed constituent quarks [9]. If all observables of intermediate p_T hadrons can be explained by recombination of only thermal quarks, this would essentially prove the existence of a quark-gluon plasma in the early stage of the collisions.

Three essential features are predicted by recombination models. First, baryons at moderate p_T are greatly enhanced relative to mesons as their transverse momentum is the sum of 3 quarks rather than 2. Recombination dominates over parton fragmentation in this region, because, for an exponential spectrum recombination is a more efficient means of producing particles at a particular p_T. This enhancement should return to its fragmentation values at higher p_T. In the intermediate range, all mesons should behave in a similar manner re-

[8] The recombination model prediction of these models is independent of the final hadron wave function with an accuracy of about 20% for protons and 10% for pions

[9] The actual source of this mass is under discussion. It may be that the chiral phase transition is slightly above the deconfinement transition. In this case, the mass would be from the dressing of the quarks. Another possibility is that the mass is a thermal mass which happens to be similar to the constituent quark mass.

gardless of mass, as should all baryons. Secondly, recombination predicts that the collective flow of the final-state hadrons should follow the collective flow of their constituent quarks. Finally, recombination causes thermal features to extend to higher transverse momentum, $p_T >> T_C$ than one might naively expect since the underlying thermal spectrum of the constituents gets a multiplication factor of essentially 3 for baryons and 2 for mesons. A last general feature which is true for the simplest of the models, but may not necessarily be true for more complex models, is that at intermediate p_T, recombination is the dominant mechanism for the production of hadrons—particularly of baryons.

Other recombination calculations have relaxed the assumptions previously described, at the cost of much more dependence on the particular form of the hadronic wave function used. One such calculation [232,233] (Oregon model) uses a description of hadronization which assumes that all hadrons—including those from fragmentation—arise from recombination. Hard partons are allowed to fragment into a shower of partons, which can in turn recombine—both with other partons in the shower and partons in the thermal background. Another model [234] (TAMU model) uses a Monte-Carlo method to model the production of hadrons allowing recombination of hard partons with thermal partons, and includes particle decays, such as $\rho \rightarrow 2\pi$ which produces low-p_T pions.

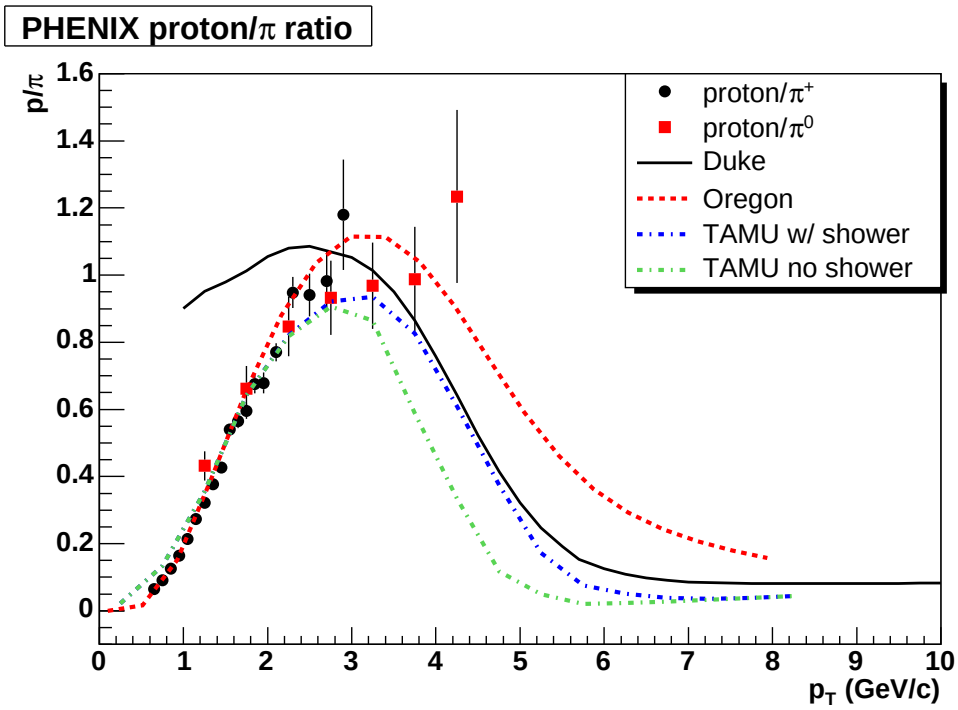

Fig. 53. The proton to pion ratio measured by PHENIX for Au+Au collisions at $\sqrt{s_{NN}} = 200$GeV. Several comparisons to recombination models as mentioned in the text are shown.

Figure 53 shows several recombination model calculations compared to the p/π

ratio from PHENIX. The general features at $p_T > 3$ GeV/c are reasonably reproduced—that is the protons show a strong enhancement at moderate p_T which disappears at $p_T > 5$ GeV/c consistent with the measured h/π ratio shown in Fig. 45. The more complicated models do a better job, as one might expect in the $p_T < 3$ GeV/c region, where the assumptions made by the Duke model begin to break down. Since the recombination model's essential ingredient is the number of constituent quarks in a hadron, the similarity of R_{CP} for the ϕ and pions is nicely explained.

Figure 54 shows the fraction of hadrons arising from recombination of only thermal quarks, as a function of p_T. For p_T between 2.5 and 4 GeV/c the fraction of protons from recombination is greater than 90% for all impact parameters, and is essentially 100% for the most central collisions. For pions the value is between 40 and 80%, depending on the centrality. This is contradicted by the data in Fig. 50 which clearly shows jet-like correlations for both pions and protons in mid-central collisions. It should be noted that the yield of particles associated with baryons in very central collisions appears to decrease, indicating a possible condition where the simple picture of recombination of purely thermal quarks may apply.

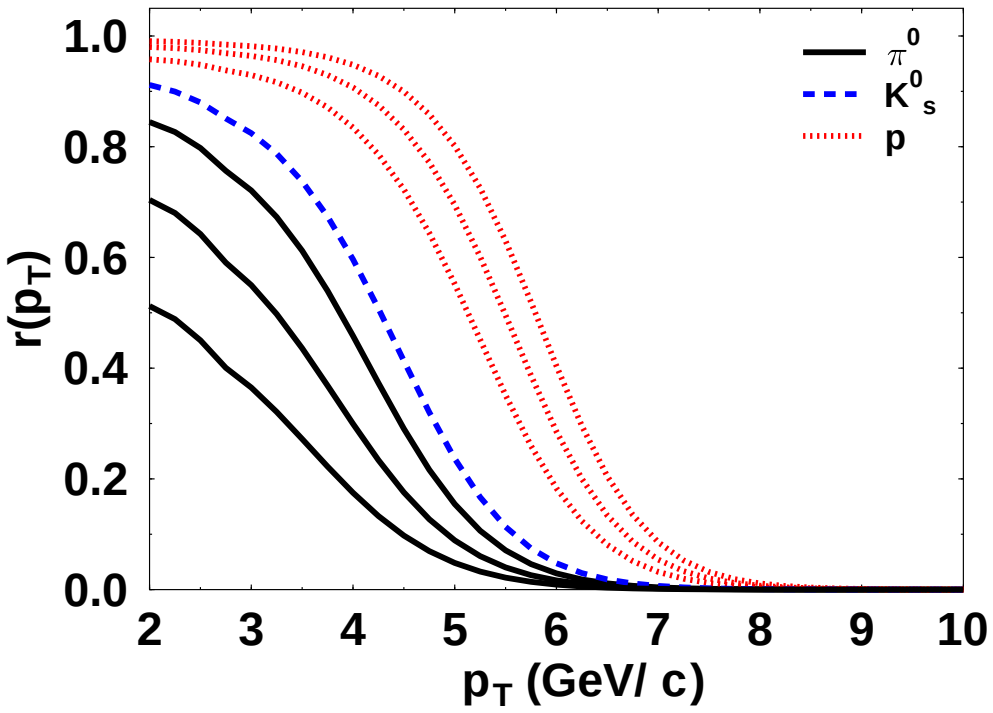

Fig. 54. The ratio r(P_T) = R/(R+F) of recombined hadrons to the sum of recombination (R) and fragmentation (F) for pions (solid), K^0s (dashed) and p (dotted lines) [231] in Au+Au collisions at $\sqrt{s_{NN}} = 200$GeV. For protons and pions different impact parameters b = 0, 7.5 and 12 fm (from top to bottom) are shown. K^0s is for b = 0 fm only.

One can examine the general prediction for the elliptic flow of identified particles by rescaling both the v_2 and the transverse momentum by the number of constituent quarks as shown in Fig. 55. This scaling was first suggested by Voloshin [235]. Above p_T/n of 1 GeV/c (corresponding to 3 GeV/c in the proton transverse momentum) all particles essentially plateau at a value of about 0.35 presumably reflecting the elliptic flow of the underlying partons. Interestingly, even at lower values of the transverse momentum, all particles also fall on the same curve aside from pions.

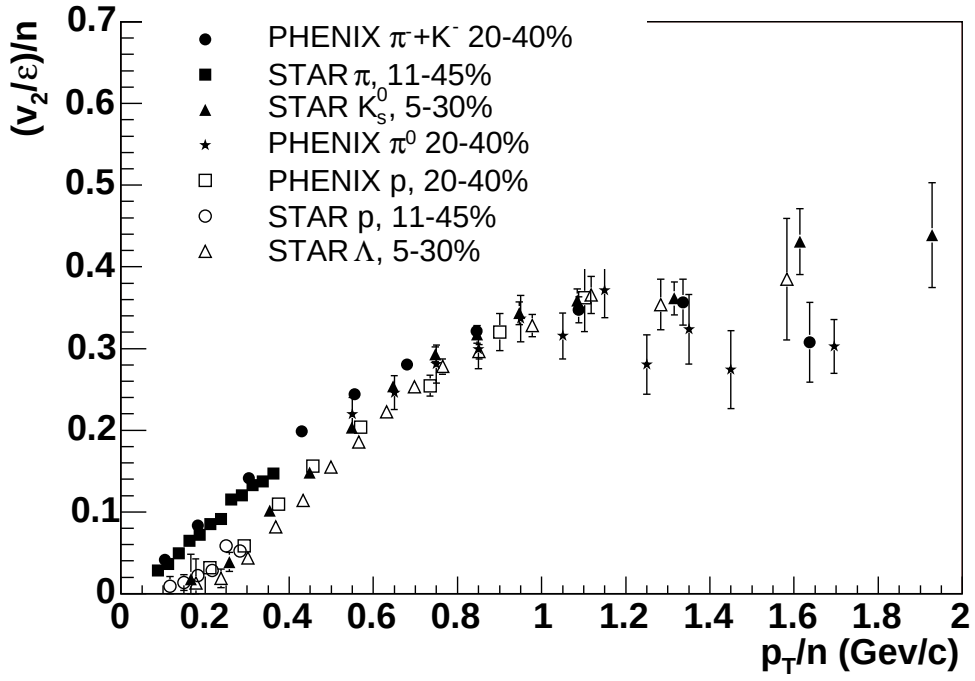

Fig. 55. v_2 as a function of transverse momentum for a variety of particles for Au + Au collisions where both v_2 and p_T have been scaled by the number of constituent quarks in the particle. The meson data are shown with filled symbols; $\pi^- + K^-$ from PHENIX at $\sqrt{s_{NN}}$ = 200GeV [50] (filled circles), charged π from STAR at $\sqrt{s_{NN}}$ = 130GeV [95] (filled squares), K^0_s from STAR at $\sqrt{s_{NN}}$ = 200GeV [236] (filled triangles), and π^0 from PHENIX at $\sqrt{s_{NN}}$ = 200GeV [237] (filled stars). While the baryons are shown with open symbols; p from PHENIX at $\sqrt{s_{NN}}$ = 200GeV [50] (open squares), p from STAR at $\sqrt{s_{NN}}$ = 130GeV [95] (open circles), and Λ from STAR at $\sqrt{s_{NN}}$ = 200GeV [236] (open triangles).

It is clear from the jet correlations observed that the majority of moderate p_T baryons in peripheral and mid-central collisions cannot arise from a purely thermal source, as that would dilute the per-trigger partner yield. The jet structure and collision scaling indicate that at least some of the baryon excess is jet-like in origin. The relatively short formation time for baryons of such momenta suggests that allowing recombination of fragmentation partons with those from the medium may solve the problem and better reproduce the data. Both the Oregon and TAMU models have mechanisms to do this. However,

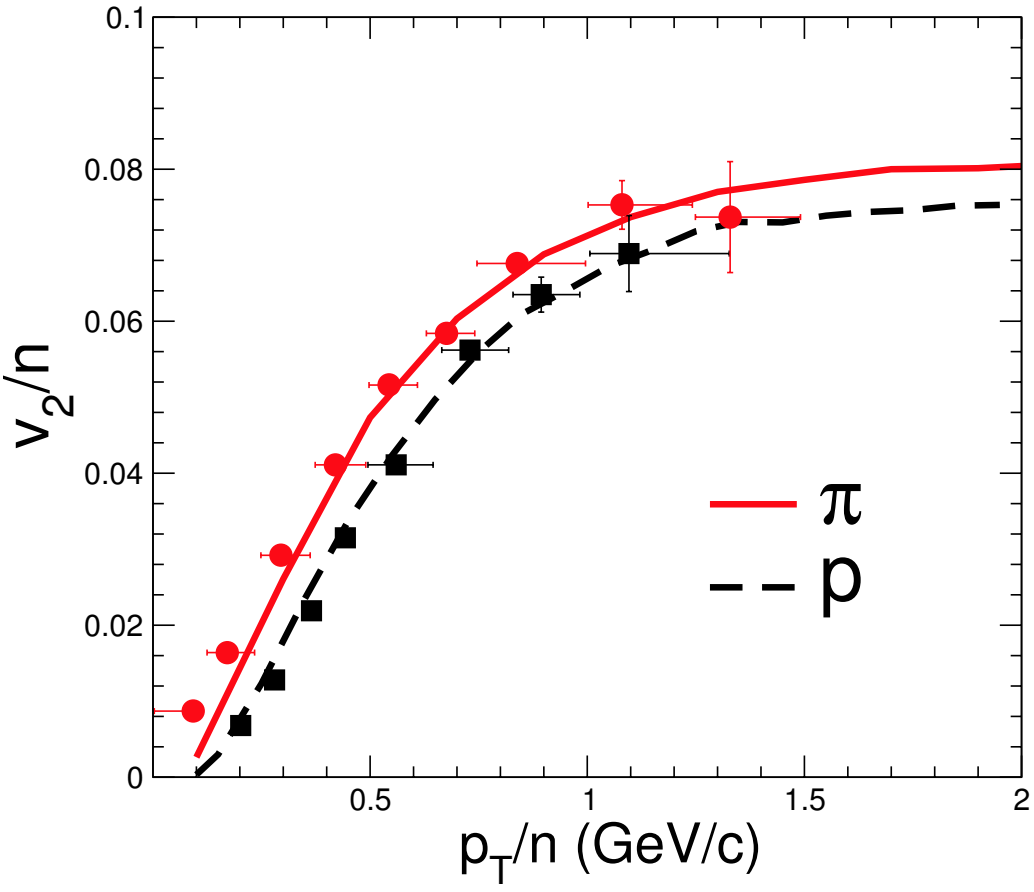

Fig. 56. v_2/n in the TAMU model, where n is the number of constituent quarks in a particle for protons and pions. Scaled pion (dashed line) and proton (dotted line) results from the TAMU model are shown in addition to measurements from the PHENIX experiment from minimum bias Au+Au reactions at $\sqrt{s_{NN}}$ = 200GeV [50]. This model allows for the recombination of hard partons and soft partons, as well as the decay of resonances such as the two pion decay of the ρ meson. One sees that, at least in this calculation, the addition of processes which mix hard and soft partons do not destroy the agreement for the model with v_2/n which is presumably a soft process.

such modification of the jet fragmentation function must also modify the elliptic flow, and could break the quark scaling needed to reproduce the observed v_2 trends. Hence, the jet structure of hadrons at 2–5 GeV/c p_T presents a challenge to models of the hadron formation.

Figure 56 shows a comparison of the elliptic flow calculated by the TAMU model [238] with PHENIX data from Au+Au collisions at $\sqrt{s_{NN}}$ = 200GeV. The model includes the recombination of hard and soft partons, as well as the decay of resonances such as the ρ. In this model, at least, the agreement of v_2 with the data is preserved—in addition a simple explanation is given for the excess of pion v_2 at low p_T. A similar conclusion in shown in [239]. This would seemingly attribute all the elliptic flow to the partonic phase leaving no room

for additional flow to be produced in the later, hadronic stage—which may be in contradiction to hydrodynamic interpretations of the hadronic state as demanded by a variety of signatures such as the p_T spectra of the protons and pions (see Section 3). It is clear that a more comprehensive comparison of observables should be undertaken to check the validity of these models. Higher-statistics jet studies with different identified particles by PHENIX in Run-4 will help clarify the situation.

7.5 Hadron Formation Time

In the discussion of the suppression of pions for $p_T > 2$GeV/c, we treat the pions as resulting from the fragmentation of hard-scattered quarks and gluons. The explanation of this suppression in terms of partonic energy loss assumes that the hadronic wave function only becomes coherent outside the medium. Protons have a different hadronic structure and larger mass, and so may have a different, shorter time scale for coherence.

Following [214], we can estimate the formation time for the different mass hadrons at moderate p_T in two different ways. According to the uncertainty principle, the formation time in the rest frame of the hadron can be related to the hadron size, R_h. In the laboratory frame, the hadron formation time is then given by

$$\tau_f \approx R_h \frac{E_h}{m_h} \tag{33}$$

where R_h is taken to be 0.5–1 fm. For a 10 GeV/c pion, this gives a formation time of 35–70 fm/c. For the p_T =2.5 GeV/c pions considered in this section, the formation time is 9–18 fm/c, well outside the collision region. However for p_T =2.5 GeV/c protons, the corresponding formation time is only 2.7 fm/c in the vacuum, suggesting the possibility that the hadronization process may begin inside the medium. However the formation of such heavy particles would presumably be delayed in a deconfined medium until the entire system began to hadronize.

If quarks and antiquarks from gluon splitting are assumed to combine into dipole color singlets leading to the final hadrons, the formation time may be estimated from the gluon emission time. Then the formation time for a hadron carrying a fraction z of the parton energy is given by

$$\tau_f \approx \frac{2E_h(1-z)}{k_T^2 + m_h^2}. \tag{34}$$

If z is 0.6–0.8 and $k_T \approx \Lambda_{QCD}$, proton formation times in the range of 1–4 fm result [214]. Such values again imply formation of the proton within the medium. Thus, it is possible that differing (and perhaps complicated) interactions with the medium may produce different scalings of proton and pion production and result in modified fragmentation functions in Au+Au collisions. However, most expectations are that this should lead to greater suppression rather than less. In fact, modified fragmentation functions measured in electron deep-inelastic scattering on nuclei by the HERMES experiment are often interpreted in terms of additional suppression for hadrons forming in the nuclear material.

7.6 Hard-Scattering Physics

If the dominant source of (anti)protons at intermediate p_T is not soft physics, is the explanation a medium-modified hard-process source? The near-side partner yields indicate that a significant fraction of the baryons have jet-like partners. However, in the parton energy loss scenario as described in Section 6, hard-scattered partons lose energy in medium prior to hadronization. Thus one would expect the same suppression for baryons and mesons. Furthermore, we know that the (anti)protons are as suppressed above $p_T = 5$GeV/c in a manner similar to pions . Hence for this explanation to be correct, there must exist a mechanism by which only partons leading to baryons between 2 and 5 GeV/c in p_T escape suppression.

Another key piece of information is that the elliptic flow v_2 for protons is large for p_T in the range 2-4 GeV/c. At low p_T this collective motion is attributed to different pressure gradients along and perpendicular to the impact parameter direction in semi-central collisions. At higher p_T it has been hypothesized that one could observe a v_2 due to smaller partonic energy loss for partons traveling along the impact parameter direction (shorter path in the medium) as opposed to larger partonic energy loss in the perpendicular direction (larger path in the medium). However, the data suggest that the pions have a large energy loss (a factor of five suppression in central Au+Au reactions) , while the protons do not. In this case one might expect that if the source of proton v_2 were energy loss, then proton v_2 would be significantly less than the v_2 for the pions. In fact, the opposite is experimentally observed: for $p_T > 2$ GeV/c, the proton v_2 is always larger than the pion v_2.

The contradictions the data create for both the "soft"- and "hard"-physics explanations may indicate that the correct physics involves an interplay between the two.

The anomalous enhancement of (anti)protons relative to pions at intermediate p_T = 2–5 GeV remains a puzzle. At lower transverse momentum particle production is a long-wavelength "soft" process and the transport of these hadrons and their precursor partons is reasonably described by hydrodynamics. As observed at lower energies, soft particles emitted from an expanding system receive a collective velocity boost to higher p_T resulting in an enhanced p/π and $\overline{p}/\pi$ ratio relative to proton-proton reactions at the same energy. We observe a similar phenomena at RHIC, for which the (anti) proton spectra and v_2 are roughly described in some hydrodynamic models up to approximately 2 GeV/c. Another class of calculations, referred to as recombination models, also boosts soft physics to higher p_T by coalescence of "dressed" partons. In the hydrodynamic models the quanta which are flowing are initially partons and then hadrons. The recombination models describe comoving valence partons which coalesce into hadrons, and do not reinteract. These two points of view may not be entirely contradictory, since both include a flowing partonic phase. If fact, it may be that the recombination models provide a mechanism by which hydrodynamics works to a much higher p_T than one might expect. The simplifying assumption of hadrons which do not interact is most probably an oversimplification and further refinement of the models will include this, though it may be that the hadronic phase will not modify the spectra as much as the hydrodynamic models might predict.

In both models, the (anti)proton enhancement as a function of centrality can be tuned to reproduce the apparent binary collision scaling observed in the data. An important distinction between the two is that in one case this enhancement is mass dependent and in the other it comes from the combination of quark momenta and thus distinguishes between baryons and mesons[10]. R_{CP} for the ϕ is similar to other mesons despite the fact that they are more massive than protons. This scaling with quark content, as opposed to mass, favors recombination models.

Further investigations into these intermediate p_T baryons reveals a near-angle correlation between particles, in a fashion characteristic of jet fragmentation. The near-angle associated particle yield increases by almost a factor of two in going from proton-proton and deuteron-gold reactions to gold-gold peripheral collisions. In addition, the partner yield is similar for trigger pions and protons, except in the most central gold-gold reactions. This appears to indicate a hard process source for a significant fraction of these baryons in contrast to the

[10] A caveat to this fact is that in the recombination models, it is the constituent-quark mass that is important, thereby giving a slightly larger mass to the strange quark.

previous mentioned physics scenarios. Quantifying the precise contribution is an important goal for future measurements.

The large (anti) baryon to pion excess relative to expectations from parton fragmentation functions at intermediate $p_T = 2 - 5$ GeV/c remains one of the most striking unpredicted experimental observations at RHIC. The data clearly indicate a new mechanism other than universal parton fragmentation as the dominant source of baryons and anti-baryons at intermediate p_T in heavy ion collisions. The boosting of soft physics, that dominates hadron production at low p_T, to higher transverse momentum has been explored with the context of hydrodynamic and recombination models. However, investigations into these intermediate p_T baryons reveals a near-angle correlation between particles, in a fashion characteristic of jet fragmentation. If instead these baryons have a partonic hard scattering followed by fragmentation source, this fragmentation process must be significantly modified. It is truly remarkable that these baryons have a large v_2 (typically 20%) indicative of strong collective motion and also a large "jet-like" near-side partner yield. At present, no theoretical framework provides a complete understanding of hadron formation in the intermediate p_T region.

8 FUTURE MEASUREMENTS

The previous sections have documented the breadth and depth of the PHENIX data from the first three years of RHIC operations, along with the physics implications of those results. Here we describe those measurements required to further define and characterize the state of matter formed at RHIC. In particular, we note that the study of penetrating probes, which are the most sensitive tools in this endeavor, is just beginning. The PHENIX experiment was specifically designed to address these probes with capabilities that are unique within the RHIC program and unprecedented in the field of relativistic heavy ion physics.

One can distinguish two broad classes of penetrating probes:

(1) Hard probes created at the very early stage of the collision which propagate through, and could be modified by, the medium. These are the QCD hard-scattering probes and the main observables are high-p_T particles coming from the fragmentation of jets, hidden charm (J/ψ production), open charm and eventually also bottom quark and Υ production.
(2) Electromagnetic probes (either real or virtual photons) which are created by the medium. Due to their large mean free path these probes can leave the medium without final-state interaction thus carrying direct information about the medium's conditions and properties. The main observables

here are low-mass e^+e^- pairs and the thermal radiation of the medium.

By their very nature, penetrating probes are also rare probes and consequently depend on the development of large values of the integrated luminosity. In the present data set the reach for high-p_T particles in PHENIX extends to roughly 10 GeV/c, and lower-cross-section measurements such as charmonium are severely limited. The dramatic improvement of the machine performance in the year 2004 run provides confidence that both this data set and those from future RHIC runs will dramatically extend our reach in the rare probes sector.

As part of a decadal planning of the RHIC operation, PHENIX has prepared a comprehensive document that outlines in great detail its scientific goals and priorities for the next 10 years together with the associated detector upgrade program needed to achieve them. The decadal plan [240] is centered around the systematic study of the penetrating probes listed above. The program is broad and can accommodate additions or modifications provided that a compelling physics case can be made. Measurements are mainly planned in Au+Au collisions at the full RHIC energy but they will be supplemented by other measurements varying the energy and/or the species and by the necessary reference measurements of $p + p$ and $p + A$ collisions. A short summary is given below.

8.1 High-p_T Suppression and Jet Physics

The most exciting results to date at RHIC are the discovery of high-p_T suppression of mesons, interpreted in terms of energy loss of quarks in a high-density medium, and the nonsuppression of baryons or equivalently, the anomalously high p/π ratio which still awaits a clear explanation. These two topics were extensively discussed in Sections 6 and 7, respectively.

The data collected so far are superb. However, they suffer from limited reach in transverse momentum, limited particle identification capabilities and limited statistics in particular for detailed studies of jet correlations. PHENIX has a program for further studies of the high-p_T-suppression phenomena and jet physics which aims at overcoming these limitations.

It will be necessary to trace the suppression pattern to much higher p_T to determine whether (and if so, when) the suppression disappears and normal perturbative QCD behavior sets in. High-luminosity runs will be needed, with at least a factor of 50 more statistics. PHENIX is particularly able to perform these measurements with its excellent capability of triggering on high-momentum π^0's.

PHENIX has performed several particle correlation analyses and has demonstrated that the experiment's aperture at mid-rapidity is sufficient to conduct these studies. Currently, these analyses are limited by the available statistics. Again, increasing the data sample by a factor of 50–100 will allow a variety of correlation studies using trigger particles with much-higher-momentum than studied to date. A particularly interesting case is the study of high-momentum γ-jet correlations, which have vastly reduced trigger bias, since the trigger photons propagate through the medium with a very long mean free path.

To further elucidate the baryon puzzle, additional data is required with better separation between baryons and mesons. An upgrade consisting of an aerogel Cerenkov counter and a high-resolution TOF detector is expected to be completed in time for the year 2006. A portion of this aerogel counter was already installed prior of the year 2004 run and performed according to expectations. Once completed, this high-p_T detector will allow identification of $\pi, K/p$ to beyond 8 GeV/c in p_T.

8.2 J/ψ Production

Suppression of heavy quarkonia is one of the earliest and most striking proposed signatures of deconfinement. The suppression mechanism follows directly from the Debye screening expected in the medium, which reduces the range of the potential between charm quark and anti-quark pairs [241]. The NA38 and NA50 experiments have carried out a systematic study of J/ψ and ψ' at the CERN-SPS in $p+p$, $p+A$, light ion, and Pb+Pb collisions providing some of the most intriguing results of the relativistic heavy ion program for more than ten years. The NA50 experiment observed an anomalous suppression of J/ψ in central Pb+Pb collisions at $\sqrt{s_{NN}}$=17.2 GeV [242]. The suppression, which is of the order of 25% with respect to the normal suppression in nuclear matter, has been interpreted by the NA50 authors as evidence for deconfinement of quarks and gluons. Although this interpretation is not universally shared [243,244], the results of NA38 and NA50 demonstrate the utility and great interest in understanding the fate of charmonium in dense nuclear matter.

The theoretical expectations at RHIC energies are not at all clear. They range from total suppression in the traditional Debye screening scenario to enhancement in coalescence models [245–247] and in statistical hadronization models [248,249], of c and $\overline{c}$ quarks. Although some versions of the coalescence model seem disfavored from our very limited data set [51], a more conclusive statement on these models has to await the much larger data set of the year 2004 run.

PHENIX has unprecedented capabilities for the study of the J/ψ in Au+Au collisions. The J/ψ can be measured via its $\mu^+\mu^-$ decay channel at forward and backward rapidities in the muon spectrometers and via its e^+e^- decay channel at mid-rapidity in the central arm spectrometers. From the recorded luminosity of the year 2004 run, we expect several thousand and $\sim$500 J/ψ in the muon and central arms, respectively. This data set will allow us a first look at the J/ψ production pattern at RHIC. However, it could well be marginal for a complete characterization as a function of centrality and p_T, so that it is likely that further higher-luminosity runs will be required. Also the $p+p$ and d+Au baseline measurements performed in the year 2001 – 2003 runs have large statistical uncertainties, and higher-statistics versions for these colliding species will be needed. A high-luminosity $p+p$ run is planned in the year 2005 and high-luminosity $d+A$ or $p+A$ are still to be scheduled in the next years.

8.3 Charm Production

Charm quarks are expected to be produced in the initial hard collisions between the incoming partons. The dominant mechanism is gluon fusion and thus the production cross section is sensitive to the gluon density in the initial state. The $c\overline{c}$ production cross section is sizable at RHIC energies with a few $c\overline{c}$ pairs and therefore several open charm mesons per unit of rapidity in central Au+Au collisions. As a result, charm observables become readily accessible at RHIC and offer additional and extraordinarily valuable diagnostic tools. For example, it is vitally important to perform measurements of charm flow and to determine the energy loss of charm quarks in the medium. Such measurements will determine if the bulk dynamics observed for light quarks extend to charm quarks, which could in fact have very different behavior due to their much larger mass. Again the potential of PHENIX in this domain is unique with its capability of measuring open charm in a broad rapidity range, in the central and muon arms, via both the electron and muon decay channels. An additional unique feature is the possibility to measure correlated semileptonic charm decays by detecting $e-\mu$ coincidences from correlated $D\overline{D}$ decays. Such a measurement is particularly interesting for the study of charm-quark energy loss which may differ significantly from that observed for lighter quarks [250–252]. A first study of $e-\mu$ coincidences should be feasible with the year 2004 data.

To date PHENIX has measured charm production cross section in an indirect way through high-p_T single electrons [42] assuming that all electrons (after measuring and subtracting the contributions from light hadrons and photon conversions) originate from the semileptonic decays of charm quarks. Although the charm cross section has large uncertainties, the centrality dependence of the charm rapidity density demonstrates that charm production follows binary

scaling as shown in Fig. 34. Improvements and additional information are expected from the much higher statistic of the year 2004 data.

A qualitatively new advance for PHENIX in the charm and also the beauty sector will be provided by the implementation of the silicon vertex detector. An upgrade project is underway to install in the next five years a silicon vertex tracker, including a central arm barrel and two end caps in front of the two muon spectrometers. The vertex tracker will allow us to resolve displaced vertices and therefore to directly identify open charm mesons via hadronic, e.g. $D \rightarrow K\pi$, as well as semi-leptonic decays. The heavy-quark physics topics accessible with the vertex tracker include production cross section and energy loss of open charm and open beauty, and spectroscopy of charmonium and bottomonium states, each of which should provide incisive new details on the properties of the created medium.

8.4 Low-Mass Dileptons

Low-mass dileptons are considered the most sensitive probe of chiral symmetry restoration primarily through ρ meson decays. Due to its very short lifetime (τ = 1.3 fm/c) compared to that of the typical fireball of $\sim$ 10 fm/c, most of the ρ mesons decay inside the medium providing an unique tool to observe in-medium modifications of its properties (mass and/or width) which could be linked to chiral symmetry restoration. The situation is somewhat different but still interesting for the ω and ϕ mesons. Because of their much longer lifetimes (τ = 23 fm/c and 46 fm/c for the ω and ϕ, respectively) they predominantly decay outside the medium, after regaining their vacuum properties, with only a small fraction decaying inside the medium. Since the measurement integrates over the history of the collision, this may result in a small modification of the line shape of these two mesons which PHENIX might be able to observe with its excellent mass resolution. PHENIX also has the unprecedented capability of simultaneously measuring within the same apparatus the ϕ meson decay through e^+e^- and K^+K^- channels. The comparison of the branching ratios to these two channels provides a very sensitive tool for in-medium modifications of the ϕ and K mesons.

The CERES experiment at CERN has confirmed the unique physics potential of low-mass dileptons [253–255]. An enhancement of electron pairs was observed in the mass region m = 0.2–0.6 GeV/c^2 in Pb+Au collisions at $\sqrt{s_{NN}}$=17.2 GeV with respect to $p+p$ collisions. The results have triggered a wealth of theoretical activity and can be explained by models which invoke in-medium modification of the ρ meson (dropping of its mass and/or broadening of its width) [256]. The precision of the CERES data has been so far insufficient to distinguish between the different models. Results with higher

statistics and better mass resolution are expected from the NA60 experiment that is studying the production of low-mass dimuons in In+In collisions [257]. Theoretical calculations [258] show that the enhancement should persist at RHIC energies and that PHENIX with its excellent mass resolution has an unique opportunity to do precise spectroscopy of the light vector mesons and to shed more light on the origin of the enhancement of the low-mass-pair continuum.

The measurement of low-mass electron pairs is however a very challenging one. The main difficulty stems from the huge combinatorial background created by the pairing of e^+ and e^- tracks from unrecognized π^0 Dalitz decays and γ conversions. PHENIX is developing a novel Cerenkov detector that, in combination with the recently installed coil which makes the magnetic field zero close to the beam axis, will effectively reduce this combinatorial background by almost two orders of magnitude [259]. The detector, operated in pure CF_4, consists of a 50-cm-long radiator directly coupled, in a windowless configuration, to a triple GEM detector which has a CsI photocathode evaporated on the top face of the first GEM foil and pad read out at the bottom of the GEM stack [260]. The R&D phase to demonstrate the validity of the concept is nearing completion. The detector construction phase is starting now with installation foreseen in time for the year 2006 — 2007. With this detector PHENIX will have the unprecedented ability to perform high-quality measurements over the whole dilepton mass range from the π^0 Dalitz decay up to the charmonium states.

8.5 Thermal Radiation

A prominent topic of interest in the field of relativistic heavy-ion collisions is the identification of the thermal radiation emitted by the system and in particular the thermal radiation emitted by the quark-gluon plasma via $q\overline{q}$ annihilation. Such radiation is a direct fingerprint of the matter formed and is regarded as a very strong signal of deconfinement. Its spectral shape should provide a direct measurement of the plasma temperature.

In principle the thermal radiation can be studied through real photons or dileptons, since real and virtual photons carry basically the same physics message. In practice the measurements are extremely challenging. The thermal radiation is expected to be a small signal compared to the large background from competing processes, hadron decays for real photons and Dalitz decays and γ conversions for dileptons, the former being larger by orders of magnitude compared to the latter. But in both cases, a very precise knowledge of all these sources is an absolutely necessary prerequisite. After subtracting these sources, one still needs to disentangle other contributions which might be

comparable or even stronger, mainly the contributions of initial hard-parton scattering to direct photons and of semileptonic decays of charm mesons to dileptons.

Theoretical calculations have singled out the dilepton mass range m = 1–3 GeV/c^2 as the most appropriate window where the QGP radiation could dominate over other contributions [261,262]. Measurements in this intermediate mass range carried out at the CERN SPS by HELIOS and NA50 have revealed an excess of dileptons, but this excess could be explained by hadronic contributions [263].

There is no conclusive evidence for QGP thermal photons from the CERN experiments (for a recent review see [264]). From the theoretical point of view it is clear that in the low-p_T region ($p_T < 2$ GeV/c) the real photon spectrum is dominated by hadronic sources and the thermal radiation from the hadron gas. It is only in the high-p_T region where one might have a chance to observe the thermal radiation from the QGP.

Preliminary PHENIX results show evidence for direct real photons at $p_T > 4$ GeV/c from the initial hard scatterings. The errors are relatively large leaving room for a comparable contribution of thermal photons. The high statistics of the year 2004 run will provide the first real opportunity to search for the QGP thermal radiation in PHENIX both in the dilepton and real photon channels. However, the search for this elusive signal might take some time as it will probably require equally-high-statistics runs of reference data in $p + p$ and $p + A$ collisions for a precise mapping of all the other contributions (hadronic + pQCD for real photons and hadronic + charm for dileptons).

9 SUMMARY AND CONCLUSIONS

The PHENIX data set from the first three years of RHIC operation provides an extensive set of measurements, from global variables to hadron spectra to high-p_T physics to heavy-flavor production. From this rich menu we have reviewed those aspects of the present data that address the broad features of the matter created in Au+Au collisions at RHIC, namely, energy and number density, thermalization, critical behavior, hadronization, and possible deconfinement.

We first investigated whether the transverse energy and multiplicity measurements of PHENIX demonstrate that a state of high-energy-density matter is formed in Au+Au collision at RHIC. We estimated from our $dE_T/d\eta$ measurement that the peak energy density in the form of created secondary particles is at least 15 GeV/fm^3. If we use a thermalization time of 1 fm/c provided by the hydrodynamic models from the elliptic flow, then the value of the energy

density of the first thermalized state would be in excess of 5 GeV/fm^3. These values are well in excess of the $\sim$1 GeV/fm^3 obtained in lattice QCD as the energy density needed to form a deconfined phase. Naïve expectations prior to RHIC turn-on that $dE_T/d\eta$ and $dN_{ch}/d\eta$ could be factorized into a "soft" and a pQCD jet component are not supported by the data. Results from a new class of models featuring initial-state gluon saturation compare well with RHIC multiplicity and E_T data.

We then examined our data and various theoretical models to investigate the degree to which the matter formed at RHIC appears to be thermalized. The measured yields and spectra of hadrons are consistent with thermal emission from a strongly expanding source, and the observed strangeness production is consistent with predictions based on complete chemical equilibrium. The scaling of the strength of the elliptic flow v_2 with eccentricity shows that a high degree of collectivity is built up at a very early stage of the collision. The hydro models which include both hadronic and QGP phases reproduce the qualitative features of the measured $v_2(p_T)$ of pions, kaons, and protons. These hydro models require early thermalization ($\tau_{therm} \leq 1$ fm/c) and high initial energy density $\varepsilon \geq 10$ GeV/fm^3. These points of agreement between the data and the hydrodynamic and thermal models can be interpreted as strong evidence for formation of high-density matter that thermalizes very rapidly.

However several of the hydro models fail to reproduce the $v_2(p_T)$ of pions, protons, and spectra of pions and protons simultaneously. Given this disagreement it is not yet possible to make an unequivocal statement regarding the presence of a QGP phase based on comparisons to hydrodynamic calculations. The experimentally measured HBT source parameters, especially the small value of $R_{\rm long}$ and the ratio $R_{\rm out}/R_{\rm side} \approx 1$, are not reproduced by the hydrodynamic calculations. Hence we currently do not have a consistent picture of the space-time dynamics of reactions at RHIC as revealed by spectra, v_2 and HBT. These inconsistencies prevent us from drawing firm conclusions on properties of the matter such as the equation of state and the presence of a mixed phase.

Critical behavior near the phase boundary can produce nonstatistical fluctuations in observables such as the net-charge distribution and the average transverse momentum. Our search for charge fluctuations has ruled out the most naïve model of charge fluctuations in a QGP, but it is unclear if the charge fluctuation signature can survive hadronization. Our measurement of $\langle p_T \rangle$ fluctuations is consistent with the effect expected of high-p_T jets, and it gives a severe constraint on the fluctuations that were expected for a sharp phase transition.

Many of these observables—for instance, large $dE/d\eta$ and $dN_{ch}/d\eta$, strangeness enhancement, strong radial flow, and elliptic flow—have been observed in

heavy ion collisions at lower energies. We have found smooth changes in these observables as a function of $\sqrt{s_{NN}}$ from AGS energies to SPS energies to RHIC energy. The $dE_T/d\eta$ increases by about 100% and the strength of the elliptic flow increase by about 50% from SPS to RHIC. The strangeness suppression factor γ_s and the radial expansion velocity $\langle\beta_T\rangle$ vary smoothly from AGS to RHIC energies. No sudden change with collision energy has been observed.

The strong suppression of high-p_T particle production at RHIC is a unique phenomenon that has not been previously observed. Measurements of two-hadron azimuthal-angle correlations at high p_T and the x_T scaling in Au+Au collisions confirm the dominant role of hard scattering and subsequent jet fragmentation in the production of high-p_T hadrons. Measurements in deuteron-gold collisions demonstrate that any initial-state modification of nuclear parton distributions causes little or no suppression of hadron production for $p_T > 2$ GeV/c at mid-rapidity. This conclusion is further strengthened by the observed binary scaling of direct photon and open charm yields in Au+Au. Combined together, these observations provide direct evidence that Au+Au collisions at RHIC have produced matter at extreme densities.

Medium-induced energy loss, predominantly via gluon bremsstrahlung emission, is the only currently known physical mechanism that can fully explain the magnitude of the observed high-p_T suppression. The approximately flat suppression factor $R_{AA}(p_T)$ observed in the data, which was predicted by the GLV energy loss model, rules out the simplest energy loss models which predicted a constant energy loss per unit length. However, the model by Wang *et al.* obtains the same flat $R_{AA}(p_T)$ from apparently different physics. From the GLV model, the initial gluon number density, $dn_g/dy \approx 1000$ and initial energy density, $\varepsilon_0 \approx 15\text{GeV/fm}^3$, have been obtained. These values are consistent with the energy density obtained from our $dE_T/d\eta$ measurement as well as ones from the hydro models.

The large (anti)baryon to pion excess relative to expectations from parton fragmentation functions at intermediate p_T (2 — 5 GeV/c) is both an unpredicted and one of the most striking experimental observation at RHIC. The data clearly indicates that a mechanism other than universal parton fragmentation is the dominant source of (anti-)baryons in the intermediate p_T range in heavy ion collisions. The boosting of soft physics to higher transverse momentum has been explored within the context of hydrodynamics and recombination models. Hydrodynamic models can readily explain the baryon to meson ratio as a consequence of strong radial flow, but these models have difficulties reproducing the difference in v_2 between protons and mesons above 2 GeV/c. Recombination models provide a natural explanation for the large baryon to meson ratio as well as the apparent quark-number scaling of the elliptic flow. However, investigations into these intermediate p_T baryons reveal a near-angle correlation between particles, in a fashion characteristic of

jet fragmentation. If instead these baryons have a partonic hard scattering followed by fragmentation, this fragmentation process must be significantly modified. It is truly remarkable that these baryons have a large v_2 of ≈ 20 % typically indicative of strong collective motion and also a large jet-like near-side partner yield. At present, no model provides a complete understanding of hadron formation in the intermediate p_T regime.

The initial operation of RHIC has produced the impressive quantity of significant results described above. These striking findings call for additional efforts to define, clarify and characterize the state of matter formed at RHIC. Further study of the collisions using hard probes such as high-p_T particles, open charm, and J/ψ, and electromagnetic probes such as direct photons, thermal photons, thermal dileptons, and low-mass lepton pairs are particularly important. The utilization of these penetrating probes is just beginning, and we expect these crucial measurements based on the very-high-statistics data of the year 2004 run will provide essential results towards understanding of the dense matter created at RHIC.

Advances in the theoretical understanding of relativistic heavy ion collisions is vital for the quantitative study of the dense matter formed at RHIC. While there is rapid and significant progress in this area, a coherent and consistent picture of heavy ion collisions at RHIC, from the initial formation of the dense matter to the thermalization of the system to the hadronization to the freezeout, remains elusive. With such a consistent model, it will become possible to draw definitive conclusions on the nature of the matter and to quantitatively determine its properties. The comprehensive data sets from global variables to penetrating probes provided by PHENIX at present and in the future will prove essential in constructing and constraining a consistent model of heavy ion collisions to determine the precise nature of the matter created at RHIC.

In conclusion, there is compelling experimental evidence that heavy-ion collisions at RHIC produce a state of matter characterized by very high energy densities, density of unscreened color charges ten times that of a nucleon, large cross sections for the interaction between strongly interacting particles, strong collective flow, and early thermalization. Measurements indicate that this matter modifies jet fragmentation and has opacity that is too large to be explained by any known hadronic processes. This state of matter is not describable in terms of ordinary color-neutral hadrons, because there is no known self-consistent theory of matter composed of ordinary hadrons at the measured densities. The most economical description is in terms of the underlying quark and gluon degrees of freedom. Models taking this approach have scored impressive successes in explaining many, but not all, of the striking features measured to date. There is not yet irrefutable evidence that this state of matter is characterized by quark deconfinement or chiral symmetry restora-

tion, which would be a direct indication of quark-gluon plasma formation. The anticipated program of additional incisive experimental measurements combined with continued refinement of the theoretical description is needed to achieve a complete understanding of the state of matter created at RHIC.

ACKNOWLEDGEMENTS

We thank the staff of the Collider-Accelerator and Physics Departments at Brookhaven National Laboratory and the staff of the other PHENIX participating institutions for their vital contributions. We acknowledge support from the Department of Energy, Office of Science, Nuclear Physics Division, the National Science Foundation, Abilene Christian University Research Council, Research Foundation of SUNY, and Dean of the College of Arts and Sciences, Vanderbilt University (U.S.A), Ministry of Education, Culture, Sports, Science, and Technology and the Japan Society for the Promotion of Science (Japan), Conselho Nacional de Desenvolvimento Científico e Tecnológico and Fundaç ao de Amparo à Pesquisa do Estado de S ao Paulo (Brazil), Natural Science Foundation of China (People's Republic of China), Centre National de la Recherche Scientifique, Commissariat à l'Énergie Atomique, Institut National de Physique Nucléaire et de Physique des Particules, and Association pour la Recherche et le Développement des Méthodes et Processus Industriels (France), Ministry of Industry, Science and Tekhnologies, Bundesministerium für Bildung und Forschung, Deutscher Akademischer Austausch Dienst, and Alexander von Humboldt Stiftung (Germany), Hungarian National Science Fund, OTKA (Hungary), Department of Atomic Energy and Department of Science and Technology (India), Israel Science Foundation (Israel), Korea Research Foundation and Center for High Energy Physics (Korea), Russian Ministry of Industry, Science and Tekhnologies, Russian Academy of Science, Russian Ministry of Atomic Energy (Russia), VR and the Wallenberg Foundation (Sweden), the U.S. Civilian Research and Development Foundation for the Independent States of the Former Soviet Union, the US-Hungarian NSF-OTKA-MTA, and the US-Israel Binational Science Foundation.

References

[1] G. F. Chapline, M. H. Johnson, E. Teller, M. S. Weiss, Phys. Rev. D8 (1973) 4302.

[2] T. D. Lee, G. C. Wick, Phys. Rev. D9 (1974) 2291.

[3] T. D. Lee, Rev. Mod. Phys. 47 (1975) 267.

[4] T. D. Lee, cU-TP-170, Published in Trans.N.Y.Acad.Sci.Ser.2 **v.40** 1980:0111. (1979).

[5] J. C. Collins, M. J. Perry, Phys. Rev. Lett. 34 (1975) 1353.

[6] N. Itoh, Prog. Theor. Phys. 44 (1970) 291.

[7] E. V. Shuryak, Phys. Rept. 61 (1980) 71.

[8] M. Creutz, Phys. Rev. D15 (1977) 1128.

[9] K. G. Wilson, Phys. Rev. D10 (1974) 2445.

[10] E. Laermann, O. Philipsen, Ann. Rev. Nucl. Part. Sci. 53 (2003) 163.

[11] F. Karsch, Lect. Notes Phys. 583 (2002) 209.

[12] K. Rajagopal, Acta Phys. Polon. B31 (2000) 3021.

[13] Z. Fodor, S. D. Katz, JHEP 0404 (2004) 050.

[14] S. Ejiri, et al., Prog. Theor. Phys. Suppl. 153 (2004) 118.

[15] W. Greiner, S. Schramm, E. Stein, 2nd Edition, Springer-Verlag, 2002.

[16] V. V. Klimov, Sov. Phys. JETP 55 (1982) 199.

[17] H. A. Weldon, Phys. Rev. D26 (1982) 1394.

[18] S. Datta, F. Karsch, P. Petreczky, I. Wetzorke, Nucl. Phys. Proc. Suppl. 119 (2003) 487.

[19] M. Asakawa, T. Hatsuda, Phys. Rev. Lett. 92 (2004) 012001.

[20] S. Datta, F. Karsch, P. Petreczky, I. Wetzorke, Phys. Rev. D69 (2004) 094507.

[21] F. Karsch, et al., Nucl. Phys. A715 (2003) 701.

[22] E. V. Shuryak, I. Zahed, Phys. Rev. D70 (2004) 054507.

[23] B. Müller, we wish to acknowledge B. Müller for this observation. (2004).

[24] E. Shuryak, Prog. Part. Nucl. Phys. 53 (2004) 273.

[25] M. Gyulassy, L. McLerran, Nucl. Phys. A750 (2005) 30.

[26] G. Baym, in Proceedings of the Bielefeld Workshop on *Quark Matter Formation and Heavy Ion Collisions*, M. Jacob and H. Satz, ed. (May, 1982). (1982).

[27] M. Plümer, S. Raha, R. Weiner, Nucl. Phys. A418 (1984) 549c.

[28] B. Müller (1992).

[29] K. Kajantie, M. Laine, K. Rummukainen, Y. Schroder, Phys. Rev. D67 (2003) 105008.

[30] A. D. Linde, Phys. Lett. B96 (1980) 289.

[31] D. J. Gross, R. D. Pisarski, L. G. Yaffe, Rev. Mod. Phys. 53 (1981) 43.

[32] Bear-Mountain, nearly the entire history of the various experimental efforts is documented in the proceedings of the various "Quark Matter" conferences, which began in 1981. A seminal document in the history of the field is the report of the "Bear Mountain" conference: *Report of the workshop on BeV/nucleon collisions of heavy ions– how and why*, Bear Mountain, New York, Nov. 29-Dec. 1, 1974 (BNL-AUI, 1975), (1974).

[33] G. Baym, Nucl. Phys. A698 (2002) XXIII.

[34] NSAC, 2002 NSAC Long-Range Plan: *Opportunities in Nuclear Science*, A Long-Range Plan for the Next Decade (April 2002). Available from http://www.sc.doe.gov/henp/np/nsac/nsac.html, (2002).

[35] PHENIX Collaboration, PHENIX ≡ Pioneering High Energy Nuclear Interaction eXperiment. Full details are available from http://www.phenix.bnl.gov/ . (2004).

[36] PHENIX, pHENIX Conceptual Design Report 1993 (PX20, BNL48922, internal report), (1993).

[37] K. Adcox, et al., Phys. Rev. Lett. 86 (2001) 3500.

[38] K. Adcox, et al., Phys. Rev. Lett. 87 (2001) 052301.

[39] K. Adcox, et al., Phys. Rev. Lett. 88 (2002) 022301.

[40] K. Adcox, et al., Phys. Rev. Lett. 88 (2002) 242301.

[41] K. Adcox, et al., Phys. Rev. Lett. 88 (2002) 192302.

[42] K. Adcox, et al., Phys. Rev. Lett. 88 (2002) 192303.

[43] K. Adcox, et al., Phys. Rev. Lett. 89 (2002) 092302.

[44] K. Adcox, et al., Phys. Rev. Lett. 89 (2002) 082301.

[45] K. Adcox, et al., Phys. Rev. C 66 (2002) 024901.

[46] K. Adcox, et al., Phys. Rev. Lett. 89 (2002) 212301.

[47] K. Adcox, et al., Phys. Lett. B561 (2003) 82.

[48] K. Adcox, et al., Phys. Rev. C69 (2004) 024904.

[49] S. S. Adler, et al., Phys. Rev. Lett. 91 (2003) 072301.

[50] S. S. Adler, et al., Phys. Rev. Lett. 91 (2003) 182301.

[51] S. S. Adler, et al., Phys. Rev. C69 (2004) 014901.

[52] S. S. Adler, et al., Phys. Rev. Lett. 91 (2003) 172301.

[53] S. S. Adler, et al., Phys. Rev. C69 (2004) 034910.

[54] S. S. Adler, et al., Phys. Rev. C69 (2004) 034909.

[55] S. S. Adler, et al., Phys. Rev. Lett. 93 (2004) 092301.

[56] S. S. Adler, et al., Phys. Rev. Lett. 91 (2003) 241803.

[57] S. S. Adler, et al., Phys. Rev. Lett. 92 (2004) 051802.

[58] S. S. Adler, et al., Phys. Rev. Lett. 91 (2003) 072303.

[59] I. Arsene, et al., Phys. Rev. Lett. 91 (2003) 072305.

[60] B. B. Back, et al., Phys. Rev. Lett. 91 (2003) 072302.

[61] J. Adams, et al., Phys. Rev. Lett. 91 (2003) 072304.

[62] S. S. Adler, et al. (2004).

[63] S. S. Adler, et al., Phys. Rev. Lett. 93 (2004) 152302.

[64] J. D. Bjorken, Phys. Rev. D27 (1983) 140.

[65] L. Ahle, et al., Phys. Lett. B332 (1994) 258.

[66] T. Alber, et al., Phys. Rev. Lett. 75 (1995) 3814.

[67] S. S. Adler, et al. (2004).

[68] A. Krasnitz, Y. Nara, R. Venugopalan, Nucl. Phys. A717 (2003) 268.

[69] P. F. Kolb, J. Sollfrank, U. W. Heinz, Phys. Rev. C62 (2000) 054909.

[70] S.-y. Li, X.-N. Wang, Phys. Lett. B527 (2002) 85.

[71] B. B. Back, et al., Phys. Rev. Lett. 85 (2000) 3100.

[72] X.-N. Wang, M. Gyulassy, Phys. Rev. Lett. 86 (2001) 3496.

[73] A. Bazilevsky, Nucl. Phys. A715 (2003) 486.

[74] V. Topor Pop, et al., Phys. Rev. C68 (2003) 054902.

[75] D. Kharzeev, M. Nardi, Phys. Lett. B507 (2001) 121.

[76] D. Kharzeev, E. Levin, Phys. Lett. B523 (2001) 79.

[77] K. J. Eskola, K. Kajantie, P. V. Ruuskanen, K. Tuominen, Nucl. Phys. B570 (2000) 379.

[78] K. J. Eskola, P. V. Ruuskanen, S. S. Rasanen, K. Tuominen, Nucl. Phys. A696 (2001) 715.

[79] F. Becattini, Z. Phys. C69 (1996) 485.

[80] F. Becattini, U. W. Heinz, Z. Phys. C76 (1997) 269 (e).

[81] P. Braun-Munzinger, K. Redlich, J. Stachel (2003).

[82] M. Kaneta, N. Xu (2004).

[83] J. Cleymans, B. Kampfer, M. Kaneta, N. Wheaton, S.and Xu (2004).

[84] J. Adams, et al., Phys. Rev. Lett. 92 (2004) 182301.

[85] P. Braun-Munzinger, D. Magestro, K. Redlich, J. Stachel, Phys. Lett. B518 (2001) 41.

[86] D. Magestro, J. Phys. G28 (2002) 1745.

[87] F. Becattini, M. Gazdzicki, A. Keranen, J. Manninen, R. Stock, Phys. Rev. C69 (2004) 024905.

[88] E. Schnedermann, J. Sollfrank, U. W. Heinz, Phys. Rev. C48 (1993) 2462.

[89] G. Rai, Nucl. Phys. A681 (2001) 181.

[90] H. Dobler, J. Sollfrank, U. W. Heinz, Phys. Lett. B457 (1999) 353.

[91] C. Alt, et al., J. Phys. G30 (2004) S119.

[92] T. Peitzmann, Eur. Phys. J. C26 (2003) 539.

[93] M. M. Aggarwal, et al., Phys. Rev. C67 (2003) 014906.

[94] J. Adams, et al., Phys. Rev. Lett. 92 (2004) 112301.

[95] C. Adler, et al., Phys. Rev. Lett. 87 (2001) 182301.

[96] C. Alt, et al., Phys. Rev. C68 (2003) 034903.

[97] G. Agakichiev, et al., Phys. Rev. Lett. 92 (2004) 032301.

[98] D. Teaney, J. Lauret, E. V. Shuryak (2001).

[99] P. Huovinen, P. F. Kolb, U. W. Heinz, P. V. Ruuskanen, S. A. Voloshin, Phys. Lett. B503 (2001) 58.

[100] D. H. Rischke, M. Gyulassy, Nucl. Phys. A597 (1996) 701.

[101] G. F. Bertsch, Nucl. Phys. A498 (1989) 173c.

[102] S. Pratt, Phys. Rev. D33 (1986) 1314.

[103] S. Pratt, Phys. Rev. Lett. 53 (1984) 1219.

[104] A. N. Makhlin, Y. M. Sinyukov, Z. Phys. C39 (1988) 69.

[105] S. Pratt, T. Csoergoe, J. Zimanyi, Phys. Rev. C42 (1990) 2646.

[106] J. Adams, et al., Phys. Rev. Lett. 93 (2004) 012301.

[107] F. Retiere, J. Phys. G30 (2004) S827.

[108] M. Csanad, T. Csorgo, B. Lorstad, A. Ster, J. Phys. G30 (2004) S1079.

[109] P. F. Kolb, R. Rapp, Phys. Rev. C67 (2003) 044903.

[110] T. Hirano, K. Tsuda, Phys. Rev. C66 (2002) 054905.

[111] T. Hirano, Y. Nara, Nucl. Phys. A743 (2004) 305.

[112] P. F. Kolb, U. Heinz (2003).

[113] D. Molnar, P. Huovinen, Phys. Rev. Lett. 94 (2005) 012302.

[114] D. A. Teaney, J. Phys. G30 (2004) S1247.

[115] U. W. Heinz, P. F. Kolb (2002).

[116] Y. M. Sinyukov, S. V. Akkelin, Y. Hama, Phys. Rev. Lett. 89 (2002) 052301.

[117] F. Grassi, Y. Hama, S. S. Padula, J. Socolowski, Octavio, Phys. Rev. C62 (2000) 044904.

[118] F. Cooper, G. Frye, Phys. Rev. D10 (1974) 186.

[119] S. Soff, S. A. Bass, A. Dumitru, Phys. Rev. Lett. 86 (2001) 3981.

[120] D. Zschiesche, S. Schramm, H. Stocker, W. Greiner, Phys. Rev. C65 (2002) 064902.

[121] F. Karsch, E. Laermann .

[122] S. Soff (2002).

[123] G. N. Fowler, R. M. Weiner, Phys. Lett. B70 (1977) 201.

[124] G. N. Fowler, E. M. Friedlander, R. M. Weiner, Phys. Lett. B104 (1981) 239.

[125] L. Van Hove, Physica 147A (1987) 19.

[126] G. J. Alner, et al., Phys. Lett. B160 (1985) 193.

[127] S. Jeon, V. Koch, Phys. Rev. Lett. 85 (2000) 2076.

[128] M. Asakawa, U. W. Heinz, B. Muller, Phys. Rev. Lett. 85 (2000) 2072.

[129] H. Heiselberg, A. D. Jackson, Phys. Rev. C63 (2001) 064904.

[130] R. Albrecht, et al., Z. Phys. C45 (1989) 31.

[131] P. Carruthers, C. C. Shih, Phys. Lett. B165 (1985) 209.

[132] H. Sorge, Phys. Rev. C52 (1995) 3291.

[133] M. J. Tannenbaum, Phys. Lett. B498 (2001) 29.

[134] R. Korus, S. Mrowczynski, M. Rybczynski, Z. Wlodarczyk, Phys. Rev. C64 (2001) 054908.

[135] J. T. Mitchell, J. Phys. G30 (2004) S819.

[136] E. G. Ferreiro, F. del Moral, C. Pajares, Phys. Rev. C69 (2004) 034901.

[137] S. Gavin, Phys. Rev. Lett. 92 (2004) 162301.

[138] J. F. Owens, Rev. Mod. Phys. 59 (1987) 465.

[139] G. Bunce, N. Saito, J. Soffer, W. Vogelsang, Ann. Rev. Nucl. Part. Sci. 50 (2000) 525.

[140] R. Cutler, D. W. Sivers, Phys. Rev. D17 (1978) 196.

[141] R. Cutler, D. W. Sivers, Phys. Rev. D16 (1977) 679.

[142] B. L. Combridge, J. Kripfganz, J. Ranft, Phys. Lett. B70 (1977) 234.

[143] F. Aversa, P. Chiappetta, M. Greco, J. P. Guillet, Nucl. Phys. B327 (1989) 105.

[144] B. Jager, A. Schafer, M. Stratmann, W. Vogelsang, Phys. Rev. D67 (2003) 054005.

[145] E. D. Bloom, et al., Phys. Rev. Lett. 23 (1969) 930.

[146] M. Breidenbach, et al., Phys. Rev. Lett. 23 (1969) 935.

[147] J. D. Bjorken, Phys. Rev. 179 (1969) 1547.

[148] M. May, et al., Phys. Rev. Lett. 35 (1975) 407.

[149] M. Arneodo, et al., Nucl. Phys. B481 (1996) 3.

[150] D. Antreasyan, et al., Phys. Rev. D19 (1979) 764.

[151] A. Krzywicki, J. Engels, B. Petersson, U. Sukhatme, Phys. Lett. B85 (1979) 407.

[152] M. Lev, B. Petersson, Z. Phys. C21 (1983) 155.

[153] C. N. Brown, et al., Phys. Rev. C54 (1996) 3195.

[154] A. L. S. Angelis, et al., Phys. Lett. B185 (1987) 213.

[155] M. M. Aggarwal, et al., Eur. Phys. J. C23 (2002) 225.

[156] J. Slivova, Ph.D thesis, Charles University, Prague, 2003, from the CERES experiment. (2003).

[157] R. Albrecht, et al., Eur. Phys. J. C5 (1998) 255.

[158] D. d'Enterria, Phys. Lett. B596 (2004) 32.

[159] D. Kharzeev, Y. V. Kovchegov, K. Tuchin, Phys. Rev. D68 (2003) 094013.

[160] H. Baer, J. Ohnemus, J. F. Owens, Phys. Rev. D42 (1990) 61.

[161] P. Aurenche, A. Douiri, R. Baier, M. Fontannaz, D. Schiff, Phys. Lett. B140 (1984) 87.

[162] P. Aurenche, R. Baier, M. Fontannaz, D. Schiff, Nucl. Phys. B297 (1988) 661.

[163] L. E. Gordon, W. Vogelsang, Phys. Rev. D48 (1993) 3136.

[164] S. S. Adler .

[165] J. Frantz, J. Phys. G30 (2004) S1003.

[166] S. S. Adler, et al., Phys. Rev. Lett. 94 (2004) 082301.

[167] J. D. Bjorken, fERMILAB-PUB-82-059-THY (1982).

[168] M. Gyulassy, M. Plumer, Phys. Lett. B243 (1990) 432.

[169] X.-N. Wang, M. Gyulassy, Phys. Rev. Lett. 68 (1992) 1480.

[170] X.-N. Wang, M. Gyulassy, M. Plumer, Phys. Rev. D51 (1995) 3436.

[171] R. Baier, Y. L. Dokshitzer, S. Peigne, D. Schiff, Phys. Lett. B345 (1995) 277.

[172] R. Baier, Y. L. Dokshitzer, A. H. Mueller, S. Peigne, D. Schiff, Nucl. Phys. B483 (1997) 291.

[173] R. Baier, Y. L. Dokshitzer, A. H. Mueller, D. Schiff, Phys. Rev. C58 (1998) 1706.

[174] M. Gyulassy, P. Levai, I. Vitev, Phys. Rev. Lett. 85 (2000) 5535.

[175] M. Gyulassy, P. Levai, I. Vitev, Nucl. Phys. B594 (2001) 371.

[176] C. Adler, et al., Phys. Rev. Lett. 89 (2002) 202301.

[177] J. Adams, et al., Phys. Rev. Lett. 91 (2003) 172302.

[178] B. B. Back, et al., Phys. Lett. B578 (2004) 297.

[179] X.-N. Wang, Phys. Lett. B595 (2004) 165.

[180] J.-w. Qiu, I. Vitev, Phys. Lett. B570 (2003) 161.

[181] E. Wang, X.-N. Wang, Phys. Rev. Lett. 87 (2001) 142301.

[182] E. Wang, X.-N. Wang, Phys. Rev. Lett. 89 (2002) 162301.

[183] J. W. Cronin, et al., Phys. Rev. D11 (1975) 3105.

[184] D. Antreasyan, et al., Phys. Rev. Lett. 39 (1977) 513.

[185] M. Gyulassy, P. Levai, Phys. Lett. B442 (1998) 1.

[186] X.-N. Wang, Phys. Rev. C61 (2000) 064910.

[187] G. Papp, P. Levai, G. I. Fai, Phys. Rev. C61 (2000) 021902.

[188] I. Vitev, M. Gyulassy, Phys. Rev. Lett. 89 (2002) 252301.

[189] I. Vitev, Phys. Lett. B562 (2003) 36.

[190] X.-N. Wang, Phys. Lett. B565 (2003) 116.

[191] P. Levai, G. Papp, G. G. Barnafoldi, G. I. Fai (2003).

[192] D. Kharzeev, E. Levin, L. McLerran, Phys. Lett. B561 (2003) 93.

[193] C. Adler, et al., Phys. Rev. Lett. 90 (2003) 032301.

[194] C. Adler, et al., Phys. Rev. Lett. 90 (2003) 082302.

[195] J. Rak, J. Phys. G30 (2004) S1309.

[196] M. Chiu, Nucl. Phys. A715 (2003) 761.

[197] S. A. Bass, et al., Nucl. Phys. A661 (1999) 205.

[198] A. Kovner, U. A. Wiedemann (2003).

[199] M. Gyulassy, I. Vitev, X.-N. Wang, B.-W. Zhang (2003).

[200] M. Gyulassy, M. Plumer, M. Thoma, X. N. Wang, Nucl. Phys. A538 (1992) 37c.

[201] B. G. Zakharov, JETP Lett. 65 (1997) 615.

[202] R. Baier, D. Schiff, B. G. Zakharov, Ann. Rev. Nucl. Part. Sci. 50 (2000) 37.

[203] M. Gyulassy, P. Levai, I. Vitev, Nucl. Phys. B571 (2000) 197.

[204] P. Levai, et al., Nucl. Phys. A698 (2002) 631.

[205] I. Vitev, M. Gyulassy, P. Levai (2001).

[206] I. Vitev, J. Phys. G30 (2004) S791.

[207] M. Gyulassy, I. Vitev, X.-N. Wang, P. Huovinen, Phys. Lett. B526 (2002) 301.

[208] X.-f. Guo, X.-N. Wang, Phys. Rev. Lett. 85 (2000) 3591.

[209] A. Airapetian, et al., Eur. Phys. J. C20 (2001) 479.

[210] K. J. Eskola, V. J. Kolhinen, C. A. Salgado, Eur. Phys. J. C9 (1999) 61.

[211] X.-N. Wang, Nucl. Phys. A750 (2005) 98.

[212] K. Gallmeister, C. Greiner, Z. Xu, Phys. Rev. C67 (2003) 044905.

[213] W. Cassing, K. Gallmeister, C. Greiner, Nucl. Phys. A735 (2004) 277.

[214] X.-N. Wang, Phys. Lett. B579 (2004) 299.

[215] M. Gyulassy, P. Levai, I. Vitev, Phys. Lett. B538 (2002) 282.

[216] R. Baier, Y. L. Dokshitzer, A. H. Mueller, D. Schiff, JHEP 0109 (2001) 033.

[217] B. R. Webber, Int. J. Mod. Phys. A15S1 (2000) 577.

[218] B. Alper, et al., Nucl. Phys. B100 (1975) 237.

[219] P. Abreu, et al., Eur. Phys. J. C17 (2000) 207.

[220] S. S. Adler, et al., Phys. Rev. Lett. 91 (2003) 172301.

[221] I. G. Bearden, et al., Phys. Rev. C66 (2002) 044907.

[222] T. Anticic, et al., Phys. Rev. C69 (2004) 024902.

[223] L. Ahle, et al., Phys. Rev. C55 (1997) 2604.

[224] L. Ahle, et al., Nucl. Phys. A638 (1998) 427.

[225] S. S. Adler, et al. (2004).

[226] S. S. Adler, et al. (2004).

[227] K. P. Das, R. C. Hwa, Phys. Lett. B68 (1977) 459.

[228] R. G. Roberts, R. C. Hwa, S. Matsuda, J. Phys. G5 (1979) 1043.

[229] E. Braaten, Y. Jia, T. Mehen, Phys. Rev. Lett. 89 (2002) 122002.

[230] R. J. Fries, B. Muller, C. Nonaka, S. A. Bass, Phys. Rev. Lett. 90 (2003) 202303.

[231] R. J. Fries, B. Muller, C. Nonaka, S. A. Bass, Phys. Rev. C68 (2003) 044902.

[232] R. C. Hwa, C. B. Yang, Phys. Rev. C70 (2004) 024905.

[233] R. C. Hwa, C. B. Yang, Phys. Rev. C67 (2003) 034902.

[234] V. Greco, C. M. Ko, P. Levai, Phys. Rev. Lett. 90 (2003) 202302.

[235] S. A. Voloshin, Nuclear Physics A715 (2003) 379c.

[236] J. Adams, et al., Phys. Rev. Lett. 92 (2004) 052302.

[237] M. Kaneta, J. Phys. G30 (2004) S1217–S1220.

[238] V. Greco, C. M. Ko, Phys. Rev. C70 (2004) 024901.

[239] X. Dong, S. Esumi, P. Sorensen, N. Xu, Z. Xu, Phys. Lett. B597 (2004) 328.

[240] PHENIX Collaboration, BNL 72162-2004, internal report (2003).

[241] T. Matsui, H. Satz, Phys. Lett. B178 (1986) 416.

[242] M. C. Abreu, et al., Phys. Lett. B477 (2000) 28.

[243] A. Capella, E. G. Ferreiro, A. B. Kaidalov, Phys. Rev. Lett. 85 (2000) 2080.

[244] A. Capella, A. B. Kaidalov, D. Sousa, Phys. Rev. C65 (2002) 054908.

[245] R. L. Thews, M. Schroedter, J. Rafelski, Phys. Rev. C63 (2001) 054905.

[246] R. L. Thews, J. Phys. G30 (2004) S369.

[247] A. P. Kostyuk, M. I. Gorenstein, H. Stocker, W. Greiner, Phys. Rev. C68 (2003) 041902.

[248] P. Braun-Munzinger, J. Stachel, Phys. Lett. B490 (2000) 196.

[249] A. Andronic, P. Braun-Munzinger, K. Redlich, J. Stachel, Phys. Lett. B571 (2003) 36.

[250] M. G. Mustafa, D. Pal, D. K. Srivastava, M. Thoma, Phys. Lett. B428 (1998) 234.

[251] Z.-w. Lin, R. Vogt, X.-N. Wang, Phys. Rev. C57 (1998) 899.

[252] Y. L. Dokshitzer, D. E. Kharzeev, Phys. Lett. B519 (2001) 199.

[253] G. Agakishiev, et al., Phys. Rev. Lett. 75 (1995) 1272.

[254] G. Agakishiev, et al., Phys. Lett. B422 (1998) 405.

[255] D. Adamova, et al., Phys. Rev. Lett. 91 (2003) 042301.

[256] R. Rapp, J. Wambach, Adv. Nucl. Phys. 25 (2000) 1.

[257] R. Arnaldi, et al. (2005).

[258] R. Rapp (2002).

[259] Z. Fraenkel, B. Khachaturov, A. Kozlov, A. Milov, D. Mukhopadhyay, D. Pal, I. Ravinovich, I. Tserruya, S. Zhou, PHENIX Technical Note 391, internal report (2001).

[260] A. Kozlov, et al., Nucl. Instrum. Meth. A523 (2004) 345.

[261] R. Rapp, Phys. Rev. C63 (2001) 054907.

[262] P. V. Ruuskanen, Nucl. Phys. A544 (1992) 169.

[263] G.-Q. Li, C. Gale, Phys. Rev. Lett. 81 (1998) 1572.

[264] S. Turbide, R. Rapp, C. Gale, Phys. Rev. C69 (2004) 014903.

PHOBOS

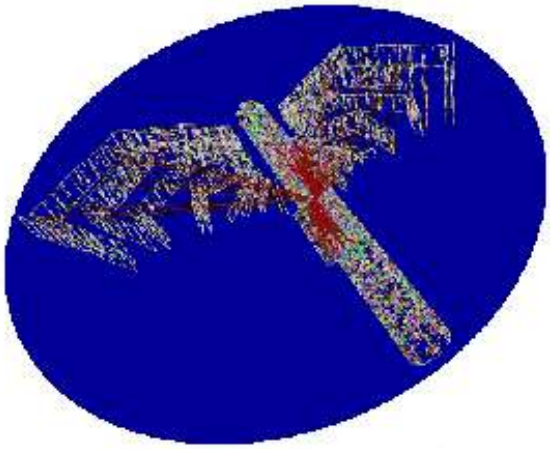

The PHOBOS Perspective on Discoveries at RHIC

B.B.Back [a] M.D.Baker [b] M.Ballintijn [d] D.S.Barton [b] B.Becker [b] R.R.Betts [f] A.A.Bickley [g] R.Bindel [g] A.Budzanowski [c] W.Busza [d] A.Carroll [b] Z.Chai [b] M.P.Decowski [d] E.García [f] T.Gburek [c] N.K.George [a,b] K.Gulbrandsen [d] S.Gushue [b] C.Halliwell [f] J.Hamblen [h] A.S.Harrington [h] M.Hauer [b] G.A.Heintzelman [b] C.Henderson [d] D.J.Hofman [f] R.S.Hollis [f] R.Hołyński [c] B.Holzman [b,f] A.Iordanova [f] E.Johnson [h] J.L.Kane [d] J.Katzy [d,f] N.Khan [h] W.Kucewicz [f] P.Kulinich [d] C.M.Kuo [e] J.W.Lee [d] W.T.Lin [e] S.Manly [h] D.McLeod [f] A.C.Mignerey [g] R.Nouicer [b,f] A.Olszewski [c] R.Pak [b] I.C.Park [h] H.Pernegger [d] C.Reed [d] L.P.Remsberg [b] M.Reuter [f] C.Roland [d] G.Roland [d] L.Rosenberg [d] J.Sagerer [f] P.Sarin [d] P.Sawicki [c] H.Seals [b] I.Sedykh [b] W.Skulski [h] C.E.Smith [f] M.A.Stankiewicz [b] P.Steinberg [b] G.S.F.Stephans [d] A.Sukhanov [b] J.-L.Tang [e] M.B.Tonjes [g] A.Trzupek [c] C.M.Vale [d] G.J.van Nieuwenhuizen [d] S.S.Vaurynovich [d] R.Verdier [d] G.I.Veres [d] E.Wenger [d] F.L.H.Wolfs [h] B.Wosiek [c] K.Woźniak [c] A.H.Wuosmaa [a] B.Wysłouch [d] J.Zhang [d]

PHOBOS collaboration
www.phobos.bnl.gov

[a] *Argonne National Laboratory, Argonne, IL 60439-4843, USA*

[b] *Brookhaven National Laboratory, Upton, NY 11973-5000, USA*

[c] *Institute of Nuclear Physics PAN, Kraków, Poland*

[d] *Massachusetts Institute of Technology, Cambridge, MA 02139-4307, USA*

[e] *National Central University, Chung-Li, Taiwan*

[f] *University of Illinois at Chicago, Chicago, IL 60607-7059, USA*

[g] *University of Maryland, College Park, MD 20742, USA*

[h] *University of Rochester, Rochester, NY 14627, USA*

Preprint submitted to Nuclear Physics A *7 April 2005*

Abstract

This paper describes the conclusions that can be drawn from the data taken thus far with the PHOBOS detector at RHIC. In the most central Au+Au collisions at the highest beam energy, evidence is found for the formation of a very high energy density system whose description in terms of simple hadronic degrees of freedom is inappropriate. Furthermore, the constituents of this novel system are found to undergo a significant level of interaction. The properties of particle production at RHIC energies are shown to follow a number of simple scaling behaviors, some of which continue trends found at lower energies or in simpler systems. As a function of centrality, the total number of charged particles scales with the number of participating nucleons. When comparing Au+Au at different centralities, the dependence of the yield on the number of participants at higher p_T ($\sim$4 GeV/c) is very similar to that at low transverse momentum. The measured values of charged particle pseudorapidity density and elliptic flow were found to be independent of energy over a broad range of pseudorapidities when effectively viewed in the rest frame of one of the colliding nuclei, a property we describe as "extended longitudinal scaling". Finally, the centrality and energy dependences of several observables were found to factorize to a surprising degree.

Key words:
PACS: 25.75.-q

1 Introduction

Currently, there exists a good understanding of the basic building blocks of normal matter, and of the fundamental forces or interactions between them. The bulk of hadronic matter is comprised of partons (quarks and gluons) bound into neutrons, protons, and subsequently nuclei by the strong force mediated by the field quanta, the gluons. The fundamental interactions between these partons are described by the theory of quantum chromodynamics (QCD) [1] and are reasonably well understood. However, because of the strength and non-Abelian nature of the interactions, finding solutions to the QCD equations remains notoriously difficult. As a result, the current understanding of the phase structure of strongly interacting matter (what phases exist, what are the properties of the matter in each phase, and what is the nature of the transitions between phases) is only partly based on theoretical QCD calculations. Instead, it is driven, to a large extent, by experiment. Among many examples of the significance of the properties of QCD "matter" is the fact

Email address: PHOBOS Spokesperson:busza@mit.edu (W.Busza).

that more than 98% of the mass of all normal hadronic matter in the universe arises from the interactions (i.e. the gluons and the sea quarks), not from the (current) mass of the valence quarks in the hadrons [2]. This mass is generated predominantly by the lower energy interactions which are most difficult to study quantitatively. Areas of impact outside nuclear physics include the evolution of the early universe, as well as the overall properties and interior structure of compact stars and stellar remnants. Both theory and experiment suggest the existence of a very rich "condensed matter" governed by QCD.

At very short distances ($\ll$hadronic sizes) the QCD coupling constant between partons is weak and decreases as the distance between the partons decreases, a phenomenon known as "asymptotic freedom" [3–5]. An expected consequence of asymptotic freedom is that a system created by heating the vacuum to high temperatures should have the properties of an almost ideal relativistic gas in which color is deconfined (first pointed out by [6] using the term "quark soup", see also [7–9]). The high temperature of this medium entails an extremely high concentration of partons, whose thermodynamics follows the Stefan-Boltzmann law. Such a system has traditionally been designated the Quark-Gluon Plasma (QGP), a term proposed in [7]. To specifically recognize its ideal, weakly interacting nature, we use the term wQGP. The current consensus is that the whole universe was in the wQGP state at an early stage following the big bang.

At another extreme, it is known that the only stable configuration of strongly interacting matter at low temperatures and densities is the multitude of varieties of color neutral objects, namely the hadrons, as well as conglomerates of hadrons such as atomic nuclei. In addition, the QCD Lagrangian (and the wQGP solution of that Lagrangian) is understood to have a higher symmetry than the observed hadron states. The solutions of QCD at temperatures and densities which correspond to normal matter, i.e. the world of hadrons and nuclei, spontaneously break this so-called "chiral symmetry" (see, for example, [10–12]). The questions of what forms and phases of QCD matter exist between the two extremes and what symmetries, properties, and interactions characterize these phases, are currently the subject of very active theoretical and experimental research (see, for example, [13]).

On both the experimental and the theoretical fronts, there are very few tools available for the study of QCD matter as a function of density and temperature. To date, the most fruitful approach to the theoretical study of high temperature QCD has been the use of numerical calculations based on the techniques of lattice gauge theory. These calculations suggest that at low baryon densities there is a phase difference in QCD matter below and above a critical temperature T_c $\sim$150–200 MeV or energy density $\sim$1 GeV/fm^3 (see, for example, [14], which quotes a T_c of 175 MeV and an energy density of 700 MeV/fm$^3\pm$50%). At another extreme, theoretical progress has been made

in recent years in the understanding of cold, ultra-dense, QCD matter which must be in some color superconducting state [15–17]. For example, there are indications that a dense, cold system of equal numbers of u, d and s quarks can form a "color-flavor locked" superconducting phase. This regime is currently out of range of experimentation using accelerators, but such phenomena might be manifested in the dense cores of neutron stars and, therefore, might be open to study through astronomical observation. The possible connection of QCD and neutron stars has a long history (see, for example, [18,19]).

The most useful experimental approach in the area of high temperature QCD matter is the detailed analysis of heavy ion collisions. In fact, the suggestion of the use of heavy ion collisions to create high density states of matter predates the full development of QCD [20]. The value of $\sim$1 GeV/fm^3 is not much higher than the energy density inside nucleons ($\sim$500 MeV/fm^3) and nuclei ($\sim$150 MeV/fm^3), and it is also comparable to estimates of the initial energy density created in hadronic collisions at high energy accelerators. In heavy ion collisions at relativistic velocities, there is both compression of the baryonic matter in the nuclei and also the release of a large amount of energy within a small volume from the almost simultaneous collisions of many nucleons. One or the other, or both, of these consequences of the interactions have the potential to produce new forms or phases of QCD matter. This is one of the prime reasons why in the past few decades much effort has been spent studying collisions of heavy ions at higher and higher energies. Extensive information can be found in the proceedings of the Quark Matter series of conferences [21] and in recent reviews [22–25]. The conditions created may be similar to those of the early universe at about 10 μsec after the big bang. Another important aspect of such studies is the extraction of valuable information about the mechanisms of particle production in small and large systems at high energies.

The most recent experimental facility for the study of heavy ion collisions is the Relativistic Heavy Ion Collider (RHIC) at Brookhaven National Laboratory. Since the inception of the physics program in July, 2000, four experiments at RHIC, namely BRAHMS, PHENIX, PHOBOS, and STAR, have studied collisions of p+p, d+Au, and Au+Au at center-of-mass collision energies per incident nucleon pair, $\sqrt{s_{NN}}$, from 19.6 to 200 GeV. Note that, for technical reasons discussed in Appendix B.1, $\sqrt{s_{NN}}$ for d+Au was actually larger by about 0.35% but, for simplicity, this tiny difference is omitted in the text and figure labels of this document. Data from all four detectors are being studied to get a better understanding of the physics of heavy ion collisions, and, in particular, to search for evidence of the creation of new forms of QCD matter [26]. To the best of our knowledge, where there is overlap, there are no major differences in the data and extracted results obtained by the four experiments at RHIC. The level of agreement is a testament to the quality of the detectors and the analyses performed by the collaborations and is a great strength of

the whole RHIC research program. This paper summarizes the most important results obtained to date by the PHOBOS collaboration and the conclusions that can be drawn from PHOBOS results, augmented where necessary by data from other experiments.

One of the most important discoveries at RHIC is the evidence that, in central Au+Au collisions at ultra-relativistic energies, an extremely high energy density system is created, whose description in terms of simple hadronic degrees of freedom is inappropriate. Furthermore, the constituents of this system experience a significant level of interaction with each other inside the medium. These conclusions are based on very general and, to a large extent, model independent arguments.

It is not claimed that the observed phenomena are unique to RHIC energies. Nor is it claimed that there is direct evidence in the data analyzed so far for color deconfinement or chiral symmetry restoration. It should be noted that interpretations of the data which invoke a high density of gluons or other non-hadronic components are certainly consistent with, and could be construed to provide at least circumstantial evidence for, deconfinement. Also, the definition of the concept of deconfinement is not so clear when the particles in the medium interact significantly. No convincing evidence has been found for the creation at RHIC of the wQGP, in contrast to the expectations of a large part of the heavy ion community in the era before the start of the RHIC physics program. This expectation may have partly resulted from a misinterpretation of the lattice results. The calculations reveal that the pressure and energy density reach 70–80% of the Stefan-Boltzmann value (i.e. the value for a non-interacting gas) for temperatures above the critical temperature (see, as one recent example, [27]). This observation was typically assumed to imply the presence of a weakly interacting system although questions were occasionally raised (for one early example, see [28]). More recently, this conclusion has been seriously challenged (see, for example, [29,30]). As an aside, some string theory models which have been shown to be related to QCD can be solved exactly in the strong-coupling limit and yield a result comparable to $\sim$75% of the Stefan-Boltzmann value [31,32]. This recent reversal of opinion was to a large degree driven by the experimental results from RHIC. Recent lattice QCD studies have shown that the quarks do retain a degree of correlation above the critical temperature (see, for example, [33,34]). However, at extremely high energy density (for example, the very early universe), the theoretical expectation remains that the system will become weakly interacting [35].

Another equally interesting result from RHIC arose from the studies of the mechanism of particle production in nuclear collisions. Specifically, it has been discovered that much of the data in this new regime can be expressed in terms of simple scaling behaviors. Some of these behaviors had been noted in data

at lower energies or for simpler systems. These observations suggest either the existence of strong global constraints or some kind of universality in the mechanism of the production of hadrons in high energy collisions, possibly connected to ideas of parton saturation. The data strongly suggest that the initial geometry and very early evolution of the system establish conditions which determine the final values of many observables. The most concise formulation of this discovery is the statement that the overall properties of the data appear to be much simpler than any of the models invoked to explain them. A full exploration and detailed analysis of all aspects of the data will be required for a complete understanding of the properties of QCD physics in the interesting regime probed by heavy ion collisions at relativistic velocities.

Section 2 of this paper describes the derived properties of the state formed shortly after the collisions at RHIC, Sect. 3 describes the evidence that the constituents of this state interact significantly, and Sect. 4 discusses the broad range of scaling behaviors that have been discovered.

As a useful reference, the PHOBOS detector and its properties are briefly described in Appendix A. Variables used in the description of the data, in particular those relating to event characterization, are defined in Appendix B. The precise determination of the collision impact parameter or centrality is critical to heavy ion physics in general and the PHOBOS program in particular. Appendix C describes how centrality and the biases associated with triggering and various elements of the data analysis are derived from measurements and simulations for the various colliding systems and beam energies.

2 Properties of the initial state produced at RHIC

The primary goal of the RHIC accelerator was the study of QCD matter under extreme conditions. In particular, it was expected that the center-of-mass energies more than an order of magnitude higher than achieved at the SPS accelerator at CERN would lead to the creation of a system with significantly higher energy density. An additional consequence of the higher beam energy compared to the SPS was the displacement of the projectile baryons a factor of two farther apart in rapidity. This was expected to lead to a lower baryon chemical potential in the high energy density region at midrapidity. Although progress has been made recently in lattice calculations which include the effects of a non-zero baryon chemical potential (see, for example, [27,36–41] and references therein), the most extensively studied system remains one with a value close to zero (see, for example, [42,43] and references therein). Therefore, creation of a system with a lower baryon chemical potential might offer the potential for more reliable comparisons of experimental data to the fundamental QCD predictions. This section describes the conclusions that can

be drawn from PHOBOS data concerning these two critical properties of the state formed in collisions of heavy ions at RHIC.

2.1 Energy density

In very high energy heavy ion interactions, the maximum energy density occurs just as the two highly Lorentz contracted nuclei collide. Clearly this system is very far from being equilibrated and, as a result, the value of the energy density, although well defined, may not be very interesting. In any reference frame, the potentially more interesting quantity is the energy density carried by particles which are closer to equilibrium conditions, i.e. those particles which have, on average, comparable longitudinal and transverse momenta. These conditions are roughly equivalent to restricting the particles to a range of pseudorapidity $|\eta| \leq 1$. Unfortunately, there are no direct measures of energy density and, therefore, it must be inferred from the properties of the detected particles. PHOBOS data have been used to investigate what range of initial energy densities are consistent with the observations. Studies of pseudorapidity and transverse momentum distributions, as well as elliptic flow, have been combined to constrain assumptions about the energy in the system and the time evolution of the volume from which the particles emanate.

Figure 1 shows distributions of charged particle pseudorapidity densities, $dN_{ch}/d\eta$, for Au+Au collisions at $\sqrt{s_{NN}}$=19.6, 130, and 200 GeV for various centralities [44]. The produced particle densities are at their maximum near midrapidity and increase with both collision energy and centrality. The right panel of Fig. 2 is a compilation of the evolution of the midrapidity charged particle density, $dN_{ch}/d\eta\rfloor_{|\eta|\leq 1}$, per participating nucleon pair, $N_{part}/2$, as a function of collision energy from PHOBOS [44–49] and lower energy heavy ion reactions at the SPS [50,51] and AGS [52–56]. The PHOBOS data are for the 6% most central Au+Au interactions. For most of the SPS and AGS data, the $dN_{ch}/d\eta$ values were obtained using sums of dN/dy results for a variety of identified particles. The data follow a simple logarithmic extrapolation from lower energies as shown by the line drawn to guide the eye. The PHOBOS apparatus allows several independent techniques to be used to measure centrality and the number of particles emitted near midrapidity, all of which provide results that differ by no more than a small fraction of their separate systematic errors. The values of $dN_{ch}/d\eta\rfloor_{|\eta|\leq 1}$ per participating nucleon pair, 1.94±0.15, 2.47±0.27, 3.36±0.17 and 3.81±0.19 for the 6% most central Au+Au collisions at 19.6, 56, 130, and 200 GeV, respectively, represent weighted averages of the published results. It is notable that multiplicity measurements were initially obtained by PHOBOS and later confirmed by the other experiments at every new beam energy and species provided during the first three RHIC runs, from the first Au+Au collisions [45] through the d+Au collisions [57].

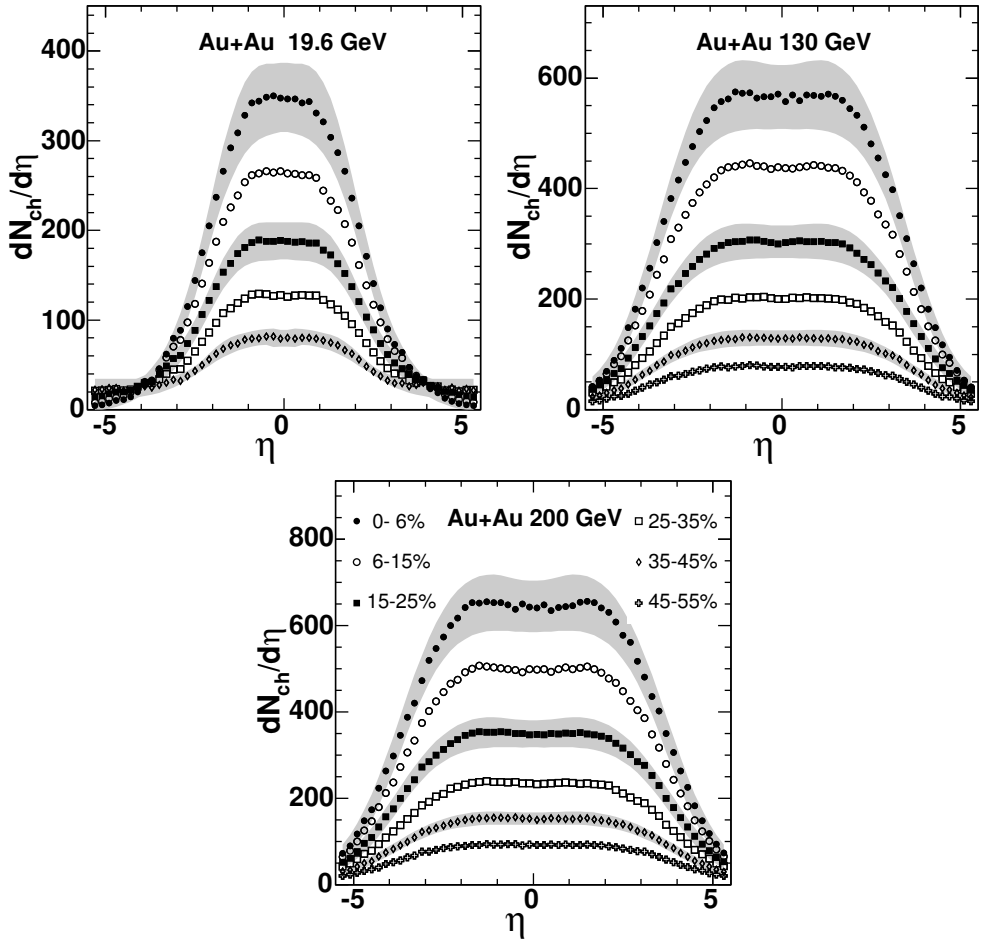

Fig. 1. Pseudorapidity density of charged particles emitted in Au+Au collisions at three different values of the nucleon-nucleon center-of-mass energy [44]. Data are shown for a range of centralities, labeled by the fraction of the total inelastic cross section in each bin, with smaller numbers being more central. Grey bands shown for selected centrality bins indicate the typical systematic uncertainties (90% C.L.). Statistical errors are smaller than the symbols.

It is interesting to note that the measured midrapidity charged particle density at RHIC is lower than the prediction of most models (see the left panel of Fig. 2, as well as [58,59]. From top to bottom, the references for the models are [60–63,59,64–73]). The authors of [58] quoted a factor of 1.1 for converting $dN/d\eta$ to dN/dy for comparison of data and theory. For consistency, the PHOBOS $dN_{ch}/d\eta$ has been multiplied by the same factor to obtain the value shown in the figure.

Among the models which predicted a value close to that seen in the data were two which invoked the concept of saturation in either the initial state [73] or the produced partons [70]. Related concepts were used in more recent formulations which describe the formation of a Color Glass Condensate (CGC). This newer CGC model successfully related the pseudorapidity and energy

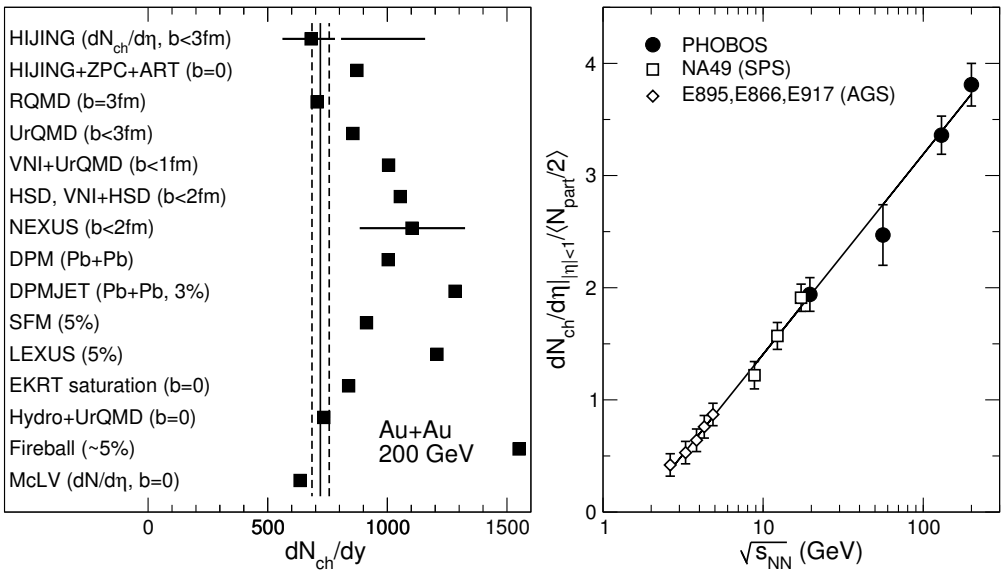

Fig. 2. (Left panel) Results of PHOBOS measurements of the charged particle density near midrapidity in central Au+Au at $\sqrt{s_{NN}}$=200 GeV [44,47–49] (shown by the vertical line with the dashed lines denoting the systematic uncertainty) compared to theoretical predictions. This panel is adapted from [58]. From top to bottom, the references for the models are [60–63,59,64–73]. See text for discussion. (Right panel) Normalized pseudorapidity density of charged particles emitted within $|\eta| \leq 1$ in central Au+Au (AGS [52–56] and PHOBOS at RHIC [44–49]) and Pb+Pb (SPS [50,51]) collisions as a function of nucleon-nucleon center-of-mass energy. See text for discussion.

dependences of charged particle production to the gluon structure function measured in e+p collisions [74]. It should be noted that this model also made predictions for the properties of particle production at high p_T in d+Au collisions [75,76] which agreed qualitatively with the pattern of hadron suppression in the d+Au data at middle to forward rapidities [77–79], but which cannot explain the excess of particle production at high p_T for backward rapidities [80,81]. The search for other evidence for possible parton saturation effects remains a topic of interest at RHIC but a more detailed discussion is beyond the scope of this paper.

Before attempting to make detailed estimates of the energy density, it is important to stress that the midrapidity particle density at the top RHIC energy is about a factor of two higher than the maximum value seen at the SPS [47] and there is evidence that the transverse energy per particle has not decreased [82,83]. Thus, with little or no model dependence, it can be inferred that the energy density has increased by at least a factor of two from $\sqrt{s_{NN}}$=17 to 200 GeV.

In addition to the measured particle multiplicities, estimating the energy density more precisely requires knowledge of the average energy per particle, as well as the volume from which they originate. PHOBOS data for the trans-

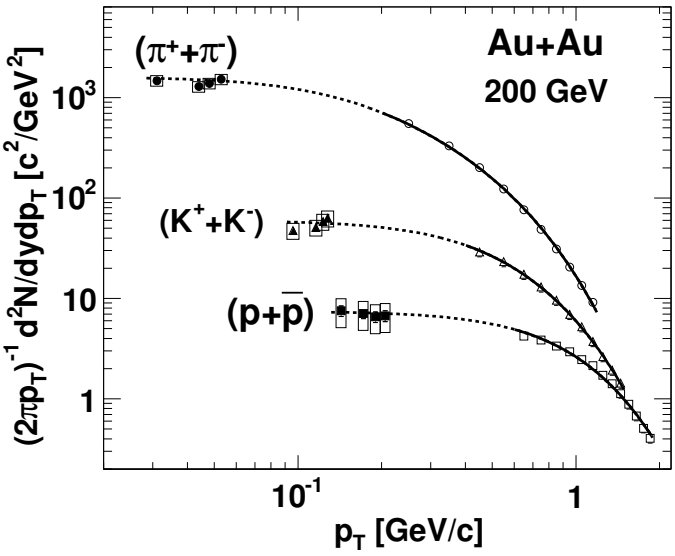

Fig. 3. Transverse momentum distributions of identified charged particles emitted near midrapidity in central Au+Au collisions at $\sqrt{s_{NN}}$=200 GeV. Invariant yield data shown are from PHENIX at higher momenta [86] and PHOBOS at lower momenta [85]. Boxes around the PHOBOS data indicate systematic uncertainties. Fits to PHENIX measurements are shown by solid curves ($\propto 1/[e^{(m_T/T_i)}+\epsilon]$, where $\epsilon = -1$ and $+1$ for mesons and baryons, respectively, m_T is the transverse mass, and T_i is the fit parameter for each species). Note that the extrapolations (dashed curves) of the fit to the data at higher momenta are consistent with the low momentum yields.

verse momentum distribution of charged particles [84] can be used to find a mean transverse momentum but these data only extend down to a few hundred MeV/c. Alternatively, Fig. 3 compares identified particle yields at very low transverse momentum measured by PHOBOS [85] to PHENIX data [86] for higher momenta. Both data sets are for particles emitted near midrapidity in central Au+Au collisions at $\sqrt{s_{NN}}$=200 GeV. The PHOBOS data clearly demonstrate that the fits shown hold over the full range of transverse momentum and that extrapolation should give a correct value for the average. The low momentum identified particle data shown in Fig. 3 are in non-overlapping regions of p_T for the three different species. Thus, without additional assumptions it is not possible to merge them into a low p_T charged particle value for comparison to PHOBOS spectra for charged particles at higher p_T.

Accounting for the yields of the various particles, an average transverse momentum for all charged particles of $\langle p_T \rangle$ ~500 MeV/c can be derived. The value found from the PHOBOS unidentified charged particle distributions is the same to within 5%. Averaging over the pions, kaons, and nucleons, and assuming the yields for the unobserved neutral particles, an average transverse mass, m_T, of ~570 MeV/c^2 can be extracted. Under the assumption of a spherically symmetric distribution in momentum space, which would have equal average transverse and longitudinal momenta, the average en-

ergy per particle is equal to the transverse mass ($m_{_T}$) at midrapidity (i.e. $\langle E^2 \rangle = \langle m_0^2 + p_{_T}^2 + p_{_\parallel}^2 \rangle \approx \langle m_0^2 + p_{_T}^2 \rangle \rfloor_{\eta=0}$). Alternatively, assuming that transverse momentum is independent of pseudorapidity, the contribution due to the longitudinal momentum can be found by averaging $p_{_\parallel} = p_{_T} \cot(\theta)$. Over the range $0 < \eta < 1$, this results in $\langle p_{_\parallel}^2 \rangle$ which is approximately 30–40% of $\langle p_{_T}^2 \rangle$ and would, therefore, raise the average energy by about 10–15%. Since there are significant theoretical uncertainties in this and other elements of the calculation, and we are interested in a lower limit, a rounded estimate of 600 MeV per particle will be used.

The total energy in the system created near midrapidity in central Au+Au collisions at $\sqrt{s_{_{NN}}}$=200 GeV can be found from

$$E_{tot} = 2 E_{part} dN_{ch}/d\eta \rfloor_{|\eta| \leq 1} f_{neut} f_{4\pi},$$

where E_{part} is the average energy per particle, $dN_{ch}/d\eta \rfloor_{|\eta| \leq 1}$=655$\pm$35(syst) is the midrapidity charged particle density for the 6% most central collisions, f_{neut} is a factor of 1.6 to roughly account for undetected neutral particles, and the factor of 2 integrates over $-1 \leq \eta \leq +1$. One further issue to consider is that there are particles with similar total momentum in the center-of-mass system but which are not traveling predominantly in the transverse direction. The correction for these additional particles, $f_{4\pi}$, is trivially estimated from the fraction of solid angle outside $\theta = 40°$–$140°$ (i.e. outside $|\eta| \leq 1$) and equals about 1.3. It should be stressed that this methodology does not suggest that the entire distribution of particles is isotropic; in fact, the data shown in Fig. 1 clearly contradict any such idea. Instead, the goal is to obtain the energy density for the component of the distribution which is consistent with isotropic emission from a source at midrapidity. Combining all of these terms, the total energy contained in all particles emitted near midrapidity, with transverse and longitudinal momenta consistent with emission from an equilibrated source, is about 1600 GeV. This is roughly 4% of the total energy of 39.4 TeV in the colliding system.

Converting this to a density in the rest frame of the system consisting of these particles requires knowledge of the volume within which this energy is contained at the earliest time of approximate equilibration. For central collisions, a transverse area equal to that of the Au nuclei ($\approx$150 fm^2) can be assumed, but which value to use for the longitudinal extent is not as clear. One extreme is to take the very first instant when the two Lorentz contracted nuclei overlap (longitudinal size $\approx$0.1 fm), which yields an upper limit on the energy density in excess of 100 GeV/fm^3. There is, however, no reason to assume that at such an early instant the system is in any way close to equilibrium. A second commonly-used assumption is that proposed by Bjorken [87], namely a transverse size equal to the colliding nuclei and a longitudinal size of 2 fm

(corresponding to a time of the order of $\tau \sim 1$ fm/c since the collision) which implies an energy density of about 5 GeV/fm^3. [1] Finally, the elliptic flow results discussed below suggest that an upper limit of the time for the system to reach approximate equilibrium is of the order of 1–2 fm/c. Using the upper range of this estimate and further conservatively assuming that the system expands during this time in both the longitudinal and transverse directions (with expansion velocities $\beta_{\parallel} \approx 1$ and $\beta_{\perp} \approx 0.6$), one obtains a lower limit of the energy density produced when the system reaches approximate equilibrium at RHIC of ≥ 3 GeV/fm^3. Even this very conservative estimate is about six times the energy density inside nucleons and about twenty times the energy density of nuclei. Therefore, this is a system whose description in terms of simple hadronic degrees of freedom is inappropriate.

2.2 Baryon chemical potential

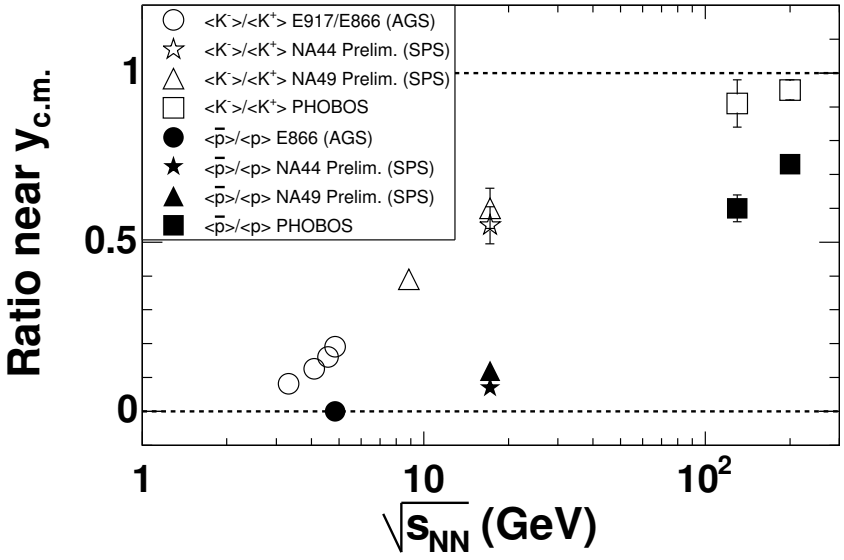

Fig. 4. Ratios of identified antiparticles over particles measured near midrapidity in central collisions of Au+Au (AGS [54,95,96] and PHOBOS at RHIC [91,92]) and Pb+Pb (SPS [93,94]) as a function of nucleon-nucleon center-of-mass energy. Error bars are statistical only.

Turning to the baryon chemical potential, μ_B, early results regarding this property of the high energy density medium produced at RHIC came from the measurement of the ratios of charged antiparticles to particles near midrapidity for central collisions. In the simplest Boltzmann approximation, the ratio of antiprotons to protons is proportional to $e^{-2\mu_B/T}$, where T is the temperature

[1] The frequently-used Bjorken approximation for the energy density with the same information from the data used here would yield a value of about 4 GeV/fm^3.

at the time of chemical freezeout. Using particle yields to deduce properties of the system is a concept that long predates QCD and heavy ion collisions [88–90]. Figure 4 compares the antiparticle to particle ratios for both protons and kaons measured at RHIC by PHOBOS [91,92] to the corresponding numbers found at lower energies [54,93–96]. Clearly, the systems formed at RHIC are much closer to having equal numbers of particles and antiparticles than was true at lower energies. The measured value of $0.73 \pm 0.02(\text{stat}) \pm 0.03(\text{syst})$ for the antiproton to proton ratio near midrapidity for central Au+Au collisions at $\sqrt{s_{NN}}$=200 GeV [92] indicates that these collisions are approaching a very low value of μ_B. Within the framework of thermal models, these ratios can be used to extract the baryon chemical potential [97]. Assuming a hadronization temperature of 165 MeV, a value of μ_B=27 MeV was found for central Au+Au at $\sqrt{s_{NN}}$=200 GeV. This baryon chemical potential is an order of magnitude lower than was obtained for Pb+Pb data at $\sqrt{s_{NN}}$=17.2 GeV from the SPS [98,99]. Although the system created near midrapidity at RHIC cannot be described as completely free of net baryons, it is clearly approaching the environment treated in most lattice calculations.

2.2.1 Comparison of particle ratios in Au+Au and d+Au

In addition to the higher center-of-mass energies, a critical element of the design of RHIC was the ability to collide asymmetric systems. This capability was first exploited with the collision of deuterons with gold nuclei at $\sqrt{s_{NN}}$=200 GeV. It is hoped that analysis of such simpler systems will serve as critical "control" experiments to aid in the understanding of the more complicated nucleus-nucleus data. As a first example, this section presents a study of the antiparticle to particle ratios.

As described above, particle ratios can be used to extract information about the properties of the system, in particular the chemical potentials. The measured values of these parameters are established at the point of chemical freezeout when inelastic interactions between the produced particles cease. However, the properties of the early evolution of the system can clearly influence final conditions. Of particular interest in this regard is the ratio of antiprotons to protons measured at midrapidity. This ratio can be interpreted as reflecting the interplay of two mechanisms, namely the transport of baryons from the two projectile nuclei to midrapidity and the production of antibaryon-baryon pairs in the interaction. By studying ratios as a function of centrality in d+Au, the effect of multiple collisions of the nucleons in the deuteron can be explored. The surprising result is shown in Fig. 5 [100].

The simple expectation, supported by various model calculations (HIJING [101], RQMD [102], and AMPT [103,104]) was that the proportion of antiprotons near midrapidity would fall slowly with collision centrality as the deuteron

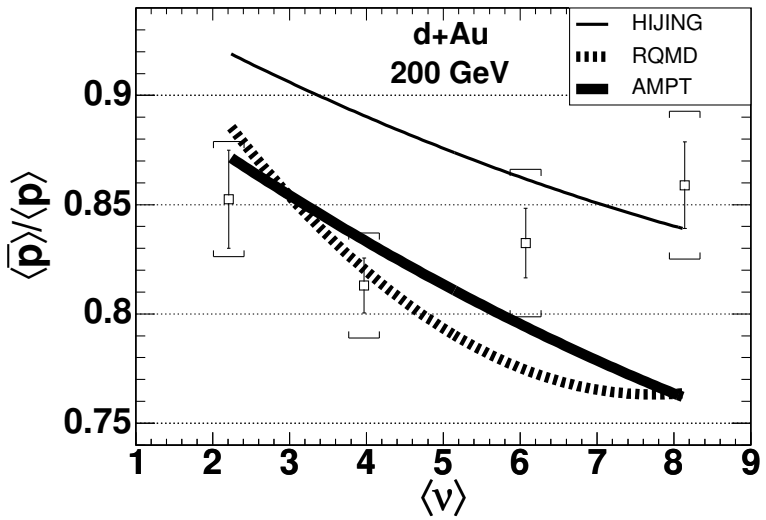

Fig. 5. The ratio of antiprotons to protons emitted in a rapidity region spanning approximately $0.0 < y < 0.8$ (where positive rapidity is in the direction of the deuteron projectile) for d+Au collisions at $\sqrt{s_{NN}}$=200 GeV [100]. Data are shown for 4 centrality ranges. The parameter $\langle\nu\rangle$ is the average number of collisions suffered by each participant in the deuteron (N_{coll}/N^{d}_{part}). Statistical and point-to-point systematic uncertainties are shown as bars and brackets, respectively. The results of several models [101–104] are shown for comparison.

participants suffered more collisions and, consequently, were effectively transported closer to the center-of-mass rapidity. In contrast, the data show a ratio which is consistent with being the same at all centralities. At present, no simple explanation or interpretation of the observed particle ratios is known.

The d+Au data at RHIC serve an important function as a control experiment since an extended volume of high density matter is presumably not formed in these collisions. Understanding the basic mechanisms of baryon transport and baryon pair production will clearly be critical to a full description of heavy ion interactions.

2.3 Nature of the transition to the high density regime

The transition to the high density state at RHIC has not been observed to create abrupt changes in any observable studied to date, including, among others, charged particle multiplicity, elliptic flow, HBT, as well as derived quantities such as energy density and freeze-out parameters. This lack of a dramatic change in character may make it more difficult to delineate the exact boundaries of the onset of significant influence from non-hadronic degrees of freedom. However, this observation may be consistent with the expectations concerning the nature of the phase transition from the most recent lattice

QCD calculations [27,36,42,105], which predict a rapid crossover in the region of the phase diagram believed to be relevant for the systems created near midrapidity at RHIC. It should be noted that the lack of dramatic shifts in observables does not necessarily rule out the presence of a phase transition with different characteristics (see, for example, the discussion in [24]).

It should be noted that indications of possible non-monotonic behavior in the energy evolution of some quantities were reported in the range $\sqrt{s_{NN}}$=5–10 GeV at the CERN SPS (see, for example, [106] and references therein). The extracted properties of the environment created near midrapidity in these lower energy collisions are significantly different from those found near midrapidity at RHIC, with energy densities at least a factor of 3–4 smaller and baryon chemical potentials an order of magnitude or more larger. A discussion of these results at lower energy falls outside the scope of this paper but future work in this area might prove important to the full exploration of the QCD phase diagram.

3 Strength of interactions in the high energy density medium

In early discussions of the high density systems formed in RHIC collisions, the expectation was that a deconfined state of quarks and gluons would be weakly interacting. This interpretation arose at least partly from the naïve assumption that any matter that attained a large fraction of the Stefan-Boltzmann limit for the pressure would act like a gas [29]. One of the most dramatic early discoveries at RHIC is the clear indication that the nature of the systems formed is very far from weakly interacting. Evidence for this conclusion is found in the magnitude of elliptic flow and in the centrality dependence of particle production at high transverse momentum. The former provides information on the manner in which particle production depends on the shape of the incident system and the latter explores how the spectrum of the produced particles is impacted by the medium. Additional evidence is provided by the yields of particles at very low transverse momentum, a measurement unique to PHOBOS.

Figure 6 shows PHOBOS measurements of the magnitude of elliptic flow, v_2, near midrapidity ($|\eta| \leq 1$) in Au+Au collisions at $\sqrt{s_{NN}}$=130 [107] and 200 GeV [108] as a function of centrality, denoted by $\langle \mathrm{N}_{part} \rangle$. Two different methods of determining the flow signal, one based on counting hits in the multiplicity detector and one based on counting tracks in the spectrometer [108], were used at the higher beam energy. Similar results were first shown for RHIC data by the STAR collaboration [109]. Figure 7 shows data from the track-based method in the rapidity interval $0 < \eta < 1.5$ for the 50% most central Au+Au collisions at $\sqrt{s_{NN}}$=200 GeV as a function of transverse

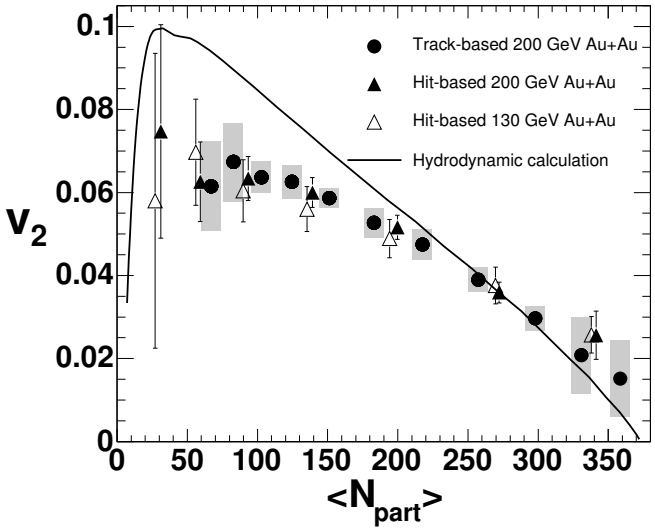

Fig. 6. Elliptic flow of charged particles near midrapidity ($|\eta| < 1$) as a function of centrality in Au+Au collisions at $\sqrt{s_{NN}}$=200 GeV using two different methods [108] (closed circles and triangles, see text for details) and at $\sqrt{s_{NN}}$=130 GeV (open triangles) [107]. Grey boxes show the systematic errors (90% C.L.) for the 200 GeV data. The curve shows the prediction from a relativistic hydrodynamics calculation [110].

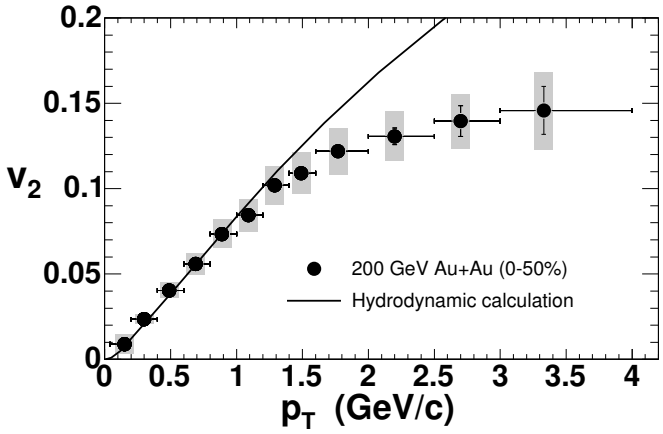

Fig. 7. Elliptic flow of charged particles emitted near midrapidity ($0 < \eta < 1.5$) in the 50% most central Au+Au collisions at $\sqrt{s_{NN}}$=200 GeV as a function of transverse momentum [108]. Grey boxes show the systematic uncertainties of the data (90% C.L.). The curve is the prediction of a relativistic hydrodynamics calculation [110].

momentum, p_T [108]. Data in both figures are compared to the predictions of a hydrodynamical calculation [110]. These results show that elliptic flow is unexpectedly large at RHIC energies. Over a wide range of centrality and transverse momentum, the value near midrapidity is as large as that calculated under the assumption that a boost-invariant relativistic hydrodynamic fluid was formed.

When two nuclei collide with non-zero impact parameter, the lenticular (or almond-shaped) overlap region has an azimuthal spatial asymmetry (see right panel of Fig. B.1). However, if the particles do not interact after their initial production (presumably with azimuthally uniform momenta), the asymmetrical shape of the source region will have no impact on the azimuthal distribution of detected particles. Therefore, observation of azimuthal asymmetry in the outgoing particles is direct evidence of interactions between the produced particles. In addition, the interactions must have occurred at relatively early times, since expansion of the source, even if uniform, will gradually erase the magnitude of the spatial asymmetry.

Qualitatively, it is clear that an asymmetric system of interacting particles will have azimuthally varying pressure gradients which can alter the observed particle directions. Hydrodynamical models can be used to calculate a quantitative relationship between a specific initial source shape and the distribution of emitted particles (see, for example, [110]). Due to the ideal nature of the fluid assumed in these models (not to be confused with the non-interacting ideal *gas*), the resulting final asymmetry is generally assumed to be an upper limit for a specific starting condition. From the strength of the observed elliptic flow and from the known dimensions of the overlap region in Au+Au collisions, it can be conservatively estimated that the pressure build-up in the initially formed medium must have occurred in a time less than about 2 fm/c (with a best-fit value from flow and other data of 0.6 fm/c) [24]. Thus, the presence of a large flow signal carries several important implications, the first of which, a limit on the timescale for equilibration, has been used previously in the discussion of energy density. In addition, one can conclude that at these early times the initially produced particles must already be interacting significantly, corresponding more closely to the conditions in a fluid rather than a gas.

Additional indirect evidence that the constituents of the system produced in heavy ion collisions at RHIC are interacting significantly is provided by the observed yield of particles with very small transverse momentum ($\leq$100 MeV/c) [85], shown previously in Fig. 3. Recall that the production of particles with p_T as low as 30 MeV/c was consistent with extrapolations from a fit to the distribution in the range of a few hundred MeV/c to a few GeV/c. If, in RHIC collisions, a medium of weakly interacting particles was initially produced, one could expect an enhancement in the production of particles with wavelengths up to the overall size of the collision volume (i.e. coherent pion production) [111]. In essence, the observation that there is no such excess is another manifestation of the high pressure gradient and significant level of interaction present in the medium, which gives rise to the large magnitude of the elliptic flow signal seen at RHIC. These properties would also produce large radial flow so that any particles initially produced with low velocity would subsequently be accelerated by the interactions.

The study of the yield of particles with large transverse momentum can be used to more directly explore the level of interactions present in the medium produced in $\sqrt{s_{NN}}$=200 GeV Au+Au collisions at RHIC. Presuming that high momentum transfer processes are induced via relatively short-range interactions, one may expect QCD factorization theorems, proven for simpler processes, to continue to hold and, therefore, a particular hard process can be induced by any binary collision in the overall nucleus-nucleus interaction [112,113]. This is the motivation for the nuclear modification factor, R_{AA}, defined in Appendix B.3 and first studied at RHIC by PHENIX [114,115], which measures how effective each particular binary collision is for inducing a hard scattering process. Strong deviations from unity indicate violations of factorization, which may be caused by initial or final state effects. In their pioneering work, the PHENIX collaboration showed that in central collisions of Au+Au at $\sqrt{s_{NN}}$=130 GeV there was significant suppression of the yield of high transverse momentum particles compared to the p+p data scaled by the number of binary collisions, N_{coll}.

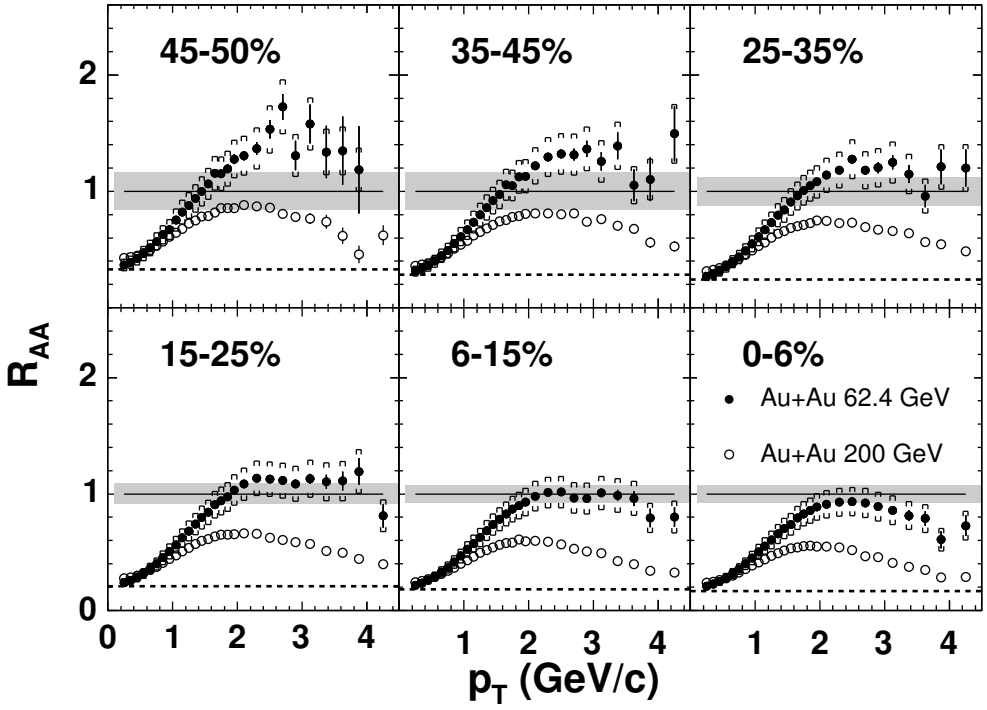

Fig. 8. Nuclear modification factor, R_{AA}, as a function of transverse momentum for Au+Au collisions at $\sqrt{s_{NN}}$=62.4 (closed symbols) and 200 GeV (open symbols), for six centrality ranges [84,116]. Centrality is expressed as a fraction of the total inelastic cross section with smaller numbers being more central. Bars and brackets show statistical and systematic uncertainties, respectively. The grey bands show the systematic error in the overall scale due to N_{coll}. The solid (dashed) line shows the expectation for scaling with N_{coll} ($N_{part}/2$) times p+p data (See discussion in Appendix B.3).

The PHOBOS collaboration has confirmed that a similar effect is present in

Au+Au collisions at 200 GeV [84], and has also performed the first similar studies at $\sqrt{s_{NN}}$=62.4 GeV [116], see Fig. 8. More importantly, as discussed later and shown in Fig. 31, the yields for Au+Au interactions at $\sqrt{s_{NN}}$=200 GeV, which span a range of more than a factor of five in the number of participants, were found to scale with the number of participants, when compared with central Au+Au collisions, to within $\leq$25% at all transverse momenta. The fact that data up to p_T of 4 GeV/c show much the same scaling as at low momentum clearly demonstrates that any scaling of the yield due to hard processes with the number of binary collisions is completely obliterated. Note the significant difference in the magnitudes and overall shapes of R_{AA} at the two energies shown in Fig. 8, as well as the fact that the difference is similar at all centralities. Additional discussion of this interesting observation, as well as other scaling properties of the data, can be found in Sect. 4.

It is important to note that, except where specifically mentioned, the reference p+p data in this and all other cases of comparison to RHIC data is for inelastic collisions. This choice is made for consistency rather than being strongly motivated by physics considerations. In most cases, the difference between the yield in non-single diffractive (NSD) and inelastic measurements is about 10% or less.

As mentioned above, the observed suppression of hard processes could result from some modification in the initial state (see, for example, [75]), as well as from interactions in the dense medium formed after the collision. To investigate this possibility, similar data were taken for d+Au collisions at the same energy. Figure 9 shows the nuclear modification factor, R_{dAu}, measured by PHOBOS in d+Au at $\sqrt{s_{NN}}$=200 GeV, in four different impact-parameter ranges [77] and the similar modification factor, R_{AA}, in central Au+Au collisions at the same energy [84]. Note the dramatic difference between the results for central d+Au and Au+Au collisions at higher transverse momentum shown in the lower right panel of the figure. For 2 GeV/c $\leq p_T \leq$ 6 GeV/c the yield of charged particles in d+Au is consistent with binary collision scaling of p+p data, whereas in Au+Au collisions the yield is clearly suppressed.

The observation that the data points at higher p_T in Fig. 9 are similar at all centralities and all lie near unity may be evidence for binary collision scaling at higher p_T in d+Au. However, this interpretation is unclear since the characteristics of the data may be a consequence of the interplay of an enhancement (similar to the so-called "Cronin effect" [81,117–120]), and some suppression, due to either energy loss in the final state or parton saturation effects in the initial state. Furthermore, several effects complicate the assumed connection between binary collision scaling and the magnitude and centrality independence of R_{dAu}. First, it should be noted that the number of participants and the number of collisions do not deviate as much with centrality in d+Au as

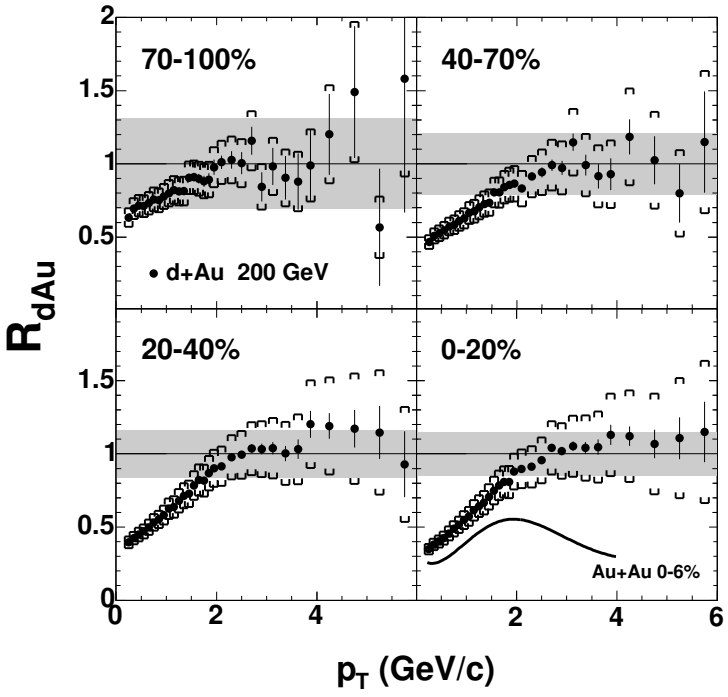

Fig. 9. Nuclear modification factor, R_{dAu}, as a function of transverse momentum for d+Au collisions at $\sqrt{s_{NN}}$=200 GeV, for four centrality ranges [77]. Centrality is expressed as a fraction of the total inelastic cross section with smaller numbers being more central. Bars and brackets show statistical and systematic uncertainties, respectively. The shaded area shows the uncertainty (90% C.L.) in R_{dAu} due to the systematic uncertainty in N_{coll} and the scale uncertainty in the proton-proton data. In the bottom right panel, the nuclear modification factor, R_{AA}, for the 6% most central Au+Au collisions at the same energy [84] is shown as a dark curve for comparison.

in Au+Au. Using the number of participant pairs as the scaling variable (i.e. using $R_{dAu}^{N_{part}}$ defined in Appendix B.3) would raise the values at all transverse momenta by an average factor of about 1.65. However, the factor would differ only by 29%, 14%, and 6% for centrality bins of 70–100%, 40–70%, and 20–40%, respectively, compared to the 0–20% data. These shifts are comparable to, or smaller than, the systematic uncertainties in the overall scale of the modification factors. Thus, the observation of similar values of R_{dAu} at all centralities does not necessarily imply scaling with the number of collisions.

To further complicate the interpretation, the value of the nuclear modification factor was found to depend on the pseudorapidity of the emitted particles. This was first inferred from the comparison of the PHOBOS results [77] to those of the other experiments [121–123]. It can also be seen from PHOBOS results directly as shown in Fig. 10 [78]. Data from BRAHMS suggest that this trend may continue to higher positive pseudorapidity [79] while preliminary PHENIX data suggests that R_{dAu} may even continue rising for negative pseu-

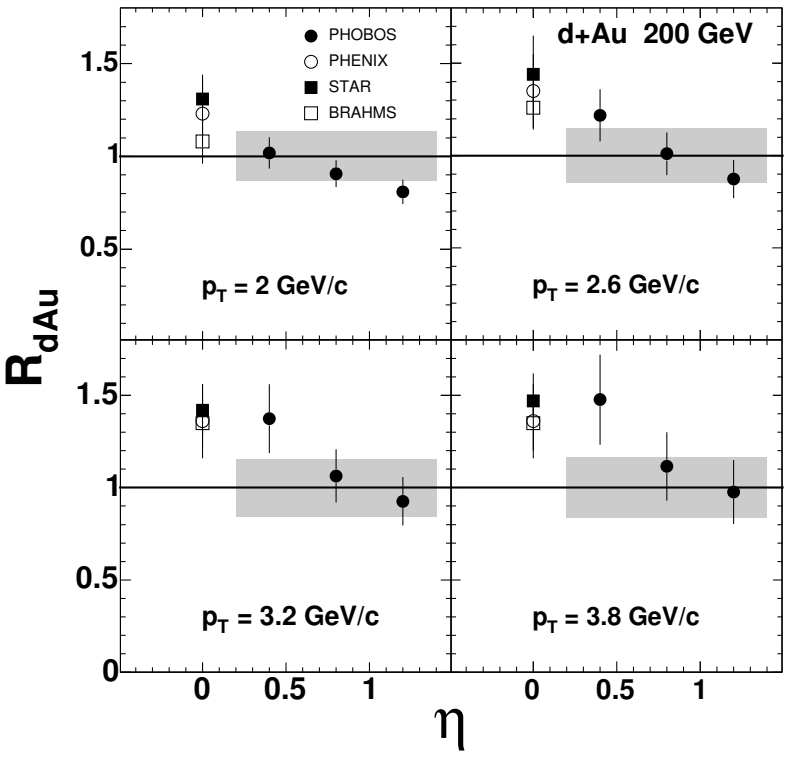

Fig. 10. Nuclear modification factor, R_{dAu}, for four different values of p_T as a function of pseudorapidity in d+Au collisions at $\sqrt{s_{NN}}$=200 GeV. PHOBOS results away from midrapidity [78] are compared to data near η=0 from BRAHMS [121], PHENIX [122], and STAR [123]. For the PHOBOS points, the error bars are the point-to-point systematic errors (90% C.L.). The systematic errors in the overall scale of the PHOBOS R_{dAu} are shown as grey bands.

dorapidity (i.e. towards the Au projectile rapidity) [80]. The trend seen in the PHOBOS and BRAHMS data has been interpreted as support for the CGC model, but this conclusion is far from clear and the PHENIX data at negative pseudorapidity remain even more poorly understood [81]. For this reason, the observation of the particular value of R_{dAu}=1 at higher p_T is a consequence of the PHOBOS acceptance and again does not necessarily imply N_{coll} scaling.

Therefore, the important feature is not the possible scaling of the particle yields in d+Au with N_{coll} times p+p yields, but instead the very significant difference between the transverse momentum dependence of the d+Au and Au+Au nuclear modification factors. The larger system appears to lead to a strong suppression while the smaller system does not. Very similar results were reported simultaneously by all four RHIC experiments [77,121–123]. Part of the difference in the behavior of the two colliding systems may be attributed to initial state effects. However, it is difficult to avoid the conclusion that the majority of the difference in R_{AA} compared to R_{dAu} results from the impact of the high energy density matter on the yield of particles with p_T in this measured range. Clearly, the constituents of the medium produced in the

central Au+Au collisions experience a significant level of interaction. Since, as discussed above, the system at this early stage cannot be primarily hadronic in nature, one can conclude that the high energy density matter created at RHIC interacts very significantly with high p_T partons (or with whatever constituents comprise the dominant degrees of freedom at this early stage). It certainly does not appear to be a weakly interacting parton or hadron gas.

In related measurements, the STAR experiment has studied back-to-back correlations of high p_T particles. Measuring the yield of particles as a function of the azimuthal angle relative to a very high p_T trigger particle, a suppression was found in particles emitted on the opposite side [124]. This suppression was found to depend on the azimuthal angle of the trigger particles with respect to the reaction plane [125]. One strength of the correlation analysis is that it is essentially self-normalizing in the sense that the result does not depend on any assumptions about the scaling of the primary production of particles. One can interpret this as additional support for the conclusions that are being drawn from the single particle data.

Further evidence that the system may be both non-hadronic in nature and also characterized by a significant level of interaction comes from flow data for identified particles. PHENIX [126] and STAR [127] have measured the elliptic flow and its dependence on transverse momentum for a variety of mesons and baryons. These data appear to be consistent with an interpretation that the flow of produced particles results from the recombination of quarks which are themselves flowing [128]. The impact of this flow of quarks is that the v_2 parameter divided by the number of valence quarks scales as a function of the transverse momentum, also divided by the number of valence quarks. It should be noted that this recombination model only holds for elliptic flow at higher values of $p_T \geq 1 - 2$ GeV/c. If this interpretation is correct, it lends support to the presumption that the system has a component of constituent quarks which experience significant interactions early in the evolution of the collision.

In conclusion, the data from RHIC collisions provide strong evidence for the creation of a very high energy density, low baryon chemical potential, medium which cannot simply be described in terms of hadrons and whose constituents experience significant interactions with each other.

4 Simple scaling behaviors of particle production

The wide range of systems and energies provided by the RHIC accelerator, combined with the unique capabilities of the PHOBOS detector, has allowed a study of the properties of particle production over a very broad range of pseu-

dorapidity and transverse momentum for a wide variety of initial conditions. This work continues a long history of investigations to understand particle production under a variety of conditions. In the process of this study, a surprising result was discovered. It emerged that an enormous span of data for charged particles emitted in d+Au and Au+Au collisions at RHIC energies could, to a large extent, be described using only a few simple unifying features. Some of these scaling behaviors had been observed previously, either at lower energies or for less complicated systems than heavy ion collisions. Although a direct theoretical connection between these observed trends in the data and the nature of the systems created is not presently apparent, it is clear that the unifying features must reflect important aspects of the dynamics of the evolution starting from the earliest stages of the collision. In addition, these observations shed light on broader aspects of particle production under a variety of conditions. This section describes the extent to which these scaling behaviors and other unifying features apply to charged particle production at RHIC energies.

In order to achieve the broadest possible coverage in pseudorapidity and transverse momentum, most of these measurements rely on detection techniques which do not differentiate between the production of different species of particles. Therefore, it is generally not known at this time to what extent the production of any specific particle exhibits the scaling behaviors described in this section. However, the degree to which one particular species deviates from any of the observed dependencies must be compensated by the sum of all the other species, a correspondence between particle types that is interesting in itself. The occurrence of such balancing could contain important information about the global influences on the processes taking place during particle production.

In a wide variety of systems (hadron+A up to A+A), the total number of emitted charged particles is observed to have a very simple dependence on energy and centrality. In all cases, the total multiplicity appears to scale linearly with the number of participant pairs, $N_{part}/2$. It should be noted that throughout this document the generic term "participant pairs" refers simply to the total number of participants divided by 2, i.e. a quantity that is unity in p+p, and does not imply a matched pair from the two colliding species. The total multiplicity of charged particles emitted in hadron+A (including p+A) and d+A is equal to $N_{part}/2$ times the multiplicity observed in p+p. In contrast, for heavier nucleus-nucleus interactions, the constant of proportionality is the multiplicity produced in e^++e^- annihilations, which is approximately equal to that measured in p+p at twice the center-of-mass energy. This is suggestive of a universal energy dependence of charged particle multiplicities in strong interactions. Centrality, as reflected by the number of participants (both the total number and, for asymmetric systems, the number in each of the nuclei) appears to have a strong influence on the shape of the pseudorapid-

ity distributions. In addition, the yield of high transverse momentum particles ($p_T \geq 4$ GeV/c) shows a dependence on the number of participants that is surprisingly similar to that for low momentum particles when comparing Au+Au at different centralities.

Over a broad range of emission angles, the distributions of pseudorapidity density and the elliptic flow signal, when measured as a function of the variable $\eta' = \eta - y_{beam}$ (i.e. when shifted by y_{beam} and thereby effectively viewed in the approximate rest frame of one of the colliding particles), appear to be identical both in shape and magnitude at all beam energies over a large range of η'. The details of the shape of the distributions depend on the impact parameter, but again in an energy-independent way. In addition to this extended longitudinal scaling, no evidence is seen for a boost invariant central plateau in the pseudorapidity distributions of either particle multiplicity or elliptic flow.

Another aspect of the centrality dependence is the observation that many differences between data for Au+Au and p+p, for example in the multiplicity per participant or in the shape of the transverse momentum distributions, persist essentially unchanged over a centrality range corresponding to a number of participants that spans a factor of 5 or more. Finally, many properties of particle production exhibit separate dependences on the energy and centrality of the collisions which factorize to a surprising degree. In other words, the centrality dependence of data such as pseudorapidity density and transverse momentum spectra was found to be identical even at center-of-mass energies separated by up to an order of magnitude.

4.1 Energy dependence of total multiplicity

The most basic observable in the study of multiplicity is the total number of produced particles. Collisions at RHIC extend the center-of-mass energy range available in heavy ion interactions by more than an order of magnitude. Section 2.1 described the energy dependence of the midrapidity particle density. In this section, the total integrated particle yield is discussed. As is clearly shown in Fig. 1, the PHOBOS multiplicity detector extends over a uniquely broad range of pseudorapidity and, therefore, the extrapolation to account for missing regions of solid angle is small even at the highest RHIC energy. The total multiplicity of charged particles per participant pair in A+A collisions over a wide range of energies [44,50,129,130] is shown in Fig. 11, along with data from d+Au [57], p($\bar{p}$)+p, and e^++e^- annihilation into hadrons (the latter two compiled from references in [131]). The d+Au value has also been divided by the number of participant pairs. The nucleus-nucleus data are for central collisions. However, this choice is inconsequential since, as will be discussed in the following section, the total multiplicity per participant pair appears to be

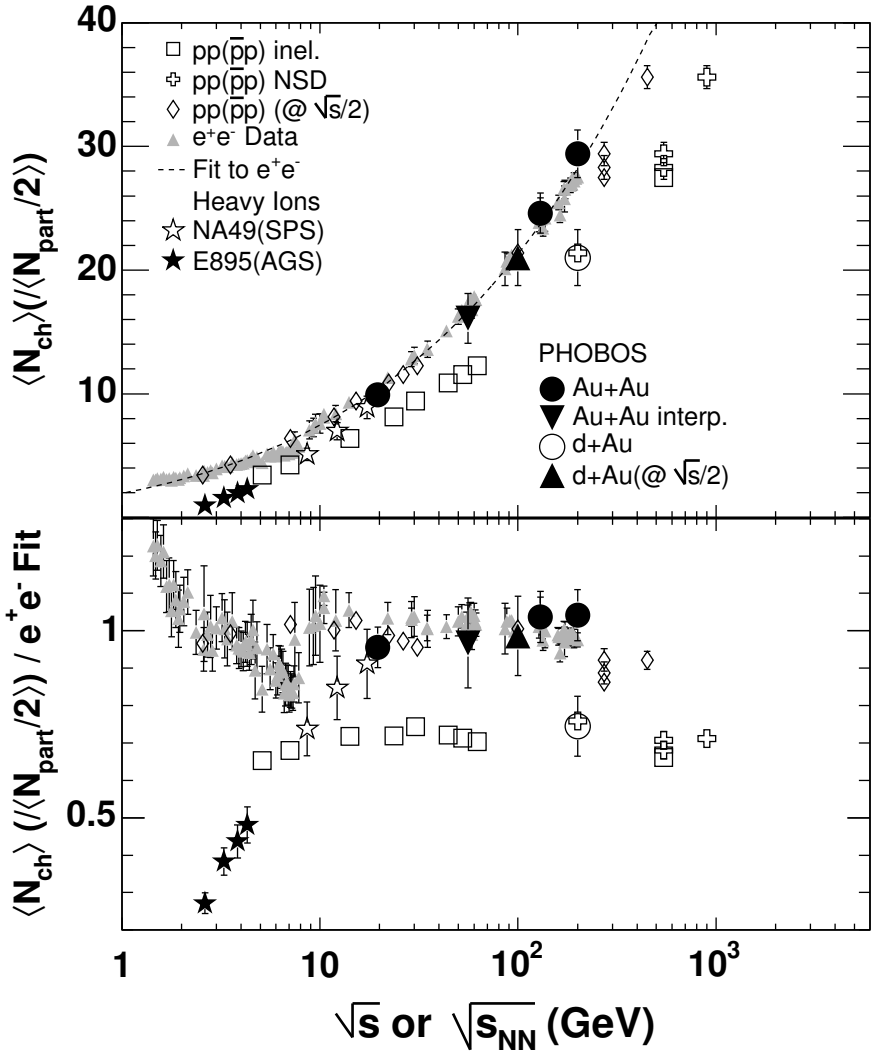

Fig. 11. (Top panel) Normalized total multiplicities of charged particles emitted in e^++e^-, p($\bar{p}$)+p (compiled from references in [131]), d+Au [57], Au+Au (AGS [130] and PHOBOS at RHIC [129,44]) and Pb+Pb (SPS [50]) collisions at a variety of nucleon-nucleon center-of-mass energies. Nucleus-nucleus data are all for central collisions and the multiplicities have been divided by the number of participating nucleon pairs. (Bottom panel) The values for all systems are shown divided by a fit to the e^++e^- data.

approximately independent of centrality.

The various sets of data have very different trends. The p+p (open squares and crosses) and d+Au (open circle) data are consistently about 30% below the e^++e^- data, as shown in the lower panel where all of the data points are divided by a fit to the e^++e^- data. Starting at the lowest energies, the A+A data rise much faster than both p+p and e^++e^- but then the slope of the energy dependence changes and above $\sqrt{s_{NN}}$ ~20–30 GeV, the A+A data

follow the trend of the e^++e^- data. The lower panel of the figure shows that these two sets agree to within 10% over a span of an order of magnitude in center-of-mass energy.

One proposed explanation for the difference between the p+p and e^++e^- data is that one must properly account for the "leading particle effect" which is present in hadron-hadron collisions, but not in e^++e^- annihilation. The distribution of protons in x_F (see Appendix B.2 for definition) for p+p collisions at different energies was found to be approximately flat (with a spike at x_F=1 for elastic and diffractive events; a summary of these data can be found in [132]). One interpretation of these data is that a leading nucleon typically carries away half of the beam energy. In p+p collisions, the x_F of the leading proton was found to directly anticorrelate with the particle multiplicity, as if the leading particle simply removed energy that would otherwise go into particle production [133–135]. By rescaling the center-of-mass energy for the p+p data by a factor of two (see open diamonds in Fig. 11), one observes that the multiplicities of p+p and e^++e^- reactions agree more closely over much of the energy range.

In contrast with the p+p data, which agree with the e^++e^- data over a large energy range only after rescaling, there is reasonable agreement of the total charged particle multiplicities between e^++e^- and A+A collisions over $\sqrt{s}$ and $\sqrt{s_{NN}}$ of about 20 to 200 GeV with no rescaling. At lower energies, one sees an apparent "suppression" of the A+A multiplicity compared to both p+p and e^++e^-. This might be explained by reference to the substantial baryon excess found in the particle yields at these lower energies (e.g. the antiproton/proton ratio $\ll$1, see references in [92]). The relatively larger number of baryons compared to pions should tend to suppress the overall multiplicity, since the baryon chemical potential reduces the entropy. Essentially, the net baryons take up an increasing fraction of the available energy. Additionally, the overlap of the peak of the rapidity distributions of the net baryons and the produced pions [136] could result in increased pion absorption during the evolution of the system.

The arguments made here suggest that the total multiplicity per participant pair is a universal function of the available energy, irrespective of the colliding system [129]. All of the heavy ion data shown in Fig. 11 are for central collisions, but as shown in Sec. 4.2 the numbers remain constant over a broad range of impact parameter. This is a surprising result if p+p collisions are expected to be a "reference system", while the enhanced multiplicity in A+A is related to more exotic physics. Moreover, the prediction of the energy dependence of the e^++e^- multiplicity is widely understood as a paradigmatic success of perturbative QCD [137], while a broader range of processes are expected to contribute in heavy ion collisions.

This interpretation of the comparison of p+p and Au+Au systems is validated by the $\sqrt{s_{NN}}$=200 GeV d+Au results from PHOBOS [138] shown in Fig. 11 for the most central collisions. If it takes more than one collision in order for all of the energy to be available for particle production, then one would expect the participants in the deuteron to contribute approximately half the multiplicity of an e^++e^- collision (i.e. with effective energy of $\sqrt{s}$), while the participants in the gold nucleus would contribute half a p+p collision. For a central d+Au collision, the ratio of gold to deuteron participants is approximately 8, so the "p+p-like" collisions should dominate, making the multiplicity closer to p+p, an expectation that is validated by the data.

It should be emphasized that this result applies mainly to the total multiplicity and not necessarily to other details of particle production. In other words, this argument does not imply that A+A collisions are merely scaled up e^++e^- annihilations. The presence of elliptic flow and strangeness enhancement, along with other observations, precludes this possibility. Furthermore, it is not argued that all observables in A+A collisions should be compared to similar data from p+p at twice the center-of-mass energy. Still, the similarities between the total charged particle multiplicities of these various systems raise the question of what are the decisive differences between the larger and smaller systems. Some insight may come from studying the role of the size and shape of the collision volume, which will be addressed in later sections.

While the physics scenario as stated is consistent with a broad range of multiplicity data, it is complicated somewhat by the recent BRAHMS result on the net baryon distribution, which is interpreted in terms of the net rapidity loss of the incoming baryons [139]. Although the measurements do not include the bulk of the net baryons, the data can constrain the shape of the distributions substantially. The BRAHMS analysis finds that the average rapidity loss of the net baryons in central Au+Au collisions at $\sqrt{s_{NN}}$=200 GeV is $\Delta y \sim 2$ units [139], which is consistent with values extracted from p+A data at lower energy [140,141]. When translated into "available" energy, i.e. the total incoming energy minus the energy of the net outgoing baryons, only about 75% of the energy is left for particle production in central A+A collisions. It should be noted that this value is a lower limit based on the assumption that the effects of longitudinal expansion can be ignored. If this reduced available energy is accounted for in the Au+Au data as was done for p+p, the resulting data points in the bottom panel of Fig. 11 would increase by about 15%. This would imply that Au+Au collisions are, in fact, able to convert the same amount of energy into a slightly larger number of particles than are produced in e^++e^- annihilations at the same center-of-mass energy. Given the systematic uncertainties in the various data sets, it is difficult to determine which of these interpretations is correct. Furthermore, given the current lack of understanding of the longitudinal dynamics in RHIC collisions (see Sect. 4.5), the validity of the assumption that all of the energy carried by the net baryons is "unavailable"

for particle production is far from obvious. What is unambiguous is the surprisingly close correspondence of all systems despite the common assumption that somewhat different physics dominates in each case.

In summary, the data show that the systematics of the total charged-particle multiplicities are suggestive of a universal mechanism which affects "bulk" features of particle production in strongly-interacting systems. The dominant control variable in this picture appears to be the available or "effective" energy, per participant pair, which is apparently 50% of $\sqrt{s_{NN}}$ in a p+p or d+Au collision, but appears to be a significantly larger fraction of $\sqrt{s_{NN}}$ in A+A and presumably all of $\sqrt{s}$ in e^++e^- reactions. This may simply be related to the fact that typical participants in an A+A collision are multiply struck when passing through the oncoming nucleus. A more complete description would involve a full explanation of the nature and origin of the outgoing baryons in both nucleon-nucleon and nucleus-nucleus collisions. All of these issues thus require a more comprehensive understanding of the early-time dynamics of the collision process, including both the dynamics of baryon-number transport and entropy production.

4.2 Centrality dependence of total multiplicity

One of the key tools for understanding particle production in high energy p+A and A+A collisions is the study of the system-size dependence, either by varying the size of the colliding nuclei or by classifying the collisions according to centrality. Variation of the collision centrality not only changes the volume of the particle production region, but also the number of binary collisions per participant (see Appendix B.3 for more discussion of this topic). In addition to changing the collision energy, varying centrality therefore provides another handle, in principle, for changing the balance of particle production between 'soft' low-momentum processes and point-like 'hard' processes with large momentum transfer.

One of the more striking features of total particle production in Au+Au collisions at RHIC is the proportionality of the total charged-particle multiplicity to the number of participant pairs [129], as shown in Fig. 12 and compared to $\bar{p}$+p [142] and d+Au collisions [138]. The figure also shows that the total charged particle multiplicity is proportional to the number of participating nucleons in Au+Au collisions at all three energies from $\sqrt{s_{NN}}$=19.6 to 200 GeV. The data suggest that the transition between p+p collisions and Au+Au is probably not controlled simply by the number of participants, as even very central d+Au collisions do not show any sign of trending up towards the level of the Au+Au data. As discussed in the preceding section, this aspect of the total multiplicity is expected in the "available energy" *ansatz*, since the Au

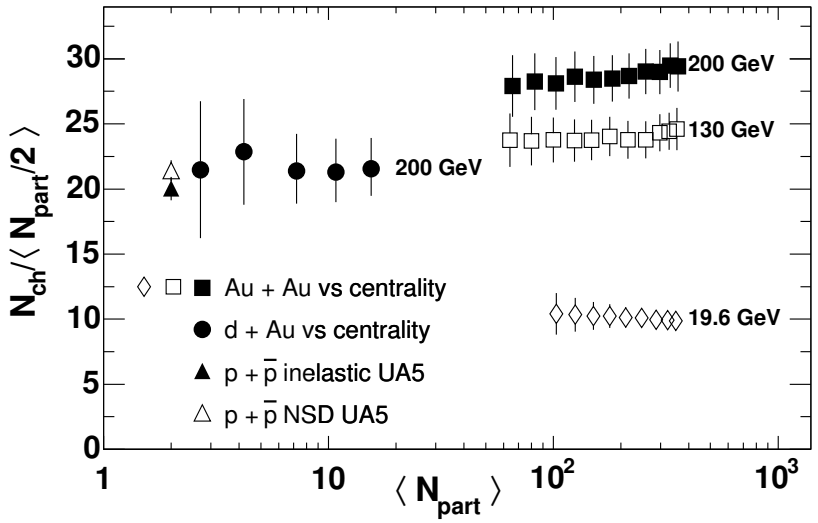

Fig. 12. Total integrated charged particle multiplicity per participant pair as a function of number of participants. Data are shown for Au+Au collisions at $\sqrt{s_{NN}}$ of 19.6, 130 and 200 GeV [129], as well as d+Au [138] and $\bar{p}+p$ at 200 GeV [142]. The vertical bars include both statistical and systematic (90% C.L.) uncertainties.

participants, which dominate the total number of participants in d+Au, are expected to be more "p+p-like".

This topic represents one area where data for collisions of lighter nuclei at RHIC could make an important contribution. Extrapolation of Au+Au analysis to very peripheral collisions inevitably suffers from considerable systematic uncertainty in the number of participants. Lessons learned from analysis of lower energies and smaller systems such as d+Au are currently being applied in an attempt to reduce those uncertainties. However, it is clear that data from lighter systems, currently being collected in Run V at RHIC, will provide vital input to the interpretation of these results.

Further information about the centrality dependence is shown in Fig. 13, the inset of which shows a detailed comparison of the PHOBOS d+Au results at $\sqrt{s_{NN}}$=200 GeV [138] with π+A, K+A, and p+A for $\sqrt{s_{NN}}$ ≈10–20 GeV [143]. In all cases in the inset, the total charged particle multiplicity in hadron-nucleus collisions is divided by the p+p multiplicity at the same collision energy. Within the experimental uncertainty, the ratios all fall on the indicated line, demonstrating that the total charged particle multiplicity scales with the number of participant pairs times the data for p+p at the same energy for all hadron-nucleus systems, as was first recognized in earlier work [144,145]. This feature of the data led to the "wounded nucleon" model of Białas, Bleszyński and Czyż [146]. The range in N_{part} over which this scaling is shown to apply is extended significantly by the PHOBOS charged particle multiplicity in d+Au collisions versus centrality.

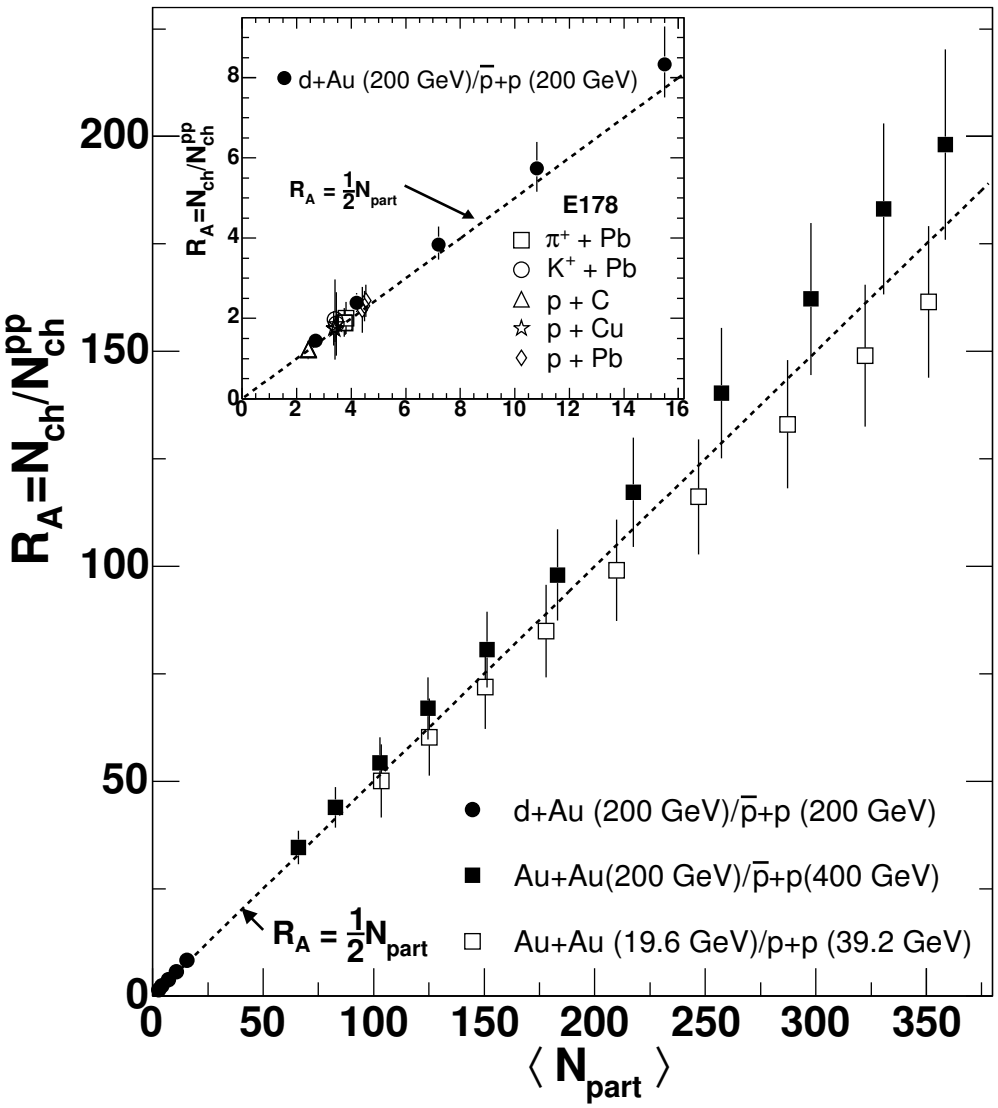

Fig. 13. Ratios of total particle multiplicity data for a wide range of hadron-nucleus [143], and nucleus-nucleus collisions [49,138] over the multiplicity in proton(antiproton)-proton interactions [147–149,142] are plotted versus the number of participating nucleons. The denominator for interactions induced by mesons, protons, or deuterons is proton-proton data at the same center-of-mass energy. For Au+Au interactions, the denominator is proton(antiproton)-proton data at twice the center-of-mass energy. The error bars include both statistical and systematic effects. Furthermore, they are partially correlated due to common errors in N_{ch}^{pp}. Note that all the data fall on a common line with a slope of 1/2 (as expected since p+p has two participants) and zero intercept.

A similar analysis of Au+Au data for collisions at $\sqrt{s_{NN}}$=19.6 GeV and 200 GeV is shown in the main part of Fig. 13 [138]. As for the hadron-nucleus data, the points fall along the line, exhibiting scaling of the total multiplicity with the number of participant pairs, but in this case multiplied by p($\bar{p}$)+p data at twice the center-of-mass energy [142,147–149]. A particularly striking

feature, as discussed in Section 4.1, is the fact that, for all these systems and energies, the total number of charged particles is directly given by the number of participant pairs times the number seen in p+p after accounting correctly for the energy carried away by the leading baryon.

This continuation of the previously-observed approximate N_{part} scaling, which is now seen to apply to all systems and over an expanded range of energies from $\sqrt{s_{NN}}$ below 10 GeV to the highest at RHIC, represents one of the more surprising features of particle production at RHIC.

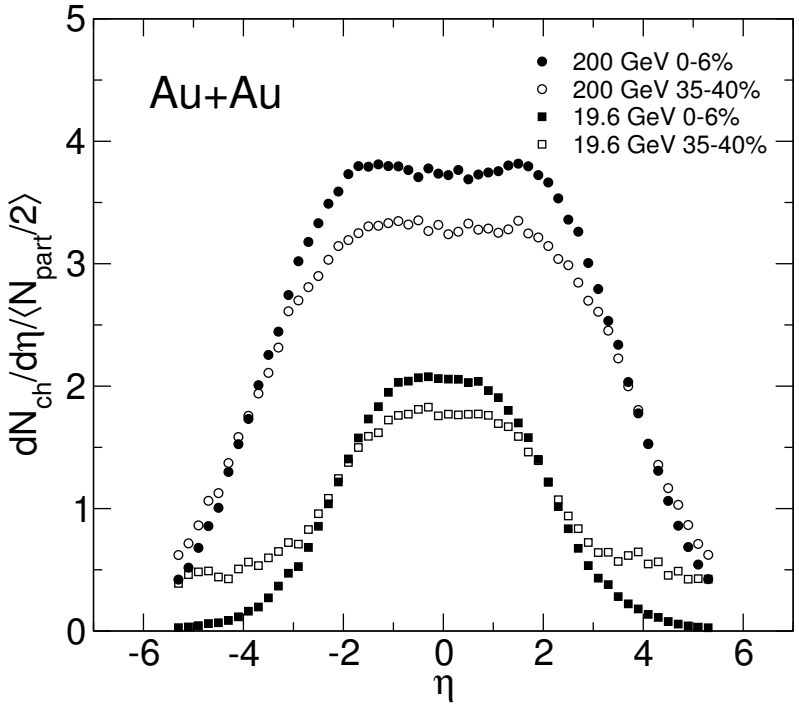

Fig. 14. Distributions of normalized pseudorapidity densities of charged particles emitted in Au+Au collisions at two energies and two ranges of centrality [44]. The data have been divided by the average number of pairs of participating nucleons for each energy and centrality range. The centrality is designated by the fraction of the total inelastic cross section, with smaller numbers being more central. Systematic errors are omitted for clarity. Statistical errors are smaller than the symbols.

4.3 Centrality dependence of pseudorapidity distributions

It should be stressed that the universal N_{part} scaling of the total number of particles produced in Au+Au collisions does not result from rapidity distributions whose shape is independent of centrality, or N_{part}. The rapidity distributions do depend on both centrality and on the nature of the colliding systems, as is evident from Fig. 14 for Au+Au [44] and Figs. 15 and 16 for d+Au [138]. However, the dependence of the shape on centrality, as first reported in [150], is very specific.

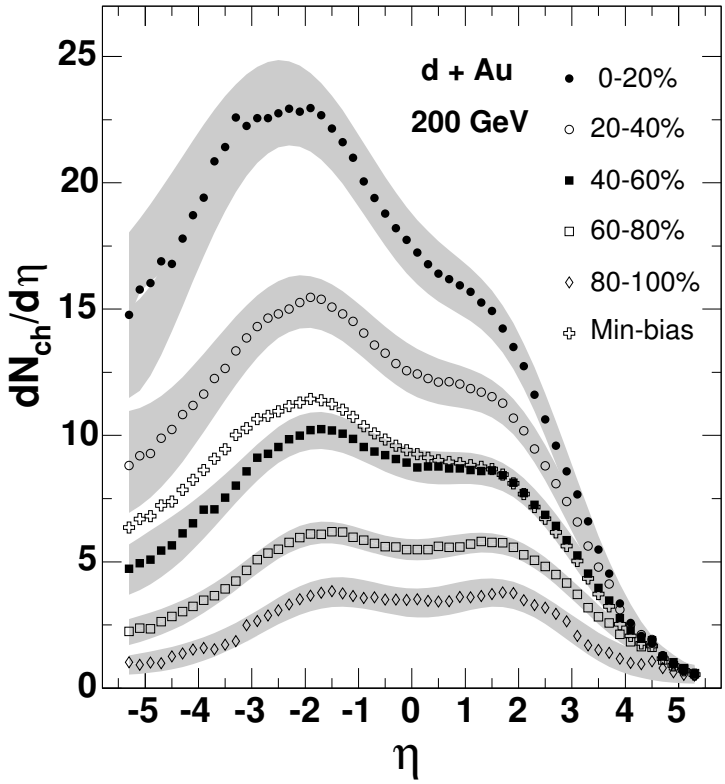

Fig. 15. Distributions of pseudorapidity densities of charged particles emitted in d+Au collisions at $\sqrt{s_{NN}}$=200 GeV for a variety of centralities [138,57]. The positive pseudorapidity direction is that of the deuteron. The centrality is designated by the fraction of the total inelastic cross section, with smaller numbers being more central. Grey bands indicate the systematic uncertainties (90% C.L.).

The Au+Au pseudorapidity distributions shown in Fig. 14 appear to exhibit a sort of incompressibility in rapidity space. Thus, a reduction in the number of particles at midrapidity is balanced by a similar increase of the number of particles at high rapidities, with the total number remaining constant. Obviously, moving particles around in rapidity changes the total longitudinal energy in the system. If the total energy available for produced particles depends only on the number of participants, energy must be conserved by changes in the distribution of transverse momentum.

The centrality dependence of pseudorapidity distributions in asymmetric systems can be studied using PHOBOS data for d+Au collisions as shown in Figs. 15 and 16 [57,138]. With increasing centrality, an increase in particle production (see Fig. 15) and a significant change in shape of the distributions (see Fig. 16) is observed. It should be stressed that the appearance of a "double-hump" structure in the d+Au distributions is primarily due to the effect of the Jacobian associated with the transformation to $dN/d\eta$ from dN/dy (see related discussion in Section 4.5.3). Although the shape changes in a non-trivial way, the integral of these distributions, when extrapolated to full solid

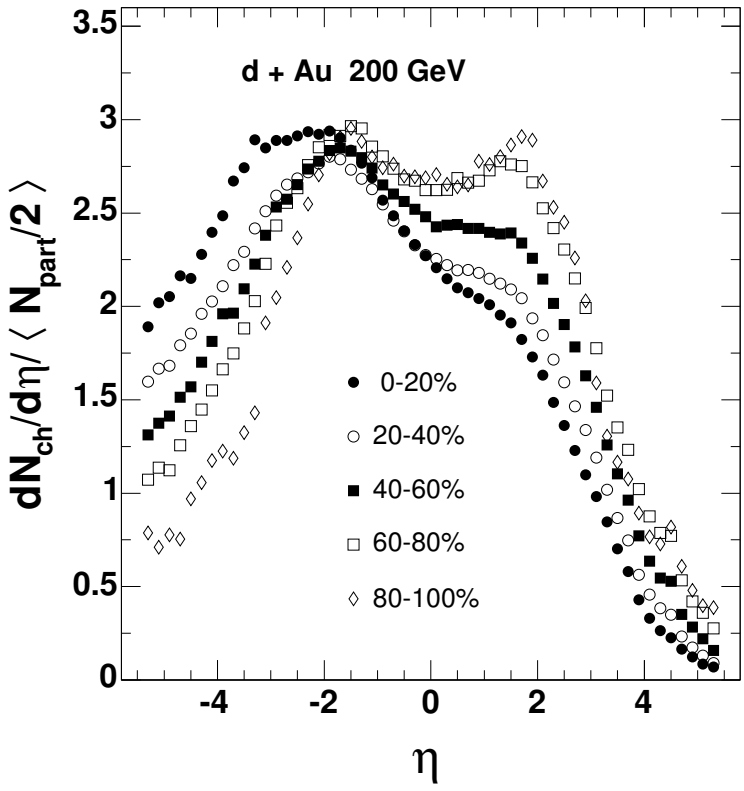

Fig. 16. The data of Fig. 15 are shown but in this case divided by the average number of participant pairs in each centrality bin [138]. Systematic errors are not shown.

angle, is found to be proportional to the number of participating nucleons, as was shown for many systems and energies in Section 4.2.

The comparison of total particle multiplicity in d+Au and p+p can be extended by studying the ratio $dN/d\eta$(d+Au)/$dN/d\eta$(p+p) as a function of pseudorapidity, as shown in Fig. 17 [138,142]. The main panel of the figure shows this ratio for various d+Au centralities, as a function of pseudorapidity. The inset and the arrows at the lower right demonstrate that, as was seen in p+A at lower energy [143,145,151–153], the data are consistent with a picture in which the density of produced particles which have a rapidity in the vicinity of the incident deuteron (gold) is proportional to the number of deuteron (gold) participants. The data suggest that the overall rapidity distribution, not just the integral of the distribution, is strongly influenced by the collision geometry.

In light of the discussion of particle production as a function of available energy in Sect. 4.1, one might initially expect the ratio at positive rapidity in Fig. 17 to increase faster than the number of deuteron participants. This is because each deuteron participant interacts with multiple Au participants and is therefore "Au+Au-like", while each Au participant suffers far fewer

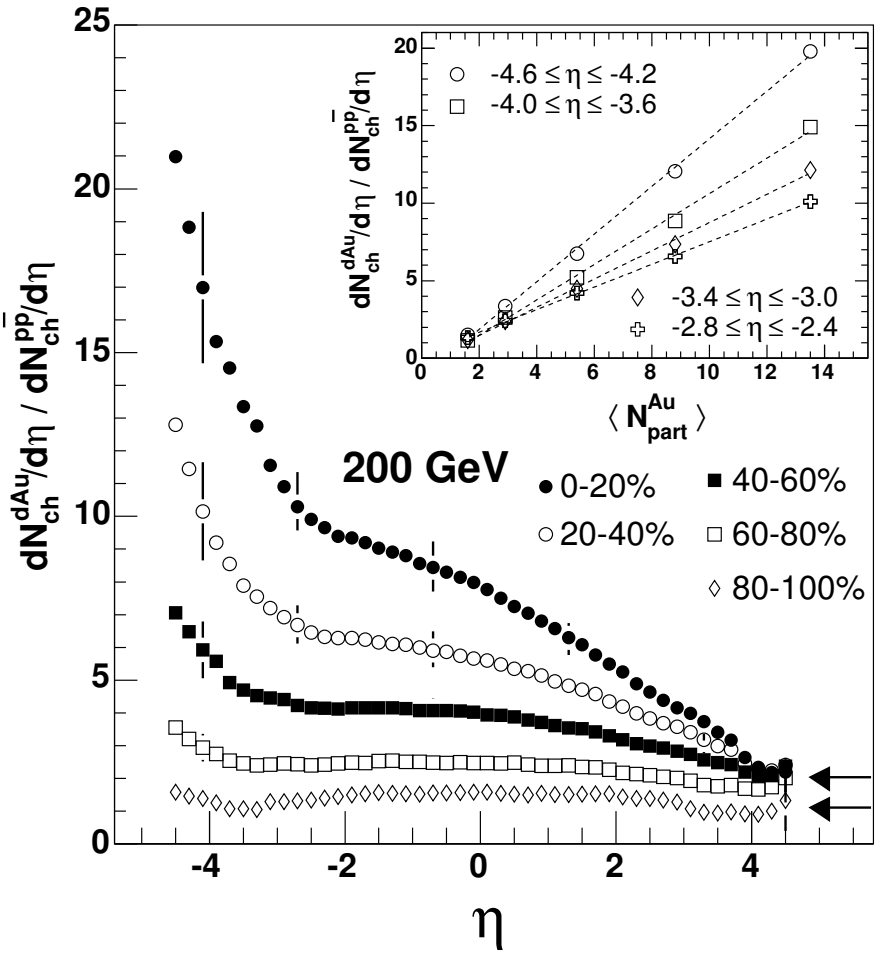

Fig. 17. The main panel shows the distributions of pseudorapidity densities of charged particles emitted in d+Au collisions with $\sqrt{s_{NN}}$=200 GeV at various centralities [138] (see Fig. 15) divided by the distribution for inelastic $\bar{p}+p$ collisions at the same energy [142]. The positive pseudorapidity direction is that of the deuteron. Centralities are labeled by the fraction of total inelastic cross section in each bin, with smaller numbers being more central. The lower and upper arrows on the right show the average number of participants in the deuteron for the most peripheral (80–100%) and most central (0–20%) bin, respectively. The inset shows the values averaged over several bins in negative pseudorapidity plotted versus the average number of participants in the Au nucleus for the five centrality bins.

collisions and is therefore "p+p-like". Recall that the normalized multiplicity per participant pair in Au+Au collisions was higher than that in p+p collisions at the same center-of-mass energy. However, it is important to keep in mind that the detailed shape of the distribution, not just the relative height at the two ends, is a complicated function of centrality. For example, it has long been known that in p+A collisions, the yield of all particles with rapidity within a unit or so of that of the proton falls with increasing target mass [154]. Thus, one should not expect conclusions from integrated yields to apply simply to narrow fixed regions of pseudorapidity.

The longitudinal properties of particle production, and in particular the dependence on center-of-mass energy, are discussed in more detail in Sect. 4.5.

4.4 Comparison of Au+Au and other systems

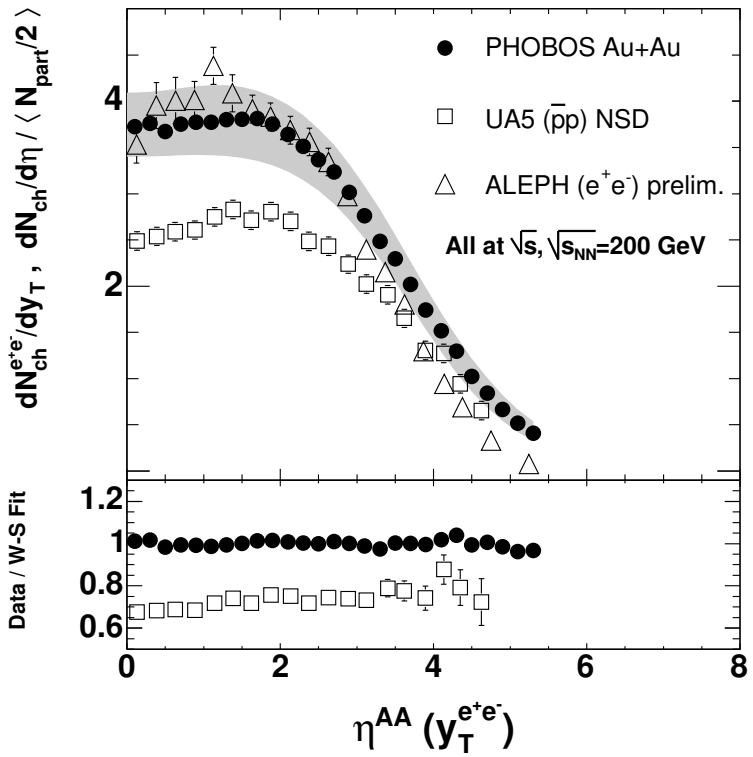

Fig. 18. (Top panel) The dN/dy_T distribution for charged particles emitted in e^++e^- collisions [156] is compared to the $dN/d\eta$ distribution for charged particles emitted in $\bar{p}$+p [155] and the normalized $dN/d\eta$ distribution for charged particles emitted in the 3% most central Au+Au collisions [44]. All three systems are at $\sqrt{s_{NN}}$ or $\sqrt{s}$ of 200 GeV. (Bottom panel) The Au+Au and p+p data are both shown divided by a fit to the former [129].

Figure 11 showed that the total charged particle multiplicities in the e^++e^- and A+A systems are very similar at a given center-of-mass energy, while those for p+p are somewhat smaller. To expand the comparison of these three very different systems, it is interesting to consider the full distributions in pseudorapidity. However, this study is complicated by the fact that the shapes of the Au+Au data vary dramatically with centrality (as is most clearly evident in Fig. 14). Figure 18 compares $dN_{ch}/d\eta$ normalized by the number of participant pairs for the 3% most central Au+Au collisions [44] to inelastic data for $\bar{p}$+p [155] and the distribution of dN_{ch}/dy_T (see definition in Appendix B.2) in the e^++e^- data [156], all at a $\sqrt{s_{NN}}$ or $\sqrt{s}$ of 200 GeV [129]. The bottom panel of the figure demonstrates that the lower total multiplicity seen in

$\bar{p}$+p results from a pseudorapidity distribution that is suppressed by roughly a constant factor over all emission angles. The figure shows agreement in the overall rapidity distribution between A+A and e^++e^-. In comparing the two distributions, one should keep in mind the centrality dependence in the shape for Au+Au, as well as the difference between dN/dy_T and $dN/d\eta_T$. Studies using JETSET [157] show that, for this data, the extracted dN/dy_T is about 10% larger than $dN/d\eta_T$ for $|y_T| \sim 0$ and about 10% smaller than $dN/d\eta_T$ for $|y_T| \sim 4$.

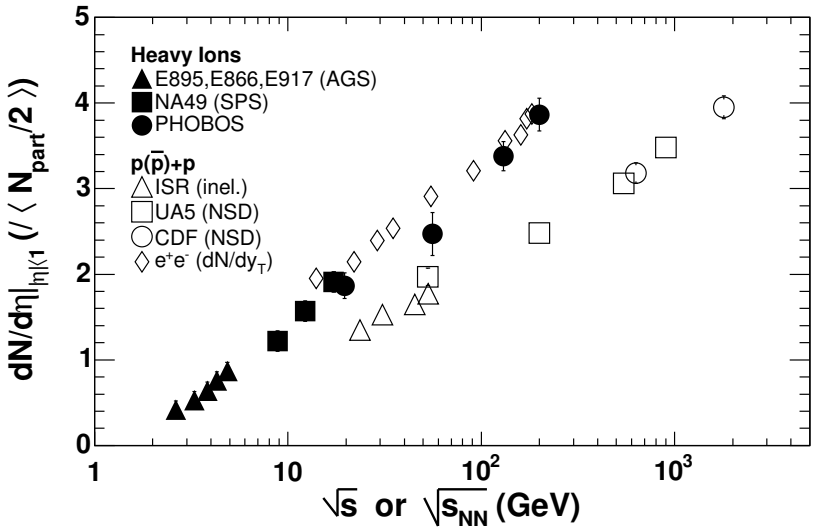

Fig. 19. Pseudorapidity particle density near midrapidity as a function of energy for p($\bar{p}$)+p, A+A and e^++e^- reactions (where the e^++e^- density is dN/dy_T, as explained in the text). Data for p($\bar{p}$)+p and e^++e^- were extracted from results compiled in [131]. Nucleus-nucleus data, shown for central collisions [44–56], have been divided by the number of participating nucleon pairs. Note that midrapidity particle densities are not available for lower energy p+p or e^++e^- collisions, in the latter case due to the lack of a well defined jet structure.

The similarity of the integrated multiplicity, as well as the shapes of the pseudorapidity distributions, for e^++e^- and the most central Au+Au data suggests that there should be a similarity in the evolution of the midrapidity density with collision energy, an expectation that is verified by the data. Figure 19 shows midrapidity particle density data from central heavy ion collisions [44–56] and from elementary collisions compiled from references in [131]. This additional close correspondence between the properties of central Au+Au and e^++e^- multiplicity data suggests that the agreement results from some underlying feature of particle production, as opposed to being an accidental coincidence. In particular, an understanding of why the shape of the pseudorapidity distribution for Au+Au collisions approaches that of e^++e^- for more central interactions might prove particularly enlightening.

The arguments presented in Sect. 4.1 concerning total charged particle multi-

plicities should not be interpreted to imply that all observables in A+A will match those in p+p at a factor of two higher $\sqrt{s}$. The midrapidity particle densities provide an instructive counterexample. Since the same total number of particles in p+p at a higher $\sqrt{s}$ are distributed over a broader range of pseudorapidity (see, for example, the top panel of Fig. 21), a factor of two shift in the p+p center-of-mass energy obviously cannot result in midrapidity densities equal to those measured in A+A. An examination of Fig. 19 reveals that the data confirm this expectation.

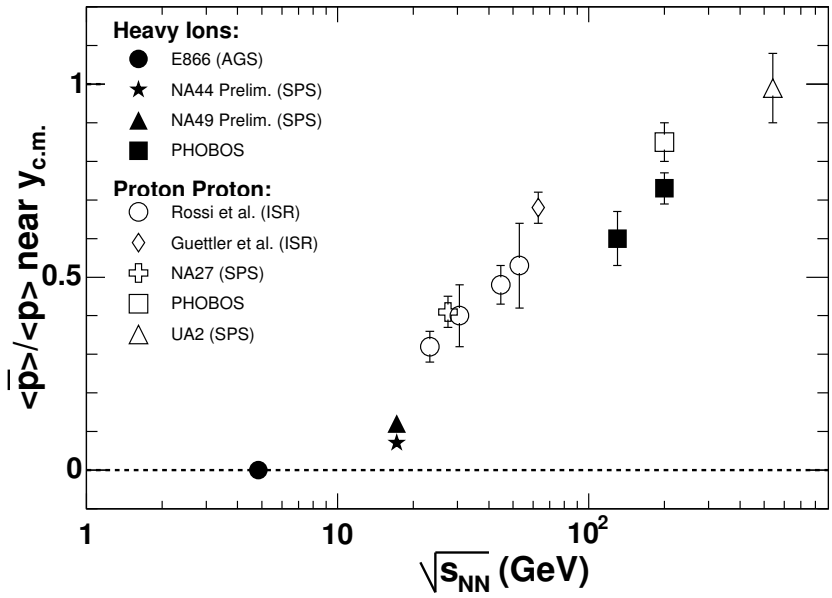

Fig. 20. Antiproton to proton ratios near midrapidity as a function of $\sqrt{s_{NN}}$ for p($\bar{p}$)+p collisions (open symbols) [158–162] and central A+A collisions (filled symbols) [91–94,54,95,96]. Error bars include both statistical and systematic errors.

A less trivial counterexample is illustrated in Fig. 20 which shows ratios of the yields of antiprotons over protons emitted near midrapidity in p($\bar{p}$)+p, as measured by PHOBOS at RHIC [158] and experiments at other energies [159–162], and in A+A collisions [54,91–96] as a function of $\sqrt{s_{NN}}$. The ratios for d+Au at $\sqrt{s_{NN}}$=200 GeV [100] (discussed in Sect. 2.2.1 and shown in Fig. 5) are consistent with the value shown on the figure for p+p. As discussed in Section 2.2, the relevant physics for understanding this ratio involves the interplay of baryon transport and antibaryon-baryon pair creation. In this case, in contrast to the situation for particle multiplicities, it is clear that the ratios for the nucleus-nucleus data are comparable to those in nucleon-nucleon collisions at significantly *lower* center-of-mass energies. Although this result may not be unexpected given the larger baryon rapidity loss in A+A as compared to p+p, it serves to illustrate the importance of a systematic study to unravel the dynamical differences between the simpler and more complicated systems.

Finally, the extraction of nuclear modification factors, R_{AA}, requires the explicit use of a p+p reference spectrum. The conventional choice is to use minimum bias data from inelastic interactions of p+p at the same collision energy, and all of the PHOBOS analyses have adhered to this standard. On the other hand, it was shown in Fig. 19 of this section and Fig. 11 of Sect. 4.1 that the charged particle multiplicity per participant (both at midrapidity and integrated over all solid angle) is larger in A+A than in p+p at the same energy. At $\sqrt{s}$ values of 200 GeV and above, it is known that the p_T spectra in p+p events with higher than average total multiplicity fall off less steeply than those for minimum bias events [163–165]. It should be stressed that we do not claim that an alternative p+p reference spectra is in any way inherently more appropriate. However, since the physics that determines the shapes of the transverse momentum spectra in p+p and A+A is not fully understood, such an alternative comparison could prove instructive. Therefore, one should keep these ambiguities in mind when interpreting data for the R-factors, particularly the specific value of the factors at large transverse momentum.

It should be noted that, although the relative yield at low and high p_T changes with multiplicity in p+p collisions, there is evidence that the change in shape is relatively small above p_T ~2 GeV/c [165]. In addition, the question of what p+p reference spectrum to use does not affect modification factors such as $R_{PC}^{N_{part}}$ which directly compare A+A at different centralities. Therefore, any possible ambiguities in nuclear modification factors due to the variation of the p_T distribution with multiplicity in p+p do not significantly impact any of the conclusions presented in this paper.

Of course, for very peripheral A+A collisions, all observables must evolve to match those in p+p (or, to be exact, the appropriate mix of p+p, p+n, n+p, and n+n) collisions at the same $\sqrt{s}$. The current PHOBOS analysis of Au+Au collisions typically spans a range of impact parameters corresponding to a variation in the average number of participants in each centrality bin of more than a factor of 5–6, i.e. from roughly 60 up to 350 or more. One remarkable aspect of this broad data set is that, over this range, the total particle multiplicity deviates very little from its central value when suitably normalized by the number of participants (see Fig. 12). The normalized pseudorapidity density near midrapidity does vary and is tending towards the p+p value but is still far above it for the most peripheral collisions studied to date (see discussion in Sect. 4.6). The shape and magnitude of the transverse momentum distributions also vary but only slightly and they show little sign of tending towards the p+p distribution (see Fig. 8). One can speculate that these deviations between peripheral Au+Au and p+p collisions might result from the fact that the number of collisions per participant (or the fraction of the participants that are multiply struck) rises extremely rapidly with decreasing impact parameter for these most grazing collisions (See Appendix B.1 and Fig. B.2).

In summary, comparisons of data for A+A and more elementary systems reveal an intriguing array of similarities and differences. Clearly, it is not possible to describe A+A collisions as trivial combinations of any other simpler systems. Rather than assuming that a single data set, such as p+p data at the same $\sqrt{s_{NN}}$, can serve as an ideal "reference" set for interpreting the complete dynamics of A+A interactions, the properties of a variety of systems should be studied over a range of energies and centralities to elucidate the similarities and differences among them. Such a study will lead to a more complete understanding of the salient features of the underlying physics, especially how the characteristics of the exciting regime of high energy density created in central Au+Au collisions at RHIC energies relate to those for other types of interactions.

4.5 Extended longitudinal scaling

This section describes several features of the pseudorapidity dependence of observables in a variety of systems. In particular, the distributions of particle yield and elliptic flow are found to be largely independent of center-of-mass energy over a broad region of pseudorapidity when shifted by y_{beam} and thereby effectively viewed in the rest frame of one of the colliding particles. In addition, no evidence is found for a broad region near midrapidity displaying the characteristic constant value of observables expected for a boost-invariant scenario.

4.5.1 Longitudinal dependence of particle production: Elementary systems

Before considering the energy dependence of pseudorapidity distributions in heavy ion collisions, it is instructive to review the extensive literature devoted to interpretations of, and expectations for, such distributions in simpler systems. A very general picture of elementary hadron-hadron collisions emerged in the late 1960's, consisting of two sources of particle production. This concept led to the prediction of two types of scaling laws for the distributions of final state particles in the regions of the longitudinal momentum space which are either near to or far from the colliding partners.

Particles near beam and target rapidity were thought to be governed by the "limiting fragmentation hypothesis" [166]. In this model, the momentum distribution of particles of species "i" in the rest frame of one of the original colliding hadrons (commonly denoted with a prime to distinguish it from the center-of-mass frame), $E_i d^3N_i/dp'^3$, or equivalently $d^3N_i/p_T dy' dp_T d\phi$, becomes energy-independent at high enough collision energy. The central concept is that the "projectile" hadron, when seen in the frame of the "target",

is Lorentz-contracted into a very narrow strongly-interacting pancake which passes through the target. This interaction leaves behind a complicated excited state whose properties do not depend in detail on the energy or even identity of the projectile, and which then "fragments" into a final state distribution of particles, $E_i d^3N_i/dp'^3$. It was generally assumed that this process produced particles primarily in a restricted window of rapidity around y'=0, possibly even leading to a complete lack of particles at midrapidity in a very high energy hadron-hadron collision [167].

In contrast, particles near midrapidity in the center-of-mass frame were expected to form a rapidity plateau with a constant dN/dy, independent of energy and the nature of the hadrons in the initial collision [168,169]. Similarly, in heavy ion collisions, a boost-invariant central plateau where "the initial conditions ... are invariant with respect to [longitudinal] Lorentz transformations" (i.e. observables are independent of y) was predicted [87]. Furthermore, the extent of this boost-invariant region was expected to grow with energy.

For elementary collisions such as p+p, and even e^++e^-, this general picture failed completely. Instead, the extended longitudinal scaling, seen in the form of x_F scaling, pointed the way to the current view in terms of QCD, modeled for instance in the widely used Pythia code [170]. This formulation generalized the concept of "fragmentation", which "describes the way the creation of new quark-antiquark pairs can break up a high-mass system into lower-mass ones, ultimately hadrons" [171]. It should be noted that energy independence, or scaling, in $E_i d^3N/dp'^3$ (i.e. full "limiting fragmentation") implies scaling of both dN/dy' and dN/dx_F.

Figure 21 shows $dN/d\eta'$ for p($\bar{p}$)+p collisions [155,172] and $dN/d(y_T\text{-}y_{jet})$ for e^++e^- collisions [173] (see Appendix B.2 for definitions). Lorentz boosts of pseudorapidity, η, are not as trivial as those of rapidity, but $\eta' \equiv \eta - y_{beam}$ (or $\eta + y_{beam}$) approximates y'. Furthermore, as noted above, the limiting fragmentation concept implies scaling in the full distribution, $E_i d^3N_i/dp'^3$. Since η' is just a function of (y', p_T, m_i), scaling in $dN/d\eta'$ is also implied directly. For these elementary systems, instead of a growing boost-invariant plateau, an extended version of limiting fragmentation is found, which leads to longitudinal scaling (energy independence) over more than four units of rapidity, extending nearly to midrapidity. The entire system can be described in terms of either string "fragmentation" or in terms of a parton cascade, leading naturally to extended longitudinal scaling.

4.5.2 Longitudinal dependence of particle production: d+A and p+A

In the case of asymmetric systems, the concept of extended longitudinal scaling can be explored separately in the rest frame of the two projectiles. Such

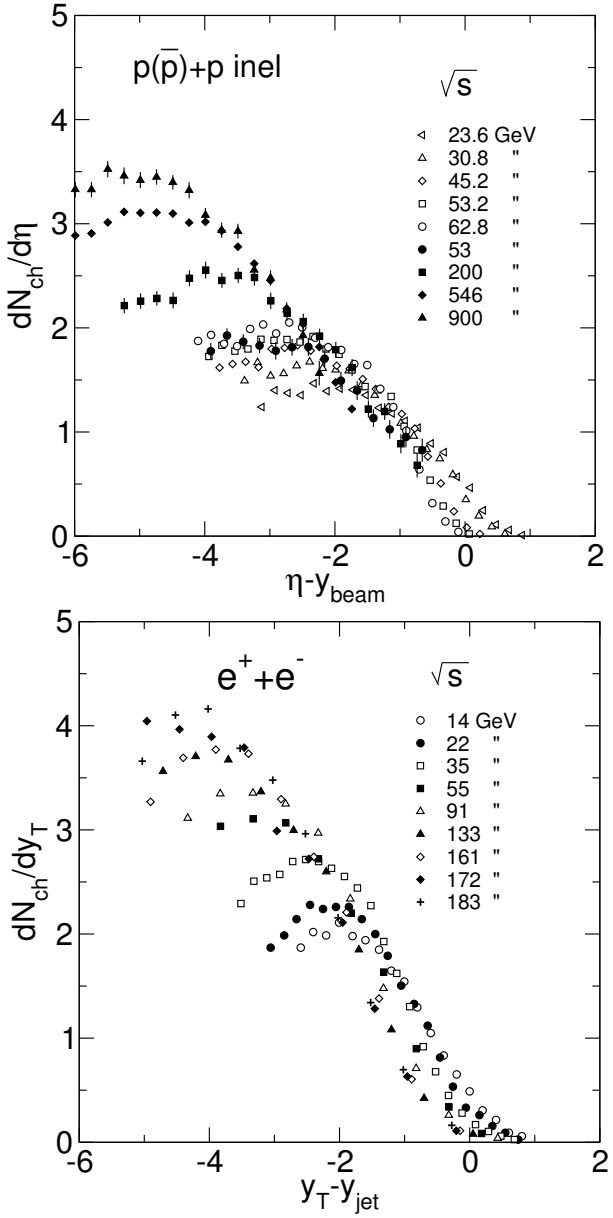

Fig. 21. (Top panel) Distributions of pseudorapidity density of charged particles emitted in p($\bar{p}$)+p collisions at a range of energies versus the variable $\eta - y_{beam}$ [172,155]. (Bottom panel) Similar data for particles emitted along the jet axis in an e^++e^- collision versus the variable $y_T - y_{jet}$, defined in Appendix B.2 [173]. In both cases, when effectively viewed in the "target" rest frame, these collisions exhibit longitudinal scaling (energy independence).

studies, applied to hadron-nucleus collisions, were of particular interest in the 1970's [145]. The specific question was whether the region of rapidity in which the particle yield is A-dependent expands with increasing collision energy [174–176]. Many models predicted that an extended A-dependent region, indicative of long-range order, should not occur. Instead, only a localized region near the rapidity of the larger collision partner would be affected by the target mass,

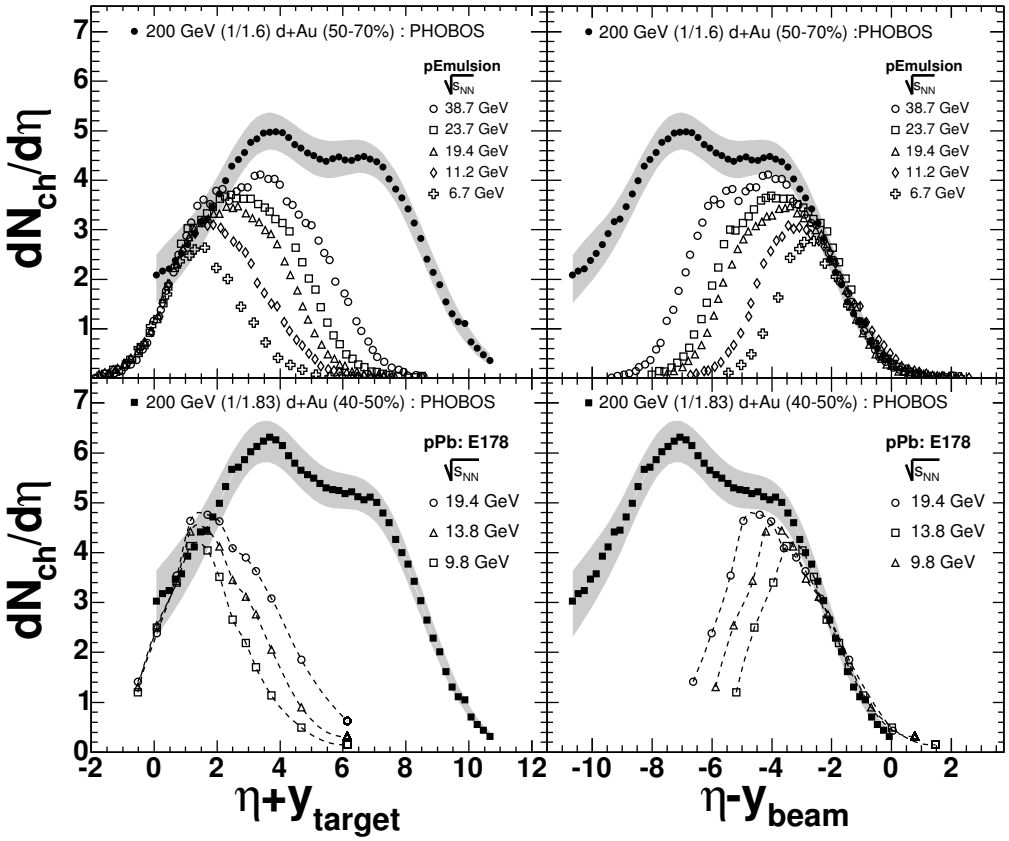

Fig. 22. A compilation of distributions of pseudorapidity densities of charged particles emitted in p+A and d+A collisions at a variety of energies[138,143,178,179]. Grey tracks are included in the distributions shown for emulsion data. The data are plotted versus the variables $\eta + y_{target}$ and $\eta - y_{beam}$ calculated using the rapidity of the larger (left panels) or smaller (right panels) of the colliding species. Note that the data at all energies and at both ends of the pseudorapidity range follow common curves.

and further, the height and width of this region was expected to be independent of, or at most weakly dependent on, beam energy. One prediction of these expectations was that the integrated yield in p+A would approach the value observed in p+p at high beam energies, since the small A-dependent region would become increasingly unimportant [177]. Instead, to the surprise of many people, a broad A-dependent region was observed, displaying characteristics very similar to the extended longitudinal scaling observed in simpler systems [141,143,151,153,178,179].

Pseudorapidity distributions from PHOBOS can be used to extend these studies to d+A collisions at RHIC energies. In Fig. 22, a compilation of pseudorapidity density data for proton+(nuclear emulsion) [178,179] and p+Pb [143] at various energies is shown, together with PHOBOS data for d+Au at $\sqrt{s_{NN}}$=200 GeV [138], with the centrality and normalization for the d+Au results chosen appropriately. To be more specific, the d+Au pseudorapidity

densities are divided by the number of participating nucleons in the deuteron (by definition this would be unity for p+A). Furthermore, the d+Au centrality bin was selected such that the ratio of the number of participating nucleons in the Au nucleus to the number in the deuteron was equal to the number of participating nucleons from the lead or emulsion in p+A. This latter quantity is commonly denoted $\bar{\nu}$, the average number of collisions per participant in the smaller projectile (see definitions in Appendix B.1). Fig. 22 clearly demonstrates that extended longitudinal scaling also is manifested in d+A collisions at RHIC energies.

4.5.3 Longitudinal dependence of particle production: Au+Au at RHIC

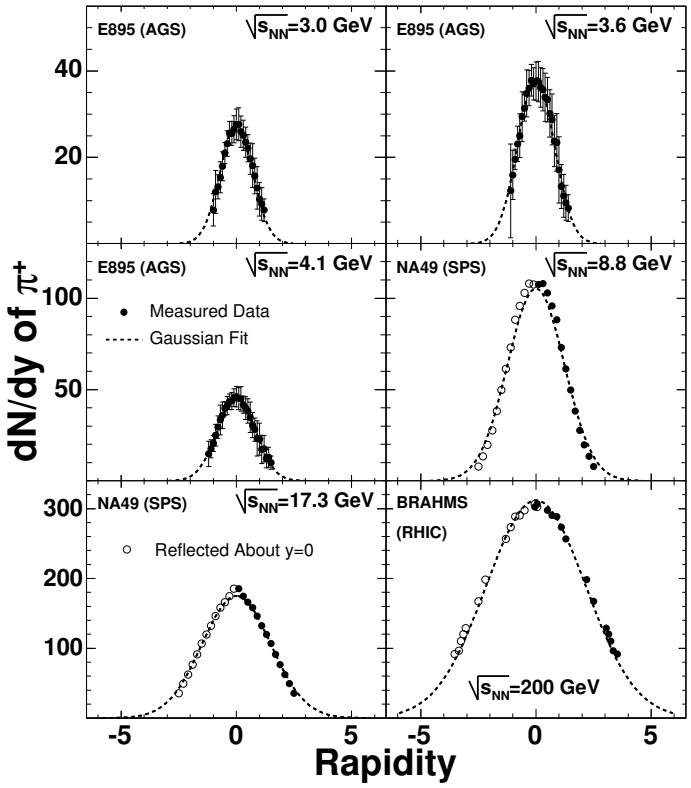

Fig. 23. Rapidity densities of positive pions emitted in central collisions of Au+Au (AGS and RHIC) [55,180] and Pb+Pb (SPS) [50] at a variety of beam energies. Note that, in contrast to Fig. 1, yields in rapidity space are well represented by Gaussians with no evidence for a broad midrapidity plateau.

The uniquely broad pseudorapidity coverage of the PHOBOS detector allows similar studies to be performed for heavy ion collisions at RHIC energies. At first the pseudorapidity distributions themselves, shown in Fig. 1, suggest that $dN_{ch}/d\eta$ may develop a small boost-invariant central plateau, but these plots are misleading for this purpose. Pseudorapidity is known to distort the rapidity distribution for production angles near 0° and 90°. Demonstrating this point, the rapidity distributions of positive pions measured by BRAHMS

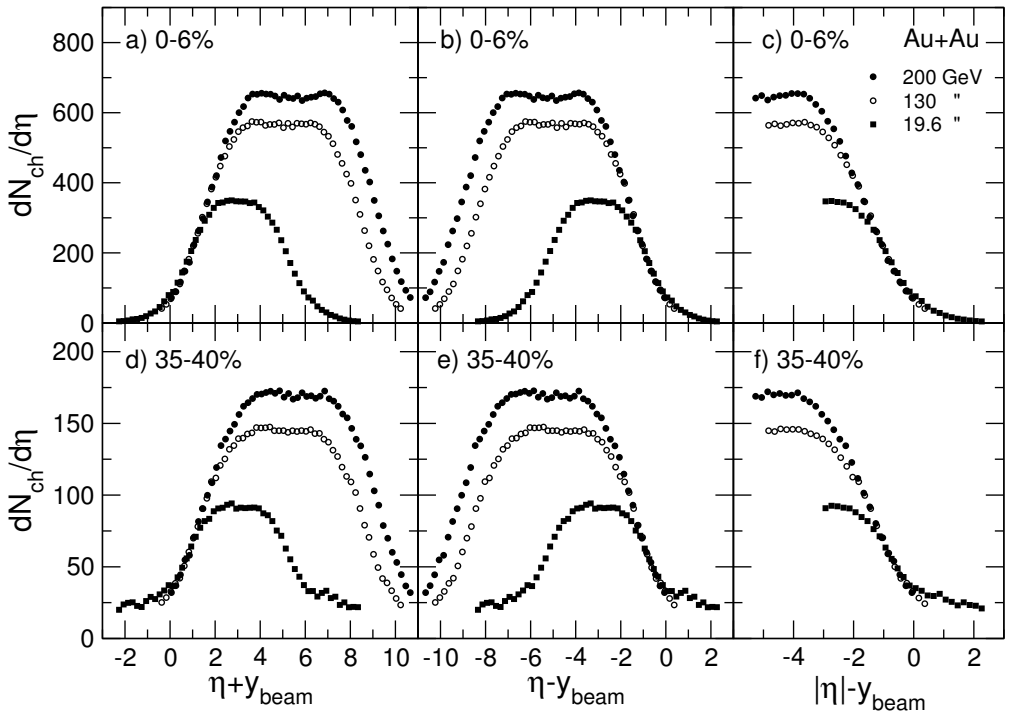

Fig. 24. Distributions of pseudorapidity densities of charged particles emitted in Au+Au collisions at three energies and two centrality ranges [44] are plotted versus $\eta' \equiv \eta - y_{beam}$ (or $\eta + y_{beam}$). In the far right panel, data for positive and negative η have been averaged to generate data versus $|\eta| - y_{beam}$. Systematic errors (identical to those on Fig. 1) are not shown and statistical errors are smaller than the symbols. Note that the data from all three energies follow a common curve.

[180], as well as similar data at lower energies [50,55], are all well represented by Gaussian fits, as shown in Fig. 23. In short, there are no indications of the existence of a broad boost-invariant central plateau in the final particle distributions.

In Fig. 24, the data shown in Fig. 1 are effectively shifted to the rest frame of one of the gold nuclei [44]. The data at both centralities show an extended scaling with the longitudinal velocity in the rest frame of one of the projectiles, identical behavior to that seen in simpler systems (see, for example, [147,148,142,153]). Similar behavior in nucleus-nucleus collisions over a narrower range in η' was first observed by BRAHMS [181,182].

Figure 24 illustrates one example of how the scaling behaviors can be used to infer the properties of particle production which lie outside the experimental acceptance at large collision energies. If one accepts the assumption that the η' distributions at all energies are identical in the region corresponding to larger η, the data from lower energies can be used to constrain the extrapolation of the higher energy data to the full solid angle. In addition, it should be noted that the corrections to the PHOBOS multiplicity data depend strongly on emission angle of the particles and also are significantly asymmetric between

positive and negative pseudorapidities. The latter effect results primarily from the offset of the PHOBOS magnet from the center of the interaction region (see Fig. A.1). The good agreement seen when comparing particles emitted at different angles and for both signs of pseudorapidity indicates the robustness of the analysis procedure, as well as providing interesting physics insight.

Fig. 24 illustrates the observation that longitudinal scaling holds over an even more extended range of pseudorapidity in these seemingly complex high energy A+A collisions at RHIC. Based on the pseudorapidity distribution (and, as will be discussed in following sections, elliptic flow and perhaps even HBT), no evidence is seen in any hadron-hadron or ion-ion collisions for two energy independent fragmentation regions separated by a boost invariant central plateau which grows in extent with increasing collision energy. Thus, the expectation from the boost-invariant description of the energy evolution of rapidity distributions is not valid for heavy ion collisions either. In fact, there is no boost invariant central plateau and, instead, the rapidity distribution appears to be dominated by two broad "fragmentation-like" regions, whose extent increases with energy. We call this effect "extended longitudinal scaling".

4.5.4 Longitudinal dependence of elliptic flow: Au+Au at RHIC

In addition to the pseudorapidity distributions of yields of produced particles, longitudinal scaling can also be seen in the elliptic flow of particles produced in heavy ion collisions. As discussed in Section 3, the elliptic flow parameter, v_2, provides a sensitive probe of the properties in the early stages of the collision, one of which is the presence or absence of boost-invariance. Boost invariant "initial conditions" (i.e. right after the collision) should lead to a boost-invariant $v_2(y)$. Kinematic effects result in a difference between $v_2(y)$ and $v_2(\eta)$, but the changes are small (<10% at 200 GeV to <20% at 19.6 GeV)[183,184]. The small magnitudes of these differences mean that they do not affect the conclusions discussed here and that a boost-invariant scenario (in rapidity) should also result in elliptic flow which is approximately flat over a large region of pseudorapidity. In Fig. 25, the pseudorapidity dependence of the elliptic flow parameter, v_2, is shown for semi-central Au+Au events at various energies [184]. Clearly, no boost invariant central plateau is seen. Thus, there are no indications of the existence of a broad boost-invariant central plateau in the final particle distributions or in the state formed shortly after the collision, as reflected by v_2.

In Fig. 26, the elliptic flow data from Fig. 25 are replotted effectively in the rest frame of one of the gold nuclei. Once again the phenomenon of extended longitudinal scaling is revealed, this time for v_2 [184]. As discussed above, there is a small modification of the shape if v_2 is plotted versus rapidity instead of η but this change does not significantly impact the comparison of

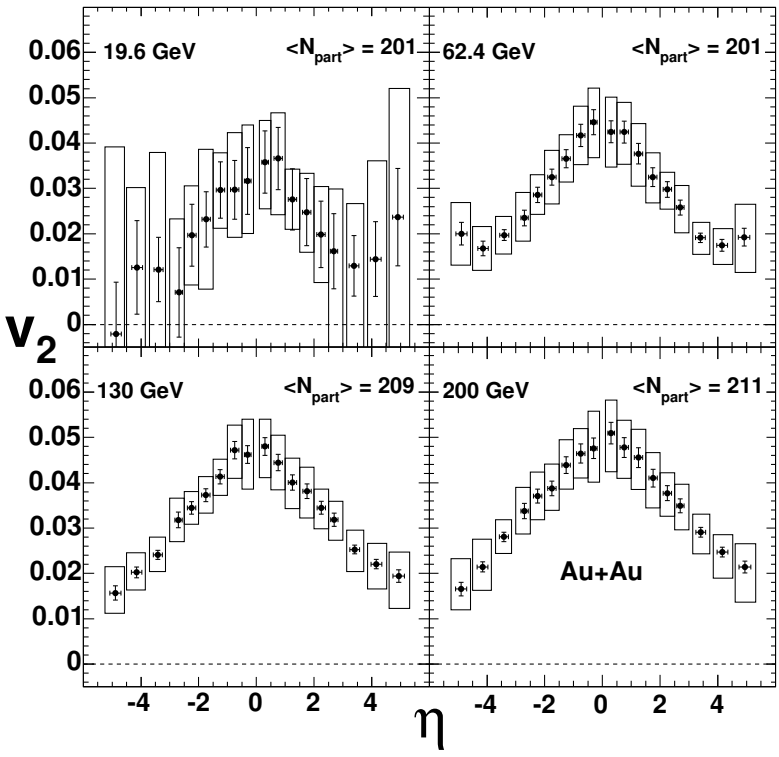

Fig. 25. Pseudorapidity dependence of elliptic flow of charged particles for the 40% most central collisions of Au+Au (average number of participating nucleons indicated) at a variety of beam energies [184]. Note the linear fall-off at higher $|\eta|$ and the lack of evidence for a constant value over a broad midrapidity region. Boxes indicate systematic uncertainties (90% C.L.).

different energies. There appears to be a single universal curve governing the elliptic flow as a function of η' over a broad range down to midrapidity at each energy studied. This extended longitudinal scaling behavior of elliptic flow in Fig. 26 has further implications since elliptic flow builds up early in the collision. Therefore, the dependence on the location in η' space must reflect the conditions very shortly after the collision, and then these early conditions lead to the measured elliptic flow.

4.5.5 Longitudinal dependence: Lessons from HBT

Particle interferometry, in the form of Hanbury-Brown Twiss (HBT) correlations [185,186], provides an extra, although much more indirect, test of the ideas of boost-invariance in heavy ion collisions. Since pions are bosons, they constructively interfere when they are near to each other in phase space. Correlation measurements in momentum space can therefore reveal the source size in position space. In particular, HBT correlations are sensitive to the spatiotemporal distributions of particles at thermal freeze-out (i.e. the point of the last elastic interactions). See [187] for a recent review. Appendix B.3 contains

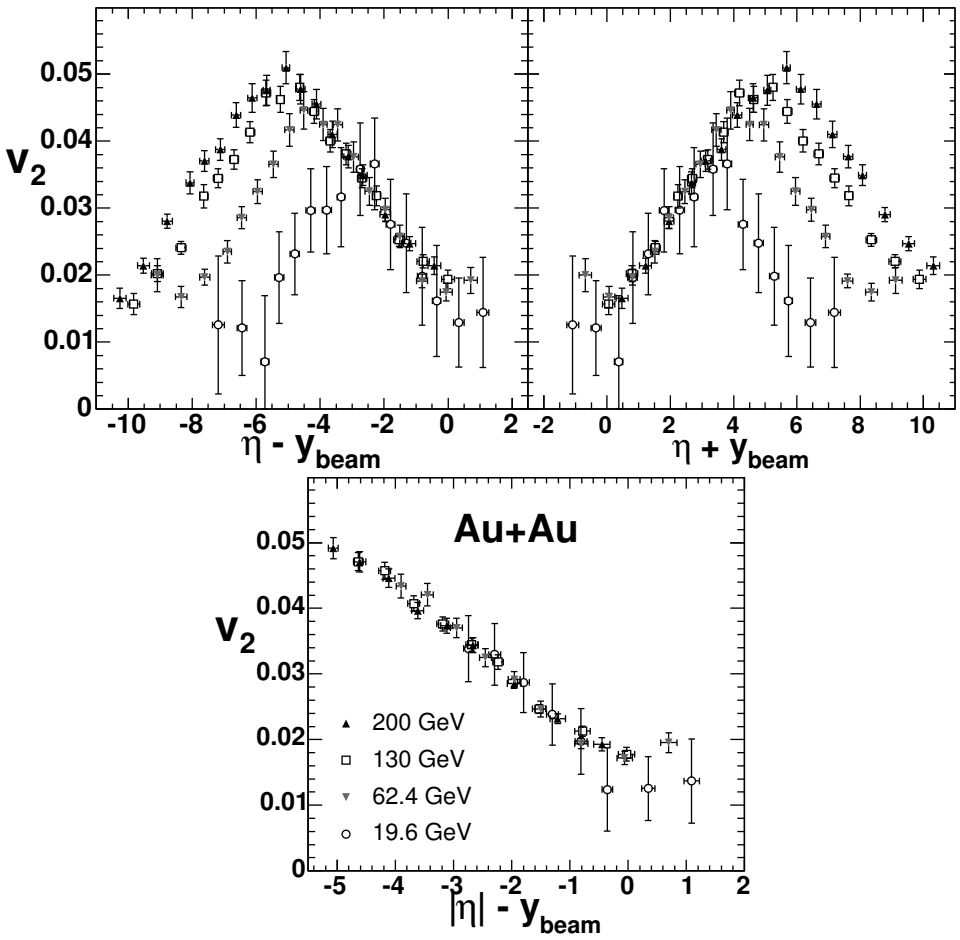

Fig. 26. The flow data of Fig. 25 are shown in the top left (top right) panel versus the variable $\eta' = \eta - y_{beam}$ ($\eta' = \eta + y_{beam}$) [184]. In the bottom panel, data at positive and negative pseudorapidity have been averaged to give v_2 as a function of $|\eta|$. These results were then plotted versus the variable $\eta' = |\eta| - y_{beam}$. As for the particle densities shown in Fig. 24, the flow data at all energies follow a common curve. In the case of flow, this curve holds over the entire range from beam or target to midrapidity.

more details including a description of the source parameterizations. Most theoretical studies of HBT assume ideal (i.e. non-viscous) hydrodynamics and a boost-invariant source which exhibits longitudinal Hubble flow ($z = v_z t$, where z and v_z are the longitudinal position and velocity, respectively). These assumptions simplify the coupled differential equations and allow the use of 2D transverse expansion overlaid on the boost-invariant longitudinal expansion (a scenario often called 2+1D hydrodynamics). While this basic hydrodynamic picture was roughly successful in describing some aspects of the elliptic flow (see Figs. 6 and 7), these models have failed to describe the HBT data from RHIC [188–190].

The influence of a possible new phase on HBT measurements has a long history

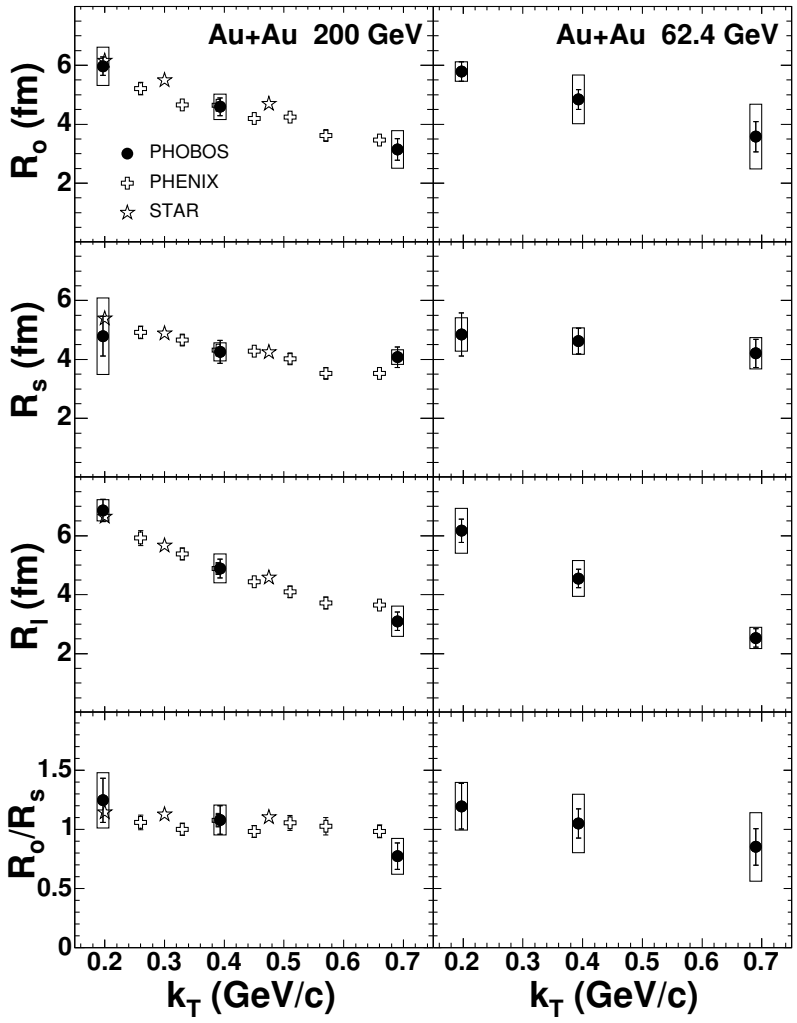

Fig. 27. Bertsch-Pratt parameters R_o, R_s, and R_l, and the ratio R_o/R_s for $\pi^-\pi^-$ pairs emitted in central collisions of Au+Au at $\sqrt{s_{NN}}$ of 200 GeV (left panels) and 62.4 GeV (right panels) as a function of pair transverse momentum k_T [192]. For comparison, data from STAR [193] (open stars) and PHENIX [194] (open crosses) are presented at $\sqrt{s_{NN}}$=200 GeV. PHOBOS systematic errors are shown as boxes; systematic errors from STAR and PHENIX are not shown.

[191]. Under the assumptions of boost-invariant hydrodynamics, the R_o/R_s ratio should be large if a long-lived source is formed and should typically be larger than $\sqrt{2}$ in any case. Figure 27 shows the results of fits using the Bertsch-Pratt parameterization, along with the R_o/R_s ratio from $\sqrt{s_{NN}}$=62.4 and 200 GeV Au+Au collisions [192] (see Appendix B.3 for definitions). The data at 200 GeV are compared to the results of other RHIC experiments [193,194]. In contrast to expectations, the ratio of R_o/R_s appears to be close to unity in heavy ion collisions. Similar results were found in heavy ion collisions at lower energies (see references in [192]). The smallness of both R_o/R_s and R_l has come to be known as the "HBT puzzle". It has been postulated that relaxing the assumption of boost-invariance [195,196], or allowing non-zero

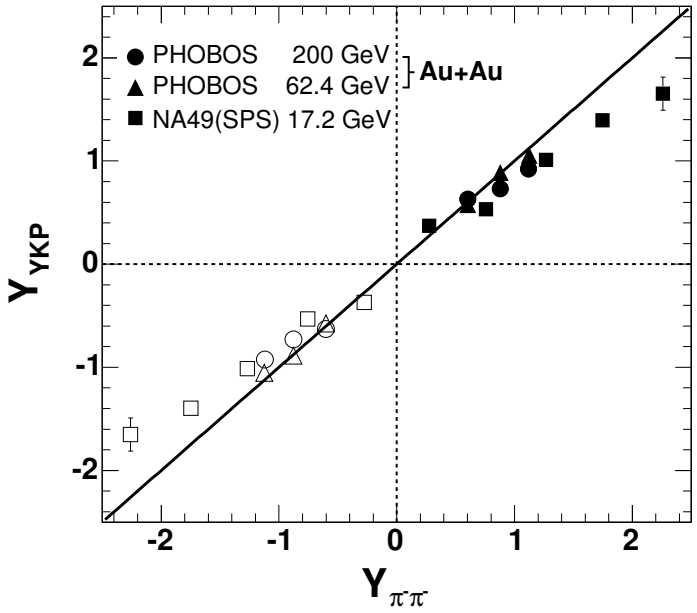

Fig. 28. The rapidity source parameters for $\pi^-\pi^-$ pairs emitted in central Au+Au collisions at RHIC [192] and Pb+Pb collisions at the SPS [198]. This element of the Yano-Koonin-Podgoretskii parameterization specifies the rapidity (in the nucleus-nucleus center-of-mass system) of the source, Y_{YKP}, from which the pions were emitted. The abscissa of this plot is the average rapidity of the pions themselves. The filled symbols are the measured data, the open symbols have been reflected about midrapidity. The line with a slope of 1 is drawn to guide the eye.

viscosity [197], may resolve this discrepancy.

The detailed nature of the longitudinal properties of particle production can also be explored by HBT measurements, in this case in a very direct way as shown in Fig. 28. The data show the average rapidity of the source of the pions (derived from the source velocity in the Yano-Koonin-Podgoretskii parameterization) as a function of the rapidity of the pions themselves [192]. A clear systematic trend is observed, and again the results are very similar to what was found at the SPS [198]. Under the simple assumption of all pions being emitted from a single source located at the center of mass, the ordinate of all points would be equal to zero. If, instead, the system consisted of a series of independent sources at different rapidities (i.e. a strong longitudinal position-momentum correlation) the points would fall on the line. The "locality" revealed by HBT studies of pion correlations in rapidity space suggests that the longitudinal distribution of particle properties is established very early, with the subsequent evolution and freezeout having only short range correlations in rapidity.

4.5.6 Extended longitudinal scaling: Summary

To summarize this section, the data demonstrate that extended longitudinal scaling, reminiscent of "limiting fragmentation" over a broad region of longitudinal momentum, seems to be a dominant feature of particle production for all colliding systems. Based on all of the data, no evidence is seen in any hadron-hadron or ion-ion collisions for two energy independent fragmentation regions separated by a boost invariant central plateau which grows in extent with increasing collision energy. The lack of a broad boost-invariant central plateau is seen in both the final particle distributions and in the state formed shortly after the collision as reflected by v_2. It is difficult to reconcile this with the common assumption that particle production at midrapidity results from different physics than that in the fragmentation region, particularly at the higher energies. Furthermore, the similarity of the longitudinal scaling of both particle densities and elliptic flow suggests the possibility of some direct connection between the two, implying that the final particle multiplicities also result from the properties of the very early evolution.

A good way to appreciate the significance of these results is to consider what would be observed in the detectors if a collider could operate its two beams at different energies. For simplicity, the conventional RHIC designation for the two counter-rotating beams, namely "blue" and "yellow", will be used. If the energy of the blue beam was set to a rapidity of 2, for example, the results show that, as the rapidity of the yellow beam was increased up to a little beyond 2, the particle density and elliptic flow seen in the detectors covering the blue beam hemisphere would show a gradual increase and then reach a limiting value. With the blue beam fixed at a rapidity of 2, the particle density would not increase beyond this limiting value on the blue beam side even if the yellow beam was set to infinite rapidity. The only way to further increase the particle density or elliptic flow in the blue beam hemisphere would be to increase the energy of the blue beam.

In p+p collisions, extended longitudinal scaling was understood to be a consequence of x_F scaling in string fragmentation (or, equivalently, in parton cascades). No similar, widely accepted, explanation exists for the observation of this behavior in the more complex p+A, d+A, and A+A collisions.

4.6 Factorization of energy and centrality dependence

The previous sections have described separately the dependencies of a variety of observables on energy and centrality. These independent discussions may have obscured the remarkable extent to which these two dependencies factorize. This section will describe several aspects of PHOBOS data which display

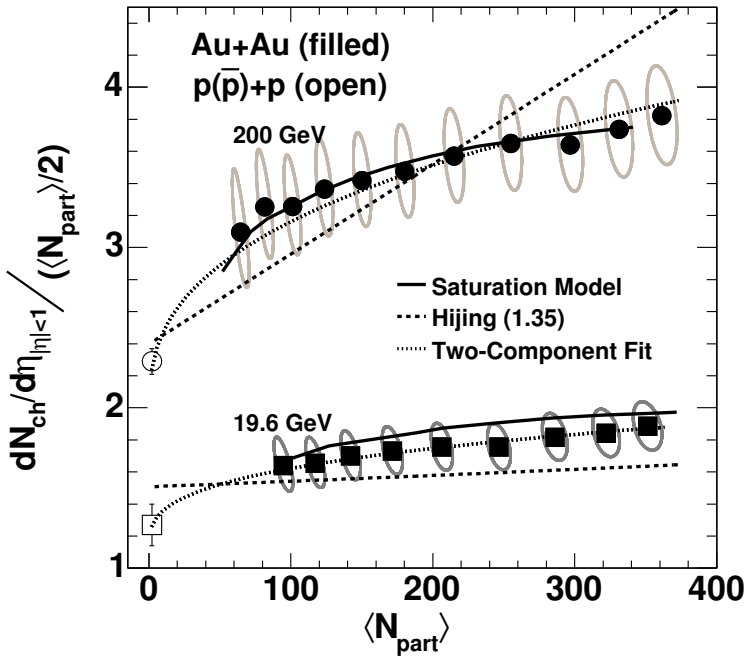

Fig. 29. Pseudorapidity density of charged particles emitted near midrapidity divided by the number of participant pairs as a function of the number of participants. Data are shown for Au+Au at collision energies of 19.6 and 200 GeV [49]. Data for p($\bar{p}$)+p [155,199,172] measured at 200 GeV and an interpolated value at 19.6 GeV are shown as open symbols. The grey ellipses show the 90% C.L. systematic errors. The results of two models [101,74,201] and one parameterized fit [200] are shown for comparison.

this phenomenon.

One simple example of factorization was revealed by the PHOBOS measurements of the total charged particle multiplicity divided by the number of pairs of participating nucleons in Au+Au collisions at three energies, from 19.6 to 200 GeV (see Fig. 12). The data for the different energies are separated by a factor that is constant as a function of centrality. In other words, the centrality and energy dependence of the yield per participant in Au+Au collisions factorize over the range of the two control variables. In this case, the factorization occurs trivially, as the total charged particle yield per participant is centrality-independent at all energies. Whether this factorization is a fundamental property of particle production in Au+Au collisions can be tested by studying the yields per participant more differentially in pseudorapidity and transverse momentum.

In Fig. 29, the pseudorapidity density of charged particles per participant pair near midrapidity is shown as a function of centrality for collision energies of 19.6 GeV and 200 GeV [49]. Data for $\bar{p}$+p collisions at 200 GeV and

an interpolated value at 19.6 GeV are also plotted [155,172,199]. Over the centrality range shown here, the normalized yield at midrapidity increases by approximately 25% from mid-peripheral to central collisions. Early theoretical explanations attributed this increase to the contribution of the hard component of particle production, which would grow with the relative increase in the number of binary nucleon-nucleon collisions in more central events. As an example of such a superposition of soft and hard particle production, the results of a HIJING calculation [101] are shown as dashed lines. The model shows an increase in the yield per participant pair, although steeper than that seen in the higher energy data.

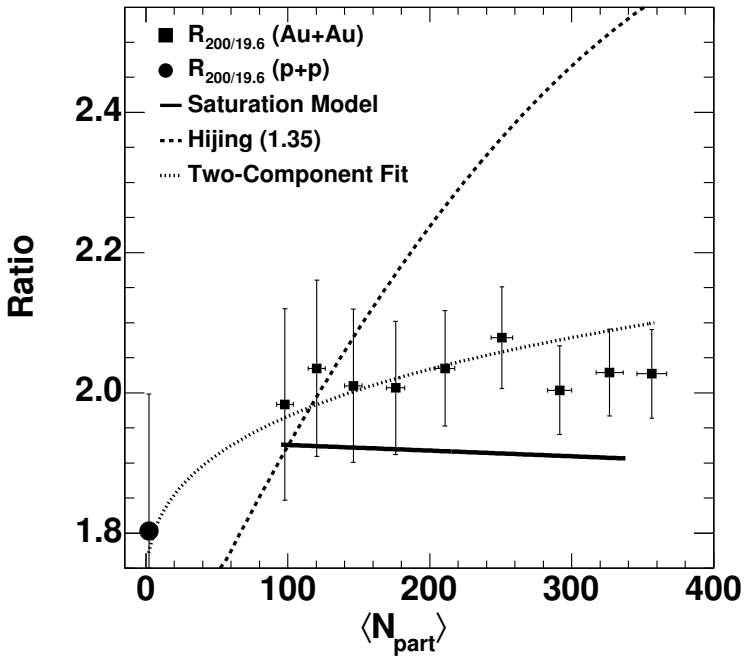

Fig. 30. Ratio of the pseudorapidity densities of charged particles emitted near midrapidity for Au+Au at 200 GeV over 19.6 GeV as a function of the number of participants [49]. The closed circle shows the ratio for collisions of protons. The error bars include both statistical and 1-σ systematic errors. The ratios for the same two models and one fit shown in Fig. 29 are displayed for reference.

However, this explanation is challenged by the detailed study of the energy dependence of midrapidity particle yields shown in Fig. 30, where the centrality dependence of the ratio of the data for 200 over 19.6 GeV is plotted [49]. Within the experimental uncertainty, this ratio is independent of centrality, whereas the contribution from hard processes would be expected to show a large increase over this collision energy range. This is illustrated by the HIJING prediction for this ratio (shown as a dashed line), which completely fails to capture the factorization of energy and centrality dependence for the midrapidity yield per participant. A similar result was found earlier (over a smaller span in beam energy) using the centrality dependence of normalized

midrapidity yields from Au+Au at $\sqrt{s_{NN}}$=130 GeV [46,48].

The results of an attempt to investigate the interplay of hard and soft scattering without invoking a complicated model are shown as dotted lines. In this case, a very simplistic two component fit [200] was performed to separately extract the fractions of the particle yield which scaled with the number of participants (soft scattering) and the number of collisions (hard scattering). A reasonably good fit to the data is found but the fitted parameters suggest that, within the uncertainties, there would be an identical contribution from hard scattering at both beam energies, a result which is totally unexpected for minijet dominated physics.

Also shown in Figs. 29 and 30 is the result of a saturation model calculation [74,201]. This model, which, as mentioned in Section 2.1, yields a reasonably good match to the energy evolution of particle yields at RHIC energies, also does a much better job of describing the centrality evolution than the HIJING model.

Another example of non-trivial centrality dependence that is energy independent was shown by the pseudorapidity distributions in Figs. 14 and 24. The former showed that the shape of the distributions differed significantly as a function of centrality. The latter demonstrated that the distributions at different beam energies were found to line up when plotted in the approximate rest frame of one of the incoming nuclei, i.e. using the variable $\eta' \equiv \eta - y_{beam}$. Thus, the shape evolution with centrality is independent of beam energy over a very broad range in η'.

Additional evidence for factorization is provided by the transverse momentum distributions briefly mentioned in Sect. 3. In the absence of medium effects, one would expect that the volume scaling (i.e. proportionality to N_{part}) observed for the bulk production of hadrons turns into scaling with the number of binary collisions (N_{coll}) when measuring reaction products of point-like hard processes. This transition should be visible when studying particle production as a function of transverse momentum. However, as is now known (see Fig. 8), particle production at large transverse momenta seems to be significantly modified in the presence of the medium in heavy ion collisions. The strength of this modification is more clearly illustrated in Fig. 31 which shows the nuclear modification factor for charged hadrons in six bins of p_T as a function of N_{part} [84]. In the figure, yields at a given transverse momentum in collisions of varying centrality were normalized by the number of participant pairs and then divided by a fit to the same quantity in central data (see Appendix B.3 for definition). Data for p+p collisions from UA1 [164] are shown with the same normalization factor. It is striking to see that the medium modification results in charged particle yields that, over the centrality range studied here, more closely scale with N_{part} than with the number of binary collisions, even

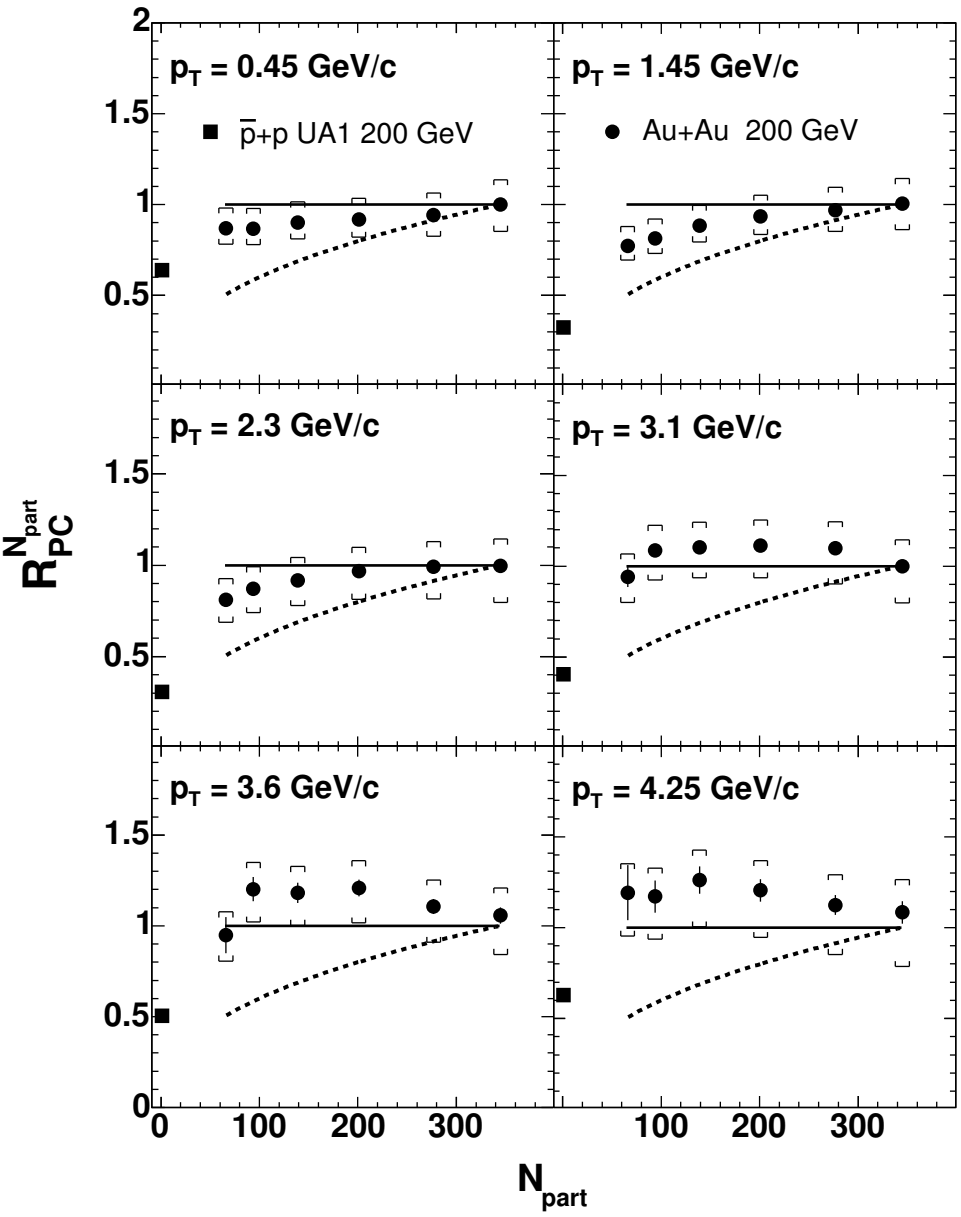

Fig. 31. Particle yield normalized by the number of participant pairs and then divided by a fit to the central data (see definitions in Appendix B.3) as a function of centrality for Au+Au collisions at $\sqrt{s_{NN}}$=200 GeV, for six transverse momentum ranges [84]. Bars and brackets show statistical and systematic uncertainties, respectively. The solid (dashed) line shows the expectation for N_{part} (N_{coll}) scaling from peripheral to central collisions. Squares show data for p+p collisions from UA1 [164] with the same normalization factor.

for transverse momenta above 4 GeV/c.

The observation of N_{part} scaling at high transverse momentum suggests that the medium is almost completely "black" or "absorbing" to produced fast particles. This conclusion follows if one assumes N_{coll} scaling of the primary

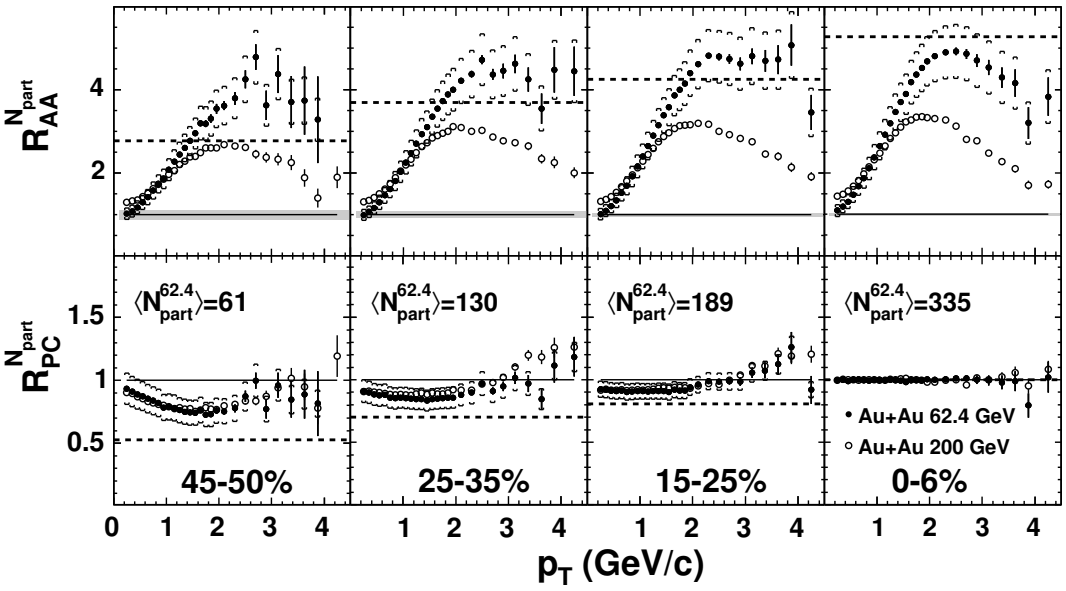

Fig. 32. Nuclear modification factors versus transverse momentum for Au+Au at two beam energies and a variety of centralities [116] calculated using two different reference distributions: (top row) $N_{part}/2$ times p+p yields [202,203,164], or (bottom row) the ratio of N_{part} times a fit to the distribution for central Au+Au. Filled symbols are for $\sqrt{s_{NN}}$=62.4 GeV, open symbols are for 200 GeV. Bars and brackets show statistical and systematic uncertainties, respectively. The grey bands in the top row show the systematic error in the overall scale due to N_{part}. Centralities are labeled by the fraction of total inelastic cross section in each bin, with smaller numbers being more central and the number of participants at the lower energy are indicated. The solid (dashed) line shows the expectation for N_{part} (N_{coll}) scaling (See discussion in Appendix B.3). Note the small variations with centrality in both the magnitude and shape of the ratios calculated using N_{part} and also that R-factors normalized using central Au+Au data (bottom row) are identical at the two beam energies.

production throughout the entire volume of the collision zone followed by complete absorption except on the surface. The volume to surface ratio (proportional to the nuclear radius R or equivalently $A^{1/3}$) has a centrality dependence that is similar to the dependence for the ratio of the number of collisions to the number of participants. However, since the centrality dependence of particle production is seen to be very similar at all transverse momenta, it is also possible that the usual simplistic assumption of participant dominance at low p_T evolving into collision dominance at higher values needs to be reconsidered.

Data from the most recent RHIC run have been used to study the evolution of the transverse momentum distributions as a function of both collision centrality and energy. The measurements were performed near midrapidity at collision energies of 62.4 GeV and 200 GeV [116]. In Fig. 32, particle production as a function of centrality and p_T is shown for these two energies in terms

of $R_{AA}^{N_{part}}$ and $R_{PC}^{N_{part}}$ (Ref. [116] shows additional centrality bins). As defined in Appendix B.3, $R_{AA}^{N_{part}}$ shows the variation in the yield per participant pair relative to p+p collisions [164,202,203] (upper row of Fig. 32) and $R_{PC}^{N_{part}}$ shows the variation in yield per participant pair relative to central Au+Au collisions (bottom row).

As discussed earlier, the range in p_T from a few hundred MeV/c to more than 4 GeV/c is assumed to cover very different regimes of particle production, from soft coherent processes to independent binary scattering. Over the collision energy range from 62.4 to 200 GeV, overall particle production in p+p increases by less than a factor 2, whereas the yield at p_T=4 GeV/c increases by an order of magnitude. This clearly shows the change in the balance of lower and higher transverse momenta particles, which presumably reflects the different energy dependencies of soft and hard particle production in p+p collisions over this energy range. For central Au+Au collisions however, the ratio of the yields between 200 GeV and 62.4 GeV at p_T=4 GeV/c is only about 4 (with a factor of 1.6 increase in the p_T-integrated multiplicity), i.e. the huge increase in the yield of high p_T particles in p+p is not reflected in Au+Au.

The top row of Fig. 32 clearly demonstrates that the overall shape and magnitude of $R_{AA}^{N_{part}}$ depend strongly on beam energy and, to a lesser extent, also on centrality. In particular, at both energies the yield per participant at any given p_T changes by less than 25% over the centrality range from 60 to 340 participants, with an even smaller variation at the highest p_T. Even more surprisingly, the comparison in terms of $R_{PC}^{N_{part}}$ in the bottom row of the figure shows that the remaining variation of the yield per participant pair is the same for both energies over the full p_T and centrality range. This means that the energy and centrality dependences of particle production also factorize over this entire range in energy, centrality, and p_T. This is particularly striking, as the factorization therefore covers both the bulk particle production at low p_T, as well as rare particle production at intermediate and high p_T, believed to be governed by different particle production mechanisms. In particular, at intermediate p_T above 1 GeV, particle production is thought to be influenced by the effects of radial hydrodynamic flow, the p_T broadening due to initial and final state multiple scattering ("Cronin effect"), the balance between 'soft' and 'hard' particle production, parton recombination and fragmentation, and the in-medium energy loss of fast partons. All of these contributions to the overall particle yields are expected to show distinctly different centrality and energy dependencies at different p_T, yet the overall result is a factorization of energy and centrality dependence at all p_T within the experimental uncertainty.

The observed factorization in the energy and centrality dependencies of transverse momentum spectra, combined with similar observations for total and midrapidity yields as well as the rapidity distributions, strongly suggests that the data reflect the dominant influence of yet-to-be-explained overall global

constraints in the particle production mechanism in A+A collisions.

5 Conclusion

PHOBOS data and results from the other RHIC experiments, combined with very general arguments which are either model independent or depend on fairly simple model assumptions, lead to a number of significant conclusions.

In central Au+Au collisions at RHIC energies, a very high energy density medium is formed. Conservative estimates of the energy density at the time of first thermalization yield a number in excess of 3 GeV/fm^3, and the actual density could be significantly larger. This is far greater than hadronic densities and so it is inappropriate to describe such a medium in terms of simple hadronic degrees of freedom. Unlike the weakly interacting QGP expected by a large part of the community before RHIC turn-on, the constituents of the produced medium were found to experience a significant level of interactions. If this medium is a new form of QCD matter, as one would expect from lattice gauge calculations for such a high energy density system, the transition to the new state does not appear to produce any signs of discontinuities in any of the observables that have been studied. To the precision of the measurements, all quantities evolve smoothly with energy, centrality, and rapidity. Although it does not provide strong evidence against other possibilities, this feature of the data is consistent with the results of recent lattice QCD calculations which suggest that the transition from this novel high energy density medium to a hadronic gas is a crossover.

An equally interesting result was the discovery that much of the data can be expressed in terms of simple scaling behaviors. In particular, the data clearly demonstrate that proportionality to the number of participating nucleons, N_{part}, is a key concept which describes much of the phenomenology. Further, the total particle yields per participant from different systems are close to identical when compared at the same available energy; the longitudinal velocity dependences of elliptic flow and particle yield are energy independent over a very broad range, when effectively viewed in the rest frame of one of the colliding nuclei; and many characteristics of the produced particles factorize to a surprising degree into separate dependences on centrality and beam energy.

All of these observations point to the importance of the geometry of the initial state and the very early evolution of the colliding system in determining many of the properties of the final observables. Future data at RHIC, most especially collisions of lighter nuclei, as well as higher energy nucleus-nucleus data from the LHC, will help to further evaluate the range of validity of these scaling behaviors. It is possible that models which describe the initial state in terms

of parton saturation will play a role in explaining some or all of these scaling properties, but such an identification is not yet clear. What is clear is that these simple scaling features will constitute an integral component or essential test of models which attempt to describe the heavy ion collision data at ultra-relativistic energies. These unifying features may, in fact, provide some of the most significant inputs to aid the understanding of QCD matter in the region of the phase diagram where a very high energy density medium is created.

Acknowledgements

The PHOBOS collaboration would like to express our gratitude to the RHIC management and construction personnel and to the operations staff of the BNL Collider-Accelerator Department for their hard work and truly spectacular success. Without the broad range of colliding species and energies, and continually increasing luminosities, provided by RHIC over a very short span of time, the PHOBOS physics program would not have been nearly so rich. We would like to express special thanks to S.Basilev, B.D.Bates, R.Baum, A.Białas, M.Ceglia, Y.-H.Chang, A.E.Chen, T.Coghen, C.Conner, J.Corbo, W.Czyż, B.Dąbrowski, M.Despet, P.Fita, J.Fitch, M.Friedl, K.Gałuszka, R.Ganz, J.Godlewski, C.Gomes, E.Griesmayer, J.Halik, P.Haridas, A.Hayes, D.Hicks, W.Kita, J.Kotuła, H.Kraner, C.Law, M.Lemler, J.Ligocki, J.Michałowski, J.Mülmenstädt, M.Neal, M.Nguyen, A.Noell, M.Patel, M.Plesko, M.Rafelski, M.Rbeiz, D.Ross, J.Ryan, A.Sanzgiri, J.Scaduto, J.Shea, J.Sinacore, S.G.Steadman, M.Stodulski, Z.Stopa, A.Straczek, M.Strek, K.Surowiecka, R.Teng, B.Wadsworth, K.Zalewski, and P.Żychowski without whose efforts the PHOBOS experiment would not have been possible. We would like to thank Krishna Rajagopal for many valuable suggestions and enlightening discussions. We acknowledge the generous support of the Collider-Accelerator Department (including RHIC project personnel) and Chemistry Department at BNL. We thank Fermilab and CERN for help in silicon detector assembly. We thank the MIT School of Science and LNS for financial support. This work was partially supported by U.S. DOE grants DE-AC02-98CH10886, DE-FG02-93ER40802, DE-FC02-94ER40818, DE-FG02-94ER40865, DE-FG02-99ER41099, and W-31-109-ENG-38, by U.S. NSF grants 9603486, 0072204, and 0245011, by Polish KBN grant 1-P03B-062-27(2004-2007), and by NSC of Taiwan Contract NSC 89-2112-M-008-024.

A The PHOBOS detector

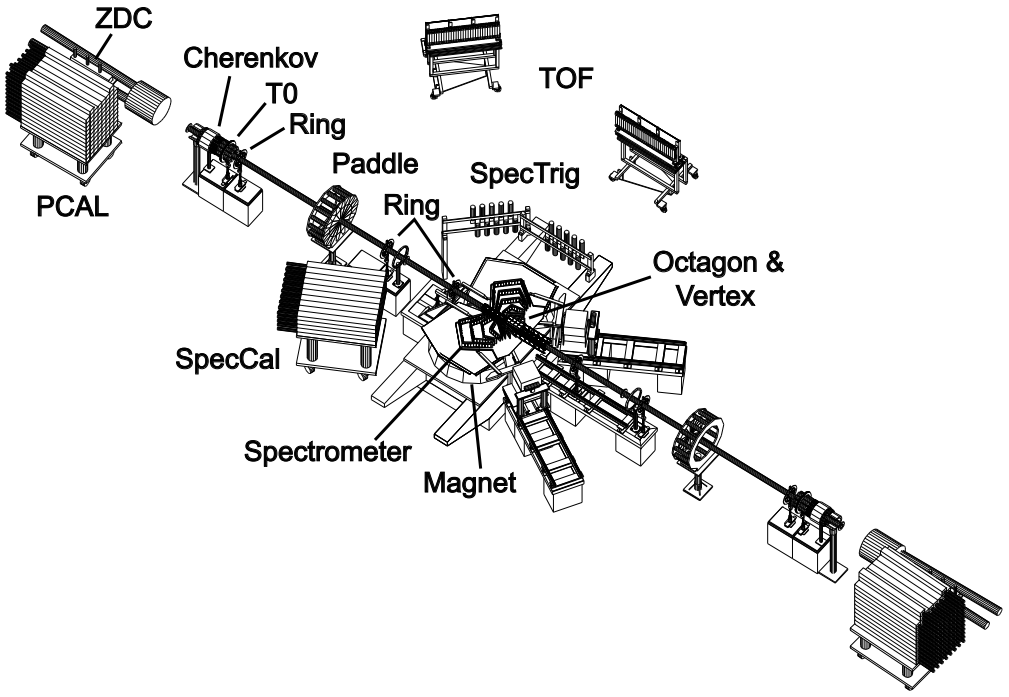

Fig. A.1. The layout of the PHOBOS detector during the RHIC run in early 2004. The beams collide at a point just to the right of the double-dipole magnet, the top of which is not shown. The PCAL and ZDC calorimeters are drawn to scale but are located about 3 times farther from the interaction point than shown.

The PHOBOS experimental setup is composed of three major sub-systems: a charged particle multiplicity detector covering almost the entire solid angle, a two arm magnetic spectrometer with particle identification capability, and a suite of detectors used for triggering and centrality determination. More details can be found in [204]. The active elements of the multiplicity detector and tracking detectors in the spectrometer are constructed entirely of highly segmented Si wafers with individual readout of the energy deposited in each pad [205–207]. The layout of the experiment during the 2004 run is shown in Fig. A.1. An enlarged view of the region around the beam collision point is shown in Fig. A.2. Table A.1 lists the colliding systems, center-of-mass energies, and data samples collected by PHOBOS during the first four RHIC runs.

The Si pad detectors used to measure multiplicity consist of a single layer covering almost the entire 4π solid angle. These detectors measure the total number of charged particles emitted in the collisions, as well as detailed information about their distribution in azimuthal and polar angle (or equivalently pseudorapidity, η). The Si modules are mounted onto a centrally located octagonal frame (Octagon) covering $|\eta| \leq 3.2$, as well as three annular frames (Rings) on either side of the collision vertex, extending the coverage out to

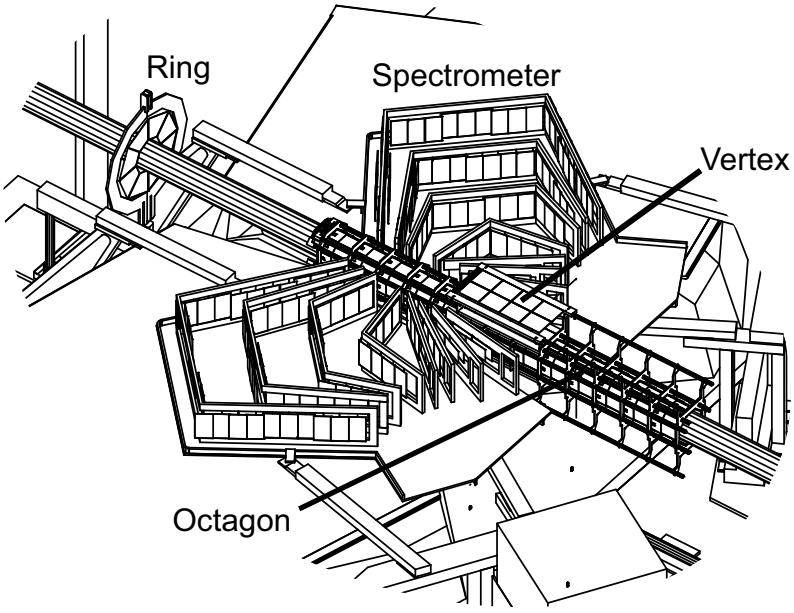

Fig. A.2. The elements of the PHOBOS detector in the vicinity of the beam collision point.

$|\eta| \leq 5.4$.

The Si modules forming the arms of the spectrometer are mounted on eight frames. Depending on the trajectory, charged particles traverse between 13 and 16 layers of Si as they pass through the spectrometer. The first layer is only 10 cm from the nominal interaction vertex. The magnet pole tips are arranged to produce almost no magnetic field in the vicinity of the first six layers. The field then rises rapidly to a roughly constant value of $\sim$2 Tesla for the remaining layers. The Si wafers are finely segmented to provide 3-dimensional space points used in the track finding. The solid angle covered depends on the vertex location along the beam direction and extends over about 3/4 of a unit of η for any given vertex location, with a total coverage of roughly $0 < \eta < 2$. Each arm covers approximately 0.1 radians in azimuth for particles that traverse all of the layers. The momentum resolution is close to 1% for particles with momenta near 0.5 GeV/c and rises about 1% for each additional 3 GeV/c.

Particle identification is provided using two techniques. Charged particle energy loss is measured in each Si layer. Combining this information with the momentum from the tracking can separate pions from kaons out to about 700 MeV/c and pions from protons out to about 1.2 GeV/c. Additional particle identification is provided by two Time-of-Flight (TOF) walls, each consisting of 120 plastic scintillator slats. Before the start of the 2003 RHIC run, these walls were moved farther from the interaction point, extending particle identification capability out to momenta roughly 2-3 times that achievable using energy loss in the silicon detector. In their new locations, the TOF walls

RHIC Run	Colliding System	$\sqrt{s_{NN}}$	Beam Rapidity	Dates of PHOBOS Data Taking	Total Events (M)
1	Au+Au	55.87 GeV	4.094	6/13/00–6/16/00	1.8*
	Au+Au	130.4 GeV	4.942	8/15/00–9/4/00	4.3
2	Au+Au	130.4 GeV	4.942	7/8/01	0.044
	Au+Au	200.0 GeV	5.370	7/20/01–11/24/01	34
	Au+Au	19.59 GeV	3.044	11/25/01–11/26/01	0.76*
	p+p	200.0 GeV	5.362	12/28/01–1/25/02	23
3	d+Au	200.7 GeV	5.370	1/6/03–3/23/03	146
	p+p	200.0 GeV	5.362	4/13/03–5/24/03	50
4	Au+Au	200.0 GeV	5.370	1/5/04–3/24/04	215
	Au+Au	62.40 GeV	4.205	3/24/04–4/2/04	22
	p+p	200.0 GeV	5.362	4/18/04–5/14/04	28

Table A.1
Summary of data collected by PHOBOS during the first four RHIC runs. Note that event totals given in the last column represent the number summed over the entire variety of triggering conditions, including minimum-bias events, interactions occurring in a restricted range of the collision vertex, collisions selected to be more central or more peripheral, and collisions satisfying the high-p_T spectrometer trigger. Note that triggers for the Au+Au runs at 19.6 and 56 GeV (marked with *) had very loose requirements on timing with the result that only a relatively small fraction of the events were usable in the currently published analysis.

cover roughly half the azimuthal acceptance of the spectrometer.

Before the 2004 run, a small hadronic calorimeter (SpecCal) was installed behind one of the spectrometer arms. Consisting of 50 lead/scintillator modules, each 10 cm square by about 120 cm long, this detector can be used to measure the energy of high momentum particles traversing part of the spectrometer acceptance.

The primary event trigger for all colliding systems was provided by two sets of 16 plastic scintillator slats (Paddles) covering $3.2 < |\eta| < 4.5$. Imposing an upper limit on the time difference between the signals in the two arrays eliminated most beam-gas interactions and provided a rough selection of collision vertex locations along the beam line. To enhance the data sample of useful events, a more precise measure of vertex location was generated using two arrays of 10 Čerenkov counters (T0s). This was necessary because the range of vertex positions for which the multiplicity and tracking detectors have reasonable acceptance is considerably shorter than that created by the overlap of the colliding beam bunches. For different colliding systems, the T0 detectors

could be moved to different locations along the beam line in order to optimize the efficiency of the vertex determination while minimizing the number of events with multiple particles traversing a single counter. A more precise vertex location is found off-line using signals from the Vertex detector, which is composed of two sets of two layers each of Si modules. With high segmentation along the beam direction, correlating hits in the inner and outer layer can be used to determine the vertex along the beam line to an accuracy of better than 0.4 mm. This detector also determines the height of the beam but with limited resolution. The vertical position and horizontal position perpendicular to the beam can be found using tracks from the spectrometer.

Colliding systems such as p+p or d+Au, which produce smaller numbers of particles, have fewer events with tracks traversing the spectrometer. The spectrometer trigger uses an additional array of scintillator slats (SpecTrig) mounted between the tracking detectors and the TOF walls. Coincidences between the SpecTrig and TOF hit slats, combined with the vertex location from T0, were used online to select events containing a high momentum track in the acceptance of both the spectrometer and the TOF.

The Zero-Degree-Calorimeters (ZDC) have a cross-sectional area of 10×12 cm^2 centered on the direction of the beam and are located about 18 m from the nominal interaction point. Particles hitting these detectors must first traverse the initial RHIC accelerator magnet which separates the two counter-circulating beams. Therefore, the ZDC signal results almost exclusively from spectator neutrons which are not bound in nuclear fragments and whose transverse momentum remains close to zero after the interaction. Due to the response time of this detector, partly resulting from its long distance from the collision point, it was not possible to use ZDC signals in the primary event trigger for the bulk of the physics data. However, this device was used on-line in special runs to check triggering efficiency for the other detectors and also off-line in studies of centrality determination.

Similar to the ZDC, the Proton Calorimeters (PCAL) are located behind the first accelerator magnets, but in this case next to the outer edge of one of the beam pipes. The magnets bend spectator protons to an angle of more than twice that of the beam particles so these protons will exit the beam pipe and shower in the PCAL. As with the ZDC, only individual protons, as opposed to those bound in clusters, can be detected. The PCAL is particularly useful for studies of d+Au collisions. On the side of the outgoing deuteron, the combination of PCAL and ZDC signals can be used to divide the event sample into p+Au, n+Au, and d+Au subsets, i.e. events in which only one or both of the incoming nucleons interacted. On the side of the outgoing Au nucleus, the PCAL is primarily sensitive to protons knocked out of the Au, which is a measure of the total number of collisions suffered by the interacting nucleons in the deuteron.

B Definitions of terms

In this section, detailed definitions are given for the important event and particle characterization parameters, as well as a number of the critical observables used in the physics analysis.

B.1 Event characterization

In interpreting data from heavy ion collisions, the primary event characterization parameters are the energy of the collision and the overlap of the two nuclei at the moment when they interact, commonly referred to as centrality. In order to compare fixed target, colliding beam, symmetric, and asymmetric systems all on a common footing, the collision energy is defined using the center-of-mass energy available when a single nucleon from one projectile collides with a single nucleon from the other projectile, ignoring Fermi motion. The standard notation for this quantity is $\sqrt{s_{NN}}$, referred to as the nucleon-nucleon center-of-mass energy. For symmetric colliding beams, each of which has the same energy per nucleon, $\sqrt{s_{NN}}$ is simply twice that value and the nucleon-nucleon frame is also the lab frame. When colliding deuterons and gold at RHIC, both beams were run at the same relativistic γ (and therefore the same rapidity) as the gold beams in the 200 GeV Au+Au collisions. The mass difference caused by the binding energy is responsible for the fact that the d+Au collisions are slightly asymmetric in the lab frame. The deuteron has a total energy of 100.7 GeV/nucleon, only 0.7% larger than the gold beam value of 100.0 GeV/nucleon. Consequently, the nucleon-nucleon frame does not coincide with the lab frame, but the shift in rapidity is only +0.004 units. For collisions of p+p, in contrast, the relativistic γ (and hence the rapidity) were adjusted in order to compensate for the small mass difference and, thereby, to achieve the same $\sqrt{s_{NN}}$ of 200 GeV as for the highest energy Au+Au collisions. At RHIC, data have been taken for a wide range of $\sqrt{s_{NN}}$ (see Table A.1) ranging from a value close to the maximum achieved at the SPS up to a value more than 10 times larger.

A direct measure of the collision geometry is given by the impact parameter, b, which is the transverse distance between the centers of the colliding heavy ions. It is defined such that $b = 0$ for central collisions, see Fig. B.1.

In most physics analyses of heavy ion collision data at highly relativistic energies, the impact parameter is not considered particularly useful in characterizing the important influence of geometry on the outcome of a given interaction. Instead, two parameters which quantify the critical distinctions are used: namely the number of participating nucleons, N_{part}, and the number of binary

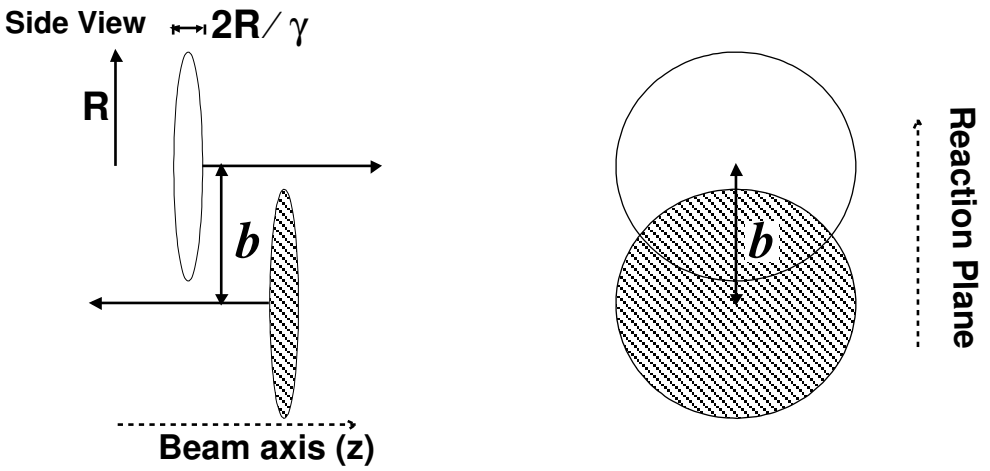

Fig. B.1. (Left panel) A side view in the nucleon-nucleon center-of-mass frame of two relativistic heavy ions colliding. (Right panel) A view along the beam axis, where the cross-hatched almond-like overlap region is indicated. The reaction plane for a particular collision is the plane defined by the impact parameter, b, and the beam axis (z).

nucleon-nucleon collisions, N_{coll}. In defining these variables, two important assumptions are made. First, since the collision duration at such high energies is very short compared to the typical time-scale for nuclear rearrangement or movement of nucleons within the nucleus, it is assumed that only the nucleons in the overlap region (the cross-hatched area in the right panel of Fig. B.1) experience any substantial interactions (i.e. participate) in the collision. Second, the collisions suffered by a given nucleon as it traverses the other nucleus may not be distinct sequential events, and thus it may be most meaningful to simply count the total number of collisions. For observables such as elliptic flow which are sensitive to the shape of the initial overlap region, a third parameter, namely the spatial asymmetry of this region derived from the impact parameter and the radii of the colliding nuclei, can be used.

In determining the number of participating nucleons, or equivalently the number of nucleons which interact, only those which are struck by nucleons from the other nucleus (as opposed to ones which were hit only in secondary scatterings) are counted. This is the same quantity as "wounded nucleons" introduced by Białas, Bleszyński and Czyż [146]. In some publications, the notation N_{wound} is used for what is herein referred to as N_{part} and the notation N_{part} includes nucleons suffering secondary scatterings. When comparing PHOBOS data with results from other experiments, care has been taken to use the appropriate values. N_{part} depends on the collision geometry and is typically calculated using a Glauber model of the collision. The key ingredients in this calculation are (1) nucleons are distributed according to a nucleon density function (e.g. Woods-Saxon), (2) nucleons in each nucleus travel in straight lines through the colliding system, and (3) nucleons interact according to the inelastic cross section, $\sigma_{_{NN}}$, as measured in proton-proton collisions. For the

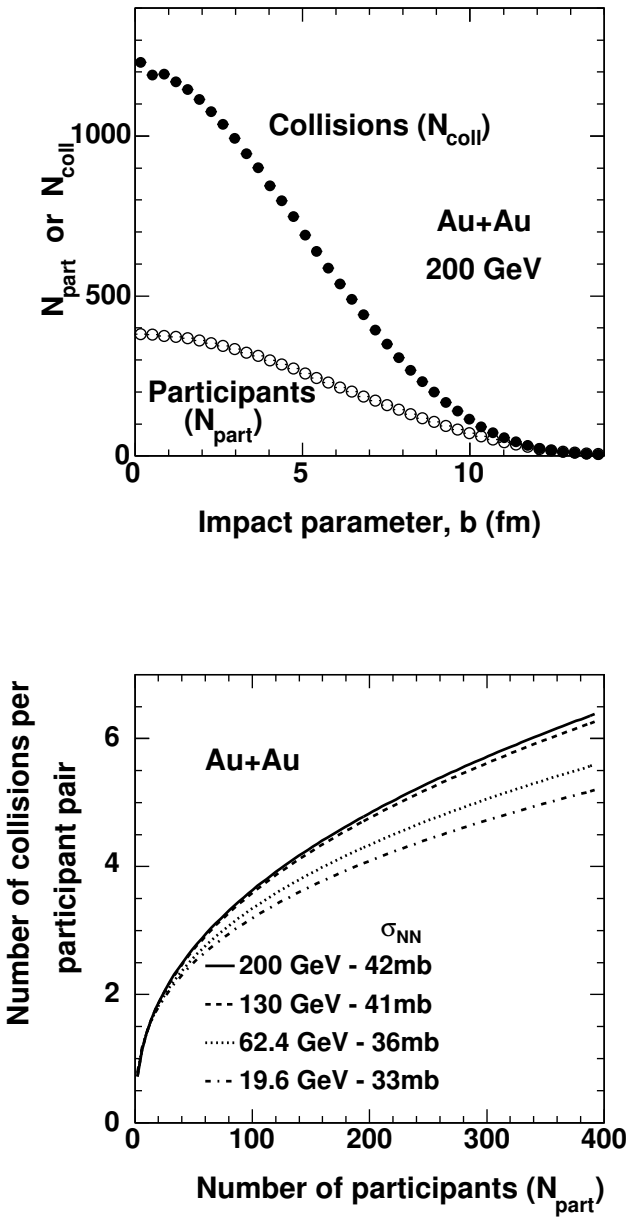

Fig. B.2. (Top panel) N_{part} and N_{coll} vs. impact parameter, b, for Au+Au collisions at $\sqrt{s_{NN}}$=200 GeV. (Bottom panel) The average number of collisions, N_{coll}, divided by the average number of participant pairs versus N_{part} for Au+Au at a variety of beam energies. See text for discussion.

energies at RHIC, the values assumed for σ_{NN} were 33, 36, 41, and 42 mb for $\sqrt{s_{NN}}$=19.6, 62.4, 130, and 200 GeV, respectively. In all cases, the nucleons were assumed to be hard spheres distributed according to a Wood-Saxon

functional form of

$$P(R) = R^2 \left(1 + e^{\frac{(R-r_0)}{a}}\right)^{-1},$$

where r_0=6.38 fm and a=0.535 fm for all energies. The open circles in the top panel of Fig. B.2 show an example of the results of such a model calculation relating N_{part} and impact parameter for Au+Au collisions at one of the RHIC energies. The number of participants is usually assumed to have a strong influence on the bulk properties of particle production but it is shown in the physics sections of this paper that N_{part} (or $N_{part}/2$) provides a convenient benchmark to study the effects of the collision geometry on many measured experimental quantities.

As introduced above, N_{coll} denotes the number of binary nucleon-nucleon collisions in a heavy ion reaction. As in the calculation of N_{part}, only primary collisions, i.e. those occurring along the straight-line trajectory of nucleons through the opposing nucleus, are counted. This quantity can also be calculated in a Glauber model, with typical results being shown as closed circles in the top panel of Fig. B.2. The yield from hard scattering (i.e. large momentum transfer) processes is expected to scale as N_{coll}. For symmetric A+A collisions, simple geometrical arguments imply that N_{coll} would scale as roughly $A^{4/3}$. Thus, for collisions of more than two participants, the number of binary nucleon-nucleon collisions is larger than the number of participants, with the difference increasing dramatically for smaller impact parameters.

One possibly important aspect of centrality in heavy ion collisions which goes beyond the simple increase in the number of participants or collisions is shown in the bottom panel of Fig. B.2. There, the number of collisions is divided by the number of participating pairs to derive the average number of collisions suffered by each participant. A similar parameter, typically denoted $\bar{\nu}$ and calculated from $\bar{\nu} = (A\sigma_{pp})/\sigma_{pA}$ where the σ's are inelastic cross sections, is commonly used to characterize centrality or target dependences of observables in p+A collisions [145]. In nucleus-nucleus collisions, the calculated average number of collisions per participant varies by a large factor as a function of centrality and also has some dependence on energy due to the varying nucleon-nucleon cross section.

B.2 Particle characterization

In describing the trajectories of particles emitted in heavy ion collisions, a distinction is typically made between longitudinal (i.e. along the beam direction) and transverse motion. The former may reflect some remnant of the original

motion of the beam while the latter is largely generated in the interaction. The physics variable typically associated with the longitudinal motion is rapidity, denoted y and defined as $y = \frac{1}{2}\ln((E+p_{\parallel})/(E-p_{\parallel})) = \ln((E+p_{\parallel})/m_{T})$ with E and $p_{\parallel}$ being the total energy and the component of the particle's momentum along the beam, respectively, and m_{T} being the transverse mass defined below. Rapidity has the important property of being additive in Lorentz transformations from one reference frame to another which differ by velocity along the beam. Thus, the shape of the distribution of any quantity plotted versus rapidity is the same in any such frame. Unfortunately, it is frequently difficult to experimentally determine the particle identification, or in some cases even the momentum itself, necessary to calculate rapidity. In such instances, it is common to replace rapidity with pseudorapidity, denoted η and defined as $\eta = -\ln(\tan(\theta/2))$, where θ is the polar angle to the beam axis. For particles whose total momentum is large compared to their mass, i.e. for particles whose velocity is close to the speed of light ($\beta = v/c \approx 1$), the two measures are close to identical, except for polar angles very close to zero. Since the produced particles are typically dominated by pions whose transverse momentum alone averages a few hundred MeV/c or more, the use of pseudorapidity is a quite reasonable approximation. A variable frequently used in elementary collisions is the Feynman x_{F} variable given by the ratio of the momentum along the beam to the maximum possible value, $x_{F} = p_{\parallel}/p_{\parallel max}$.

Another aspect of the distributions as a function of longitudinal velocity that proves to be very interesting is the comparison of distributions at a variety of beam energies but viewed in the rest frame of one of the projectile particles. For distributions as a function of rapidity, this can be done exactly and trivially by simply subtracting the rapidity of the beam from the rapidity of each particle. In the case of pseudorapidity distributions, the transformation is not exact but a reasonably close approximation is found using the shifted pseudorapidity, denoted η' and defined as $\eta' = \eta - y_{beam}$, where η is the pseudorapidity of a particle and y_{beam} is the beam rapidity. The quantity y_{beam}, which is given by $\frac{1}{2}\ln((E+p)/(E-p)) = \ln((E+p)/M)$ with E, p, and M being the energy, momentum, and mass of the beam, respectively, is given in Table A.1 for the various colliding systems and energies. Fermi motion of 300 MeV/c would spread the nucleons out by typically $\approx$0.3 units in rapidity.

The transverse motion is most often characterized using simply the component of the momentum, denoted p_{T}, that is perpendicular to the beam axis. Occasionally, the so-called transverse mass, $m_{T} = \sqrt{p_{T}^2 + m_0^2}$, is used where m_0 is the rest mass of the particle. The use of this more complicated variable is motivated by its appearance as the natural scaling parameter for particles emitted by a thermal source. It can also be used to combine energy, transverse momentum, and rapidity of a particle via the identity $E = m_{T}\cosh(y)$.

The various particle characterization variables can be related using the fol-

lowing identities:

$$p_{\parallel} = m_{T} \sinh(y) = p_{T} \sinh(\eta).$$

For relativistic beam energies, $p_{\parallel} \approx (\sqrt{s}/2)\, x_{F}$ and for y larger than about 1–2, $\sinh(y) \approx (e^{y})\,/2$ so that:

$$\eta' \equiv \eta - y_{beam} \approx \ln(x_{F}) - \ln\left(\frac{p_{T}}{M}\right)$$

$$y' \equiv y - y_{beam} \approx \ln(x_{F}) - \ln\left(\frac{m_{T}}{M}\right),$$

where M is the nucleon mass.

In the case of jets emitted in e^{+}+e^{-} annihilation, the motions of individual particles along and transverse to the beam are not the most interesting quantities. Instead, distributions are characterized by the trajectories of particles relative to the jet direction, the so-called thrust axis. Since data exist most frequently in the form of unidentified charged particles, the motion along the thrust axis is traditionally defined using y_{T}, the rapidity calculated using the momentum parallel to the jet direction and assuming the pion mass. The required shift to compare different beam energies in a common frame, as was done for y' or η', is not intuitively obvious. In this paper, the somewhat arbitrary choice was made to replace y_{beam} in the formulas above with y_{jet} which is the rapidity calculated using the center-of-mass energy combined with the assumption of the proton mass. Therefore, the same shift was used in both e^{+}+e^{-} and p+p at the same $\sqrt{s}$.

B.3 Notation for observables

The most basic observable characterizing particle production is the total number of particles emitted. Two experimental hurdles complicate the extraction of this number from the data. The first is that only charged particles are easily detected. Although assumptions can be made concerning the ratio of charged and neutral particles, the multiplicity data is almost always presented in terms of the number of charged particles. Adjustments for the number of unobserved neutrals is typically only done when needed in a specific calculation, for example in the discussion of the energy density presented in Sect. 2.1. The notation N_{ch}(A+B) is used to denote the total charged particle yield, integrated over all solid angle, in collisions of species A with species B. To date, PHOBOS has measured N_{ch}(d+Au) at a variety of centralities for one center-of-mass energy and N_{ch}(Au+Au) over a broad range of both centrality and beam energy. Note

that in all cases the multiplicity is defined to be "primary", i.e. those particles emitted in the initial interaction. Corrections are applied to the data to remove all other "secondary" particles, which are created in weak or electromagnetic decays of primary particles and interactions of primary particles with material in the detector. The second complication in extracting total numbers is that no detector can be fully hermetic, i.e. capable of detecting every single particle emitted. As a result, it is always necessary to measure distributions of particles and extrapolate into the unmeasured regions.

Because the PHOBOS multiplicity detector measures only the emission angle of charged particles, the extracted distribution is the number of charged particles per unit pseudorapidity, denoted $dN_{ch}/d\eta$. The experimental layout is designed to minimize the amount of material between the collision vertex and the active elements and, therefore, the cut-off in transverse momentum is low and the losses of particles with low $p_{_T}$ are small. The correction for secondary particles which are added to the total by decays or interactions in the material is typically much larger than the correction for particles that are lost. In addition, the very broad coverage in η provided by the PHOBOS setup results in a relatively small extrapolation for particles emitted at small angles with respect to the beam. Thus, PHOBOS can provide information about $dN_{ch}/d\eta$ and N_{ch} which are unique at RHIC. As mentioned above, it is also interesting to study particle distributions shifted into the rest frame of one of the projectiles. The shifted distribution, $dN_{ch}/d\eta'$, can be used as a measure of the charged particle pseudorapidity density as effectively viewed in the rest frame of one of the colliding nuclei, although one should keep in mind that such a shift is, in principle, associated with a small distortion of the distributions.

As discussed in the main body of this paper, the particle density is highest near y or η of zero and, therefore, it is generally assumed that the potential for creation of any new state of matter is also highest in that region. As a result, the properties of observables "near midrapidity" are of particular interest. For the midrapidity multiplicity distribution, the range chosen is ± 1 unit in η so the pseudorapidity distribution is averaged over this range to generate $dN_{ch}/d\eta\rfloor_{|\eta|\leq 1}$.

In cases where the momentum and angle of the particles are measured, distributions in both transverse momentum and rapidity (or pseudorapidity in cases without particle identification) can be generated. The transverse distributions are commonly presented in a form which is Lorentz invariant given by $Ed^3\sigma/dp^3$, with E and p being the total energy and vector momentum of the particle, respectively. Since the interesting quantity is typically the number of particles in a given event, i.e. the distribution that integrates to give multiplicity, this is more commonly expressed as invariant yield Ed^3N/dp^3. When integrating over all orientations of the reaction plane, azimuthal symmetry can be assumed and the differential momentum volume can be expressed in

cylindrical coordinates as $dp^3 \rightarrow 2\pi p_T dp_T dp_\parallel$. Furthermore, the component of the momentum parallel to the beam can be transformed using $dp_\parallel = Edy$ where y is the rapidity, resulting in the final form $d^2N/2\pi p_T dp_T dy$. When using transverse mass, the transformation is trivial since $p_T dp_T = m_T dm_T$ and only the horizontal axis changes in the distributions. In cases without particle identification, rapidity is approximated by pseudorapidity, yielding $d^2N/2\pi p_T dp_T d\eta$.

When comparing transverse momentum distributions for more complicated systems to data from proton-proton collisions, one could simply take the ratio of the two distributions as a function of p_T to study the change in magnitude or shape. This ratio is called the nuclear modification factor since it is a measure of the modification of the properties of the emitted particles resulting from the presence of the nucleus in the interaction. In order to test specific theories of how the yield should scale, the standard procedure is to normalize the A+A (or, equivalently, scale the p+p) data by some factor. The resulting ratio comparing collisions of species A with species B to p+p is typically denoted R_{AB} defined as

$$R_{AB} = \frac{1}{Norm} \frac{dN_{A+B}/dp_T}{dN_{p+p}/dp_T} = \frac{1}{N_{coll}} \frac{dN_{A+B}/dp_T}{dN_{p+p}/dp_T}.$$

The most common normalization, and the one usually indicated by the simple notations R_{AA}, R_{dAu}, etc., is N_{coll} as shown in the rightmost formula above. This arises from the interest in studying the behavior of high transverse momentum particles and the belief that the yield from such "hard" processes should scale with the number of binary nucleon-nucleon collisions. Analysis by the PHOBOS collaboration has demonstrated that the number of pairs of participating nucleons is often the more appropriate scaling variable. To avoid confusion, ratios using this latter normalization are denoted

$$R_{AB}^{N_{part}} = \frac{1}{N_{part}/2} \frac{dN_{A+B}/dp_T}{dN_{p+p}/dp_T}.$$

Note that a p+p collision has one pair of participants. This normalization will be generically referred to as the number of participant pairs even in asymmetric collisions.

It is frequently of interest to study the evolution of the shape and magnitude of these distributions as a function of centrality for nucleus-nucleus collisions. The most direct display of this evolution involves dividing data from one centrality bin by that from a different bin. In this case, both distributions need to be suitably normalized. The notation PC (CP) is used for ratios where peripheral (central) data is divided by central (peripheral). The PHOBOS collaboration has recently advocated the use of R_{PC} since different experiments

have different reach in centrality and the central data typically have significantly smaller statistical and systematic errors. In keeping with the convention described above, the definitions with the different normalizations are

$$R_{PC} = \frac{N_{coll}^{central}}{N_{coll}^{periph}} \frac{dN_{A+B}^{periph}/dp_T}{dN_{A+B}^{central}/dp_T}$$

and

$$R_{PC}^{N_{part}} = \frac{N_{part}^{central}}{N_{part}^{periph}} \frac{dN_{A+B}^{periph}/dp_T}{dN_{A+B}^{central}/dp_T}.$$

Note that the practical application of these definitions typically uses a fit to the distribution that appears in the denominator in order to avoid propagating statistical point-to-point fluctuations.

In the case of pure N_{coll} scaling, R_{AB} and R_{PC} would be unity while $R_{AB}^{N_{part}}$ and $R_{PC}^{N_{part}}$ would be unity for perfect N_{part} scaling. The variation of R_{AB} for N_{part} scaling (see, for example, Fig. 8) or the variation of $R_{PC}^{N_{part}}$ and $R_{AB}^{N_{part}}$ for N_{coll} scaling (see Figs. 31 and 32) depends on the ratio of N_{coll} to N_{part}. Careful examination of the numbers in Tables C.2 and C.3 in Appendix C.1 reveals that, for a given centrality, this ratio depends slightly on beam energy. When comparing data at 62.4 and 200 GeV, the difference is never more than 15%. For clarity, the dashed lines in Figs. 8 and 32 show only the value for the lower beam energy.

Using an event-by-event measurement of the orientation of the two colliding nuclei, the study of particle distributions can be extended to include a third coordinate, namely the azimuthal angle. In relativistic heavy ion collisions, the generic terms "directed flow" and "elliptic flow" are used for the measurement of anisotropy in the azimuthal distributions of particles relative to the reaction plane. The reaction plane for a particular collision is the plane defined by the impact parameter and the beam axis (b and z in Fig. B.1). In flow analyses, the distribution of particles in the azimuthal angle, ϕ, (always taken relative to the reaction plane for a particular collision) is measured and expressed in terms of a Fourier expansion, $dN_{ch}/d\phi = N_0(1 + 2v_1 cos(\phi) + 2v_2 cos(2\phi) + \ldots)$. The amplitude of the first ϕ-dependent term, v_1, is called directed flow. Elliptic flow is the name given to the amplitude of the second term of the Fourier expansion, v_2. This latter anisotropy in the form of a variation in particle yield in momentum space results primarily from the non-spherical shape in position space of the initial collision volume (see the cross-hatched region in the right panel of Fig. B.1).

Moving beyond single particle distributions, additional information can be

obtained by studying the correlations of particles. In heavy ion collisions, the most common multi-particle observable studied is the HBT correlation, named for Hanbury-Brown and Twiss who pioneered an analogous technique for studying the size of objects in astronomy [185,186]. The procedure is most often applied to pairs of like-sign pions and depends on the quantum mechanical connection between separation in coordinate and momentum space for identical particles. The data are presented as the ratio of the distribution of pairs in some relative-momentum variable divided by a distribution which matches the correct occupancy of the two-particle phase space but which does not contain the effects of the two-particle correlation. This normalization is obtained by pairing particles found in different events which have been matched for centrality and other event-characterization variables. The resulting correlation functions can be fit using a variety of parameterizations of the source distributions. From such parameterizations, information about the spatiotemporal extent of the emission source can be extracted. One commonly used system is the so-called Bertsch-Pratt coordinates [191,208,209]. For a given pair of identical particles with average momentum k, the coordinates are: longitudinal (R_l) along the beam direction (z), outwards (R_o) in the (z, k) plane perpendicular to z, and sidewards (R_s) perpendicular to the other two directions. The Yano-Koonin-Podgoretskii parameterization also includes spatial parameters for the longitudinal and transverse sizes of the source, as well as parameters describing the duration and longitudinal velocity of the source [210,211].

C Techniques for determining centrality

As briefly discussed in Appendix B, determining the centrality of a heavy ion collision is extremely important for event characterization. Knowing the centrality provides a geometrical scale for use in any studies of the underlying collision dynamics and affords the possibility of a more meaningful comparison to "baseline" data from elementary proton or electron collisions. The primary event centrality in PHOBOS is determined by utilization of signals from the Paddle scintillator counters, as well as the Octagon and Ring silicon detectors, all of which are sensitive to charged particle multiplicities in various regions of pseudorapidity. These signals, through bins in the percentage of total cross section, provide a measure of centrality. The validity of this technique is based on the experimental observation of a strong correlation between the charged particle multiplicity signals in, for example, the Paddle scintillator counters and neutral beam "remnants" (spectator neutrons) as measured in the Zero-Degree-Calorimeters (ZDCs). This correlation is shown in Fig. C.1 for $\sqrt{s_{NN}}$=200 GeV Au+Au collisions at PHOBOS.

The specific methods developed within PHOBOS to determine centrality de-

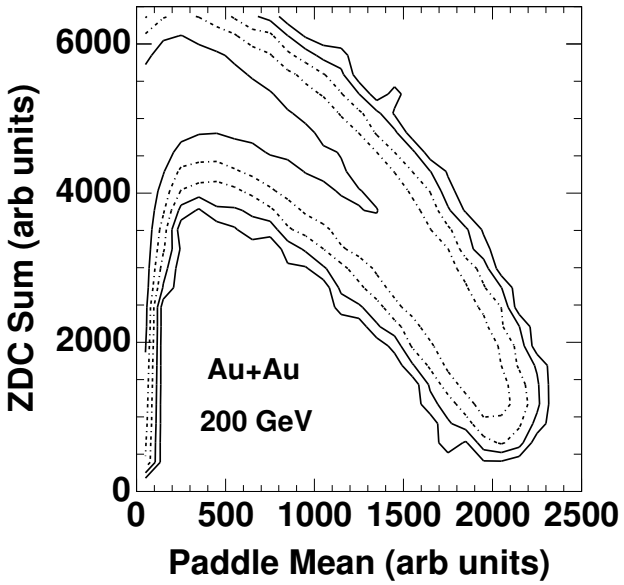

Fig. C.1. Correlation between spectator neutrons measured in the PHOBOS ZDC's (ZDC Sum) and charged particle multiplicity measured in the Paddle counters (Paddle Mean) for $\sqrt{s_{NN}}$=200 GeV Au+Au collisions. The contours are logarithmic with a factor of 4 in yield between adjacent levels.

pend on both the collision species (Au+Au versus d+Au) and the collision energy. The technique is to associate an experimentally measured signal to a well-defined centrality related variable, such as the number of participating nucleons, N_{part}. For this technique to be meaningful, a monotonic relation must exist between the multiplicity signals in the chosen region of pseudorapidity and N_{part}. This assumption is justified by the experimental correlation shown in Fig. C.1 (the remnant neutrons are anti-correlated with N_{part} for the 50% most central collisions). Additional evidence for the validity of this technique has been obtained using extensive Monte Carlo (MC) studies using event generators (such as HIJING, AMPT, RQMD, and Venus) and a full GEANT simulation of the PHOBOS detector. An outline of some of these techniques follows.

C.1 Centrality determination in Au+Au collisions

There are four main considerations that must be addressed in the course of determining the event centrality: the event selection, detection efficiency, choice of pseudorapidity region to utilize, and the event generator simulations to extract N_{part}.

The initial event selection must cleanly identify and separate true Au+Au collisions from numerous background sources, such as beam-gas interactions,

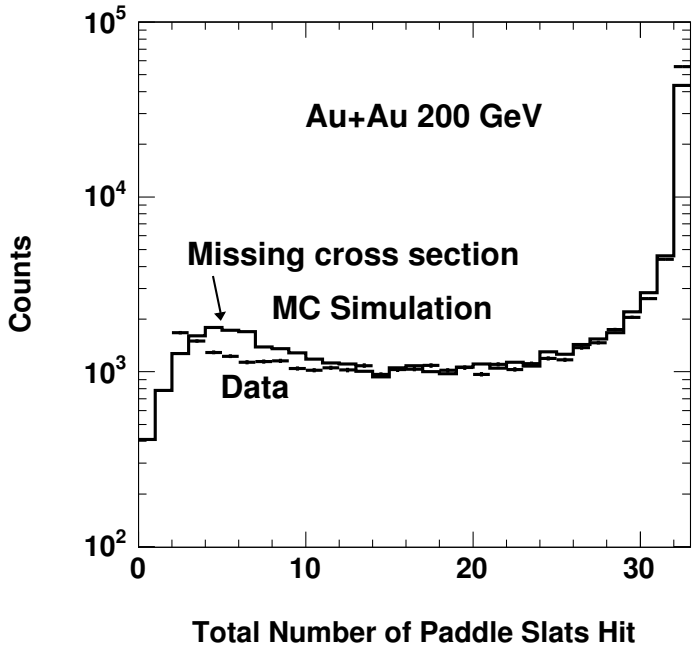

Fig. C.2. Illustration of the detection efficiency determination in Au+Au collisions using a comparison between Monte Carlo (MC) simulation and data for the number of Paddle slats hit. Data are shown for Au+Au collisions at $\sqrt{s_{NN}}$=200 GeV. The same technique was used for $\sqrt{s_{NN}}$=62.4 and 130 GeV Au+Au collisions.

while simultaneously providing the smallest possible bias on the resulting data set. In PHOBOS this was accomplished by using a combination of energy and time signals from the Paddle counters and the ZDCs. A selection of events with less than 4 ns time-difference between the two Paddle signals was combined with cuts on the ZDC individual and summed timing signals. Additional logic ensured no loss of very central events that have a high Paddle signal and correspondingly few numbers of spectator neutrons available to hit the ZDCs. This selection provided a basic "valid collision" definition for Au+Au collisions at $\sqrt{s_{NN}}$=62.4, 130 and 200 GeV. For the lowest energy Au+Au collision of $\sqrt{s_{NN}}$=19.6 GeV, the ZDC timing requirement had to be modified due to the substantially reduced efficiency for detection of the lower energy neutrons.

The detector efficiency was determined for two "minimum-bias" trigger configurations of at least one (two) hits in each scintillator Paddle counter array. For both configurations, a loss of peripheral events had to be accounted for before bins in percentage of total cross section could be correctly fashioned. The fraction of lost peripheral events was determined using comparisons of the total number of Paddle slats hit in both data and the full MC simulations (see Fig. C.2). This analysis yielded a total detection efficiency of 97% and 88% for the two trigger configurations, respectively, for Au+Au collisions at

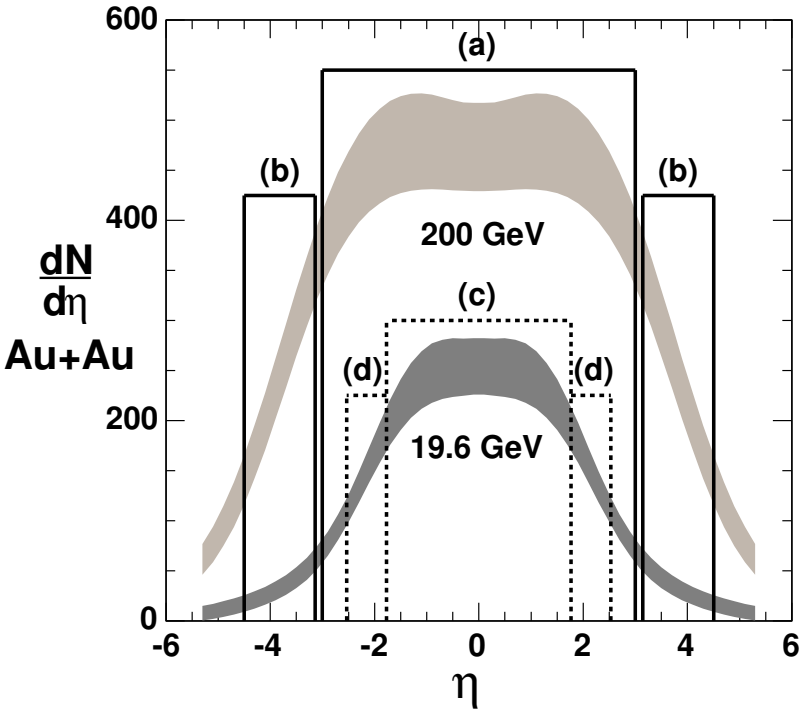

Fig. C.3. Pseudorapidity density distributions from $\sqrt{s_{NN}}$=200 (light, top band) and 19.6 (dark, bottom band) GeV Au+Au collisions, for the most central 25% of the cross section [44]. The boxed areas (a–d) illustrate the separate regions in pseudorapidity used in the centrality determination for each collision energy. Region (b) illustrates the pseudorapidity coverage of the Paddle scintillator counters, and the other regions were developed for centrality determination using the Octagon silicon detector.

$\sqrt{s_{NN}}$=200 GeV.

Using the collision event selection criteria outlined above and the deduced trigger detection efficiency, the next task is to find an appropriate experimental quantity for use in determining the event centrality. For Au+Au collisions, a consistent centrality determination was found to be relatively independent of the choice of detector (and hence the pseudorapidity limits), as long as the chosen region contained substantial particle multiplicity. The signal from the Paddle counters, with a pseudorapidity coverage of $3.2 < |\eta| < 4.5$ (region (b) of Fig. C.3), worked well as a centrality measure for collision energies of $\sqrt{s_{NN}}$=62.4, 130 and 200 GeV.

For the lowest energy of 19.6 GeV, new pseudorapidity regions had to be chosen due to a reduction in the monotonicity between the multiplicity signals in the Paddle counters and both the number of spectator neutrons seen in

the ZDCs and N_{part}, as determined from MC simulations. In addition, the Paddles are traversed by significantly fewer particles at 19.6 than 200 GeV (see dark grey band in Fig. C.3 or the bottom panel of Fig. 1) and, consequently, a different pseudorapidity region had to be chosen. In order to create a centrality measure at 19.6 GeV similar to that obtained from the Paddles at 200 GeV, the Paddle pseudorapidity range was scaled down to a smaller region by the ratio of beam rapidities $y_{19.6}^{beam}/y_{200}^{beam} = 0.563$ (region (d) of Fig. C.3). The resulting η region, $1.8 \leq |\eta| \leq 2.5$, lies wholly within the Octagon silicon detector coverage of $|\eta| \leq 3.2$ for collisions which occur within ± 10 cm of the nominal vertex position. Thus, the charged particle multiplicity measured in the region (d) was used as a centrality measure for 19.6 GeV and allowed for a direct centrality comparison to the original Paddle-based method at 200 GeV. Additional centrality measures were developed at both energies, in pseudorapidity regions close to midrapidity, which used the multiplicity signals of charged particles traversing the Octagon in the pseudorapidity regions (a) and (c), where region (c) is scaled by a factor of 0.563 compared to region (a). This technique of matching centrality regions allowed direct comparisons of midrapidity and away from midrapidity centrality determinations across a factor of ten in collision energy. Also, both pseudorapidity regions have been found to have very different rates of particle production and intrinsic dependences on N_{part}. By utilizing these two independent regions, the assumption that the centrality measure and N_{part} have to be only monotonic and not necessarily linear can be explicitly tested. An insignificant difference was found when analyzing data with both methods, at both energies [49].

Use of the Octagon silicon detector signals as a centrality measure introduces an additional complication not present for the Paddle counters. The precise vertex position of each event is required for the merging and angle correction of valid hits in the Octagon. PHOBOS has developed several techniques to determine the primary collision vertex, including use of the Vertex detector and straight-line tracks in the first six planes of the Spectrometer. However, due to the requirement of any of these valid vertices, the resulting data set is not only biased by the intrinsic trigger efficiency, but also by the vertex reconstruction efficiency. Additional inefficiencies are introduced for low multiplicity events and this fact is the primary reason that PHOBOS has, thus far, only published data for the top 50% of cross section for Au+Au data, where there are no such inefficiencies. Despite these additional complications, exploiting the Octagon detector signals as a centrality measure greatly expands the available solid angle for centrality determination. As shown in Fig. C.4, a good match between the data and MC simulations in all regions of pseudorapidity shown in Fig. C.3 gives confidence in the validity of the procedure.

Once the choice of pseudorapidity region for the centrality determination is made and the corresponding efficiency is determined, the resulting multiplicity related distribution can be divided into percentile of total cross section bins,

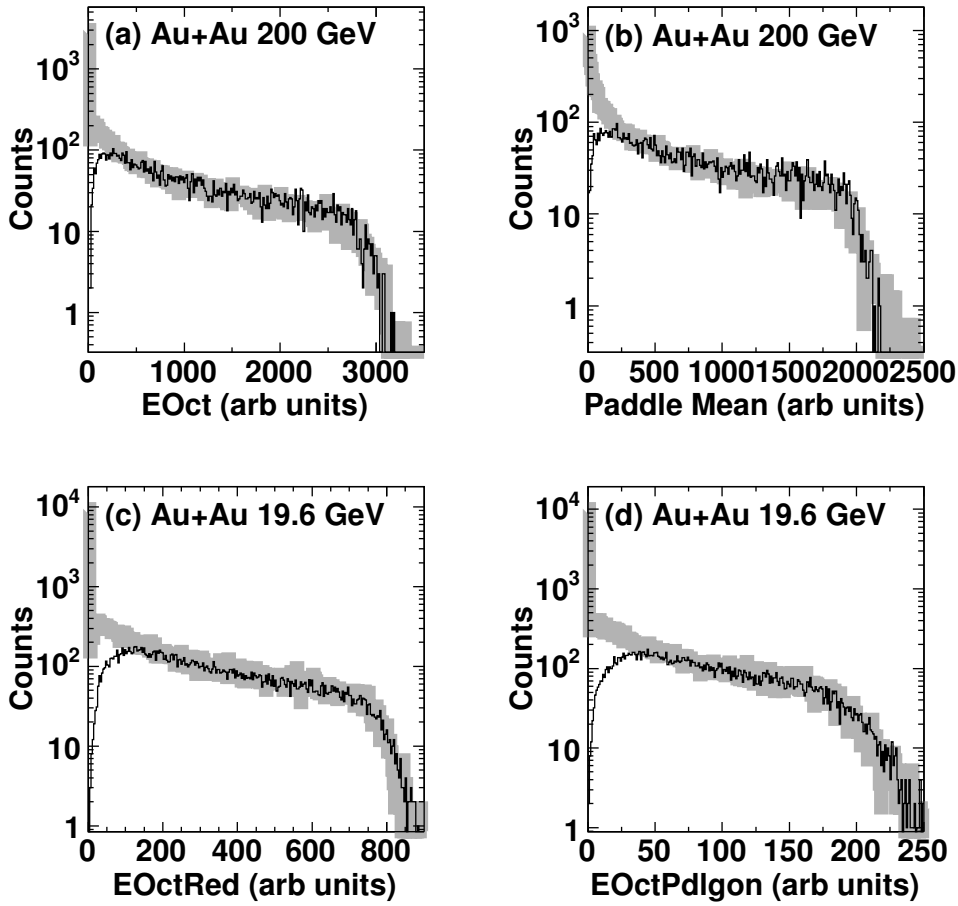

Fig. C.4. Charged particle multiplicity signal distributions measured in the four pseudorapidity regions (boxes labeled (a–d) in Fig. C.3) used in the centrality determination. Black histograms are data and the grey distributions are MC simulations for Au+Au at two energies. All data are shown for a restricted collision vertex of $|z| \leq 10$ cm, and thus have an additional inefficiency for low multiplicities as evident from the figures where the data falls below the (unbiased) MC simulations for peripheral events.

as illustrated in Fig. C.5, panels (a) and (b). Comprehensive MC simulations of these signals, that include Glauber model calculations of the collision geometry, allow the estimation of N_{part} for a cross section bin, as illustrated in Fig. C.5, panels (c) and (d). The most central collisions (b$\sim$0, see Fig. B.1) will have the largest number of participants with the obvious upper limit of N_{part}=394 for a "perfectly central" Au+Au collision, where all nucleons interact.

Systematic uncertainties on the extracted values of N_{part} were determined with MC simulations that included possible errors in the overall detection efficiency and also utilized different types of event generators. The uncertainty on the deduced N_{part} increased from $\sim$3% for central collisions to $\sim$9% for

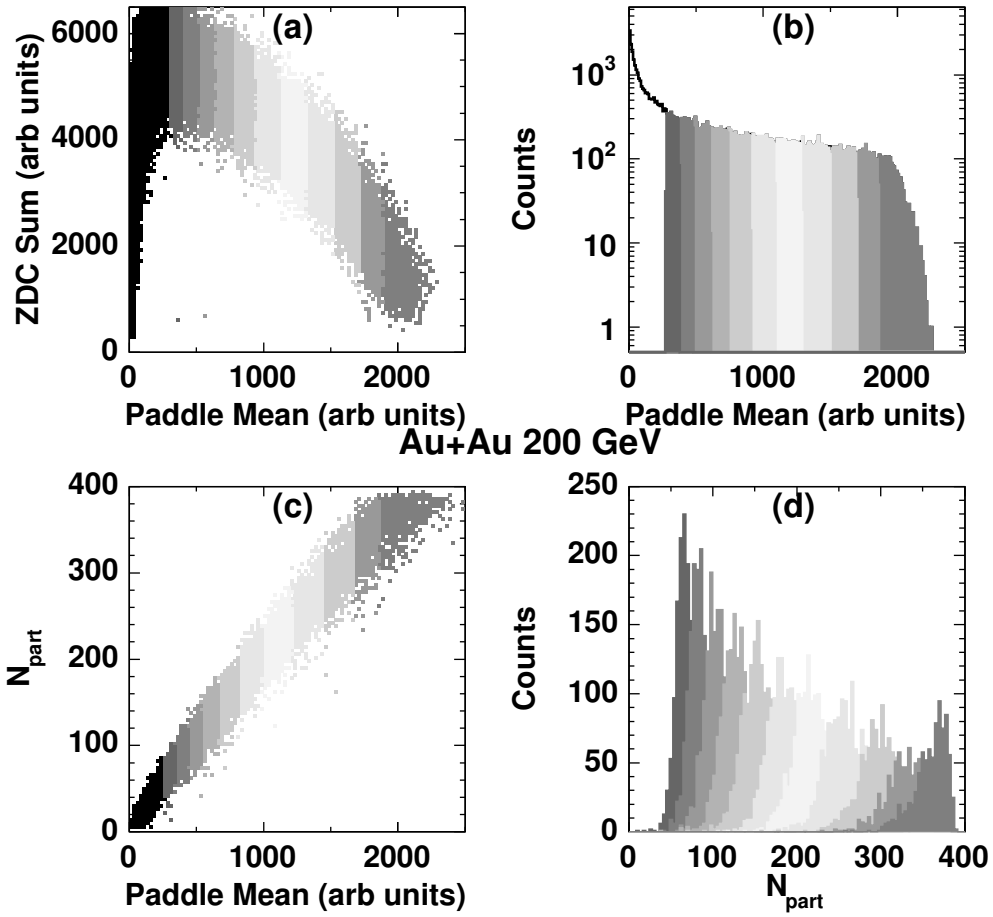

Fig. C.5. Illustration of how the centrality of a heavy ion Au+Au collision is defined (results for $\sqrt{s_{NN}}$=200 GeV are shown). Only the top 50% of cross section, where there is 100% detection and vertex reconstruction efficiency, is used. Panel (a) shows the experimental correlation between the charged particle multiplicity signals in the Paddle counters (Paddle Mean) and the signals in the ZDC's from spectator neutrons. The shaded bands represent bins in percentile of cross section cut on the Paddle Mean signal. Panel (b) is a projection of (a) onto the Paddle Mean axis. Panel (c) shows a corresponding MC calculation where a monotonic relation is observed between the Paddle Mean signal and N_{part}, the number of participating nucleons. From this correlation, the average N_{part} (see panel (d)) can be extracted for each bin in percentile of cross section.

mid-peripheral.

In principle, N_{coll} could be extracted from the same elaborate simulation procedure used for N_{part}. In practice, however, three issues arise. First, the ratio of N_{coll} over N_{part} varies dramatically with centrality (see bottom panel of Fig. B.2), but the experimental observables used in the centrality determination, when normalized by N_{part}, depend only weakly on centrality (see, for example, Figs. 12 and 29). Secondly, while the relationship between N_{coll} and

Energy	σ_{NN}	A	syst	stat	B	syst	stat
19.6	33	0.310	0.013	0.001	1.356	0.007	0.001
62.4	36	0.296	0.012	0.001	1.376	0.007	0.001
130	41	0.274	0.016	0.001	1.408	0.010	0.001
200	42	0.271	0.016	0.001	1.413	0.010	0.001

Table C.1
List of the nucleon-nucleon cross section used for the four Au+Au energies followed by the parameters of the power law fit to N_{coll} vs N_{part}, $N_{coll} = A \times (N_{part})^B$, along with their systematic and statistical errors. The systematic errors between the two parameters are highly correlated.

N_{part} is very sensitive to the assumed nucleon-nucleon cross-section, the correspondence between the observables and N_{part} is relatively insensitive to such changes. In contrast, factors which strongly impact the extraction of N_{part}, such as the overall detection efficiency and the detailed properties of the produced particles, have no influence on the correspondence between N_{coll} and N_{part}. For these reasons, it was found more effective to determine the values and systematic uncertainties for N_{coll} from the derived values of N_{part} by using a parameterization of the results of a Glauber calculation (see Appendix B.1 and Fig. B.2). Specifically, the results of the simulation are fit to a power law of the form $N_{coll} = A \times (N_{part})^B$ with the parameters given in Table C.1. The systematic errors of the fit procedure are determined by fitting different ranges of the data. Since the two parameters are highly anti-correlated (the normalized correlation coefficient ranges from -0.997 to -0.998), the changes observed in the different fits, and hence the deduced systematic errors, are highly correlated. This functional form works well down to values of $N_{part} \sim 20 - 30$ but begins to deviate by ~10–20% for smaller values. Tables C.2 and C.3 summarize the values of N_{part} and N_{coll} and their systematic uncertainties for the centrality bins used for Au+Au at $\sqrt{s_{NN}}$=62.4 and 200 GeV.

It should be noted that additional physics considerations may impact the extracted value of N_{coll}. As one example, the results of a straightforward Glauber simulation can be compared to the output of the HIJING code for Au+Au at $\sqrt{s_{NN}}$=200 GeV. At all impact parameters, the numbers for N_{part} are equal in the two cases to within 10 particles or less (with the HIJING value consistently higher). In contrast, N_{coll} from HIJING is found to be lower by roughly 10% (resulting from the particular implementation of nuclear shadowing in the code [101]), with a slight increase in the difference for more central collisions.

Bin	N_{part}	syst	N_{coll}	syst 1	syst 2	syst 3	syst T
45-50%	61	7	85	13	3	4	14
35-45%	86	9	136	20	4	7	22
25-35%	130	10	240	26	7	12	29
15-25%	189	9	402	27	12	20	36
6-15%	266	9	643	30	19	32	48
0-6%	335	11	883	40	26	44	65

Table C.2
List of centrality parameters extracted for each of the fractional cross section bins used in the analysis of Au+Au at $\sqrt{s_{NN}}$=62.4 GeV. Bins are labeled by the percentage of the total inelastic cross section with smaller numbers being more central. The systematic error in N_{part} is found as described in the text. There are three components of the systematic error in N_{coll}: 1) the propagation of the uncertainty in N_{part} through the power law function, 2) the value from the systematic uncertainty in the fit, 3) an estimate of the systematic uncertainty in the Glauber model itself, and T) total found by summing contributions in quadrature.

Bin	N_{part}	syst	N_{coll}	syst 1	syst 2	syst 3	syst T
45-50%	65	4	99	9	3	5	11
35-45%	93	5	164	12	5	8	15
25-35%	138	6	286	18	9	14	25
15-25%	200	8	483	28	15	24	40
6-15%	276	9	762	35	23	38	57
0-6%	344	11	1040	47	31	52	77

Table C.3
List of centrality parameters extracted for each of the fractional cross section bins used in the analysis of Au+Au at $\sqrt{s_{NN}}$=200 GeV. Bins are labeled by the percentage of the total inelastic cross section with smaller numbers being more central. The systematic error in N_{part} is found as described in the text. There are three components of the systematic error in N_{coll}: 1) the propagation of the uncertainty in N_{part} through the power law function, 2) the value from the systematic uncertainty in the fit, 3) an estimate of the systematic uncertainty in the Glauber model itself, and T) total found by summing contributions in quadrature.

C.2 Centrality determination in d+Au collisions

The centrality determination for d+Au collisions at $\sqrt{s_{NN}}$=200 GeV incorporates the same considerations necessary for Au+Au collisions, however the details of the analysis techniques differ.

The initial definition of a 'valid collision' took on a different form, as the most basic event selection could not be defined cleanly from the timing signals of the Paddles. The asymmetric nature of the collision system resulted in very different particle multiplicities impinging on the two symmetrically located Paddle trigger counters, which caused an overall reduction in the timing resolution compared to that of the Au+Au collision system. Previous requirements of a ZDC detector timing coincidence were also no longer possible due to the unacceptable bias that would be imposed on the dataset. To ensure that the events analyzed were real collisions occurring in a usable proximity to the detector, a reconstructed collision vertex was required.

Lower total multiplicities precluded the high resolution track-based vertex reconstruction algorithms developed for Au+Au collisions ($\sigma_z \leq$0.04 cm for central collisions) as it became increasingly inefficient. A more efficient, but less accurate ($\sigma_z \sim$0.8 cm for central collisions) vertex reconstruction method based on global averaging techniques across the entire Octagon was created. This selection coupled with the intrinsic triggering of the system was estimated to have an overall efficiency of 83% for d+Au collisions at 200 GeV. This high efficiency data set was used for more global physics analyses, such as the centrality dependence of the $dN_{ch}/d\eta$ distribution.

In addition to the Octagon-based vertex determination, a new on-line fast vertex position derived from the T0 Čerenkov counters (see Appendix A) was developed for the d+Au collision data. This T0 time-difference-based method was utilized as a primary trigger for some of the data sets. In addition, the fully calibrated T0 signals were used in an off-line vertex-finding algorithm which, combined with the new Octagon-based algorithm discussed above, provided a very clean event selection. An additional benefit of on-line vertex triggering from the T0 detectors was the enhancement of the fraction of data occurring near the center of the detector ($|z| < 20$ cm). A Paddle-triggered dataset in d+Au allowed data to be written for collisions occurring within approximately 2 m of the center of the interaction region. The additional (T0) requirement forced a larger bias on the data than the Paddles and Octagon vertices alone and further reduced the overall trigger+vertex efficiency to 49%, but resulted in a much higher fraction of usable data that provided significantly improved statistics necessary for many Spectrometer-based analyses.

The more significant challenge in the d+Au data analysis was to extract the centrality dependence of various physics analyses without the centrality measure itself directly influencing the outcome as a result of strong auto-correlations. This issue is not a major factor when measuring quantities for a minimum-bias configuration [57], but it becomes a significant consideration for any detailed studies requiring a centrality definition. In these cases, unlike Au+Au collisions, the centrality determination for d+Au collisions was found to be strongly dependent on the choice of pseudorapidity region utilized

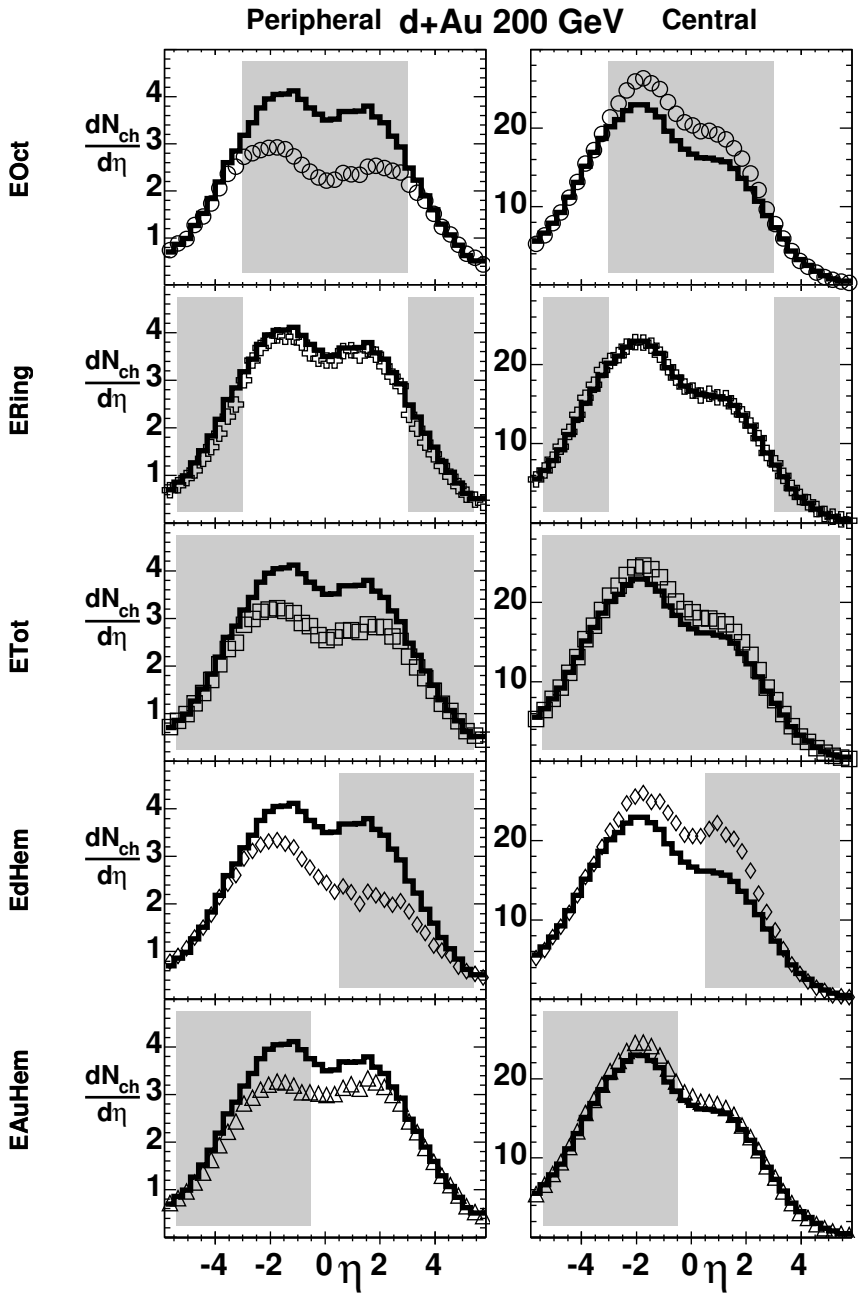

Fig. C.6. Reconstructed MC simulated pseudorapidity distributions (open symbols) for d+Au collisions at $\sqrt{s_{NN}}$=200 GeV for peripheral (left panels) and central (right panels) collisions where the centrality definition is taken from different regions of pseudorapidity (see text for discussion). MC simulations shown utilized the HIJING event generator coupled to a complete GEANT simulation of the PHOBOS detector. The unbiased HIJING output (truth values) is shown as histograms. The shaded areas indicate the pseudorapidity region covered by each centrality measure.

in the analysis. This fact is illustrated with MC simulated data in Fig. C.6, where strong auto-correlation biases are seen in the reconstructed pseudora-

pidity distributions for four of the five different centrality methods explored. Specifically a suppression of midrapidity yields ($|\eta| < 3$) in the reconstructed spectrum for peripheral collisions is observed (left column of Fig. C.6). The opposite effect is observed for central collisions, i.e. enhancement at midrapidity (right column of Fig. C.6). This study utilized five different centrality definitions that each covered different regions of pseudorapidity: the Octagon detector ($E_{Oct}, |\eta| \leq 3.0$), the Ring detectors ($E_{Ring}, 3.0 \leq |\eta| \leq 5.4$), the combined coverage of Octagon and Rings ($E_{Tot}, |\eta| \leq 5.4$), the deuteron direction ($E_{dHem}, 0.5 \leq \eta \leq 5.4$) and the gold direction ($E_{AuHem}, -5.4 \leq \eta \leq -0.5$). Both HIJING and AMPT based MC simulations indicated that a centrality measure based on the signals in the Ring counters provided the least bias on the measurement.

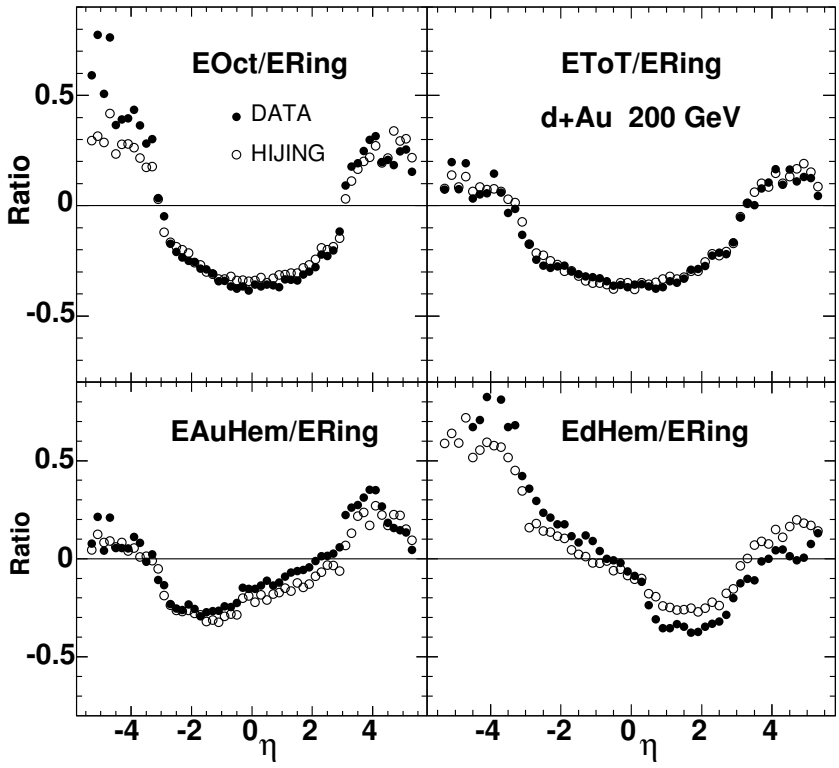

Fig. C.7. Ratios of reconstructed $dN_{ch}/d\eta$ distributions in d+Au collisions at $\sqrt{s_{NN}}$=200 GeV for both data and MC simulations using different centrality measures, each of which is selecting on the same percentile of central collisions. The good agreement in these ratios gives confidence that the MC simulations are providing a good basis on which to study the effects of biases created in the data that result from using different regions of pseudorapidity for the centrality determination.

Additional support for using the MC based simulations to select the best centrality measure is given in Fig. C.7. Ratios of the reconstructed $dN_{ch}/d\eta$ distributions obtained from four centrality measures relative to that obtained using the E_{Ring} variable are shown for both MC simulations and data. These ratios are found to be in very good agreement. This information, which is based

on data and MC simulation independently, provides the necessary confidence that using the Ring detectors for the centrality measure will provide the most accurate experimental result. It is important to point out that this study only provided guidance as to the choice of the Rings for the experimental centrality measure, and the final experimentally measured $dN_{ch}/d\eta$ distributions do not rely on the details of the MC simulation.

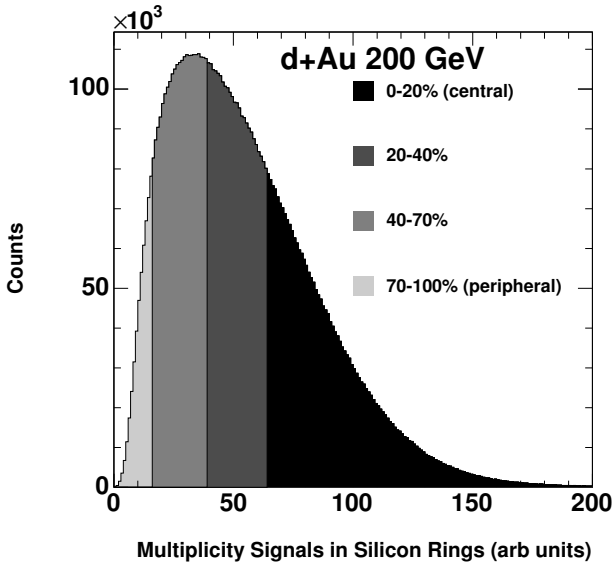

Fig. C.8. Illustration of how the centrality is defined for a d+Au collision. The entire cross section range is used in the analysis. The shaded bands represent bins in percentile of cross section based on the multiplicity signals in the Ring detectors. The data are shown for an online vertex (T0) restricted data set (see text).

The choice of the Ring detectors for use in the centrality determination for d+Au collisions, along with the extracted efficiency, allows for the creation of centrality bins based on percentage of cross section. For d+Au, a centrality determination is desired over the entire range of peripheral to central collisions. Thus, corrections must be made to both the location of the E_{Ring} bins and the extracted N_{part} values to properly account for the inefficiencies in detecting peripheral collisions. These corrections were made based on extensive MC simulations using both the HIJING and AMPT event generators. For the case of the T0 triggered dataset, the centrality determination was reanalyzed in terms of the efficiency associated with each cross section bin and the associated N_{part}. The additional requirement of hits (particles) in the T0 detectors serves to push the average N_{part} higher, with the largest shifts for lower centrality classes. An example of the resulting centrality bins on the Ring signal distributions for four-bins of cross section are shown in Fig. C.8. The decreasing efficiency for more peripheral collisions is immediately evident.

Systematic uncertainties on the deduced average N_{part} values for each percentile bin of cross section were determined with additional simulations. In these studies, the N_{part} distribution taken directly from Glauber model calculations was matched to the measured centrality related variable, i.e. E_{Ring}, distribution from data, and the average corresponding N_{part} was extracted for each centrality bin. Many different effects, including various types of detector resolution smearing, possible non-linear dependencies of the measured centrality variable on N_{part}, and different deuteron wave functions, were included and the analysis repeated. These studies showed that the mean value of N_{part} estimated from the full HIJING (or AMPT) + GEANT detector simulation was reasonable and the systematic error on N_{part} reaches $\sim$30% for the most peripheral centrality bin, where the overall bias is greatest.

References

[1] H. Kastrup, P. Zerwas, eds., QCD 20 Years Later (World Scientific, Singapore, 1993).

[2] S. Eidelman, et al., (Particle Data Group), Phys. Lett. B 592 (2004) 1.

[3] D. J. Gross, F. Wilczek, Phys. Rev. Lett. 30 (1973) 1343.

[4] H. Politzer, Phys. Rev. Lett. 30 (1973) 1346.

[5] The work in references [3] and [4] was recognized by the 2004 Nobel Prize in Physics; http://nobelprize.org/physics/laureates/2004/.

[6] J. C. Collins, M. J. Perry, Phys. Rev. Lett. 34 (1975) 1353.

[7] E. V. Shuryak, Phys. Reports 61 (1980) 71.

[8] H. Satz, ed., Statistical Mechanics of Quarks and Hadrons, (North-Holland, 1981).

[9] D. J. Gross, R. D. Pisarski, L. G. Yaffe, Rev. Mod. Phys. 53 (1981) 43.

[10] H. Pagels, Phys. Reports 16 (1975) 219.

[11] W. Marciano, H. Pagels, Phys. Reports 36 (1978) 137.

[12] R.D. Pisarski, F. Wilczek, Phys. Rev. D 29 (1984) 338.

[13] K. Rajagopal, Acta Phys. Pol. B 31 (2000) 3021; arXiv:hep-ph/0009058 (2000).

[14] F. Karsch, Nucl. Phys. A 698 (2002) 199.

[15] T. Schäfer, arXiv:hep-ph/0304281 (2003).

[16] M. G. Alford, Ann. Rev. Nucl. Part. Sci. 51 (2001) 131.

[17] K. Rajagopal, F. Wilczek, arXiv:hep-ph/0011333 (2000).

[18] G. Baym, S. A. Chin, Phys. Lett. B 62 (1976) 241.

[19] G. Chapline, M. Nauenberg, Phys. Rev. D 16 (1977) 450.

[20] G. F. Chapline, M. H. Johnson, E. Teller, M. S. Weiss, Phys. Rev. D 8 (1973) 4302.

[21] See Proceedings of the International Conference on Ultra-Relativistic Nucleus-Nucleus Collisions:Quark Matter; J. Phys. G 30 (2004) S633; Nucl. Phys. A 715 (2003) 1c; *ibid.* A 698 (2002) 1c; *ibid.* A 661 (1999) 1c; *ibid.* A 638 (1998) 1c; *ibid.* A 610 (1996) 1c; *ibid.* A 590 (1995) 1c; *ibid.* A 566 (1994) 1c; *ibid.* A 544 (1992) 1c; *ibid.* A 525 (1991) 1c; *ibid.* A 498 (1989) 1c; Z. Phys. C 38 (1988) 1; Nucl. Phys. A 461 (1987) 1c; "Quark Matter '84", K. Kajantie, ed. (Springer Verlag, 1985); Nucl. Phys. A 418 (1984) 1c; Quark Matter Formation and Heavy Ion Collisions, Proceedings of the Bielefeld Workshop 1982, M. Jacob, H. Satz, eds. (WSPC, Singapore, 1983); Phys. Reports 88 (1982) 321; Workshop on future relativistic heavy ion experiments, R. Bock, R. Stock, eds., (Darmstadt, 1980).

[22] P. M. Jacobs, X. -N. Wang, Prog. Part. Nucl. Phys. 54 (2005) 443; arXiv:hep-ph/0405125 (2004).

[23] R. C. Hwa, X. -N. Wang, eds., Quark Gluon Plasma 3 (World Scientific, Singapore, 2003).

[24] P. F. Kolb, U. Heinz, in Quark-Gluon Plasma 3 (World Scientific, Singapore, 2003); arXiv:nucl-th/0305084 (2003).

[25] D. H. Rischke, Prog. Part. Nucl. Phys. 52 (2004) 197.

[26] White Papers from BRAHMS, PHENIX, and STAR, submitted to Nucl. Phys. A.

[27] K. Kanaya, Nucl. Phys. A 715 (2003) 233c.

[28] M. Plümer, S. Raha, R. M. Weiner, Nucl. Phys. A 418 (1984) 549c.

[29] E. V. Shuryak, Nucl. Phys. A 750 (2005) 64.

[30] E. V. Shuryak, Prog. Part. Nucl. Phys. 53 (2004) 273.

[31] G. T. Horowitz, A. Strominger, Nucl. Phys. B 360 (1991) 197.

[32] S. S. Gubser, I. R. Klebanov, A. A. Tseytlin, Nucl. Phys. B 534 (1998) 202.

[33] F. Karsch, S. Datta, E. Laermann, P. Petreczky, S. Stickan, I. Wetzorke, Nucl. Phys. A 715 (2003) 701.

[34] E. V. Shuryak, I. Zahed, Phys. Rev. C 70 (2004) 021901R.

[35] K. Kajantie, M. Laine, K. Rummukainen, Y. Schröder, Phys. Rev. D 67 (2003) 105008.

[36] F. Karsch, J. Phys. G 30 (2004) S887.

[37] M. D'Elia, M. P. Lombardo, arXiv:hep-lat/0409010 (2004).

[38] S. Ejiri, C. R. Allton, M. Doering, S. J. Hands, O. Kaczmarek, F. Karsch, E. Laermann, K. Redlich, arXiv:hep-lat/0408046 (2004).

[39] Z. Fodor, S. D. Katz, Jour. High Ener. Phys. 0404 (2004) 50; arXiv:hep-lat/0402006 (2004).

[40] P. de Forcrand, O. Philipsen, Prog. Theor. Phys. Suppl. 153 (2004) 127.

[41] C. T. H. Davies, et al., (HPQCD and UKQCD), Phys. Rev. Lett. 92 (2004) 022001.

[42] E. Laermann, O. Philipsen, Ann. Rev. Nucl. Part. Sci. 53 (2003) 163.

[43] F. Karsch, Lect. Notes Phys. 583 (2002) 209.

[44] B. B. Back, et al., (PHOBOS), Phys. Rev. Lett. 91 (2003) 052303.

[45] B. B. Back, et al., (PHOBOS), Phys. Rev. Lett. 85 (2000) 3100.

[46] B. B. Back, et al., (PHOBOS), Phys. Rev. C 65 (2002) 031901R.

[47] B. B. Back, et al., (PHOBOS), Phys. Rev. Lett. 88 (2002) 022302.

[48] B. B. Back, et al., (PHOBOS), Phys. Rev. C 65 (2002) 061901R.

[49] B. B. Back, et al., (PHOBOS), Phys. Rev. C 70 (2004) 021902R.

[50] S. V. Afanasiev, et al., (NA49), Phys. Rev. C 66 (2002) 054902.

[51] T. Anticic, et al., (NA49), Phys. Rev. C 69 (2004) 024902.

[52] L. Ahle, et al., (E866), Phys. Rev. C 57 (1998) 466R.

[53] B. B. Back, et al., (E917), Phys. Rev. C 66 (2002) 054901.

[54] L. Ahle, et al., (E866), Phys. Lett. B 490 (2000) 53.

[55] J. L. Klay, et al., (E895), Phys. Rev. C 68 (2003) 054905.

[56] J. Dunlop, Mass. Inst. of Tech. PhD. Thesis (1999).

[57] B. B. Back, et al., (PHOBOS), Phys. Rev. Lett. 93 (2004) 082301.

[58] K. J. Eskola, Nucl. Phys. A 698 (2002) 78c.

[59] S. A. Bass, et al., Nucl. Phys. A 661 (1999) 205c.

[60] X.-N. Wang, in [59], 210c (1999).

[61] B. Zhang, in [59], 220c (1999).

[62] H. Sorge, in [59], 217c (1999); arXiv:nucl-th/9905008 (1999).

[63] M. Bleicher, in [59], 218c (1999).

[64] W. Cassing, in [59], 222c (1999).

[65] H. J. Drescher, in [59], 216c (1999).

[66] A. Capella, A. Kaidalov, J. Tran Thanh Van, Heavy Ion Phys. 9 (1999) 169; arXiv:hep-ph/9903244 (1999).

[67] J. Ranft, arXiv:hep-ph/9911213 (1999).

[68] N. Armesto, C. Pajares, Int. J. Mod. Phys. A 15 (2000) 2019; arXiv:hep-ph/0002163 (2000).

[69] S. Jeon, J. Kapusta, Contest on the RHIC predictions, June 2000.

[70] K. J. Eskola, K. Kajantie, P. V. Ruuskanen, K. Tuominen, Nucl. Phys. B 570 (2000) 379.

[71] S. A. Bass, et al., Phys. Rev. C 60 (1999) 021902.

[72] J. Stachel, in [59], 226c (1999).

[73] A. Krasnitz, R. Venugopalan, Phys. Rev. Lett 86 (2001) 1717.

[74] D. Kharzeev, E. Levin, Phys. Lett. B 523 (2001) 79.

[75] D. Kharzeev, E. Levin, L. McLerran, Phys. Lett. B 561 (2003) 93.

[76] D. Kharzeev, Y.V. Kovchegov, K. Tuchin, Phys. Lett. B 599 (2004) 23.

[77] B. B. Back, et al., (PHOBOS), Phys. Rev. Lett. 91 (2003) 072302.

[78] B. B. Back, et al., (PHOBOS), Phys. Rev. C 70 (2004) 061901(R).

[79] I. Arsene, et al., (BRAHMS), Phys. Rev. Lett. 93 (2004) 242303.

[80] M.X. Liu, et al., (PHENIX), J. Phys. G 30 (2004) S1193.

[81] A. Accardi, arXiv:nucl-th/0405046 (2004).

[82] K. Adcox, et al., (PHENIX), Phys. Rev. Lett. 87 (2001) 052301.

[83] J. Adams, et al., (STAR), Phys. Rev. C 70 (2004) 054907.

[84] B. B. Back, et al., (PHOBOS), Phys. Lett. B 578 (2004) 297.

[85] B. B. Back, et al., (PHOBOS), Phys. Rev. C 70 (2004) 051901(R).

[86] S. S. Adler, et al., (PHENIX), Phys. Rev. C 69 (2004) 034909.

[87] J. D. Bjorken, Phys. Rev. D 27 (1983) 140.

[88] E. Fermi, Prog. Theor. Phys. 5 (1950) 570.

[89] R. Hagedorn, Nuovo Cim. Suppl. 3 (1965) 147.

[90] R. Hagedorn, J. Ranft, Nuovo Cim. Suppl. 6 (1968) 169.

[91] B. B. Back, et al., (PHOBOS), Phys. Rev. Lett. 87 (2001) 102301.

[92] B. B. Back, et al., (PHOBOS), Phys. Rev. C 67 (2003) 021901R.

[93] I. G. Bearden, et al., (NA44), Phys. Lett. B 388 (1996) 431.

[94] J. Bächler, et al., (NA49), Nucl. Phys. A 661 (1999) 45.

[95] L. Ahle, et al., (E866), Phys. Rev. C 60 (1999) 064901.

[96] L. Ahle, et al., (E866), Phys. Rev. Lett. 81 (1998) 2650.

[97] F. Becattini, J. Cleymans, A. Keränen, E. Suhonen, K. Redlich, Phys. Rev. C 64 (2001) 024901.

[98] F. Becattini, Z. Phys. C 69 (1996) 485.

[99] P. Braun-Munzinger, I. Heppe, J. Stachel, Phys. Lett. B 465 (1999) 15.

[100] B. B. Back, et al., (PHOBOS), Phys. Rev. C 70 (2004) 011901R.

[101] M. Gyulassy, X. N. Wang, Comput. Phys. Commun. 83 (1994) 307; HIJING v1.383 used for d+Au, and v1.35 used for Au+Au.

[102] H. Sorge, Phys. Rev. C 52 (1995) 3291; version 2.4 including rope formation was used.

[103] Z. W. Lin, S. Pal, C. M. Ko, B. A. Li, B. Zhang, Phys. Rev. C 64 (2001) 011902.

[104] B. Zhang, C. M. Ko, B. A. Li, Z. Lin, Phys. Rev. C 61 (2000) 067901.

[105] C. Bernard, et al., (MILC), Phys. Rev. D 71 (2005) 034504.

[106] F. Becattini, M. Gazdzicki, A. Keränen, J. Manninen and R. Stock, Phys. Rev. C 69 (2004) 024905.

[107] B. B. Back, et al., (PHOBOS), Phys. Rev. Lett. 89 (2002) 222301.

[108] B. B. Back, et al., (PHOBOS), submitted to Phys. Rev. C (RC); arXiv:nucl-ex/0407012 (2004).

[109] K. H. Ackermann, et al., (STAR), Phys. Rev. Lett. 86 (2001) 402.

[110] P. Huovinen, private communication of a calculation using the results of P. F. Kolb, P. Huovinen, U. W. Heinz, H. Heiselberg, Phys. Lett. B 500 (2001) 232.

[111] W. Busza, in Particle Production in Highly Excited Matter, H. H. Gutbrod, J. Rafelski, eds., (Plenum Press, Proceedings of a NATO Advanced Study Institute on Particle Production in Highly Excited Matter, 1993) p. 149.

[112] J. C. Collins, D. E. Soper, G. Sterman, Nucl. Phys. B 261 (1985) 104.

[113] J. C. Collins, D. E. Soper, G. Sterman, in Perturbative QCD, A.H. Mueller, ed., (World Scientific, 1988); Adv. Ser. Direct. High Energy Phys. 5 (1988) 1.

[114] K. Adcox, et al., (PHENIX), Phys. Rev. Lett. 88 (2002) 022301.

[115] K. Adcox, et al., (PHENIX), Phys. Lett. B 561 (2003) 82.

[116] B. B. Back, et al., (PHOBOS), Phys. Rev. Lett. 94 (2005) 082304.

[117] J. W. Cronin, H. J. Frisch, M. J. Shochet, J. P. Boymond, P. A. Piroué, R. L. Sumner, Phys. Rev. D 11 (1975) 3105.

[118] D. Antreasyan, J. W. Cronin, H. J. Frisch, M. J. Shochet, L. Kluberg, P. A. Piroué, R. L. Sumner, Phys. Rev. D 19 (1979) 764.

[119] A. Accardi, arXiv:hep-ph/0212148 (2002).

[120] I. Vitev. Phys. Lett. B 562 (2003) 36.

[121] I. Arsene, et al., (BRAHMS), Phys. Rev. Lett. 91 (2003) 072305.

[122] S. S. Adler, et al., (PHENIX), Phys. Rev. Lett. 91 (2003) 072303.

[123] J. Adams, et al., (STAR), Phys. Rev. Lett. 91 (2003) 072304.

[124] C. Adler, et al., (STAR), Phys. Rev. Lett. 90 (2003) 082302.

[125] J. Adams, et al., (STAR), Phys. Rev. Lett. 93 (2004) 252301.

[126] S. S. Adler, et al., (PHENIX), Phys. Rev. Lett. 91 (2003) 182301.

[127] J. Adams, et al., (STAR), Phys. Rev. Lett. 92 (2004) 052302.

[128] D. Molnar, S. A. Voloshin, Phys. Rev. Lett. 91 (2003) 092301.

[129] B. B. Back, et al., (PHOBOS), submitted to Phys. Rev. C(RC); arXiv:nucl-ex/0301017 (2003).

[130] J. Klay, U.C. Davis PhD. Thesis (2001).

[131] S. Eidelman, et al., (Particle Data Group), Phys. Lett. B 592 (2004) 1.

[132] G. I. Veres, Eötvös Loránd University PhD. Thesis, http://na49info.cern.ch/cgi-bin/wwwd-util/NA49/NOTE?292 (2002).

[133] A. E. Brenner, et al., Phys Rev D 26 (1982) 1497.

[134] M. Basile, et al., Phys. Lett. B 92 (1980) 367.

[135] M. Basile, et al., Phys. Lett. B 95 (1980) 311.

[136] B. B. Back, et al., (E917), Phys. Rev. Lett. 86 (2001) 1970.

[137] A. H. Mueller, Nucl. Phys. B 213 (1983) 85.

[138] B. B. Back, et al., (PHOBOS), submitted to Phys. Rev. Lett.; arXiv:nucl-ex/0409021 (2004).

[139] I. G. Bearden, et al., (BRAHMS), Phys. Rev. Lett. 93 (2004) 102301.

[140] W. Busza, A. S. Goldhaber, Phys. Lett. B 139 (1984) 235.

[141] W. Busza, R. Ledoux, Ann. Rev. Nucl. Part. Sci. 38 (1988) 119.

[142] G. J. Alner, et al., (UA5), Phys. Rep. 154 (1987) 247.

[143] J. E. Elias, et al., (E178), Phys. Rev. D 22 (1980) 13.

[144] W. Busza, et al., (E178), Phys. Rev. Lett. 34 (1975) 836.

[145] W. Busza, Acta Phys. Pol. B 8 (1977) 333.

[146] A. Białas, M. Bleszyński, W. Czyż, Nucl. Phys. B 111 (1976) 461.

[147] J. Whitmore, Phys. Rep. 10 (1974) 273.

[148] J. Whitmore, Phys. Rep. 27 (1976) 187.

[149] H. Bøggild, T. Ferbel, Ann. Rev. Nucl. Sci. 24 (1974) 247.

[150] B. B. Back, et al., (PHOBOS), Phys. Rev. Lett. 87 (2001) 102303.

[151] D. H. Brick, et al., (E565/570), Phys. Rev. D 41 (1990) 765.

[152] C. DeMarzo, et al., (NA5), Phys. Rev. D 29 (1984) 2476.

[153] C. Halliwell, et al., (E178), Phys. Rev. Lett. 39 (1977) 1499.

[154] D. S. Barton, et al., (E451), Phys. Rev. D 27 (1983) 2580.

[155] G. J. Alner, et al., (UA5), Z. Phys. C 33 (1986) 1.

[156] H. Stenzel, (ALEPH), Contributed paper to ICHEP2000 (2000).

[157] PYTHIA manual, T. Sjöstrand, Comp. Phys. Comm. 82 (1994) 74. JETSET 7.4 is currently part of the PYTHIA code.

[158] B. B. Back, et al., (PHOBOS), Phys. Rev. C 71 (2005) 021901(R).

[159] A. M. Rossi, G. Vannini, A. Bussire, E. Albini, D. D'Alessandro, and G. Giacomelli, Nucl. Phys. B 84 (1975) 269.

[160] K. Guettler, et al., Nucl. Phys. B 116 (1976) 77.

[161] M. Banner, et al., (UA2), Phys. Lett. B 122 (1983) 322.

[162] M. Aguilar-Benitez, et al., Z. Phys. C 50 (1991) 405.

[163] G. Arnison, et al., (UA1), Phys. Lett. B 118 (1982) 167.

[164] C. Albajar, et al., (UA1), Nucl. Phys. B 335 (1990) 261.

[165] G. Bocquet, et al., (UA1), Phys. Lett. B 366 (1996) 434.

[166] J. Benecke, T. T. Chou, C. N. Yang, E. Yen, Phys. Rev. 188 (1969) 2159.

[167] T. T. Chou, C.-N. Yang, Phys. Rev. Lett. 25 (1970) 1072.

[168] R. P. Feynman, Phys. Rev. Lett. 23 (1969) 1415.

[169] R. P. Feynman, Photon-Hadron Interactions (W.A. Benjamin Inc., 1972) p. 237-249.

[170] T. Sjöstrand, P. Edén, C. Friberg, L. Lönnblad, G. Miu, S. Mrenna, E. Norrbin, Comp. Phys. Comm. 135 (2001) 238.

[171] T. Sjöstrand, L. Lönnblad, S. Mrenna, P. Skands, arXiv:hep-ph/0308153 (2003).

[172] W. Thomé, et al., Nucl. Phys. B 129 (1977) 365.

[173] P. Abreu, et al., (DELPHI), Phys. Lett. B 459 (1999) 397.

[174] B. Andersson, in Proceedings VII International Colloquium on Multiparticle Reactions, Tutzing, 1976, and references therein.

[175] K. Gottfried, in Proceedings V International Colloquium on Multiparticle Reactions, Uppsala, 1974.

[176] N. N. Nikolaev, Sov. J. Part. Nucl. 12 (1981) 63, and references therein.

[177] L. Stodolsky, in Proceedings VI International Colloquium on Multiparticle Reactions, Oxford, 1975.

[178] I. Otterlund, et al., Nucl. Phys. B 142 (1978) 445, and references therein.

[179] S. Fredriksson, et al., Phys. Rep. 144 (1987) 187, and references therein.

[180] I. G. Bearden, et al., (BRAHMS), arXiv:nucl-ex/0403050 (2004).

[181] I. G. Bearden, et al., (BRAHMS), Phys. Lett. B 523 (2001) 227.

[182] I. G. Bearden, et al., (BRAHMS), Phys. Rev. Lett. 88 (2002) 202301.

[183] P. F. Kolb, Proceedings of the 17th Winter Workshop on Nuclear Dynamics, Park City Utah 2001. Acta Phys. Hung. New Ser. Heavy Ion Phys. 15 (2002) 279; arXiv:nucl-th/0104089 (2001).

[184] B. B. Back, et al., (PHOBOS), Phys. Rev. Lett. 94 (2005) 122303.

[185] R. Hanbury-Brown, R. Q. Twiss, Phil. Mag. Ser. 7, Vol. 45, No. 366 (1954) 663.

[186] R. Hanbury-Brown, R. Q. Twiss, Nature 178 (1956) 1046.

[187] B. Tomasik, U. A. Wiedemann, in Quark-Gluon Plasma 3 (World Scientific, Singapore, 2003); arXiv:hep-ph/0210250.

[188] D. Rischke, M. Gyulassy, Nucl. Phys. A 597 (1996) 701.

[189] T. Hirano, K. Tsuda, Phys. Rev. C 66 (2002) 054905.

[190] S. Soff, arXiv:hep-ph/0202240 (2002).

[191] S. Pratt, Phys. Rev. D 33 (1986) 1314.

[192] B. B. Back, et al., (PHOBOS), submitted to Phys. Rev. C (RC); arXiv:nucl-ex/0409001 (2004).

[193] J. Adams, et al., (STAR), Phys. Rev. Lett. 93 (2004) 012301.

[194] S. S. Adler, et al., (PHENIX), Phys. Rev. Lett. 93 (2004) 152302.

[195] M. D. Baker, Proc. of the Eighteenth Lake Louise Winter Institute; arXiv:nucl-ex/0309002 (2003).

[196] T. Renk, Phys. Rev. C 70 (2004) 021903R.

[197] D. Teaney, arXiv:nucl-th/0301099 (2003).

[198] H. Appelshäuser, et al., (NA49), Eur. Phys. J. C 2 (1998) 661.

[199] R. E. Ansorge, et al., Z. Phys. C 43 (1989) 357.

[200] D. Kharzeev, M Nardi, Phys. Lett. B 507 (2001) 121.

[201] D. Kharzeev, E. Levin, M. Nardi, arXiv:hep-ph/0111315 (2001).

[202] A. Breakstone, et al., Z. Phys. C 69 (1995) 55.

[203] D. Drijard, et al., Nucl. Phys. B 208 (1982) 1.

[204] B. B. Back, et al., (PHOBOS), Nucl. Inst. Meth. A 499 (2003) 603.

[205] B. B. Back, et al., (PHOBOS), Nucl. Inst. Meth. A 447 (2000) 257.

[206] B. B. Back, et al., (PHOBOS), Nucl. Phys. B Proc. Sup. 78 (1999) 245.

[207] B. B. Back, et al., (PHOBOS), Nucl. Inst. Meth. A 419 (1998) 549.

[208] G. F. Bertsch, Nucl. Phys. A 498 (1989) 173.

[209] U. Heinz, Nucl. Phys. A 610 (1996) 264.

[210] F. Yano, S. Koonin, Phys. Lett. B 78 (1978) 556.

[211] M. Podgoretskii, Sov. J. Nucl. Phys. 37 (1983) 272.

STAR

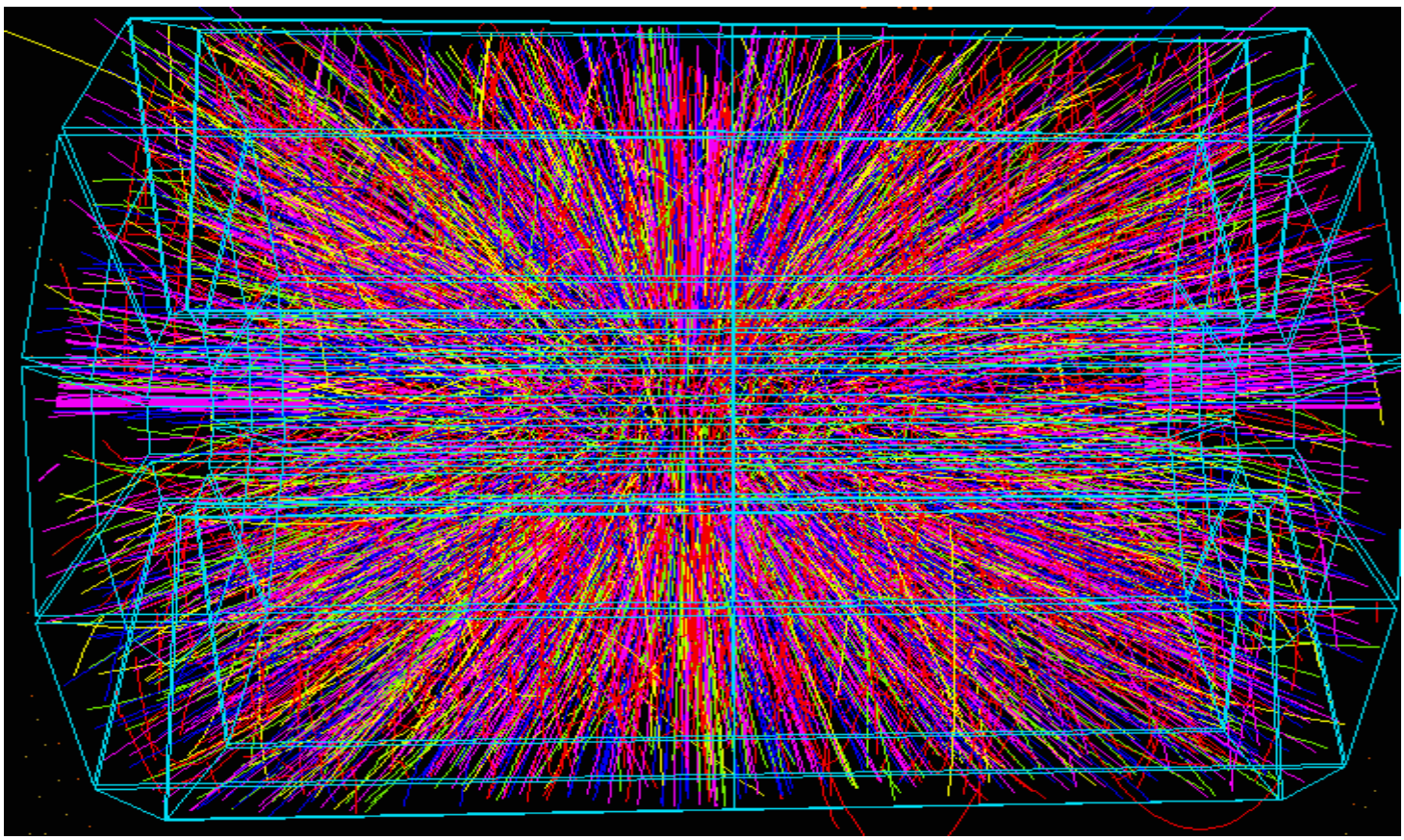

Experimental and Theoretical Challenges in the Search for the Quark Gluon Plasma:

The STAR Collaboration's Critical Assessment of the Evidence from RHIC Collisions

J. Adams [c] M.M. Aggarwal [ac] Z. Ahammed [aq] J. Amonett [t]
B.D. Anderson [t] D. Arkhipkin [m] G.S. Averichev [ℓ] S.K. Badyal [s]
Y. Bai [aa] J. Balewski [q] O. Barannikova [af] L.S. Barnby [c]
J. Baudot [r] S. Bekele [ab] V.V. Belaga [ℓ]
A. Bellingeri-Laurikainen [aℓ] R. Bellwied [at] J. Berger [n]
B.I. Bezverkhny [av] S. Bharadwaj [ag] A. Bhasin [s] A.K. Bhati [ac]
V.S. Bhatia [ac] H. Bichsel [as] J. Bielcik [av] J. Bielcikova [av]
A. Billmeier [at] L.C. Bland [d] C.O. Blyth [c] B.E. Bonner [ah]
M. Botje [aa] A. Boucham [aℓ] J. Bouchet [aℓ] A.V. Brandin [y]
A. Bravar [d] M. Bystersky [k] R.V. Cadman [a] X.Z. Cai [ak]
H. Caines [av] M. Calderón de la Barca Sánchez [q] J. Castillo [u]
O. Catu [av] D. Cebra [g] Z. Chajecki [ab] P. Chaloupka [k]
S. Chattopadhyay [aq] H.F. Chen [aj] Y. Chen [h] J. Cheng [ao]
M. Cherney [j] A. Chikanian [av] W. Christie [d] J.P. Coffin [r]
T.M. Cormier [at] J.G. Cramer [as] H.J. Crawford [f] D. Das [aq]
S. Das [aq] M.M. de Moura [ai] T.G. Dedovich [ℓ]
A.A. Derevschikov [ae] L. Didenko [d] T. Dietel [n] S.M. Dogra [s]
W.J. Dong [h] X. Dong [aj] J.E. Draper [g] F. Du [av] A.K. Dubey [o]
V.B. Dunin [ℓ] J.C. Dunlop [d] M.R. Dutta Mazumdar [aq]
V. Eckardt [w] W.R. Edwards [u] L.G. Efimov [ℓ] V. Emelianov [y]
J. Engelage [f] G. Eppley [ah] B. Erazmus [aℓ] M. Estienne [aℓ]
P. Fachini [d] J. Faivre [r] R. Fatemi [q] J. Fedorisin [ℓ] K. Filimonov [u]
P. Filip [k] E. Finch [av] V. Fine [d] Y. Fisyak [d] J. Fu [ao]
C.A. Gagliardi [am] L. Gaillard [c] J. Gans [av] M.S. Ganti [aq]

Preprint submitted to Nuclear Physics A *28 March 2005*

F. Geurts [ah] V. Ghazikhanian [h] P. Ghosh [aq] J.E. Gonzalez [h]
H. Gos [ar] O. Grachov [at] O. Grebenyuk [aa] D. Grosnick [ap]
S.M. Guertin [h] Y. Guo [at] A. Gupta [s] T.D. Gutierrez [g]
T.J. Hallman [d] A. Hamed [at] D. Hardtke [u] J.W. Harris [av]
M. Heinz [b] T.W. Henry [am] S. Hepplemann [ad] B. Hippolyte [r]
A. Hirsch [af] E. Hjort [u] G.W. Hoffmann [an] H.Z. Huang [h]
S.L. Huang [aj] E.W. Hughes [e] T.J. Humanic [ab] G. Igo [h]
A. Ishihara [an] P. Jacobs [u] W.W. Jacobs [q] M. Jedynak [ar]
H. Jiang [h] P.G. Jones [c] E.G. Judd [f] S. Kabana [b] K. Kang [ao]
M. Kaplan [i] D. Keane [t] A. Kechechyan [ℓ] V.Yu. Khodyrev [ae]
J. Kiryluk [v] A. Kisiel [ar] E.M. Kislov [ℓ] J. Klay [u] S.R. Klein [u]
D.D. Koetke [ap] T. Kollegger [n] M. Kopytine [t] L. Kotchenda [y]
M. Kramer [z] P. Kravtsov [y] V.I. Kravtsov [ae] K. Krueger [a]
C. Kuhn [r] A.I. Kulikov [ℓ] A. Kumar [ac] R.Kh. Kutuev [m]
A.A. Kuznetsov [ℓ] M.A.C. Lamont [av] J.M. Landgraf [d] S. Lange [n]
F. Laue [d] J. Lauret [d] A. Lebedev [d] R. Lednicky [ℓ] S. Lehocka [ℓ]
M.J. LeVine [d] C. Li [aj] Q. Li [at] Y. Li [ao] G. Lin [av]
S.J. Lindenbaum [z] M.A. Lisa [ab] F. Liu [au] H. Liu [aj] L. Liu [au]
Q.J. Liu [as] Z. Liu [au] T. Ljubicic [d] W.J. Llope [ah] H. Long [h]
R.S. Longacre [d] M. Lopez-Noriega [ab] W.A. Love [d] Y. Lu [au]
T. Ludlam [d] D. Lynn [d] G.L. Ma [ak] J.G. Ma [h] Y.G. Ma [ak]
D. Magestro [ab] S. Mahajan [s] D.P. Mahapatra [o] R. Majka [av]
L.K. Mangotra [s] R. Manweiler [ap] S. Margetis [t] C. Markert [t]
L. Martin [aℓ] J.N. Marx [u] H.S. Matis [u] Yu.A. Matulenko [ae]
C.J. McClain [a] T.S. McShane [j] F. Meissner [u] Yu. Melnick [ae]
A. Meschanin [ae] M.L. Miller [v] N.G. Minaev [ae] C. Mironov [t]
A. Mischke [aa] D.K. Mishra [o] J. Mitchell [ah] B. Mohanty [aq]
L. Molnar [af] C.F. Moore [an] D.A. Morozov [ae] M.G. Munhoz [ai]
B.K. Nandi [aq] S.K. Nayak [s] T.K. Nayak [aq] J.M. Nelson [c]
P.K. Netrakanti [aq] V.A. Nikitin [m] L.V. Nogach [ae]
S.B. Nurushev [ae] G. Odyniec [u] A. Ogawa [d] V. Okorokov [y]
M. Oldenburg [u] D. Olson [u] S.K. Pal [aq] Y. Panebratsev [ℓ]
S.Y. Panitkin [d] A.I. Pavlinov [at] T. Pawlak [ar] T. Peitzmann [aa]
V. Perevoztchikov [d] C. Perkins [f] W. Peryt [ar] V.A. Petrov [at]
S.C. Phatak [o] R. Picha [g] M. Planinic [aw] J. Pluta [ar] N. Porile [af]

J. Porter [as] A.M. Poskanzer [u] M. Potekhin [d] E. Potrebenikova [ℓ]
B.V.K.S. Potukuchi [s] D. Prindle [as] C. Pruneau [at] J. Putschke [w]
G. Rakness [ad] R. Raniwala [ag] S. Raniwala [ag] O. Ravel [aℓ]
R.L. Ray [an] S.V. Razin [ℓ] D. Reichhold [af] J.G. Reid [as]
J. Reinnarth [aℓ] G. Renault [aℓ] F. Retiere [u] A. Ridiger [y]
H.G. Ritter [u] J.B. Roberts [ah] O.V. Rogachevskiy [ℓ] J.L. Romero [g]
A. Rose [u] C. Roy [aℓ] L. Ruan [aj] M. Russcher [aa] R. Sahoo [o]
I. Sakrejda [u] S. Salur [av] J. Sandweiss [av] M. Sarsour [q] I. Savin [m]
P.S. Sazhin [ℓ] J. Schambach [an] R.P. Scharenberg [af] N. Schmitz [w]
J. Seger [j] P. Seyboth [w] E. Shahaliev [ℓ] M. Shao [aj] W. Shao [e]
M. Sharma [ac] W.Q. Shen [ak] K.E. Shestermanov [ae]
S.S. Shimanskiy [ℓ] E Sichtermann [u] F. Simon [w] R.N. Singaraju [aq]
N. Smirnov [av] R. Snellings [aa] G. Sood [ap] P. Sorensen [u]
J. Sowinski [q] J. Speltz [r] H.M. Spinka [a] B. Srivastava [af]
A. Stadnik [ℓ] T.D.S. Stanislaus [ap] R. Stock [n] A. Stolpovsky [at]
M. Strikhanov [y] B. Stringfellow [af] A.A.P. Suaide [ai]
E. Sugarbaker [ab] C. Suire [d] M. Sumbera [k] B. Surrow [v]
M. Swanger [j] T.J.M. Symons [u] A. Szanto de Toledo [ai] A. Tai [h]
J. Takahashi [ai] A.H. Tang [aa] T. Tarnowsky [af] D. Thein [h]
J.H. Thomas [u] S. Timoshenko [y] M. Tokarev [ℓ] S. Trentalange [h]
R.E. Tribble [am] O.D. Tsai [h] J. Ulery [af] T. Ullrich [d]
D.G. Underwood [a] G. Van Buren [d] M. van Leeuwen [u]
A.M. Vander Molen [x] R. Varma [p] I.M. Vasilevski [m]
A.N. Vasiliev [ae] R. Vernet [r] S.E. Vigdor [q] Y.P. Viyogi [aq]
S. Vokal [ℓ] S.A. Voloshin [at] W.T. Waggoner [j] F. Wang [af]
G. Wang [t] G. Wang [e] X.L. Wang [aj] Y. Wang [an] Y. Wang [ao]
Z.M. Wang [aj] H. Ward [an] J.W. Watson [t] J.C. Webb [q]
G.D. Westfall [x] A. Wetzler [u] C. Whitten Jr. [h] H. Wieman [u]
S.W. Wissink [q] R. Witt [b] J. Wood [h] J. Wu [aj] N. Xu [u] Z. Xu [d]
Z.Z. Xu [aj] E. Yamamoto [u] P. Yepes [ah] V.I. Yurevich [ℓ]
I. Zborovsky [k] H. Zhang [d] W.M. Zhang [t] Y. Zhang [aj]
Z.P. Zhang [aj] R. Zoulkarneev [m] Y. Zoulkarneeva [m]
A.N. Zubarev [ℓ]

STAR Collaboration

[a] *Argonne National Laboratory, Argonne, Illinois 60439, USA*
[b] *University of Bern, 3012 Bern, Switzerland*
[c] *University of Birmingham, Birmingham, United Kingdom*
[d] *Brookhaven National Laboratory, Upton, New York 11973, USA*
[e] *California Institute of Technology, Pasadena, California 91125, USA*
[f] *University of California, Berkeley, California 94720, USA*
[g] *University of California, Davis, California 95616, USA*
[h] *University of California, Los Angeles, California 90095, USA*
[i] *Carnegie Mellon University, Pittsburgh, Pennsylvania 15213, USA*
[j] *Creighton University, Omaha, Nebraska 68178, USA*
[k] *Nuclear Physics Institute AS CR, 250 68 Řež/Prague, Czech Republic*
[ℓ] *Laboratory for High Energy (JINR), Dubna, Russia*
[m] *Particle Physics Laboratory (JINR), Dubna, Russia*
[n] *University of Frankfurt, Frankfurt, Germany*
[o] *Institute of Physics, Bhubaneswar 751005, India*
[p] *Indian Institute of Technology, Mumbai, India*
[q] *Indiana University, Bloomington, Indiana 47408, USA*
[r] *Institut de Recherches Subatomiques, Strasbourg, France*
[s] *University of Jammu, Jammu 180001, India*
[t] *Kent State University, Kent, Ohio 44242, USA*
[u] *Lawrence Berkeley National Laboratory, Berkeley, California 94720, USA*
[v] *Massachusetts Institute of Technology, Cambridge, MA 02139-4307*
[w] *Max-Planck-Institut für Physik, Munich, Germany*
[x] *Michigan State University, East Lansing, Michigan 48824, USA*
[y] *Moscow Engineering Physics Institute, Moscow Russia*
[z] *City College of New York, New York City, New York 10031, USA*
[aa] *NIKHEF and Utrecht University, Amsterdam, The Netherlands*
[ab] *Ohio State University, Columbus, Ohio 43210, USA*
[ac] *Panjab University, Chandigarh 160014, India*
[ad] *Pennsylvania State University, University Park, Pennsylvania 16802, USA*
[ae] *Institute of High Energy Physics, Protvino, Russia*
[af] *Purdue University, West Lafayette, Indiana 47907, USA*
[ag] *University of Rajasthan, Jaipur 302004, India*
[ah] *Rice University, Houston, Texas 77251, USA*
[ai] *Universidade de Sao Paulo, Sao Paulo, Brazil*
[aj] *University of Science & Technology of China, Anhui 230027, China*

[ak] *Shanghai Institute of Applied Physics, Shanghai 201800, China*
[al] *SUBATECH, Nantes, France*
[am] *Texas A&M University, College Station, Texas 77843, USA*
[an] *University of Texas, Austin, Texas 78712, USA*
[ao] *Tsinghua University, Beijing 100084, China*
[ap] *Valparaiso University, Valparaiso, Indiana 46383, USA*
[aq] *Variable Energy Cyclotron Centre, Kolkata 700064, India*
[ar] *Warsaw University of Technology, Warsaw, Poland*
[as] *University of Washington, Seattle, Washington 98195, USA*
[at] *Wayne State University, Detroit, Michigan 48201, USA*
[au] *Institute of Particle Physics, CCNU (HZNU), Wuhan 430079, China*
[av] *Yale University, New Haven, Connecticut 06520, USA*
[aw] *University of Zagreb, Zagreb, HR-10002, Croatia*

Abstract

We review the most important experimental results from the first three years of nucleus-nucleus collision studies at RHIC, with emphasis on results from the STAR experiment, and we assess their interpretation and comparison to theory. The theory-experiment comparison suggests that central Au+Au collisions at RHIC produce dense, rapidly thermalizing matter characterized by: (1) initial energy densities above the critical values predicted by lattice QCD for establishment of a Quark-Gluon Plasma (QGP); (2) nearly ideal fluid flow, marked by constituent interactions of very short mean free path, established most probably at a stage preceding hadron formation; and (3) opacity to jets. Many of the observations are consistent with models incorporating QGP formation in the early collision stages, and have not found ready explanation in a hadronic framework. However, the measurements themselves do not yet establish unequivocal evidence for a transition to this new form of matter. The theoretical treatment of the collision evolution, despite impressive successes, invokes a suite of distinct models, degrees of freedom and assumptions of as yet unknown quantitative consequence. We pose a set of important open questions, and suggest additional measurements, at least some of which should be addressed in order to establish a compelling basis to conclude definitively that thermalized, deconfined quark-gluon matter has been produced at RHIC.

Key words:
PACS: 25.75.-q

Contents

1 Introduction

The Relativistic Heavy Ion Collider was built to create and investigate strongly interacting matter at energy densities unprecedented in a laboratory setting – matter so hot that neutrons, protons and other hadrons are expected to "melt". Results from the four RHIC experiments already demonstrate that the facility has fulfilled its promise to reach such extreme conditions during the early stages of nucleus-nucleus collisions, forming matter that exhibits heretofore unobserved behavior. These results are summarized in this work and in a number of excellent recent reviews [1–5]. They afford RHIC the exciting scientific opportunity to discover the properties of matter under conditions believed to pertain during a critical, though fleeting, stage of the universe's earliest development following the Big Bang. The properties of such matter test fundamental predictions of Quantum ChromoDynamics (QCD) in the non-perturbative regime.

In this document we review the results to date from RHIC experiments, with emphasis on those from STAR, in the context of a narrower, more pointed question. The specific prediction of QCD most often highlighted in discussions of RHIC since its conception is that of a transition from hadronic matter to a Quark-Gluon Plasma (QGP) phase, defined below. Recent theoretical claims [6–8] that a type of QGP has indeed been revealed by RHIC experiments and interest in this subject by the popular press [9,10] make it especially timely to evaluate where we are with respect to this particular goal. The present paper has been written in response to a charge (see Appendix A) from the STAR Collaboration to itself, to assess whether RHIC results yet support a compelling discovery claim for the QGP, applying the high standards of scientific proof merited by the importance of this issue. We began this assessment before the end of the fourth successful RHIC running period, and we have based our evaluation on results from the first three RHIC runs, which are often dramatic, sometimes unexpected, and generally in excellent agreement among the four RHIC experiments (and we utilize results from all of the experiments here). Since we began, some analyses of data from run 4 have progressed to yield publicly presented results that amplify or quantify some of our conclusions in this work, but do not contradict any of them.

In addressing our charge, it is critical to begin by defining clearly what we mean by the QGP, since theoretical expectations of its properties have evolved significantly over the 20 years since the case for RHIC was first made. For our purposes here, we take the QGP to be **a (locally) thermally equilibrated state of matter in which quarks and gluons are deconfined from hadrons, so that color degrees of freedom become manifest over *nuclear*, rather than merely nucleonic, volumes**. In concentrating on thermalization and deconfinement, we believe our definition to be consistent

with what has been understood by the physics community at large since RHIC was first proposed, as summarized by planning documents quoted in Appendix B. In particular, thermalization is viewed as a necessary condition to be dealing with a state of matter, whose properties can be meaningfully compared to QCD predictions or applied to the evolution of the early universe. Observation of a deconfinement transition has always been a primary goal for RHIC, in the hope of illuminating the detailed mechanism of the normal color confinement in QCD. For reasons presented below, we do significantly omit from our list of necessary conditions some other features discussed as potentially relevant over the years since RHIC's conception.

- We do not demand that the quarks and gluons in the produced matter be non-interacting, as has been considered in some conceptions of the QGP. Lattice QCD calculations suggest that such an ideal state may be approached in static bulk QGP matter only at temperatures very much higher than that required for the deconfinement transition. Furthermore, attainment of thermalization on the ultra-short timescale of a RHIC collision must rely on frequent interactions among the constituents during the earliest stages of the collision – a requirement that is not easily reconcilable with production of an ideal gas. While the absence of interaction would allow considerable simplifications in the calculation of thermodynamic properties of the matter, we do not regard this as an essential feature of color-deconfined matter. In this light, some have suggested [6–8] that we label the matter we seek as the sQGP, for strongly-interacting Quark-Gluon Plasma. Since we regard this as the form of QGP that should be normally anticipated, we consider the 's' qualifier to be superfluous.
- We do not require evidence of a first- or second-order phase transition, even though early theoretical conjecture [11] often focused on possible QGP signatures involving sharp changes in experimental observables with collision energy density. In fact, the nature of the predicted transition from hadron gas to QGP has only been significantly constrained by quite recent theory. Our definition allows for a QGP discovery in a thermodynamic regime beyond a possible critical point. Most modern lattice QCD calculations indeed suggest the existence of such a critical point at baryon densities well above those where RHIC collisions appear to first form the matter. Nonetheless, such calculations still predict a rapid (but unaccompanied by discontinuities in thermodynamic observables) crossover transition in the bulk properties of strongly interacting matter at zero baryon density.
- We consider that evidence for chiral symmetry restoration would be sufficient to demonstrate a new form of matter, but is not *necessary* for a compelling QGP discovery. Most lattice QCD calculations do predict that this transition will accompany deconfinement, but the question is certainly not definitively decided theoretically. If clear evidence for deconfinement can be provided by the experiments, then the search for manifestations of chiral symmetry restoration will be one of the most profound goals of

further investigation of the matter's properties, as they would provide the clearest evidence for fundamental modifications to the QCD vacuum, with potentially far-reaching consequences.

The above "relaxation" of demands, in comparison to initial expectations before initiation of the RHIC program, makes a daunting task even more challenging. The possible absence of a first- or second-order phase transition reduces hopes to observe some well-marked changes in behavior that might serve as an experimental "smoking gun" for a transition to a new form of matter. Indeed, even if there were a sharp transition as a function of bulk matter temperature, it would be unlikely to observe non-smooth behavior in heavy-ion collisions, which form finite-size systems spanning some range of local temperatures even at fixed collision energy or centrality. We thus have to rely more heavily for evidence of QGP formation on the comparison of experimental results with theory. But theoretical calculation of the properties of this matter become subject to all the complexities of strong QCD interactions, and hence to the technical limitations of lattice gauge calculations. Even more significantly, these QCD calculations must be supplemented by other models to describe the complex dynamical passage of heavy-ion collision matter into and out of the QGP state. Heavy ion collisions represent our best opportunity to make this unique matter in the laboratory, but we place exceptional demands on these collisions: they must not only produce the matter, but then must serve "pump and probe" functions somewhat analogous to the modern generation of condensed matter instruments – and they must do it all on distance scales of femtometers and a time scale of 10^{-23} seconds!

There are two basic classes of probes at our disposal in heavy ion collisions. In studying electroweak collision products, we exploit the *absence* of final-state interactions (FSI) with the evolving strongly interacting matter, hoping to isolate those produced during the early collision stages and bearing the imprints of the bulk properties characterizing those stages. But we have to deal with the relative scarcity of such products, and competing origins from hadron decay and interactions during later collision stages. Most of the RHIC results to date utilize instead the far more abundant produced hadrons, where one exploits (but then must understand) the FSI. It becomes critical to distinguish *partonic* FSI from *hadronic* FSI, and to distinguish both from initial-state interactions and the effects of (so far) poorly understood parton densities at very low momentum fraction in the entrance-channel nuclei. Furthermore, the formation of hadrons from a QGP involves soft processes (parton fragmentation and recombination) that cannot be calculated from perturbative QCD and are *a priori* not well characterized (nor even cleanly separable) inside hot strongly interacting matter.

In light of all these complicating features, it is remarkable that the RHIC experiments have already produced results that appear to confirm some of the

more striking, and at least semi-quantitative, predictions made on the basis of QGP formation! Other, unexpected, RHIC results have stimulated new models that explain them within a QGP-based framework. The most exciting results reveal phenomena not previously observed or explored at lower center-of-mass energies, and indeed are distinct from the observations on which a circumstantial case for QGP formation was previously argued at CERN [12]. In order to assess whether a discovery claim is now justified, we must judge the robustness of both the new experimental results and the theoretical predictions they seem to bear out. Do the RHIC data *demand* a QGP explanation? Can they alternatively be accounted for in a hadronic framework? Are the theories and models used for the predictions mutually compatible? Are those other experimental results that currently appear to deviate from theoretical expectations indicative of details yet to be worked out, or rather of fundamental problems with the QGP explanation?

We organize our discussion as follows. In Chapter 2 we briefly summarize the most relevant theoretical calculations and models, their underlying assumptions, limitations and most robust predictions. We thereby identify the *crucial* QGP features we feel must be demonstrated experimentally to justify a compelling discovery claim. We divide the experimental evidence into two broad areas in Chapters 3-4, focusing first on what we have learned about the bulk thermodynamic properties of the early stage collision matter from such measures as hadron spectra, collective flow and correlations among the soft hadrons that constitute the vast majority of outgoing particles. We discuss the consistency of these results with thermalization and the exposure of new (color) degrees of freedom. Next we provide an overview of the observations of hadron production yields and angular correlations at high transverse momentum ($p_T \gtrsim 4$ GeV/c), and what they have taught us about the nature of FSI in the collision matter and their bearing on deconfinement. In discussing the evidence, we occasionally rely on preliminary STAR data presented at conferences or in preprints, but not yet published on their own. While it is conceivable that small changes may yet occur in the precise values or uncertainties of experimental results in the preliminary figures, we are confident that the conclusions drawn from these data in this paper would not be affected.

In Chapter 5 we focus on open questions for experiment and theory, on important crosschecks and quantifications, on predictions not yet borne out by experiment and experimental results not yet accommodated by theory. Finally, we provide in Chapter 6 an extended summary, conclusions and outlook, with emphasis on additional measurements and theoretical improvements that we feel are needed to strengthen the case for QGP formation. The summary of results in Chap. 6 is extended so that readers already familiar with most of the theoretical and experimental background material covered in Chaps. 2-5 can skip to the concluding section without missing the arguments central to our assessment of the evidence.

The STAR detector and its capabilities have been described in detail elsewhere [13], and will not be discussed.

2 Predicted Signatures of the QGP

The promise, and then the delivery, of experimental results from the AGS, SPS and RHIC have stimulated impressive and important advances over the past decade in the theoretical treatment of the thermodynamic and hydrodynamic properties of hot strongly interacting matter and of the propagation of partons through such matter. However, the complexities of heavy-ion collisions and of hadron formation still lead to a patchwork of theories and models to treat the entire collision evolution, and the difficulties of the strong interaction introduce significant quantitative ambiguities in all aspects of this treatment. In support of a possible compelling QGP discovery claim, we must then identify the most striking qualitative predictions of theory, which survive the quantitative ambiguities, and we must look for a congruence of various observations that confirm such robust predictions. In this chapter, we provide a brief summary of the most important pieces of the theoretical framework, their underlying assumptions and quantitative limitations, and what we view as their most robust predictions. Some of these predictions will then be compared with RHIC experimental results in later chapters.

2.1 Features of the Phase Transition in Lattice QCD

The phase diagram of bulk thermally equilibrated strongly interacting matter should be described by QCD. At sufficiently high temperature one must expect hadrons to "melt", deconfining quarks and gluons. The exposure of new (color) degrees of freedom would then be manifested by a rapid increase in entropy density, hence in pressure, with increasing temperature, and by a consequent change in the equation of state (EOS). In the limit where the deconfined quarks and gluons are non-interacting, and the quarks are massless, the (Stefan-Boltzmann) pressure P_{SB} of this partonic state, as a function of temperature T at zero chemical potential (*i.e.*, zero net quark density), would be simply determined by the number of degrees of freedom [2]:

$$\frac{P_{SB}}{T^4} \;=\; [2(N_c^2-1)+\frac{7}{2}N_cN_f]\frac{\pi^2}{90}, \qquad (1)$$

where N_c is the number of colors, N_f the number of quark flavors, the temperature is measured in energy units (throughout this paper), and we have taken $\hbar = c = 1$. The two terms on the right in Eq. 1 represent the gluon and quark contributions, respectively. Refinements to this basic expectation, to incorporate effects of color interactions among the constituents, as well as of non-vanishing quark masses and chemical potential, and to predict the location and nature of the transition from hadronic to partonic degrees of freedom,

are best made via QCD calculations on a space-time lattice (LQCD).

In order to extract physically relevant predictions from LQCD calculations, these need to be extrapolated to the continuum (lattice spacing $\rightarrow 0$), chiral (actual current quark mass) and thermodynamic (large volume) limits. While computing power limitations have restricted the calculations to date to numbers of lattice points that are still considered somewhat marginal from the viewpoint of these extrapolations [2], enormous progress has been made in recent years. Within the constraints of computing cost, there have been important initial explorations of sensitivity to details of the calculations [2]: *e.g.*, the number and masses of active quark flavors included; the technical treatment of quarks on the lattice; the presence or absence of the $U_A(1)$ anomaly in the QGP state. Additional numerical difficulties have been partially overcome to allow first calculations at nonzero chemical potential and to improve the determination of physical quark mass scales for a given lattice spacing [2].

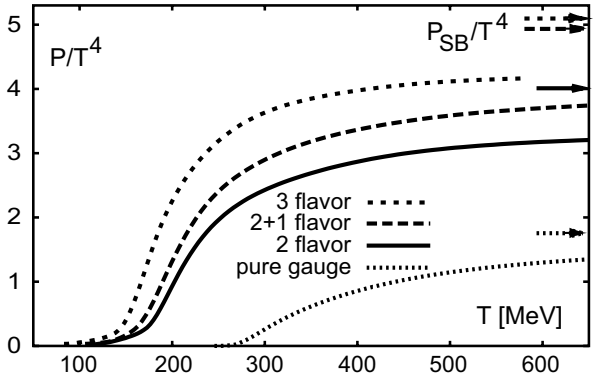

Fig. 1. *LQCD calculation results from Ref. [14] for the pressure divided by T^4 of strongly interacting matter as a function of temperature, and for several different choices of the number of dynamical quark flavors. The arrows near the right axis indicate the corresponding Stefan-Boltzmann pressures for the same quark flavor assumptions.*

Despite the technical complications, LQCD calculations have converged on the following predictions:

- There is indeed a predicted transition of some form between a hadronic and a QGP phase, occurring at a temperature in the vicinity of $T_c \simeq 160$ MeV for zero chemical potential. The precise value of the transition temperature depends on the treatment of quarks in the calculation.
- The pressure divided by T^4 rises rapidly above T_c, then begins to saturate by about $2T_c$, but at values substantially below the Stefan-Boltzmann limit (see Fig. 1) [14]. The deviation from the SB limit indicates substantial remaining interactions among the quarks and gluons in the QGP phase.
- Above T_c, the effective potential between a heavy quark-antiquark pair takes the form of a screened Coulomb potential, with screening mass (or inverse screening length) rising rapidly as temperature increases above T_c

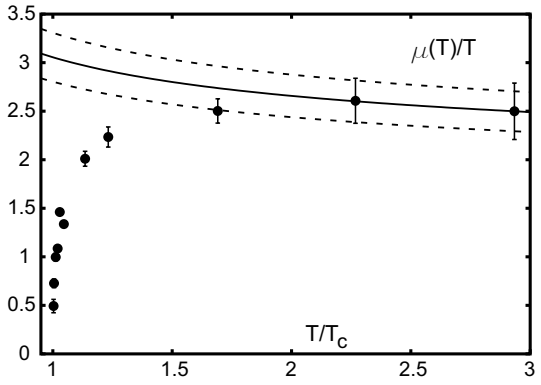

Fig. 2. *Temperature-dependence of the heavy-quark screening mass (divided by temperature) as a function of temperature (in units of the phase transition temperature), from LQCD calculations in Ref. [15]. The curves represent perturbative expectations of the temperature-dependence.*

(see Fig. 2) [15]. As seen in the figure, the screening mass deviates strongly from perturbative QCD expectations in the vicinity of T_c, indicating large non-perturbative effects. The increased screening mass leads to a shortening of the range of the $q\overline{q}$ interaction, and to an anticipated suppression of charmonium production, in relation to open charm [16]. The predicted suppression appears to set in at substantially different temperatures for J/ψ $(1.5 - 2.0T_c)$ and ψ' $(\sim 1.0T_c)$ [17].

- In most calculations, the deconfinement transition is also accompanied by a chiral symmetry restoration transition, as seen in Fig. 3 [14]. The reduction in the chiral condensate leads to significant predicted variations in in-medium meson masses. These are also affected by the restoration of $U_A(1)$ symmetry, which occurs at higher temperature than chiral symmetry restoration in the calculation of Fig. 3.
- The nature of the transition from hadronic to QGP phase is highly sensitive to the number of dynamical quark flavors included in the calculation and to the quark masses [18]. For the most realistic calculations, incorporating two light (u, d) and one heavier (s) quark flavor relevant on the scale of T_c, the transition is most likely of the crossover type (with no discontinuities in thermodynamic observables – as opposed to first- or second-order phase transitions) at zero chemical potential, although the ambiguities in tying down the precise values of quark masses corresponding to given lattice spacings still permit some doubt.
- Calculations at non-zero chemical potential, though not yet mature, suggest the existence of a critical point such as that illustrated in Fig. 4 [19]. The numerical challenges in such calculations leave considerable ambiguity about the value of μ_B at which the critical point occurs (*e.g.*, it changes from $\mu_B \approx 700$ to 350 MeV between Refs. [20] and [19]), but it is most likely above the value at which RHIC collision matter is formed, consistent with the crossover nature of the transition anticipated at RHIC.
- Even for crossover transitions, the LQCD calculations still predict a rapid

temperature-dependence of the thermodynamic properties, as revealed in all of the figures considered above. However, in basing experimental expectations on this feature, it must be kept in mind that the early collision temperature varies slowly with collision energy and is not directly measured by any of the probes studied most extensively to date.

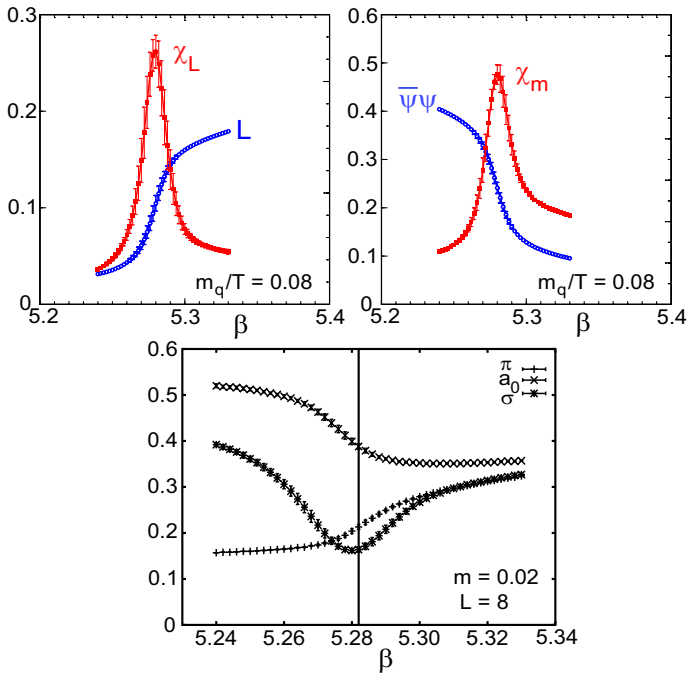

Fig. 3. *LQCD calculations for two dynamical quark flavors [14] showing the coincidence of the chiral symmetry restoration (marked by the rapid decrease of chiral condensate $\langle\overline{\psi}\psi\rangle$ in the upper right-hand frame) and deconfinement (upper left frame) phase transitions. The lower plot shows that the chiral transition leads toward a mass degeneracy of the pion with scalar meson masses. All plots are as a function of the bare coupling strength β used in the calculations; increasing β corresponds to decreasing lattice spacing and to increasing temperature.*

2.2 Hydrodynamic Signatures

In order to determine how the properties of bulk QGP matter, as determined in LQCD calculations, may influence observable particle production spectra from RHIC collisions, one needs to model the time evolution of the collision "fireball". To the extent that the initial interactions among the constituents are sufficiently strong to establish local thermal equilibrium rapidly, and then to maintain it over a significant evolution time, the resulting matter may be treated as a relativistic fluid undergoing collective, hydrodynamic flow [3]. The application of hydrodynamics for the description of hadronic fireballs has a long history [21,22]. Relativistic hydrodynamics has been extensively applied to heavy ion collisions from BEVALAC to RHIC [3,22,23], but with

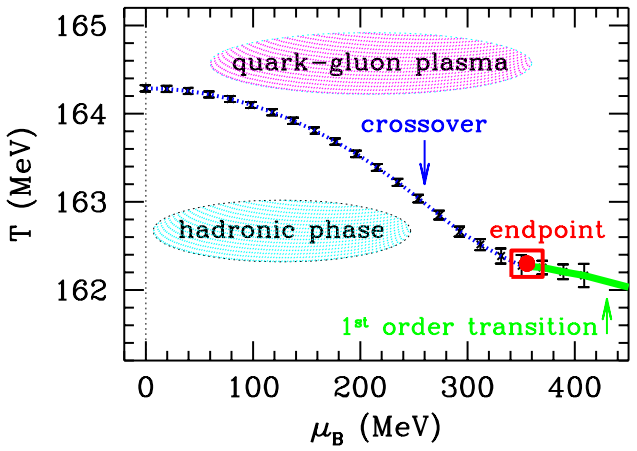

Fig. 4. *LQCD calculation results for non-zero chemical potential [19], suggesting the existence of a critical point well above RHIC chemical potential values. The solid line indicates the locus of first-order phase transitions, while the dotted curve marks crossover transitions between the hadronic and QGP phases.*

the most striking successes at RHIC. The applicability of hydrodynamics at RHIC may provide the clearest evidence for the attainment of local thermal equilibrium at an early stage in these collisions. (On the other hand, there are alternative, non-equilibrium treatments of the fireball evolution that have also been compared to RHIC data [24].) The details of the hydrodynamic evolution are clearly sensitive to the EOS of the flowing matter, and hence to the possible crossing of a phase or crossover transition during the system expansion and cooling. It is critical to understand the relative sensitivity to the EOS as compared with that to other assumptions and parameters of the hydrodynamic treatment.

Traditional hydrodynamics calculations cannot be applied to matter not in local thermal equilibrium, hence they must be supplemented by more phenomenological treatments of the early and late stages of the system evolution. These parameterize the initial conditions for the hydrodynamic flow and the transition to freezeout, where the structureless matter flow is converted into final hadron spectra. Since longitudinal flow is especially sensitive to initial conditions beyond the scope of the theory, most calculations to date have concentrated on *transverse* flow, and have assumed longitudinal boost-invariance of the predictions [3]. Furthermore, it is anticipated that hadrons produced at sufficiently high transverse momentum in initial partonic collisions will not have undergone sufficient rescatterings to come to thermal equilibrium with the surrounding matter, so that hydrodynamics will be applicable at best only for the softer features of observed spectra. Within the time range and momentum range of its applicability, most hydrodynamics calculations to date have treated the matter as an *ideal*, non-viscous fluid. The motion of this fluid is completely determined given the three components of the fluid velocity $\vec{v}$, the

pressure (P) and the energy and baryon densities (e and n_B). The hydrodynamic equations of motion for an ideal fluid are derived from the exact local conservation laws for energy, momentum, and baryon number by assuming an ideal-fluid form for the energy-momentum tensor and baryon number current; they are closed by an equation of state $P(e, n_B)$ [21].

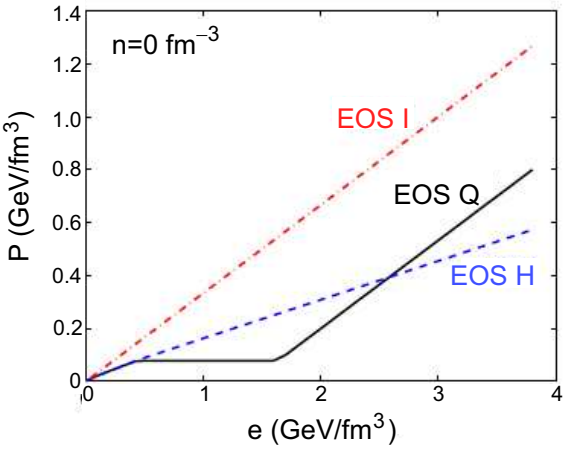

Fig. 5. *Pressure as a function of energy density at vanishing net baryon density for three different equations of state of strongly interacting matter: a Hagedorn resonance gas (EOS H), an ideal gas of massless partons (EOS I) and a connection of the two via a first-order phase transition at T_c=164 MeV (EOS Q). These EOS are used in hydrodynamics calculations in Ref. [3], from which the figure is taken.*

The EOS in hydrodynamics calculations for RHIC has been implemented using simplified models inspired by LQCD results, though not reproducing their details. One example is illustrated by the solid curve in Fig. 5, connecting an ideal gas of massless partons at high temperature to a Hagedorn hadron resonance gas [25] at low temperatures, via a first-order phase transition chosen to ensure consistency with ($\mu_B = 0$) LQCD results for critical temperature and net increase in entropy density across the transition [3]. In this implementation, the slope $\partial P/\partial e$ (giving the square of the velocity of sound in the matter) exhibits high values for the hadron gas and, especially, the QGP phases, but has a soft point at the mixed phase [3,22]. This generic softness of the EOS during the assumed phase transition has predictable consequences for the system evolution.

In heavy ion collisions, the measurable quantities are the momenta of the produced particles at the final state and their correlations. Transverse flow measures are key observables to compare quantitatively with model predictions in studying the EOS of the hot, dense matter. In non-central collisions, the reaction zone has an almond shape, resulting in azimuthally anisotropic pressure gradients, and therefore a nontrivial elliptic flow pattern. Experimentally, this elliptic flow pattern is usually measured using a Fourier decompo-

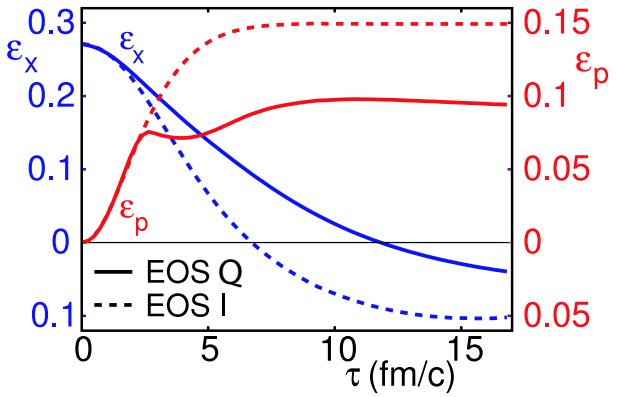

Fig. 6. *Hydrodynamics calculations for the time evolution of the spatial eccentricity ϵ_x and the momentum anisotropy ϵ_p for non-central (7 fm impact parameter) Au+Au collisions at RHIC [3]. The solid and dashed curves result, respectively, from use of EOS Q and EOS I from Fig. 5. The gradual removal of the initial spatial eccentricity by the pressure gradients that lead to the buildup of ϵ_p reflects the self-quenching aspect of elliptic flow. The time scale runs from initial attainment of local thermal equilibrium through freezeout in this calculation.*

sition of momentum spectra relative to the event-by-event reaction plane, in which the second Fourier component v_2 is the dominant contribution. The important feature of elliptic flow is that it is "self-quenching" [26,27], because the pressure-driven expansion tends to reduce the spatial anisotropy that causes the azimuthally anisotropic pressure gradient in the first place. This robust feature is illustrated in Fig. 6, which compares predictions for the spatial and resulting momentum eccentricities as a function of time during the system's hydrodynamic evolution, for two different choices of EOS [3]. The self-quenching makes the elliptic flow particularly sensitive to earlier collision stages, when the spatial anisotropy and pressure gradient are the greatest. In contrast, hadronic interactions at later stages may contribute significantly to the radial flow [28,29].

The solid momentum anisotropy curve in Fig. 6 also illustrates that entry into the soft EOS mixed phase during a transition from QGP to hadronic matter stalls the buildup of momentum anisotropy in the flowing matter. An even more dramatic predicted manifestation of this stall is shown by the dependence of p_T-integrated elliptic flow on produced hadron multiplicity in Fig. 7, where a dip is seen under conditions where the phase transition occupies most of the early collision stage. Since the calculations are carried out for a fixed impact parameter, measurements to confirm such a dip would have to be performed as a function of collision energy. In contrast to early (non-hydrodynamic) projections of particle multiplicities at RHIC (represented by horizontal arrows in Fig. 7), we now know that the multiplicity at the predicted dip is approximately achieved for appropriate centrality in RHIC Au+Au collisions at full energy. However, comparisons of predicted with measured excitation functions

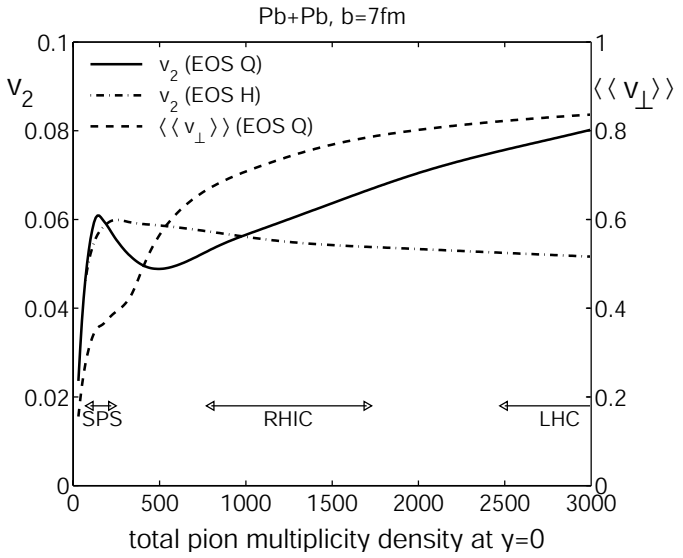

Fig. 7. *Predicted hydrodynamic excitation function of p_T-integrated elliptic (v_2, solid curve, left axis) and radial ($\langle\langle v_\perp \rangle\rangle$, dashed, right axis) flow for non-central Pb+Pb collisions [30]. The calculations assume a sharp onset for freezeout along a surface of constant energy density corresponding to temperature $\approx$ 120 MeV. The soft phase transition stage in EOS Q gives rise to a dip in the elliptic flow. The horizontal arrows at the bottom reflect early projections of particle multiplicity for different facilities, but we now know that RHIC collisions produce multiplicities in the vicinity of the predicted dip.*

for elliptic flow are subject to an overriding ambiguity concerning where and when appropriate conditions of initial local thermal equilibrium for hydrodynamic applicability are actually achieved. Hydrodynamics itself has nothing to say concerning this issue.

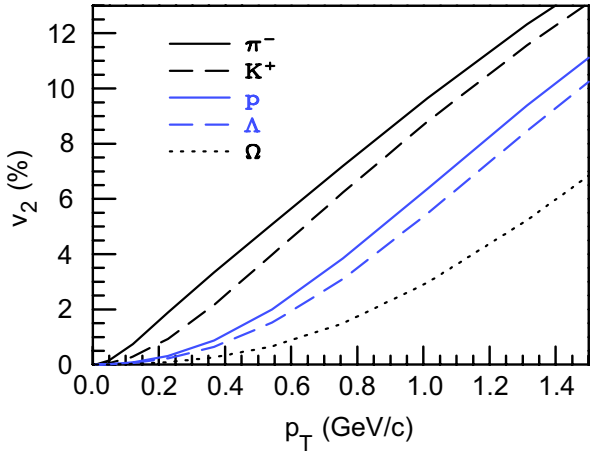

Fig. 8. *Hydrodynamics predictions [32] of the p_T and mass-dependences of the elliptic flow parameter v_2 for identified final hadrons from Au+Au collisions at $\sqrt{s_{NN}}$=130 GeV. The calculations employ EOS Q (see Fig. 5) and freezeout near 120 MeV.*

One can alternatively attain sensitivity to the EOS in measurements for given

collision energy and centrality by comparing to the predicted dependence of elliptic flow strength on hadron p_T and mass (see Fig. 8). The mass-dependence is of simple kinematic origin [3], and is thus a robust feature of hydrodynamics, but its quantitative extent, along with the magnitude of the flow itself, depends on the EOS [3].

Of course, the energy- and mass-dependence of v_2 can also be affected by species-specific hadronic FSI at and close to the freezeout where the particles decouple from the system, and hydrodynamics is no longer applicable [28,29]. A combination of macroscopic and microscopic models, with hydrodynamics applied at the early partonic and mixed-phase stages and a hadronic transport model such as RQMD [31] at the later hadronic stage, may offer a more realistic description of the whole evolution than that achieved with a simplified sharp freezeout treatment in Figs. 6,7,8. The combination of hydrodynamics with RQMD [29] has, for example, led to predictions of a substantially different, and monotonic, energy-dependence of elliptic flow, as can be seen by comparing Fig. 9 to Fig. 7. The difference between the two calculations may result primarily [6] from the elimination in [29] of the assumption of ideal fluid expansion even in the hadronic phase. In any case, this comparison suggests that the energy dependence of elliptic flow in the quark-hadron transition region is at least as sensitive to the late hadronic interaction details as to the softening of the EOS in the mixed-phase region. Flow for multi-strange and charmed particles with small hadronic interaction cross sections may provide more selective sensitivity to the properties of the partonic and mixed phases [29,33,34]. There may be non-negligible sensitivity as well to the addition of such other complicating features as viscosity [35] and deviations from longitudinal boost-invariance, studies of the latter effect requiring computationally challenging (3+1)-dimensional hydrodynamics calculations [36]. Certainly, the relative sensitivities to EOS variations vs. treatments of viscosity, boost-invariance, and the evolution of the hadronic stage must be clearly understood in order to interpret agreement between hydrodynamics calculations and measured flow.

In addition to predicting one-body hadron momentum spectra as a function of many kinematic variables, hydrodynamic evolution of the matter is also relevant for understanding two-hadron Hanbury-Brown-Twiss (HBT) quantum correlation functions [5]. From these correlation measurements one can extract information concerning the size and shape of the emitting surface at freezeout, *i.e.*, at the end of the space-time evolution stage treated by hydrodynamics. While the detailed comparison certainly depends on improving models of the freezeout stage, it is reasonable to demand that hydrodynamics calculations consistent with the one-body hadron measurements be also at least roughly consistent with HBT results.

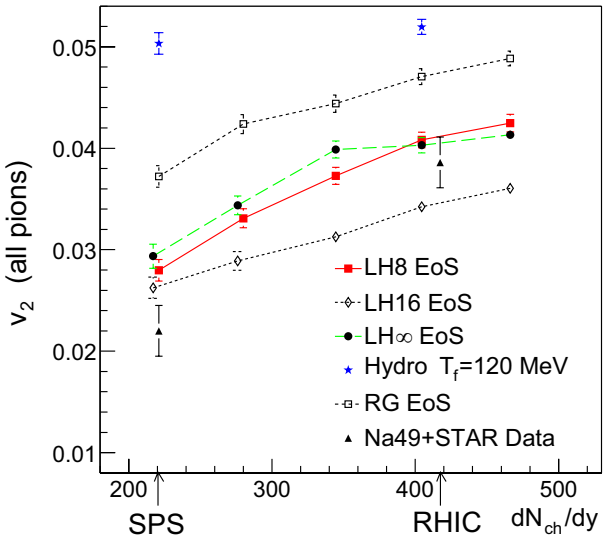

Fig. 9. *Predictions [29] from a hybrid hydrodynamics-RQMD approach for the elliptic flow as a function of charged particle multiplicity in Pb+Pb collisions at an impact parameter $b = 6$ fm. Curves for different choices of EOS (LH8 is most similar to EOS Q in Fig. 7) are compared to experimental results derived [29] from SPS and RHIC measurements. The replacement of a simplified freezeout model for all hadron species and of the assumption of ideal hadronic fluid flow with the RQMD hadron cascade appears to remove any dip in v_2 values, such as seen in Fig. 7.*

2.3 Statistical Models

The aim of statistical models is to derive the equilibrium properties of a macroscopic system from the measured yields of the constituent particles [37,38]. Statistical models, however, do not describe how a system approaches equilibrium [38]. Hagedorn [25] and Fermi [39] pioneered their application to computing particle production yield ratios in high energy collisions, where conserved quantities such as baryon number and strangeness play important roles [40]. Statistical methods have become an important tool to study the properties of the fireball created in high energy heavy ion collisions [37,41], where they succeed admirably in reproducing measured yield ratios. Can this success be taken as evidence that the matter produced in these collisions has reached thermal and chemical equilibrium before hadronization? Can the temperature and chemical potential values extracted from such statistical model fits be interpreted as the equilibrium properties of the collision matter?

The answer to both of the above questions is "not on the basis of fits to integrated yields alone." The essential condition for applicability of statistical models is phase-space dominance in determining the distribution of a system with many degrees of freedom among relatively few observables [39,42], and this does not necessarily reflect a process of thermodynamic equilibration via interactions of the constituents. Indeed, statistical model fits can describe

the observed hadron abundances well (albeit, only by including a strangeness undersaturation factor, $\gamma_s < 1$) in p+p, $e^+ + e^-$ and p+A collisions, where thermal and chemical equilibrium are thought not to be achieved [37] . It is thus desirable to distinguish a system driven towards thermodynamic equilibrium from one born at hadronization with statistical phase space distributions, where "temperature" and "chemical potential" are simply Lagrange multipliers [43]. In order to make this distinction, it is necessary and sufficient to measure the extensive interactions among particles and to observe the change from canonical ensemble in a small system with the size of a nucleon (p+p, $e^+ + e^-$) and tens of produced particles, to grand canonical ensemble in a large system with extended volume and thousands of produced particles (central Au+Au) [37,40].

The evolution of the system from canonical to grand canonical ensemble can be observed, for example, via multi-particle correlations (especially of particles constrained by conservation laws [42]) or by the centrality dependence of the strangeness suppression factor γ_s. The interactions among constituent particles, necessary to attainment of *thermal* equilibrium, can be measured by collective flow of many identified particles [29,44] and by resonance yields [45] that follow their hadronic rescattering cross sections. (Collective flow and resonance formation could, in principle, proceed via the dominant hadronic interactions that do not change hadron species, and hence are not strictly sufficient to establish *chemical* equilibration among hadrons, which would have to rely on relatively weak *inelastic* processes [43].)

If other measurements confirm the applicability of a grand canonical ensemble, then the hadron yield ratios can be used to extract the temperature and chemical potential of the system [37] at chemical freezeout. The latter is defined as the stage where hadrons have been created and the net numbers of stable particles of each type no longer change in further system evolution. These values place constraints on, but do not directly determine, the properties of the matter when thermal equilibrium was first attained in the wake of the collision. Direct measurement of the temperature at this early stage requires characterization of the yields of particles such as photons that are produced early but do not significantly interact on their way out of the collision zone.

2.4 Jet Quenching and Parton Energy Loss

Partons from the colliding nuclei that undergo a hard scattering in the initial stage of the collision provide colored probes for the colored bulk matter that may be formed in the collision's wake. It was Bjorken [46] who first suggested that partons traversing bulk partonic matter might undergo significant energy loss, with observable consequences on the parton's subsequent fragmentation

into hadrons. More recent theoretical studies have demonstrated that the elastic parton scattering contribution to energy loss first contemplated by Bjorken is likely to be quite small, but that gluon radiation induced by passage through the matter may be quite sizable [4]. Such induced gluon radiation would be manifested by a significant softening and broadening of the jets resulting from the fragmentation of partons that traverse substantial lengths of matter containing a high density of partons – a phenomenon called "jet quenching". As will be documented in later chapters, some of the most exciting of the RHIC results reveal jet quenching features quite strikingly. It is thus important to understand what features of this phenomenon may distinguish parton energy loss through a QGP from other possible sources of jet softening and broadening.

Several different theoretical evaluations of the non-Abelian radiative energy loss of partons in dense, but finite, QCD matter have been developed [47–50]. They give essentially consistent results, including the non-intuitive prediction that the energy loss varies with the square (L^2) of the thickness traversed through static matter, as a consequence of destructive interference effects in the coherent system of the leading quark and its first radiated gluon as they propagate through the matter. The overall energy loss is reduced, and the L-dependence shifted toward linearity, by the expansion of the matter resulting from heavy ion collisions. The significant deformation of the collision zone for non-central collisions, responsible for the observed elliptic flow (hence also for an azimuthal dependence of the rate of matter expansion), should give rise to a significant variation of the energy loss with angle with respect to the impact parameter plane. The scale of the net energy loss depends on factors that can all be related to the rapidity density of gluons (dN_g/dy) in the matter traversed.

The energy loss calculated via any of these approaches is then embedded in a perturbative QCD (pQCD) treatment of the hard parton scattering. The latter treatment makes the standard factorization assumption (untested in the many-nucleon environment) that the cross section for producing a given final-state high-p_T hadron can be written as the product of suitable initial-state parton densities, pQCD hard-scattering cross section, and final-state fragmentation functions for the scattered partons. Nuclear modifications must be expected for the initial parton densities as well as for the fragmentation functions. Entrance-channel modifications – including both nuclear shadowing of parton densities and the introduction by multiple scattering of additional transverse momentum to the colliding partons – are capable of producing some broadening and softening of the final-state jets. But these effects can, in principle, be calibrated by complementing RHIC A+A collision studies with p+A or d+A, where QGP formation is not anticipated.

The existing theoretical treatments of the final-state modifications attribute

the changes in effective fragmentation functions to the parton energy loss. That is, they assume vacuum fragmentation (as characterized phenomenologically from jet studies in more elementary systems) of the degraded parton and its spawned gluons [4]. This assumption may be valid in the high-energy limit, when the dilated fragmentation time should exceed the traversal time of the leading parton through the surrounding matter. However, its justification seems questionable for the soft radiated gluons and over the leading-parton momentum ranges to which it has been applied so far for RHIC collisions. In these cases, one might expect hadronization to be aided by the pickup of other partons from the surrounding QGP, and not to rely solely on the production of $q\overline{q}$ pairs from the vacuum. Indeed, RHIC experimental results to be described later in this document hint that the distinction between such recombination processes and parton fragmentation in the nuclear environment may not be clean. Furthermore, one of the developed models of parton energy loss [48] explicitly includes energy *gain* via absorption of gluons from the surrounding thermal QGP bath.

The assumption of vacuum fragmentation also implies a neglect of FSI effects for the hadronic fragmentation products, which might further contribute to jet broadening and softening. Models that attempt to account for *all* of the observed jet quenching via the alternative description of hadron energy loss in a hadronic gas environment are at this time still incomplete [51]. They must contend with the initial expectation of *color transparency* [52], *i.e.*, that high momentum hadrons formed in strongly interacting matter begin their existence as point-like color-neutral particles with very small color dipole moments, hence weak interactions with surrounding nuclear matter. In order to produce energy loss consistent with RHIC measurements, these models must then introduce *ad hoc* assumptions about the rate of growth of these "prehadron" interaction cross sections during traversal of the surrounding matter [51].

The above caveats concerning assumptions of the parton energy loss models may call into question some of their quantitative conclusions, but are unlikely to alter the basic qualitative prediction that substantial jet quenching is a *necessary* result of QGP formation. The more difficult question is whether the observation of jet quenching can also be taken as a *sufficient* condition for a QGP discovery claim? Partonic traversal of matter can, in principle, be distinguished from effects of *hadronic* traversal by detailed dependences of the energy loss, *e.g.*, on azimuthal angle and system size (reflecting the nearly quadratic length-dependence characteristic of gluon radiation), on p_T (since hadron formation times should increase with increasing partonic momentum [53]), or on type of detected hadron (since hadronic energy losses should depend on particle type and size, while partonic energy loss should be considerably reduced for heavy quarks [53,54]). However, the energy loss calculations do not (with the exception of the small quantitative effect of *ab-*

sorption of thermal gluons [48]) distinguish confined from deconfined quarks and gluons in the surrounding matter. Indeed, the same approaches have been applied to experimental results from semi-inclusive deep inelastic scattering [55] or Drell-Yan dilepton production [56] experiments on nuclear targets to infer quark energy losses in *cold*, confined nuclear matter [57]. Baier, *et al.* [58] have shown that the energy loss is expected to vary smoothly with energy density from cold hadronic to hot QGP matter, casting doubt on optimistic speculations [53] that the QGP transition might be accompanied by a rapid change in the extent of jet quenching with collision energy. Thus, the relevance of the QGP can only be inferred indirectly, from the magnitude of the gluon density dN_g/dy needed to reproduce jet quenching in RHIC collision matter, vis-a-vis that needed to explain the energy loss in cold nuclei. Is the extracted gluon density consistent with what one might expect for a QGP formed from RHIC collisions? To address this critical question, one must introduce new theoretical considerations of the initial state for RHIC collisions.

2.5 Saturation of Gluon Densities

In a partonic view, the initial conditions for the expanding matter formed in a RHIC collision are dominated by the scattering of gluons carrying small momentum fractions (Bjorken x) in the nucleons of the colliding nuclei. Gluon densities in the proton have been mapped down to quite small values of $x \sim 10^{-4}$ in deep inelastic scattering experiments at HERA [59]. When the measurements are made with high resolving power (*i.e.*, with large 4-momentum transfer Q^2), the extracted gluon density $xg(x, Q^2)$ continues to grow rapidly down to the lowest x values measured. However, at moderate $Q^2 \sim$ few $(\mathrm{GeV})^2$, there are indications from the HERA data that $xg(x, Q^2)$ begins to saturate, as might be expected from the competition between gluon fusion ($g + g \rightarrow g$) and gluon splitting ($g \rightarrow g + g$) processes. It has been conjectured [60–63] that the onset of this saturation moves to considerably higher x values (for given Q^2) in a nuclear target, compared to a proton, and that a QGP state formed in RHIC collisions may begin with a saturated density of gluons. Indeed, birth within this saturated state might provide a natural mechanism for the rapid achievement of thermal equilibrium in such collisions [60].

The onset of saturation occurs when the product of the cross section for a QCD process (such as gluon fusion) of interest ($\sigma \sim \pi\alpha_s(Q^2)/Q^2$) and the areal density of partons (ρ) available to participate exceeds unity [66]. In this so-called Color Glass Condensate region (see Fig. 10), QCD becomes highly non-linear, but amenable to classical field treatments, because the coupling strength remains weak ($\alpha_s << 1$) while the field strength is large [60–63]. The borderline of the CGC region is denoted by the "saturation scale" $Q_s^2(x, A)$. It depends on both x and target mass number A, because the target gluon density

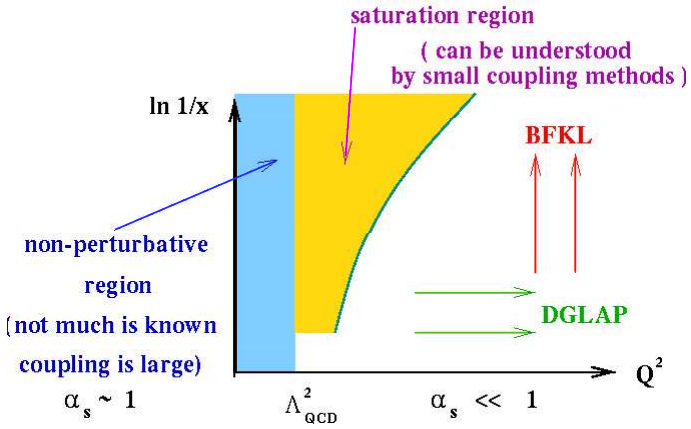

Fig. 10. *Schematic layout of the QCD landscape in $x - Q^2$ space. The region at the right is the perturbative region, marked by applicability of the linear DGLAP[64] and BFKL[65] evolution equations for the Q^2- and x-dependence, respectively, of the parton distribution functions. At $Q^2 < \Lambda^2_{QCD}$, the coupling constant is large and non-perturbative methods must be used to treat strongly interacting systems. The matter in RHIC collisions may be formed in the intermediate region, where gluon densities saturate, the coupling is still weak, but very strong color fields lead to non-linear behavior describable by classical field methods. The curve separating the saturation and perturbative regimes sets the saturation scale. Figure courtesy of Y. Kovchegov.*

depends on both factors. In particular, at sufficiently low x and moderate Q^2, ρ is enhanced for a nucleus compared to a nucleon by a factor $\sim A^{1/3}$: the target sees the probe as having a longitudinal coherence length ($\ell_c \sim 1/m_N x$) much greater, but a transverse size ($\sim 1/Q^2$) much smaller, than the nuclear diameter. The probe thus interacts coherently with all the target gluons within a small diameter cylindrical "core" of the nucleus. The HERA data [59] suggest a rather slow variation – $xg(x) \propto x^{-\lambda}$, with $\lambda \sim 0.3$ at $Q^2 \sim$ few $(\mathrm{GeV})^2$ – of gluon densities with x at low x. Consequently, one would have to probe a proton at roughly two orders of magnitude lower x than a Au nucleus to gain the same factor growth in gluon densities as is provided by $A^{1/3}$.

Under the assumption that QGP formation in a RHIC collision is dominated by gluon-gluon interactions below the saturation scale, saturation models predict the density of gluons produced per unit area and unit rapidity [60]:

$$\frac{d^2N}{d^2b dy} = C\frac{N_c^2 - 1}{4\pi^2 \alpha_s(Q_s^2) N_c} Q_s^2(x, N_{part}), \tag{2}$$

where A has been replaced by N_{part}, the number of nucleons participating in an A+A collision at given impact parameter b, and $\hbar = c = 1$. The x-dependence of the saturation scale is taken from the HERA data,

$$Q_s^2(x) = Q_0^2 (\frac{x_0}{x})^{\lambda}, \tag{3}$$

and the same values of $\lambda \sim 0.2 - 0.3$ are generally assumed to be valid inside the nucleus as well. However, the multiplicative factor C above, parameterizing the number of outgoing hadrons per initially present gluon, is typically adjusted to fit observed outgoing hadron multiplicities from RHIC collisions. (Variations in C are clearly not distinguishable, in the context of Eqn. (2), from changes to the overall saturation scale Q_0^2.) Once this parameter is fixed, gluon saturation models should be capable of predicting the dependence of hadron multiplicity on collision energy, rapidity, centrality and mass number. Furthermore, the initial QGP gluon densities extracted can be compared with the independent values obtained from parton energy loss model fits to jet quenching observations or from hydrodynamics calculations of elliptic flow.

While it is predictable within the QCD framework that gluon saturation should occur under appropriate conditions, and the theoretical treatment of the CGC state is highly evolved [60–63], the dependences of the saturation scale are not yet fully exposed by supporting data. Eventual confirmation of the existence of such a scale must come from comparing results for a wide range of high energy experiments from Deep Inelastic Scattering in ep and eA (HERA, eRHIC) to pA and AA (RHIC, LHC) collisions.

2.6 Manifestations of Quark Recombination

The concept of quark recombination was introduced to describe hadron production in the forward region in p+p collisions [67]. At forward rapidity, this mechanism allows a fast quark resulting from a hard parton scattering to recombine with a slow anti-quark, which could be one in the original sea of the incident hadron, or one excited by a gluon [67]. If a QGP is formed in relativistic heavy ion collisions, then one might expect recombination of a different sort, namely, coalescence of the abundant thermal partons, to provide another important hadron production mechanism, active over a wide range of rapidity and transverse momentum [68]. In particular, at moderate p_T values (above the realm of hydrodynamics applicability), this hadron production "from below" (recombination of lower p_T partons from the thermal bath) has been predicted [69] to be competitive with production "from above" (fragmentation of higher p_T scattered partons). It has been suggested [70] that the need for substantial recombination to explain observed hadron yields and flow may be taken as a signature of QGP formation.

In order to explain observed features of RHIC collisions, the recombination models [68,69] make the central assumption that coalescence proceeds via *constituent* quarks, whose number in a given hadron determines its production rate. The constituent quarks are presumed to follow a thermal (exponential) momentum spectrum and to carry a collective transverse velocity distribution.

This picture leads to clear predicted effects on baryon and meson production rates, with the former depending on the spectrum of thermal constituent quarks and antiquarks at roughly one-third the baryon p_T, and the latter determined by the spectrum at one-half the meson p_T. Indeed, the recombination model was recently re-introduced in the RHIC context, precisely to explain an anomalous abundance of baryons vs. mesons observed at moderate p_T values [69]. If the observed (saturated) hadronic elliptic flow values in this momentum range result from coalescence of collectively flowing constituent quarks, then one can expect a similarly simple baryon vs. meson relationship [69]: the baryon (meson) flow would be 3 (2) times the quark flow at roughly one-third (one-half) the baryon p_T.

As will be discussed in later chapters, RHIC experimental results showing just such simple predicted baryon vs. meson features would appear to provide strong evidence for QGP formation. However, the models do not spell out the connection between the inferred spectrum and flow of constituent quarks and the properties of the essentially massless partons (predominantly gluons) in a chirally restored QGP, where the chiral condensate (hence most of the constituent quark mass) has vanished. One may guess that the constituent quarks themselves arise from an earlier coalescence of gluons and *current* quarks during the chiral symmetry breaking transition back to hadronic matter, and that the constituent quark flow is carried over from the partonic phase.

However, alternative guesses concerning the relation of partons to the recombination degrees of freedom are also conceivable. Perhaps it is valence current, rather than constituent, quarks that recombine to determine hadron flow and momentum in this moderate-p_T range. In that case, hadronization might proceed through the formation of "pre-hadrons" (*e.g.*, the pointlike color singlet objects discussed in connection with color transparency [52]) from the leading Fock (valence quark only) configurations, giving rise to the same 3-to-2 baryon-to-meson ratios as for constituent quarks. The internal pre-hadron wave functions would then subsequently evolve toward those of ordinary hadrons on their way out of the collision zone, so that the little-modified hadron momentum would in the end be shared substantially among sea quarks and gluons, as well as the progenitor valence quarks. Either of the above speculative (and quite possibly not orthogonal) interpretations of recombination would suggest that the hadron flow originates in, but is two steps removed from, *partonic* collectivity. But it is difficult to draw firm conclusions in light of the present ambiguity in connecting the effective degrees of freedom in coalescence models to the quarks and gluons treated by LQCD.

In addition, it is yet to be demonstrated that the coexistence of coalescence and fragmentation processes is quantitatively consistent with hadron angular correlations observed over p_T ranges where coalescence is predicted to dominate. These correlations exhibit prominent (near-side) peaks with angular

widths (at least in azimuthal difference between two moderate-p_T hadrons) and charge sign ordering characteristic of jets from vacuum fragmentation of hard partons [71]. The coalescence yield might simply contribute to the background underlying these peaks, but one should also expect contributions from the "fast-slow" recombination (hard scattered parton with QGP bath partons) [72] for which the model was first introduced, and these could produce charge sign ordering. The latter effects – part of in-medium, as opposed to vacuum, fragmentation – complicate the interpretation of the baryon/meson comparisons and, indeed, muddy the distinction between fragmentation and recombination processes.

Finally, the picture provided by recombination is distinctly different from ideal hydrodynamics at a hadronic level, where velocity (mass) of a hadron is the crucial factor determining flow, rather than the number of constituent (or valence) quarks. At low momentum, energy and entropy conservations become a serious problem for quark coalescence, placing an effective lower limit on the p_T range over which the models can be credibly applied. The solution of this problem would require a dynamical, rather than purely kinematic treatment of the recombination process [69]. Such parton dynamics at low momentum might account for the thermodynamic properties of the macroscopic system discussed earlier, but we do not yet have a unified partonic theoretical framework.

3 Bulk properties

The multiplicities, yields, momentum spectra and correlations of hadrons emerging from heavy-ion collisions, especially in the soft sector comprising particles at transverse momenta $p_T \lesssim 1.5$ GeV/c, reflect the properties of the bulk of the matter produced in the collision. In particular, we hope to infer constraints on its initial conditions, its degree of thermalization and its Equation of State from measurements of soft hadrons.

The measured hadron spectra reflect the properties of the bulk of the matter at kinetic freezeout, after elastic collisions among the hadrons have ceased. At this stage the system is already relatively dilute and "cold". However from the detailed properties of the hadron spectra at kinetic freezeout, information about the earlier hotter and denser stage can be obtained. Somewhat more direct information on an earlier stage can be deduced from the integrated yields of the different hadron species, which change only via *inelastic* collisions. These inelastic collisions cease already (at so-called chemical freezeout) before kinetic freezeout.

The transverse momentum distributions of the different particles reflect a random and a collective component. The random component can be identified with the temperature of the system at kinetic freezeout. The collective component arises from the matter density gradient from the center to the boundary of the fireball created in high-energy nuclear collisions. Interactions among constituents push matter outwards; frequent interactions lead to a common constituent velocity distribution. This so-called *collective flow* is therefore sensitive to the strength of the interactions. The collective flow is additive and thus accumulated over the whole system evolution, making it potentially sensitive to the Equation of State of the expanding matter. At lower energies the collective flow reflects the properties of dense hadronic matter [73], while at RHIC energies a contribution from a pre-hadronic phase is anticipated.

In non-central heavy-ion collisions the initial transverse density gradient has an azimuthal anisotropy that leads to an azimuthal variation of the collective transverse flow velocity with respect to the impact parameter plane for the event. This azimuthal variation of flow is expected to be self-quenching (see Sec. 2.2), hence, especially sensitive to the interactions among constituents in the *early* stage of the collision [26,74], when the system at RHIC energies is anticipated to be well above the critical temperature for QGP formation.

Study of quantum (boson) correlations among pairs of emerging hadrons utilizes the Hanbury-Brown-Twiss effect to complement measurements of momentum spectra with information on the spatial size and shape of the emitting system. The measurement of more general two-particle correlations and

of event-wise fluctuations can illuminate the degree of equilibration attained in the final hadronic system, as well as the dynamical origin of any observed non-equilibrium structures. Such dynamical correlations are prevalent in high-energy collisions of more elementary particles – where even relatively soft hadrons originate in large part from the fragmentation of partons – but are expected to be washed out by thermalization processes that produce phase space dominance of the final distribution probabilities.

In this section, we review the most important implications and questions arising from RHIC's vast body of data on soft hadrons. We also discuss some features of the transition region ($1.5 \lesssim p_T \lesssim 6$ GeV/c), where the spectra gradually evolve toward the characteristic behavior of the hard parton fragmentation regime. In the process of going through the measured features of hadron spectra in the logical sequence outlined above, we devote special attention to a few critical features observed *for the first time* for central and near-central Au+Au collisions at STAR, that bear directly on the case for the QGP:

- hadron yields suggestive of chemical equilibration across the u, d and s quark sectors;
- elliptic flow of soft hadrons attaining the strength expected for an ideal relativistic fluid thermalized very shortly after the collision;
- elliptic flow results at intermediate p_T that appear to arise from the flow of quarks in a pre-hadronic stage of the matter.

3.1 Rapidity Densities

Much has been made of the fact that predictions of hadron multiplicities in RHIC collisions before the year 2000 spanned a wide range of values, so that even the earliest RHIC measurements had significant discriminating power [7,75]. Mid-rapidity charged hadron densities measured in PHOBOS [76] and in STAR [77] are plotted in Fig. 11 as a function of collision centrality, as characterized by the number of participating nucleons, N_{part}, inferred from the fraction of the total geometric cross section accounted for in each analyzed bin. The solid curves in the figure represent calculations within a gluon saturation model [66], while the dashed curves in frames (a) and (b) represent two-component fits to the data [76] and in frames (c) and (d) represent an alternative model [78] assuming saturation of final-state mini-jet production. The apparent logarithmic dependence of the measured pseudorapidity densities on $\langle N_{part} \rangle$ is a characteristic feature of the gluon saturation model [66]. Consequently, the model's ability to reproduce the measured centrality and energy dependences have been presented as evidence for the relevance of the Color Glass Condensate to the initial state for RHIC collisions, and used to

constrain the saturation scale for initial gluon densities. This scale is in fair agreement with the scale extrapolated from HERA e-p measurements at low Bjorken x [7].

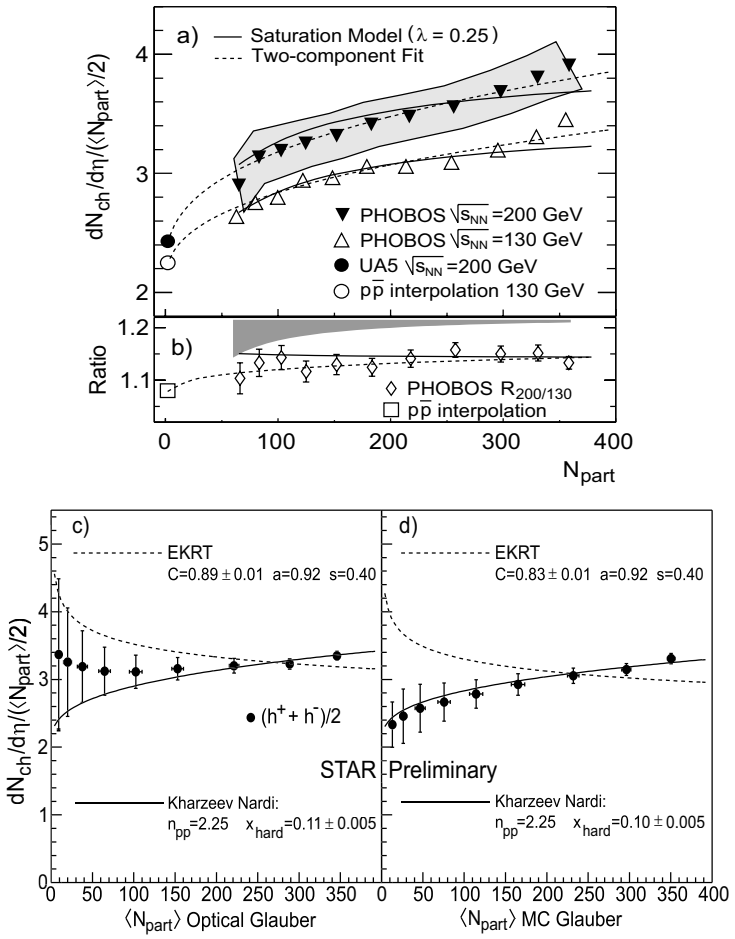

Fig. 11. *Measured and calculated pseudorapidity densities* $dN_{ch}/d\eta_{|\eta|\leq 1}/(\langle N_{part}\rangle/2)$ *of charged particles from RHIC Au+Au collisions as a function of* N_{part}. *PHOBOS data [76] at* $\sqrt{s_{\rm NN}}$= *130 GeV (open triangles) and 200 GeV (closed triangles) are shown in frame (a), and their ratio is plotted in (b). The open and solid circles in (a) are* $\overline{p}p$ *collision results. STAR data for 130 GeV [77] are shown in frames (c) and (d), plotted with two different Glauber model treatments to deduce* $\langle N_{part}\rangle$. *The data plotted in frames (a), (b) and (d) utilize the preferred Monte-Carlo Glauber approach. However, the initial-state gluon saturation model calculations [66] shown as solid curves in all frames have been carried out utilizing the questionable optical approximation to the Glauber treatment, which is applied as well to the experimental results only in frame (c). The dashed curves in frames (a) and (b) represent two-component fits to the data [76] and in frames (c) and (d) represent an alternative model [78] assuming saturation of final-state mini-jet production.*

However, these arguments are compromised because the particle multiplicity appears not to have strong discriminating power once one allows for adjustment of theoretical parameters. Furthermore, $\langle N_{part}\rangle$, which affects the scale

on both axes in Fig. 11, is not a direct experimental observable. Glauber model calculations to associate values of $\langle N_{part} \rangle$ with given slices of the geometric cross section distribution have been carried out in two different ways, leading to an inconclusive theory *vs.* experiment comparison in Figs. 11(a) and (b). The preferred method for evaluating Glauber model cross sections in nucleus-nucleus collisions [79] invokes a Monte Carlo approach for integrating over all nucleon configurations, and has been used for the experimental results in frames (a), (b) and (d). However, the gluon saturation model calculations in *all* frames of Fig. 11 have employed the optical approximation, which ignores non-negligible correlation effects [79]. Comparison of the *experimental* results in frames (c) and (d), where the same STAR data have been plotted using these two Glauber prescriptions, illustrates the significant sensitivity to the use of the optical approximation. The "apples-to-apples" comparison of experiment and theory in frame (c) does not argue strongly in favor of initial-state gluon saturation, although an analogous "apples-to-apples" comparison within the Monte Carlo Glauber framework is clearly desirable.

Furthermore, over a much broader energy range, the charged particle multiplicity is found to vary quite smoothly from AGS energies ($\sqrt{s_{\rm NN}} \approx$ few GeV) to the top RHIC energy ($\sqrt{s_{\rm NN}}$=200 GeV)[80] (see Fig. 35). One would not expect CGC conditions to be dominant in collisions over this entire range [7], so the apparent success of CGC arguments for RHIC hadron multiplicities is less than compelling. Other evidence more directly relevant to CGC predictions will be discussed in Chap. 4.

Whatever physics ultimately governs the smooth increase in produced particle multiplicity with increasing collision energy and centrality seems also to govern the growth in total transverse energy per unit pseudorapidity ($dE_T/d\eta$). PHENIX measurements at $\sqrt{s_{\rm NN}} = 130$ GeV [81] first revealed that RHIC collisions generate ≈ 0.8 GeV of transverse energy per produced charged particle near mid-rapidity, independent of centrality – essentially the same value that is observed also in SPS collisions at an order of magnitude lower center-of-mass energy [82]. This trend persists to $\sqrt{s_{\rm NN}} = 200$ GeV [83]. For RHIC central Au+Au collisions, this translates to the conversion of nearly 700 GeV per unit rapidity (dE_T/dy) from initial-state longitudinal to final-state transverse energy [81]. Under simplifying assumptions (longitudinal boost-invariance, free-streaming expansion in which the matter does no work) first suggested by Bjorken [84], one can extract from this observation a crude estimate of the initial spatial energy density of the bulk matter at the start of its transverse expansion:

$$e_{Bj} \;=\; \frac{dE_T}{dy}\frac{1}{\tau_0 \pi R^2}, \tag{4}$$

where τ_0 is the formation time and R the initial radius of the expanding system.

With reasonable guesses for these parameter values ($\tau_0 \approx 1$ fm/c, $R \approx 1.2A^{1/3}$ fm), the PHENIX $dE_T/d\eta$ measurements suggest an initial energy density ~ 5 GeV/fm^3 for central Au+Au collisions at RHIC, well above the critical energy density ~ 1 GeV/fm^3 expected from LQCD for the transition to the QGP phase. This estimate of the initial energy density is larger than that in SPS collisions, since the particle multiplicity grows at RHIC, but by a modest factor (≈ 1.6 [81] at $\sqrt{s_{\rm NN}} = 130$ GeV).

3.2 Hadron Yields and Spectra

Figure 12 compares STAR and some PHENIX measurements of integrated hadron yield ratios for central Au+Au collisions to statistical model fits and to results for p+p collisions. In comparison to p+p the relative yield of multi-strange baryons Ξ and Ω is seen to be considerably enhanced at RHIC [85,86]. The measured ratios are used to constrain the values of system temperature and baryon chemical potential at chemical freezeout, under the statistical model assumption that the system is in thermal and chemical equilibrium at that stage. The excellent fit obtained to the ratios in the figure, including stable and long-lived hadrons through multi-strange baryons, is consistent with the light flavors, u, d, and s, having reached chemical equilibrium (for central and near-central collisions only) at $T_{ch} = 160 \pm 10$ MeV [37,85–87]. (The deviations of the short-lived resonance yields, such as those for Δ and K* collected near the right side of Fig. 12, from the statistical model fits, presumably result from hadronic rescattering after the chemical freezeout.)

Although the success of the statistical model in Fig. 12 might, in isolation, indicate hadron production mechanisms dominated by kinematic phase space in elementary collisions (see Sec. 2.3), other measurements to be discussed below suggest that true thermal and chemical equilibration is at least approximately achieved in heavy-ion collisions at RHIC by interactions among the system's constituents. The saturation of the strange sector yields, attained for the first time in near-central RHIC collisions, is particularly significant. The saturation is indicated quantitatively by the value obtained for the non-equilibrium parameter γ_s for the strange sector [88], included as a free parameter in the statistical model fits. As seen in the inset of Fig. 12, γ_s rises from ≈ 0.7 in peripheral Au+Au collisions to values statistically consistent with unity [85,86] for central collisions. The temperature deduced from the fits is essentially equal to the critical value for a QGP-to-hadron-gas transition predicted by LQCD [2,14], but is also close to the Hagedorn limit for a hadron resonance gas, predicted without any consideration of quark and gluon degrees of freedom [25]. [1] If thermalization is indeed achieved by the bulk matter *prior* to

[1] Note that Hagedorn himself considered the Hagedorn temperature and the LQCD

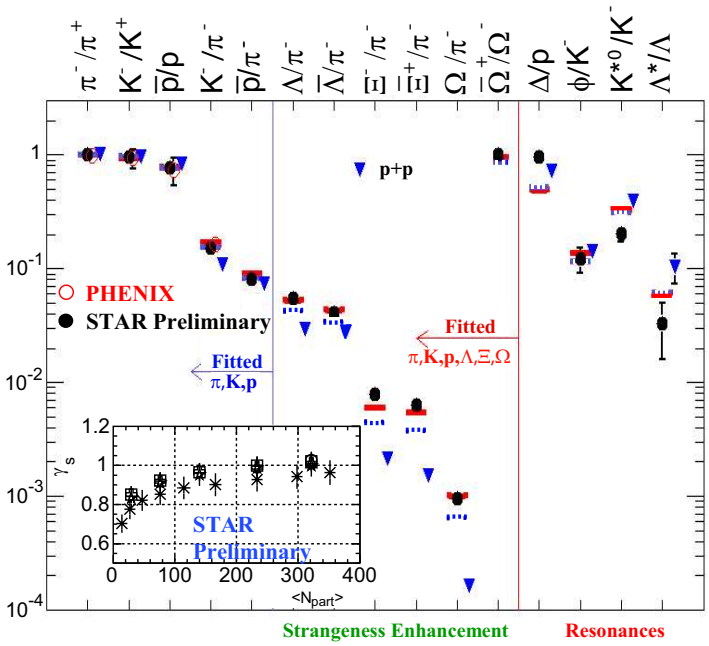

Fig. 12. *Ratios of p_T-integrated mid-rapidity yields for different hadron species measured in STAR (filled symbols) and PHENIX (open symbols), for central Au+Au (circles) and p+p (triangles) collisions at $\sqrt{s_{\rm NN}}$ = 200 GeV. The horizontal bars represent statistical model expectations based on fits to measured yield ratios for π, K and p only (blue dotted lines) and for π, K, p, Λ, Ξ and Ω (red solid lines). In the latter case, the fit parameters are $T_{ch} = 160 \pm 5$ MeV, $\mu_B = 24 \pm 4$ MeV, $\gamma_s = 0.99 \pm 0.07$ [86]. The variation of γ_s with centrality is shown in the inset, where the asterisk symbols represent fits to π, K and p yields only, while all other symbols represent the addition of various other hadrons containing strange valence quarks.*

chemical freezeout, then the deduced value of T_{ch} represents a lower limit on that thermalization temperature.

The characteristics of the system at *kinetic* freezeout can be explored by analysis of the transverse momentum distributions for various hadron species, some of which are shown in Fig. 13. In order to characterize the transverse motion, hydrodynamics-motivated fits [90] have been made to the measured spectra, permitting extraction of model parameters characterizing the random (generally interpreted as a kinetic freezeout temperature T_{fo}) and collective (radial flow velocity $\langle\beta_T\rangle$) aspects. Results for these parameters are shown for different centrality bins and different hadron species in Fig. 14. (While theoretical studies [90] suggest caution in interpreting spectrum fits made without correction for resonance feed-down, as is the case in Fig. 14, auxiliary STAR analyses show little quantitative effect of the feed-down within the STAR p_T coverage.)

As the collisions become more and more central, the bulk of the system, dom-

critical temperature to be identical [89].

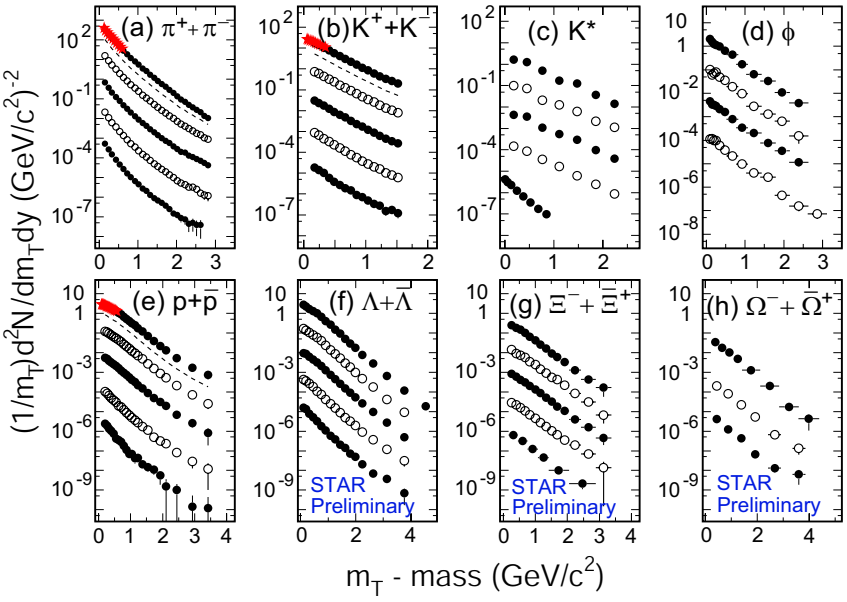

Fig. 13. *Mid-rapidity hadron spectra from* $\sqrt{s_{\rm NN}}$ *= 200 GeV Au+Au collisions, as reported in Refs. [87,94–96]. The spectra are displayed for steadily decreasing centrality from the top downwards within each frame, with appropriate scaling factors applied to aid visual comparison of the results for different centralities. For* K^* *only, the lowest spectrum shown is for 200 GeV* $p+p$ *collisions. The dashed curves in frames (a), (b) and (e) represent spectra from minimum-bias collisions. The invariant spectra are plotted as a function of* $m_T - \text{mass} \equiv \sqrt{p_T^2/c^2 + \text{mass}^2} - \text{mass}$.

inated by the yields of π, K, p, appears from Fig. 14 to grow cooler at kinetic freezeout and to develop stronger collective flow. These results may indicate a more rapid expansion after chemical freezeout with increasing collision centrality. On the other hand, even for the most central collisions, the spectra for multi-strange particles ϕ and Ω appear, albeit with still large uncertainties, to reflect a higher temperature [86]. The ϕ and Ω results suggest diminished hadronic interactions with the expanding bulk matter after chemical freezeout [85,86,91,92], as predicted [28,33,93] for hadrons containing no valence u or d quarks. If this interpretation is correct, the substantial radial flow velocity inferred for ϕ and Ω would have to be accumulated prior to chemical freezeout, giving the multi-strange hadrons perhaps greater sensitivity to collective behavior during earlier partonic stages of the system evolution.

As one moves beyond the soft sector, the p_T - and centrality dependences of the observed hadron spectra develop a systematic difference between mesons and baryons, distinct from the mass-dependence observed at lower p_T. This difference is illustrated in Fig. 15 by the binary-scaled ratio R_{CP} of hadron yields for the most central vs. a peripheral bin, corrected by the expected ratio of contributing binary nucleon-nucleon collisions in the two centrality bins [96]. The results are plotted as a function of p_T for mesons and baryons separately in panels (a) and (b), respectively, with the ratio of binary collision-scaled

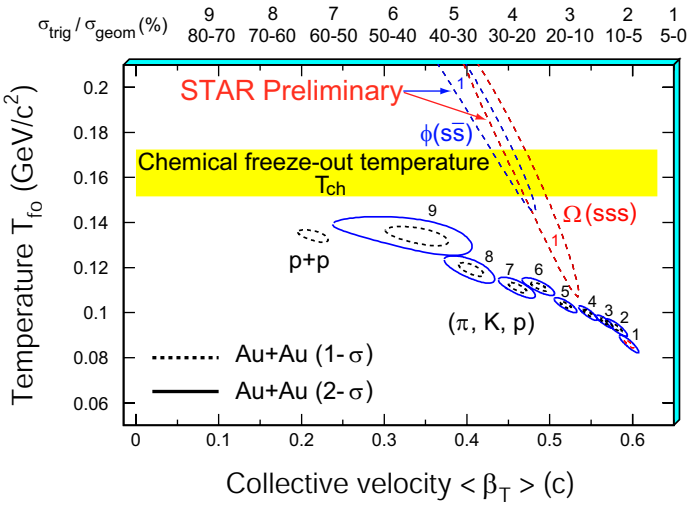

Fig. 14. *The χ^2 contours, extracted from thermal + radial flow fits (without allowance for resonance feed-down), for copiously produced hadrons π, K and p and multi-strange hadrons ϕ and Ω. On the top of the plot, the numerical labels indicate the centrality selection. For π, K and p, 9 centrality bins (from top 5% to 70-80%) were used for $\sqrt{s_{NN}} = 200$ GeV Au+Au collisions [87]. The results from $p+p$ collisions are also shown. For ϕ and Ω, only the most central results [86] are presented. Dashed and solid lines are the 1-σ and 2-σ contours, respectively.*

yields of all charged hadrons indicated in both panels by a dot-dashed curve to aid comparison. If the centrality-dependence simply followed the number of binary collisions, one would expect $R_{CP} = 1$. This condition is nearly achieved for baryons near $p_T \approx 2.5$ GeV/c, but is never reached for mesons. The initial results for ϕ-mesons and Ω-baryons included in Fig. 15 suggest that the difference is not very sensitive to the mass of the hadron, but rather depends primarily on the number of valence quarks contained within it. The meson and baryon values appear to merge by $p_T \approx 5$ GeV/c, by which point $R_{CP} \approx 0.3$.

The origin of this significant shortfall in central high-p_T hadron production will be discussed at length in Sec. 4. Here, we want simply to note that the clear difference seen in the centrality dependence of baryon vs. meson production is one of the defining features of the intermediate p_T range from ~ 1.5 to ~ 6 GeV/c in RHIC heavy-ion collisions, and it cannot be understood from $p+p$ collision results [97]. Another defining feature of this medium p_T range, to be discussed further below, is a similar meson-baryon difference in elliptic flow. Both facets of the meson-baryon differences can be explained naturally in quark recombination models for hadron formation [69].

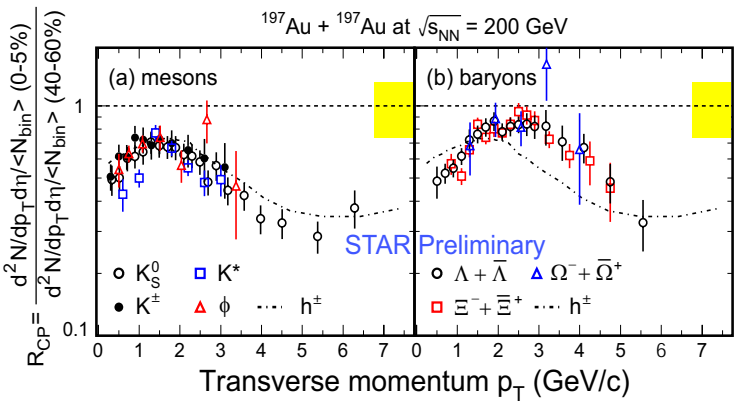

Fig. 15. *STAR preliminary results [96] from* $\sqrt{s_{\rm NN}}$ *= 200 GeV Au+Au collisions for the ratio of mid-rapidity hadron yields* R_{CP} *in a central (0-5%) over a peripheral (40-60%) bin, plotted vs.* p_T *for mesons (a) and baryons (b). The yields are scaled in each centrality region by the calculated mean number* $\langle N_{bin}\rangle$ *of binary contributing nucleon-nucleon collisions, calculated within a Monte Carlo Glauber model framework. The width of the shaded band around the line at unity represents the systematic uncertainty in model calculations of the centrality dependence of* $\langle N_{bin}\rangle$*.* R_{CP} *for the sample of all charged hadrons is also shown by dot-dashed curves in both plots. The error bars on the measured ratios include both statistical and systematic uncertainties.*

3.3 Hadron yields versus the reaction plane

In non-central heavy-ion collisions, the beam direction and the impact parameter define a reaction plane for each event, and hence a preferred azimuthal orientation. The orientation of this plane can be estimated experimentally by various methods, *e.g.*, using 2- or 4-particle correlations [98,99], with different sensitivities to azimuthal anisotropies not associated with collective flow. The observed particle yield versus azimuthal angle with respect to the event-by-event reaction plane promises information on the early collision dynamics [27,74]. The anisotropy of the particle yield versus the reaction plane can be characterized in a Fourier expansion. Due to the geometry of the collision overlap region the second coefficient of this Fourier series – v_2, often referred to as the elliptic flow – is expected to be the dominant contribution.

Figure 16 shows the mid-rapidity elliptic flow measurements, integrated over transverse momentum, as a function of collision centrality for one SPS [100] and two RHIC [101,102] energies. One clearly observes a characteristic centrality dependence that reflects the increase of the initial spatial eccentricity of the collision overlap geometry with increasing impact parameter. The integrated elliptic flow value for produced particles increases about 70% from the top SPS energy to the top RHIC energy, and it appears to do so smoothly as a function of energy (see Fig. 34), so far exhibiting no obvious "dip" of the sort predicted [30] by ideal hydrodynamics in Fig. 7.

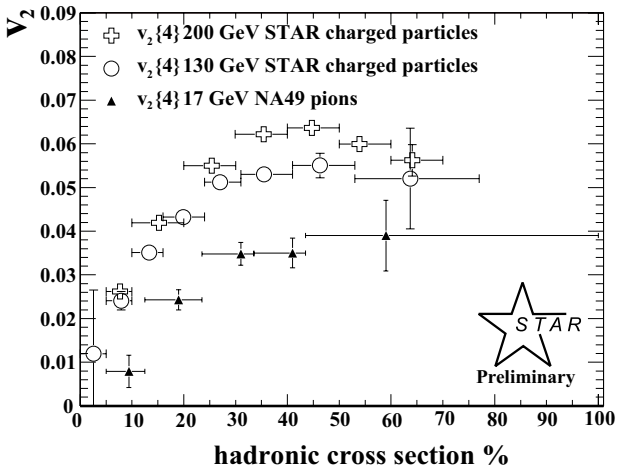

Fig. 16. *Centrality dependence of v_2, integrated over p_T. The triangles are the NA49 measurements for pions at $\sqrt{s_{NN}}$ = 17 GeV [100]. The circles and crosses are STAR measurements for charged particles at $\sqrt{s_{NN}}$ = 130 GeV [101] and 200 GeV [102], respectively. The 4-particle cumulant method has been used to determine v_2 in each case.*

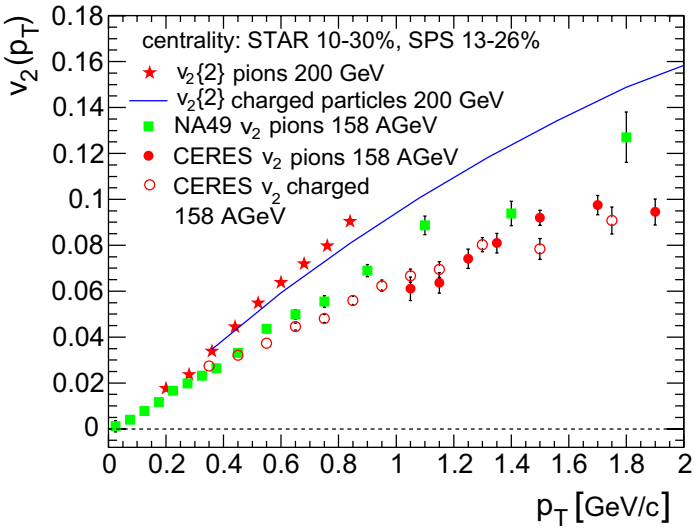

Fig. 17. *$v_2(p_t)$ for one centrality (10-30%) range. The circles and squares are the CERES [103] and NA49 [100] measurements, respectively, at $\sqrt{s_{NN}}$ = 17 GeV. The stars and the solid line are STAR measurements [102] for pions and for all charged particles, respectively, at $\sqrt{s_{NN}}$ = 200 GeV (evaluated here by the 2-particle correlation method).*

The origin of the energy dependence can be discerned by examining the differential $v_2(p_t)$, shown for the centrality selection 10–30% in Fig. 17. The comparison of the results for pions at $\sqrt{s_{NN}}$ = 200 GeV and at the top SPS energy clearly reveals an increase in slope vs. p_T that accounts for part of the increase in p_T -integrated v_2 from SPS to RHIC. The remaining part of the change is due to the increase in $\langle p_t \rangle$. As measurements become available at

more collision energies, it will be important to remove kinematic effects, such as the increase in $\langle p_t \rangle$, from comparisons of results, as they might mask finer, but still significant, deviations from smooth energy dependence.

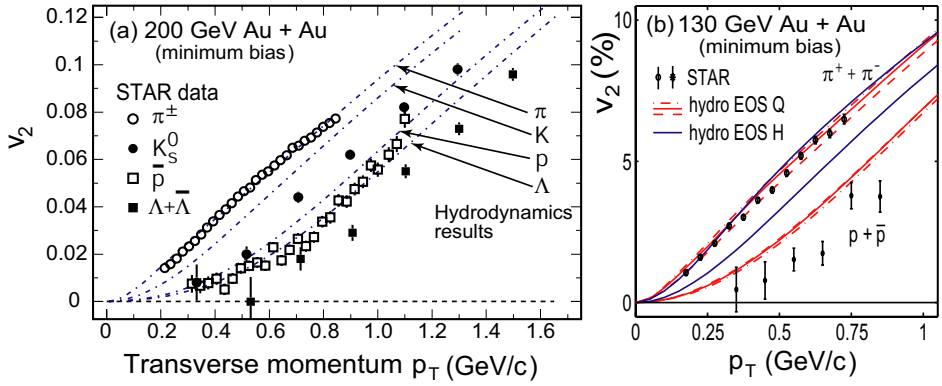

Fig. 18. *(a) STAR experimental results of the transverse momentum dependence of the elliptic flow parameter in 200 GeV Au+Au collisions for charged* $\pi^+ + \pi^-$, K^0_s, $\overline{p}$, *and* Λ *[104]. Hydrodynamics calculations [32,106] assuming early thermalization, ideal fluid expansion, an equation of state consistent with LQCD calculations including a phase transition at* T_c*=165 MeV (EOS Q in [32] and Fig. 5), and a sharp kinetic freezeout at a temperature of 130 MeV, are shown as dot-dashed lines. Only the lower* p_T *portion (*$p_T \leq 1.5$ *GeV/c) of the distributions is shown. (b) Hydrodynamics calculations of the same sort as in (a), now for a hadron gas (EOS H) vs. QGP (EOS Q) equation of state (both defined in Fig. 5) [3,32], compared to STAR* v_2 *measurements for pions and protons in minimum bias 130 GeV Au+Au collisions [105]. Predictions with EOS Q are shown for a wider variety of hadron species in Fig. 8.*

Collective motion leads to predictable behavior of the shape of the momentum spectra as a function of particle mass, as reflected in the single inclusive spectra in Fig. 13. It is even more obvious in the dependence of $v_2(p_t)$ for the different mass particles. Figure 18 shows the measured low-p_T v_2 distributions from 200 and 130 GeV Au+Au minimum bias collisions. Shown are the measurements for charged pions, K^0_S, antiprotons and Λ[104,105]. The clear, systematic mass-dependence of v_2 shown by the data is a strong indicator that a common transverse velocity field underlies the observations. This mass-dependence, as well as the absolute magnitude of v_2, is reproduced reasonably well (*i.e.*, at the $\pm$30% level) by the hydrodynamics calculations shown in Fig. 18. Parameters of these calculations have been tuned to achieve good agreement with the measured spectra for different particles, implying that they account for the observed radial flow and elliptic flow simultaneously. In particular, since the parameters are tuned for zero impact parameter, the theory-experiment comparison for v_2 as a function of centrality represents a significant test of these hydrodynamics calculations.

The agreement of these hydrodynamics calculations, which assume *ideal* relativistic fluid flow, with RHIC spectra and v_2 results is one of the centerpieces

of recent QGP discovery claims [6–8]. The agreement appears to be optimized (though still with some quantitative differences, see Fig. 18) when it is assumed that local thermal equilibrium is attained very early ($\tau < 1$ fm/c) during the collision, and that the hydrodynamic expansion is characterized by an EOS (labeled Q in Fig. 18) containing a soft point roughly consistent with the LQCD-predicted phase transition from QGP to hadron gas [3,29,32]. When the expanding matter is treated as a pure hadron gas (EOS H in Fig. 18(b)), the mass-dependence of v_2 is significantly underpredicted. The inferred early thermalization suggests that the collision's early stages are dominated by very strongly interacting matter with very short constituent mean free paths – essentially a "perfect liquid" [107], free of viscosity. Similar QGP-based calculations that invoke ideal hydrodynamics up to freezeout overpredict the elliptic flow for more peripheral RHIC collisions and for lower energies. One possible interpretation of this observation is that thermalized, strongly interacting QGP matter dominates near-central Au+Au collisions at or near the full RHIC energy.

In assessing these claims, it is critical to ask how unique and robust the hydrodynamics account is in detail for the near-central RHIC collision flow measurements (radial and elliptic). Might the observed v_2 result alternatively from a harder EOS (such as EOS H) combined with later achievement of thermalization or with higher viscosity [35] (both conditions impeding the development of collective flow)? How does the sensitivity to the EOS in the calculations compare quantitatively with the sensitivity to other ambiguities or questionable assumptions in the hydrodynamics treatments? For example, the particular calculations in Fig. 18 [32,106] invoke a simplified treatment with a sharp onset of kinetic freezeout along a surface of constant energy density corresponding to $T_{fo} \approx 130$ MeV. The sensitivity to the assumed value of T_{fo}, if it is kept within the range spanned by the measurements in Fig. 14, is relatively weak [32]. However, alternative approaches combining ideal hydrodynamics for the partonic stage with a hadron transport (RQMD) treatment of the presumably viscous hadronic stage [29] yield similar success in accounting for RHIC results, but certainly predict a dependence of v_2 on collision energy differing significantly from the sharp-freezeout predictions (compare Fig. 7 and Fig. 9). While the combination of partonic hydrodynamics and hadron transport offers the promise of a reasonable QGP-based account for the observed smooth energy dependence of p_T -integrated v_2 (see Figs. 9,34), it also serves to emphasize that quantitative ambiguities of scale comparable to the EOS sensitivity remain to be understood.

In addition to questions about the thermalization time, viscosity and freezeout treatment, one also needs to address the robustness of the standard assumption of longitudinal boost-invariance in hydrodynamics calculations [3]. There is growing evidence at RHIC for significant deviations from boost-invariance. This is illustrated by PHOBOS results for v_2 as a function of pseudorapidity

in Fig. 19, where one sees no evidence for a mid-rapidity plateau in elliptic flow strength [108]. Thus, while the successes of QGP-based hydrodynamics calculations at RHIC are tantalizing, substantially greater systematic investigation of their sensitivities – including computationally challenging full three-dimensional treatments – would be needed to make a compelling QGP claim on their basis alone.

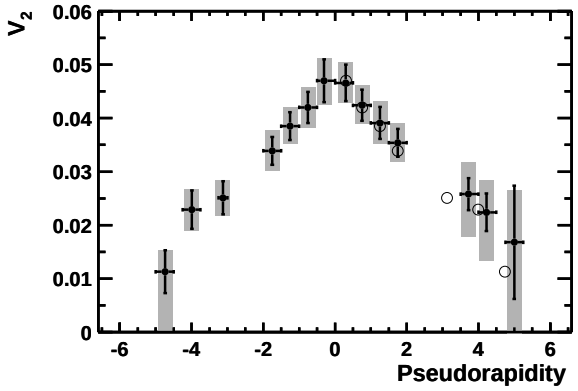

Fig. 19. *Azimuthal anisotropies v_2 measured by the PHOBOS collaboration [108] for Au+Au collisions at $\sqrt{s_{\rm NN}}$=130 GeV, as a function of pseudorapidity. Within each pseudorapidity bin, the results are averaged over all charged particles, over all centralities and over all p_T . The black error bars are statistical and the grey bands systematic uncertainties. The points on the negative side are reflected about $\eta = 0$ and plotted as open circles on the positive side, for comparison. Figure taken from Ref. [108].*

At higher p_T values, as shown by experimental results from 200 GeV Au+Au minimum bias collisions in Fig. 20, the observed values of v_2 saturate and the level of the saturation differs substantially between mesons and baryons. Hydrodynamics calculations overpredict the flow in this region. The dot-dashed curves in Fig. 20(a)-(c) represent simple analytical function fits to the measured K^0_S and $\Lambda+\bar{\Lambda}$ v_2 distributions [104,109]. It is then seen in Fig. 20 (b) and (c) that STAR's most recent v_2 results for the multi-strange baryons Ξ and Ω [110] are consistent with that of Λ's within still sizable statistical uncertainties.

In Fig. 20 (d), particle-identified elliptic flow measurements for the 200 GeV Au+Au minimum-bias sample are combined by dividing both v_2 and p_T by the number of valence quarks (n_q) in the hadron of interest. The apparent scaling behavior seen in this figure for $p_T/n_q > 1$ GeV/c is intriguing, as the data themselves seem to be pointing to constituent quarks (or at least to valence quarks sharing the full hadron momentum, see Sec. 2.6) as the most effective degree of freedom in determining hadron flow at intermediate p_T values. The data need to be improved in statistical precision and p_T extent for more identified mesons and baryons in order to establish this scaling more definitively. Within error bars the size of those for $p_T/n_q > 1$ GeV/c, the low

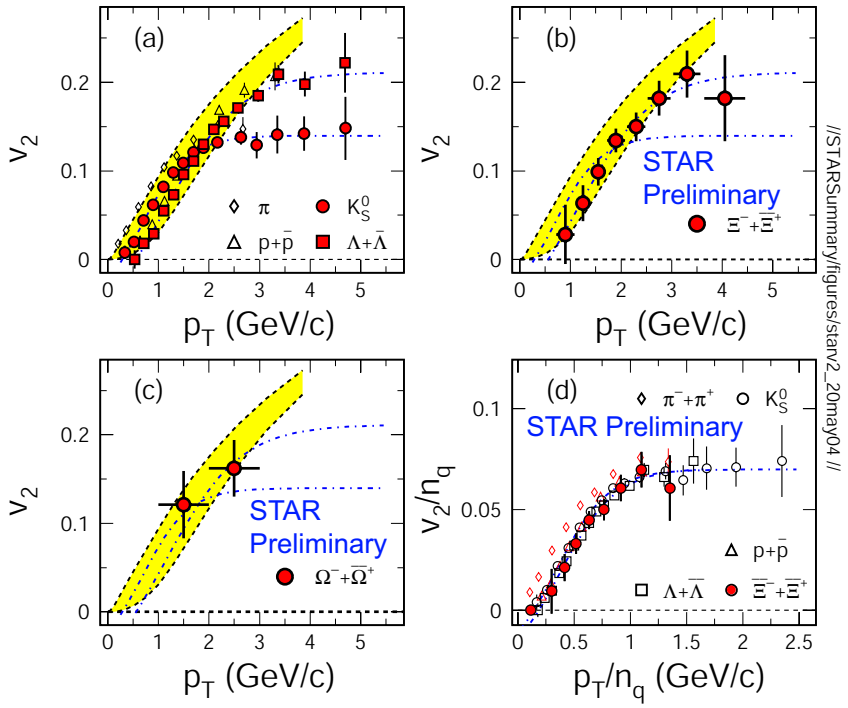

Fig. 20. *(a) Experimental results of the transverse momentum dependence of the event elliptic anisotropy parameter for* π *and* $p + \overline{p}$ *from PHENIX [111] and for* K^0_S *and* $\Lambda + \overline{\Lambda}$ *from STAR [104], all produced in minimum-bias Au+Au collisions at* $\sqrt{s_{NN}} = 200$ *GeV. Dot-dashed lines are fits to the data using simple analytic functions. Hydrodynamic calculations are indicated by the shaded bands. STAR multi-strange baryon elliptic flow [110] is shown in (b) for* Ξ *and (c) for* Ω*. (d) Flow results for all of the above hadrons (except the statistically limited* Ω*) combined by scaling both* v_2 *and* p_T *by the number of valence quarks* (n_q) *in each hadron. The figure is an update of one in [109].*

p_T data would also look as though they scale with the number of constituent quarks, whereas we already have seen in Fig. 18 that there is rather a clear hydrodynamic mass-dependence in the low p_T region. (Note that the pion data barely extend into the scaling region at $p_T/n_q > 1$ GeV/c.)

If the scaling behavior at intermediate p_T is confirmed with improved data, it will provide a very important clue to the origin of the meson-baryon differences (see also Fig. 15) that characterize this p_T range. In particular, both the v_2 scaling and the meson-baryon R_{CP} differences can be explained [69,112] (see Fig. 21) by assuming that hadron formation at moderate p_T proceeds via two competing mechanisms: the coalescence of n_q constituent quarks at transverse momenta $\sim p_T/n_q$, drawn from a thermal (exponential) spectrum [69], plus more traditional fragmentation of hard-scattered partons giving rise to a power-law component of the spectrum. Note that, as discussed in section 2.6, these models are not expected to apply at low p_T. It is not yet clear that the same models could simultaneously account as well for another observed feature characteristic of this intermediate p_T range, namely, a jet-like azimuthal

correlation of hadron pairs that will be discussed further in Sec. 4.

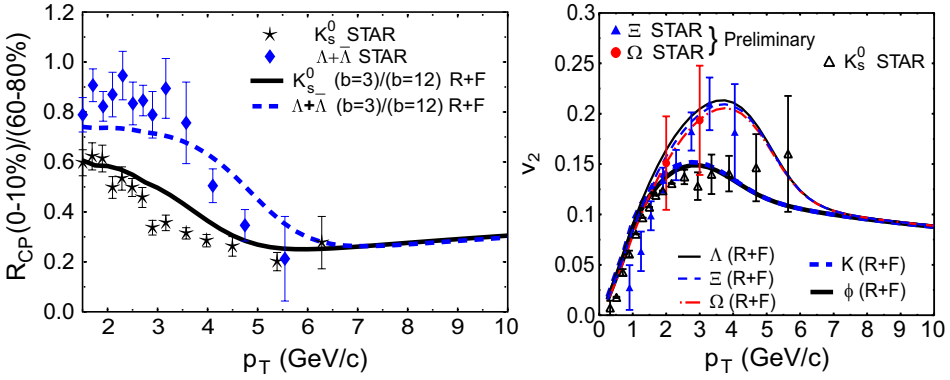

Fig. 21. *Comparisons of calculations in the Duke quark recombination model [69,112] with STAR measurements [104,110] of (a) R_{CP} and (b) v_2 for strange mesons and baryons. "R+F" denotes the sum of recombination and fragmentation contributions. Comparison of the solid and broken curves in (b) reveals a weak mass-dependence in the calculations, superimposed on the predominant meson-baryon differences. Figures taken from Ref. [70].*

.

In these coalescence models, the constituent quarks carry their own substantial azimuthal anisotropy, which is then summed to give the hadron v_2. The establishment of clearer evidence for such pre-hadronic collective flow would be an important milestone in elucidating the nature of the matter produced in RHIC collisions. In interpreting such evidence, it must be kept in mind that constituent quarks are not partons: they are effective degrees of freedom normally associated with chiral symmetry breaking and confinement, rather than with the deconfinement of a QGP. Until the mechanism for the emergence of these effective degrees of freedom from a QCD plasma of current quarks and gluons is clarified (see Sec. 2.6), collectively flowing constituent quarks should not be taken as definitive proof of a QGP stage, as we have defined it in Sec. 1. It is unclear, for example, whether the characteristic time scale for constituent quarks to coalesce from current quarks and gluons might not be shorter than that for the establishment of thermalization in the collision (leading to a sort of "constituent quark plasma", as opposed to a QGP). Furthermore, the constituent quark v_2 values needed to account for the observed hadron v_2 saturation might arise in part from differential energy loss of their progenitor partons in traversing the spatially anisotropic matter of non-central collisions [47], rather than strictly from the partonic hydrodynamic flow assumed in [112]. The unanticipated RHIC results in this intermediate p_T range thus raise a number of important and fascinating questions that should be addressed further by future measurements and theoretical calculations.

In summary, the measured yields with respect to the reaction plane are among the most important results to date from RHIC: they provide critical hints of the properties of the bulk matter at early stages. They indicate that it

behaves collectively, and is consistent with rapid (*i.e.*, very short mean free path) attainment of at least approximate local thermal equilibrium in a QGP phase. Hydrodynamic accounts for the mass- and p_T-dependence of v_2 for soft hadrons appear to favor system evolution through a soft, mixed-phase EOS. The saturated v_2 values observed for identified mesons and baryons in the range $1.5 \lesssim p_T \lesssim 6$ GeV/c suggest that hadronization in this region occurs largely via coalescence of collectively flowing constituent quarks. What has yet to be demonstrated is that these interpretations are unique and robust against improvements to both the measurements and the theory. In particular, it must be demonstrated more clearly that the sensitivity to the role of the QGP outweighs that to other, more mundane, ambiguities in the theoretical treatment.

3.4 Quantum Correlation Analyses

Two-hadron correlation measurements in principle should provide valuable information on the phase structure of the system at freezeout. From the experimentally measured momentum-space two-particle correlation functions, a Fourier transformation is then performed in order to extract information on the space-time structure [113]. Bertsch-Pratt parameterization [114] is often used to decompose total momentum in such measurements into components parallel to the beam (*long*), parallel to the pair transverse component (*out*) and along the remaining third direction (*side*). In this Cartesian system, information on the source duration time is mixed into the *out* components. Hence, the ratio of inferred emitting source radii R_{out}/R_{side} is sensitive to the time duration of the source emission. For example, if a QGP is formed in collisions at RHIC, a long duration time and consequently large value of R_{out}/R_{side} are anticipated [115].

Measured results for Hanbury-Brown-Twiss (HBT) pion interferometry, exploiting the boson symmetry of the two detected particles at low relative momenta, are shown in Figs. 22 and 23. A clear dependence of the 'size' parameters on the pair transverse momentum k_T is characteristic of collective expansion of the source [116,117], so the results are plotted vs. k_T in Fig. 22. As indicated by the set of curves in the figure, hydrodynamics calculations that can account for hadron spectra and elliptic flow at RHIC systematically over-predict R_{out}/R_{side} [116,118]. One possible implication of this discrepancy is that the collective expansion does not last as long in reality as in the hydrodynamics accounts. However, shorter expansion times are difficult to reconcile with the observed magnitude of R_{side}, and are not supported by a recent systematic study of HBT correlations relative to the event-by-event reaction plane [117]. The source eccentricity at freezeout inferred from these azimuthally sensitive measurements is shown in Fig. 23 to retain a significant

fraction of the initial spatial eccentricity characteristic of the impact parameter for each centrality bin. The observed eccentricity retention is, in fact, quantitatively consistent with hydrodynamics expectations for the *time-integrated* pion emission surface to which HBT is sensitive [119]. Thus, the deformations in Fig. 23 tend to support the hydrodynamics view of the expansion pressure and timeline (see Fig. 6), which lead to an eventual complete quenching of the initial configuration-space anisotropy by the end of the freezeout process.

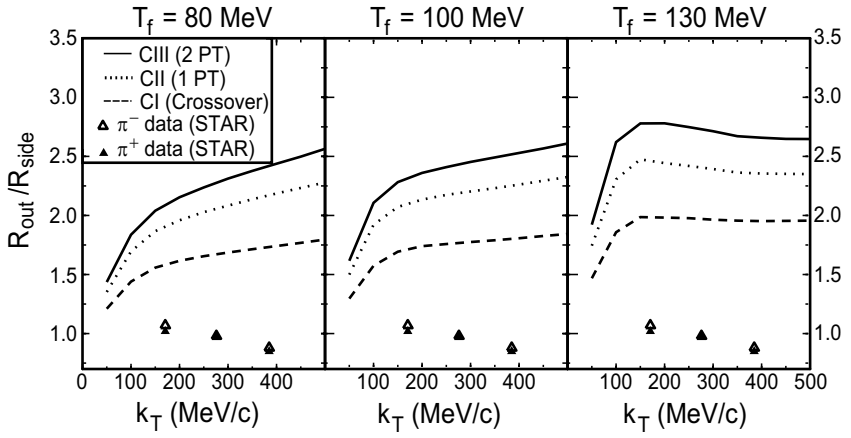

Fig. 22. *STAR measurements [116] of R_{out}/R_{side} from pion HBT correlations for central Au+Au collisions, plotted as a function of the pion pair transverse momentum k_T. The experimental results are identical in the three frames, but are compared to hydrodynamics calculations [118] performed for a variety of parameter values.*

The failure of the hydrodynamics calculations to account for the HBT results in Fig. 22 raises another significant issue regarding the robustness of the hydrodynamics success in reproducing v_2 and radial flow data. Although the HBT interference only emerges after the freezeout of the strong interaction, whose treatment is beyond the scope of hydrodynamics, the measured correlation functions receive contributions from all times during the collision process. Furthermore, these HBT results are extracted from the low p_T region, where soft bulk production dominates. It is thus reasonable to expect the correct hydrodynamics account of the collective expansion to be consistent with the HBT source sizes. If improved treatment of the hadronic stage and/or the introduction of finite viscosity during the hydrodynamic expansion [35] are necessary to attain this consistency, then it is important to see how those improvements affect the agreement with elliptic flow and spectra.

STAR has also measured two-hadron momentum-space correlation functions for *non*-identical particles [121]. These are sensitive to differences in the average emission time and position for the different particle species. Such differences are very clearly revealed by the measured correlations between pions and kaons [121], and provide additional strong evidence for a collective transverse flow of the produced hadrons.

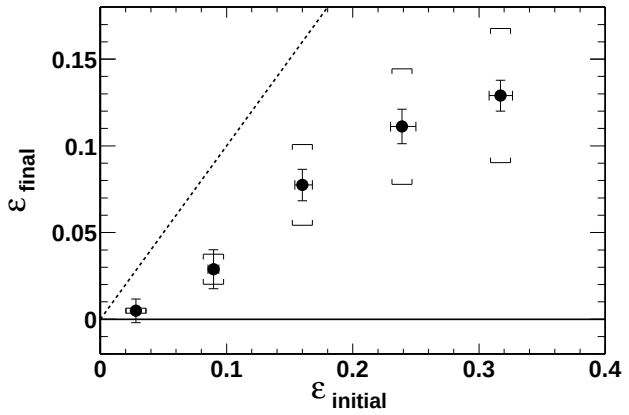

Fig. 23. *The eccentricity ϵ_{final} of the time-integrated emitting source of soft pions, inferred from STAR HBT correlations measured with respect to the reaction plane, plotted versus the initial spatial eccentricity $\epsilon_{initial}$ deduced from a Glauber calculation for five different Au+Au centrality bins. The dotted line represents $\epsilon_{final} = \epsilon_{initial}$. See [117] for details.*

3.5 Correlations and fluctuations

A system evolving near a phase boundary should develop significant dynamical fluctuations away from the mean thermodynamic properties of the matter. For high-energy heavy ion collisions, it has been predicted that the general study of two-particle correlations and event-wise fluctuations might provide evidence for the formation of matter with partonic degrees of freedom [122–127]. In addition, nonstatistical correlations and fluctuations may be introduced by incomplete equilibrium [128]. With its large acceptance and complete event-by-event reconstruction capabilities, the STAR detector holds great potential for fluctuation analyses of RHIC collisions.

An approach that has been used previously [129,130] to search for the presence of dynamical correlations involves extraction of measures of the excess variance of some observable above the statistical fluctuations that show up even in mixed-event samples. An example shown in Fig. 24 utilizes the square root of the covariance in p_T for charged-particle pairs from collisions at SPS (CERES [129]) and at STAR [131]. The presence of dynamical 2-particle correlations is revealed by non-zero values of this quantity, whose gross features exhibit a magnitude and a smooth centrality-dependence that are essentially independent of collision energy, once the variations of the inclusive mean p_T values ($<< p_T >>$) with centrality and energy have been divided out. However, the detailed nature of the dynamical correlations is best probed by fully exploiting the impressive statistical precision at STAR to investigate finer, multi-dimensional aspects of the correlation densities themselves, rather than of the integrals of correlation densities represented by excess variance measures.

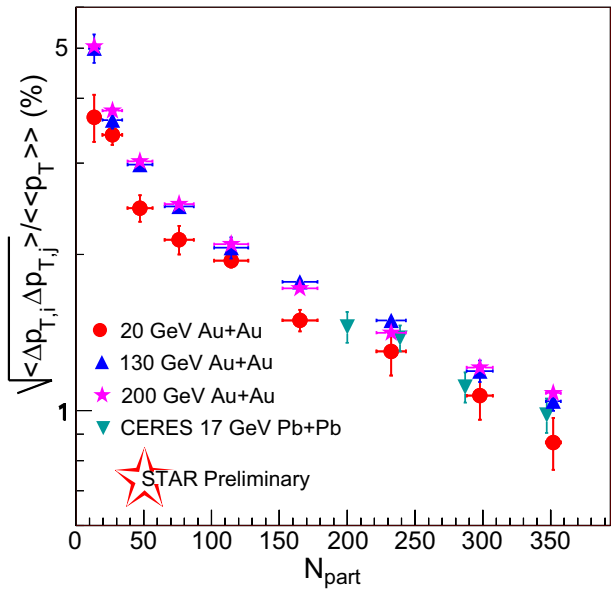

Fig. 24. *The square root of the transverse momentum covariance for charged particle pairs, scaled by the inclusive mean p_T value for each centrality and collision energy, plotted vs. centrality for SPS [129] and RHIC [131] data at several energies. Both the centrality-dependence (nearly $\propto 1/N_{part}$) and magnitude of this quantity are essentially unchanged from SPS to RHIC energies, but its implicit integration of correlation densities over the full detector acceptance masks other interesting correlation features.*

For example, emerging STAR angular correlation results are already suggesting that there is appreciable soft hadron emission before the attainment of local thermal equilibrium, even in the most central RHIC collisions. The upper left-hand frame of Fig. 25 shows measurements for p+p collisions at RHIC of the joint autocorrelation on the angular difference variables $\Delta\eta \equiv \eta_1 - \eta_2$ (pseudorapidity) and $\Delta\phi \equiv \phi_1 - \phi_2$ (azimuthal angle) for all but the softest pairs of charged hadrons [132]. This plot makes clear the central role of parton fragmentation in p+p collisions, even down to hadron transverse momenta of 0.5 GeV/c, resulting in a prominent near-side jet peak symmetric about $\Delta\eta = \Delta\phi = 0$ and a broad $\Delta\eta$-independent away-side jet ridge. One certainly anticipates some remnants of these correlations to survive in heavy-ion collisions at sufficiently high hadron p_T , and these correlations will be discussed in the next chapter. In the soft sector, however, attainment of a fully equilibrated state of all emerging hadrons at freezeout would wash out such initial hard-scattering dynamical correlations. Instead, the observed soft-hadron-pair correlation for central Au+Au collisions shown in the upper right-hand frame of Fig. 25, after removal of multipole components representing elliptic flow (v_2) and momentum conservation (v_1) [132], exhibits a substantially modified remnant of the jet correlation on the near side, affecting typically 10-30% of the detected hadrons. Contributions to this near-side peak from HBT correlations and Coulomb final-state interactions between hadrons have been suppressed

by cuts to remove pairs at very low relative momentum, reducing the overall strength of the correlation near $\Delta\eta = \Delta\phi = 0$ by $\sim$10% [132]. Simulations demonstrate that resonance decays make no more than a few percent contribution to the remaining near-side correlation strength. (The lack of evidence for any remaining away-side correlation will be discussed further in the high-p_T context in Sec. 4.)

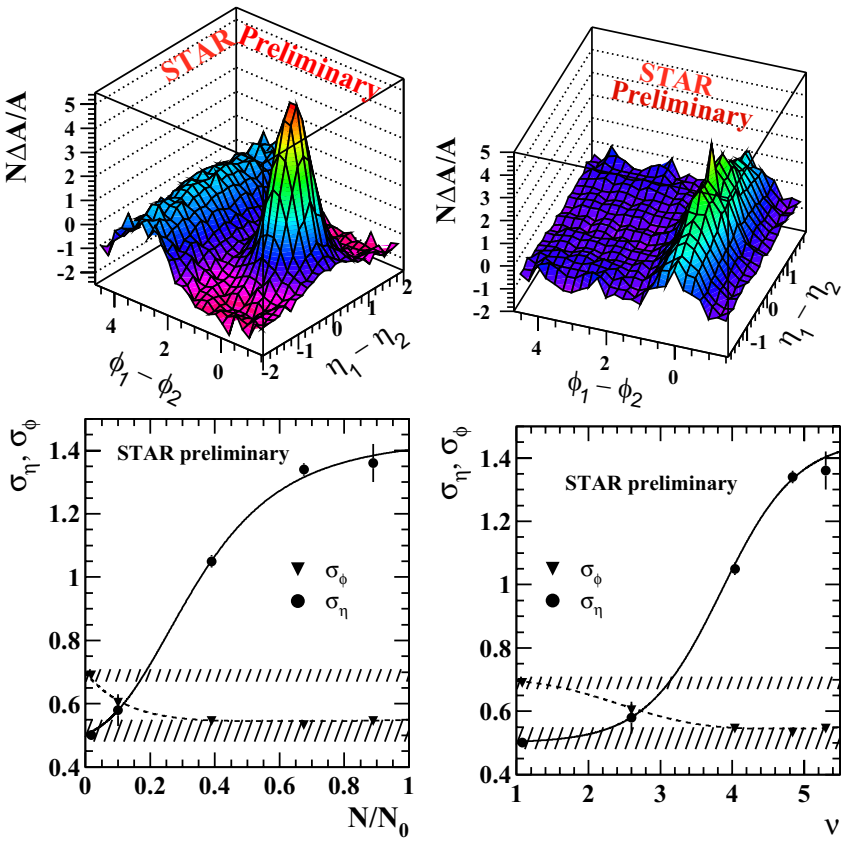

Fig. 25. *Upper frames: joint autocorrelations measured by STAR, as a function of the hadron pair angle differences $\eta_1 - \eta_2$ and $\phi_1 - \phi_2$, for 200 GeV p+p (left) and 130 GeV central Au+Au (right) collisions. The quantity $N\Delta A/A$ plotted on the vertical axes represents the average multiplicity for the selected centrality bin multiplied by the relative difference in charged particle pair yields between same events and mixed events. The Au+Au measurements include hadrons in the range $0.15 \leq p_T \leq 2.0$ GeV/c, and have elliptic flow and momentum conservation long-range correlations removed. The p+p measurements include hadrons in the range $0.5 \leq p_T \leq 6$ GeV/c. Lower frames: centrality-dependence of the Au+Au pseudorapidity and azimuthal widths from two-dimensional gaussian fits to the near-side correlation structure seen for one centrality bin in the upper right frame. The same extracted widths for Au+Au collisions are plotted* vs. *two different measures of centrality: the observed charged-particle multiplicity divided by its maximum value (on the left), and the mean number ν of nucleons encountered by a typical participant nucleon (right). The hatched bands indicate the widths observed for p+p collisions, and the curves guide the eye. See [132] for details.*

The observed near-side correlation in central Au+Au is clearly much broader in $\Delta\eta$ than that in p+p (or peripheral Au+Au) collisions. The pseudorapidity spread, as characterized by the $\Delta\eta$ width of a two-dimensional gaussian function fitted to the structure (ignoring the $\Delta\eta = \Delta\phi = 0$ bin, where conversion electron pairs contribute), grows rapidly with increasing collision centrality, as revealed in the lower frames of Fig. 25. This trend suggests that while some parton fragments are not yet fully equilibrated in the soft sector, they are nonetheless rather strongly coupled to the longitudinally expanding bulk medium. The onset of this coupling appears especially dramatic when the results are plotted (lower right-hand frame) *vs.* the alternative centrality measure $\nu \equiv (N_{part}/2)^{1/3}$ (estimating the mean number of nucleons encountered by a typical participant nucleon along its path through the other nucleus), rather than the more traditional charged-particle multiplicity (lower left frame). The latter comparison serves as a reminder that, as we seek evidence for a transition in the nature of the matter produced in RHIC collisions, it is important to consider carefully the optimal variables to use to characterize the system.

The coupling to the longitudinal expansion can be seen more clearly as an equilibration mechanism from measurements of the power spectra P^{λ} of local fluctuations in the density of charged hadrons with respect to a mixed-event counterpart P^{λ}_{mix}. The λ superscript distinguishes different directions (modes) of density variation, orthogonal in the wavelet decomposition used [134] for the analysis: along η, along ϕ, and along the diagonal $\eta\phi$. The so-called "dynamic texture" [133] of the event, used to characterize the non-statistical excess in density fluctuations, is defined as $P^{\lambda}_{dyn}/P^{\lambda}_{mix}/N$, where $P^{\lambda}_{dyn} = P^{\lambda} - P^{\lambda}_{mix}$ and N is the average number of tracks in a given p_T interval per event. The dynamic texture is shown as a function of p_T for three different modes and for both central and peripheral collisions in Fig. 26 [134]. HIJING simulations [136] shown in the figure cannot account for the observed fluctuations, even when jet quenching is included, although they do suggest qualitatively that the rising trends in the data with increasing p_T are signals of "clumpiness" in the particle density caused by jets. In the absence of a successful model for these fluctuations, we can at least search for interesting centrality dependences. The box symbols in the figure represent what we would expect for the dynamic texture in central collisions, based on what STAR measures for peripheral collisions, if the correlation structure were independent of centrality. The strong suppression observed with respect to this expectation for the central collision η-mode fluctuations is interpreted as another manifestation of the coupling of parton fragments to the longitudinally expanding bulk medium [134].

The results in Figs. 25 and 26 are averaged over all charged hadrons without consideration of the sign of the charge. Detailed information on the hadronization of the medium can be obtained from the study of charge-*dependent* (CD) correlations, *e.g.*, by examining the difference between angle-dependent correlations of like- *vs.* unlike-sign pairs. One method focuses on the "balance

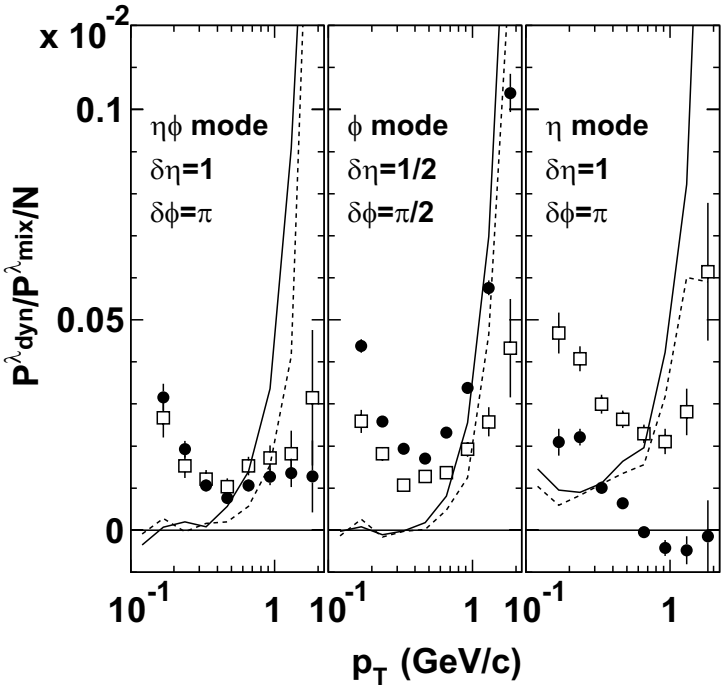

Fig. 26. *STAR measurements (filled circles) of dynamic texture for the 4% most central Au+Au collisions at* $\sqrt{s_{\rm NN}}$*= 200 GeV, compared to STAR peripheral (60-84%) collision data (boxes) renormalized for direct comparison, and to HIJING calculations with (dashed curves) and without (solid curves) inclusion of jet quenching. The dynamic texture measures the non-statistical excess in point-to-point fluctuations in the local density of charged hadrons in an event, averaged over the event ensemble. Figure taken from Ref. [134].*

function", constructed [126,135] to measure the excess of unlike- over like-sign pairs as a function of their (pseudo)rapidity difference $\Delta\eta$. The results in Fig. 27 show that the width of this function in $\Delta\eta$ steadily decreases with increasing Au+Au centrality [131], in contrast to HIJING simulations [136]. A related trend is observed in the CD two-dimensional autocorrelation [132] (not plotted) analogous in format to the charge-independent results shown in Fig. 25. The CD peak amplitude increases, and its width decreases, dramatically with increasing centrality. These trends indicate a marked change in the formation mechanism of charged hadron pairs in central Au+Au, relative to p+p, collisions. The implications of that change for the nature of the medium produced are now under intensive study with a growing array of correlation techniques.

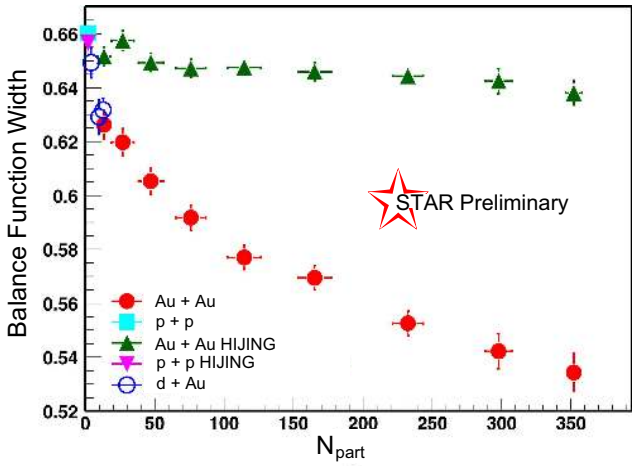

Fig. 27. *Width of the measured charged hadron balance function from p+p (filled square), d+Au (open circles) and Au+Au (filled circles) collisions at* $\sqrt{s_{\rm NN}}$*=200 GeV, plotted as a function of centrality via the calculated mean number of participating nucleons for each analyzed bin. The triangle symbols represent the results of HIJING simulations [136] of the balance function width measured within STAR for 200 GeV Au+Au collisions. The figure is from Ref. [131].*

3.6 Summary

In this chapter, we have presented important results on the bulk matter properties attained in Au+Au collisions at RHIC. The measured hadron spectra, yield ratios, and low p_T v_2, are all consistent from all experiments at RHIC. STAR, in particular, has made pioneering measurements of elliptic flow, of multi-strange baryons, and of dynamical hadron correlations that bear directly on the matter properties critical to establishing QGP formation. The yield ratios are consistent with chemical equilibration across the u, d and s sectors. The spectra and v_2 clearly reveal a collective velocity field in such collisions. The combined evidence for near-central Au+Au collisions at RHIC suggests that thermal equilibrium is largely, though not quite completely, attained, and that collective flow is established, at an early collision stage when sub-hadronic degrees of freedom dominate the matter. However, the quality of some of the data, and the constraints on ambiguities in some of the theoretical models used for interpretation, are not yet sufficient to demonstrate convincingly that thermalized, deconfined matter has been produced.

In particular, the unprecedented success of hydrodynamics in providing a reasonable quantitative account for collective flow at RHIC, and of the statistical model in reproducing hadron yields through the strange sector, together argue for an early approach toward thermalization spanning the u, d and s sectors. On the other hand, measurements of angle difference distributions for soft hadron pairs reveal that some (admittedly heavily modified) remnants of jet-like dynamical correlations survive the thermalization process, and indicate its

incompleteness. The fitted parameters of the statistical model analyses, combined with inferences from the produced transverse energy per unit rapidity, suggest attainment of temperatures and energy densities at least comparable to the critical values for QGP formation in LQCD calculations of bulk, static strongly interacting matter.

The data in this chapter provide two hints of deconfinement that need to be sharpened in future work. One is the improvement in hydrodynamics accounts for measured low-p_T flow when the calculations include a soft point in the EOS, suggestive of a transition from partonic to hadronic matter. It needs to be better demonstrated that comparable improvement could not be obtained alternatively by addressing other ambiguities in the hydrodynamics treatment. One indication of such other ambiguities is the failure of hydrodynamics calculations to explain the emitting source sizes inferred from pion interferometry. The second hint is the apparent relevance of (constituent or valence) quark degrees of freedom in determining the observed meson-baryon differences in flow and yield in the intermediate-p_T region. Here the data need improved precision to establish more clearly the quark scaling behavior expected from coalescence models, while the theory needs to establish a clearer connection between the effective quarks that seem to coalesce and the current quarks and gluons of QCD.

4 Hard Probes

Due to the transient nature of the matter created in high energy nuclear collisions, external probes cannot be used to study its properties. However, the dynamical processes that produce the bulk medium also produce energetic particles through hard scattering processes. The interaction of these energetic particles with the medium provides a class of unique, penetrating probes that are analogous to the method of computed tomography (CT) in medical science.

For $p_T \gtrsim 5$ GeV/c the observed hadron spectra in Au+Au collisions at RHIC exhibit the power-law falloff in cross section with increasing p_T that is characteristic of perturbative QCD hard-scattering processes [137]. The parameters of this power-law behavior vary systematically with collision centrality, in ways that reveal important properties of the matter traversed by these penetrating probes [137]. While we focus for the most part in this chapter on hadrons of p_T above 5 GeV/c, we do also consider data in the intermediate p_T range down to 2 GeV/c, when those data allow more statistically robust measurements of effects we associate with hard scattering.

4.1 Inclusive hadron yields at high p_T

There are several results to date from RHIC exhibiting large and striking effects of the traversed matter on hard probes in central collisions. Figures 28 and 29 show the most significant high p_T measurements made at RHIC thus far. Both figures incorporate measurements of $\sqrt{s_{\rm NN}}$=200 GeV p+p, d+Au and centrality-selected Au+Au collisions at RHIC, with the simpler p+p and d+Au systems providing benchmarks for phenomena seen in the more complex Au+Au collisions.

Figure 28 shows $R_{AB}(p_T)$, the ratio of inclusive charged hadron yields in A+B (either Au+Au or d+Au) collisions to p+p, corrected for trivial geometric effects via scaling by $\langle N_{bin} \rangle$, the calculated mean number of binary nucleon-nucleon collisions contributing to each A+B centrality bin:

$$R_{AB}(p_T) = \frac{dN_{AB}/d\eta d^2p_T}{T_{AB} d\sigma_{NN}/d\eta d^2p_T}. \qquad (5)$$

where the overlap integral $T_{AB} = \langle N_{bin} \rangle / \sigma^{pp}_{inelastic}$. A striking phenomenon is seen: large p_T hadrons in central Au+Au collisions are suppressed by a factor ≈ 5 relative to naive (binary scaling) expectations. Conventional nuclear effects, such as nuclear shadowing of the parton distribution functions and initial state multiple scattering, cannot account for the suppression. Further-

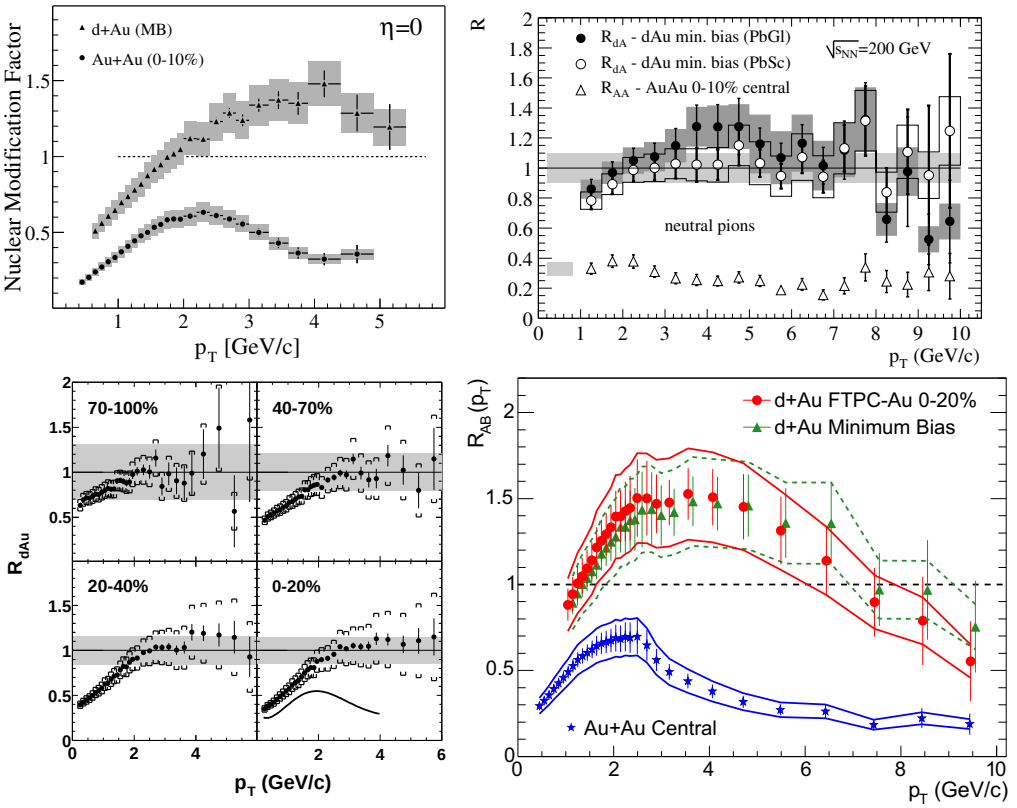

Fig. 28. *Binary-scaled ratio $R_{AB}(p_T)$ (Eq. 5) of charged hadron and π^0 inclusive yields from 200 GeV Au+Au and d+Au relative to that from p+p collisions, from BRAHMS[138] (upper left), PHENIX[139] (upper right), PHOBOS[140] (lower left) and STAR[141] (lower right). The PHOBOS data points in the lower left frame are for d+Au, while the solid curve represents PHOBOS central (0-6%) Au+Au data. The shaded horizontal bands around unity represent the systematic uncertainties in the binary scaling corrections.*

more, the suppression is not seen in d+Au but is unique to Au+Au collisions, proving experimentally that it results not from nuclear effects in the initial state (such as gluon saturation), but rather from the final state interaction (FSI) of hard scattered partons or their fragmentation products in the dense medium generated in Au+Au collisions [138–141].

These dominant FSI in Au+Au are presumably superimposed on a variety of interesting initial-state effects revealed by the d+Au results. The enhancement seen in Fig. 28 in R_{dAu} for moderate p_T and mid-rapidity, known as the Cronin effect [142], is generally attributed [143] to the influence of multiple parton scattering through cold nuclear matter *prior to* the hard scattering that produces the observed high-p_T hadron. Other effects, revealed by the strong *rapidity*-dependence of R_{dAu}, will be discussed in Sec. 4.4.

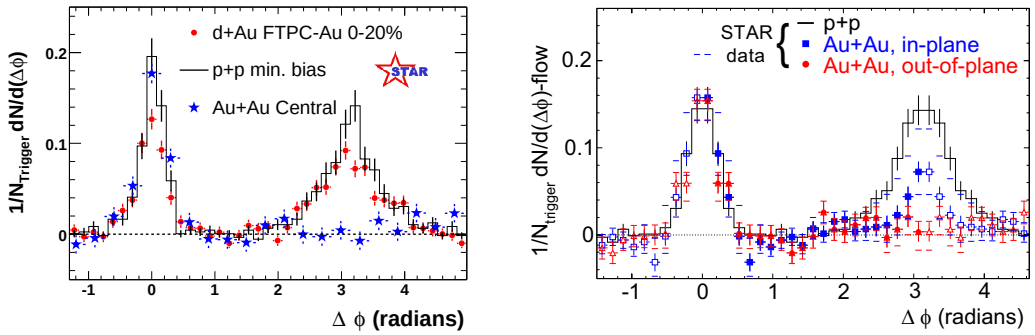

Fig. 29. *Dihadron azimuthal correlations at high p_T. Left panel shows correlations for p+p, central d+Au and central Au+Au collisions (background subtracted) from STAR [141,71]. Right panel shows the background-subtracted high p_T dihadron correlation for different orientations of the trigger hadron relative to the Au+Au reaction plane [144].*

4.2 Dihadron azimuthal correlations

Figure 29 shows seminal STAR measurements of correlations between high p_T hadrons. The left panel shows the azimuthal distribution of hadrons with p_T>2 GeV/c relative to a trigger hadron with $p_T{}^{\rm trig}$>4 GeV/c. A hadron pair drawn from a single jet will generate an enhanced correlation at $\Delta\phi \approx 0$, as observed for p+p, d+Au and Au+Au, with similar correlation strengths, widths and (not shown) charge-sign ordering (the correlation is stronger for oppositely charged hadron pairs [71]). A hadron pair drawn from back-to-back dijets will generate an enhanced correlation at $\Delta\phi \approx \pi$, as observed for p+p and for d+Au with somewhat broader width than the near-side correlation peak. However, the back-to-back dihadron correlation is strikingly, and uniquely, absent in central Au+Au collisions, while for peripheral Au+Au collisions the correlation appears quite similar to that seen in p+p and d+Au. If the correlation is indeed the result of jet fragmentation, the suppression is again due to the FSI of hard-scattered partons or their fragmentation products in the dense medium generated in Au+Au collisions [141]. In this environment, the hard hadrons we do see (and hence, the near-side correlation peak) would arise preferentially from partons scattered outward from the surface region of the collision zone, while the away-side partons must burrow through significant lengths of dense matter.

The qualification concerning the dominance of jet fragmentation is needed in this case, because the correlations have been measured to date primarily for hadrons in that intermediate p_T range (2-6 GeV/c) where sizable differences in meson vs. baryon yields have been observed (see Fig. 15), in contrast to expectations for jets fragmenting in vacuum. The systematics of the meson-baryon differences in this region suggest sizable contributions from softer mechanisms, such as quark coalescence [69]. Where the azimuthal correlation measurements

have been extended to trigger particles above 6 GeV/c, they show a similar pattern to the results in Fig. 29, but with larger statistical uncertainties [145]. This suggests that the peak structures in the correlations do, indeed, reflect dijet production, and that the back-to-back suppression is indeed due to jet quenching. Coalescence processes in the intermediate p_T range may contribute predominantly to the smooth background, with only long-range (*e.g.*, elliptic flow) correlations, that has already been subtracted from the data in Fig. 29.

It remains an open challenge for the quark coalescence models to account for the observed $\Delta\phi$ distributions at moderate p_T at the same time as the meson *vs.* baryon yield and elliptic flow differences discussed in Sec. 3 (see Fig. 21 and associated discussion). Can the size of the jet peaks seen in Fig. 29 be reconciled with the modest fragmentation contributions implied by the coalescence fits near $p_T \approx 4$ GeV/c (Fig. 21)? Do the jet $\Delta\phi$ peaks rather require substantial contributions also from recombination of a hard-scattered parton with thermal partons from the bulk matter [72]? Are models of the latter type of contributions, of constituent quark coalescence in a thermal ensemble [112] and of vacuum fragmentation [4] mutually compatible? They would appear to contain non-orthogonal contributions and to employ incompatible degrees of freedom. Until these questions are successfully addressed, some ambiguity remains in physics conclusions drawn from the intermediate-p_T region, including the dihadron correlations in Fig. 29.

A more differential probe of partonic energy loss is the measurement of high p_T dihadron correlations relative to the reaction plane orientation. The right panel of Fig. 29 shows a study from STAR of the high p_T dihadron correlation from 20-60% centrality Au+Au collisions, with the trigger hadron situated in the azimuthal quadrants centered either in the reaction plane ("in-plane") or orthogonal to it ("out-of-plane") [144]. The same-side dihadron correlation in both cases is similar to that in p+p collisions. In contrast, the suppression of the back-to-back correlation depends strongly on the relative angle between the trigger hadron and the reaction plane. This systematic dependence is consistent with the picture of partonic energy loss: the path length in medium for a dijet oriented out of the reaction plane is longer than in the reaction plane, leading to correspondingly larger energy loss. The dependence of parton energy loss on path length is predicted [4] to be substantially stronger than linear. The orientation-dependence of the energy loss should be further affected by different rates of matter expansion in-plane *vs.* out-of-plane.

The energy lost by away-side partons traversing the collision matter must appear, in order to conserve transverse momentum, in the form of an excess of softer emerging hadrons. An analysis of azimuthal correlations between hard and *soft* hadrons has thus been carried out for both 200 GeV p+p and Au+Au collisions [146] in STAR, as a first attempt to trace the degree of degradation on the away side. With trigger hadrons still in the range $4 < p_T^{trig} < 6$ GeV/c,

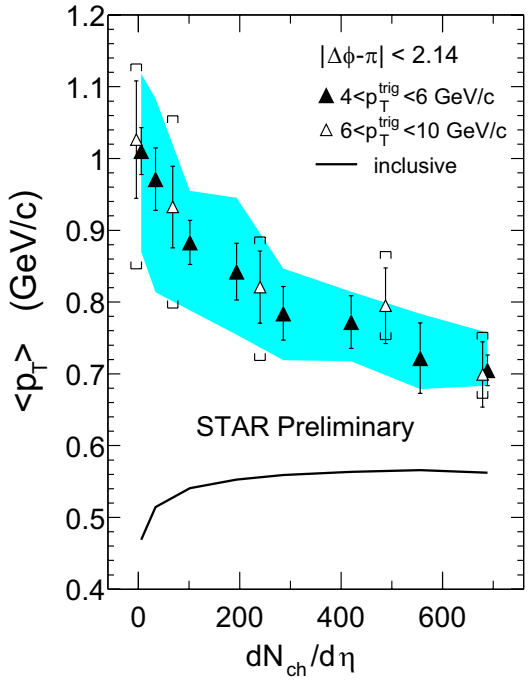

Fig. 30. *Associated charged hadron <p_T> from the away-side in 200 GeV p+p (two leftmost points) and Au+Au collisions at various centralities, in each case opposite a trigger hadron with p_T in the 4–6 GeV/c (filled triangles) or 6–10 GeV/c (open triangles) range [146]. The shaded band and the horizontal caps represent the systematic uncertainties for the filled and open symbols, respectively. <p_T> for inclusive hadron production in the Au+Au collisions is indicated by the solid curve.*

but the associated hadrons now sought over 0.15< p_T <4 GeV/c, combinatorial coincidences dominate these correlations, and they must be removed statistically by a careful mixed-event subtraction, with an elliptic flow correlation correction added by hand [146]. The results demonstrate that, in comparison with p+p and peripheral Au+Au collisions, the momentum-balancing hadrons opposite a high-p_T trigger in central Au+Au are greater in number, much more widely dispersed in azimuthal angle, and significantly softer. The latter point is illustrated in Fig. 30, showing the centrality dependence of <p_T> of the associated away-side charged hadrons in comparison to that of the bulk inclusive hadrons. While in peripheral collisions the values of <p_T> for the away-side hadrons are significantly larger than that of inclusive hadrons, the two values approach each other with increasing centrality. These results are again subject to the ambiguity arising from possible soft (*e.g.*, coalescence) contributions to the observed correlations, as the away-side strength shows little remnant of jet-like behavior [146]. But again, preliminary results for higher trigger-hadron p_T values, shown in Fig. 30, appear to be consistent within larger uncertainties. If a hard-scattering interpretation framework turns out to be valid, the results suggest that even a moderately hard parton traversing a significant path length through the collision matter makes substantial progress toward equilibration with the bulk. The rapid attainment of thermalization via the

multitude of softer parton-parton interactions in the earliest collision stages would then not be surprising.

4.3 Theoretical interpretation of hadron suppression

Figure 31 shows $R_{CP}(p_T)$, the binary scaled ratio of yields from central relative to peripheral collisions for charged hadrons from 200 GeV Au+Au interactions. $R_{CP}(p_T)$ is closely related to $R_{AB}(p_T)$, using as reference the binary-scaled spectrum from peripheral Au+Au collisions rather than p+p collisions. The substitution of the reference set allows a slight extension in the p_T range for which useful ratios can be extracted. The error bars at the highest p_T are dominated by statistics and are therefore, to a large extent, uncorrelated from point to point. The suppression for central collisions is again seen to be a factor ≈ 5 relative to the most peripheral collisions, and for $p_T \gtrsim 6$ GeV/c it is independent of p_T within experimental uncertainties. Also shown in Fig. 31 are results from theoretical calculations based on pQCD incorporating partonic energy loss in dense matter (pQCD-I [147], pQCD-II [148]) and on suppression at high p_T due to gluon saturation effects (Saturation [150], with implications discussed further in the following subsection). The negligible p_T-dependence of the suppression at high p_T is a prediction of the pQCD models [147,148], resulting from the subtle interplay of partonic energy loss, Cronin (initial-state multiple scattering) enhancement, and nuclear shadowing. The variation in the suppression for $p_T \lesssim 5$ GeV/c is related to differences in suppression in this region for mesons and baryons (see Fig. 15). It is accounted for in the pQCD-I calculation by the introduction of an additional non-fragmentation production mechanism for kaons and protons [147]. The magnitude of the hadron suppression in the pQCD calculations is adjusted to fit the measurements for central collisions, as discussed further below.

In order to deduce the magnitude of *partonic* energy loss in the medium it is essential to establish the degree to which *hadronic* interactions, specifically the interaction of hadronic jet fragments with the medium, can at least in part generate the observed high p_T phenomena and contribute substantially to the jet quenching [51,152,153]. Simple considerations already argue against this scenario. The dilated formation time of hadrons with energy E_h and mass m_h is $t_f = (E_h/m_h)\tau_f$, where the rest frame formation time $\tau_f \sim 0.5 - 0.8$ fm/c. Thus, a 10 GeV/c pion has formation time ~ 50 fm/c and is unlikely to interact as a fully formed pion in the medium. Since the formation time depends on the boost, the suppression due to hadronic absorption with constant or slowly varying cross section should turn off with rising p_T, at variance with observations (Fig. 31). A detailed hadronic transport calculation [51] leads to a similar conclusion: the absorption of formed hadrons in the medium fails by a large factor to account for the observed suppression. Rather, this calculation

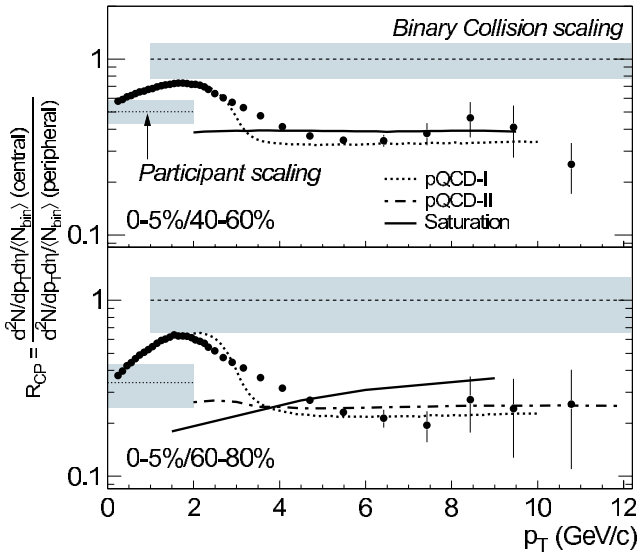

Fig. 31. *Binary-scaled yield ratio $R_{CP}(p_T)$ for central (0-5%) relative to peripheral (40-60%, 60-80%) collisions for charged hadrons from 200 GeV Au+Au collisions [151]. The shaded bands show the multiplicative uncertainty of the normalization of $R_{CP}(p_T)$ relative to binary collision and participant number scaling.*

attributes the suppression to *ad hoc* medium interactions of "pre-hadrons" with short formation time and constant cross section. The properties of these "pre-hadrons" are thus similar to those of colored partons [51], and not to the expected color transparency of hadronic matter to small color singlet particles that might evolve into normal hadrons [52].

Additional considerations of the available high p_T data [53] also support the conclusion that jet quenching in heavy ion collisions at RHIC is the consequence of partonic energy loss. In particular, large v_2 values observed at high p_T and the systematics of the small-angle dihadron correlations are difficult to reconcile with the hadronic absorption scenario. While further theoretical investigation of this question is certainly warranted, we conclude that there is no support in the data for *hadronic* absorption as the dominant mechanism underlying the observed suppression phenomena at high p_T and we consider *partonic* energy loss to be well established as its primary origin. It is conceivable that there may be minor hadronic contributions from the fragments of soft gluons radiated by the primary hard partons during their traversal of the collision matter. In any case, we emphasize that while the jet quenching results seem to favor partons over hadrons *losing* energy, they do not allow any direct conclusion regarding whether the energy is lost *to* partonic or hadronic matter.

The magnitude of the suppression at high p_T in central collisions is fit to the data in the pQCD-based models with partonic energy loss, by adjusting the initial gluon density of the medium. The agreement of the calculations with the measurements at p_T>5 GeV/c is seen in Fig. 31 to be good. In order to

describe the observed suppression, these models require an initial gluon density about a factor 50 greater than that of cold nuclear matter [147–149]. This is the main physics result of the high p_T studies carried out at RHIC to date. It should be kept in mind that the actual energy loss inferred for the rapidly expanding Au+Au collision matter is not very much larger than that inferred for static, cold nuclear matter from semi-inclusive deep inelastic scattering data [57]. But in order to account for this slightly larger energy loss *despite* the rapid expansion, one infers the much larger *initial* gluon density at the start of the expansion [147,148]. Certainly, then, the quantitative extraction of gluon density is subject to uncertainties from the theoretical treatment of the expansion and of the energy loss of partons in the entrance-channel cold nuclear matter before they initially collide.

The gluon density derived from energy loss calculations is consistent with estimates from the measured rapidity density of charged hadrons [154] using the Bjorken scenario [84], assuming isentropic expansion and duality between the number of initial gluons and final charged hadrons. Similar values are also deduced under the assumption that the initial state properties in central Au+Au RHIC collisions, and hence the measured particle multiplicities, are determined by gluon-gluon interactions below the gluon density saturation scale in the initial-state nuclei [66]. Additionally, the energy density is estimated from global measurements of transverse energy (see Sec. 3.1) to be of order 50-100 times that in cold nuclear matter, consistent with the values inferred from hydrodynamics accounts of measured hadron spectra and flow. The consistency among all these estimates, though only semi-quantitative at present, is quite significant. These inferred densities fall well into the regime where LQCD calculations predict equilibrated matter to reside in the QGP phase.

4.4 Rapidity-dependence of high p_T hadron yields in d+Au collisions

It had been proposed recently [150] that gluon saturation effects can extend well beyond the saturation momentum scale Q_s, resulting in hadron suppression relative to binary scaling ($R_{AB}(p_T)$<1) for $p_T \sim 5-10$ GeV/c mid-rapidity hadron production at RHIC energies, in apparent agreement with the data in Fig. 31. However, since this predicted suppression originates in the properties of the incoming nuclear wave function, hadron production in d+Au collisions should also be suppressed by this mechanism [150]. Experimentally, an *enhancement* in mid-rapidity hadron production in d+Au is seen instead (Fig. 28 [138–141]), even in central d+Au collisions [141] where saturation effects should be most pronounced. The observed enhancement is at variance with saturation model expectations at high p_T [150].

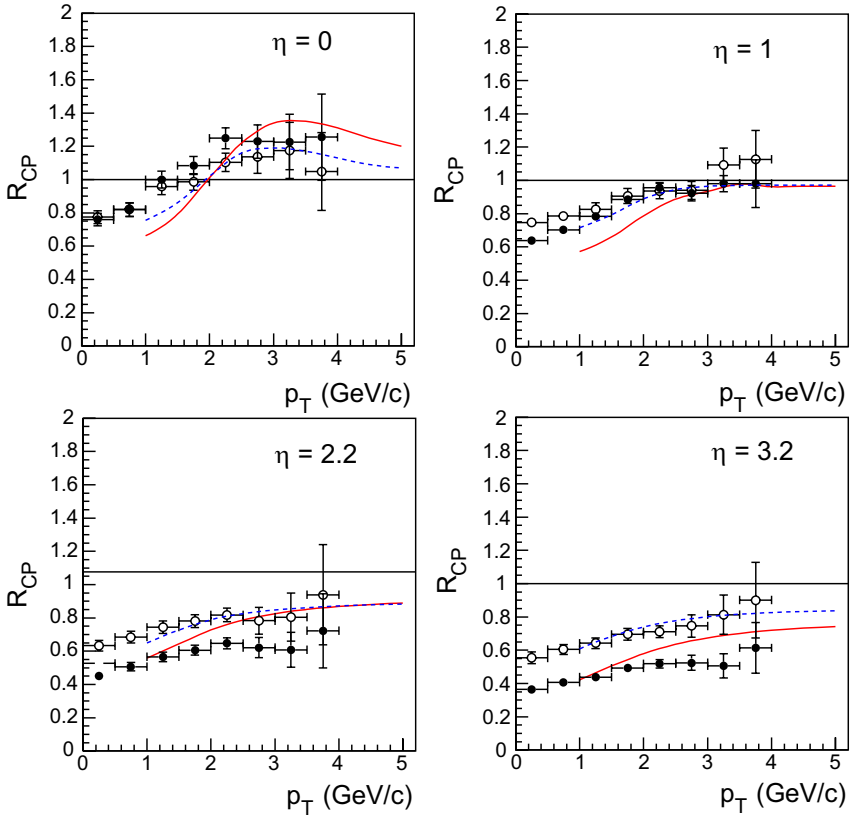

Fig. 32. *The ratio R_{CP} of binary-scaled central to peripheral hadron yields for d+Au collisions at $\sqrt{s_{\rm NN}}$=200 GeV, plotted as a function of p_T for four different pseudo-rapidity bins, centered at $\eta = 0$, $\eta = 1$, $\eta = 2.2$ and $\eta = 3.2$. The measurements are from the Brahms Collaboration [155], for all charged hadrons (negative hadrons only) in the case of the former (latter) two η bins. The curves represent gluon saturation model fits from [157]. The filled circles and solid curves compare yields in the 0-20% to 60-80% centrality bins, while the open circles and dashed curves compare 30-50% to 60-80%. The figure is taken from Ref. [157].*

However, at large rapidities in the deuteron direction, a suppression of the highest p_T hadrons studied is indeed observed in d+Au collisions, as revealed by the results from the Brahms experiment in Fig. 32 [155]. This is not true of large rapidities in the Au direction [158,159]. This distinct behavior is consistent with gluon saturation models, as seen by the fits [157] to these results in Fig. 32. High-p_T hadrons produced at small angles with respect to the deuteron beam arise preferentially from asymmetric partonic collisions involving gluons at low Bjorken x in the Au nucleus. (For example, in a next-to-leading order leading-twist perturbative QCD calculation, the mean x-value of partons probed in the Au nucleus has been found to be 0.03-0.05 when selecting on hadrons at $\eta = 3.2$ and $p_T = 1.5$ GeV/c [156]. Note, however, that such a calculation may have limited validity in the regime of strong gluonic fields.) It is precisely at low x in heavy nuclei that gluon saturation, and the resultant suppression in high-p_T hadron production, should set in. Thus, gluon satura-

tion models predicted the qualitative behavior of increasing suppression with increasing rapidity in the deuteron direction before the experimental results became available [160], although parameter values had to be tuned after the fact [157] to adjust the saturation scale to obtain the fits shown in Fig. 32.

At the moderate p_T values kinematically accessible at large pseudorapidity, one may worry legitimately that softer hadron production mechanisms (*e.g.*, quark recombination) and initial-state multiple scattering of partons before hard collisions complicate the interpretation of the d+Au results. The same basic suppression of hadrons in the deuteron, relative to the Au, direction can be seen extending to higher p_T in the mid-rapidity backward/forward yield ratios from STAR [159], shown in Fig. 33. The same gluon saturation model calculations [157] shown in Fig. 32 are seen in Fig. 33 to be qualitatively, but not quantitatively, consistent with the observed dependences of the hadron yields on pseudorapidity, p_T and centrality. In particular, both measurements and calculations suggest that the mid-rapidity suppression fades away at transverse momenta above 5-6 GeV/c, as one probes higher-x partons in the Au nucleus.

The results in Fig. 32 and 33 represent the strongest evidence yet available for the applicability of Color Glass Condensate concepts within the kinematic range spanned by RHIC collisions. Nonetheless, more mundane origins of this forward hadron suppression in d+Au have not been ruled out. Di-hadron correlation measurements involving these forward hadrons in d+Au collisions may help to distinguish between CGC and other explanations [161]. A critical characteristic of the CGC is that it can be treated as a classical gluon field. Forward hadrons that result from the interaction of a quark from the deuteron beam with this gluon field may have their transverse momentum balanced not by a single recoiling parton (and therefore a jet), but rather by a number of relatively soft hadrons with a much more smeared angular correlation than is characteristic of di-jet processes. Such a "mono-jet" signature would not be expected from more conventional sources of shadowing of gluon densities in the Au nucleus [162], which still allow individual quark-gluon, rather than quark-gluon field, scattering. On the other hand, kinematic limits on the accessible p_T values for forward hadrons imply that one is dealing, even in a di-jet framework, with unconventional away-side jets of only a few GeV/c [163]. In this regime, a suitable reference is needed, using p+p or d+A with a sufficiently light nucleus A to place the contributing parton x-range above the anticipated gluon saturation regime. The discriminating power of di-hadron correlations for CGC mono-jets must be demonstrated by modifications in d+Au with respect to this reference.

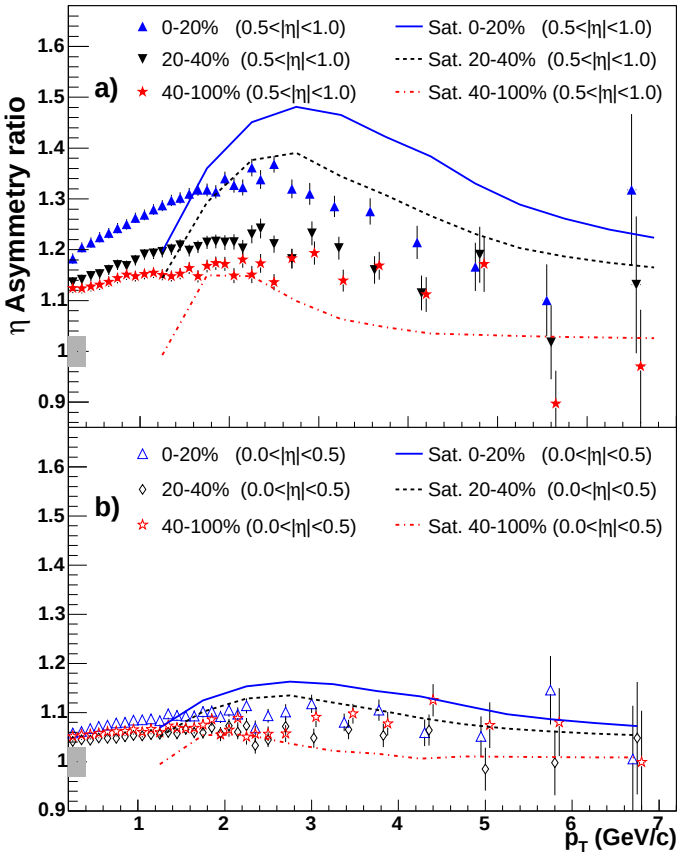

Fig. 33. *Comparison of STAR measurements [159] with gluon saturation model calculations [157] for backward (Au side) to forward (d side) charged hadron yield ratios at mid-rapidity in d+Au collisions at* $\sqrt{s_{\rm NN}}$*=200 GeV. Results are shown as a function of hadron* p_T *for two different pseudorapidity ranges, (a)* $0.5 < |\eta| < 1.0$ *and (b)* $0.0 < |\eta| < 0.5$*, and three different centrality ranges. Centrality is determined experimentally from the measured charged particle multiplicity in the forward Au direction, for* $-3.8 < \eta < -2.8$*. Figure is taken from Ref. [159].*

4.5 Outlook

While large effects have been observed and the phenomenon of jet quenching in dense matter has been firmly established, precision data in a larger p_T range are needed to fully explore the jet quenching phenomena and their connection to properties of the dense matter. The region $2<p_T<6$ GeV/c has significant contributions from non-perturbative processes other than vacuum fragmentation of partons, perhaps revealing novel hadronization mechanisms. Most studies to date of azimuthal anisotropies and correlations of "jets" have by necessity been constrained to this region, with only the inclusive spectra extending to the range where hard scattering is expected to dominate the inclusive yield. High statistics data sets for much higher p_T hadrons are needed to fully exploit azimuthal asymmetries and correlations as measurements of partonic energy loss. Dihadron measurements probing the details of the frag-

mentation process may be sensitive to the *energy* density, in addition to the gluon density that is probed with the present measurements. Heavy quark suppression is theoretically better controlled, and measurement of it will provide a critical check on the understanding of partonic energy loss. The *differential* measurement of energy loss through measurement of the emerging away-side jet and the recovery of the energy radiated in soft hadrons is still in its initial phase of study. A complete mapping of the modified fragmentation with larger initial jet energy and with a direct photon trigger will crosscheck the energy dependence of energy loss extracted from single inclusive hadron suppression. Experiments at different colliding energies are also useful to map the variation of jet quenching with initial energy density and the lifetime of the dense system.

At the same time as we extend the p_T range for jet quenching studies on the high side, it is crucial also to pursue further (particle-identified) hadron correlation measurements in the soft sector, in order to understand better how jets are modified by interactions with the dense bulk matter. Measurements such as those presented in Figs. 25 and 30 are just beginning to illuminate the dissipative processes leading to thermalization of parton energy. The properties of particles that have been substantially degraded, but not completely thermalized, by passage through the bulk may provide particularly fertile ground for exposing possible fundamental modifications (*e.g.*, symmetry violations or restoration) of strong interactions in RHIC collision matter.

5 Some Open Issues

It should be clear from the detailed discussions of experimental and theoretical results in the preceding chapters that some open questions need to be addressed before we can judge the evidence in favor of QGP formation at RHIC to be compelling. In this chapter we collect a number of such open questions for both experiment and theory. Convincing answers to even a few of these questions might tip the balance in favor of a QGP discovery claim. But even then, it will be important to address the remaining questions to solidify our understanding of the properties of the matter produced in RHIC collisions.

Lattice QCD calculations suggest that a confined state is impossible in bulk, thermodynamically equilibrated matter at the energy densities apparently achieved at RHIC. Indeed, several experimental observations are *consistent* with the creation of deconfined matter. However, a discovery as important as the observation of a fundamentally new state of matter surely demands proof beyond circumstantial evidence for deconfinement. Can we do better?

One response that has been offered is that the EOS of strongly interacting matter is already known from lattice QCD calculations, so that only the conditions initially attained in heavy-ion collisions, and the degree of thermalization in the matter produced, are open to doubt. Such a view tends to trivialize the QGP search by presuming the answer. Indeed, an important aspect of the original motivation for the experimental program at RHIC was to explore the Equation of State of strongly interacting matter under these extreme conditions of energy density. Lattice QCD, in addition to its technical difficulties and attendant numerical uncertainties, attempts to treat bulk, static, thermodynamically equilibrated quark-gluon systems. The relationship of such idealized matter to the finite, rapidly evolving systems produced in relativistic heavy-ion collisions is not *a priori* clear. One would prefer, then, to take LQCD calculations as guideposts to the transition properties to search for experimentally, but not as unassailable truth. On the other hand, there are sufficient complexities in the theoretical treatment of heavy-ion collisions that one would like to apply all credible constraints in parameterizing the problem. This dichotomy leads to our first question:

- **To what extent should LQCD results be used to constrain the Equations of State considered in model treatments of RHIC collisions? How does one allow for independent checks of the applicability of LQCD to the dynamic environment of a RHIC collision?**

Experimentally, to verify the creation of a fundamentally new state of matter at RHIC one would like crosschecks demonstrating that the matter behaves

qualitatively *differently* than "normal" (hadronic) matter in a system known or believed to be in a confined state. Although such a demonstration might be straightforward in bulk matter, it becomes an enormous challenge with the limited experimental control one has over thermodynamic variables in heavy-ion collisions. The finite size and lifetime of the matter produced in the early collision stages, coupled with the absence of global thermal equilibrium and of measurements (to date) of local temperature, all work to obscure the hallmark of QGP formation predicted by lattice QCD: a rapid transition around a critical temperature leading to deconfinement and, quite possibly, chiral symmetry restoration (the latter considered here as a sufficient, but not necessary, QGP manifestation). Given these complications, the underlying challenge to theory and experiment is:

- **Can we make a convincing QGP discovery claim without clear evidence of a rapid transition in the behavior of the matter produced? Can we devise probes with sufficient sensitivity to early, local system temperature to facilitate observation of such an onset at RHIC? Can we predict, based on what we now know from SPS and RHIC collisions, at what energies or under what conditions we might produce matter below the critical temperature, and which observables from those collisions should not match smoothly to SPS and RHIC results?**

At the most basic level, it is conceivable that there is no rapid deconfinement transition in nature (or at least in the matter formed fleetingly in heavy-ion collisions), but rather a gradual evolution from dominance of hadronic toward dominance of partonic degrees of freedom. It is not yet clear that we could distinguish such behavior of QCD matter from the blurring of a well-defined QGP transition by the use of tools with insufficient resolution or control.

5.1 What experimental crosschecks can be performed on apparent QGP signatures at RHIC?

Below we briefly discuss some of the key observations that underlie theoretical claims [6–8] that deconfined matter has been produced at RHIC, and ask what crosschecks might be carried out to test this hypothesis.

5.1.1 Jet quenching

As discussed in Sec. 4, inclusive hadron spectra and two-particle azimuthal correlations at moderate and high p_T clearly demonstrate that jets are suppressed in central RHIC Au+Au collisions, relative to scaled NN collisions. The lack

of suppression (indeed, the enhancement, due to the Cronin effect) in d+Au collisions at RHIC provides a critical crosscheck that the quenching is not an initial-state effect. Measurements with respect to the event reaction plane orientation (see Fig. 29) provide another important crosscheck, demonstrating that the magnitude of the suppression depends strongly on the amount of matter traversed. Such jet quenching was first predicted [46] within the framework of parton energy loss in traversing a QGP. However, more recent theoretical work [58] casts doubt that deconfinement of the medium is essential to the phenomenon, or would be manifested clearly in the energy-dependence of quenching. Nonetheless, experimental hints of a possibly interesting energy dependence to quenching phenomena should be pursued as a potential crosscheck on formation of a new state of matter.

Moderate-p_T (up to 4 GeV/c) yields from Pb-Pb collisions at the SPS [164] appear to show an enhancement over a scaled *parameterized* p-p reference spectrum. However, questions raised about the p-p parameterization [165], combined with the unavailability of measurements constraining the initial-state (Cronin) enhancement at these energies, leave open the possibility that even at SPS, jets in central A+A collisions may turn out to be suppressed *relative to expectations*. Indeed, the data in [164] do demonstrate hadron suppression in central relative to semi-peripheral collisions. Also, it is unclear whether the suppression of away-side two-particle correlations out of the reaction plane, observed at RHIC (see Fig. 29), might be of similar origin as the away-side out-of-plane broadening observed at the SPS [103]. These ambiguities are amplified by the limited p_T range covered in SPS measurements, spanning only a region where RHIC results suggest that hard parton scattering and fragmentation may not yet be the dominant contributing hadron production mechanism. These observations lead to the following question:

- **Is there a qualitative change in the yield of high-p_T hadrons in A+A collisions between SPS and RHIC energies? Or does hadron suppression rather evolve smoothly with energy, reflecting a gradual growth in initial gluon density and parton energy loss? Is it feasible to make meaningful measurements of hard probes at sufficiently low collision energy to test for the absence or gross reduction of jet quenching in matter believed to be in a hot hadronic (*i.e.*, confined) gas state?**

5.1.2 Constituent-quark scaling of yields and anisotropies

The baryon *vs.* meson systematics of R_{CP} (Fig. 15) and the apparent scaling of elliptic flow with the number of constituent quarks (Fig. 20) in the intermediate p_T range strongly suggest collective behavior at a pre-hadronic level, a necessary aspect of QGP formation and thermalization in heavy-ion collisions.

Once again, one would like to observe the *absence* of this behavior for systems in which QGP is not formed. High-quality, particle-identified elliptic flow data do not yet exist at SPS (or lower) energies in this p_T region.

- **Should constituent-quark scaling of v_2 in the intermediate p_T sector be broken if a QGP is *not* formed? If so, is an appropriate statistically meaningful, particle-identified measurement of v_2 at intermediate p_T feasible at $\sqrt{s_{NN}}$ below the QGP formation threshold?**

Alternatively, we could seek to establish the role of constituent quarks more convincingly by additional predictions of the quark coalescence models introduced to characterize this intermediate p_T region. For this purpose it may be helpful to integrate the coalescence models with other (e.g., gluon saturation or hydrodynamics) models that might serve to constrain the anticipated initial conditions and coalescence parameters as a function of centrality or collision energy.

- **Coalescence models have provided a simple ansatz to recognize the possible importance of constituent quark degrees of freedom in the hadronization process in A+A collisions at RHIC, and to suggest that these constituent quarks exhibit collective flow. Once model parameters have been adjusted to account for the observed ratios of yields and elliptic flow strengths for baryons vs. mesons, can integration of key features from other models enhance predictive power? For example, can the centrality-dependence of these ratios, or meson vs. baryon correlations (angular or otherwise) at moderate p_T be predicted?**

5.1.3 Strong elliptic flow in agreement with hydrodynamics

In contrast to the above signatures, which require access to moderate-to-high p_T values, observables in the soft sector have already been extensively explored, even from Bevalac energies. The only soft-sector observable selected as a "pillar" of the QGP claim at RHIC, in Ref. [6], is the strong elliptic flow, whose magnitude, mass and p_T-dependence for mid-central collisions are in reasonable agreement with expectations based on ideal hydrodynamic flow (see Fig. 18). Furthermore, the agreement appears better for an Equation of State that includes passage through a phase transition from partonic to hadronic matter.

This success leads to the claim [3,6] that the elliptic flow has finally, in near-central collisions at RHIC energies, reached the ideal hydrodynamic "limit," suggesting creation of equilibrated, low-viscosity matter at an early stage in

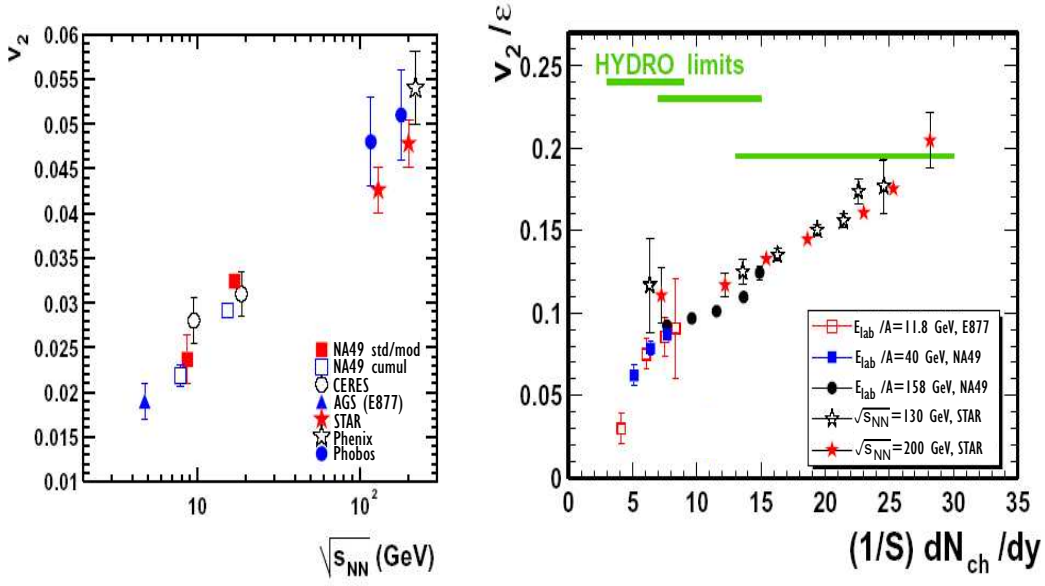

Fig. 34. *(a) Energy dependence of elliptic flow measured near mid-rapidity for mid-central collisions ($\sim 12-34\%$ of the geometric cross section) of $A \sim 200$ nuclei at the AGS, SPS and RHIC. (b) Mid-rapidity elliptic flow measurements from various energies and centralities combined in a single plot of v_2 divided by relevant initial spatial eccentricity vs. charged-particle rapidity density per unit transverse area in the $A+A$ overlap region. The figures, taken from Ref. [100], highlight the smooth behavior of flow vs. energy and centrality. The rightmost points represent near-central STAR results, where the observed v_2/ϵ ratio becomes consistent with limiting hydrodynamic expectations for an ideal relativistic fluid. The hydrodynamic limits are represented by horizontal lines [100] drawn for AGS, SPS and RHIC energies (from left to right), for one particular choice of EOS that assumes no phase transition in the matter produced.*

the collision (when geometric anisotropy is still large). However, the results from many experiments clearly indicate a smoothly rising $v_2(\sqrt{s_{NN}})$, while the hydrodynamic limit for given initial spatial eccentricity and fixed EOS is falling with increasing energy (see Fig. 34). It is thus unclear from the available data whether we are observing at RHIC the interesting onset of saturation of a simple physical limit particularly relevant to QGP matter, or rather an accidental crossing point of experiment with a necessarily somewhat simplified theory. It is of major significance that ideal hydrodynamics appears to work at RHIC for the first time. This conclusion – and in particular the evidence for an Equation of State containing a phase change – would be much strengthened if the hydrodynamic limit were demonstrated to be relevant as well under conditions far removed from those in RHIC measurements to date. Future measurements in central collisions of heavier and highly deformed nuclei (*e.g.*, U+U [3]) possible after a planned upgrade of the ion source for RHIC, or at significantly lower or higher energy (the latter awaiting LHC turn-on) will

provide the possibility of additional crosschecks of this important conclusion.

- **Is the ideal hydrodynamic limit for elliptic flow relevant to heavy-ion collisions over a broad range of conditions, within which near-central Au+Au collisions at full RHIC energy represent merely a first "sighting"? Will v_2 at LHC energies surpass the hydrodynamic limit? Is thermalization likely to be sufficiently established in collisions below $\sqrt{s_{\rm NN}}\approx 100$ GeV to permit meaningful tests of hydrodynamics? If so, will measurements at lower RHIC energies reveal a non-trivial energy dependence of v_2, such as that predicted in Fig. 7 by ideal hydrodynamics incorporating a phase transition? Can one vary the initial spatial eccentricity of the bulk matter independently of centrality and degree of thermalization, via controlled changes in the relative alignment of deformed colliding nuclei such as uranium?**

5.1.4 Dependence of observables on system size

The above questions focused on excitation function measurements, which traditionally have played a crucial role in heavy-ion physics. It is also desirable to explore the appearance and disappearance of possible QGP signatures as a function of system size. To date, system size variations have been examined at RHIC primarily via the centrality dependence of many observables. A number of variables have been observed to change rapidly from the most peripheral to mid-peripheral collisions, and then to saturate for mid-central and central collisions. Examples of this type of behavior include: the strength (I_{AA} in Ref. [71]) and $\Delta\eta$ width (Fig. 25) of near-side di-hadron correlations; the ratio of measured v_2 to the hydrodynamic limit for relevant impact parameter [105]; the strangeness saturation parameter γ_s deduced from statistical model fits to measured hadron yield ratios (inset in Fig. 12) [86]. Do these changes reflect a (QGP) transition with increasing centrality in the nature of the matter first produced, or merely the gradual growth in importance of hadronic initial- and final-state interactions, and in the degree of thermalization achieved, as the number of nucleon participants increases? One's answer to this question may depend on how rapid the variation with centrality appears, but this in turn depends on what measure one uses for centrality, as emphasized in the lower frames of Fig. 25.

As the centrality changes for given colliding nuclei, so, unavoidably, does the initial shape of the overlap region. In order to unravel the influence of different initial conditions on the evolution of the matter formed in heavy-ion collisions, it will be important to measure as well the dependence of observables such as those above on the size of the colliding nuclei.

- **Do RHIC measurements as a function of centrality already contain hints of the onset of QGP formation in relatively peripheral regions? Will future measurements for lighter colliding nuclei permit more definitive delineation of these apparently rapid changes with system size?**

5.2 Do the observed consistencies with QGP formation demand a QGP-based explanation?

Because it is difficult to control the degree of thermalization achieved in heavy-ion collisions, and to measure directly the temperature at which it is initially achieved, it is possible that none of the crosschecks discussed in the preceding subsection for RHIC energies and below may provide definitive experimental resolution concerning QGP formation. In this case, our reliance on the comparison with theory would be significantly increased, and the questions posed below become especially important. Here, we question the *uniqueness* of a QGP-based explanation. In other words, do the data *demand* a scenario characterized by thermalized, deconfined matter?

5.2.1 Strong elliptic flow

The hydrodynamic overestimate of elliptic flow at energies below RHIC has been attributed either to a failure to achieve complete thermalization in those collisions [3] or to their earlier transition to a viscous hadronic phase [6]. These interpretations suggest that the observed energy-dependence of flow (Fig. 34) is dominated by the complex dynamics of early thermalization and late hadronic interactions. While application of hydrodynamics relies on local thermal equilibrium, it is not obvious that agreement with data after parameter adjustment necessarily proves thermalization. The following question is posed in this light.

- **The unprecedented success of hydrodynamics calculations assuming ideal relativistic fluid behavior in accounting for RHIC elliptic flow results has been interpreted as evidence for both early attainment of local thermal equilibrium and an Equation of State with a soft point, characteristic of the predicted phase transition. How do we know that the observed elliptic flow can't result, alternatively, from a harder EOS coupled with incomplete or late thermalization and/or significant viscosity in the produced matter?**

Even if we *assume* thermalization (and hence the applicability of hydrodynamics), it is clear that a complete evaluation of the "theoretical error bars"

has yet to be performed. When parameters are adjusted to reproduce spectra, agreement with v_2 measurements in different centrality bins is typically at the 20-30% level. The continuing systematic discrepancies from HBT results, and from the energy dependence of elliptic flow when simplified freezeout parameterizations are applied, suggest some level of additional ambiguity from the treatment of late-stage hadronic interactions and from possibly faulty assumptions of the usual hydrodynamics calculations (see Sec. 2.2). When theoretical uncertainties within hydrodynamics are fairly treated, does a convincing signal for an EOS with a soft point survive?

- **The indirect evidence for a phase transition of some sort in the elliptic flow results comes primarily from the sensitivity in hydrodynamics calculations of the magnitude and hadron mass-dependence of v_2 to the EOS. How does the level of this EOS sensitivity compare quantitatively to that of uncertainties in the calculations, gleaned from the range of parameter adjustments, from the observed deviations from the combination of elliptic flow, spectra and HBT correlations, and from the sensitivity to the freezeout treatment and to such normally neglected effects as viscosity and boost non-invariance?**

5.2.2 Jet quenching and high gluon density

The parton energy loss treatments do not directly distinguish passage through confined vs. deconfined systems. Although effects of deconfinement must exist at some level, *e.g.*, on the propagation of radiated soft gluons, their inclusion in the energy loss models might well be quantitatively masked by other uncertainties in the calculations. Evidence of deconfinement must then be indirect, via comparison of the magnitude of inferred gluon or energy densities early in the collision to those suggested by independent partonic treatments such as gluon saturation models. The actual energy loss inferred from fits to RHIC data, through the rapidly expanding collision matter, is only slightly larger than that indicated through static cold nuclei by fits to semi-inclusive deep inelastic scattering data. The significance of the results is then greatly magnified by the correction to go from the expanding collision matter to an equivalent static system at the time of the initial hard scattering. The quantitative uncertainties listed in the question below will then be similarly magnified. What, then, is a reasonable guess of the range of initial gluon or energy densities that can be accommodated, and how does one demonstrate that those densities can only be reached in a deconfined medium?

- **Does the magnitude of the parton energy loss inferred from RHIC hadron suppression observations *demand* an explanation in terms of traversal through deconfined matter? The answer must take**

into account quantitative uncertainties in the energy loss treatment arising, for example, from the uncertain applicability of factorization in-medium, from potential differences (other than those due to energy loss) between in-medium and vacuum fragmentation, and from effects of the expanding matter and of energy loss of the partons through cold matter preceding the hard scattering.

Gluon saturation models set a QCD scale for anticipated gluon densities, that can then be compared to values inferred from parton energy loss treatments, modulo the questions asked above and below. An important question, given that RHIC multiplicity data are used as input to the models (*e.g.*, to fix the proportionality between gluon density and hadron yields) is whether they provide information truly independent from the initial energy density inferred via the simple Bjorken hydrodynamic expansion scenario (Eq. 4) from measured rapidity densities of transverse energy.

- **If there is a truly universal gluon density saturation scale, determined already from HERA e-p deep inelastic scattering measurements, why can't RHIC A+A particle multiplicities be predicted a priori without input from RHIC experimental data? Is not the A- (or N_{part}-) dependence of the gluon densities at the relevant Bjorken x-ranges predicted in gluon saturation treatments? Can saturated entrance-channel gluon densities in overlapping cold nuclei be directly compared to the early gluon densities in thermalized hot matter, inferred from parton energy loss treatments of jet quenching?**

6 Overview and Outlook

6.1 What have we learned from the first three years of RHIC measurements?

Already in their first three years, all four RHIC experiments have been enormously successful in producing a broad array of high-quality data illuminating the dynamics of heavy-ion collisions in a new regime of very high energy densities. STAR, in particular, has established a number of seminal, striking results highlighted in Secs. 3 and 4 of this document. In parallel, there have been significant advances in the theoretical treatment of these collisions. The theory-experiment comparison indicates that central Au+Au collisions at RHIC produce a unique form of strongly interacting matter, with some dramatic and surprisingly simple properties. A number of the most striking experimental results have been described to a reasonable quantitative level, and in some cases even predicted beforehand, using theoretical treatments inspired by QCD and based on QGP formation in the early stages of the collisions.

The observed hadron spectra and correlations at RHIC reveal three transverse momentum ranges with distinct behavior: a soft range ($p_T \lesssim$1.5 GeV/c) containing the vast majority of produced hadrons, representing most of the remnants of the bulk collision matter; a hard-scattering range ($p_T \gtrsim 6$ GeV/c), providing partonic probes of the early collision matter; and an intermediate range ($1.5 \lesssim p_T \lesssim 6$ GeV/c) where hard processes coexist with softer ones. The behavior in each of these ranges is quite different than would be expected from an incoherent sum of independent nucleon-nucleon collisions; for the hard sector, in particular, this is one of the most important new observations at RHIC. Below we summarize the major findings described in earlier chapters within each of these three ranges, in each case listing them in approximate decreasing order of what we judge to be their level of robustness with respect to current experimental and theoretical ambiguities. This is not intended necessarily to represent order of importance, as some of the presently model-dependent conclusions are among the strongest arguments in favor of QGP formation.

6.1.1 Soft sector

- The matter produced exhibits **strong collective flow**: most hadrons at low p_T reflect a communal transverse velocity field resulting from conditions early in the collision, when the matter was clearly expanding rapidly under high, azimuthally anisotropic, pressure gradients and frequent interactions among the constituents. The commonality of the velocity is clearest from

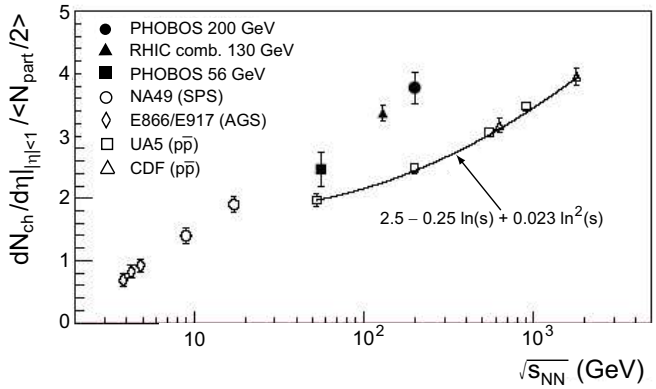

Fig. 35. *Measured mid-rapidity charged particle densities, scaled by the calculated number of participant nucleons, for central collisions of $A \sim 200$ nuclei at AGS, SPS and RHIC, plotted as a function of the center-of-mass energy. Results for $\overline{p}+p$ collisions are shown for comparison. Figure from [80].*

the systematic dependence of elliptic flow strength on hadron mass at low p_T (see Fig. 18), from the common radial flow velocities extracted by fitting observed spectra (Fig. 14), and from the measurements of HBT and non-identical particle correlations [121]. All of these features fit naturally, at least in a qualitative way, within a hydrodynamic description of the system evolution.

- Most bulk properties measured appear to fall on quite smooth curves with similar results from lower-energy collisions. Examples shown include features of integrated two-hadron p_T correlations (Fig. 24), elliptic flow (Fig. 34), charged particle density (Fig. 35) and emitting source radii inferred from HBT analyses (Fig. 36). Similarly, the centrality-dependences observed at RHIC are generally smooth (but see Fig. 25 for a possible exception). These experimental results contrast with theoretical speculations and predictions made before RHIC start-up, which often [11,30,166] suggested strong energy dependences accompanying the hadron-to-QGP transition. The observed smooth general behavior has been primarily attributed to the formation of matter over a range of initial local conditions, even at a given collision energy or centrality, and to the absence of any direct experimental determination of early temperature. In any case, the results clearly highlight **the difficulty of observing any rapid "smoking-gun" onset of a transition to a new form of matter**.
- Despite the smoothness of the energy and centrality dependences, two important milestones related to the attainment of thermal equilibrium appear to be reached for the first time in near-central RHIC collisions at or near full energy. The first is that **the yields of different hadron species, *up to and including multi-strange hadrons*, become consistent with a Grand Canonical statistical distribution** at a chemical freezeout temperature of 160 ± 10 MeV and a baryon chemical potential ≈ 25 MeV

(see Fig. 12). This result places an effective lower limit on the temperatures attained if thermal equilibration is reached during the collision stages preceding this freezeout. This lower limit is **essentially equal to the QGP transition temperature predicted by lattice QCD calculations** (see Fig. 1).

- At the same time (*i.e.*, for near-central RHIC collisions) the mass- and p_T-dependence of the observed hadron spectra and of the strong elliptic flow in the soft sector become **consistent, at the** $\pm 20-30\%$ **level, with hydrodynamic expectations for an *ideal* relativistic fluid** formed with an initial eccentricity characteristic of the impact parameter. These hydrodynamic calculations have not yet succeeded in also quantitatively explaining the emitting hadron source size inferred from measured HBT correlations (see Fig. 22). Nonetheless, their overall success suggests that the interactions among constituents in the initial stages of these near-central collisions are characterized by very short mean free paths, leading to **quite rapid** ($\tau \lesssim 1$ **fm/c) attainment of at least approximate local thermal equilibrium**. The short mean free path in turn suggests a very dense initial system.
- Based on the rapid attainment of thermal equilibrium, and making the assumption of longitudinal boost-invariant expansion, one can extract [84] a rough lower bound on the initial energy density from measured rapidity densities [81,83] of the total transverse energy (dE_T/dy) produced in the collisions. These estimates suggest that in central Au+Au collisions at RHIC, **matter is formed at an initial energy density well above the critical density** (~ 1.0 GeV/fm^3) predicted by LQCD for a transition to the QGP.
- Measurements of two-hadron angular correlations and of the power spectrum of local charged-particle density fluctuations reveal strong near-side correlations surviving in the soft sector, reminiscent of jet-like behavior in some aspects, but with a strong pseudorapidity broadening introduced by the presence of the collision matter. The observed structure (see Fig. 25) suggests that **soft jet fragments are not fully thermalized with the bulk matter, but nonetheless show the effects of substantial coupling to that matter** in a considerable broadening of the jet "peak" in pseudorapidity difference between two hadrons.
- Hydrodynamics calculations are best able to reproduce RHIC results for hadron spectra and the magnitude and mass-dependence of elliptic flow (Fig. 18) by utilizing **an Equation of State incorporating a soft LQCD-inspired phase transition from QGP to hadronic matter**. However, the calculations also exhibit comparable sensitivity to other *a priori* unknown features, *e.g.*, the details of the hadronic final-state interactions and the time at which thermal equilibrium is first attained. In light of these competing sensitivities, it is not yet clear if the experimental results truly *demand* an EOS with a soft point.

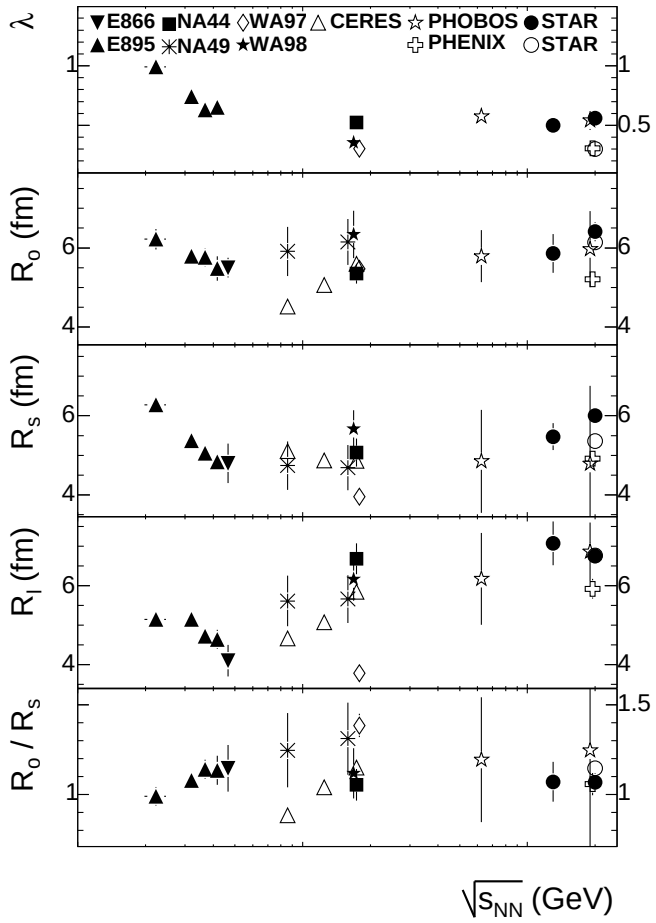

Fig. 36. *Energy dependence of HBT parameters extracted from pion pair correlations in central $A + A$ ($A \sim 200$) collisions at mid-rapidity and pair $k_T \approx 0.2$ GeV/c. The data span the AGS, SPS and RHIC. Figure from [167].*

6.1.2 Intermediate sector

- In the intermediate p_T range, the elliptic flow strength v_2 saturates and we see systematic meson vs. baryon differences (rather than a systematic mass-dependence) in both yield (see Fig. 15) and v_2 value (Figs. 20). In the same region we also observe clear jet-like angular correlation peaks in the near-side azimuthal difference distributions between pairs of hadrons (see Fig. 29). The most natural interpretation for this combination of characteristics is that **the intermediate-p_T yield arises from a mixture of partonic hard-scattering (responsible for the jet-like correlations) and softer processes (responsible for the meson-baryon differences)** .
- **The saturated v_2 values appear to scale with the number of constituent (or valence) quarks n in the hadron studied**, *i.e.*, v_2/n vs. p_T/n falls on a common curve for mesons and baryons (see Fig. 20). If this trend persists as the particle-identified intermediate-p_T data are improved in

statistical precision for a suitable variety of hadron types, it would provide direct experimental evidence for the relevance of sub-hadronic degrees of freedom in determining flow for hadrons produced at moderate p_T in RHIC collisions.

- Quark recombination models are able to provide a reasonable account of the observed meson and baryon spectra, as well as the v_2 systematics, in the intermediate sector by **a sum of contributions from coalescence of thermalized constituent quarks following an exponential p_T spectrum and from fragmentation of initially hard-scattered partons with a power-law spectrum** [70]. It is not yet clear if the same mixture can also account quantitatively for the azimuthal dihadron correlation (including background under the jet-like peaks) results as a function of p_T. Other models [69,72] mix the above contributions by also invoking recombination of hard-scattered with thermal partons.

6.1.3 Hard sector

- The dominant characteristic of the hard regime is **the strong suppression of hadron yields in central Au+Au collisions**, in comparison to expectations from p+p or peripheral Au+Au collisions, scaled by the number of contributing binary (nucleon-nucleon) collisions (see Fig. 31). Such suppression sets in already in the intermediate sector, but saturates and remains constant as a function of p_T throughout the hard region explored to date. Such suppression was not seen in d+Au collisions at RHIC, indicating that it is **a final-state effect associated with the collision matter produced in Au+Au**. It is consistent with effects of parton energy loss in traversing dense matter, predicted before the data were available [147,148].
- Azimuthal correlations of moderate- (see Fig. 29) and high-p_T [145] hadrons exhibit clear jet-like peaks on the near side. However, **the anticipated away-side peak associated with dijet production is suppressed** by progressively larger factors as the Au+Au centrality is increased, and for given centrality, as the amount of (azimuthally anisotropic) matter traversed is increased (see Fig. 29). Again, no such suppression is observed in d+Au collisions. The suppression of hadron yields and back-to-back correlations firmly establish that **jets are quenched by very strong interactions with the matter produced in central Au+Au collisions**. The jet-like near-side correlations survive presumably because one observes preferentially hard fragments of partons scattered outward from the surface region of the collision zone. Effects of interaction with the bulk matter are nonetheless still seen on the near side, primarily by the broadened distribution in pseudorapidity of softer correlated fragments (see Fig. 25 and Ref. [146]).
- Many features of the observed suppression of high-p_T hadrons, including the centrality-dependence and the p_T-independence, can be described efficiently by **perturbative QCD calculations incorporating parton en-**

ergy loss in a thin, dense medium (see Fig. 31). To reproduce the magnitude of the observed suppression, despite the rapid expansion of the collision matter the partons traverse, these treatments need to assume that **the initial gluon density when the collective expansion begins is more than an order of magnitude greater than that characteristic of cold, confined nuclear matter** [147]. The inferred gluon density is consistent, at a factor ~ 2 level, with the saturated densities needed to account for RHIC particle multiplicity results in gluon saturation models (see Fig. 11).

- The yields of hadrons at moderate-to-high p_T in central d+Au collisions exhibit a systematic dependence on pseudorapidity, marked by **substantial suppression, with respect to binary scaling expectations, of products near the deuteron beam direction, in contrast to substantial enhancement of products at mid-rapidity and near the Au beam direction** (see Figs. 32 and 33). This pattern suggests a depletion of gluon densities at low Bjorken x in the colliding Au nucleus, and is **qualitatively consistent with predictions of gluon saturation models**. Measurements to date cannot yet distinguish interactions with a classical gluon field (Color Glass Condensate) from interactions with a more conventionally shadowed density of individual gluons.
- Angular correlations between moderate-p_T and soft hadrons have been used to explore how transverse momentum balance is achieved, in light of jet quenching, opposite a high-p_T hadron in central Au+Au collisions. The results show the balancing hadrons to be significantly larger in number, softer (see Fig. 30) and more widely dispersed in angle compared to p+p or peripheral Au+Au collisions, with **little remnant of away-side jet-like behavior**. To the extent that hard scattering dominates these correlations at moderate and low p_T, the results could signal an approach of the away-side parton toward thermal equilibrium with the bulk matter it traverses. As mentioned earlier, progress toward thermalization of jet fragments on the near-side is also suggested by soft-hadron correlations.
- The hard sector was not accessed in SPS experiments, so any possible energy dependence of jet quenching can only be explored via the hadron nuclear modification factor in the intermediate-p_T range. While the results (see Fig. 37) leave open the possibility of a rapid transition [53], one is not expected on the basis of theoretical studies of parton energy loss [58]. Furthermore, serious questions have been raised [165] about the validity of the p+p reference data used to determine the SPS result in the figure.

In summary, the RHIC program has enabled dramatic advances in the study of hot strongly interacting matter, for two basic reasons. With the extended reach in initial energy density, the matter produced in the most central RHIC collisions appears to have attained conditions that considerably simplify its theoretical treatment: essentially ideal fluid expansion, and approximate local thermal equilibrium beyond the LQCD-predicted threshold for QGP formation. With the extended reach in particle momentum, the RHIC experiments

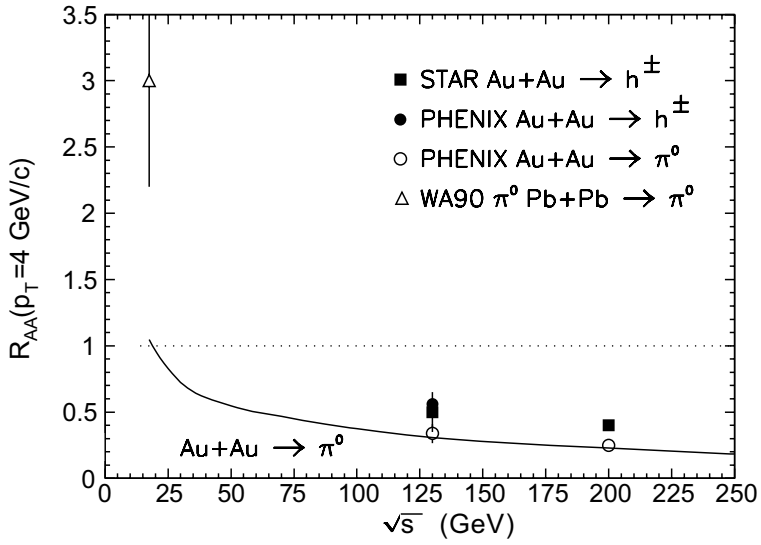

Fig. 37. *The nuclear modification factor measured for 4 GeV/c hadrons in central $A + A$ ($A \sim 200$) collisions at SPS and two RHIC energies, showing (Cronin) enhancement at the lower energy and clear jet-quenching suppression at RHIC. The small difference between RHIC charged hadron and identified π^0 results reflects meson vs. baryon differences in this p_T range. The solid curve represents a parton energy loss calculation under simplifying assumptions concerning the energy-dependence, as described in [147].*

have developed probes for behavior that was difficult to access at lower collision energies: jet quenching and apparent constituent quark scaling of elliptic flow. These results indicate, with fairly modest reliance on theory, that RHIC collisions produce highly opaque and dense matter that behaves collectively. The magnitude of the density inferred from parton energy loss treatments, together with the hints of constituent quark collective flow, argue against the effectiveness of a purely hadronic treatment of this unique strongly interacting matter. It appears from the most robust signals to evolve for a significant fraction of its lifetime as a low-viscosity, pre-hadronic liquid.

If one takes seriously all of the theoretical successes mentioned above, they suggest the following more detailed overall picture of RHIC collisions: Interactions of very short mean free path within the gluon density saturation regime lead to a rapidly thermalized partonic system at energy densities and temperatures above the LQCD critical values. This thermalized matter expands collectively and cools as an ideal fluid, until the phase transition back to hadronic matter begins, leading to a significant pause in the build-up of elliptic flow. During the phase transition, constituent quarks emerge as the effective degrees of freedom in describing hadron formation at medium p_T out of this initially partonic matter. Initially hard-scattered partons (with lower color interaction cross sections than the bulk partons) traversing this matter lose substantial energy to the medium via gluon radiation, and thereby approach, but do not quite reach, equilibration with the bulk matter. Thus,

some evidence of degraded jets survives (*e.g.*, see Fig. 29), depending on the amount of matter traversed. Any claim of QGP discovery based on RHIC results to date requires an assessment of the robustness, internal consistency, quantitative success and predictive power of this emerging picture.

6.2 Are we there yet?

The consistency noted above of many RHIC results with a QGP-based theoretical framework is an important and highly non-trivial statement! Indeed, it is the basis of some claims [6–8] that the Quark-Gluon Plasma has already been discovered at RHIC. However, these claims are associated with QGP definitions [6,7] that do not specifically highlight deconfinement as an essential property to be demonstrated. In our judgment, for reasons mentioned below, and also reflected in the list of open questions provided in Chap. 5 of this document, it is premature to conclude definitively that the matter produced in central RHIC collisions is a Quark-Gluon Plasma, as this term has been understood by the scientific community for the past 20 years (see Appendix B).

- The RHIC experiments have not yet produced *direct* evidence for deconfinement, or indeed for any clear transition in thermodynamic properties of the matter produced. It may be unreasonable to expect a clear onset of deconfinement in heavy-ion systems as a function of collision energy, because the matter, even if locally thermalized, is presumably formed over a range of initial temperatures at any given collision energy. Thus, in the emerging theoretical picture, the matter produced in heavy-ion collisions at SPS was probably also formed in part above the critical energy density, but over a smaller fraction of the volume and with shorter-lived (or perhaps never attained) thermal equilibrium, in comparison with RHIC collisions. At still lower collision energies, where the critical conditions might never be reached, various aspects of the theoretical framework applied at RHIC become inapplicable, precluding a simple theory-experiment comparison over a range from purely hadronic to allegedly QGP-dominated matter.
- The indirect evidence for a thermodynamic transition and for attainment of local thermal equilibrium in the matter produced at RHIC are intertwined in the hydrodynamics account for observed hadron spectra and elliptic flow results. The uniqueness of the solution involving early thermalization and an EOS with a soft mixed phase is not yet demonstrated. Nor is its robustness against changes in the treatment of the late hadronic stage of the evolution, including the introduction of viscosity and other modifications that might be needed to reduce discrepancies from HBT measurements.
- The indirect evidence for deconfinement rests primarily on the large initial gluon densities inferred from parton energy loss fits to the observed hadron

suppression at high p_T, and on the supposition that such high densities could only be achieved in deconfined matter. The latter supposition has yet to be demonstrated in a compelling theoretical argument. The agreement with initial gluon densities suggested by Color Glass Condensate approaches is encouraging, but is still at a basically qualitative level. The measurements suggest that matter is formed at initial temperatures and energy densities at or above the critical values predicted by LQCD for a deconfinement transition. But they do not establish the detailed relevance of the lattice calculations to the fleeting dynamic matter produced in heavy-ion collisions.

- The role of collectively flowing constituent quarks in hadron formation at intermediate p_T is not yet well established experimentally. If it becomes so established by subsequent measurements and analyses, this will hint at the existence of a collective, thermalized partonic stage in the system evolution. However, that hint will fall short of a conclusive QGP demonstration until some interpretational ambiguities are resolved: Is it really *constituent*, rather than *current* (valence) quarks that coalesce? If the former, do the constituent quarks then merely represent the effective degrees of freedom for hadronization of a QGP, or do they indicate an intermediate, pre-hadronic evolutionary stage, after the abundant gluons and current quarks have coalesced and dynamical chiral symmetry breaking has been re-introduced? If there is a distinct constituent quark formation stage, is thermalization achieved before, or only during, that stage?
- The theory remains a patchwork of different treatments applied in succession to each stage of the collision evolution, without yet a clear delineation of the different aspects as distinct limits of one overarching, seamless theory. The theoretical claims of QGP discovery in [8], considered together, rely on five "pillars of wisdom" for RHIC central Au+Au collisions, and each invokes a separate model or theoretical approach for its interpretation: (i) statistical model fits to measured hadron yields to infer possible chemical equilibrium across the u, d and s sectors; (ii) hydrodynamics calculations of elliptic flow to suggest early thermalization and soft EOS; (iii) quark recombination models to highlight the role of thermalized constituent quarks in intermediate-sector v_2 scaling; (iv) parton energy loss models to infer an initial gluon density from high-p_T hadron suppression observations; (v) gluon saturation model fits to observed hadron multiplicities and yields at large rapidity, to suggest how high-density QCD may predetermine the achieved initial gluon densities. Each movement of the theoretical suite has its own assumptions, technical difficulties, adjusted parameters and quantitative uncertainties, and they fit together somewhat uneasily. Until they are assimilated into a more self-consistent whole with only a few overall parameters fitted to existing data, it may be difficult to assess theoretical uncertainties quantitatively or to make non-trivial quantitative predictions whose comparison with future experimental results have the potential to prove the theory wrong.

The bottom line is that in the absence of a direct "smoking gun" signal of deconfinement revealed by experiment alone, a QGP discovery claim must rest on the comparison with a promising, but still not yet mature, theoretical framework. In this circumstance, clear predictive power with quantitative assessments of theoretical uncertainties are necessary for the present appealing picture to survive as a lasting one. The matter produced in RHIC collisions is fascinating and unique. The continuing delineation of its properties will pose critical tests for the theoretical treatment of non-perturbative QCD. But we judge that a QGP discovery claim based on RHIC measurements to date would be premature. We do not propose that a comprehensive theoretical understanding of all observed phenomena must be attained before a discovery claim is warranted, but only that at least some of the serious open questions posed above and in Sec. 5 be successfully answered.

6.3 What are the critical needs from future experiments?

The above comments make it clear what is needed most urgently from theory. But how can future measurements, analyses and heavy-ion collision facilities bring us to a clearer delineation of the fundamental properties of the unique matter produced, and hopefully to a more definitive conclusion regarding the formation of a Quark-Gluon Plasma? We briefly describe below the goals of some important anticipated programs, separated into short-term and long-term prospects, although the distinction in time scale is not always sharp. In the short term, RHIC measurements should concentrate on verifying and extending its new observations of jet quenching and v_2 scaling; on testing quantitative predictions of theoretical calculations incorporating a QGP transition at lower energies and for different system sizes; on measuring charmed-hadron and charmonium yields and flow to search for other evidence of deconfinement; and on testing more extensive predictions of gluon saturation models for forward hadron production. Some of the relevant data have already been acquired during the highly successful 2004 RHIC run – which has increased the RHIC database by an order of magnitude – and simply await analysis, while other measurements require anticipated near-term upgrades of the detectors. In the longer term, the LHC will become available to provide crucial tests of QGP-based theoretical extrapolations to much higher energies, and to focus on very high p_T probes of collision matter that is likely to be formed deep into the gluon saturation regime. Over that same period, RHIC should provide the extended integrated luminosities and upgraded detectors needed to undertake statistically challenging measurements to probe directly the initial system temperature, the pattern of production yields among various heavy quarkonium species, the quantitative energy loss of partons traversing the early collision matter, and the fate of strong-interaction symmetries in that

matter.

Important short-term goals include the following:

- **Establish v_2 scaling more definitively.** Extend the particle-identified flow measurements for hadrons in the medium-p_T region over a broader p_T range, a wider variety of hadron species, and as a function of centrality. Does the universal curve of v_2/n vs. p_T/n remain a good description of all the data? How is the scaling interpretation affected by anticipated hard contributions associated with differential jet quenching through spatially anisotropic collision matter? Can the observed di-hadron angular correlations be quantitatively accounted for by a 2-component model attributing hadron production in this region to quark coalescence (with correlations reflecting only the collective expansion) plus fragmentation (with jet-like correlations)? Do hadrons such as ϕ-mesons or Ω-baryons, containing no valence u or d quarks, and hence with quark-exchange contributions to hadronic interaction cross sections suppressed in normal nuclear matter, follow the same flow trends as other hadrons? Do the measured v_2 values for resonances reflect their constituent quark, or rather their hadron, content? These investigations have the potential to establish more clearly that constituent quarks exhibiting collective flow are the relevant degrees of freedom for hadronization at medium p_T.
- **Establish that jet quenching is an indicator of parton, and not hadron, energy loss.** Extend the measurements of hadron energy loss and di-hadron correlations to higher p_T, including particle identification in at least some cases. Do the meson-baryon suppression differences seen at lower p_T truly disappear? Does the magnitude of the suppression remain largely independent of p_T, in contrast to expectations for hadron energy loss [53]? Does one begin to see a return of away-side jet behavior, via punch-through of correlated fragments opposite a higher-p_T trigger hadron? Improve the precision of di-hadron correlations with respect to the reaction plane, and extend jet quenching measurements to lighter colliding nuclei, to observe the non-linear dependence on distance traversed, expected for radiating partons [4]. Measure the nuclear modification factors for charmed meson production, to look for the "dead-cone" effect predicted [54] to reduce energy loss for heavy quarks.
- **Extend RHIC Au+Au measurements down toward SPS measurements in energy, to test quantitative predictions of the energy-dependence.** Does the suppression of high-p_T hadron yields persist, and does it follow the gentle energy-dependence predicted in Fig. 37? Do the gluon densities inferred from parton energy loss model fits to hadron yields follow energy-dependent trends expected from gluon saturation models? Does elliptic flow remain in agreement with calculations that couple expansion of an ideal partonic fluid to a late-stage, viscous hadron cascade? Do meson-baryon differences and indications of constituent-quark scaling

persist in hadron yields and flow results at intermediate p_T? Do quark coalescence models remain viable, with inferred thermal quark spectra that change sensibly with the (presumably) slowly varying initial system temperatures? The study of the evolution with collision energy of differential measurements such as those in Fig. 25 promises to yield important insight into the dynamical processes which occur during system evolution.

- **Measure charmonium yields and open charm yields and flow, to search for signatures of color screening and partonic collectivity.** Use particle yield ratios for charmed hadrons to determine whether the apparent thermal equilibrium in the early collision matter at RHIC extends even to quarks with mass significantly greater than the anticipated system temperature. From the measured p_T spectra, constrain the relative contributions of coalescence vs. fragmentation contributions to charmed-quark hadron production. Compare D-meson flow to the trends established in the u, d and s sectors, and try to extract the implications for flow contributions from coalescence vs. possibly earlier partonic interaction stages of the collision. Look for the extra suppression of charmonium, compared to open charm, yields expected to arise from the strong color screening in a QGP state (see Fig. 2).
- **Measure angular correlations with far forward high-energy hadrons in d+Au or p+Au collisions.** Search for the mono-jet signature anticipated for quark interactions with a classical (saturated) gluon field, as opposed to di-jets from quark interactions with individual gluons. Correlations among two forward hadrons are anticipated to provide the best sensitivity to the gluon field at sufficiently low Bjorken x to probe the possible saturation regime.

Longer-term prospects, requiring much greater integrated luminosities (as anticipated at RHIC II) or other substantial facility developments, include:

- **Develop thermometers for the early stage of the collisions, when thermal equilibrium is first established.** In order to pin down experimentally where a thermodynamic transition may occur, it is critical to find probes with direct sensitivity to the temperature well before chemical freeze-out. Promising candidates include probes with little final-state interaction: direct photons – measured down to low momentum, for example, via $\gamma - \gamma$ HBT, which is insensitive to the large π^0 background – and thermal dileptons. The former would require enhanced pair production tracking and the latter the introduction of hadron-blind detectors and techniques.
- **Measure the yields and spectra of various heavy quarkonium species.** Recent LQCD calculations [17] predict the onset of charmonium melting – which can be taken as a signature for deconfinement – at quite different temperatures above T_c for J/ψ vs. ψ'. Similar differences are anticipated for the various Υ states. While interpretation of the yield for any one quarkonium species may be complicated by competition in a QGP state between

enhanced heavy quark production rates and screened quark-antiquark interactions, comparison of a measured hierarchy of yields with LQCD expectations would be especially revealing. They would have to be compared to measured yields for open charm and beauty, and to the corresponding quarkonium production rates in p+p and p+A collisions. Clear identification of ψ' and separation of Υ states require upgrades to detector resolution and vertexing capabilities.

- **Quantify parton energy loss by measurement of mid-rapidity jet fragments tagged by a hard direct photon, a heavy-quark hadron, or a far forward energetic hadron.** Such luminosity-hungry coincidence measurements will elucidate the energy loss of light quarks vs. heavy quarks vs. gluons, respectively, through the collision matter. They should thus provide more quantitative sensitivity to the details of parton energy loss calculations.
- **Test quantitative predictions for elliptic flow in U+U collisions.** The large size and deformation of uranium nuclei make this a considerable extrapolation away from RHIC Au+Au conditions, and a significant test for the details of hydrodynamics calculations that are consistent with the Au+Au results [3]. If the relative alignment of the deformation axes of the two uranium nuclei can be experimentally controlled, one would be able to vary initial spatial eccentricity largely independently of centrality and degree of thermalization of the matter.
- **Measure hadron multiplicities, yields, correlations and flow at LHC and GSI energies, and compare to quantitative predictions based on models that work at RHIC.** By fixing parameters and ambiguous features of gluon saturation, hydrodynamics, parton energy loss and quark coalescence models to fit RHIC results, and with guidance from LQCD calculations regarding the evolution of strongly interacting matter with initial temperature and energy density, theorists should make quantitative predictions for these observables at LHC and GSI before the data are collected. The success or failure of those predictions will represent a stringent test of the viability of the QGP-based theoretical framework.
- **Devise tests for the fate of fundamental QCD symmetries in the collision matter formed at RHIC.** If the nature of the QCD vacuum is truly modified above the critical temperature, then chiral and $U_A(1)$ symmetries may be restored, while parity and CP may conceivably be broken [168]. Testing these symmetries in this unusual form of strongly interacting matter is of great importance, even if we do not have a crisp demonstration beforehand that the matter is fully thermalized and deconfined. Indeed, if evidence were found for a clear change in the degree of adherence to one of the strong interaction symmetries, in comparison with normal nuclear matter, this would likely provide the most compelling "smoking gun" for production of a new form of matter in RHIC collisions. Approaches that have been discussed to date include looking for meson mass shifts in dilepton spectra as a signal of chiral symmetry restoration, and searching for

CP violation via $\Lambda - \overline{\Lambda}$ spin correlations or electric dipole distributions of produced charge with respect to the reaction plane [168]. It may be especially interesting to look for evidence among particles emerging opposite an observed high-p_T hadron tag, since the strong suppression of away-side jets argues that the fate of the away-side particles may reflect strong interactions with a maximal amount of early collision matter. These tests will begin in the short term, but may ultimately need the higher statistics available in the longer term to distinguish subtle signals from dominant backgrounds.

6.4 Outlook

The programs we have outlined above for desirable advances in theory and experiment represent a decade's worth of research, not all of which must, or are even expected to, *precede* a discovery announcement for the Quark-Gluon Plasma. We can imagine several possible scenarios leading to a more definitive QGP conclusion. Identification of a single compelling experimental signature is still conceivable, but the most promising prospects are long-term: establishment of a telling pattern of quarkonium suppression *vs.* species; observation of clear parity or CP violation, or of chiral symmetry restoration, in the collision matter; extraction of a transition signal as a function of measured early temperature. It is also possible that a single theoretical development could largely seal the case: *e.g.*, a compelling argument that gluon densities more than an order of magnitude higher than those in cold nuclear matter really do *demand* deconfinement; or sufficient hydrodynamics refinement to demonstrate that RHIC flow results really do *demand* a soft point in the EOS. Perhaps the most likely path would involve several additional successes in theory-experiment comparisons, leading to a preponderance of evidence that RHIC collisions have produced thermalized, deconfined quark-gluon matter.

In any scenario, however, RHIC has been, and should continue to be, a tremendous success in its broader role as an instrument for discovery of new features of QCD matter under extreme conditions. The properties already delineated, with seminal contributions from STAR, point toward a dense, opaque, nonviscous, pre-hadronic liquid state that was not anticipated before RHIC. Determining whether the quarks and gluons in this matter reach thermal equilibrium with one another before they become confined within hadrons, and eventually whether chiral symmetry is restored, are two among many profound questions one may ask. Further elaboration of the properties of this matter, with eyes open to new unanticipated features, remains a vital research mission, independent of the answer that nature eventually divulges to the more limited question that has been the focus of this document.

7 Appendix A: Charge

This report was prepared for the STAR Collaboration in response to the following charge from the Spokesperson, delivered to a drafting committee on March 18, 2004.

"Thank you very much for agreeing to help in preparing a draft whitepaper to serve as the starting point for a focused discussion by the STAR Collaboration of the experimental evidence regarding the role of the Quark-Gluon Plasma in RHIC heavy ion collisions."

"The charge to this panel is to make a critical assessment of the presently available evidence to judge whether it warrants a discovery announcement for the QGP, using any and all experimental and theoretical results that address this question. The white paper should pay particular attention to identifying the most crucial features of the QGP that need to be demonstrated experimentally for a compelling claim to be made. It should summarize those data that may already convincingly demonstrate some features, as well as other data that may be suggestive but with possible model-dependence, and still other results that raise questions about a QGP interpretation. If the conclusion is that a discovery announcement is at present premature, the paper should outline critical additional measurements and analyses that would make the case stronger, and the timeline anticipated to produce those new results."

"The white paper should be of sufficient quality and scientific integrity that, after incorporation of collaboration comments, it may be circulated widely within the RHIC and larger physics communities as a statement of STAR's present assessment of the evidence for the QGP."

8 Appendix B: Definitions of the Quark-Gluon Plasma in Nuclear Physics Planning Documents

One's conclusion concerning the state of the evidence in support of Quark-Gluon Plasma formation is certainly influenced by the definition one chooses for the QGP state. Recent positive claims have been based on definitions different from that chosen in this work (see Sec. 1), leaning more toward either an operational definition based on actual RHIC measurements [6], or a demonstration that experiments have reached conditions under which lattice QCD calculations predict a QGP state [7]. We have rather chosen to extract what we believe to be the consensus definition built up in the physics community from the past 20 years' worth of planning documents and proposals for RHIC. In this section, we collect relevant quotes concerning the QGP from a number of these documents.

A relativistic heavy-ion collider facility was first established as the highest priority for new construction by the 1983 Nuclear Science Advisory Committee (NSAC) Long Range Plan [169]. In discussing the motivation for such a facility, that document states:

> "Finally, under conditions of very elevated energy density, nuclear matter will exist in a wholly new phase in which there are no nucleons or hadrons composed of quarks in individual bags, but an extended *quark-gluon plasma*, within which the quarks are deconfined and move independently. ... The production and detection of a quark-gluon plasma in ultra-relativistic heavy ion collisions would not only be a remarkable achievement in itself, but by enabling one to study quantum chromodynamics (QCD) over large distance scales it would enable one to study fundamental aspects of QCD and confinement unattainable in few-hadron experiments. ... A second, chiral-symmetry restoring, transition is also expected at somewhat higher energy density, or perhaps coincident with the deconfinement transition; such a transition would be heralded by the quarks becoming effectively massless, and low mass pionic excitations no longer appearing in the excitation spectrum."

The high priority of such a collider was confirmed in the 1984-6 National Academy of Sciences survey of Nuclear Physics [170], which stated:

> "A major scientific imperative for such an accelerator derives from one of the most striking predictions of quantum chromodynamics: that under conditions of sufficiently high temperature and density in nuclear matter, a transition will occur from excited hadronic matter to a quark-gluon plasma, in which the quarks, antiquarks and gluons of which hadrons are composed become 'deconfined' and are able to move about freely. The quark-gluon

plasma is believed to have existed in the first few microseconds after the big bang, and it may exist today in the cores of neutron stars, but it has never been observed on Earth. Producing it in the laboratory will thus be a major scientific achievement, bringing together various elements of nuclear physics, particle physics, astrophysics, and cosmology."

The glossary of the above document [170] defined Quark-Gluon Plasma in the following way:

"An extreme state of matter in which quarks and gluons are deconfined and are free to move about in a much larger volume than that of a single hadron bag. It has never been observed on earth."

In the 1984 proposal for RHIC from Brookhaven National Laboratory [171], the QGP was described as follows:

"The specific motivation from QCD is the belief that we can assemble macroscopic volumes of nuclear matter at such extreme thermodynamic conditions as to overcome the forces that confine constituents in normal hadrons, creating a new form of matter in an *extended confined plasma of quarks and gluons*."

The 1989 NSAC Long Range Plan [172], in reconfirming the high priority of RHIC, states:

"The most outstanding prediction based on the theory of the strong interaction, QCD, is that the properties of matter should undergo a profound and fundamental change at an energy density only about one order of magnitude higher than that found in the center of ordinary nuclei. This change is expected to involve a transition from the confined phase of QCD, in which the degrees of freedom are the familiar nucleons and mesons and in which a quark is able to move around only inside its parent nucleon, to a new deconfined phase, called the quark-gluon plasma, in which hadrons dissolve into a plasma of quarks and gluons, which are then free to move over a large volume."

The 1994 NSAC Assessment of Nuclear Science [173] states:

"When nuclear matter is heated to extremely high temperatures or compressed to very large densities we expect it to respond with a drastic transformation, in which the quarks and gluons, that are normally confined within individual neutrons and protons, are able to move over large distances. A new phase of matter, called Quark-Gluon-Plasma (QGP), is formed. At the same time chiral symmetry is restored making particles massless at the scale of quark masses. Quantum Chromodynamics (QCD) of massless quarks is chirally (or left-right) symmetric, but in the normal world this

symmetry is spontaneously broken giving dynamical masses to quarks and the particles composed of quarks."

The 1996 NSAC Long Range Plan [174] repeats the emphasis on chiral symmetry restoration in addition to deconfinement:

"At temperatures in excess of T_c nuclear matter is predicted to consist of unconfined, nearly massless quarks and gluons, a state called the *quark-gluon plasma*. The study of deconfinement and chiral symmetry restoration is the primary motivation for the construction of the Relativistic Heavy Ion Collider (RHIC) at Brookhaven National Laboratory."

The most recent National Academy of Sciences survey of Nuclear Physics [175] puts it this way:

"At RHIC such high energy densities will be created that the quarks and gluons are expected to become deconfined across a volume that is large compared to that of a hadron. By determining the conditions for deconfinement, experiments at RHIC will play a crucial role in understanding the basic nature of confinement and shed light on how QCD describes the matter of the real world. ...Although the connection between chiral symmetry and quark deconfinement is not well understood at present, chiral symmetry is expected to hold in the quark-gluon plasma."

Finally, the 2004 NuPECC (Nuclear Physics European Collaboration Committee) Long Range Plan for nuclear physics research in Europe [176] states:

"The focus of the research in the ultra-relativistic energy regime is to study and understand how collective phenomena and macroscopic properties, involving many degrees of freedom, emerge from the microscopic laws of elementary particle-physics. ... The most striking case of a collective bulk phenomenon predicted by QCD is the occurrence of a phase transition to a deconfined chirally symmetric state, the quark gluon plasma (QGP)."

In short, every statement concerning the QGP in planning documents since the conception of RHIC has pointed to deconfinement of quarks and gluons from hadrons as the primary characteristic of the new phase. More recent definitions have tended to include chiral symmetry restoration as well. Based on the above survey, we believe that the definition used in this paper would be very widely accepted within the worldwide physics community as a "minimal" requirement for demonstrating formation of a Quark-Gluon Plasma.

Acknowledgements: We thank the RHIC Operations Group and RCF at BNL, and the NERSC Center at LBNL for their support. This work was supported in part by the HENP Divisions of the Office of Science of the U.S. DOE; the U.S. NSF; the BMBF of Germany; IN2P3, RA, RPL, and EMN of France; EPSRC of the United Kingdom; FAPESP of Brazil; the Russian Ministry of Science and Technology; the Ministry of Education and the NNSFC of China; Grant Agency of the Czech Republic, FOM of the Netherlands, DAE, DST, and CSIR of the Government of India; Swiss NSF; the Polish State Committee for Scientific Research; and the STAA of Slovakia.

References

[1] P. Jacobs and X.N. Wang, hep-ph/0405125.

[2] D.H. Rischke, Prog. Part. Nucl. Phys. 52 (2004) 197.

[3] P. F. Kolb and U. Heinz, in Quark Gluon Plasma 3, eds. R.C. Hwa and X.N. Wang (World Scientific, Singapore, 2003); nucl-th/0305084.

[4] M. Gyulassy, I. Vitev, X.N. Wang and B.W. Zhang, in Quark Gluon Plasma 3, eds. R.C. Hwa and X.N. Wang (World Scientific, Singapore, 2003), nucl-th/0302077; R. Baier, D. Schiff, B.G. Zakharov, Ann. Rev. Nucl. Part. Sci. 50 (2000) 37.

[5] B. Tomášik and U.A. Wiedemann, in Quark Gluon Plasma 3, eds. R.C. Hwa and X.N. Wang (World Scientific, Singapore, 2003); hep-ph/0210250.

[6] M. Gyulassy, nucl-th/0403032.

[7] M. Gyulassy and L. McLerran, Nucl. Phys. A750 (2005) 30.

[8] RIKEN-Brookhaven Research Center Scientific Articles, Vol. 9: New Discoveries at RHIC: the current case for the Strongly Interactive QGP (May, 2004).

[9] J. Glanz, Like Particles, 2 Houses of Physics Collide, New York Times, January 20, 2004 (Section F, page 1); K. Davidson, Universe-Shaking Discovery, or More Hot Air?, San Francisco Chronicle, January 19, 2004.

[10] G. Brumfiel, What's In a Name?, Nature, July 26, 2004.

[11] J.W. Harris and B. Müller, Ann. Rev. Nucl. Part. Sci. 46 (1996) 71.

[12] U. Heinz and M. Jacob, nucl-th/0002042.

[13] K.H. Ackermann et al., Nucl. Instrum. Methods A499 (2003) 624.

[14] F. Karsch, Lecture Notes in Physics 583 (2002) 209.

[15] O. Kaczmarek, F. Karsch, E. Laermann and M. Lütgemeier, Phys. Rev. D62 (2000) 034021.

[16] T. Matsui and H. Satz, Phys. Lett. B178 (1986) 416; F. Karsch, M.T. Mehr and H. Satz, Z. Phys. C37 (1988) 617.

[17] M. Asakawa and T. Hatsuda, Phys. Rev. Lett. 92 (2004) 012001; S. Datta et al., J. Phys. G 30 (2004) S1347.

[18] E. Laermann and O. Philipsen, Ann. Rev. Nucl. Part. Sci. 53 (2003) 163.

[19] Z. Fodor and S.D. Katz, JHEP 0404 (2004) 050.

[20] Z. Fodor and S.D. Katz, Phys. Lett. B534 (2002) 87; Z. Fodor and S.D. Katz, JHEP 0203 (2002) 014.

[21] L.D. Landau, Izv. Akad. Nauk Ser, Fiz. 17 (1953) 51; L.D. Landau and E.M. Lifshitz, Fluid Mechanics.

[22] E. Shuryak, Prog. Part. Nucl. Phys. 53 (2004) 273.

[23] R. Stock, J. Phys. G 30 (2004) S633.

[24] T. Biro and B. Müller, Phys. Lett. B 578 (2004) 78, and references therein.

[25] R. Hagedorn, Nuovo Cim. Suppl. 3 (1965) 147.

[26] H. Sorge, Phys. Lett. B402 (1997) 251.

[27] H. Sorge, Phys. Rev. Lett. 82 (1999) 2048.

[28] S.A. Bass and A. Dumitru, Phys. Rev. C61 (2000) 064909.

[29] D. Teaney, J. Lauret, and E. Shuryak, Phys. Rev. Lett. 86 (2001) 4783; nucl-th/0110037.

[30] P.F. Kolb, J. Sollfrank and U. Heinz, Phys. Rev. C62 (2000) 054909.

[31] H. Sorge, Phys. Rev. C52 (1995) 3291.

[32] P. Huovinen, P.F. Kolb, U. Heinz, P.V. Ruuskanen and S.A. Voloshin, Phys. Lett. B503 (2001) 58.

[33] H. van Hecke, H. Sorge and N. Xu, Phys. Rev. Lett. 81 (1998) 5764.

[34] N. Xu and Z. Xu, Nucl. Phys. A715 (2003) 587c.

[35] D. Teaney, Phys. Rev. C68 (2003) 034913.

[36] K. Morita, S. Muroya, C. Nonaka and T. Hirano, Phys. Rev. C66 (2004) 054904, and references therein.

[37] P. Braun-Munzinger, K. Redlich and J. Stachel, in Quark Gluon Plasma 3, eds. R.C. Hwa and X.N. Wang (World Scientific, Singapore, 2003); nucl-th/0304013.

[38] K. Huang, Statistical Mechanics (John Wiley and Sons, 1988).

[39] E. Fermi, Prog. Theor. Phys. 5 (1950) 570.

[40] E.V. Shuryak, Phys. Lett. B42 (1972) 357; J. Rafelski and M. Danos, Phys. Lett. B97 (1980) 279; R. Hagedorn and K. Redlich Z. Phys. C 27 (1985) 541.

[41] P. Braun-Munzinger, J. Stachel, J.P. Wessels and N. Xu, Phys. Lett. B365 (1996) 1.

[42] V. Koch, Nucl. Phys. A715 (2003) 108c.

[43] U. Heinz, Nucl. Phys. A661 (1999) 140c.

[44] A.M. Poskanzer and S.A. Voloshin, Phys. Rev. C58 (1998)1671.

[45] G. Torrieri and J. Rafelski, Phys. Lett. B509 (2001) 239; Z. Xu, J. Phys. G 30 (2004) S325; M. Bleicher and H. Stocker, J. Phys. G 30 (2004) S111.

[46] J.D. Bjorken, FERMILAB-PUB-82-59-THY and erratum (unpublished).

[47] M. Gyulassy, P. Levai and I. Vitev, Nucl. Phys. A661 (1999) 637; M. Gyulassy, P. Levai and I. Vitev, Nucl. Phys. B571 (2000) 197; M. Gyulassy, P. Levai and I. Vitev, Phys. Rev. Lett. 85 (2000) 5535; M. Gyulassy, P. Levai and I. Vitev, Nucl. Phys. B594 (2001) 371.

[48] E. Wang and X.N. Wang, Phys. Rev. Lett. 87 (2001) 142301.

[49] R. Baier, Y.L. Dokshitzer, A.H. Mueller, S. Peigne and D. Schiff, Nucl. Phys. B483 (1997) 291; R. Baier, Y.L. Dokshitzer, A.H. Mueller and D. Schiff, Nucl. Phys. B531 (1998) 403; R. Baier, Y.L. Dokshitzer, A.H. Mueller and D. Schiff, Phys. Rev. C60 (1999) 064902; R. Baier, Y.L. Dokshitzer, A.H. Mueller and D. Schiff, JHEP 0109 (2001) 033.

[50] U.A. Wiedemann, Nucl. Phys. B588 (2000) 303; U.A. Wiedemann, Nucl. Phys. A690 (2001) 731; C.A. Salgado and U.A. Wiedemann, Phys. Rev. Lett. 89 (2002) 092303; C.A. Salgado, U.A. Wiedemann, Phys. Rev. D68 (2003) 014008.

[51] W. Cassing, K. Gallmeister and C. Greiner, Nucl. Phys. A735 (2004) 277.

[52] G.R. Farrar, H. Liu, L.L. Frankfurt and M.I. Strikman, Phys. Rev. Lett. 61 (1998) 686; S.J. Brodsky and A.H. Mueller, Phys. Lett. B206 (1988) 685; B.K. Jennings and G.A. Miller, Phys. Lett. B236 (1990) 209; B.K. Jennings and G.A. Miller, Phys. Rev. D44 (1991) 692; B.K. Jennings and G.A. Miller, Phys. Rev. Lett. 69 (1992) 3619; B.K. Jennings and G.A. Miller, Phys. Lett. B274 (1992) 442.

[53] X.N. Wang, Phys. Lett. B579 (2004) 299.

[54] M. Djordjevic and M. Gyulassy, Phys. Lett. B560 (2003) 37.

[55] A. Airapetian et al. [HERMES Collaboration], Eur. Phys. J. C 20 (2001) 479; V. Muccifora [HERMES Collaboration], Nucl. Phys. A715 (2003) 506.

[56] J.M. Moss et al., hep-ex/0109014.

[57] X.N. Wang and X.F. Guo, Nucl. Phys. A 696 (2001) 788; B.W. Zhang and X.N. Wang, Nucl. Phys. A720 (2003) 429.

[58] R. Baier, Nucl. Phys. A715 (2003) 209c.

[59] J. Breitweg et al., Eur. Phys. J. C 7 (1999) 609.

[60] A.H. Mueller, Nucl. Phys. B335 (1990) 115; A.H. Mueller, Nucl. Phys. B572 (2002) 227.

[61] L.D. McLerran and R. Venugopalan, Phys. Rev. D49 (1994) 2233.

[62] L.D. McLerran, hep-ph/0311028.

[63] E. Iancu and R. Venugopalan, in Quark Gluon Plasma 3, eds. R.C. Hwa and X.N. Wang (World Scientific, Singapore, 2003); hep-ph/0303204.

[64] V.N. Gribov and L.N. Lipatov, Sov. J. Nucl. Phys. 15 (1972) 438 and 675; L.N. Lipatov, Sov. J. Nucl. Phys. 20 (1975) 94; G. Altarelli and G. Parisi, Nucl. Phys. B126 (1977) 298; Yu. L. Dokshitzer, Sov. Phys. JETP 46 (1977) 641.

[65] E.A. Kuraev, L.N. Lipatov and V.S. Fadin, Phys. Lett. B60 (1975) 50; Sov. Phys. JETP 44 (1976) 443; Sov. Phys. JETP 45 (1977) 199; L.N. Lipatov, Sov. J. Nucl. Phys. 23 (1976), 338; Ya. Ya. Balitsky and L.N. Lipatov, Sov. J. Nucl. Phys. 28 (1978) 822; Sov. Phys. JETP Lett. 30 (1979) 355.

[66] D. Kharzeev and M. Nardi, Phys. Lett. B507 (2001) 121; D. Kharzeev and E. Levin, Phys. Lett. B523 (2001) 79.

[67] V.V. Anisovich and V.M. Shekhter, Nucl. Phys. B55 (1973) 455; J.D. Bjorken and G.E. Farrar, Phys. Rev. D9 (1974) 1449; K.P. Das and R.C. Hwa, Phys. Lett. B68 (1977) 459; Erratum ibid. 73 (1978) 504; R.G. Roberts, R.C. Hwa and S. Matsuda, J. Phys. G 5 (1979) 1043.

[68] C. Gupt, R.K. Shivpuri, N.S. Verma and A.P. Sharma, Nuovo Cim. A75 (1983) 408; T. Ochiai, Prog. Theor. Phys. 75 (1986) 1184; T.S. Biro, P. Levai and J. Zimanyi, Phys. Lett. B347 (1995) 6; T.S. Biro, P. Levai and J. Zimanyi, J. Phys. G 28 (2002) 1561.

[69] S.A. Voloshin, Nucl. Phys. A. 715 (2003) 379c; D. Molnar and S.A. Voloshin, Phys. Rev. Lett. 91 (2003) 092301; R.J. Fries, B. Müller, C. Nonaka and S.A. Bass, Phys. Rev. Lett. 90 (2003) 202303; V. Greco, C.M. Ko and P. Levai, Phys. Rev. Lett. 90 (2003) 202302; Z.W. Lin and C.M. Ko, Phys. Rev. Lett. 89 (2002) 202302; Z.W. Lin and D. Molnar, Phys. Rev. C68 (2003) 044901.

[70] B. Müller, nucl-th/0404015.

[71] C. Adler et al. [STAR Collaboration], Phys. Rev. Lett. 90 (2003) 082302.

[72] R.C. Hwa and C.B. Yang, Phys. Rev. C66 (2002) 025205; R.C. Hwa and C.B. Yang, Phys. Rev. C67 (2003) 034902; R.C. Hwa and C.B. Yang, Phys. Rev. C70 (2004) 024905.

[73] W. Reisdorf and H.G. Ritter, Ann. Rev. Nucl. Part. Sci. 47 (1997) 663.

[74] J.-Y. Ollitrault, Phys. Rev. D46 (1992) 229.

[75] X.N. Wang and M. Gyulassy, Phys. Rev. Lett. 86 (2001) 3496.

[76] B.B. Back et al. [PHOBOS Collaboration], Phys. Rev. C65 (2002) 061901R.

[77] J. Adams et al. [STAR Collaboration], nucl-ex/0311017.

[78] K.J. Eskola, K. Kajantie, P.V. Ruuskanen and K. Tuominen, Nucl. Phys. B570 (2000) 379.

[79] W. Czyz and L.C. Maximon, Annals Phys. 52 (1969) 59.

[80] B.B. Back et al. [PHOBOS Collaboration], nucl-ex/0301017.

[81] K. Adcox et al. [PHENIX Collaboration], Phys. Rev. Lett. 87 (2001) 052301.

[82] M.M. Aggarwal et al. [WA98 Collaboration], Eur. Phys. J. C 18 (2001) 651.

[83] C. Adler et al. [STAR Collaboration], Phys. Rev. C70 (2004) 054907.

[84] J.D. Bjorken, Phys. Rev. D27 (1983) 140.

[85] J. Adams et al. [STAR Collaboration], Phys. Rev. Lett. 92, (2004) 182301.

[86] O. Barannikova et al. [STAR Collaboration], nucl-ex/0403014.

[87] C. Adler et al. [STAR Collaboration], Phys. Rev. Lett. 89 (2002) 092301; J. Adams et al. [STAR Collaboration], Phys. Lett. B595 (2004) 143; J. Adams et al. [STAR Collaboration], Phys. Rev. C70 (2004) 041901; J. Adams et al. [STAR Collaboration], nucl-ex/0406003.

[88] N. Xu and M. Kaneta, Nucl. Phys. A698 (2002) 306c.

[89] R. Hagedorn, CERN-TH-3918/84.

[90] E. Schnedermann, J. Sollfrank, and U. Heinz, Phys. Rev. C48 (1993) 2462.

[91] P. Braun-Munzinger, J. Stachel, J. Wessels, and N. Xu, Phys. Lett. B344 (1995) 43; P. Braun-Munzinger, I. Heppe, and J. Stachel, Phys. Lett. B465 (1999) 15.

[92] S.A. Bass et al., Phys. Rev. C60 (1999) 021902.

[93] A. Dumitru and S.A. Bass, Phys. Lett. B460 (1999) 411.

[94] S.S. Adler et al. [PHENIX Collaboration], Phys. Rev. C69 (2004) 034909.

[95] E. Yamamoto et al. [STAR Collaboration], Nucl. Phys. A715 (2003) 466c.

[96] K. Schweda et al. [STAR Collaboration], J. Phys. G 30 (2004) S693.

[97] K. Adcox et al. [PHENIX Collaboration], Phys. Rev. Lett. 88 (2002) 242301.

[98] A.M. Poskanzer and S.A. Voloshin, Phys. Rev. C58 (1998) 1671.

[99] N. Borghini, P.M. Dinh and J.Y. Ollitrault, Phys. Rev. C64 (2001) 054901.

[100] C. Alt et al. [NA49 Collaboration], Phys. Rev. C68 (2003) 034903.

[101] C. Adler et al. [STAR Collaboration], Phys. Rev. C66 (2002) 034904.

[102] A. Tang et al. [STAR Collaboration], AIP Conf. Proc. 698 (2004) 701; J. Adams et al. [STAR Collaboration], nucl-ex/0409033.

[103] G. Agakichiev et al. [CERES/NA45 Collaboration], Phys. Rev. Lett. 92 (2004) 032301.

[104] J. Adams et al. [STAR Collaboration], Phys. Rev. Lett. 92 (2004) 052302.

[105] C. Adler et al. [STAR Collaboration], Phys. Rev. Lett. 87 (2001) 182301.

[106] P. Huovinen, private communications (2003).

[107] E. Shuryak, Prog. Part. Nucl. Phys.53 (2004) 273.

[108] B.B. Back, et al. [PHOBOS Collaboration], Phys. Rev. Lett. 89 (2002) 222301.

[109] X. Dong, S. Esumi, P. Sorensen, N. Xu, and Z. Xu, Phys. Lett. B597 (2004) 328.

[110] J. Castillo et al. [STAR Collaboration], J. Phys. G 30 (2004) S1207.

[111] S.S. Adler et al. [PHENIX Collaboration], Phys. Rev. Lett. 91 (2003) 182301.

[112] C. Nonaka, R.J. Fries and S.A. Bass, Phys. Lett. B583 (2004) 73; C. Nonaka et al., Phys. Rev. C69 (2004) 031902.

[113] For general introduction of two-particle correlation studies, see U.A. Wiedemann and U. Heinz, Phys. Rept. 319 (1999) 145; B. Jacak and U. Heinz, Ann. Rev. Nucl. Part. Sci. 49 (1999) 529.

[114] G. Bertsch, Nucl. Phys. A498 (1989) 173c.

[115] D. Rischke and M. Gyulassy, Nucl. Phys. A597 (1996) 701; D. Rischke and M. Gyulassy, Nucl. Phys. A608 (1996) 479.

[116] C. Adler et al. [STAR Collaboration], Phys. Rev. Lett. 87 (2001) 082301; K. Adcox et al. [PHENIX Collaboration], Phys. Rev. Lett. 88 (2002) 242301.

[117] J. Adams et al. [STAR Collaboration], Phys. Rev. Lett. 92 (2003) 062301.

[118] S. Soff, hep-ph/0202240; D. Zschiesche, S. Schramm, H. Stocker, and W. Greiner, Phys. Rev. C65 (2001) 064902; S. Soff, S.A. Bass, and A. Dumitru, Phys. Rev. Lett. 86 (2001) 3981.

[119] U. Heinz, hep-ph/0407360.

[120] C.Y. Wong, J. Phys. G 30 (2004) S1053.

[121] J. Adams et. al. [STAR Collaboration], Phys. Rev. Lett. 91 (2003) 262302.

[122] M. Stephanov, K. Rajagopal, and E. Shuryak, Phys. Rev. Lett. 81 (1998) 4816.

[123] S. Voloshin, V. Koch, and H.G. Ritter, Phys. Rev. C60 (1999) 024901.

[124] S. Jeon and V. Koch, Phys. Rev. Lett. 85 (2000) 2076.

[125] M. Asakawa, U. Heinz, and B. Müller, Phys. Rev. Lett. 85 (2000) 2072.

[126] S.A. Bass, P. Danielewicz, and S. Pratt, Phys. Rev. Lett. 85 (2000) 2689.

[127] Q. Liu and T. Trainor, Phys. Lett. B567 (2003) 184.

[128] M. Gaździcki and St. Mrówczyński, Z. Phys. C54 (1999) 127.

[129] D. Adamava et al. [CERES Collaboration], Nucl. Phys. A727 (2003) 97.

[130] S.S. Adler et al. [PHENIX Collaboration], Phys. Rev. Lett. 93 (2004) 092301.

[131] G. Westfall et al. [STAR Collaboration], J. Phys. G 30 (2004) S1389.

[132] J. Adams et al. [STAR Collaboration], nucl-ex/0411003;T.A. Trainor et al. [STAR Collaboration], hep-ph/0406116.

[133] I. Bearden et al. [NA44 Collaboration], Phys. Rev. C65 (2002) 044903.

[134] J. Adams et al. [STAR Collaboration], Phys. Rev. C 71 (2005) 031901(R).

[135] J. Adams et al. [STAR Collaboration], Phys. Rev. Lett. 90 (2003) 172301.

[136] X.N. Wang and M. Gyulassy, Phys. Rev. D44 (1991) 3501; X.N. Wang and M. Gyulassy, Comput. Phys. Commun. 83 (1994) 307.

[137] C. Adler et al. [STAR Collaboration], Phys. Rev. Lett. 89 (2002) 202301.

[138] I. Arsene et al. [BRAHMS Collaboration], Phys. Rev. Lett. 91 (2003) 072305.

[139] S.S. Adler et al. [PHENIX Collaboration], Phys. Rev. Lett. 91 (2003) 072303.

[140] B.B. Back et al. [PHOBOS Collaboration], Phys. Rev. Lett. 91 (2003) 072302.

[141] J. Adams et al. [STAR Collaboration], Phys. Rev. Lett. 91 (2003) 072304.

[142] D. Antreasyan et al., Phys. Rev. D19 (1979) 764.

[143] X.N. Wang, Phys. Rept. 280 (1997) 287; M. Lev and B. Petersson, Z. Phys. C21 (1987) 155; T. Ochiai et al., Prog. Theor. Phys. 75 (1986) 288.

[144] J. Adams et al. [STAR Collaboration], Phys. Rev. Lett. 93 (2004) 252301.

[145] D. Hardtke et al. [STAR Collaboration], Nucl. Phys. A715 (2003) 272.

[146] F. Wang et al. [STAR Collaboration], J. Phys. G. 30 (2004) S1299; J. Adams et al. [STAR Collaboration], nucl-ex/0501016.

[147] X.N. Wang, Phys. Lett. B 595 (2004) 165.

[148] I. Vitev and M. Gyulassy, Phys. Rev. Lett. 89 (2002) 252301.

[149] K.J. Eskola, H. Honkanen, C.A. Salgado, and U.A. Wiedemann, Nucl. Phys. A747 (2005) 511.

[150] D. Kharzeev, E. Levin and L. McLerran, Phys. Lett. B561 (2003) 93.

[151] J. Adams et al. [STAR Collaboration], Phys. Rev. Lett. 91 (2003) 172302.

[152] T. Falter and U. Mosel, Phys. Rev. C66 (2002) 024608.

[153] K. Gallmeister, C. Greiner and Z. Xu, Phys. Rev. C67 (2003) 044905.

[154] B.B. Back et al. [PHOBOS Collaboration], Phys. Rev. Lett. 88 (2002) 022302.

[155] I. Arsene et al. [BRAHMS Collaboration], Phys. Rev. Lett. 93 (2004) 242303.

[156] V. Guzey, M. Strikman, and W. Vogelsang, Phys. Lett. B603 (2004) 173.

[157] D. Kharzeev, Y.V. Kovchegov and K. Tuchin, Phys Lett. B599 (2004) 23.

[158] A.D. Frawley et al. [PHENIX Collaboration], J. Phys. G30 (2004) S675.

[159] J. Adams et al. [STAR Collaboration], Phys. Rev. C 70 (2004) 064907.

[160] D. Kharzeev, Y.V. Kovchegov and K. Tuchin, Phys. Rev. D68 (2003) 094013.

[161] D. Kharzeev, E. Levin and L. McLerran, hep-ph/0403271.

[162] R. Vogt, hep-ph/0405060.

[163] A. Ogawa et al. [STAR Collaboration], nucl-ex/0408004.

[164] M.M. Aggarwal et al. [WA98 Collaboration], Phys. Rev. Lett. 81 (1998) 4087; M.M. Aggarwal et al. [WA98 Collaboration], Phys. Rev. Lett. 84 (2000) 578; M.M. Aggarwal et al. [WA98 Collaboration], Eur. Phys. J. C 23 (2002) 225.

[165] D. d'Enterria, J. Phys. G 30 (2004), S767.

[166] D.H. Rischke and M. Gyulassy, Nucl. Phys. A608 (1996) 479.

[167] J. Adams et al. [STAR Collaboration], nucl-ex/0411036.

[168] D. Kharzeev et al., Phys. Rev. Lett. 81 (1998) 512 (1998); D. Kharzeev, hep-ph/0406125.

[169] A Long Range Plan for Nuclear Science (NSAC Report, 1983).

[170] Physics Through the 1990s: Nuclear Physics, J. Cerny et al. (National Academy Press, Washington, D.C., 1986).

[171] RHIC and Quark Matter: Proposal for a Relativistic Heavy Ion Collider at Brookhaven National Laboratory (BNL Report 51801, August 1984).

[172] Nuclei, Nucleons, Quarks: Nuclear Science in the 1990's (NSAC Long Range Plan Report, December 1989).

[173] Nuclear Science: Assessment and Promise (NSAC Report, May 1994).

[174] Nuclear Science: A Long Range Plan (NSAC Report, February 1996).

[175] Nuclear Physics: The Core of Matter, The Fuel of Stars, J.P. Schiffer, et al. (National Academy Press, Washington, D.C., 1999).

[176] NuPECC Long Range Plan 2004: Perspectives for Nuclear Physics Research in Europe in the Coming Decade and Beyond, ed. M. Harakeh, et al. (April 2004).